

CONFIDENTIAL – DO NOT COPY

The Use of Structure-based Drug Design to Optimise Protein-Ligand Interactions

Sophie Bertrand

University of Strathclyde

Department of Pure and Applied Chemistry

April 2015



This thesis is the result of the author's original research. It has been composed by the author and has not been previously submitted for examination which has led to the award of a degree.

The copyright of this thesis belongs to GSK in accordance with the author's contract of engagement with GSK under the terms of the United Kingdom Copyright Acts. Due acknowledgement must always be made of the use of any material contained in, or derived from, this thesis.

Signed:

April 2015

Acknowledgements

Firstly, I would like to deeply thank my PhD supervisors, Dr. Craig Jamieson, Dr. Nicole Hamblin and Dr. Ian Churcher for all their support, encouragement and advice during these past four years. I really appreciated all their time in reviewing my work, their invaluable insights, discussions and questions. They have been amazing mentors and help me to become the medicinal chemist I am today.

I would like to thank all my colleagues who contributed one way or another to this work for their time, help and expertise. I would like to thank all my colleagues from the BCATm and PI3K δ teams, past and present, for their chemistry and medicinal chemistry input in the work described. I would like to thank my colleagues from the computational chemistry group for their expertise and running the biophysical assays and the X-ray crystallography experiments. I would like to thank my colleagues in the Biological Sciences department for running the biochemical assays. I would like to thank my colleagues from the Chemical Sciences group for running the physicochemical property assays. I would also like to thank my colleagues from the analytical department for their analytical expertise. I would like to thank my colleagues from the chiral purification group for their help with chiral resolution. I would like to thank my colleagues from DMPK for running *in vivo* PK assays. I would also like to thank my CRO colleagues for carrying out some experimental work.

I would like to thank my internal examiner, Prof. Billy Kerr, for his thorough review of this work and insightful comments to improve this thesis. I would also like to thank Dr. Eric Talbot, colleague and friend, for his help in preparing this thesis and all his support and encouragement.

I would like to thank Dr. Amanda Gladwin and Dr. Mark Hillier from the Legal Global Patents department for reading over the copies of this thesis. I would also like to thank Dr. David House, Dan Thomas, Dr. Máire Convery, Dr. Don Somers, Alan Hill and Chris Edwards for carrying out all the data integrity checks of this thesis.

I would also like to thank Dr. Harry Kelly and Prof. Billy Kerr for all their efforts in making this programme possible and giving me the opportunity to further develop as

a chemist. I would also like to thank them for their support and for giving so many opportunities to present my work at seminars and conferences. I also would like to thank Dr. Edith Hessel for all her support and encouragement with this thesis and my personal development.

I would like to thank all my colleagues from the fragment group and the RRI DPU for the discussions and for making the lab a great place to work.

I would also like to thank all my friends for all their encouragement, support and all the great times we shared. In particular, my friends Aurélie, Emilie, Jess and Nora, for their unending friendship and support.

I would also like to deeply thank my parents, sister and cousin, Caro, for their love, encouragement and support. They have always been there for me and supported me in all my pursuits.

Finally, a special thanks to Ali for his love and support when I needed it the most.

Abstract

High attrition rates in drug candidates represent a key problem facing the pharmaceutical industry. Several studies have shown that controlling the physicochemical properties of molecules can reduce the likelihood of toxicity and, thus, the risk of attrition. Fragment-based drug discovery (FBDD) is a new approach to discovering high quality drug candidates using structure-based design with inherent focus on physicochemical properties. This approach was applied to two biological targets, mitochondrial branched-chain aminotransferase (BCAT_m) and phosphoinositide 3-kinase delta (PI3K δ).

BCAT_m, which catalyses the first step of branched-chain amino acids catabolism, has been identified as a potential novel target for an anti-obesity drug. FBDD screening using a combination of biochemical and biophysical assays successfully identified a variety of starting points for BCAT_m inhibition. From this exercise, 11 protein-ligand

structures were solved by X-ray crystallography displaying significant diversity in their binding mode. Two fragment hits were optimised using structurebased design and fragment merging techniques to identify a high quality lead molecule for this novel target. In addition, all of the data generated contributed to the discovery of a novel series of inhibitors suitable for use in critical *in vivo* experiments to further understand the biological role of BCATm.

PI3K δ , a lipid kinase critical in immune cell signalling, has been confirmed as a promising target for respiratory diseases. Structure-based design was initially employed to improve the selectivity profile of an existing lead series. Subsequently, novel and selective PI3K δ inhibitors were identified by targeting a specific interaction with the protein demonstrating an advantage over previously disclosed inhibitors, which retain potency at a related kinase. In addition, FBDD and structurebased design were employed to optimise potency and selectivity of a fragment hit whilst keeping the physicochemical properties in good range for oral dosing. Overall, these novel inhibitors demonstrate a promising profile in relation to the discovery of a suitable oral PI3K δ inhibitor for clinical development.

Contents

Acknowledgements.....	3
Abstract.....	4
Abbreviations.....	8
Chapter 1.....	14
Fragment-based Drug Discovery	14
1.1 New Challenges for the Pharmaceutical Industry.....	14
1.2 Fragment-based Drug Discovery	20
1.2.1 Introduction.....	20
1.2.2 Screening Methods	22
1.2.2.1 Fluorescence-based Thermal Melting (T _m)	23
1.2.2.2 Isothermal Titration Calorimetry (ITC).....	24
1.2.2.3 Surface Plasmon Resonance (SPR)	26

1.2.2.4 NMR Techniques.....	27
1.2.3 X-ray Crystallography	32
1.2.4 Fragment Optimisation	34
1.2.5 Ligand Efficiency	35
1.2.6 Case Studies	40
Chapter 2.....	42
Application of FBDD to the Discovery and Optimisation of BCATm Inhibitors.....	42
2.1 Biological Background.....	42
2.1.1 Obesity and BCATm	42
2.1.2 BCATm.....	46
2.1.3 Crystal Structure of BCATm	50
2.1.4 Known Inhibitors	51
2.1.5 Aims.....	55
2.1.6 Biochemical Assay	56
2.2 Fragment Hits Identification	58
2.2.1 Screening Strategy	58
2.2.2 Evaluation of Crystal Structures	65
2.2.3 Cluster Analysis	70
2.3 Cluster 3 - From Fragment to Lead Molecules	75
2.3.1 Fragment Hit and Initial SAR.....	75
2.3.2 Optimisation Goals	83
2.3.3 Results and Discussion	87
2.3.3.1 Synthesis of Carboxylic Acid Intermediates	87
2.3.3.2 Synthesis of <i>ortho</i> -Substituted Analogues.....	90
2.3.3.3 Expanding SAR around the Lipophilic Pocket.....	96
2.3.3.4 Biological Results.....	100
2.3.3.5 Future Work.....	110
2.3.4 Conclusion	112
2.4 Cluster 6 - Fragment to Lead Optimisation.....	114
2.4.1 Fragment Hit	114
2.4.2 Research Objective	122
2.4.3 Results and Discussion	123

2.4.3.1 Pyrazolo[1,5- α]pyrimidinone Chemistry	123
2.4.3.2 Investigation of Alternative Linkers	126
2.4.3.3 Exploring the Lipophilic Pocket	141
2.4.4 Conclusion	158
2.5 Overall Conclusions	160
Chapter 3.....	163
Discovery and Optimisation of Oral PI3K δ Inhibitors.....	163
3.1 Biological Background.....	163
3.1.1 Asthma	163
3.1.2 The PI3K Family	167
3.1.3 PI3K δ Structure and Selective Inhibition.....	171
3.2 Aims	178
3.3 Lead Series – Dihydrobenzofuran Template.....	181
3.3.1 Research Objective	182
3.3.2 Results and Discussion	185
3.3.2.1 Retrosynthetic Analysis	185
3.3.2.2 Synthesis of Piperidine 247	189
3.3.2.3 Synthesis of Piperidine 248	207
3.3.2.4 Biological Results	214
3.3.2.5 Morpholine Chemistry	221
3.3.2.6 Biological Results	224
3.3.3 Summary and Conclusions	227
3.3.4 Future Work.....	229
3.4 Fragment Series – Benzoxazine Template	231
3.4.1 Background.....	231
3.4.2 Aims and Optimisation Goals.....	234
3.4.3 Results and Discussion	240
3.4.3.1 Chemistry at the 6-position.....	240
3.4.3.2 Derivatisation at the 7-position.....	256
3.4.3.3 Biological Results	259
3.4.3.4 Expanding Knowledge around 7-substituted Benzoxazines.....	271
3.4.4 Summary and Conclusions	283

3.4.5 Future Work.....	285
3.5 General Conclusions	286
Experimental.....	288
4.1 General procedures.....	290
4.2 Experimental Procedures for Cluster 3 Template	295
4.3 Experimental Procedures for Cluster 6 Template	317
4.4 Experimental Procedures for Dihydrobenzofuran Template	331
References.....	361
Appendix.....	379
Experimental Procedures for Benzoxazine Template.....	380

Abbreviations

Å	Ångstrom
Ac	acetyl
ADME	absorption distribution metabolism excretion
ADP	adenosine diphosphate
AKT/PKB	protein kinase B
aq.	aqueous
Ar	aryl
ATP	adenosine triphosphate
APC	antigen-presenting cell
AUC	area under the curve
BCAA	branched-chain amino acid
BCAT	branched-chain aminotransferase
BCKA	branched-chain α -ketoacid
BCKADH	branched-chain α -ketoacid dehydrogenase
BMI	body mass index
Bn	benzyl

Bu	butyl
°C	degree Celsius
cat.	catalyst
CDI	1,1'-carbonyldiimidazole
CHI	chromatographic hydrophobicity index
chromlogD _{pH}	chromatographic log ₁₀ (distribution coefficient at the given aqueous buffer pH)
Cl	clearance
Cl _b	blood clearance
CLND	chemiluminescent nitrogen detection
CNS	central nervous system
clogP	calculated log ₁₀ (partition coefficient between octanol and water)
CMPB	cyanomethylenetriethylphosphorane
cmpd	compound
CPME	cyclopentyl methyl ether
CoA	coenzyme A
cod	1,5-cyclooctadiene
COPD	chronic obstructive pulmonary disease
Cp	cyclopentadienyl
CSD	Cambridge structural database
CV	column volume
δ	chemical shift (NMR)
Da	Dalton
DAG	diacylglycerol
DCM	dichloromethane
DEAD	diethyl azodicarboxylate
DHB	dihydrobenzofuran
DIAD	diisopropyl azodicarboxylate
DIBAL-H	diisobutylaluminium hydride
DIPEA	diisopropylethylamine
DMF	<i>N,N</i> -dimethylformamide
DMSO	dimethylsulfoxide
DTBAD	di- <i>tert</i> -butyl azodicarboxylate

DNA	deoxyribonucleic acid
DNA-PK	DNA-dependent protein kinase
e.e.	enantiomeric excess
ELT	encoded library technology
eq.	equivalent
ESI	electrospray ionisation
Et	ethyl
F	bioavailability
FaSSIF	fasted state simulated intestinal fluid
FBDD	fragment based drug discovery
FDA	Food and Drug Administration
g	gram(s)
GPCR	G-protein coupled receptor
GTP	guanosine triphosphate
h	hour(s)
HAC	heavy atom count
HATU	<i>O</i> -(7-azabenzotriazol-1-yl)- <i>N,N,N',N'</i> -tetramethyluronium hexafluorophosphate
HBA	hydrogen bond acceptor
HBD	hydrogen bond donor
hERG	human ether-à-go-go related gene
HMBC	heteronuclear multiple bond correlation
HMQC	heteronuclear multiple quantum correlation
HPLC	high-performance liquid chromatography
HRMS	high resolution mass spectrometry
HTS	high throughput screening
hWB	human whole blood
Hz	hertz
IC ₅₀	concentration of the substance that exhibits 50% inhibition
ICS	inhaled corticosteroid
IgE	immunoglobulin E antibody
IL	interleukin

IR	infrared spectroscopy
ITC	isothermal titration calorimetry
IVC	<i>in vitro</i> clearance
<i>J</i>	coupling constant (NMR)
K _a	acid dissociation constant
K _d	dissociation constant
L	litre(s)
LABA	long-acting β ₂ -agonist
LBF	liver blood flow
LCMS	liquid chromatography mass spectroscopy
LE	ligand efficiency
LHMDS	lithium hexamethyldisilazide
LLE	ligand lipophilicity efficiency
LLE _{AT}	ligand lipophilicity efficiency defined by Astex
Lys	lysine
m	milli
M	molar
MDAP	mass directed auto-preparative
Me	methyl
MeCN	acetonitrile
Met	methionine
Met ID	metabolite identification
μ	micro
μwave	microwave
MHz	mega Hertz
min	minute(s)
mol	mole(s)
mp	melting point
mTOR	mammalian target of rapamycin
MW	molecular weight
n	nano
NAD	nicotinamide adenine dinucleotide

NBS	<i>N</i> -bromosuccinimide
NCE	new chemical entity
n.d.	not determined
NMR	nuclear magnetic resonance
NOE(SY)	nuclear Overhauser effect (spectroscopy)
Nu	nucleophile
PK1	phosphoinositide-dependent kinase-1
Perm.	permeability
Ph	phenyl
PH	pleckstrin homology
Phe	phenylalanine
PI	phosphatidylinositol
pIC ₅₀	- log ₁₀ (IC ₅₀)
pIC ₅₀ (cell)	cellular pIC ₅₀
pIC ₅₀ (d)	pIC ₅₀ for BCAT ^m decoupled assay
PIFA	phenyliodine bis(trifluoroacetate)
PI3K	phosphoinositide 3-kinase
PI4K	phosphoinositide 4-kinase
PI5K	phosphoinositide 5-kinase
PIP	phosphatidylinositol phosphate
PIPK	phosphatidylinositol phosphate kinase
pK _a	- log ₁₀ (K _a)
PK	pharmacokinetic
PLP	pyridoxal-5'-phosphate
PMB	<i>para</i> -methoxybenzyl
PMP	pyridoxamine-5'-phosphate
p.o.	per os (oral dose)
PPB	plasma protein binding
ppm	parts per million
PSA	polar surface area
PTEN	phosphatase and tensin homolog

R _f	retention factor (chromatography)
ROESY	rotating-frame nuclear Overhauser effect correlation spectroscopy
R _t	retention time
rt	room temperature
SAR	structure-activity relationship
sat.	saturated
SCX	ISOLUTE™ strong cation exchange sorbent
SFI	solubility forecast index
SH	Src-homology domain
SHIP	SH2 domain containing inositol 5'-phosphatase
S/N	signal to noise ratio for NMR
SPE	solid phase extraction
SPhos	2-dicyclohexylphosphino-2',6'-dimethoxybiphenyl
SPR	surface plasmon resonance
SSS	sub-structure search
STD-NMR	saturation transfer difference nuclear magnetic resonance
t	time
T	temperature
t _{1/2}	half-life
TBAF	tetra- <i>n</i> -butylammonium fluoride
TBDMS	<i>tert</i> -butyldimethylsilyl
TBME	<i>tert</i> -butyl methyl ether
Tf	triflate
TFA	trifluoroacetic acid
Th	T helper cell
THF	tetrahydrofuran
Thr	threonine
TLC	thin layer chromatography
T _m	thermal melt
TMS	trimethylsilyl
T ₃ P	propylphosphonic anhydride
Trp	tryptophan

Tyr	tyrosine
UV	ultraviolet
V _{dss}	volume of distribution at steady state
vdW	van der Waals
Vps34	vacuolar protein sorting-associated protein 34
WHO	World Health Organisation
w/w	by weight

Chapter 1

Fragment-based Drug Discovery

1.1 New Challenges for the Pharmaceutical Industry

The discovery and development of drugs to market has always been a costly process. However, historically this was offset by a relatively large number of new products being launched successfully. In recent times, with the number of New Chemical Entity (NCE) registrations declining, and development costs increasing steadily, the pharmaceutical industry is facing new challenges to continue to develop new drugs in an economically viable manner. There is now a real need to reduce development time

and costs, reduce high compound attrition rates and cope with increased demands imposed by regulatory authorities and less well understood targets.¹⁻³ During the last decade the pharmaceutical industry has developed new approaches to tackle these problems, for example, using data from the human genome and systems biology.⁴⁻⁶

Despite these advances, high attrition rates of drug candidates still remain and this represents one of the key problems pharmaceutical companies are facing. In their analysis, Kola and Landis² revealed that attrition from candidate to drug is estimated at 95%; and, on average, only one in nine compounds progresses from first time in human to registration. Using these figures, a 5% improvement of the success rate could potentially double the output of the pharmaceutical industry. In order to begin to solve this challenge, we must first understand the causes of attrition. The graph in Figure 1.1 shows the causes of attrition in both 1991 and 2000. From these data, it appears that pharmacokinetic and bioavailability issues have largely been addressed (they accounted for less than 10% of attrition in 2000), which can be explained by a better understanding of pharmacokinetic properties and how to optimise these. However, efficacy remains an unsolved problem very hard to predict, and toxicological and commercial reasons for compound attrition have increased during this period.²

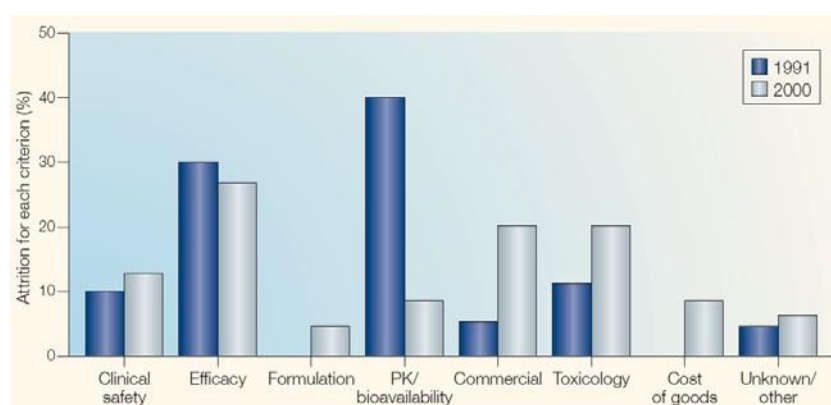


Figure 1.1 Causes of attrition in 1991 and 2000²

Toxicology and clinical safety, which accounts for approximately 30% of attrition, is now better understood and can be tackled in the early stage of the drug discovery process with increasing attention paid to this during lead optimisation.⁷⁻⁹ These are the key areas in which medicinal chemists can help to reduce attrition rates. Several studies have shown a link between the physicochemical properties of molecules and the risk of toxicity.⁷⁻¹²

In their analysis, Leeson and Springthorpe⁷ show that increasing lipophilicity as measured by clogP, which correlates with increased compound promiscuity (i.e. unwanted interactions with other targets), is a likely major cause of drug toxicity (Figure 1.2, a). Very lipophilic compounds will want to avoid water by burying themselves in proteins and, therefore, have a greater chance of binding to unwanted targets as well as their desired target. On the other hand, this analysis shows no clear correlation between MW and promiscuity (Figure 1.2, b).

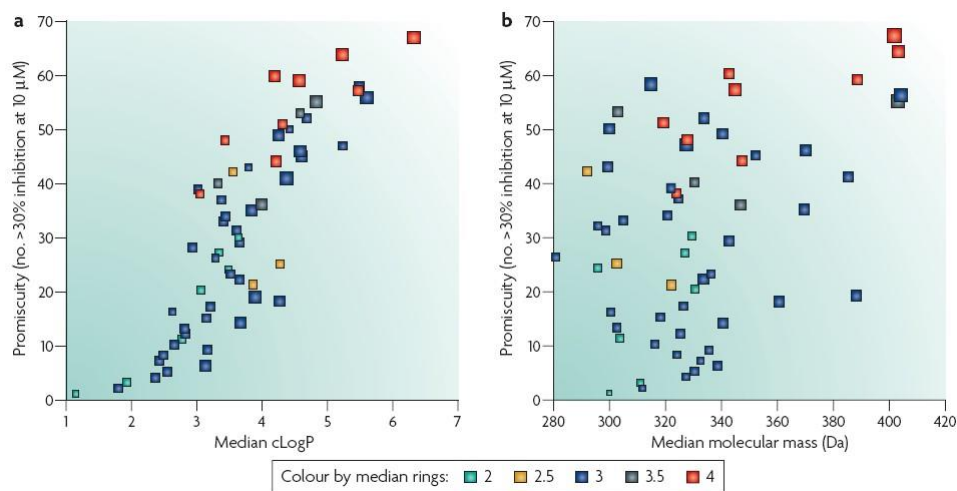


Figure 1.2 Promiscuity analysis of drugs⁷

Promiscuity was determined by the number of targets to which a compound showed activity > 30 % when assayed at 10 µM. Squares are sized by (a) median clogP or (b) median molecular weight.

Leeson and Springthorpe's analysis also shows properties of historical oral drugs, compounds in development and compounds in current patents from four major

pharmaceutical companies (Figure 1.3). The median clogP and MW varies significantly between the companies. This suggests a difference in the medicinal chemistry approaches and also in the compound portfolio between the companies. However, looking at the overall trend, compounds have moved significantly towards higher MW and higher clogP, with a median MW of 450 Da and a median clogP of 4.1, whereas recent oral drugs, discovered since 1990, have a median MW of 415 Da and a median clogP of 3.1.⁷ One possible reason is that the targets these new compounds are directed at have also changed significantly in recent years. It has been suggested that easily druggable targets have already been widely studied, possibly leaving only less druggable targets remaining. This is also supported by the difference in the means of MW and clogP between oral drugs before and after 1990. Oral drugs launched before 1990 had a median MW of 340 Da and a median clogP of 2.4. Nevertheless, this tendency towards higher lipophilicity in drug candidates needs to be addressed to offset the increase in toxicity observed in drug candidates.^{8,12}

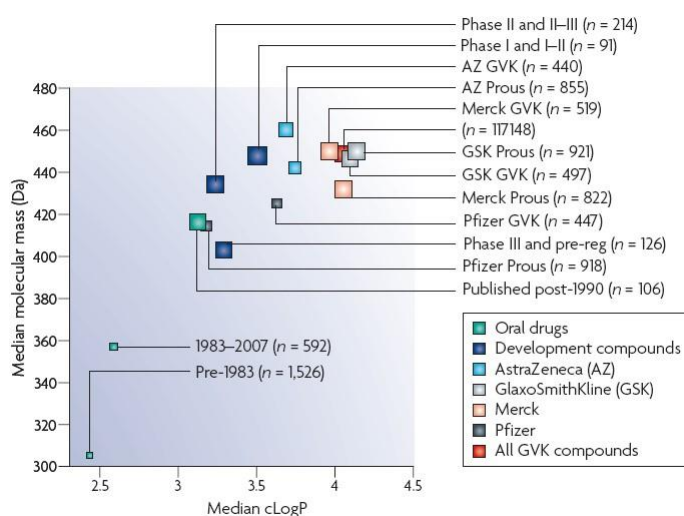


Figure 1.3 Trends in clogP and MW⁷

Squares are coloured and labelled by source, and sized by mean Lipinski score (vide infra)
 Databases used for analysis: Prous Science Integrity¹³ and GVK Bio¹⁴

While potential for attrition will depend on a wide range of factors, MW and clogP appear to be easily measured key contributors. Indeed, as discussed above,

manipulation of these physicochemical properties should provide molecules with improved ADME properties and a reduced likelihood of toxicity.

Lipophilicity of a compound is commonly estimated using the partition or distribution of a compound between two immiscible phases, often octanol and water.¹⁵ LogP corresponds to the intrinsic hydrophobicity of a compound and describes the partition of non-ionisable or un-ionised forms of a molecule. LogP is a constant in a given solvent. However, for ionisable molecules, logP will then vary with the pH as the relative proportion of species will vary depending on the pK_a. In this instance, a distribution coefficient is used, termed logD. This parameter, which represents the effective hydrophobicity, reflects the distribution of all the species present at a given pH. LogD at pH 7.4 (i.e. physiological pH) is typically used in drug discovery as it is considered to be the most relevant to a biological setting. Within our laboratory, a new parameter, called chromatographic logD_{7.4} (chromlogD_{7.4}), has been developed to assess lipophilicity of a compound.¹⁶ The chromlogD_{7.4} is derived from a chromatographic hydrophobicity index (CHI), obtained from retention times observed in a fast gradient reversed phase HPLC method.¹⁶⁻¹⁸

$$\text{chromlogD}_{7.4} = \text{CHI}_{7.4} \times 0.0857 - 2$$

Over the past 15 years, several analyses have been published with suggested guidelines to control physicochemical properties of the drug molecules. The first guide commonly used by the medicinal chemistry community was the Lipinski ‘rule of five’, a physicochemical property guideline for drug absorption.¹⁹ The ‘rule of five’ was derived from oral drugs that reached phase II clinical trials as a minimum. It states that drug candidates are more likely to have poor absorption or permeability if more than one of the following criteria is violated:

- MW greater than 500 Da,
- clogP greater than 5,

- number of HBD greater than 5, and - number of HBA is greater than 10.

Since then, several studies have been carried out highlighting the importance of physicochemical properties of the drug molecules and revised guidelines have been suggested.⁹⁻¹¹ Hughes and co-workers, at Pfizer,⁹ analysed the relationship between physicochemical properties and *in vivo* toxicity on a set of 245 compounds and demonstrated that compounds with $clogP > 3$ and $PSA < 75$ have an increased likelihood of toxicity. Gleeson¹⁰ showed that compounds with $clogP > 4$ and $MW > 400$ are more likely to have a poor ADME profile. A more recent review by Waring¹¹ on the effect of lipophilicity on ADME parameters also suggests that the optimal lipophilicity range is even more narrow and $clogP$ lies between one and three.

Additionally, new parameters have been investigated such as aromaticity and sp^2 character in molecules. An analysis of GSK molecules from Ritchie and Macdonald²⁰ revealed that an increased number of aromatic rings in drug molecules has a detrimental effect on developability parameters such as solubility, lipophilicity, plasma protein binding, CYP450 inhibition and hERG inhibition. A molecule with more than three aromatic rings is more likely to have a poor developability profile. A related parameter, the ‘Solubility Forecast Index’ (SFI), has been introduced as a useful guide to predict solubility.²¹ Based on the analysis of around 100,000 compounds, the SFI should be kept below five to have a greater likelihood of achieving good aqueous solubility ($> 100 \mu M$).

$$SFI = clogP + \text{number of aromatic rings}$$

In addition, a more general parameter, the ‘Property Forecast Index’ (PFI), has been derived as a useful predictor of developability.¹⁶ The PFI should be kept below seven to reduce the risk of toxicity through off target effects.

$$PFI = \text{chromlog}D_{7.4} + \text{number of aromatic rings}$$

These studies clearly indicate that monitoring and controlling the physicochemical properties of lead molecules from an early stage is crucial to reduce the likelihood of toxicity and, thus, the risk of attrition. However, reducing the molecular weight, the lipophilicity and the number of aromatic rings of lead molecules whilst still maintaining the desired potency and selectivity is a difficult proposition as MW and lipophilicity tend to increase during lead optimisation.^{22,23} Traditional leads from HTS tends to be large, well decorated molecules with less space for optimisation to drug molecules. As a consequence, an entirely new approach to hit and lead identification has been implemented over the past decade or so. Fragment-based Drug Discovery (FBDD) starts from much smaller molecule starting points (MW < 250 Da), which, if optimised carefully, lead to smaller, less lipophilic drug candidates. In turn, these molecules are anticipated to have lower attrition risk and higher success rates.

1.2 Fragment-based Drug Discovery

1.2.1 Introduction

Fragment-based Drug Discovery (FBDD) is a more recent structure-based approach for lead discovery that has emerged in the past decade aimed at reducing attrition and providing leads for previously intractable targets.²⁴⁻²⁶ As stated above, fragments are low molecular weight molecules (~ 100-250 Da) with low clogP and high aqueous solubility, which often bind weakly (μM to mM) to their target. Although fragments bind with lower affinity to their target, their binding efficiency per atom is usually higher than traditional HTS hits.^{24,27} The diagram in Figure 1.4 demonstrates how HTS often provides compounds that fill the enzyme pocket but not optimally. In contrast, fragment screening is anticipated to provide small molecules which bind optimally and can then be grown to a compact, yet potent lead through controlling clogP and binding

efficiency during the optimisation phase.²⁷ Thus, the lead molecule is designed to efficiently occupy the enzyme pocket.

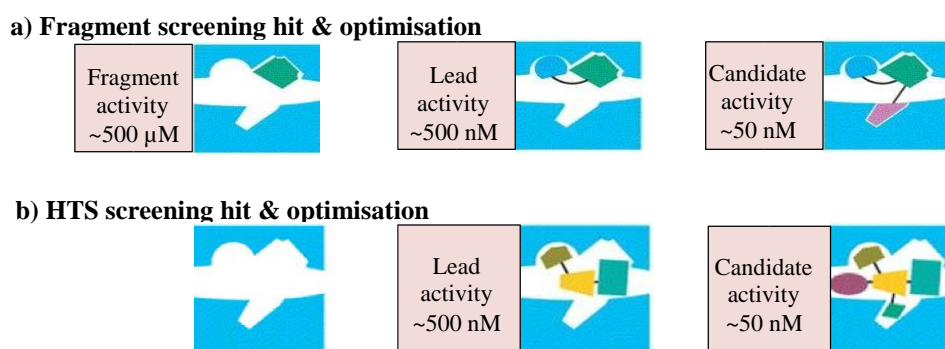


Figure 1.4 Comparison of (a) Fragment and (b) HTS approaches in drug discovery²⁴

FBDD consists of three key steps: (1) fragment library design, (2) fragment screening to identify and confirm hits and (3) fragment optimisation into leads (Figure 1.5). Each step is crucial for the success of the FBDD approach.

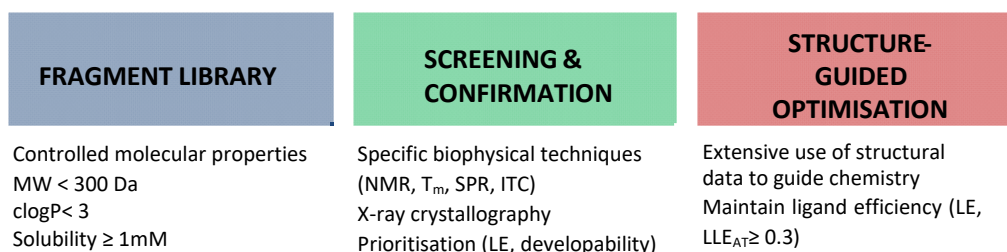


Figure 1.5 Fragment-based Drug Discovery process

Firstly, construction of the fragment library is extremely important to ensure optimal properties and maximum diversity in the screening set. Several criteria are considered when designing the library such as structural diversity, appropriate coverage of physicochemical space and solubility.²⁸ As mentioned previously, lipophilicity is also a key parameter to reduce likelihood of toxicity and a ‘rule of three’²⁹ (MW \leq 300 Da, clogP \leq 3, HBD \leq 3, HBA \leq 3) is often applied similarly to the ‘rule of five’. Solubility and purity are also crucial as fragments need to be screened at higher concentration in

order to be detected in a biological or biophysical assay. Therefore, high solubility is a pre-requisite, as is compound purity, to avoid any artefacts in the particular assay used.

Additionally, small fragments allow sampling of chemical space more efficiently than HTS-derived molecules, since chemical space increases exponentially as molecular weight increases.^{22,30} Thus, in principle, fewer fragments need to be screened to give good coverage of available chemical space. Libraries of as few as 1,000 fragments are commonly used compared to typical HTS libraries, which are generally in excess of 10^6 compounds. As fragments are less complex, they have a higher probability of binding to the target, therefore, hit rates are typically higher from fragment screening.²⁸

As fragments are weak binders (μM to mM affinity), traditional biochemical screening methods, which measure the biological activity of a molecule, are often not sensitive enough and high concentration screening ($> 100 \mu\text{M}$) will usually be required.²⁷ Although high concentration biochemical screening can be used, it can sometimes be less reliable due to potential risks of compound aggregation and interference with the assay read-out.³¹ Therefore, more specialised biophysical techniques such as X-ray crystallography, Nuclear Magnetic Resonance (NMR), Surface Plasmon Resonance (SPR) and Isothermal Titration Calorimetry (ITC) are used to screen fragments and these are discussed in some detail in the following sections.

Finally, X-ray crystallography using the fragment hits in complex with the biological target is critical to confirm their binding mode and guide the fragment to lead optimisation process. During this last stage, X-ray crystallography will give detailed structural information to drive synthetic chemistry and is pivotal in the design of ligand efficient lead molecules.

1.2.2 Screening Methods

As described above, high concentration biochemical assays are required to detect weak fragment hits but can give false positives and artefacts.³¹ Therefore, more specialised biophysical techniques are used to screen fragments as they measure a direct interaction of the molecule with their target and can detect weak binders. However, binding alone does not necessarily translate to changes in biological function. Therefore, a biochemical assay is useful to confirm that any hits identified are functionally active. Commonly, a combination of these techniques is used to triage fragment hits. Each experimental approach has different strengths and limitations, but the choice of the technique will often depend on the target. Each of the techniques described below will detect functional and non-functional binding.

1.2.2.1 Fluorescence-based Thermal Melting (T_m)

Fluorescence-based thermal melting (T_m) monitors changes in thermal stability of a protein using a fluorescent dye that binds selectively to denatured or unfolded protein.³² As the temperature rises, the protein undergoes thermal unfolding and exposes its hydrophobic region where the dye can bind and gives a fluorescent response. However, if the protein is folded, the dye is exposed to an aqueous environment and its fluorescence is quenched. Fluorescence is monitored and plotted against temperature to give a thermal melting graph shown in Figure 1.6. The melting temperature (T_m) is defined as the midpoint of the protein unfolding curve. When a molecule binds to a protein, it can stabilise its native state which reflects in an increase of its T_m . The result is given as the difference in T_m in the presence and in the absence of binding ligand (ΔT_m). An example of a typical T_m graph is shown in Figure 1.6.

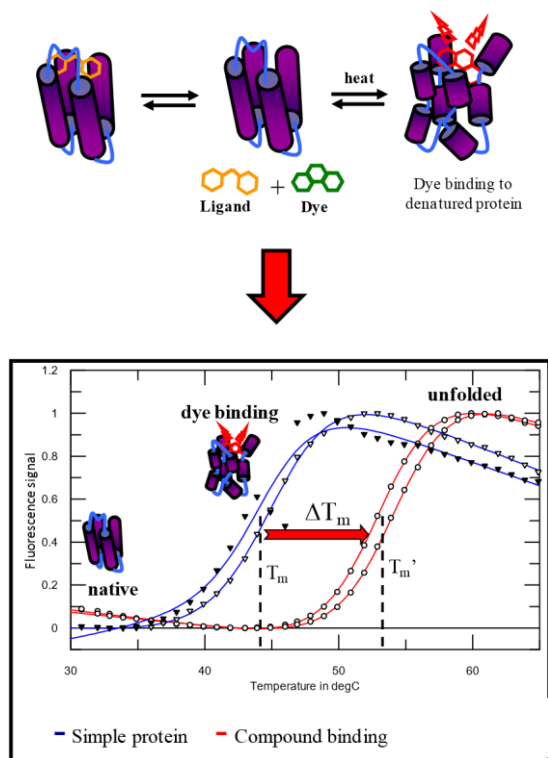


Figure 1.6 Fluorescence-based thermal melting principle³³

T_m is a high throughput technique which requires only small quantities of protein, so in a practical sense generates a large amount of data. One limitation is that weak fragments can bind without stabilising the protein and, therefore, exhibit no ΔT_m and consequently are not detectable using this methodology.

1.2.2.2 Isothermal Titration Calorimetry (ITC)

Isothermal titration calorimetry (ITC) measures the heat released or absorbed when a ligand binds to a protein.³² ITC is a quantitative technique that directly measures binding affinity (K_a), binding stoichiometry (n), enthalpy change (ΔH) and entropy (ΔS). The basic principle of ITC is shown in Figure 1.7.

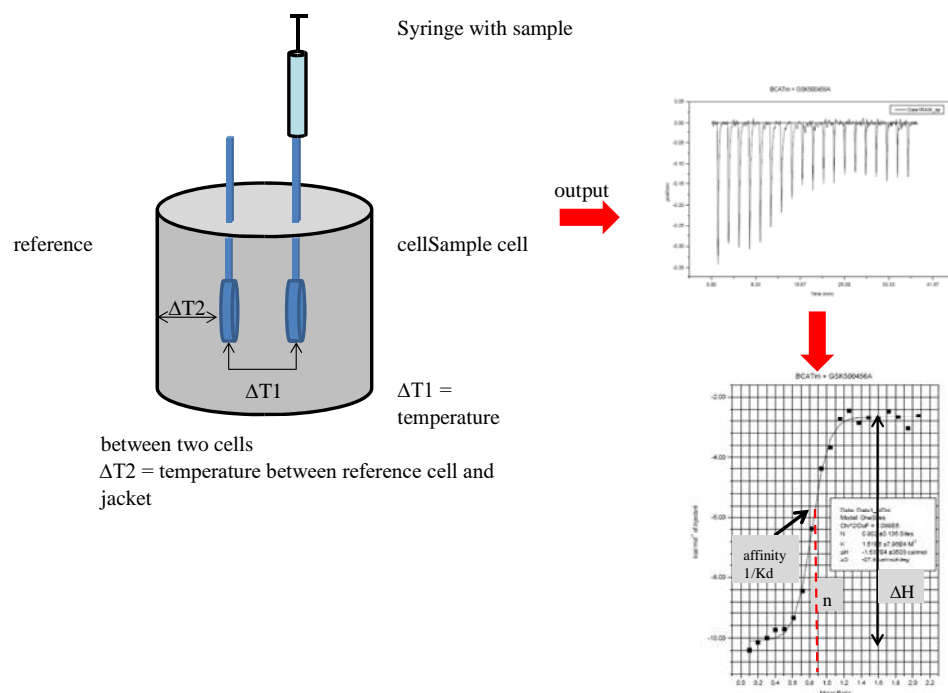


Figure 1.7 ITC principle³⁴

A solution of ligand is titrated into a cell containing a solution of the target protein. When the ligand interacts with the protein, heat is released or absorbed in direct proportion to the amount of binding. The temperature between the sample cell and the reference cell (ΔT_1) is kept at a constant value by addition or removal of heat to the sample cell. The heat change is measured over time to give an ITC spectrum. As the protein becomes saturated with ligand, the heat change decreases until only the dilution heat is observed. As a result, a series of spikes of heat flow is obtained, with each spike corresponding to one injection of ligand. These heat spikes are then integrated to give a curve of the total heat exchange per injection, which gives the thermodynamic parameters of the interaction studied.

ITC is a low throughput technique which requires a relatively large amount of protein (~1 mg per experiment) in comparison to some of the other commonly used techniques.

Therefore, this technique is not suitable for primary screening but is very useful as a hit confirmation technique.

1.2.2.3 Surface Plasmon Resonance (SPR)

Surface Plasmon Resonance (SPR) is an optical technique used to detect changes in the refractive index near the sensor surface as a result of a ligand binding. The basic principle of SPR is shown in Figure 1.8.

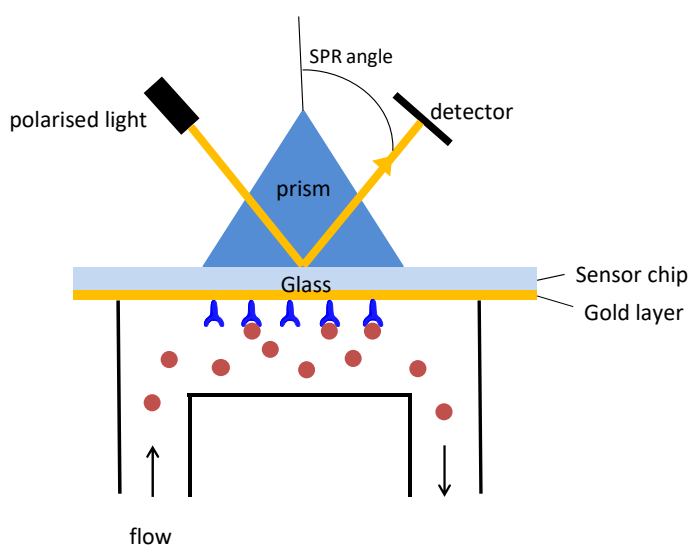


Figure 1.8 SPR principle

The target protein is immobilised onto a gold-coated glass sensor chip (50-100 nm thick). The attachment point must be selected with care to avoid disturbance in the binding site of interest. A solution of the ligand is then injected through the flow cell under continuous flow conditions. Binding of a ligand will result in a change at the sensor surface, which will lead to a change in SPR signal. To measure the SPR signal, a light is passed through a prism positioned on top of the sensor, at an angle at which the light is totally reflected and a detector monitors the intensity of the reflected light. Under these conditions, the evanescent wave (a wave formed when waves travelling in a medium undergo total internal reflection) passes into the gold layer exciting the

electrons, which then produce surface plasmons. At a specific wavelength and angle, plasmon resonance occurs at the gold surface resulting in a decrease in the intensity of the reflected light. The detector monitors the angle and intensity of the reflected light. The angle of the SPR is sensitive to any change in the gold surface. Thus, if the ligand binds to the protein, the surface mass changes resulting in a change in the refractive index. These changes are converted in a resonance unit, which ultimately generate a sensorgram as shown in Figure 1.9.

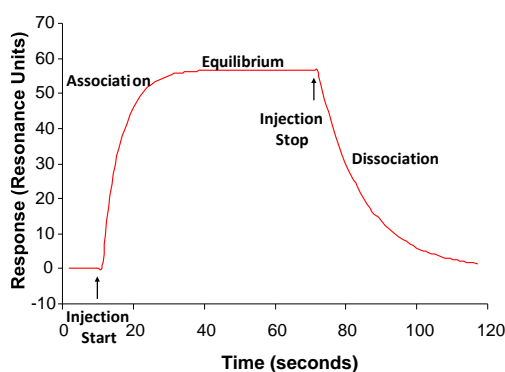


Figure 1.9 SPR sensorgram

SPR is an extremely sensitive and label-free technique to study molecular interactions, which requires very low amounts of protein and is relatively high throughput. It allows to determine a number of parameters such as binding stoichiometry, association rate constant (k_{on}), dissociation rate constant (k_{off}), binding constant (K_d) and thermodynamic parameters including free energy (ΔG), enthalpy (ΔH) and entropy (ΔS). Competition experiments can also be used to confirm binding at the desired site. A major limitation, however, is the necessity to immobilise the protein of choice without affecting its function or stability.

1.2.2.4 NMR Techniques

NMR techniques can be divided in two categories: protein-based methods and ligand-based methods. Protein-based methods require labelling of the protein, which is

expensive, and is restricted to proteins of less than 50 kDa. Thus, they are less frequently used for FBDD. However, one advantage is that they can provide information on the site of binding. On the other hand, ligand-based methods do not require labelled protein and observe changes in the NMR signals of the small molecules. Most of the ligand-based methods record 1D spectra, which are faster to acquire than 2D and thus, allow higher throughput. They provide the most simple and rapid methods of NMR screening and are therefore very popular. One major limitation is the inability to detect tight binders. For the case of a strongly bound ligands, the dissociation rates are slower preventing the transfer of the properties of the bound molecules to the bulk unbound molecules. The following section will focus on ligand-based methods, which are commonly used in our laboratory.

a. Line Broadening NMR

Line broadening NMR exploits the relaxation properties of a molecule. Relaxation depends on the tumbling rate of a molecule. Small molecules tumble fast in solution resulting in fast relaxation rate and thus sharp signals. In contrast, macromolecules tumble slower and exhibit broadened signals. When a ligand binds to a protein, it adopts the relaxation properties of the complex. This leads to a slower relaxation rate and broadening of the ligand signals. An example of spectra is shown in Figure 1.10.

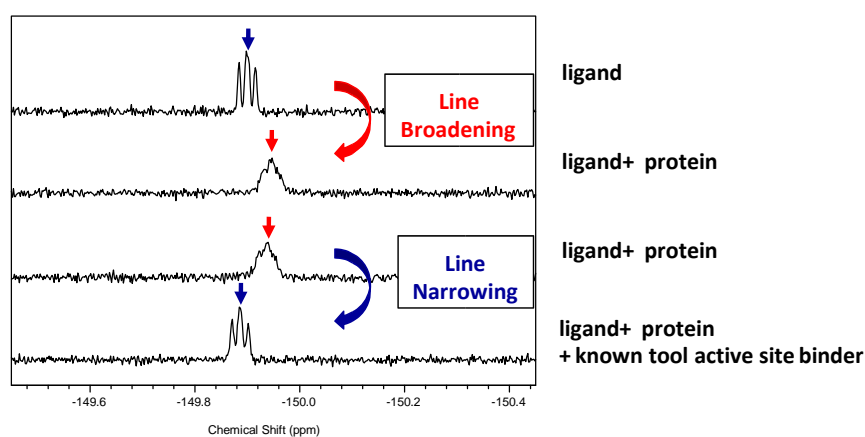


Figure 1.10 Example of line broadening ^{19}F NMR spectra

Line broadening NMR also allows the use of cocktail mixtures for screening and ranking of ligand binding affinity by comparing the extent to which the individual signals broaden.

b. Saturation Transfer Difference NMR (STD-NMR)

Saturation transfer difference NMR (STD-NMR) exploits a magnetisation transfer process from the protein to the binding ligand.^{35,36} The principle of STD-NMR is illustrated in Figure 1.11. Selective irradiation of the protein, at a chemical shift far from any ligand resonance, excites a small number of methyl protons only on the protein, which then leads to the saturation of the entire protein by intramolecular saturation transfer (spin diffusion). When a ligand binds to the protein, some of the magnetisation is transferred to the ligand by intermolecular saturation transfer. The intensity of saturation transferred depends on contact time and proximity to the protein. As shown on Figure 1.11, the saturation is more intense on the protons that more closely interact with the protein.

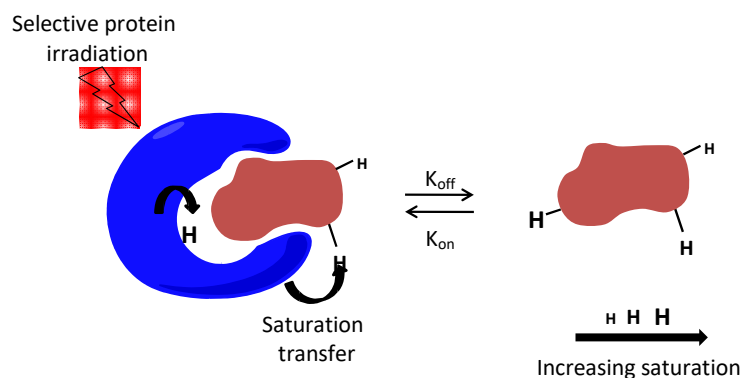


Figure 1.11 Principle of STD-NMR experiment³⁷

As a result, if the ligand binds to the protein, the intensity of a proton signal will be reduced where interaction with the target takes place. The difference between the

resulting spectrum with saturation and the reference spectrum without saturation gives an STD spectrum, showing only signals of a bound ligand as shown in Figure 1.12.

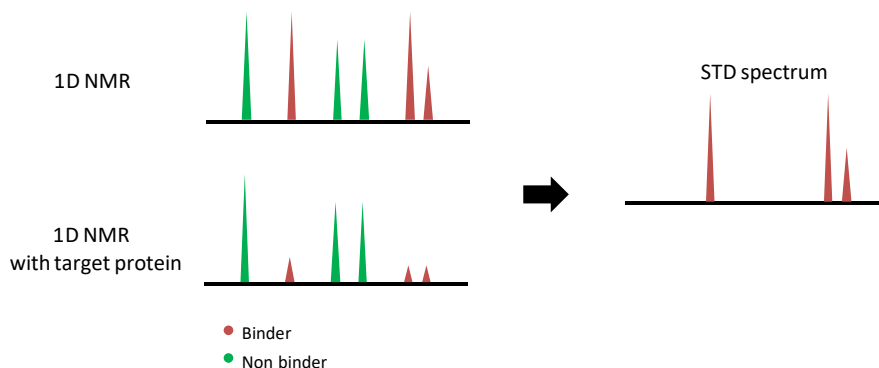


Figure 1.12 Example of an STD-NMR spectrum

The signal intensity of the STD-NMR experiment is determined as a multiple of the background and the signal to noise (S/N) ratio (Figure 1.13). The noise corresponds to the difference between the highest and lowest peak in the region of 10-11 ppm where no compound signal would usually be detected. Subsequently, the peak height in the STD-NMR is measured to give the signal intensity expressed as S/N. As shown on Figure 1.13, a peak with a S/N = 1 is 50% higher than the highest signal from the noise and can be considered significant. Therefore, compounds showing S/N > 1 will usually be considered as binders. The cut-off S/N selected for a target will then depend on the number of hits obtained. For targets that tend to give high hit rates (e.g. kinases), a higher cut-off will be applied to reduce the number of hits to a manageable quantity.

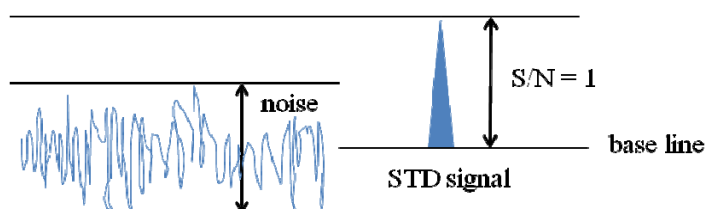


Figure 1.13 Signal intensity measurement

STD-NMR is a high sensitivity, medium throughput technique (1,000 - 10,000 compounds with pooling), which requires a small concentration of protein (usually 10-50 μM) but high ligand concentration (up to 1 mM). This technique also allows identification of ligand binding from a cocktail mixture. One major limitation of STD-NMR is that strongly bound compounds can score as apparent non-binders as STD-NMR relies on fast exchange of the ligand with the protein. If the ligand is tightly bound, fewer ligands will be saturated and exchanged into solution. Therefore, in such instances no STD signal will be observed, resulting in a false negative.

c. Water-Ligand Observation with Gradient Spectroscopy (WaterLOGSY)

The Water-LOGSY technique also exploits magnetisation transfer. However, this approach consists of exciting the bulk water molecules magnetisation. Magnetisation from the water molecules can be transferred to the protein and to the ligand. When a ligand does not interact with the protein, magnetisation will be transferred directly from the water molecules resulting in a positive NOE and thus negative signal. In contrast, when a ligand binds to the protein, water magnetisation is transferred *via* the protein resulting in a negative NOE and consequently a positive signal. Therefore, bound and unbound ligands can be differentiated as they will exhibit opposite sign signals.

Selective irradiation
of water molecules

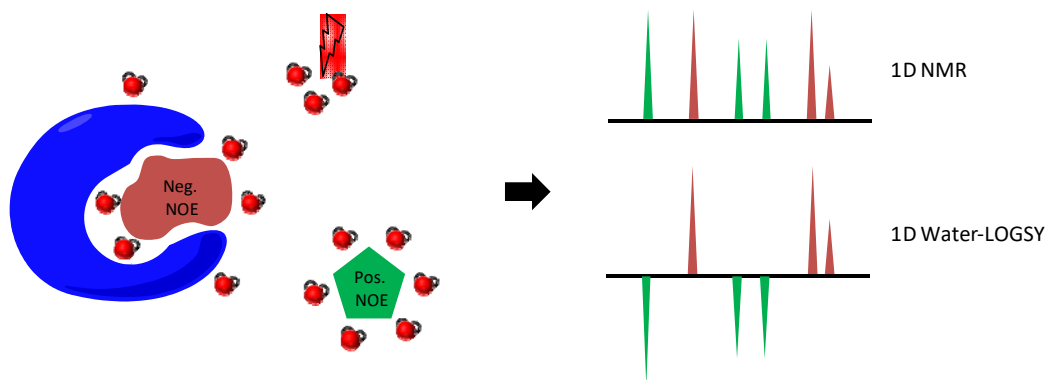


Figure 1.14 Principle of Water-LOGSY experiment

Similarly to STD-NMR, Water-LOGSY is a very sensitive method and requires small amount of protein but high concentration of ligand, which can lead to solubility issues.

1.2.3 X-ray Crystallography

As indicated above, X-ray crystallography is a critical component of fragment-based drug discovery. It enables confirmation of binding of the fragment hits to the target protein and gives detailed information of the associated interactions. X-ray crystallography is also essential to guide the design and the optimisation of the fragment hits.

X-ray crystallography is a very sensitive method, which can detect weak binders and has been used as a screening platform.^{38,39} The process to obtain crystal structures is summarised in Figure 1.15.⁴⁰ First, crystals of the ligand-protein complex need to be obtained. In the second step, the crystal is placed in a beam of X-rays generating a diffraction pattern. From these data, an electron density map is reconstructed. Finally,

the molecule is fitted in the electron density and after refinement, a crystal structure is proposed.

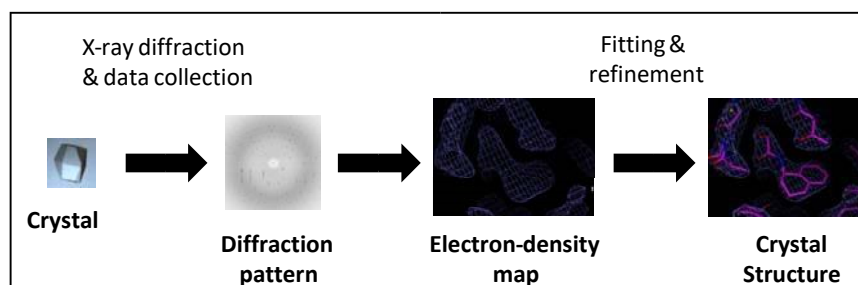


Figure 1.15 X-ray crystallography process

There are two ways to produce crystals of a small molecule with the target protein: co-crystallisation and soaking.⁴¹ Co-crystallisation consists of crystallising the molecule-protein complex pre-formed in solution, while soaking consists of exposing the pre-formed protein crystal to a solution containing the molecule. Soaking is often the method of choice as it requires only developing crystallisation conditions for the target protein. Once crystals of the protein itself have been obtained, several crystals of the ligand-protein complex can be produced. One limitation is that crystals are fragile and can often break in soaking conditions. In this instance, co-crystallisation will be more appropriate. As the complex is formed prior to crystallisation, binding-induced conformational changes can also be identified. However, this method is less suitable for high-throughput screening as separate crystallisation conditions are required for each compound.

The quality of a crystal structure is primarily judged by its resolution which defines the level of detail that the structure provides but this is predicted on accurately measured and complete X-ray diffraction data. At very high resolution (1 Å), the electron density map is clear and it is easier to fit individual atoms. At 2 Å, the resolution is still very good; ring systems can be modelled into the observed electron density in a straightforward manner. However, as the resolution decreases, the fitting becomes more difficult and uncertain (Figure 1.16). For small molecule-protein

complex X-ray crystallography, standard resolutions range between 1.5 Å to 3 Å. Generally, a resolution of around 2 Å provides an accurate structure and can be used with confidence in structure based design. By contrast, a structure based on a resolution of 3 Å should be used with care.

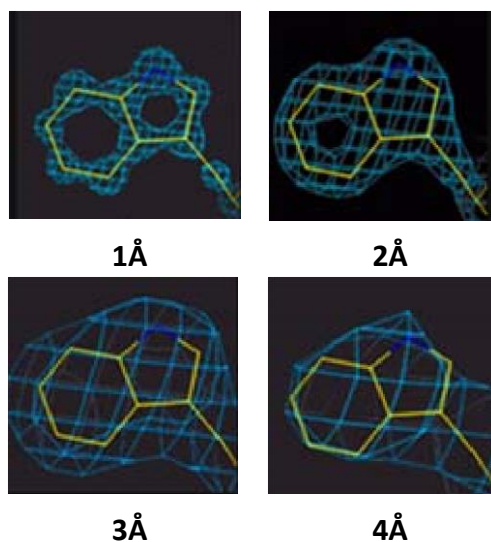


Figure 1.16 Effects of resolution on structure determination

Although X-ray crystallography gives very valuable information on the binding of a molecule and the active site, a crystal structure is only a static ‘snapshot’ of the complex. Proteins are flexible molecules, and this fact should be borne in mind during structure-based design. As prediction of conformational changes remains challenging, the crystal model needs to be challenged regularly to confirm hypotheses. Several crystal structures should be obtained during the optimisation process to confirm the binding mode of the molecules as the project progresses along the optimisation trajectory.

1.2.4 Fragment Optimisation

Once the fragment hits have been identified and confirmed by X-ray crystallography, the process of structure-based optimisation to lead can begin. Refinement of the initial fragment core is important to ensure that the fragment interacts optimally with the

pocket before adding molecular weight to the molecule. Following this, several strategies can be used to optimise fragment hits to leads which include growing, linking or merging fragments, as described in Figure 1.17.⁴²

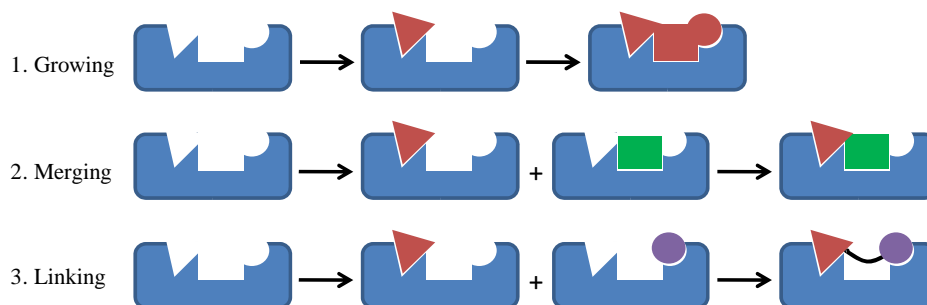


Figure 1.17 Approaches to optimise fragments⁴²

Growing, the most commonly used method, consists of designing larger molecules from the fragment hit that will have new interactions with the protein. This assumes that the fragment does not change binding mode during the process. Merging consists of combining interactions observed in other fragment hits to design new molecules with higher affinity. Finally, linking consists of linking two fragment hits together. Although linking two ligand efficient fragments is attractive to obtain higher affinity compounds, it is necessary to keep both fragments in the same orientation to conserve the key interactions, and this remains a challenge. Growing and merging have proved to be the most successful due to difficulties encountered in identifying suitable linkers.^{43,44}

1.2.5 Ligand Efficiency

Constant monitoring of binding efficiency during fragment optimisation is critical to ensure any change in size is accompanied by an appropriate improvement in potency. In this regard, ligand efficiency (LE) has emerged as a useful guide to prioritise hits and to allow optimisation of hits to leads efficiently. Kuntz⁴⁵ was first to propose the

use of normalised potencies. However, it was not until Hopkins⁴⁶ introduced the term ‘ligand efficiency’ that LE became widely used to compare the effectiveness of both fragment optimisation and also the more established process of lead optimisation.

LE estimates the efficiency of a ligand binding interaction with respect to its size and is defined as the free energy of ligand binding in relation to each heavy atom (or nonhydrogen atom).

$$LE = \frac{\Delta G}{HAC} = \frac{-RT \ln K_i}{HAC} \sim \frac{pIC_{50}}{HAC}$$

ΔG = Gibbs free energy, HAC = heavy atom count, K_i = binding constant

Based on the above, in order to achieve a 10 nM compound (a potency typical of a development candidate or drug) with molecular weight below 500 (i.e. to fulfil Lipinski’s rule, which contains on average 36 HAC), an LE of greater than or equal to 0.3 is required. The aim in FBDD is to find fragments with an LE of 0.3 or greater and monitor it through the optimisation process, aiming to keep it constant or, indeed, to improve it. If a drop of 10% or greater is observed for a small modification the change is considered not to be optimal.

Figure 1.18 illustrates the concept of ligand efficiency in a graphical manner. The figure shows the distribution of HTS hits, lead-like compounds, fragments and small molecule drugs in terms of their relative potencies and HAC. The blue area represents the region where compounds will be considered as ligand efficient ($LE \geq 0.3$). Although fragment hits have low MW and weak potencies, they often fall in the highly ligand efficient area which provides a greater opportunity for efficient optimisation. On the other hand, HTS hits which have higher potencies but higher MW tend to be in the low efficiency area (yellow zone), which make it more difficult to optimise to a highly efficient drug molecule.

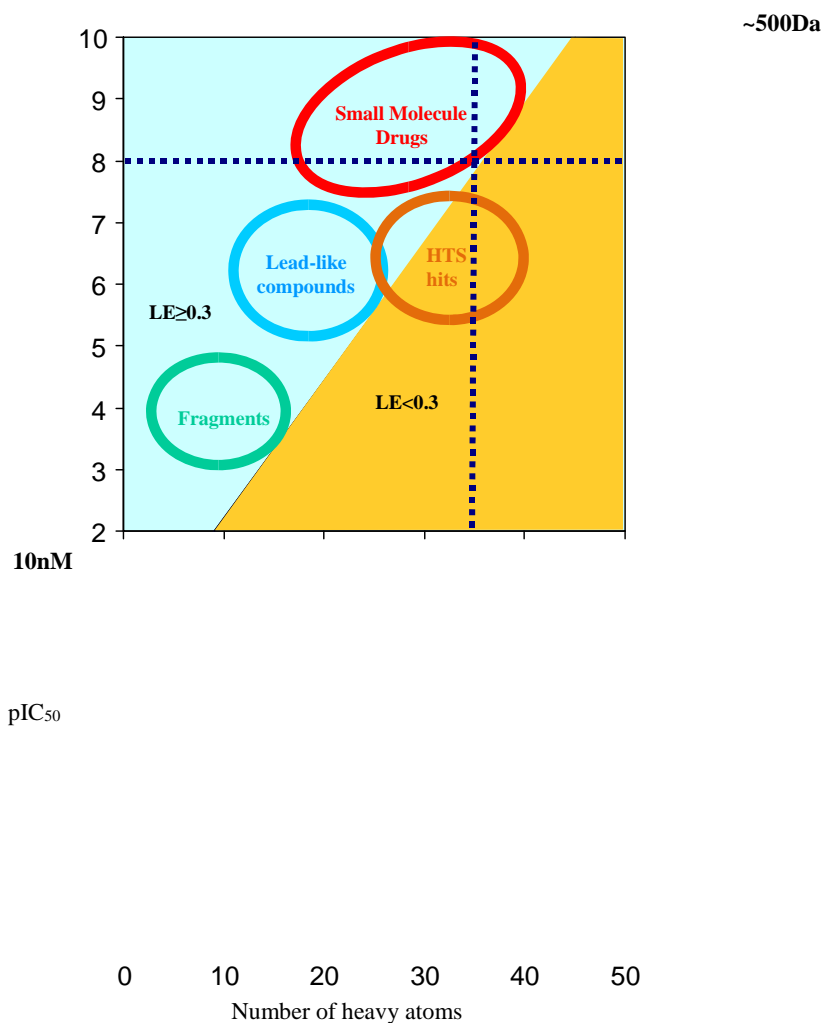


Figure 1.18 Ligand efficiency²⁴

As stated above, during lead optimisation, lipophilicity is generally observed to increase,^{22,23} and this tends to increase binding affinity due to desolvation. When a lipophilic molecule is in aqueous solution, water associates around the molecule becoming more ordered, hence decreasing entropy. However, when a molecule interacts with a protein, the ordered water molecules are displaced into bulk water where they become less ordered. This results in an increase in entropy, which from consideration of thermodynamics, results in an increase in affinity (Figure 1.19).

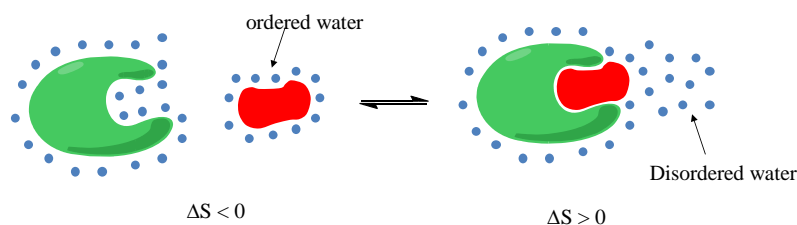


Figure 1.19 Desolvation effect

As discussed previously, high lipophilicity also increases the potential of off-target activity and toxicity. Therefore, it is also crucial to monitor lipophilicity during optimisation. Leeson and Springthorpe have proposed a new parameter, ligandlipophilicity efficiency (LLE) which takes into account lipophilicity in relation to potency.⁷ They suggest a target value of 5 or greater for development candidates based on the average oral drug with $clogP$ of 2.5 and potency of 1-10 nM.

$$LLE = (pIC_{50} \text{ or } pK_i) - clogP$$

While this parameter is very useful in lead optimisation, it is not particularly suited to fragment hits, which tend to have lower activity and higher polarity. Therefore, Mortenson and Murray have defined an alternative LLE index (LLE_{AT}), where a modified free energy term is used to remove the non-specific binding component due to lipophilicity.⁴⁷ In addition, a constant term is added to allow direct comparison with the conventional LE.

$$LLE_{AT} = 0.111 + \left(\frac{pIC_{50} - clogP}{HAC} \right) \times 1.36$$

Using this expression, LLE_{AT} has the same target value of ≥ 0.3 as LE. LLE_{AT} also enables judgement of how successful a modification has been. The more lipophilic the group, the larger fold increase in potency is required to maintain LLE_{AT} . Figure 1.20 shows the minimum fold improvement required in potency for commonly employed

substituents to maintain or improve LLE_{AT} . For example, if a *tert*-butyl group is added to a molecule, the binding affinity of the new analogue should increase by 300-fold or more to maintain or increase LLE_{AT} .

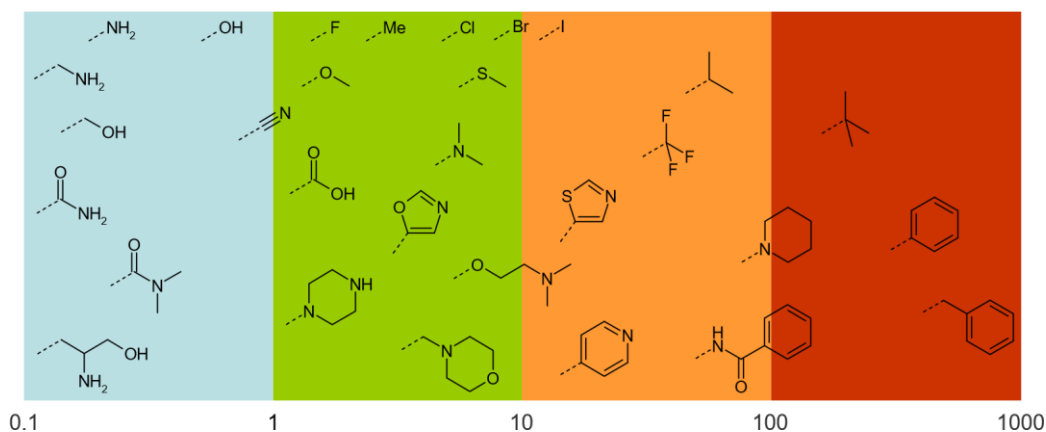


Figure 1.20 Fold improvement required in potency for common substituents to maintain constant LLE_{AT} ⁴⁷

The example below indicates why monitoring LLE_{AT} is as important as monitoring LE to optimise hits into drug candidates. Figure 1.21 shows the progression from fragment to lead of a series targeting P38 α kinase.^{39,48,49} While LE shows acceptable values in the region of 0.3 throughout the optimisation process, LLE_{AT} are well below the desired value of 0.3. These results suggest that the series will be difficult to optimise to a candidate molecule with logP in the desired range (< 3).¹¹

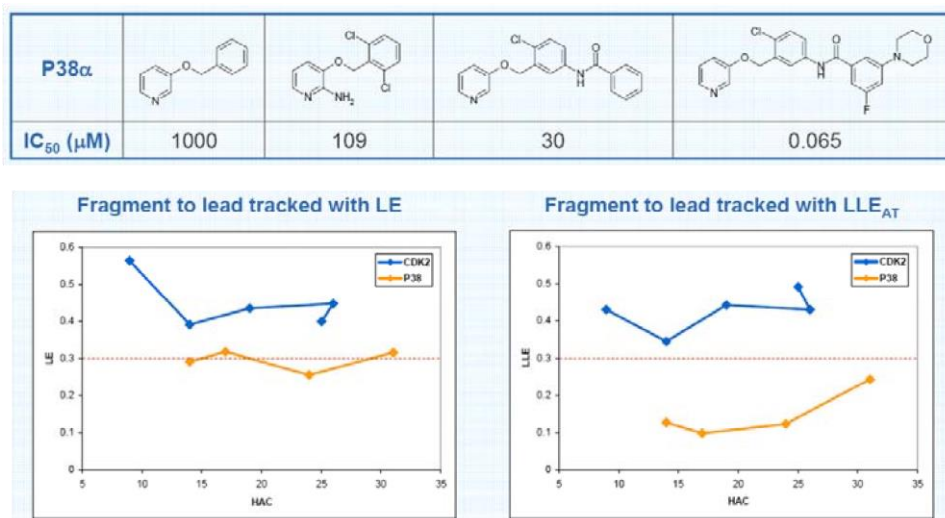


Figure 1.21 Potencies, LE and LLE_{AT} of P38 α series developed by Astex⁴⁹

Both LE and LLE_{AT} will be used in this report to follow fragment hits, both for prioritisation and optimisation.

1.2.6 Case Studies

Several fragment-derived drugs have now entered the clinic,⁵⁰⁻⁵² with almost half of them being protein kinase inhibitors. This reflects the fact that protein kinases are very tractable targets and thus, have enabled validation of FBDD as a novel valuable approach for discovering new drugs.

The first fragment-derived drug, Zelboraf (vemurafenib, PLX4032) developed by Plexxikon, has been approved by the FDA (August 2011) for the treatment of latestage metastatic melanoma.⁵³⁻⁵⁵ The target is the mutated form of the kinase B-Raf (V600E), known to be present in cancers. The discovery of vemurafenib is described in Figure 1.22.⁵⁵ The initial fragment hit was identified from a high concentration screening approach (200 μ M) through multiple structurally characterised kinases. Analysis of the data revealed that some compounds inhibited three kinases (Pim-1, p38, CSK) by at least 30% and were thus progressed to co-crystallisation. The 7azaindole **1**, which was successfully co-crystallised with Pim-1, was selected as starting point. The initial fragment hit was further validated with analogue **2**, which showed increased affinity and a single binding mode. Further structure-based optimisation led to compound PLX4720 (**3**), which showed good potency and selectivity for B-Raf V600E compared to wild-type B-Raf and other kinases. Final optimisation to improve the overall profile of the compound delivered PLX4032 (**4**). It is important to note that although the starting fragment was not selective, which would be expected with small fragment, the final grown fragment exhibited good levels of selectivity for B-Raf (V600E).

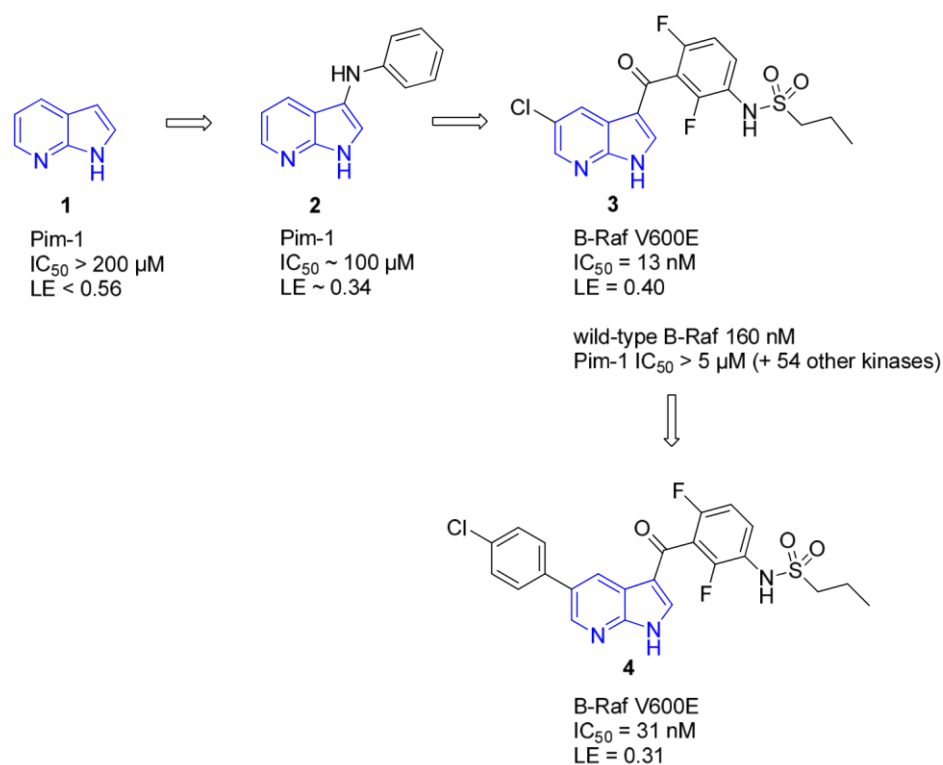


Figure 1.22 Discovery of Zelboraf

Astex has used the FBDD approach to deliver a novel chaperone protein Hsp90 inhibitors, currently in several clinical trials for oncology. The initial fragment hit **5**, also a known drug, ethamivan, was identified by water LOGSY NMR screening. Although the compound showed relatively poor ligand efficiency, its crystal structure revealed several opportunities for improvement. Focussed structure-based design led to the discovery of compound **6** with an increase in affinity over 1,000,000-fold and excellent ligand efficiency.⁵⁶ Subsequent lead optimisation efforts then delivered the clinical compound AT13387 (**7**).⁵⁷

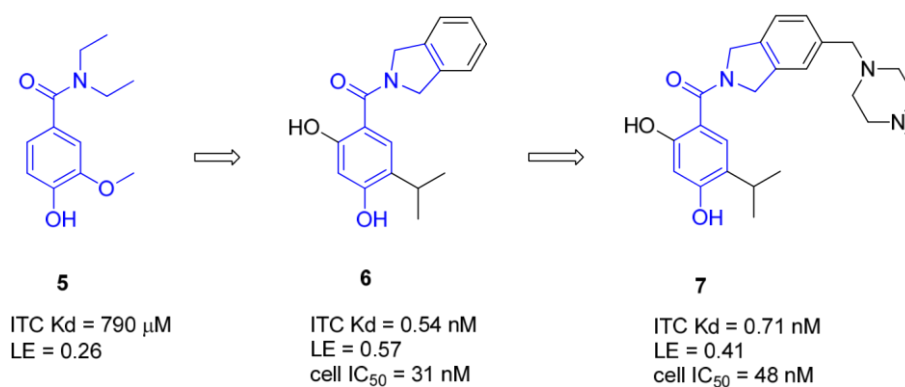


Figure 1.23 Discovery of clinical compound AT13387 (7)

As illustrated by these two examples, FBDD is a powerful approach to deliver high quality drug molecules for a range of biological targets of relevance to human health.

Chapter 2

Application of FBDD to the Discovery and Optimisation of BCAT^m Inhibitors

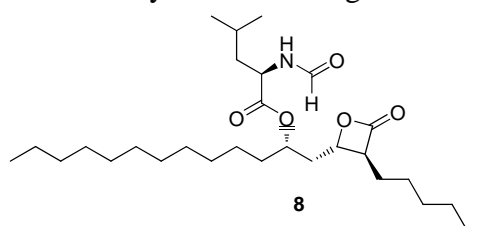
2.1 Biological Background

2.1.1 Obesity and BCAT^m

Obesity has become a serious health problem and was believed to have reached an epidemic level by 1997. According to the World Health Organisation (WHO), in 2008, more than one billion adults worldwide were overweight (Body Mass Index, BMI⁵⁸ ≥ 25) and of these, at least 500 million were obese (BMI ≥ 30).⁵⁹ Excess weight and obesity is associated with serious diseases such as diabetes, hypertension, cardiovascular diseases and certain forms of cancer.^{60,61} As a result, obesity is one of the leading preventable causes of death worldwide. More than 3.4 million people die each year from diseases linked to being overweight or obese.⁵⁹

Obesity is a consequence of an energy imbalance between the calories consumed and the calories expended. Although genetic susceptibility plays a role in weight gain, the major causes are excessive food energy intake (high in fat, sugar and salt) and reduced physical activity. Lifestyle modification (reduced caloric intake, more physical exercise) remains the main treatment for milder obesity, whilst surgery is currently the most effective treatment for severe obesity. Research in this domain has not been very successful and currently available drug treatments for obesity are extremely limited

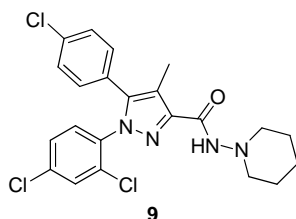
due to
efficacy
associated
effects.⁶²⁻



Orlistat
Gastrointestinal lipase inhibitor
Reduce fat uptake

lack of
and
side

only three
have been
by the
the long



Rimonabant
CB₁ receptor antagonist
Appetite suppression

⁶⁴ To date,
drugs
approved
FDA for
term

treatment of obesity: Orlistat (**8** - Xenical[®], Alli[®]), Rimonabant (**9** - Acomplia[®]) and Sibutramine (**10** - Meridia[®], Reductil[®]) and these are shown in Figure 2.1.

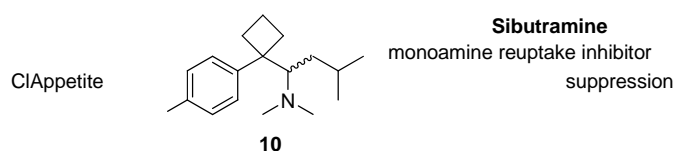


Figure 2.1 Anti-obesity drugs approved by FDA for long term treatment

Recently, two of these, Sibutramine (endocannabinoid receptor antagonist) and Rimonabant (centrally acting monoamine reuptake inhibitor), have been withdrawn due to severe adverse effects.^{65,66} Sibutramine has been associated with increased risks of serious cardiovascular effects (stroke, heart attacks) and Rimonabant with severe CNS side effects (mainly depression). Both compounds exerted their effect through appetite suppression. Consequently, only Orlistat currently remains as long term treatment for obesity. Orlistat is a gastrointestinal lipase inhibitor, which decreases dietary fat absorption (on average patients lose around 3 kg more than placebo).⁶⁵⁻⁶⁷ In term of successor compounds, few new drugs are currently in clinical trials.⁶² Most of these entities act either by appetite suppression or by inhibition of intestinal fat absorption. Therapeutic approaches, focusing on other approaches such as promoting energy expenditure have, to date, been less extensively studied.

Based on the limited efficacy of currently available drugs, the side effects associated with them and the lack of compounds in the current development pipeline suggests there is a clear and urgent need for new therapies for obesity. In terms of potential new targets for anti-obesity drugs, the enzyme mitochondrial branched-chain aminotransferase (BCATm) has come to prominence. The enzyme catalyses the first step in branched-chain amino acid (BCAA: Leu, Ile and Val) catabolism. This process is the metabolic breakdown of complex molecules into smaller molecules, often resulting in energy release and accordingly BCATm has recently been linked to obesity in knock-out studies and, thus, has been proposed as a potential new therapeutic target.⁶⁸

High-protein diets have been reported to increase energy expenditure and induce satiety resulting in weight loss.⁶⁹ These effects are believed to be mediated by BCAAs, especially leucine, which are involved in protein synthesis and inhibition of protein degradation.^{68,70} These data suggest that increasing levels of BCAAs might be beneficial as a treatment for obesity. However, studies in genetically modified obese rodents (ob/ob mice and Zucker rats) and diet-induced obese mice and humans, have shown that individuals with these characteristics have higher BCAA levels than lean animals and have lower levels of expression of BCATm.⁷¹ Interestingly, these effects are reversed in humans who lose weight following gastric bariatric surgery. BCATm knock-out (KO) studies carried out by She and co-workers revealed an interesting phenotype.⁶⁸ The KO mice appeared healthy, viable and despite eating more, they were leaner than wild-type mice and had improved insulin resistance and glucose tolerance than wild-type mice. In addition, these animals also showed increased energy expenditure. From the KO studies results, inhibition of BCATm was postulated to create a futile cycle of protein synthesis and degradation, resulting in increased energy use and ultimately weight loss.^{68,72}

Figure 2.2 represents the first step in BCAA catabolism and the potential effect of BCATm inhibition. BCAAs, which are not produced in the body, are obtained through our diet. They are then used to build proteins or metabolised. BCATm converts BCAAs to branched-chain α -ketoacids. They are either used to inhibit protein degradation or metabolised further to produce energy. Inhibition of BCATm would block the synthesis of α -ketoacids and, thus, prevents inhibition of protein degradation, promoting the cycle of protein synthesis and protein degradation, which would increase energy use and potentially result in weight loss.

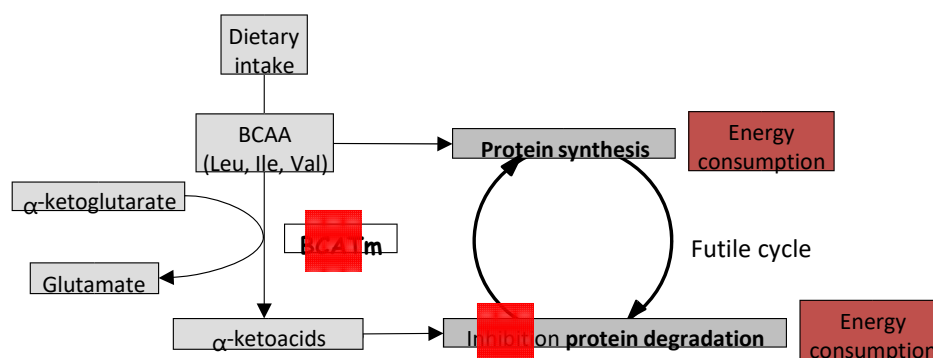


Figure 2.2 Potential effect of BCATm inhibition in the first step of BCAA metabolism

Based on all the above, BCATm may be a suitable new therapeutic target for obesity. In order to better understand BCATm pharmacology and its potential link with weight loss, the *in vivo* evaluation of small molecule inhibitors of this enzyme is an attractive prospect.

2.1.2 BCATm

Branched-chain aminotransferases (BCATs) are pyridoxal-5'-phosphate (PLP)dependent enzymes. PLP (**12**), a vitamin B6 derivative (pyridoxine, **11**), is a cofactor, small organic molecule required by the enzyme to function.⁷³ In a PLPdependent enzyme, PLP is covalently bound to a lysine residue *via* a Schiff base linkage (internal aldimine, **13**) as shown in Figure 2.3.⁷⁴

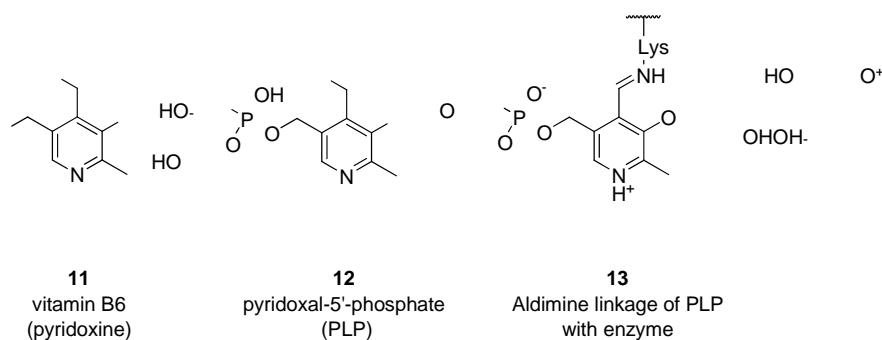


Figure 2.3 pyridoxal-5'-phosphate (PLP) structure

PLP-dependent enzymes mainly catalyse reactions of amino acids such as decarboxylation, transamination, racemisation, β,γ -elimination and β,γ -substitution. Based on their structures, they have been categorised in five groups, fold-type I to V.⁷³⁻⁷⁵ BCATs are classified as a fold-type IV PLP-dependent enzyme. A unique feature of this class is that the proton transfer at the C-4' position of the co-enzyme substrate imine intermediate occurs on the *Re*-face instead of the *Si*-face of the coenzyme, as described in Figure 2.4.⁷⁶

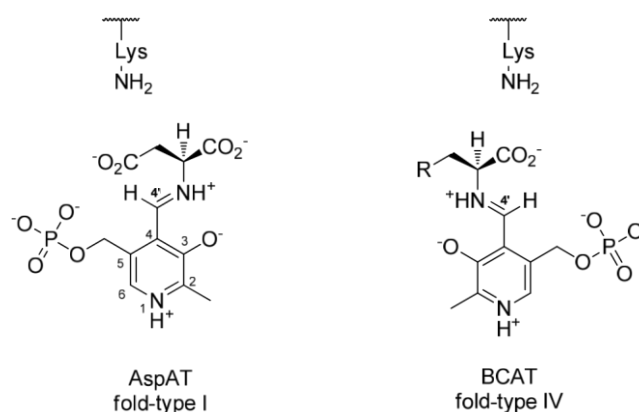


Figure 2.4 Coenzyme orientation in BCAT⁷⁷

In AspAT, the *Si*-face of the coenzyme points towards the Lys residue, while in BCAT, the *Re*-face points towards the Lys residue.

As discussed above, BCATs are involved in the first step of branched-chain amino acid (BCAA) catabolism as shown in Figure 2.5.⁷⁸ BCAAs are essential amino acids, which play an important role in protein synthesis and energy production for the body. First, BCAAs are converted by BCAT into α -ketoacids, which are involved in the inhibition of protein degradation. During this first process, BCAT also converts α -ketoglutarate to glutamate. Then, α -ketoacids are converted to Acyl-CoA derivatives by branched-chain α -ketoacid dehydrogenase (BCKDH), which also reduces NAD^+ to NADH and produce carbon dioxide. After further reactions, AcylCoA are converted into Acetyl CoA or Succinyl CoA derivatives, which are subsequently used in other cycles to generate energy.

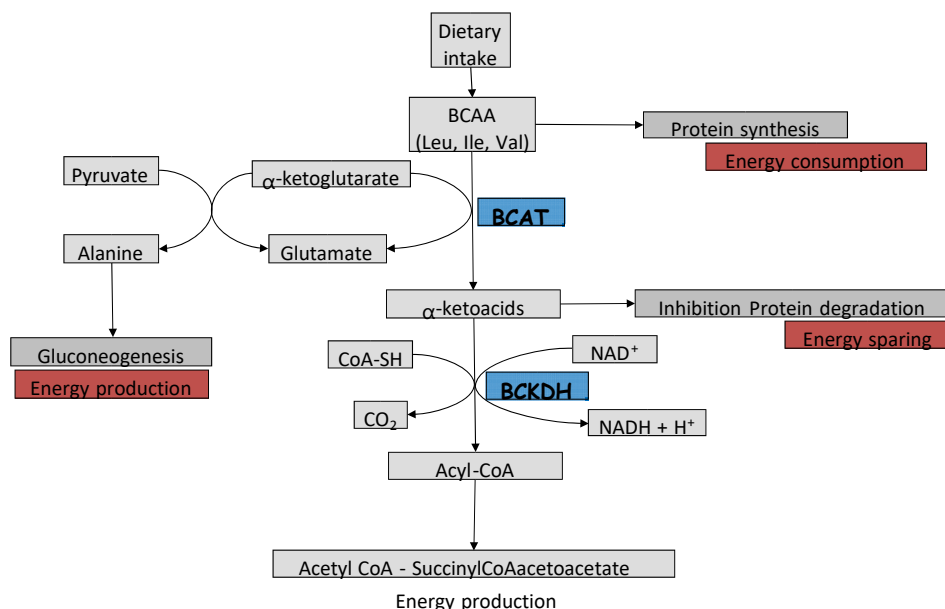


Figure 2.5 BCAA metabolic pathway

BCAA: branched-chain amino acid; BCAT: branched-chain aminotransferase;
 BCKDH: branched-chain α -ketoacid dehydrogenase; CoA-SH: reduced coenzymeA;
 NAD: nicotinamide adenine dinucleotide

As described above, BCAT catalyses the reversible transamination of BCAAs (leucine, isoleucine and valine) to their corresponding α -ketoacids (α -ketoisocaproate, α -keto- β -methylvalerate and α -ketoisovalerate, respectively).⁷⁸ This process is outlined in Figure 2.6.

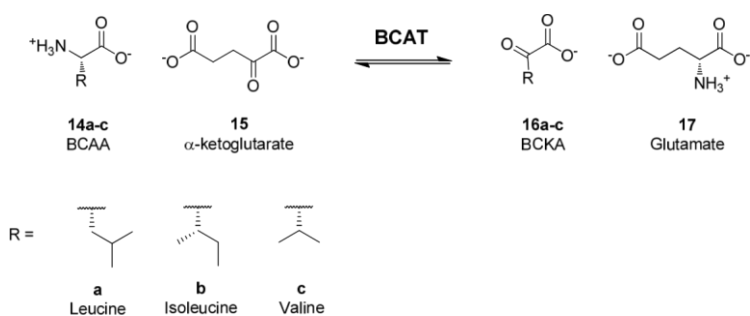


Figure 2.6 Transamination of BCAA catalysed by BCAT
 BCAA: branched-chain amino acids; BCKA: branched-chain α -ketoacids

The full catalytic cycle is described in Figure 2.7.⁷⁸ The target enzyme cycles between two forms, the PLP-form **I** (co-factor covalently bound to the protein) and the PMP-form **IV** (co-factor free). Initially, the PLP co-factor is covalently bound to the enzyme *via* the Lys202 residue (i.e. PLP-form). In the first half-reaction, the PLP-form (**I**) reacts with a BCAA to form an imine complex **II**, which then undergoes an isomerisation (**III**) and is hydrolysed to give the corresponding branched-chain α -ketoacid and the pyridoxamine-5'-phosphate (PMP) form of BCAT (**IV**) with the PMP co-factor no longer bound to the enzyme. In the complementary half-reaction, α -ketoglutarate is then converted to glutamate and the PLP-form of BCAT is regenerated to complete the catalytic cycle.

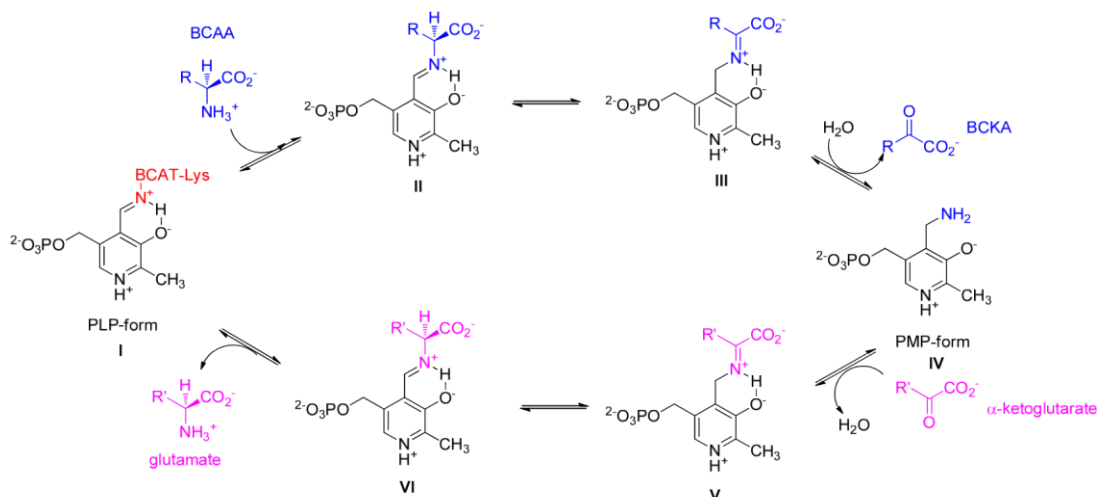


Figure 2.7 Catalytic cycle of BCAT

In mammals, there are two isoforms of BCAT: a mitochondrial form (BCATm) and a cytosolic form (BCATc).⁷⁹ From consideration of the primary sequence, the two isoforms share 58% homology. The key residues in the active sites are identical in the hBCATc and hBCATm structures, which could potentially make selectivity challenging. BCATm is the predominant form and is ubiquitously expressed except in the liver.⁸⁰ Its main sites of activity are skeletal muscle, adipose tissue and, to a lesser extent, intestine and kidney where it plays an important role in amino acid metabolism.⁸¹ On the other hand, BCATc is mainly expressed in the brain, placenta and ovaries.⁸² BCATc is the predominant form in the brain and is involved in the

synthesis of the neurotransmitter glutamate. However, due to their localisation in the body, selectivity between the two isoforms could be achieved through peripheral restriction of drug candidates through control of their physicochemical properties.

2.1.3 Crystal Structure of BCATm

The X-ray crystal structure of human BCATm shows that the enzyme is a homodimer.⁸³ Each monomer is composed of two subunits: a small domain (residues 1-175, yellow) and a large domain (residues 176-365, green), as shown in Figure 2.8.

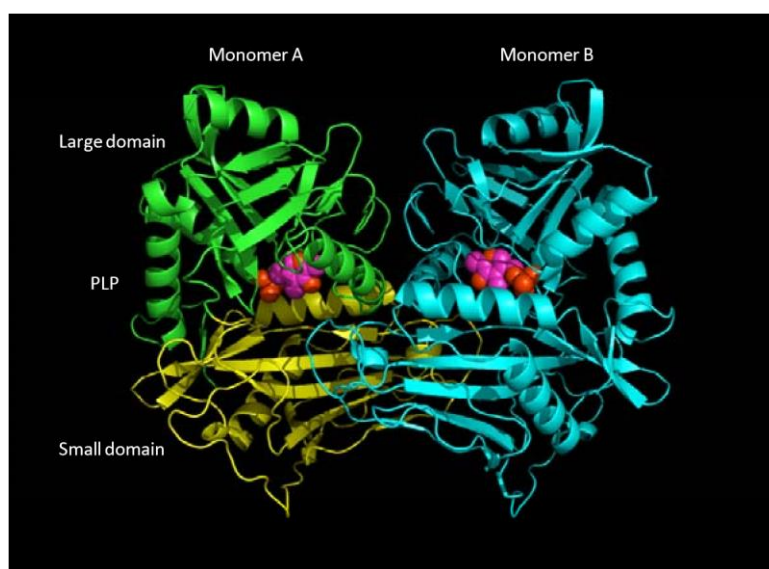


Figure 2.8 Ribbon crystal structure of hBCATm complex with PLP co-factor (pdb 1ekf)^{83,84}

The active site is at the interface of the two subunits and also close to the dimer interface. It comprises residues from both subunits of one monomer (green and yellow in Figure 2.8) and from the small domain of the other monomer (blue in Figure 2.8). The co-factor, PLP, is situated at the interface of the two subunits and at the bottom of the active site. PLP forms a Schiff base with Lys202, situated on the *Re*-face of the co-enzyme as mentioned above, and makes several interactions with the protein. The protonated nitrogen of the pyridine ring interacts with Glu237 and the oxygen with

Tyr207 (Figure 2.9). Each terminal oxygen atom of the phosphate makes two to three hydrogen bonds with protein and water molecules.

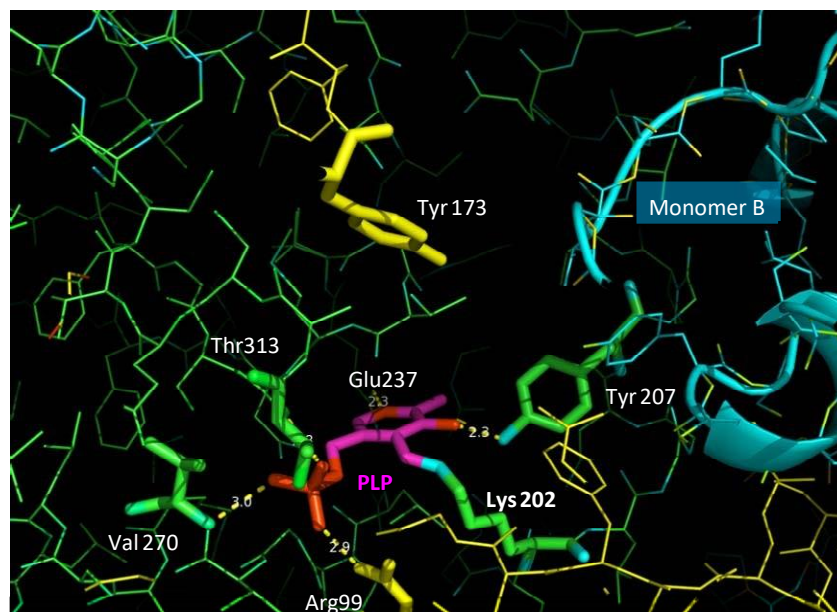


Figure 2.9 Crystal structure of active site of hBCATm complex with PLP co-factor (pdb 1ekf)^{83,84}

Shows active site of monomer A with respect to the position of monomer B

2.1.4 Known Inhibitors

At present, no selective BCATm inhibitors have been described in the literature and only a limited number of BCATc inhibitors have been reported.⁸⁵⁻⁸⁸

Gabapentin **18**, an anti-epileptic drug, has been shown to inhibit BCATc with limited inhibition of BCATm⁸⁷ (Figure 2.10) and the X-ray crystal structure of Gabapentin in both enzymes have been obtained.⁸⁵ The active sites are similar; however, the relative orientation of the small and large domains is significantly different, which could explain the selectivity observed.

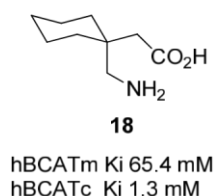


Figure 2.10 Gabapentin, anti-epileptic drug

Pfizer have reported a series of biaryl sulfonyl hydrazines as BCATc inhibitors for the treatment of neurodegenerative diseases, with modest selectivity over BCATm (10-fold).⁸⁶ Compound **19**, one of the best compounds disclosed, also demonstrated *in vitro* and *in vivo* neuroprotection. Relevant data associated with compound **19** are highlighted in Figure 2.11. The compound has high clogP giving little space for optimisation and thus, poor LLE_{AT}.

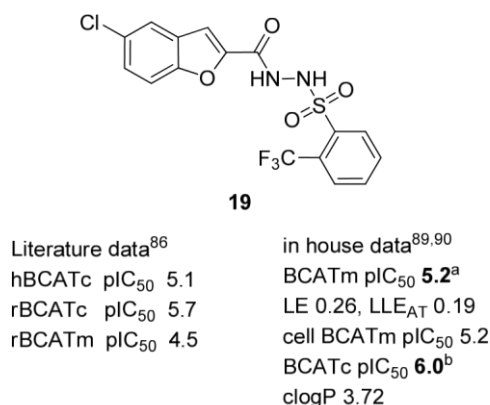


Figure 2.11 BCATc inhibitor reported by Pfizer^{86,89,90}

^aCompound reported inactive (pIC₅₀ < 4.2) in 2 test occasions and failed to fit a curve in 2 test occasions out of 112; ^bCompound failed to fit a curve in 2 out of the 52 test occasions.

The X-ray crystal structure of compound **19** was obtained in hBCATc confirming its binding mode (Figure 2.12).⁸⁴ The compound binds adjacent to the PLP co-factor and

the sulfonyl hydrazide moiety forms several hydrogen interactions: the sulfonyl and carbonyl oxygens both interact with Ala332 and both hydrazide NH with Thr258.

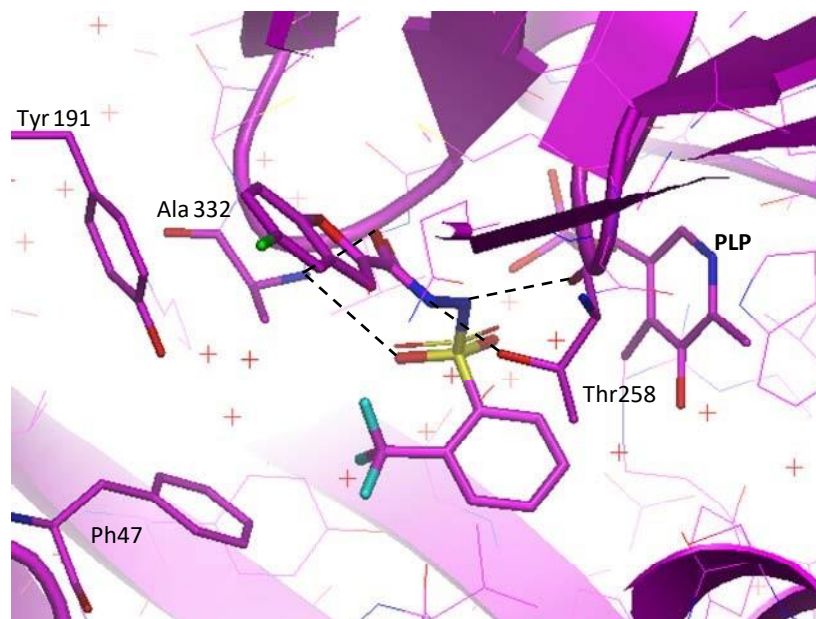


Figure 2.12 Crystal structure of hBCATc in complex with compound **19**⁸⁴

Figure 2.13 represents an overlay of compound **19** in both BCATc (●) and BCATm (●). The binding modes are very similar, which would explain the poor selectivity observed between the two isoforms. Only the two Tyr residues highlighted (Tyr191 in BCATc and Tyr173 in BCATm) showed a significant movement, but this is almost certainly due to the difference in residues in the loop.

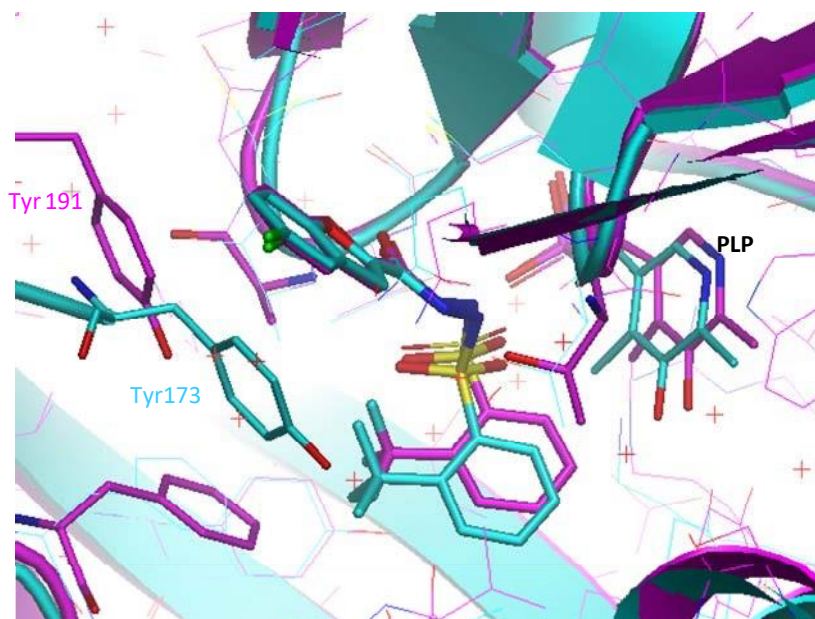


Figure 2.13 Crystal structure of compound **19** in BCATc (●) and BCATm (●)⁸⁴

More recently, an NMR-based fragment screen within the Abbott laboratories has identified six fragments as inhibitors of BCATc (IC_{50} 15 - 650 μ M).⁸⁸ Two of the molecules contain the same sulfonyl hydrazine core similar to Pfizer inhibitors.

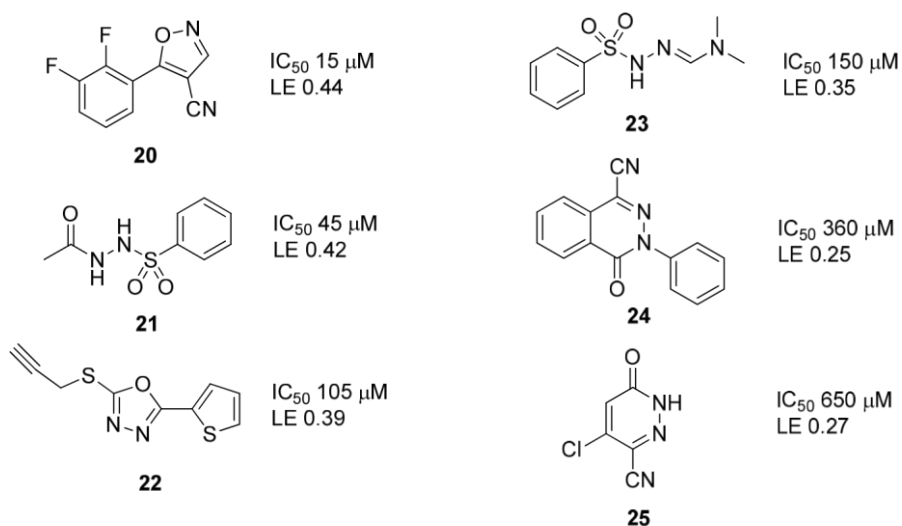


Figure 2.14 BCATc fragment inhibitors identified by NMR screening⁸⁸

From consideration of the above, the BCATm active site appears chemically tractable, although selectivity against BCATc might be challenging due to the similarity between the two isoforms. Having stated this, it is believed that selectivity could be achievable or could be facilitated through peripheral restriction.

2.1.5 Aims

The goal of this research programme was to identify a potent, selective (over BCATc and other similar enzymes) and/or non-brain penetrant inhibitor for BCATm. As BCATc is mainly expressed in the brain, a non-brain penetrant molecule would be expected to give good *in vivo* functional selectivity. Central nervous system (CNS) drugs require specific physicochemical properties to be able to cross the blood-brain barrier (BBB) and enter the brain.⁹¹⁻⁹³ Studies of the physicochemical properties of known CNS drugs have enabled the identification of optimum physicochemical properties in order to increase the potential for BBB penetration:⁹¹

- MW < 450,
- logP/logD 2-4, - PSA < 70 Å² and -
HBD 0-1.

Identifying a molecule with properties outside this range (especially PSA > 70 Å²) is expected to limit CNS penetration and, thus, avoid any *in vivo* effects due to BCATc inhibition.

The initial objective in the programme was to identify a tool molecule suitable for investigating the biological profile of BCATm inhibition using appropriate *in vivo* models as, at present, no selective small molecule inhibitors of the target of interest have been reported. It should be noted that the properties of a tool molecule can differ slightly from the properties required for a candidate drug,⁹⁴ with the latter profile often being more stringent, for example, in terms of pharmacokinetic properties.

The desired profile for a tool molecule to enable an *in vivo* study is summarised in Table 2.1.

Parameter	Desired value
BCATm enzyme pIC ₅₀	≥ 6.5
BCATm cellular pIC ₅₀	≥ 6.5
Selectivity BCATc	> 10-fold or non brain-penetrant
LE, LLE _{AT}	> 0.3
Physicochemical properties for oral dosage	chromlogD _{7.4} ≤ 3 Ar ring ≤ 3 CLND > 100 µg/mL
p.o. AUC	high
Half life T _{1/2}	Compatible with once or twice a day dose
<i>in vivo</i> clearance in whole blood in mouse (Cl _b)	< 5 mL/min/kg

Table 2.1 Desired profile for a tool molecule inhibitor

2.1.6 Biochemical Assay

Four main biochemical assays were used during this programme. The primary enzyme activity was measured by a combination of coupled and decoupled assays as the reaction catalysed by the target enzyme (BCATm) does not result in a change of absorbance of light, hampering direct detection by standard photometric means. BCATm catalyses the transamination of branched-chain amino acids to the corresponding α -keto acids and simultaneously converts α -ketoglutarate to glutamate. In the coupled assay, glutamate becomes the substrate of a second reaction catalysed by glutamate oxidase. This second reaction produces α -ketoglutarate and hydrogen

peroxide. Amplex Red can then react with hydrogen peroxide in presence of horseradish peroxidase to produce a highly fluorescent compound, Resorufin. Hence, inhibition of the compound against BCATm can be measured indirectly *via* fluorescence (Figure 2.15). The potency in the coupled assay will be referred to as pIC_{50} , representing $-\log$ of the concentration at which there is 50% inhibition of the fluorescence response.

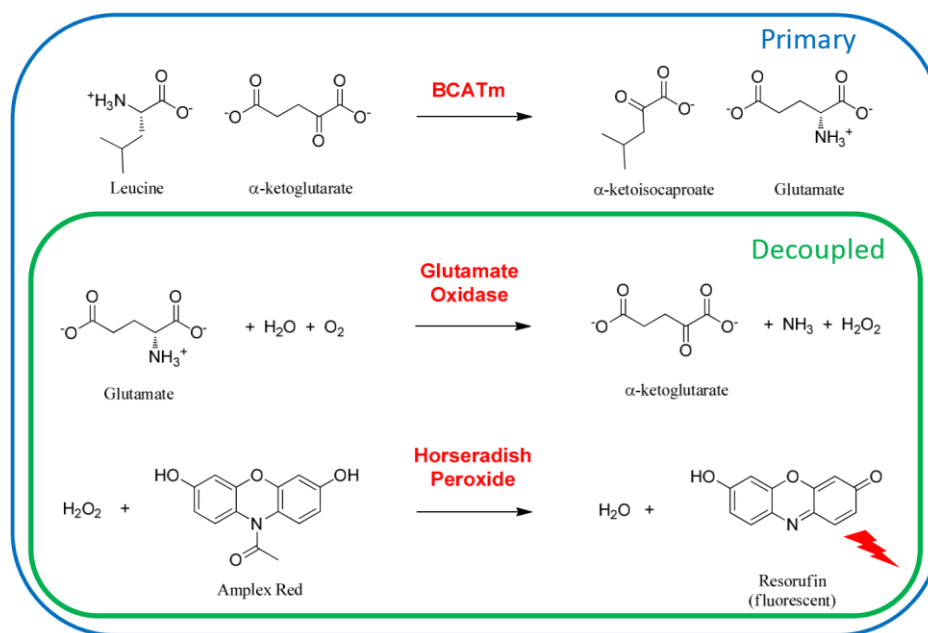


Figure 2.15 Biochemical assay format

In order to exclude false positives due to the inhibition of the other enzymes present (glutamate oxidase and horseradish peroxidase), a decoupled assay is used. The decoupled assay consists of testing the compound against the two other enzymes alone in the absence of BCATm (Figure 2.15, green cycle). If compounds show activity in this assay, this will be an undesired, off-target mechanism. The potency of the decoupled assay will be referred as $pIC_{50}(d)$ and will be specified only if compounds show activity. Most of the compounds identified showed no activity in the decoupled assay, however, it is important to rule out such artificial effects.

When more potent compounds ($BCATm\ pIC_{50} \geq 6$) were identified, they were tested in a cellular assay. This assay gives information on compound potency in a more

physiologically-relevant system, and may highlight issues associated with membrane permeability as the compound will have to cross the cell membrane to reach the target. The associated potency will be referred to as cell pIC₅₀. Additionally, compounds prepared in the programme will also be tested against BCATc. The potency in this selectivity assay will be referred as BCATc pIC₅₀.

2.2 Fragment Hits Identification

2.2.1 Screening Strategy

Given the fact that X-ray structures of BCATm had previously been solved and that the related BCATc system had previously been shown to be amenable to FBDD, it was decided to pursue this approach for BCATm.

As described in Chapter 1, although biochemical screening is more relevant to enzyme activity, in some cases high concentration biochemical assays could give less reliable results than biophysical techniques, which measure direct binding to the target enzyme and are often more sensitive allowing detection of weak affinity hits. The choice of biophysical techniques relies not only on the protein used and the type of assay format required, but also on the technology available. For this project Saturation Transfer Difference NMR (STD-NMR) and Thermal Melt (T_m) were selected as primary screening techniques as they are relatively high throughput techniques and could be readily developed for this specific protein. The STD-NMR assay was carried out on a mixture of the PLP and PMP forms of the enzyme, while the T_m screen was carried out on both forms independently. An NMR hit may therefore have bound to either, or both, PLP and PMP forms of the protein but the precise mechanism of inhibition was not initially determined. A biochemical assay was also used as a complementary technique to evaluate their functional activity and help prioritise fragment hits for X-ray crystallography. Fragments which show activity in two or more of the T_m , STD-NMR or biochemical assays were progressed to X-ray crystallography as previous experience within our laboratory suggests that the crystal success rate tends to be higher with such

compounds.⁹⁵ However, depending on the hit rate observed, fragments which show activity in only one technique may also be progressed.

In collaboration with another member of our laboratory⁹⁶ and biology colleagues,⁹⁷ a cascade of assays was designed to identify fragment hits. The research operating plan considered is summarised in Figure 2.16.

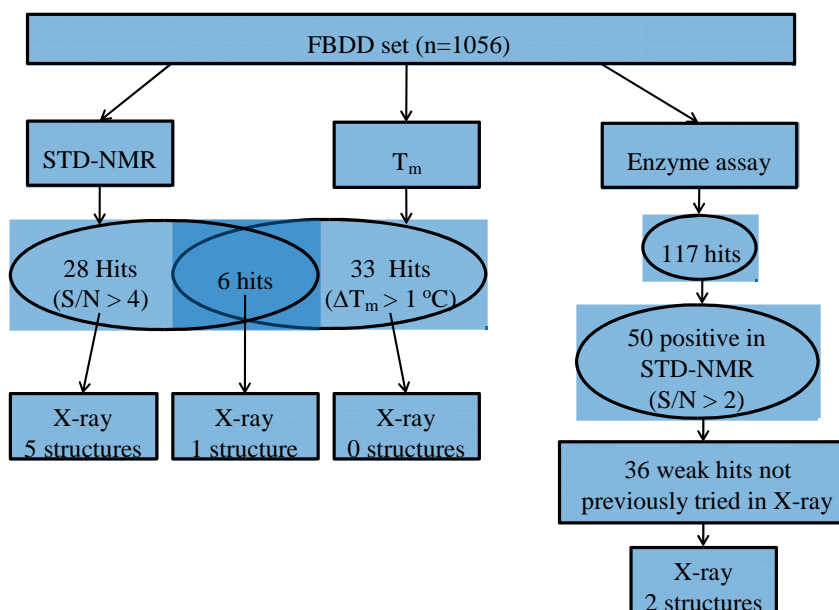


Figure 2.16 Fragment screening cascade

Our fragment library of 1056 compounds was screened in parallel through the two biophysical assays by other members of our laboratories.^{34,98} STD-NMR gave 34 binding fragments (with signal to noise $S/N > 4$).⁹⁸ As discussed previously, STDNMR can detect very weak binding; therefore, the S/N cut-off was chosen to match the capacity available in downstream assays. In this case, a signal to noise of greater than 4 was selected as it gave a reasonable number of hits to progress to crystallography. The T_m assay gave 39 binding fragments ($\Delta T_m > 1$ °C).³⁴ Overall, the combined hit rate for these assays was 6%, which was consistent with expectations for a fragment screen and higher than the hit rate observed with the complementary HTS screening approach used for this target ($\leq 1\%$ in general).²⁸ However, inspection of the two data sets

showed that the overlap between the two techniques was low. As the fragments identified have binding affinities around the limit of detection of the techniques, the outcome might be different for each screening method employed. Depending on the cut-off selected, a fragment active in one technique might not be detected in another technique. Furthermore, STD-NMR is sensitive to lower percentage occupancy, while T_m is less sensitive, leading to further differences in the composition of the hit sets identified for each technique. This highlights the importance of using multiple, complementary techniques for the initial screening phase, which will ensure that maximum chemical diversity is generated from the screen and should be borne in mind when conducting future fragment screening efforts.

Both NMR and T_m hits were progressed to X-ray crystallography. For this target protein, crystallography was carried out by soaking at a high concentration (4060 mM) of the ligand of interest into preformed protein crystals.⁸⁴ From the 34 NMR hits, six crystal structures were obtained. From the 39 T_m hits, only one structure was obtained, which was a dual hit (**26**). In this particular case, the STD-NMR assay demonstrated better correlation with X-ray crystallography than the T_m assay. The compounds obtained from the biophysical screens that were amenable to X-ray crystallography are summarised in Figure 2.17.

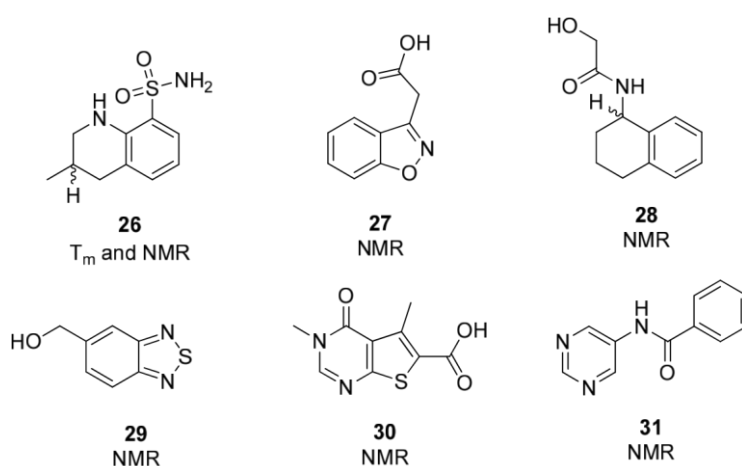


Figure 2.17 Fragment hits solved by crystallography

The overall success rate of X-ray crystallography was relatively low (around 10%). One possible explanation could be that only the PLP-form of the protein was used for crystallography whereas compounds were tested in both forms of the enzyme. The PMP-form of the enzyme was less stable and could not be crystallised for soaking experiments needed in the biostructural work. In addition, fragments were tested against the protein in solution where the bound conformations might be different from those observed in the solid state. Another potential issue associated with the soaking experiment used in this programme is that the compound might destroy the crystals. As the soaking was carried out at high compound concentration (4060 mM), compound solubility might also be an issue. In addition, crystallography requires reasonable percentage occupancy of the active site (50%). However, fragments might have different binding modes with similar energy meaning it can be difficult to define the precise binding mode by X-ray crystallography, particularly at lower resolutions, therefore making structural refinement difficult.

From the high concentration functional biochemical assay, a high number of specific hits were identified (117 hits, $pIC_{50} \geq 3$), which could not all be progressed to crystallography.⁹⁰ Therefore, the STD-NMR data were used to triage the biochemical hits. To progress new compounds to crystallography and increase our structural knowledge, the STD-NMR cut off was revisited and lowered to $S/N > 2$. With this new cut-off, 36 weak fragments, which were not previously examined in X-ray crystallography, were identified and progressed to structural studies. Two new structures (**32** and **33**) were solved and these are depicted in Figure 2.18.⁸⁴

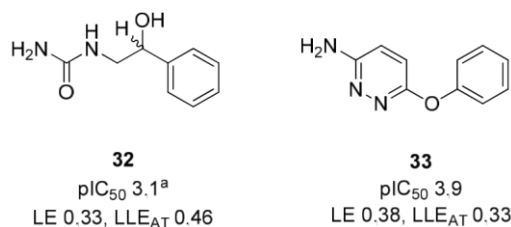
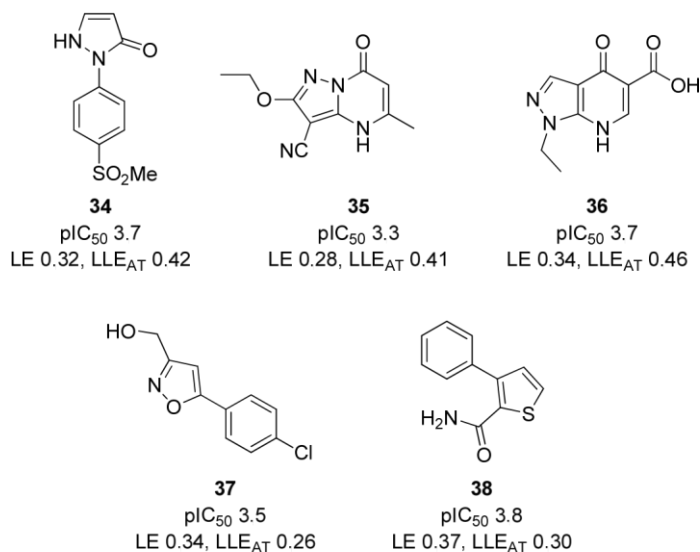


Figure 2.18 Fragment hits identified from biochemical assay and solved by X-ray crystallography

^a

Compound reported inactive ($pIC_{50} < 2.9$) in one out of two test occasions.

In order to increase further the number of fragment crystal structures, substructure searches (SSS) were carried out on the five compounds (**34-38**)⁹⁹ that were identified as dual hits in STD-NMR and T_m but failed to generate crystal structures (Figure 2.19). As they were detected in both biophysical assays and showed biochemical activity, they were more likely to be genuinely binding to the protein.



m

Figure 2.19 Dual hits in T and

STD-NMR

a

Compound reported inactive ($pIC_{50} < 2.9$) in one out of two test occasions.

Substructure searching consists of finding compounds structurally related to the fragment hit of interest using compound collection available in our laboratories and SOBAX database (preferred supplier's compound library). 80 analogues were identified from this SSS exercise, and STD-NMR⁹⁸ of these analogues identified 32 binding fragments from which three (**39-41**) were successfully solved by X-ray crystallography⁸⁴ (Figure 2.20). As previously observed, the X-ray crystallography success rate was around 10%.

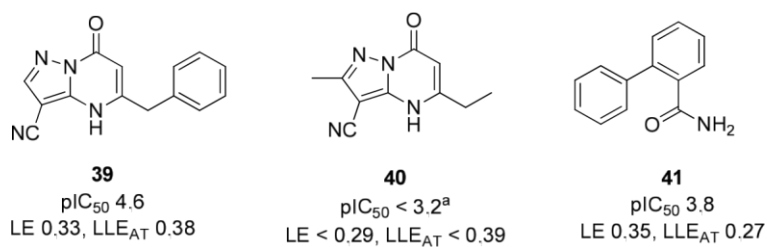


Figure 2.20 Fragment hits identified by follow-up STD-NMR screening and solved by X-ray crystallography

^acompound reported active (pIC₅₀ = 4.4) in one out of the three test occasions

This exercise highlights the importance of using related compounds available both internally and externally to identify further hits, which subsequently can provide structural insight in terms of binding mode. Such information adds additional value to the particular chemotype of interest and enables more straightforward optimisation using a structure-based approach through building confidence in a series of interest without investment in wet chemistry.

Overall, eleven crystal structures were solved⁸⁴ and the respective compounds are summarised in Table 2.2, along with their LE, LLE_{AT} and clogP.

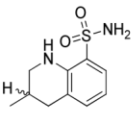
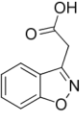
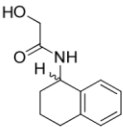
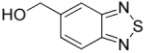
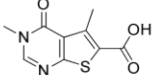
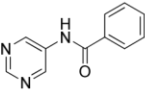
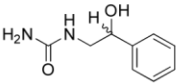
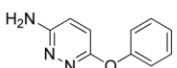
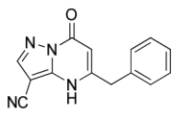
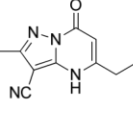
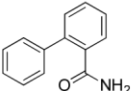
Cmpd	Structure	T _m	NMR	pIC ₅₀	LE, LLE _{AT}	clogP	X-ray res. (Å)
26		√	√	< 2.9	< 0.27 < 0.26	1.3	2.31
27		x	√	< 2.9	< 0.31 < 0.33	0.8	2.06
28		x	√	< 2.9	< 0.27 < 0.23	1.6	2.40
29		x	√	< 2.9	< 0.36 < 0.35	1.0	2.16
30		x	√	4.2 ^a	0.38 0.44	0.6	1.94
31		x	√	3.0 ^b	0.27 0.26	1.3	2.40
32		n.d.	√	3.1 ^b	0.33 0.45	-0.2	2.00
33		n.d.	√	3.9	0.38 0.33	1.6	2.12
39		n.d.	√	4.6	0.33 0.38	0.8	2.20
40		n.d.	√	< 3.2 ^c	< 0.29 < 0.39	0.1	2.20
41		n.d.	√	3.8	0.35 0.27	2.1	2.17

Table 2.2 Summary of fragment hits solved by X-ray crystallography

^a Compound reported inactive (pIC₅₀ < 4.2) in 3 of the 34 test occasions.

^b Compounds reported inactive (pIC₅₀ < 2.9) in 1 of the 2 test occasions.

^c

Compound reported active ($pIC_{50} = 4.4$) in 1 out of the 3 test occasions.

2.2.2 Evaluation of Crystal Structures

Once fragment hits were identified and confirmed to bind to the target by X-ray crystallography at acceptable resolution (1.9-2.4 Å), they were clustered using consideration of binding mode and direction of growth opportunities, in contrast to traditional clustering of screening hits which is based on 2D-structure similarity. This was anticipated to give greater insight into potential means of growing fragment hits towards more lead-like molecules.

As part of a collaborative effort within our laboratories,¹⁰⁰ fragment hit clustering and prioritisation was carried out. Compounds were overlaid and compared to each other in order to identify where they bind in the pocket, the key interactions made with the protein and also to determine potential growth vectors to access new subsites (Figure 2.21). From this structure analysis, it was found that they occupied a range of positions and significant movements in the protein were induced by the compounds.

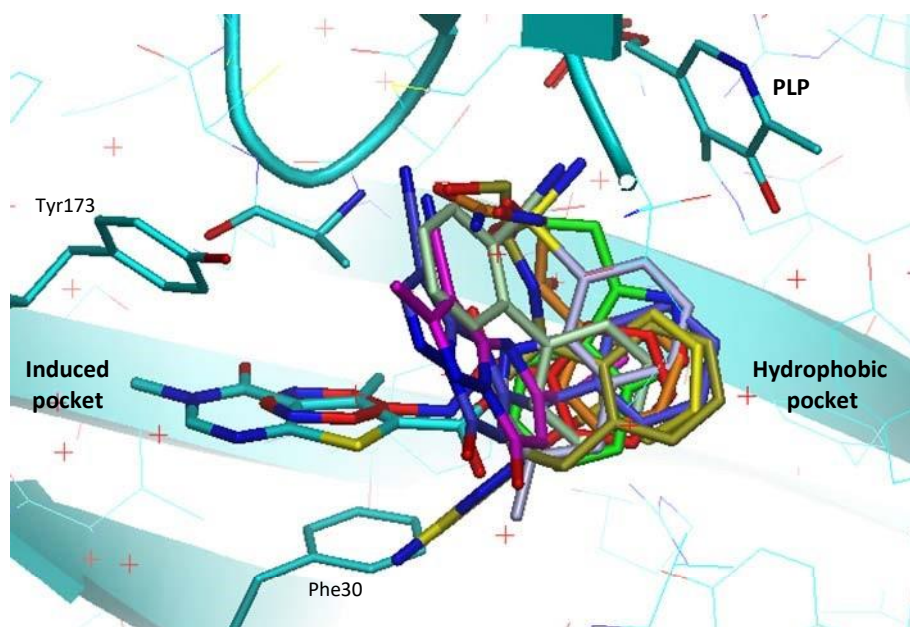







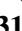




Figure 2.21 Overlay of the different fragment hits showing main binding sites 26 , 27 , 28 , 30 , 31 , 32 , 33 , 39 , 40 , 41 , 29 not bound in the catalytic site

Compound **29** did not bind in the enzyme catalytic site but was observed at the interface between the protein dimers. This binding mode was not expected to result in inhibition of the enzyme, and indeed no biochemical activity was observed with the compound and close analogues screened from substructure searching efforts.

Compounds **26**, **27**, **28** and **32** were all found to be occupying a similar binding mode (Figure 2.22). The heterocyclic cores occupy a lipophilic pocket adjacent to the PLP co-factor, where the BCAAs bind. From consideration of the refined structure, fragments showed no polar interaction with the protein in this region. However, the pendant carbonyl or sulfonyl groups interacted with Ala314. Compound **32** (●) also showed an additional H-bonding interaction between the alcohol and a tyrosine residue (Tyr141). The alcohol is observed to displace a water molecule present in other structures in order to interact directly with Tyr141 as shown in Figure 2.22.

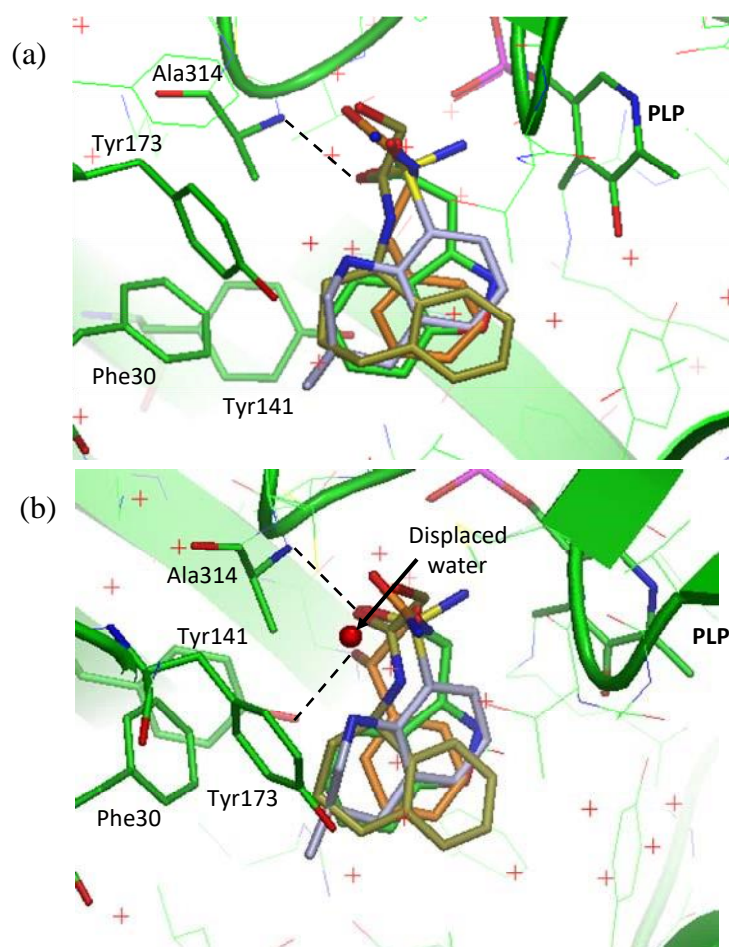


Figure 2.22

- (a) Overlaid crystal structures of compounds **26** (●), **27** (●), **28** (●) and **32** (●)
(b) Rotation - Direct interaction of compound **32** (●) with Tyr141 through displacement of water

Compound **30** (●) occupied a very distinct binding site from previous compounds (e.g. **27** (●) Figure 2.23). The crystal structure revealed a significant movement of a tyrosine loop (Tyr173) of the protein, opening a new induced lipophilic pocket. The aromatic core formed π -stacking interactions with a phenylalanine residue (Phe30). The pyrimidinone carbonyl acted as a hydrogen bond acceptor to a lysine NH (Lys79) at the back of the pocket.

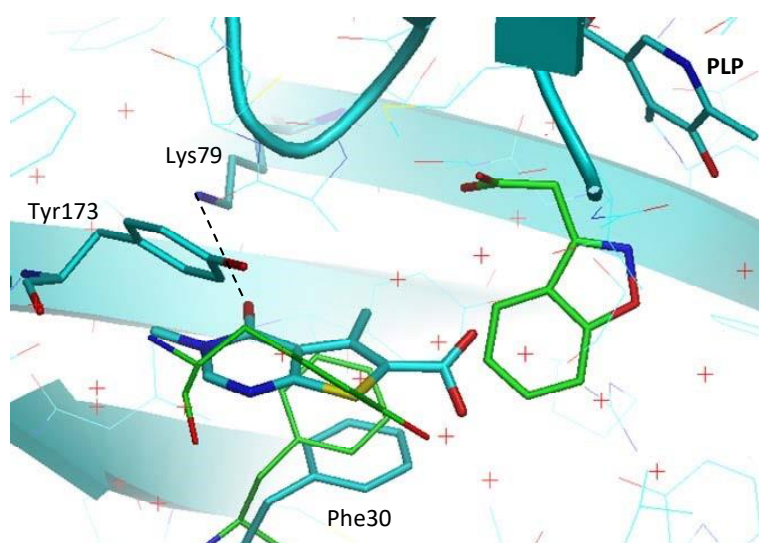


Figure 2.23 Crystal structure of compound **30** (●) overlaid with compound **27** (●). Compound **31** (●) also opened the induced lipophilic pocket but did not extend as deeply into the induced pocket as compound **30** (●) (Figure 2.24). The compound bridged two sites demonstrating that it is possible to have both regions occupied simultaneously. The crystal structure showed similar π -stacking interactions with the Phe30 residue but did not show any specific polar interactions with the heteroatoms of the fragment and the protein.

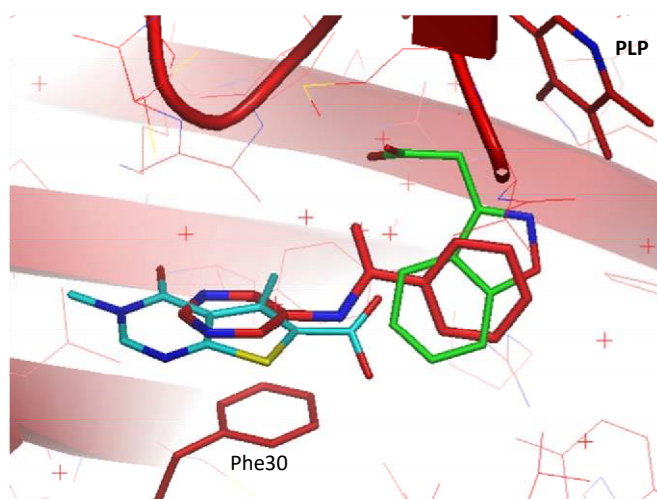


Figure 2.24 Crystal structure of compound **31** (●) overlaid with compounds **27** (●) and **31** (●)

Compound **33** (●) displayed a unique binding mode as shown in Figure 2.25. Although the phenyl ring occupied the lipophilic pocket in common with several fragments (e.g. **27** ●), the crystal structure showed a distinct movement of the Phe30 residue. The pyridazine amine opened a new pocket where Phe30 had pivoted 90° (yellow residue) from its usual position (green residue) and π -stacked with the pyridazine ring.

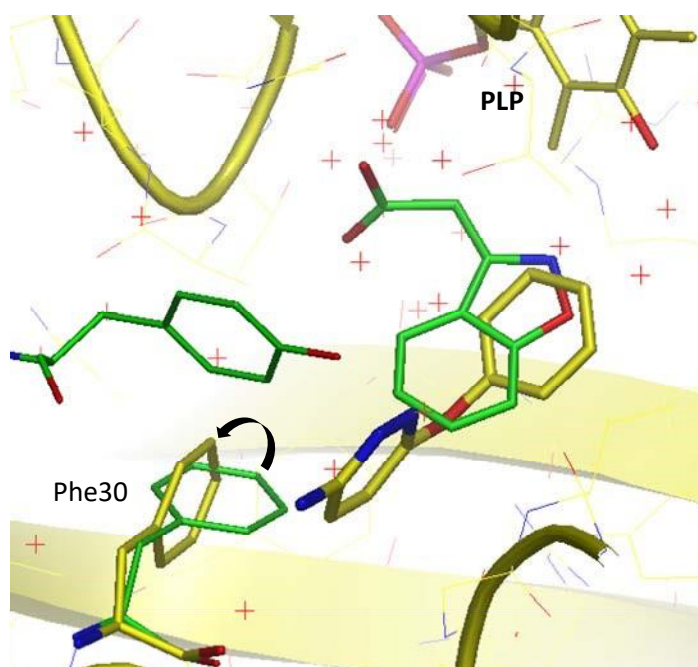


Figure 2.25 Crystal structure of compound **33** (●) overlaid with compound **27** (●)

Compounds **39** (●) and **40** (●) also exhibited a different binding mode to other fragments where the compounds bridged the lipophilic pocket to a new subsite, accessing the latter site *via* a novel vector (Figure 2.30). The crystal structure showed a potential non-ideal (in terms of geometry)¹⁰¹ hydrogen bond between the cyano nitrogen and the backbone NH of Cys315 residue (angle 118 °). The pyrimidinone carbonyl also exhibited an H-bonding interaction with Tyr173 (2.62 Å). In the crystal structure of compound **39** (●), the Tyr173 loop was disordered. The benzyl ring resided in the lipophilic pocket where several fragments bound and moved the core slightly to accommodate the ring compared to compound **40** (●).

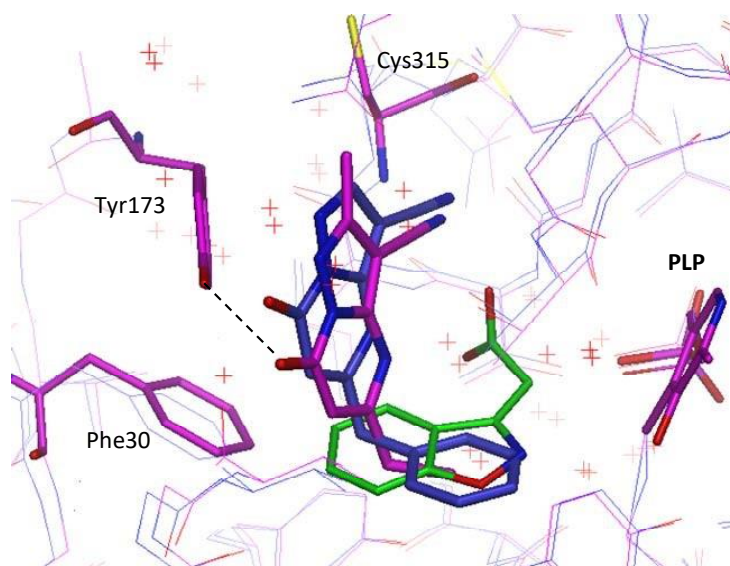


Figure 2.26 Crystal structure of compound **39** (●) and **40** (●) overlaid with compound **27** (●)

Although compound **41** (○) bound in the lipophilic pocket and made a H-bonding interaction with Ala314 similarly to compound **27** (●), the growth vectors exhibited to adjacent subsites were different. The amide NH₂ formed an additional H-bonding interaction with the carbonyl of Thr240.

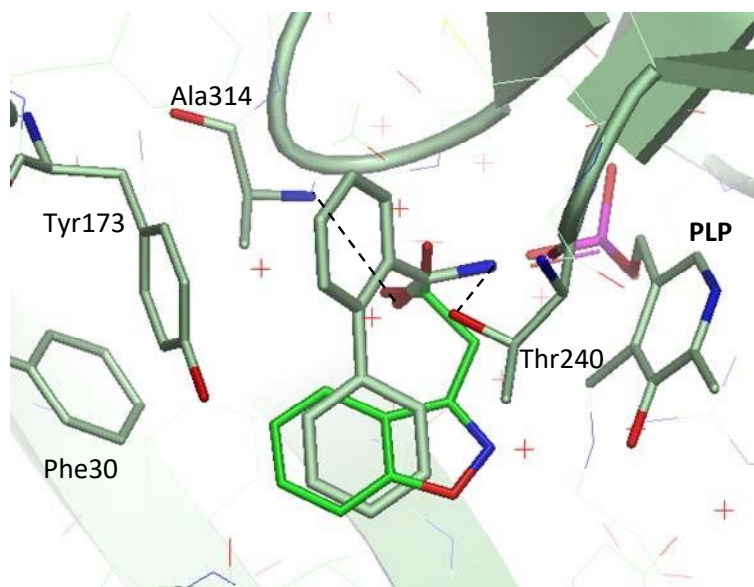


Figure 2.27 Crystal structure of compound **41** (●) overlaid with compound **27** (●)
2.2.3 Cluster Analysis

From this exercise, fragments were organised in seven distinct clusters (Figure 2.28). In this particular case, most of the clusters were singletons. The diversity of structural information obtained provided opportunities to grow the fragment hits in various ways. Fragment merging techniques¹⁰² could be used for example to exploit interactions observed within the distinct binding modes. In addition, clustering by binding mode instead of 2D-similarity allows rapid comparison of potential growth vectors and selection of a representative fragment to explore initial SAR of a cluster.

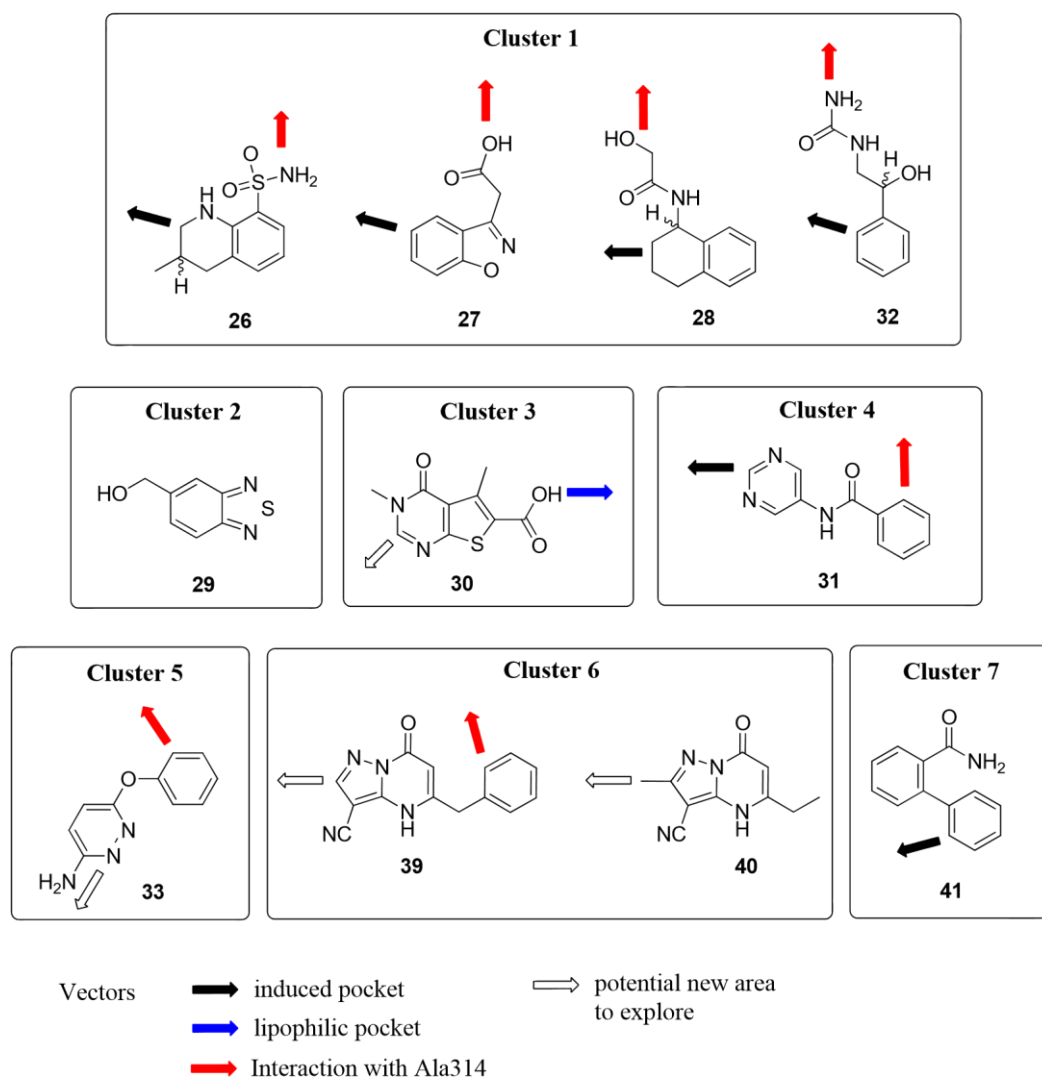


Figure 2.28 Fragment hits clustering summary

The fragments identified were then prioritised by considering crystal structure, ligand interactions, ligand efficiency, data from related analogues, potential synthetic direction and general tractability. A summary of the properties of the clusters discussed in the previous section is shown below, with green denoting good properties, yellow borderline and red potential issues for progression of the exemplar compound (Table 2.3). As discussed previously, compound **29** did not bind in the enzyme catalytic site, and showed no functional activity and, thus, was not pursued further.

Cmpd	Structure	Cluster	pIC ₅₀	LE	LLE _{AT}	clogP	tractability
26		1	< 2.9	< 0.27	< 0.26	1.3	
27		1	< 2.9	< 0.31	< 0.33	0.8	
28		1	< 2.9	< 0.27	< 0.23	1.6	
32		1	3.1 ^a	0.33	0.45	-0.2	
30		3	4.2 ^b	0.38	0.44	0.6	
31		4	3.0 ^a	0.27	0.26	1.3	
33		5	3.9	0.38	0.33	1.6	No SAR
39		6	4.6	0.33	0.38	0.1	
40		6	< 3.2 ^c	< 0.29	< 0.39	0.8	
41		7	3.8	0.35	0.27	2.1	No novelty

Table 2.3 Summary of cluster properties (Note: Cluster 2 not shown)

- ^a Compounds reported inactive (pIC₅₀ < 2.9) in 1 of the 2 test occasions.
^b Compound reported inactive (pIC₅₀ < 4.2) in 3 of the 34 test occasions.
^c Compound reported active (pIC₅₀ = 4.4) in 1 out of the 3 test occasions.

Based in their overall profile, clusters 1, 3, 4 and 6 were identified as higher priority and synthetic efforts towards these targets was initiated within our laboratory.

Although cluster 1 compounds showed no biochemical activity and, therefore, low ligand efficiency, they showed a highly conserved binding mode and gave the opportunity to grow in two directions. Overlay of cluster 1 compounds with compound **30** (●) and the literature BCATc inhibitor **19** (●) showed potential to grow toward the induced pocket and a novel area where a known BCATc inhibitor binds as shown in Figure 2.29. Given the potential for expansion of compound **27** into the subsites indicated above, optimisation efforts around this template was subsequently initiated by another member of our laboratory.⁹⁶ Compounds **26** and **28** were deemed less tractable in terms of synthetic access to the desired compounds and compound **32** was structurally of lower interest.

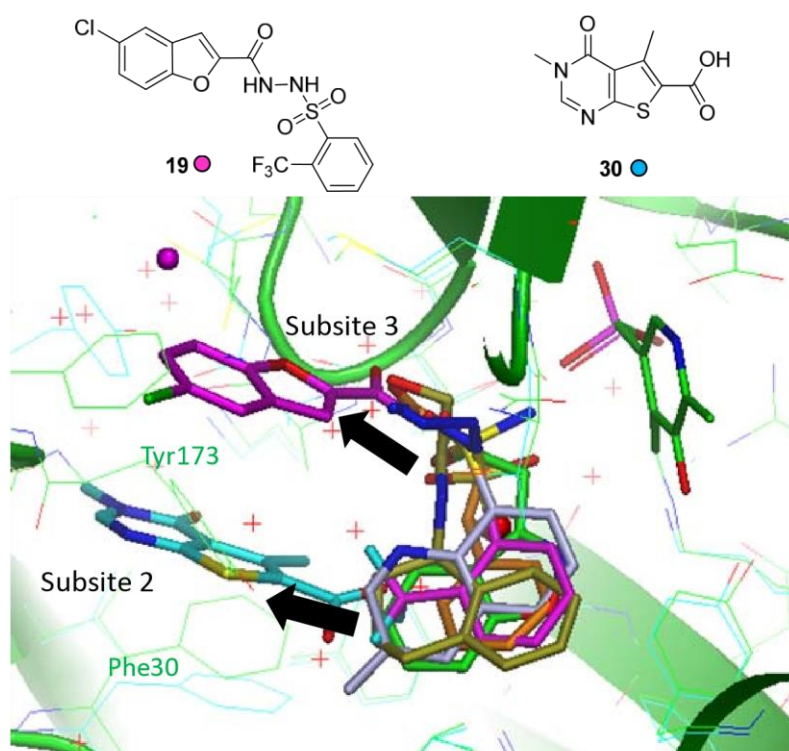


Figure 2.29 Overlaid crystal structures of compounds **26** (●), **27** (●), **28** (●), **32** (●), **30** (●) and BCATc inhibitor **19** (●)

Compound **30** (cluster 3, ●) displayed good potency, good ligand efficiency and was the only fragment to bind deeply in the newly identified induced pocket and thus

offered the opportunity to explore this novel area as well as growing toward the lipophilic pocket, where several fragments bind. These efforts will be described in the following sections. Cluster 4 (**31**) had the advantage of bridging two subsites but showed low potency and low ligand efficiency. Although chemistry on this cluster was very tractable, the biaryl amide moiety is a common feature in molecules, thus this cluster was initially progressed through analogues identified by database searching and will not be discussed further. Compound **39** from Cluster 6 had a unique binding mode and high potency with good ligand efficiency, making it an attractive starting point for further optimisation. Again work in this area will be fully described in subsequent sections.

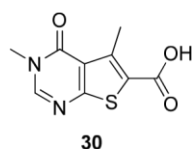
Clusters 2, 5 and 7 were of no further interest as discussed in the previous section, therefore, no further efforts were made with these. Although cluster 5 showed good potency and efficiency and a novel binding mode, this cluster showed no SAR from the initial SSS efforts and, thus, was not considered further. Lastly, Cluster 7 was considered to be quite lipophilic for a fragment and did not represent any additional novelty compared to the other clusters.

This fragment hit finding exercise highlights the importance of analogue searching in the hit finding phase, where it can be used to generate additional hits amenable to crystallography and also establish initial SAR. In addition, clustering by binding mode compared to 2D-similarity enables efficient prioritisation in the hit to lead optimisation phase, where one exemplar from each vectorial cluster was explored.

2.3 Cluster 3 - From Fragment to Lead Molecules

2.3.1 Fragment Hit and Initial SAR

The initial fragment **30** from cluster 3 was a hit in the STD-NMR assay and showed moderate biochemical activity with good ligand efficiencies. The compound was one of the most ligand efficient fragments identified with low lipophilicity, which would allow further optimisation and thus, represented an excellent starting point for hit to lead efforts. In addition, and as discussed above, compound **30** bound in the induced lipophilic pocket (Figure 2.31), which offered the opportunity to explore a novel area of the pocket, which had previously not been exploited in the literature.



pIC ₅₀	4.2*
LE	0.38
LLE _{AT}	0.44
chromlogD _{7,4}	-0.71

Figure 2.30 Cluster 3 fragment hit **30**

*Compound reported inactive (pIC₅₀ < 4.2) in 3 of the 34 test occasions.

From the crystal structure of compound **30** (●, 1.96 Å, Figure 2.31), three key interactions were observed: i) the fragment formed a π -stacking interaction with the Phe30 residue, ii) the pyrimidinone amide carbonyl participated in a hydrogen bonding interaction with the side chain NH of the Lys79 residue (3.25 Å) at the back of the pocket, and iii) the carboxylic acid formed an apparent hydrogen bonding interaction with Val155 (from the other enzyme monomer) *via* a water molecule (2.57 Å and 2.78 Å). In addition, the 3-pyrimidinone position also could provide a good vector to access a new area. Thus, this cluster offered the opportunity to grow in different directions: towards the conserved lipophilic pocket, where other fragments bound and on the pyrimidinone side of the molecule into a novel part of the catalytic site.

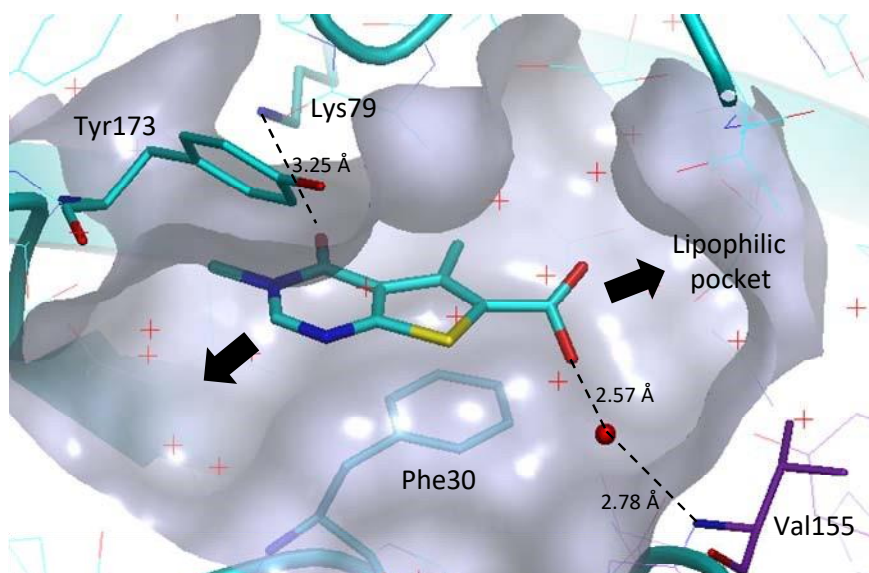
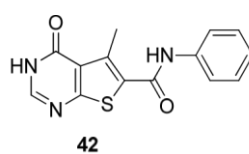


Figure 2.31 Crystal structure of fragment hit **30**

Compound **42** was identified through SSS of the related HTS data generated for BCATm in order to find related compounds with established activity against the enzyme (Figure 2.32). This analogue showed an increase in potency while maintaining good ligand efficiency giving further confidence in this cluster. This highlights the importance of exploiting information from other hit finding techniques (e.g. HTS) to enable expansion of SAR prior optimisation, and again shows the utility of substructure searching.



42

pIC₅₀ 5.2
 LE 0.36
 LLE_{AT} 0.37
 chromlogD_{7,4} 2.82

Figure 2.32 Analogue of fragment hit **30**

The crystal structure of compound **42** () confirmed that the compound bound in the same way as the initial hit **30** (, Figure 2.33).⁸⁴ The core had moved slightly; however, the key interaction with the Lys79 residue (3.13 Å) was maintained. The amide carbonyl had rotated and participated in a potential hydrogen bonding interaction *via* a

different water molecule to Tyr141 at the back of the pocket. In addition, the crystal structure showed that the phenyl ring was accommodated in the lipophilic pocket where cluster 1 compounds bound. This structure gave us confidence that growing toward the lipophilic pocket could be a successful strategy to enhance potency.

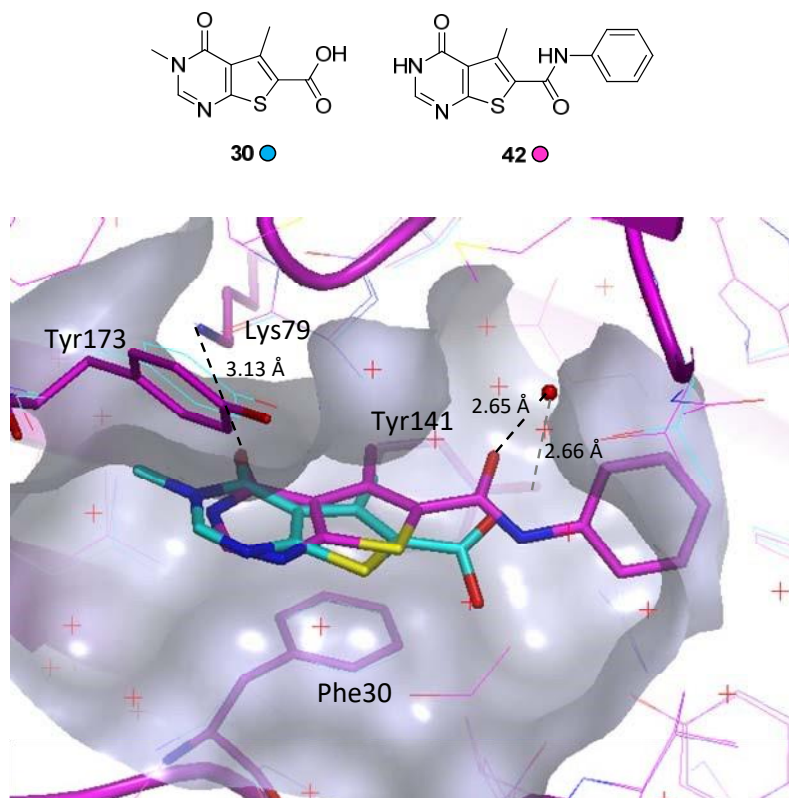


Figure 2.33 Crystal structure of BCATm in complex with compound 42 (●) and compound 30 (●)

To further expand SAR, a further SSS was carried out using commercially available compounds (from SOBAX, an in-house virtual library of compounds available from compound suppliers) and our laboratory's compound collection (2.4 M compounds, a useful resource to find analogues). As discussed previously, internal and external libraries are key asset to expand knowledge rapidly. Small modifications such as removal of the methyl groups or carboxylic acid were key to confirm the contribution of a particular group to the biological activity observed. Modification of the pyrimidinone scaffold was also examined to access the role of the electronics and

interaction points in the core. Figure 2.34 gives an overview of the various hypotheses considered to identify further analogues for testing.

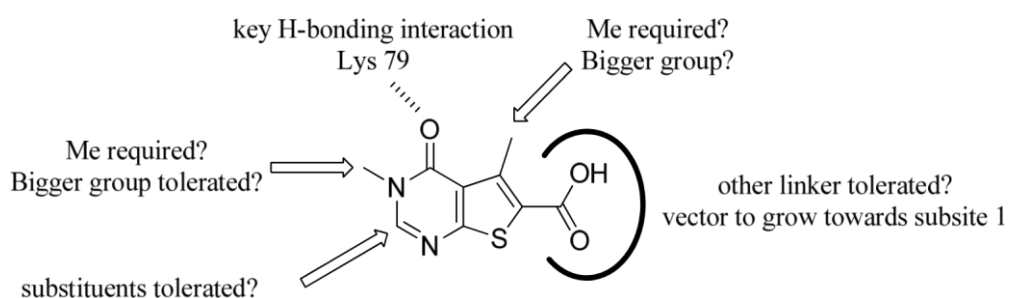


Figure 2.34 Initial SAR searches

All of the compounds identified were assessed by LCMS to confirm purity prior to testing, in accord with our laboratory's usual workflow for processing database compounds. Biological data associated with compounds selected to explore substituent modifications are shown in Table 2.4.

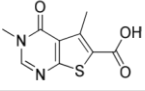
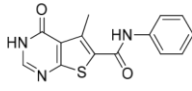
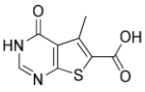
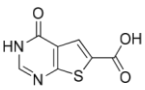
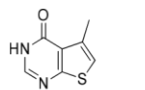
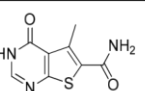
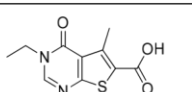
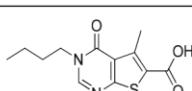
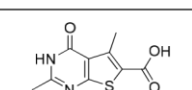
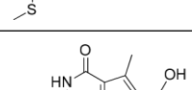
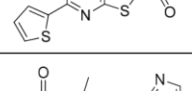
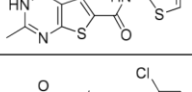
Cmpd	Structure	pIC ₅₀	LE	LLE _{AT}	clogP
30		4.2 ^a	0.38	0.44	0.61
42		5.2	0.36	0.37	1.4
43		4.3	0.42	0.49	0.39
44		< 3.2	< 0.34	< 0.43	0.19
45		< 3.2	< 0.40	< 0.43	0.62
46		< 3.2	< 0.31	< 0.49	0.67
47		3.6 ^b	0.31	0.32	1.15
48		3.7	0.28	0.22	2.21
49		4.5 ^c	0.36	≤ 0.38	1.14
50		5.1	0.37	0.31	2.38
51		4.8	0.33	0.39	0.7
52		< 4.2	< 0.26	< 0.28	1.5

Table 2.4 SSS biological results

^a Compound reported inactive (pIC₅₀ < 4.2) in 3 of the 34 test occasions.

^b Compound reported pIC₅₀ < 4.2 in 2 of the 4 test occasions.

^c Compound reported inactive (pIC₅₀ < 4.2) in 1 of the 2 test occasions.

From the data above, it can be noted that the methyl group on the pyrimidinone nitrogen (**43**) can be removed maintaining similar potency to the initial hit **30** and therefore good LE and LLE_{AT}. An ethyl substituent (**47**) reduced potency and, thus,

negatively impacted both LE and LLE_{AT}, suggesting that limited space exists to expand in this region. Having stated this, the butyl analogue (**48**) did not completely ablate potency, however, showed very poor ligand efficiencies as a result of increasing both MW and clogP. The potency of the butyl analogue **48** perhaps suggests that the protein could move to accommodate bigger groups or the compound could potentially adopt a different binding mode. The 2-methyl substituent on the thiophene seemed to be key for potency as shown by the difference in potency between compounds **43** and **44**. From the crystal structure of compound **30**, the methyl group appeared to fit optimally in the pocket (Figure 2.35), potentially making favourable hydrophobic contacts with the protein surface.¹⁰³ From consideration of literature data, a methyl group may be expected to give up to 10-fold increase in potency due to the hydrophobic effect.⁴⁵ In some instances where the methyl fits perfectly in the pocket, a bigger increase can be observed.^{104,105}

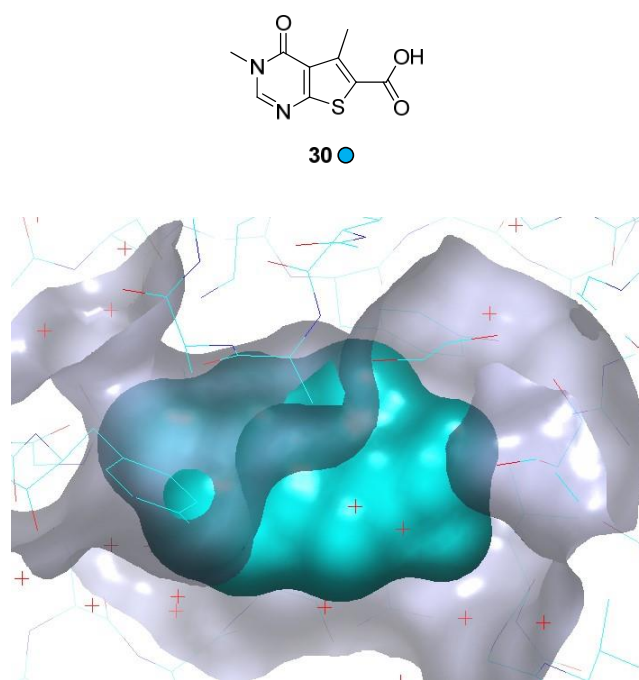


Figure 2.35 Crystal structure of compound **30** with electron density (●) and protein surface (⊙) showing good fitting of the methyl group

Based on the potency of compound **45** in comparison to **43**, the carboxylic acid at the 2-position also seemed to be beneficial for potency suggesting that the interaction *via* water molecule with Val155 is important as indicated in the X-ray (Figure 2.31). Interestingly, replacement of the carboxylic acid with a carboxamide (**46**) completely ablated the potency. From the crystal structure, it was not clear why this should be the case as the primary carboxamide should be capable of making similar H-bonding interactions with the enzyme. Solubility might be an issue with this compound, potentially impeding measurement of its biological activity at the relatively high test concentrations used.

Compounds **49** and **50** confirmed that substituents at the 3-position of the pyrimidinone ring are tolerated. Compound **50** also showed increased potency but slightly reduced ligand efficiencies. If the compounds bound to the enzyme as expected, the sulfur containing chain or the thiophene ring could potentially access a new area of the pocket. In order to determine binding mode, the two compounds were progressed to crystallography.⁸⁴ Crystal structure analysis of compound **49** () showed excellent overlay with compound **30** () (Figure 2.36). The key interactions were maintained: π -stacking interaction with Phe30, an H-bonding interaction between the pyrimidinone carbonyl and Lys79 and an H-bonding interaction of the carboxylic acid *via* a water molecule with Val155. As hypothesised, the crystal structure also indicated that a new part of the pocket could be accessed to improve potency and ligand efficiency. Polar groups on the backbone are visible around this thioether substituent (Gly171, Leu28) and are potentially accessible from this position, providing additional opportunities for interactions that could be targeted to improve potency.

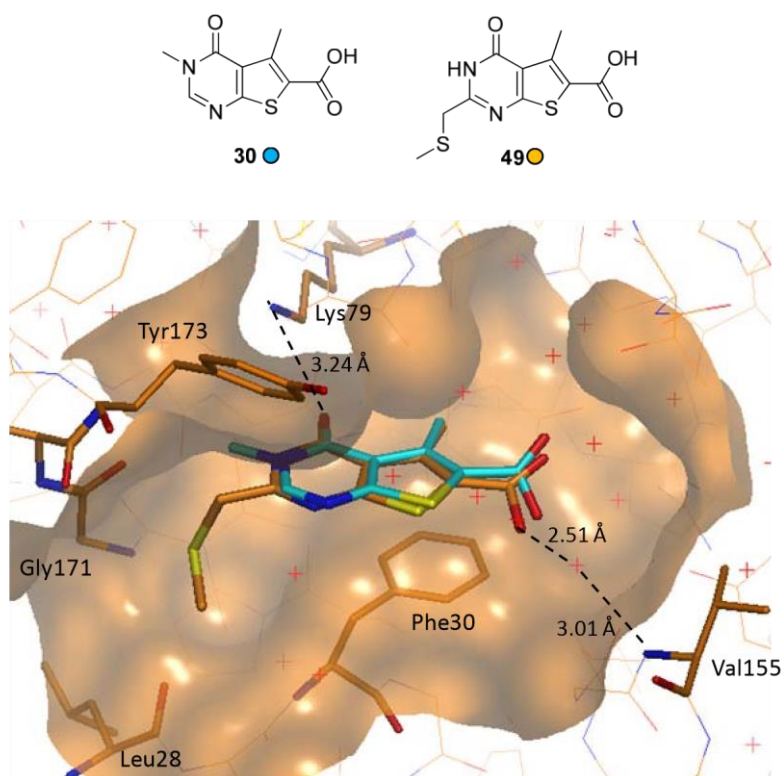


Figure 2.36 Crystal structure of compound **49** (●) overlaid with compound **30** (●)

Compound **51** confirmed that aromatic amides are tolerated in the lipophilic pocket. Interestingly, compound **52** showed no activity in the enzyme assay compared to its analogue **42** but from the crystal structure it was not clear why that would be the case.

This initial phase of fragment optimisation emphasises the importance of using SSS and HTS output to expand SAR prior to compound synthesis and increase structural knowledge to guide optimisation of the fragment hit.

2.3.2 Optimisation Goals

As outlined previously, the objective of the research was initially to demonstrate that potency could be improved to the desired level for a tool molecule (BCATm $pIC_{50} \geq 6.5$). Based on the initial results generated from the in-house collection and commercially available compounds, efforts were in the first instance focused on growing towards the lipophilic pocket, as it was believed that targeting this region offered the greatest probability of success in optimising potency. In addition, from structural data from the other clusters, it is known that H-bonding interaction with Ala314 should increase potency further.

Overlay of compound **42** (●) with compounds from cluster 1 (e.g. **27** ● and **26** ●, Figure 2.37) suggested that substituents at the *ortho*-position of the phenyl ring could potentially pick up similar interactions to the sulfonamide and acid groups observed in cluster 1 compounds (i.e. interaction with Ala314).

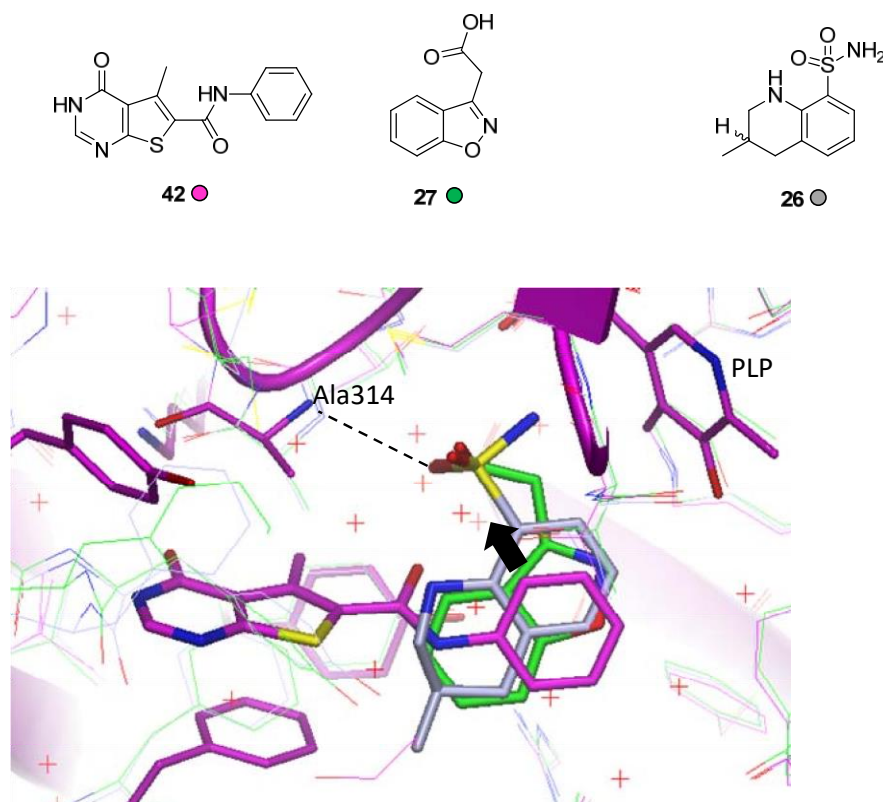


Figure 2.37 Crystal structure of BCATm in complex with compound **42** (●) and compounds **27** (●) and **26** (●) from cluster 1

Based on this, substituents reasoned to interact with Ala314 from cluster 1 were selected for synthesis (Figure 2.38).

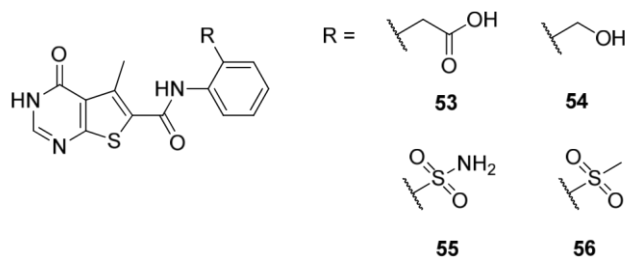


Figure 2.38 Compounds designed to interact with subsite 2 residues

A docking study was carried out by another member of our laboratories¹⁰⁶ and confirmed that substituents selected at the *ortho*-position should be in similar position to the carboxylic acid or the sulfonamide of cluster 1 compounds. In the docking studies, the core was usually shifted to the left compared to compound **42** (●, Figure 2.39) and found to be in good range to interact with Gly171, but all the key interactions were maintained. Compound **55** (●) showed that the sulfonamide was in similar position to compound **26** (●) sulfonamide, interacting with Ala 314.

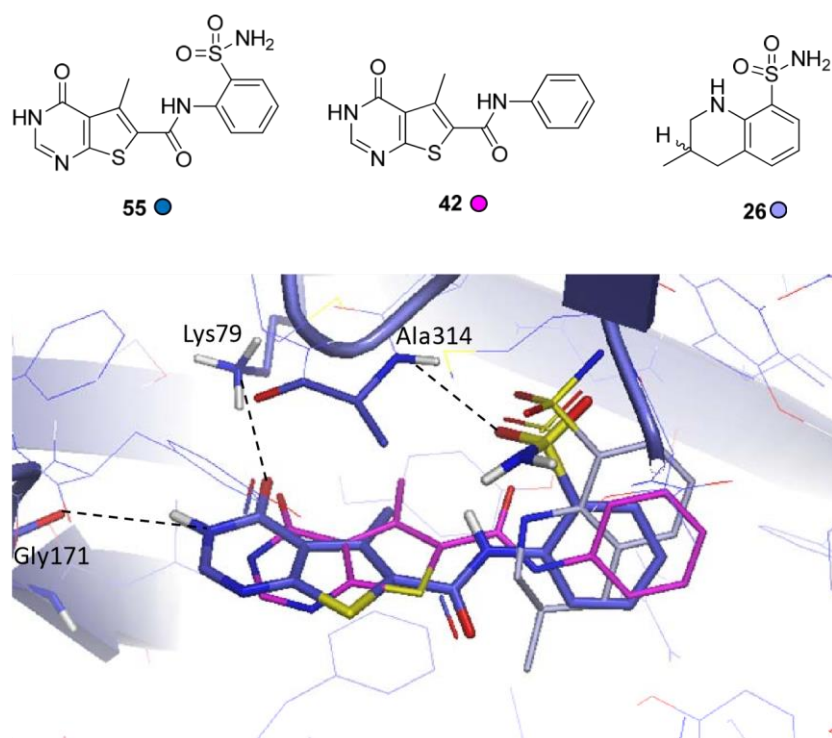


Figure 2.39 Docking of compound 55 (●) overlaid with compounds 42 (●) and 26 (●)

Compound 53 (●, Figure 2.40) did not overlay well with the available crystal structure of compound 42 (●). The core was shifted significantly to the left but still showed interaction with Lys79. Although the phenyl ring did not overlay with the corresponding ring in compound 42, the carboxylic acid still showed the potential to interact with Ala314 and Tyr141 and thus, was still of interest.

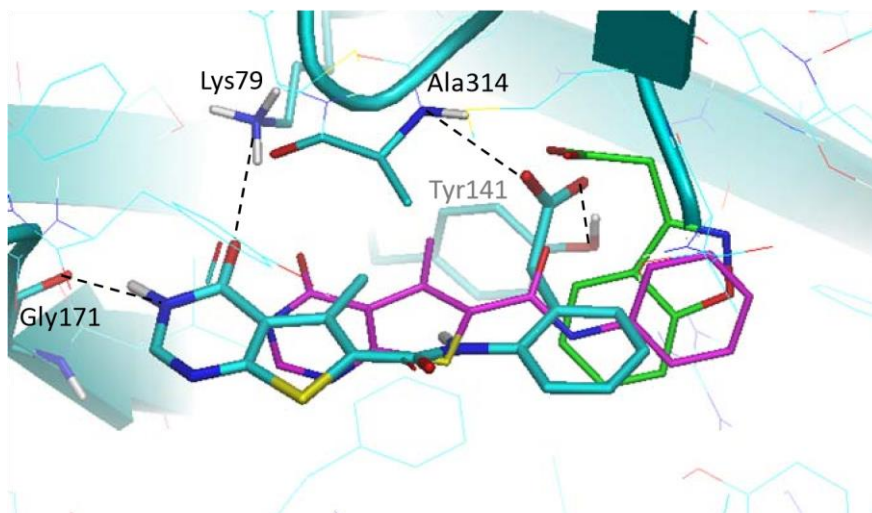
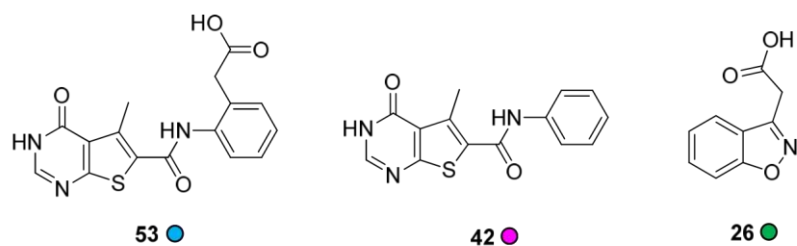
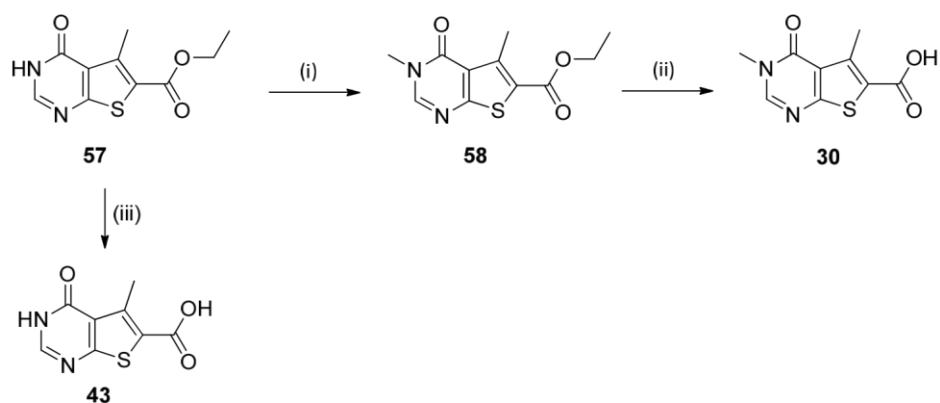


Figure 2.40 Docking of compound **53** (●) overlaid with crystal structures of **42** (●) and **26** (●)

2.3.3 Results and Discussion

2.3.3.1 Synthesis of Carboxylic Acid Intermediates

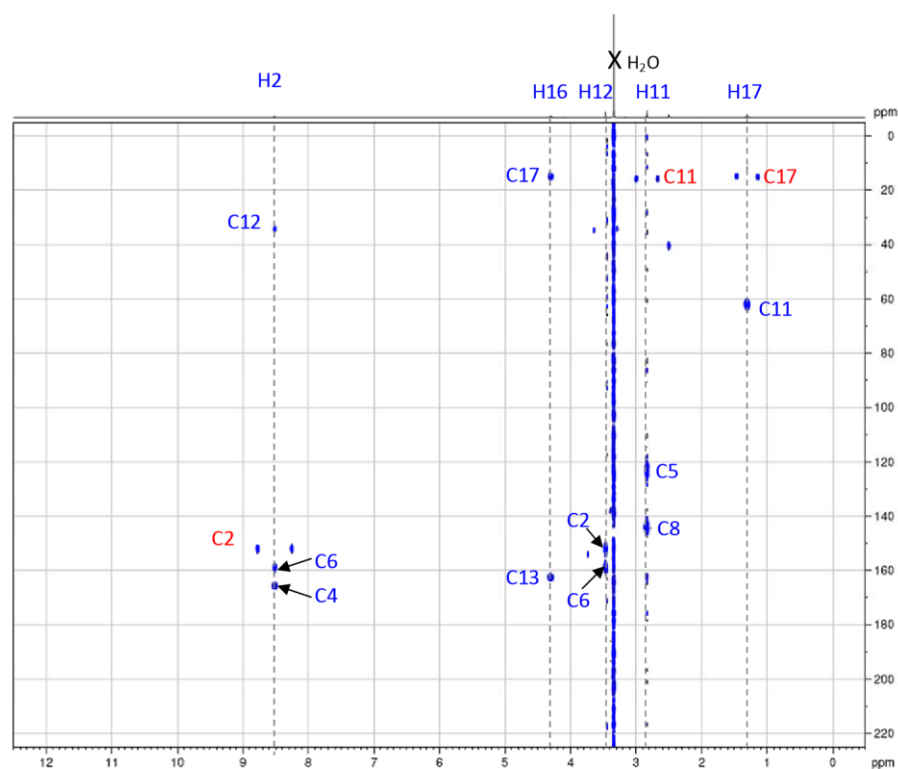
Having identified a series of derivatives with potential to enhance potency, attention then turned to synthesis of the target compounds. The fragment hit **30** and the desmethyl analogue **43** were synthesised as intermediates, which would enable further chemistry (Scheme 2.1). Additionally, the ester starting materials **57** and **58** provide further analogues to probe the role of the carboxylic acid moiety.



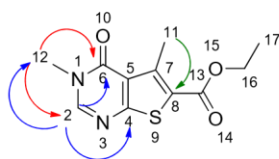
Reagents and conditions: (i) MeI, K₂CO₃, MeCN, 80 °C, 3 h, 95%; (ii) LiOH, THF/EtOH/H₂O, rt, 3 days, 86%; (iii) LiOH, THF/MeOH/H₂O, rt to 40 °C, 46 h, 99%.

Scheme 2.1

Compound **57** could be methylated using methyl iodide and potassium carbonate at 80 °C. The desired *N*-methylated product **58** was obtained as the major product in excellent yield (95%). The regioselective *N*-alkylation versus *O*-alkylation can be explained by the use of a soft alkylating agent such as methyl iodide. The structure of the *N*-alkylated compound **58** was confirmed using ¹H, ¹³C, HMQC and HMBC NMR. The methyl carbon has a significantly different chemical shift depending on the attached heteroatom in both ¹H and ¹³C NMR. A carbon chemical shift of ~30 ppm would be expected for *N*-CH₃ while a chemical shift of ~50 ppm would be expected for *O*-CH₃. The chemical shift observed in both carbon and proton environments was indicative of *N*-alkylation (33.8 ppm for C12 and 3.47 ppm for H12). Methylation of the desired nitrogen was also confirmed by HMBC which showed a key correlation between the methyl proton on N1 and the carbonyl carbon C6 and carbon C2 (Figure 2.41).



¹³C data



C4	165.7 ppm (corr. H2) key correlation
C6	159.1 ppm (corr. H2, H12) key correlation
C2	152.0 ppm (corr. H12) key correlation
C8	144.5 ppm (corr. H11)
C5	122.8 ppm (corr. H11)
C12	33.8 ppm key shift
C11	33.7 ppm

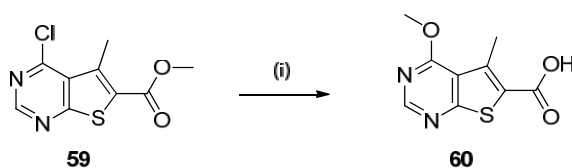
Figure 2.41 HMBC of compound **58**

The ester intermediate **58** was then hydrolysed using lithium hydroxide in a mixture of THF/EtOH/H₂O at room temperature to give the desired final product **30** in excellent yield.

Again, starting from the commercially available ester **57** hydrolysis using lithium hydroxide in a mixture of THF/MeOH/H₂O at room temperature then 40 °C gave the desired final product **43** in excellent yield.

From the crystal structure of compound **30**, the carbonyl of the pyrimidinone makes a key H-bonding interaction with Lys79. To quantify the role of this interaction, the

methoxypyrimidine analogue **60** was synthesised (Scheme 2.2). A route to convert pyrimidinones to the desired pyrimidine ethers is to use S_NAr substitution from the corresponding aryl halides (Scheme 2.2). The carbonyl group is first activated by halogenation using $POCl_3$ for example and then reacted with the desired nucleophile.¹⁰⁷ The commercially available chlorinated intermediate **59** was reacted with sodium methoxide in methanol with concomittent ester hydrolysis to give the desired final product **60**.



Reagents and conditions: (i) NaOMe, MeOH, rt, 2 h, 55%.

Scheme 2.2

2.3.3.2 Synthesis of *ortho*-Substituted Analogues

As outlined earlier, *ortho*-substituents containing HBD and HBA groups could interact with Ala314 as observed in cluster 1 compounds, and it was envisaged that the desired amides (Figure 2.42) could be prepared using standard coupling conditions using the carboxylic acid derivative **43** and suitable functionalised aniline (Figure 2.43).^{108,109} Prior to the amide coupling, however, the required carboxylic acid and aniline intermediates had to be prepared.

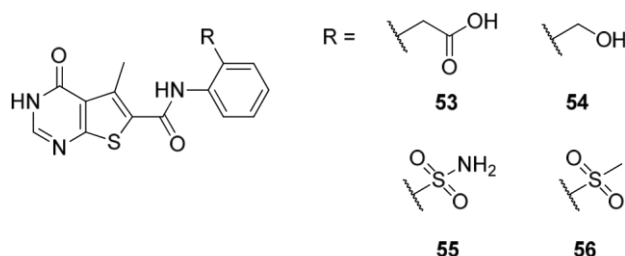


Figure 2.42

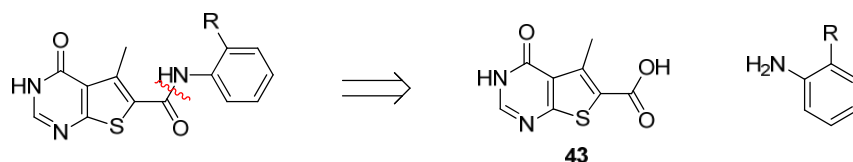
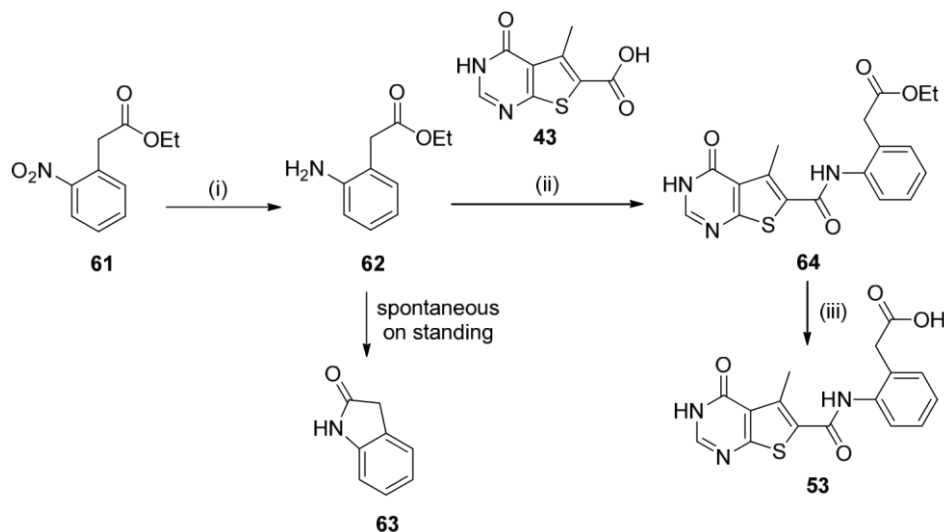


Figure 2.43 Retrosynthetic analysis

The synthesis of the first aniline derivative is shown in Scheme 2.3. The commercially available nitro compound **61** was reduced to the desired aniline **62** by hydrogenation in an H-cube using 10% Pd/C catcart cartridge. The desired aniline **62** was unstable and was observed to convert to the cyclised oxindole product **63** upon standing. It was therefore necessary for the aniline to be used immediately for the next step. The aniline **62** was then coupled with the carboxylic acid **43** using HATU and DIPEA at room temperature in modest yield. The ester intermediate **64** was then hydrolysed using lithium hydroxide in a mixture of THF/MeOH/H₂O at room temperature to give the desired final product **53**.



Reagents and conditions: (i) 10% Pd/C catcart, full H₂, EtOH, 20 °C, H-cube, 1 mL/min, 86%; (ii) HATU, DIPEA, DMF, rt, 16 h, 40%; (iii) LiOH, THF/MeOH/H₂O, rt, 2 h, 58%. **Scheme**

2.3 Synthetic route to compound 52

O-[7-Azabenzotriazol-1-yl]-1,1,3,3-tetramethyluronium hexafluorophosphate (HATU) is commonly used in our laboratory as it has proven to be a very efficient coupling agent. HATU has demonstrated to give good yields in shorter time and is very efficient even with less reactive, non-nucleophilic amines and in sterically hindered carboxylic acids.¹⁰⁸ In addition, the acylating agent is generated *in situ* using mild conditions. In solution, the uronium species is in equilibrium with the guanidinium species (Figure 2.44). The guanidinium form **66** is usually reported as the crystalline form.

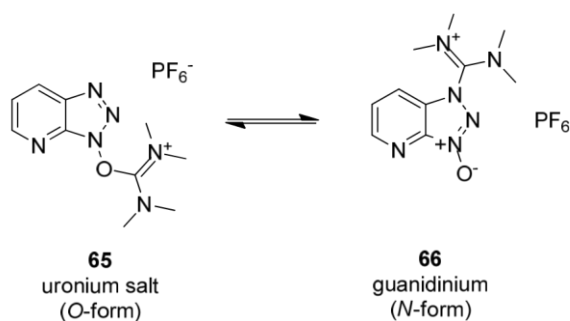


Figure 2.44 HATU coupling reagent, equilibrium between uronium and guanidinium species. The HATU coupling consists of two steps: activation and coupling (Figure 2.45). In the activation step, the carboxylic acid substrate **67** is deprotonated by a base; this base is typically diisopropylethylamine (DIPEA, **68**). HATU **66** then reacts with the deprotonated acid **69** to give a uronyl ester **71** and deprotonated HOAt (1-hydroxy azabenzotriazole) **70**. HOAt **70** reacts with the activated acid **71** to generate the reactive HOAt ester intermediate **743** and a urea by-product **72**. The driving force is the formation of a stable urea. In the coupling step, the active ester **74** reacts with the amine **73** to give the required amide **76** and reforming the HOAt **75**. The urea and HOAt by-products are water soluble and can be removed from the reaction mixture by an aqueous work-up using sodium bicarbonate solution.

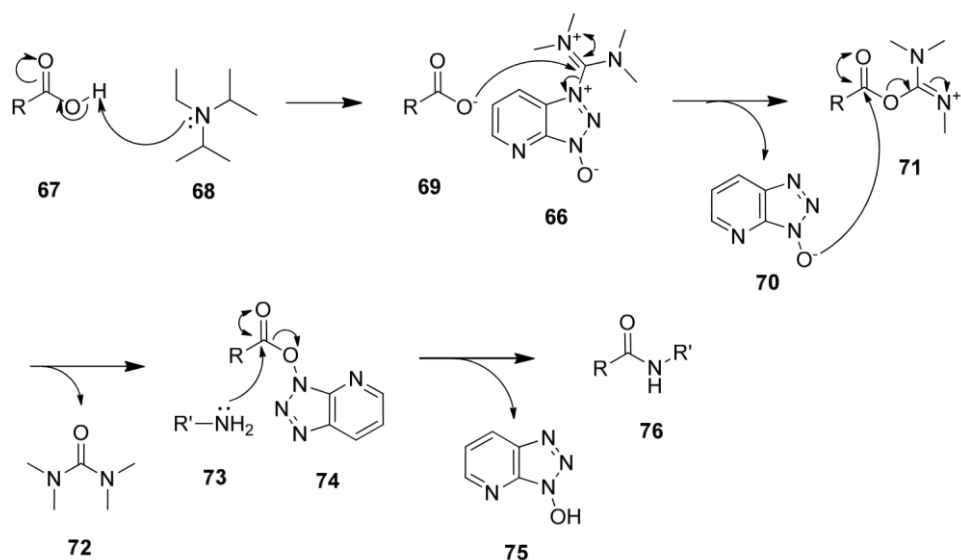


Figure 2.45 HATU coupling mechanism

In addition, as depicted in Figure 2.46, HATU has been postulated to enhance the speed of the reaction *via* the effect of the azabenzoyl nitrogen in stabilising the transition state through a neighboring group effect.¹⁰⁸

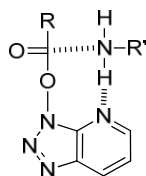
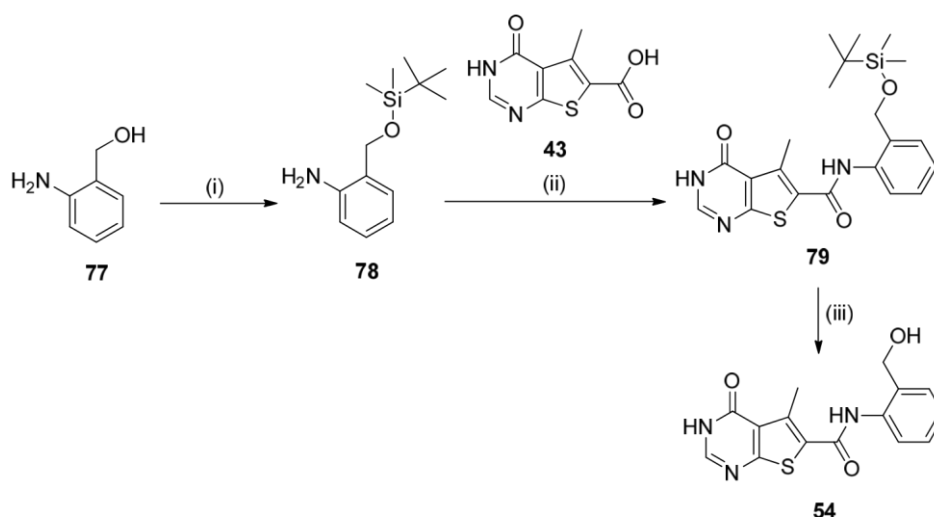


Figure 2.46 Stabilisation of transition

state

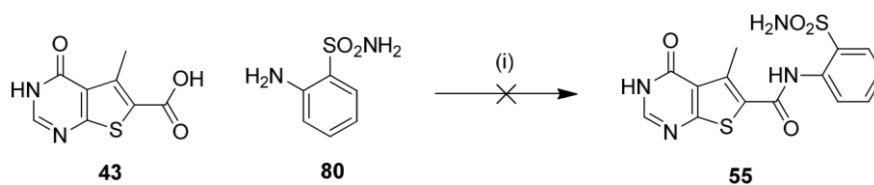
Access to the desired alcohol-containing aniline building block commenced through protection of the commercially available aniline **77** with a *tert*-butyldimethylsilyl (TBDMS) group at room temperature (Scheme 2.4).¹¹⁰ The protected intermediate **78** was then coupled to the carboxylic acid **43** in modest yield using HATU and DIPEA at room temperature. The TBDMS protecting group was then removed using TBAF at room temperature to give the desired final product **54**.



Reagents and conditions: (i) TBDMSCl, imidazole, DCM, rt, 14 h, 92%; (ii) HATU, DIPEA, DMF, rt, 18 h, 44%; (iii) TBAF 1 M in THF, THF, rt, 3 h, 59%.

Scheme 2.4 Synthetic route to compound **54**

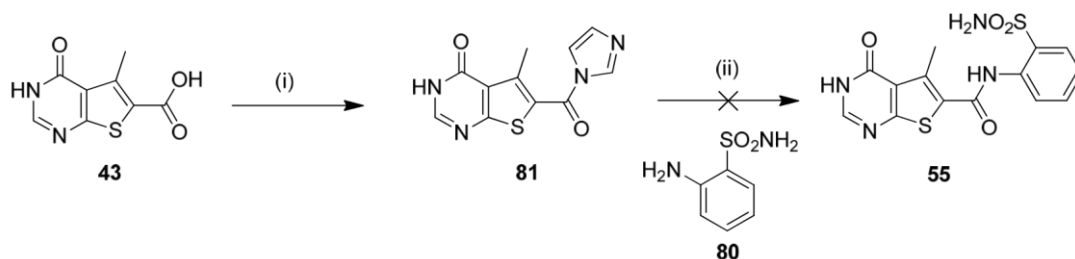
The amide coupling developed on the above systems using HATU did not prove to be effective for the sulfonamide and the sulfone anilines, due presumably to the reduced reactivity of the anilines (Scheme 2.5). Although microwave conditions offered a slight improvement, conversion to the desired product could not be further optimised under these conditions. Attempts to isolate the desired product from the reaction mixture using mass directed auto-preparative HPLC (MDAP) failed to give enough compound for biological testing. Consequently a number of alternative reagents to facilitate amide bond formation were explored.



Reagents and conditions: (i) HATU, DIPEA, DMF, rt, 12 h then 40 °C, 3 h.

Scheme 2.5

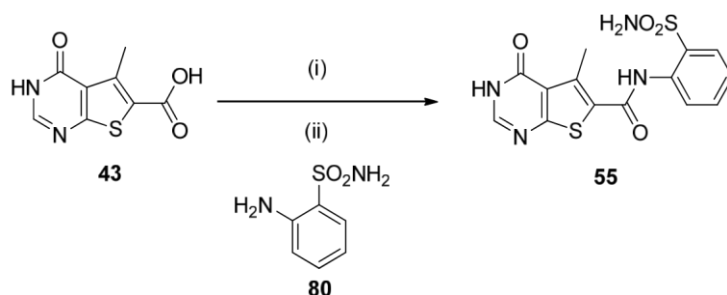
CDI was previously used to make a carboxamide analogue in the series and thus was deemed to be a viable alternative (Scheme 2.6). The carboxylic acid **43** was reacted with CDI to form the activated acyl carboxy imidazole intermediate **81**. Upon addition of the aniline, no desired product was observed following LCMS analysis of the reaction mixture; only the acyl carboxy imidazole **81** was present, suggesting that the reactivity of the intermediate was low.



Reagents and conditions: (i) CDI, THF, rt, 1 h; (ii) rt, 12 h.

Scheme 2.6 Amide coupling using CDI

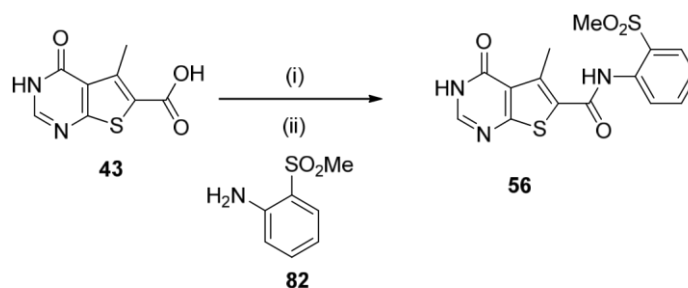
Based on the above, it was decided to convert the carboxylic acid **43** to a more reactive intermediate, specifically the acid chloride (Scheme 2.7). The carboxylic acid intermediate **43** was converted to the acid chloride using neat thionyl chloride at reflux. The acid chloride intermediate was then reacted with 2-aminobenzenesulfonamide to give the desired final product **55**. Despite the low yield, this was encouraging for an electron-deficient and relatively hindered substrate and a sufficient quantity was isolated for biological testing.



Reagents and conditions: (i) SOCl₂, reflux, 20 h; (ii) DIPEA, DMF, rt, 18 h, 11% over two steps.

Scheme 2.7 Amide coupling with acid chloride

The amide coupling conditions developed for the sulfonamide analogue were also applied to the sulfone moiety (Scheme 2.8). Again, the carboxylic acid intermediate **43** was converted to the acid chloride using thionyl chloride at 50 °C. The mixture was then reacted with the sulfone aniline to give the desired final product **56** in a disappointing yield (9%) but in sufficient quantities for downstream bioassay.



Reagents and conditions: (i) SOCl₂, 50 °C, 2 days; (ii) DIPEA, DMF, rt, 16 h then 50 °C, 16 h, 9% over two steps.

Scheme 2.8

2.3.3.3 Expanding SAR around the Lipophilic Pocket

Although the phenyl amide analogue **42** showed encouraging data and good vector to grow towards Ala314, only a small selection of amides were available from the initial substructure searching carried out at the hit evaluation stage (section 3.4). Therefore, a wider range of amides were selected for synthesis to expand our understanding of SAR in the pocket and to determine if physicochemical properties could be modulated further in this region. Accordingly, a small array of both saturated and aromatic systems were selected for synthesis. Initially the selection was limited to amines available commercially or from our laboratory's reagent collection (Figure 2.47).

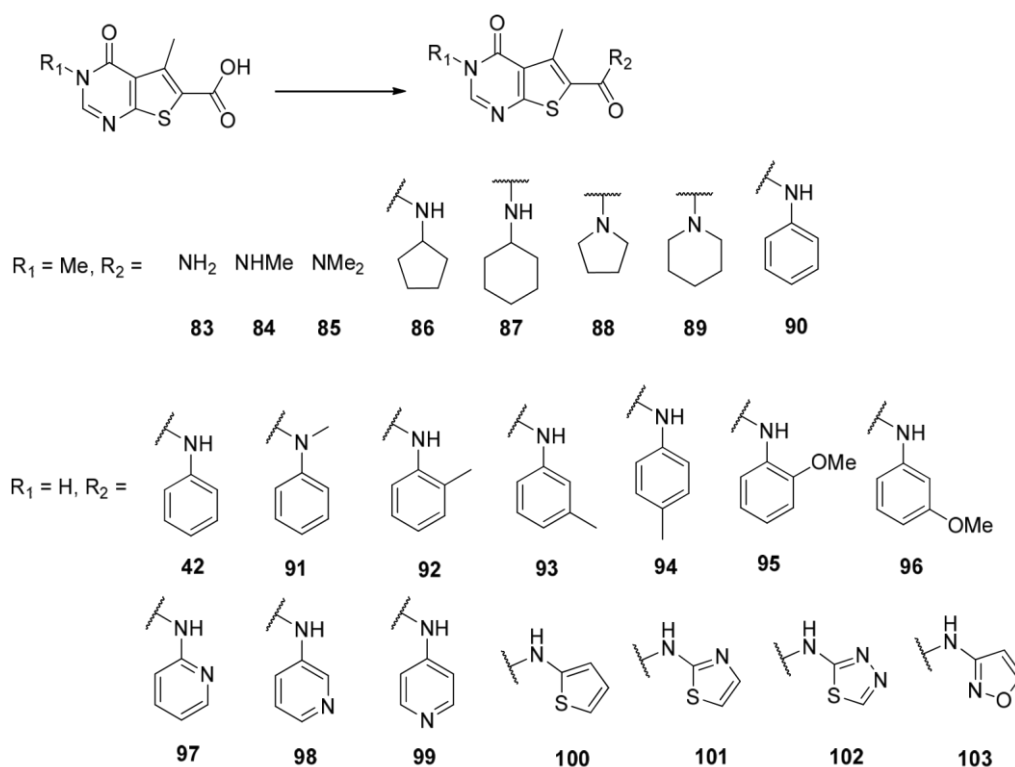


Figure 2.47 Compounds designed to explore SAR in the lipophilic pocket

In the saturated set, methyl, cyclopentyl and cyclohexyl were chosen as representative examples and both primary and secondary amides were investigated (**83-89**). As the core already contains two aromatic rings, it was important to assess if a third aromatic ring was required as this could be detrimental towards key the properties of the molecules such as solubility.^{20,111} In the aromatic set (**91-103**), a selection of substituted phenyl rings and heterocycles was made to further probe the SAR in this part of the enzyme pocket. From the crystal structure of compound **42** (●, Figure 2.48), the phenyl ring seemed to fill the pocket well, which suggested that substituents at the *meta*- and *para*-positions would clash with the protein surface. To confirm that the pocket was optimally occupied, substitution with small substituents (e.g. Me **92-94**) was investigated.

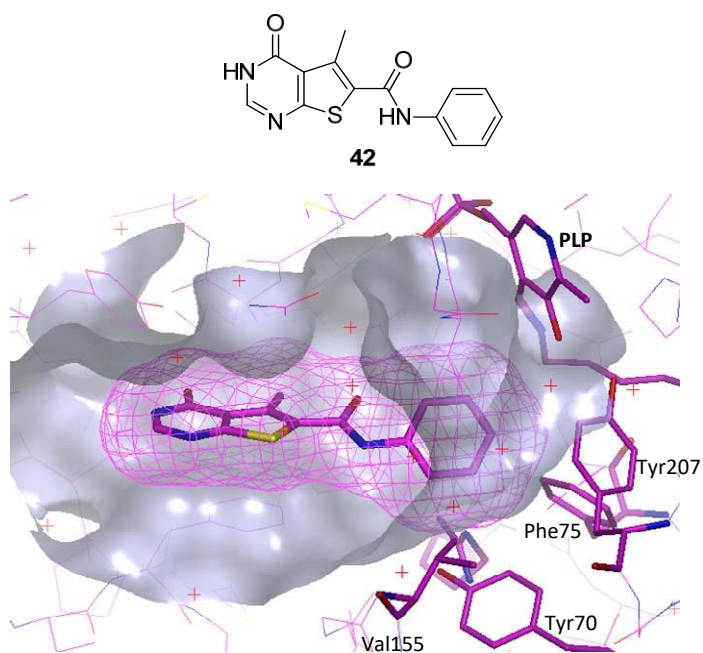
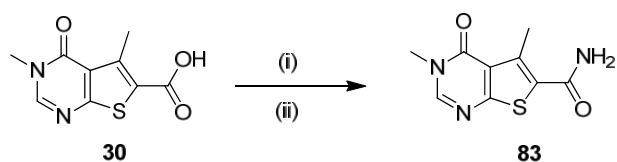


Figure 2.48 X-ray structure of BCATm in complex with compound **42** with electron density

Although the nature of the pocket appears fairly lipophilic (no polar residues appear to be within range for interaction, Figure 2.48), some additional heterocycles were selected to further explore this region (**97-103**) at the same time as maintaining acceptable physicochemical properties. Additional introduction of heteroatoms will reduce lipophilicity of the molecule and, thus, be beneficial for solubility.

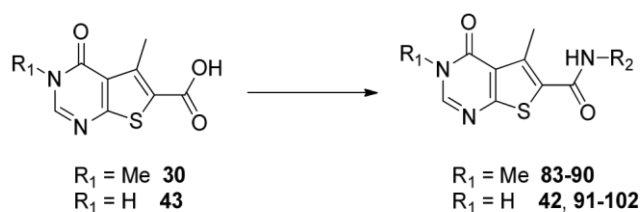
The carboxamide **83** was prepared using CDI. The carboxylic acid **30** was reacted with CDI to form the activated acyl carboxy imidazole intermediate. Ammonia gas was then bubbled through the mixture for 5 min and the mixture was stirred at room temperature for 1 h to give the desired product **83**.



Reagents and conditions: (i) CDI, THF, rt, 24 h; (ii) ammonia gas bubbled for 5 min, then 1 h stirring, rt, 28%.

Scheme 2.9

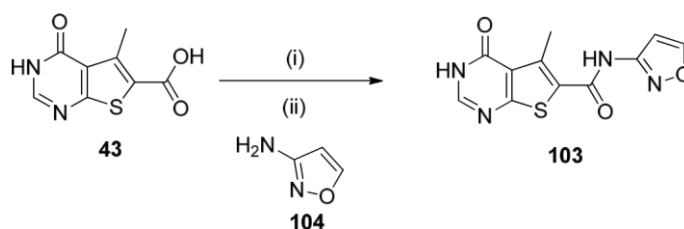
The other desired amides were prepared using HATU as coupling reagent as it has been proven to work with a variety of amines (Scheme 2.10). Isolated yields were variable (3-68%) depending on the amines used. The reaction mixtures generally showed a mixture of by-products by LCMS, however, no real trend was observed between the reactions. Ionisation of these by-products was usually weak by LCMS and did not allow identification of a clear mass ion. In some instances, the reaction did not go to completion even after heating and use of excess amine, which could also explain the lower yields.



Reagents and conditions: (i) $R_2\text{-NH}_2$, HATU, DIPEA, DMF, rt to 50 °C, 1-80 h, 3-67%.

Scheme 2.10

It was found that despite extensive experimentation, compound **103** could not be synthesised using the HATU-mediated approach described above. Consequently, thionyl chloride mediated conditions were employed as shown in Scheme 2.11.

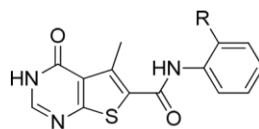


Reagents and conditions: (i) SOCl_2 , 80 °C, 3 days; (ii) DIPEA, DMF, rt, 24 h, 14%.

Scheme 2.11

2.3.3.4 Biological Results

Targetting the interactions from cluster 1 compounds showed highly encouraging results as shown in Table 2.5.



Cmpd	R	pIC ₅₀	LE	LLE _{AT}	Chrom logD _{7.4}	CLND sol. (µg/mL)
42	H	5.2	0.36	0.37	2.82	76
53		6.0	0.34	0.45	0.44	164
54		5.0	0.31	0.44	1.86	139
55		4.9	0.28	0.41	0.26	≥ 160
56		< 4.2	< 0.24	< 0.35	2.74	n.d. ^a
64		< 4.2	0.22	0.28	3.28	162

Table 2.5 Biological data on *ortho*-substituted phenyl ^ainsufficient material available to measure solubility

Introduction of hydrogen bond donating groups maintained activity as well as both LE and LLE_{AT}. Although the alcohol **54** and the sulfonamide **55** did not give an increase in potency, they did significantly improve the solubility of the molecule. Lack of enhancement in potency could be attributed to the angle or length to complete the necessary hydrogen-bonding interaction with Ala314 being suboptimal, which could be confirmed by crystallisation. Compound **56** completely ablated activity suggesting that the sulfone was not suitable to make the desired interaction with the protein. On

the other hand, the carboxylic acid **53** increased potency ~10fold while maintaining good LE and increasing LLE_{AT}. This suggested that a useful polar interaction may have been made as outlined in the design hypothesis. The carboxylic acid is potentially able to access the hydrogen-bonding interaction observed in cluster 1 as suggested by the docking. To confirm its binding mode, the compound was progressed to X-ray crystallography.⁸⁴ Interestingly, the corresponding ethyl ester (**64**) was inactive. The crystal structures available of compounds **42** (●) and compound **27** (●), as shown in Figure 2.49, suggested that the ethyl group might clash with the protein surface or modify the orientation of the substituent to accommodate the ethyl group and therefore break the key hydrogen bonding interactions, thus potentially accounting for the lack of activity.

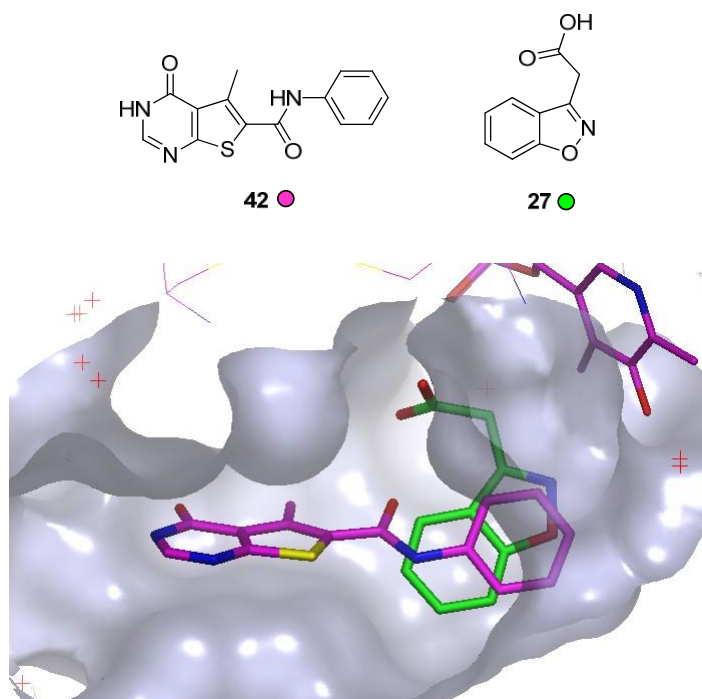


Figure 2.49 Crystal structure of compound **42** (●) overlaid with compounds **27** (●)

The X-ray crystal structure of compound **53** (●) confirmed the binding mode was conserved compared to compounds **30** (●) and **42** (●) (Figure 2.50). Compound **53**

overlays perfectly with initial hit **30** suggesting an optimal, low energy binding pose. The pyrimidinone core forms a π -stacking interaction with the Phe30 residue, and the pyrimidinone amide carbonyl forms an H-bonding interaction with the side chain NH of the Lys79 residue (2.97 Å) at the back of the pocket. The amide was observed to interact with Val155 (from the other protein dimer) *via* a water molecule as observed with fragment **30**. In addition, the carbonyl oxygen of the carboxylic acid made a key hydrogen-bonding interaction with the protein backbone NH (Ala314) as observed in cluster 1 compounds (●). The carboxylic acid is likely also to make an intramolecular hydrogen-bonding interaction with the amide NH maintaining the molecule in a desired conformation with both the acid and the amide in a preferred geometry.

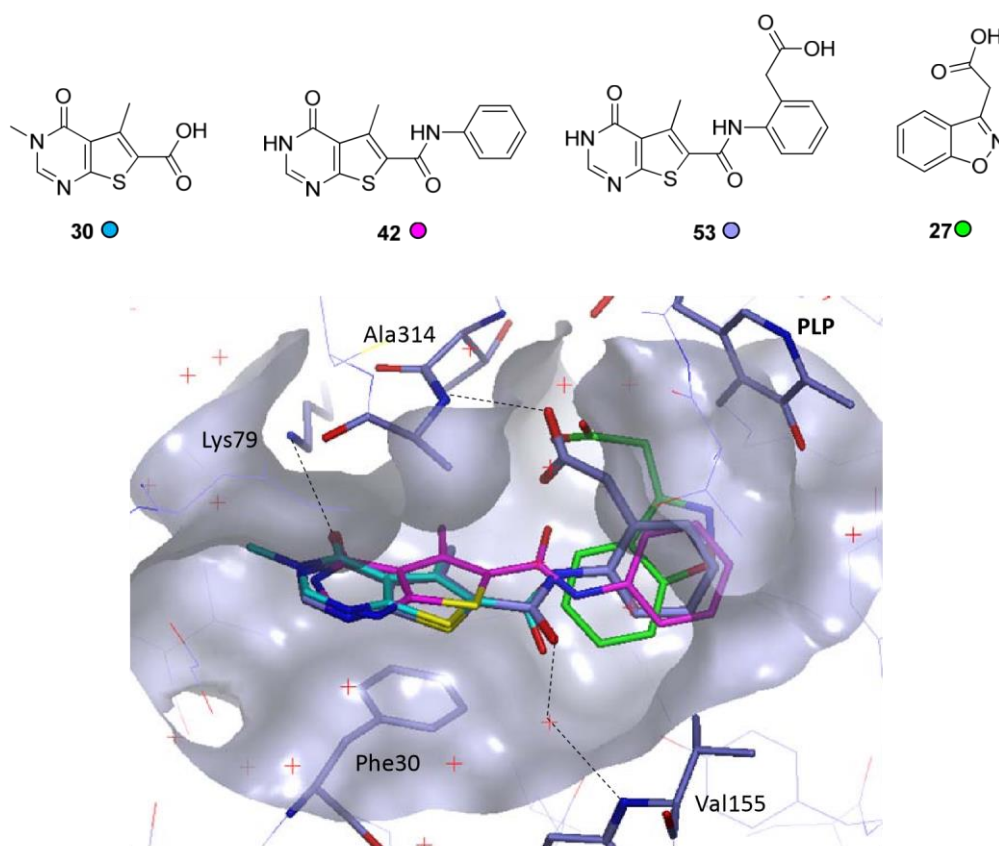


Figure 2.50 Crystal structure of compound **53** (●) overlaid with compounds **30** (●), **42** (●) and **27** (●).

Given its superior potency compared to progenitor compound **30**, compound **53** was subjected to further analysis. The full profile of the compound is summarised in Table 2.6.

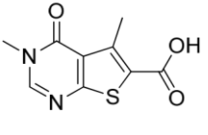
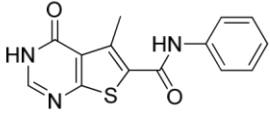
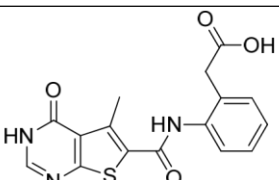
			
	30	42	53
BCATm pIC₅₀	4.2 ^a	5.2	6.0
LE, LLE_{AT}	0.38, 0.44	0.36, 0.37	0.34, 0.45
chromlogD_{7.4}	-0.71	2.82	0.44
CLND	≥ 73	76	164
BCATc pIC₅₀	3.5	4.7	5.6
Cell pIC₅₀	n.d.	n.d.	< 4.3
PSA	72	75	112

Table 2.6 Profile of compounds **42** and **53**

^aCompound reported inactive (pIC₅₀ < 4.2) in 3 of the 34 test occasions.

Compound **53** showed a 100-fold increase in potency compared to hit compound **30** and a 10-fold compared to compound **42** while maintaining good LE and LLE_{AT} demonstrating efficient binding. Lipophilicity of the molecule has been reduced and solubility increased by addition of the carboxylic acid group. Both compounds showed no selectivity over BCATc at this stage. However, as discussed in the introduction section, selectivity can also be achieved by reducing brain penetration of the compound, which is feasible given the high PSA of the acid **53**. At this stage of the programme, attention focussed on finding a cell active compound. Although the compound was close to the criteria required for a tool molecule, it showed no activity in the cell assay. However, the low lipophilicity of the molecule (measured chromlogD_{7.4} = 0.44) will more than likely prevent efficient uptake into the cell as it will almost certainly result in poor membrane permeability. Another possibility is that the compound may need to be slightly more potent as in other series of BCATm inhibitors, a cell drop-off of around 10-fold was usually observed in the cell based assay. However, in comparison to the literature BCAT inhibitor **19**, compound **53** represents a considerable advance prior art in terms of its overall profile (Table 2.7) and removes potential toxicity risk associated with hydrazide moiety.

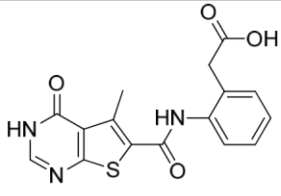
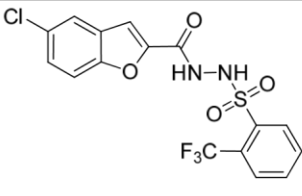
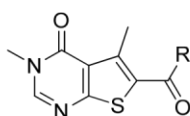
	 <p style="text-align: center;">53</p>	 <p style="text-align: center;">19</p>
BCATm pIC₅₀	6.0	5.2 ^a
LE, LLE_{AT}	0.34, 0.45	0.26, 0.19
chromlogD_{7.4}	0.44	5.20
CLND	164	n.d.
BCATc pIC₅₀	5.6	6.0 ^b
Cell pIC₅₀	< 4.3	5.2

Table 2.7 Profile of literature compound **18** and compound **52**

^aCompound reported inactive (pIC₅₀<4.2) in 2 test occasions and failed to fit a curve in 2 test occasions out of 112; ^bCompound failed to fit a curve in 2 out of the 52 test occasions.

To be able to improve further the properties of this compound, it was important to understand the SAR in the phenyl sub-pocket through analysis of the amide array targeting this region. The biological data associated with the amide analogues (**8390**) are listed in Table 2.8.



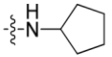
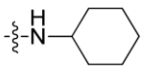
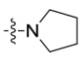
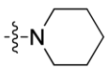
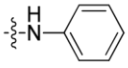
Cmpd	R	pIC ₅₀	LE	LLE _{AT}	Chrom logD _{7.4}	CLND sol. (µg/mL)
30	OH	4.2	0.38	0.44	-0.71	76
83	NH ₂	< 3.2 ^a	< 0.29	< 0.45	n.d.	n.d.
84	NHMe	< 3.2 ^b	< 0.27	< 0.40	0.66	≥ 82
85	NMe ₂	< 4.2 ^c	< 0.31	< 0.46	1.04	≥ 87
86		< 4.2	< 0.29	< 0.31	n.d.	n.d.
87		< 3.2 ^d	< 0.21	< 0.20	n.d.	n.d.
88		< 4.2	< 0.30	< 0.40	1.62	≥ 125
89		< 3.2 ^d	< 0.22	< 0.28	2.55	≥ 136
90		5.1	0.33	0.34	3.46	117

Table 2.8 Biological data on saturated rings shown with compound **30** for comparison

^a Compound reported as pIC₅₀<4.2 in 2 out of the 3 test occasions.

^b Compound reported as pIC₅₀<4.2 in 3 out of the 5 test occasions.

^c Compound reported as pIC₅₀<3.2 and pIC₅₀ = 3.9 out of the 4 test occasions.

^d Compound reported as pIC₅₀<4.2 in 1 out of the 2 test occasions.

As is apparent from the data above, most of the analogues tested exhibited negligible biological activity. Compounds **83-85** completely ablated potency which could not be clearly rationalised from consideration of the crystal structure. All the saturated rings tested (**86-89**) showed no activity suggesting that 3-dimensional shape was not tolerated. Only compound **90** showed an increase in potency with good efficiency. These results suggested that a phenyl ring system was preferred to saturated analogues.

The biological data on substituted aromatic rings and heterocyclic derivatives is shown in Table 2.9.

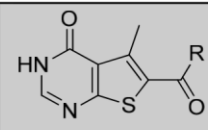
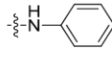
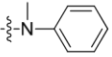
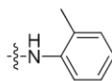
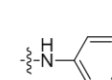
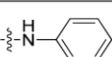
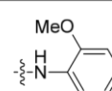
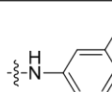
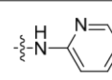
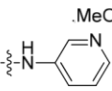
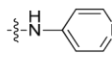
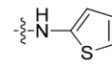
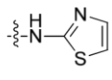
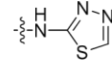
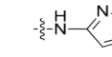
Cmpd		pIC ₅₀	LE	LLE _{AT}	Chrom logD _{7.4}	CLND sol. (µg/mL)
42		5.2	0.36	0.37	2.82	76
91		4.3	0.28	0.32	2.54	≥ 95
92		< 4.2 ^a	< 0.27	< 0.31	2.93	40
93		< 4.2	< 0.27	< 0.26	3.30	26
94		< 4.2	< 0.27	< 0.26	3.49	76
95		< 4.2	< 0.26	< 0.32	3.39	7
96		< 4.2	< 0.26	< 0.29	3.01	19
97		< 4.2	< 0.29	< 0.37	1.92	n.d.
98		< 4.2	< 0.29	< 0.37	1.04	≥ 130
99		< 4.2	< 0.29	< 0.37	1.07	2
100		5.8	0.42	0.45	2.43	40
101		< 4.2	< 0.30	< 0.40	1.46	4
102		6.7	0.48	0.63	0.10	66
103		< 4.2	< 0.30	< 0.43	1.19	23

Table 2.9 Biological data on amides

^a Compound reported active (pIC₅₀ = 4.3) in 1 out of the 3 test occasions.

Substitution on the phenyl ring usually decreased potency and consequently decreased LE and LLE_{AT} (e.g. **92** to **96**). The crystal structure data suggested that *meta*- and *para*-substituents might clash with the protein, which was in accord with the results obtained (e.g. **93**, **94**). On the other hand, and as shown previously, *ortho*-substituents with a hydrogen bond donating group targeting Ala314 residue have been successful. However, *ortho*-substituted compounds **92** and **95** showed reduced potency, suggesting that these substituents were not favoured. Without the desired hydrogen bond donating moieties, the phenyl ring might not have the optimal orientation and not fit in the pocket. Interestingly, pyridyl systems were not tolerated and ablated all potency as illustrated by compounds **97** to **99**. Consideration of the crystal structure showed the pocket to be reasonably lipophilic in nature, with most of the residues both in proximity to and pointing towards the ring being lipophilic (e.g. Tyr, Phe, Val).

The thiophene compound **100** (an isostere of phenyl ring) showed slightly better activity to the phenyl analogue **42** with good LE and LLE_{AT}. It could be attractive to combine this ring system with the carboxylic acid chain in compound **53** to confirm that the SAR is transferrable and that thiophene could be a more efficient binder. More interestingly, the thiadiazole compound **102** showed a 50-fold increase in potency, while by contrast compounds **101** and **103** were essentially inactive. The enhancement of potency observed on compound **102** could not be rationalised from the current crystal structure conformation and earlier results obtained on the other heterocycles that suggested that heteroatoms were not tolerated. As noted above, the crystal structure available showed a lipophilic pocket with no polar residues accessible for hydrogen-bonding interaction. Compound **102** was therefore submitted to crystallography to confirm its binding mode and, thus, to further understand the effect of this group.

From consideration of all these results, the SAR appeared to be somewhat flat in the lipophilic pocket. Specifically designed *ortho*-substituents showed encouraging

increases in potency and associated efficiencies, however almost all other modifications resulted in a negative impact on potency, except notably compound **102**, which was studied further.

Initial attempts to obtain a crystal structure of compound **102** by soaking were unsuccessful.⁸⁴ Poor compound solubility was thought to be a contributing factor as precipitation was observed in the soaking conditions. As the compound showed very promising data in terms of potency and efficiencies, co-crystallisation was investigated. Despite precipitation in these conditions also being observed, a crystal structure was successfully obtained with excellent resolution (1.65 Å).⁸⁴

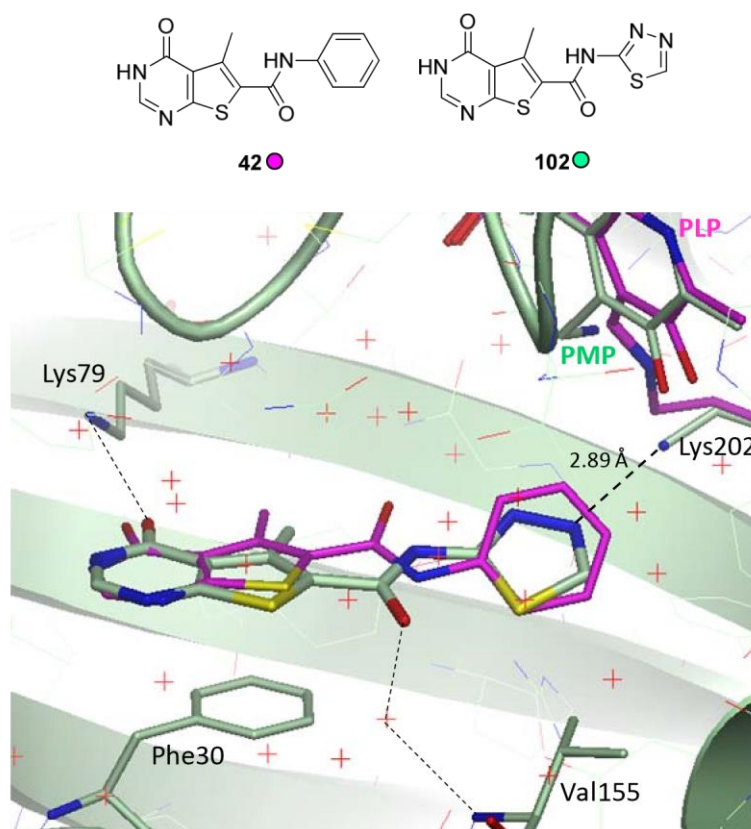


Figure 2.51 Crystal structure of compound **102** (●) overlaid with compound **42** (●).

The crystal structure of compound **102** (●), shown in Figure 2.51, revealed for the first time that the compound bound to the PMP-form of the protein, where the cofactor is unbound to Lys202. This new binding mode potentially explained the difference in

potency between the thiazole compound **101** and the thiadiazole **102**. The thiadiazole moiety makes a key new H-bonding interaction with the chain NH of Lys202, preventing this residue from forming a covalent bond with the co-factor as observed for the PLP-form of the protein (). The other nitrogen in the thiadiazole ring system appeared to form a hydrogen-bonding interaction with a network of water molecules and, thus, may also be important in terms of contributing to potency. The binding mode of the compound is otherwise very similar to compound **42** (●). The core formed a π -stacking interaction between Phe30 and makes a H-bonding interaction with the amino group of Lys79. The amide geometry had altered forming an apparent hydrogen-bonding interaction with Val155 (from the second monomer) *via* a water molecule similarly to what was observed with the initial fragment hit **30**. Compound **102** overlaid perfectly with the initial fragment hit **30** and **53** suggesting an optimal, low energy binding pose. This also suggested that the geometry of the amide observed in compound **42** might be sub-optimal. The full profile of the thiadiazole moiety **102** is summarised in Table 2.10 along with the progenitor systems **33** and **52** for comparison.

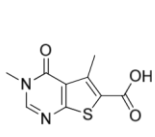
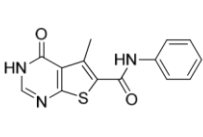
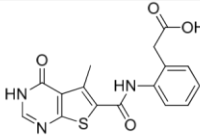
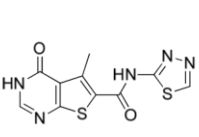
				
	30	42	53	102
BCATm pIC ₅₀	4.2 ^a	5.2	6.0	6.7
LE, LLE _{AT}	0.38, 0.44	0.36, 0.37	0.34, 0.45	0.48, 0.63
chromlogD _{7.4}	-0.71	2.82	0.44	0.10
CLND sol. (µg/mL)	≥ 73	76	164	66
BCATc pIC ₅₀	3.5	4.7	5.6	6.0
Cell pIC ₅₀	n.d.	n.d.	< 4.3	5.5

Table 2.10 Biological data of compounds **42**, **53** and **102**

^aCompound reported inactive (pIC₅₀ < 4.2) in 3 of the 34 test occasions.

Compound **102** showed nearly a 30-fold increase in potency compared to compound **42** and greater than 300-fold compared to the initial hit **30**, with excellent associated LE and LLE_{AT}, thus demonstrating very efficient binding. The compound also showed cellular potency for the first time in this series, which was particularly pleasing.

However the measured CLND solubility confirmed the poor solubility observed during the handling of the compound and would need to be improved. Measured logD was found to be low, which could reduce cell permeability perhaps accounting for the lower activity observed in the cellular assay. However, the compound potentially offers a new mode of action and further studies are ongoing to understand the difference with the other compounds. To date, all other molecules bind to the PLP-form (co-factor covalently bound to the protein), which may lead to a different pharmacological profile.

2.3.3.5 Future Work

Following this highly promising result, the next steps in this series would be to investigate other heterocycles as described in Figure 2.52 to understand if thiadiazole is the optimum ring system but also to modulate the physicochemical properties of the compound. It will also be interesting to combine the preferred *ortho*-substituent with the heterocycle (Figure 2.53). As shown by the overlay of compound **102** with compound **53** in Figure 2.54, although the angle will be different, the acid could form a similar vector to interact with Ala314.

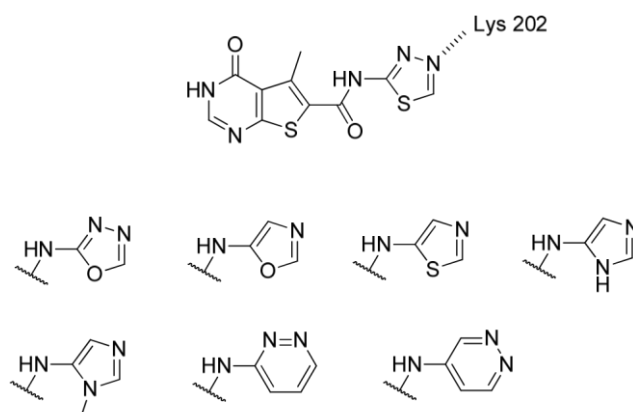


Figure 2.52

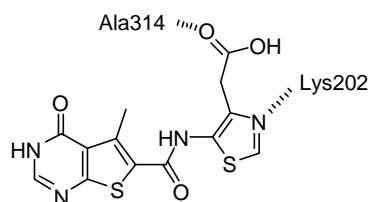


Figure 2.53

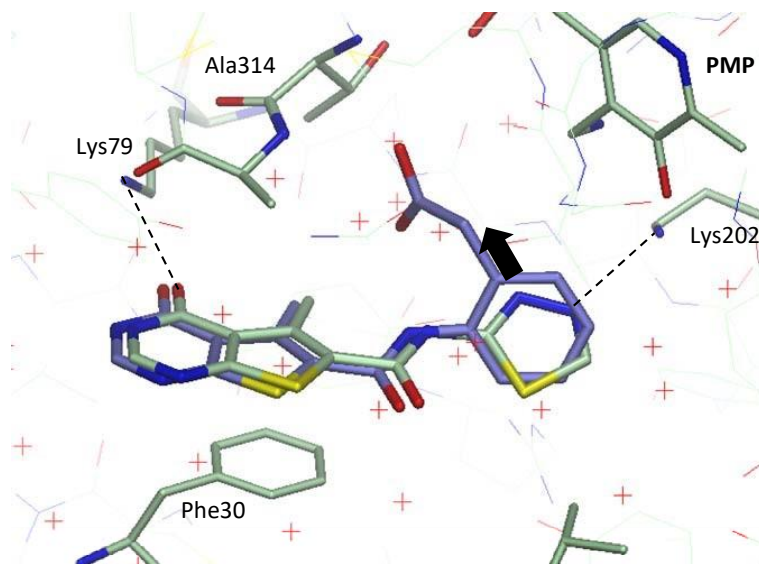


Figure 2.54 Crystal structure of compound **102** (●) overlaid with compound **53** (●).

However, and as previously discussed, the associated SAR has been widely explored in this region of the protein and based on the current data, scope for improvement seems limited in this area. Having stated this, selected areas of the protein around the thiopyrimidinone core have not been fully explored as shown in Figure 2.55 and could help to improve potency further. Solubility needs to be improved and logD should be increased to afford greater cell permeability. Substitution of the pyrimidinone NH could enable access to a new area of the subsite 1 pocket or at least, prevent intermolecular hydrogen-bonding interactions by leaving a methyl substituent. Substitution at the 2-position could allow further improvement in potency as shown by compounds **49** and **50**. However, as the compound already contained three aromatic rings, addition of aliphatic groups would be preferred in order to maintain good physicochemical properties (e.g. solubility) for developability.^{21,112}

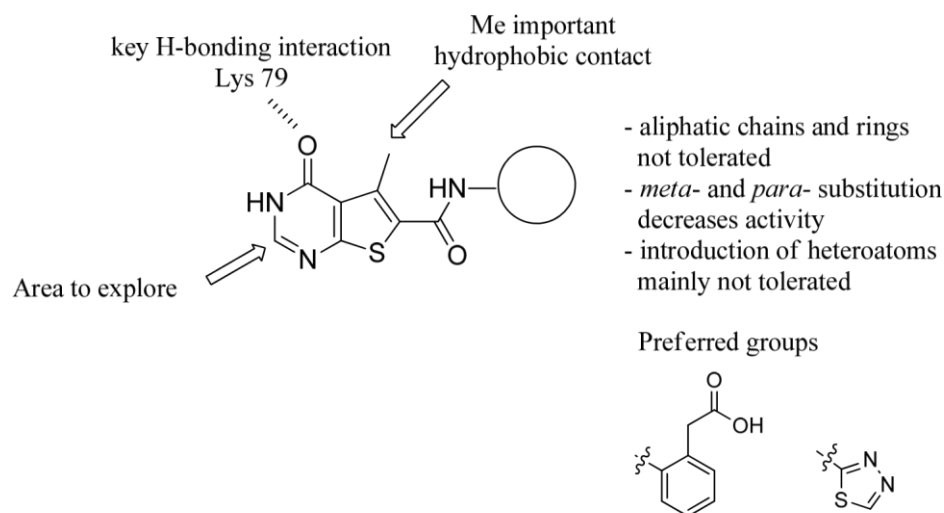


Figure 2.55 SAR summary of cluster 3

At this stage of the programme, new molecular entities derived from cluster 6 (vide infra) were considered to be more advanced. A number of promising compounds already reached the criteria for a tool molecule and initial pharmacokinetic data were very encouraging (see section 5). Against this background, chemistry efforts were subsequently prioritised on cluster 6. It was agreed that cluster 3 could be reconsidered at a later stage as a back-up series should the efforts on cluster 6 ultimately prove unsuccessful.

2.3.4 Conclusion

FBDD successfully identified cluster 3 as a new class of BCATm inhibitors with novel binding mode. A combination of structure-based design and broader SAR exploration to seek potential new interactions enabled the discovery of two lead compounds (**53** and **102**) with improved properties compared to known literature inhibitor **19**.

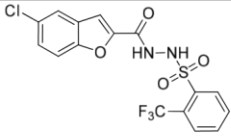
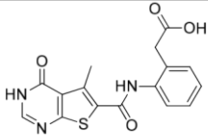
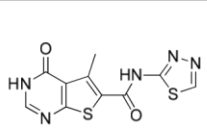
			
	19	53	102
BCATm pIC₅₀	5.2 ^a	6.0	6.7
LE, LLE_{AT}	0.26, 0.19	0.34, 0.45	0.48, 0.63
chromlogD_{7.4}	5.2	0.44	0.10
CLND	n.d.	164	66
BCATc pIC₅₀	6.0 ^b	5.6	6.0
Cell pIC₅₀	5.2	< 4.3	5.5

Table 2.11 Biological data of compounds **19**, **53** and **102**

^aCompound reported inactive (pIC₅₀<4.2) in 2 test occasions and failed to fit a curve in 2 test occasions out of 112; ^bCompound failed to fit a curve in 2 out of 52 test occasions.

Compound **53** was identified through rational design using X-ray structure information. The compound showed good potency and solubility with good LE and LLE_{AT}. Cell potency data were disappointing but could potentially be improved by increasing chromlogD of the molecule. Reduction of the number of HBD or masking the NH could help to improve cellular potency. In addition, this work highlights the importance of hybridisation of information from other clusters information in order to accelerate the optimisation process.

Compound **102** was discovered by a combination of rational design and array chemistry efforts and X-ray crystallography revealed a novel binding mode to the PMP-form of the protein. This work highlights the importance of challenging an established binding hypotheses and use of diversity-based approaches to identify novel interactions. The compound showed good potency, LE and LLE_{AT}, reaching the tool criteria for the enzyme potency. In addition, the compound also showed evidence of cell potency. The low solubility observed would need to be improved as this could negatively impact on the ADME profile.

In conclusion, a novel series of BCAT_m inhibitors has been identified, which offered the opportunity to bind to both the PLP- and PMP-form depending on the groups occupying the lipophilic pocket. Potency has been successfully improved reaching the enzyme target of 6.5. Solubility has also been enhanced by introducing solubilising groups and by adding a methyl group on the pyrimidinone to break potential intermolecular interactions. New interactions have been identified alongside new vectors (3-position of pyrimidinone ring) for further optimisation of potency within this series of compounds. In addition, compounds have shown improvement in terms of potency, efficiency and physicochemical properties compared to known literature inhibitor **19**.

2.4 Cluster 6 - Fragment to Lead Optimisation

2.4.1 Fragment Hit

As described in the introduction, the initial fragment hit **35** (Table 2.12) was identified as a dual hit from STD-NMR and T_m and showed weak activity in the biochemical assay. However, despite this the compound failed to generate a crystal structure. As the compound was detected in the two biophysical assays and the biochemical assay, this provided greater confidence that it was genuinely binding to the protein. Thus, a substructure search of our laboratory's compound collection was carried out to identify additional analogues for X-ray crystallography. Thirteen analogues with the pyrazopyrimidinone core were tested in STD-NMR and biochemical assays. From this study, seven additional compounds were progressed to crystallography, with compounds **39** and **40** being successfully solved. The overall profile of compound **39** showed good potency, LE and LLE_{AT} in comparison to the progenitor **35**, suggesting that such compounds were highly encouraging starting points for further optimisation.

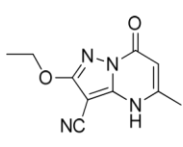
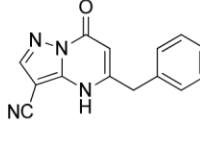
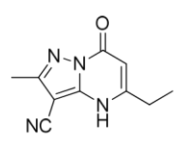
			
	35	39	40
BCATm pIC₅₀	3.3 ^a	4.6	< 3.2 ^b
LE, LLE_{AT}	0.28, 0.41	0.33, 0.38	< 0.29, < 0.39
chromlogD_{7.4}	0.52	1.43	0.21
CLND sol. (µg/mL)	≥ 96	122	≥ 92

Table 2.12 Cluster 6 fragments

^aCompound reported inactive (pIC₅₀ < 2.9) in one out of the two test occasions.

^bCompound reported active (pIC₅₀ = 4.4) in one out of three test occasions.

Crystal structures of compounds **39** (●) and **40** (●) revealed a unique binding mode compared to analogues from other clusters (e.g. **42** from cluster 3, ●), as shown in Figure 2.56.⁸⁴ The pendant benzyl ring of compound **39** and the ethyl group of compound **40** were bound in the lipophilic pocket identified from other clusters and the pyrimidinone core accessed a new pocket, perpendicular to the induced pocket (between Phe30 and Tyr173). The crystal structure of **40** showed that the pyrimidinone carbonyl was in good distance to Tyr173 (2.62 Å - disordered in compound **39**) to make an interaction. The nitrogen atom of the nitrile group was at a good distance from the backbone NH of the Cys315 residue to form an H-bonding interaction. However, the angle between the nitrile nitrogen and the backbone NH (measured angle 118 °) was not optimal,¹⁰¹ and nitriles are generally weak H-bond acceptors. With compound **39**, the core has slightly shifted to accommodate the benzyl ring and the active loop of the protein (residues 172-178) was disordered.

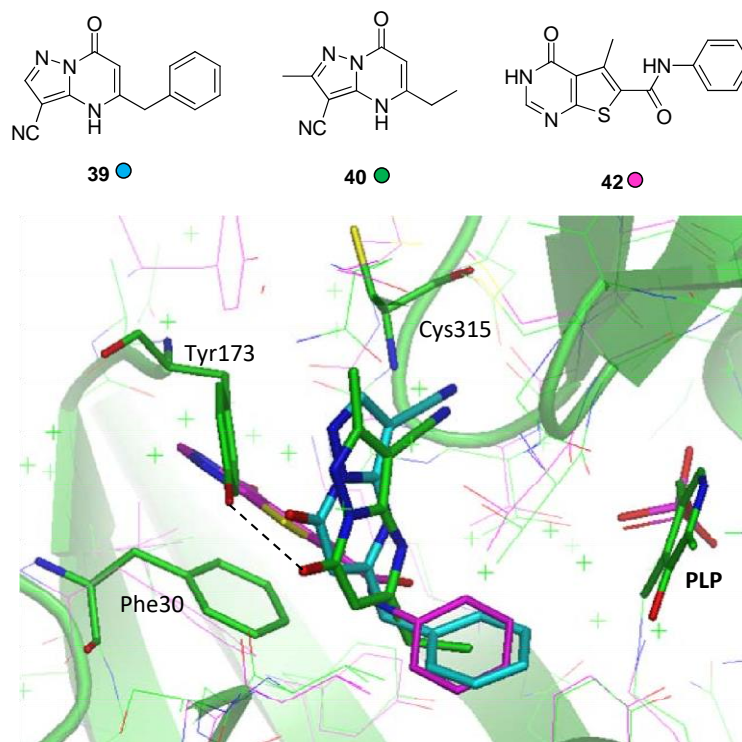


Figure 2.56 Crystal structure of BCATm in complex with compounds **39** (●), **40** (●) and **42** (●)

The compounds also showed a different binding mode compared to the literature compound **19** (○) as shown in Figure 2.57, offering potential for a novel range of interactions. The nitrile is in a similar position to the amide carbonyl of compound **19**, which made an H-bonding interaction with Cys315, again suggesting the importance of binding in this region.

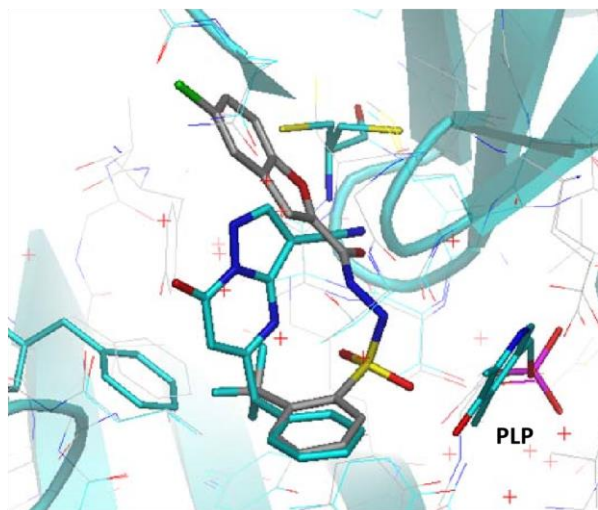
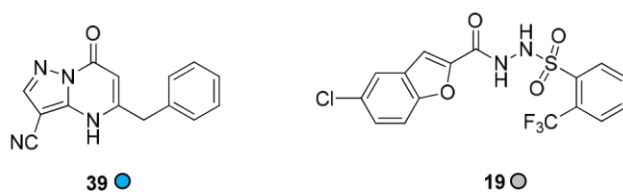


Figure 2.57 Crystal structure of compound **39** (●) overlaid with **19** (○)

A concurrent HTS campaign identified structurally related compounds **105** and **106** as efficient hits that displayed encouraging cellular potency against BCATm (Table 2.13),¹¹³ which gave us confidence that potency could be improved in this cluster.

Structure	 105	 106
BCATm pIC₅₀	6.2	5.7
LE; LLE_{AT}	0.39, 0.35	0.36; 0.32
chromlogD_{7.4}	2.92	2.86
CLND sol. (μg/mL)	54	37
Cell pIC₅₀	6.1	5.9

Table 2.13 HTS hit profile

A crystal structure of compound **105** bound into BCATm (●,Figure 2.58) confirmed a similar binding mode to the fragment hits **39** and **40** and revealed access to a novel induced pocket that accommodated the bromobenzyl substituent. This pocket is blocked by a methionine side-chain (Met241) in the protein crystal structure of **40** (●), however rotation of the thioether side-chain through 180° facilitated binding of the larger substituent. This movement had not previously been observed in any other BCATm protein structures. In the absence of this information, traditional fragment optimisation techniques may not have identified this induced pocket from fragment hits **39** and **40**, again highlighting the value of using information from other hit finding techniques.

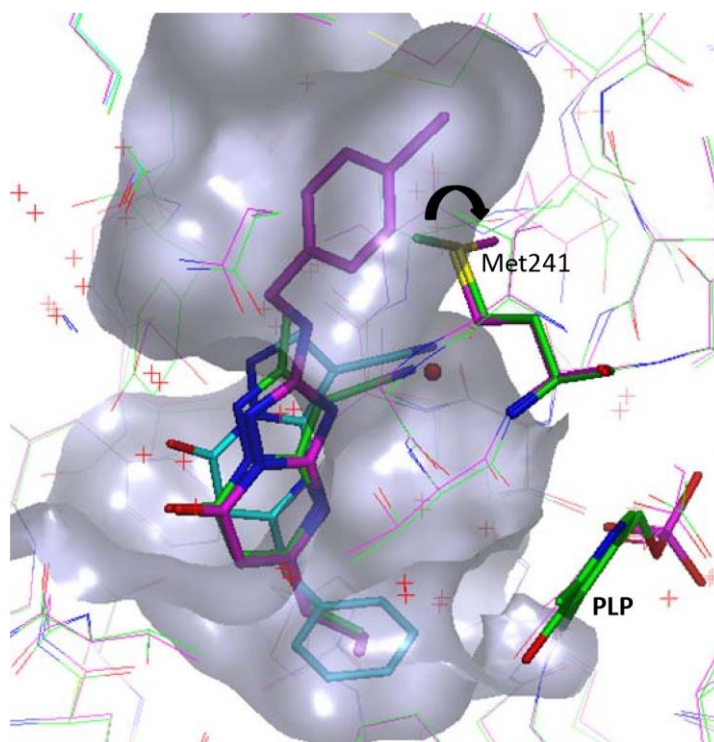
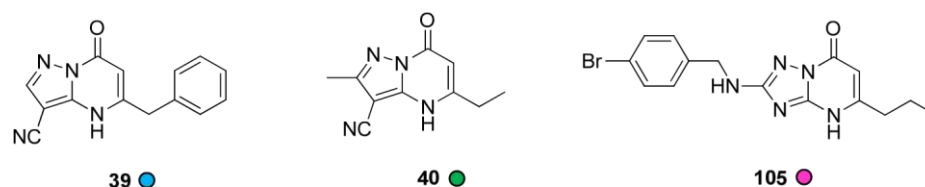


Figure 2.58 Crystal structure of BCATm in complex with compound **39** (●), **40** (●) and **105** (●)
Nitrile displaced water molecule observed in structure **105**

From consideration of this data on compound **105**, introduction of an aminobenzyl group on the pyrazolopyrimidine core was hypothesised to improve potency further of our fragment hits. Therefore, chemistry carried out elsewhere in our laboratory initially focussed on synthesising hybrid compounds, as shown in Table 2.14.¹¹⁴ The initial results were very promising, with compounds achieving tool molecule criteria: enzyme pIC_{50} values greater than 7 with high LE and LLE_{AT} values and cell pIC_{50} values greater than 6. The initial data showed that a propyl chain at the 5-position was equipotent with the benzyl ring (i.e. **107** vs. **109**), which was beneficial as it increased efficiency and reduced the number of aromatic rings, thus, improves the chance of a better DMPK profile.^{20,111} In addition, a consistent 10-15-fold increase in potency was

observed along with improvement in solubility by replacing the triazole with the 3-cyano motif on the pyrazolo fragment. The bromo analogue **108** showed a slight increase in potency compared to its chloro analogue **107**, both in the enzyme and cellular assay.

Cmpd	Structure	BCATm pIC ₅₀	LE, LLE _{AT}	Chrom logD _{7.4}	CLND sol. (µg/mL)	Cell pIC ₅₀
105		6.2	0.39, 0.35	2.92	54	6.1
106		5.7	0.36, 0.32	2.86	37	5.9
107		7.1	0.41, 0.36	2.90	144	6.2
108		7.6	0.43, 0.38	3.02	≥ 163	6.6
109		7.0	0.34, 0.30	3.23	26	5.9

Table 2.14 Evolution of hybrid molecules

A crystal structure of compound **107** (●) was obtained and confirmed that the compound bound similarly to the initial fragment hit **40** (●) and to compound **105** (●) as shown in Figure 2.59.⁸⁴ The three molecules overlaid perfectly suggesting the core may be in a preferred low energy location. Comparison with compound **105** (●) suggested the nitrile group in compound **107** displaced a water molecule observed in the structure with **105**. Displacing this water may account for the 10-fold increase in affinity indicating that this may be energetically favourable.

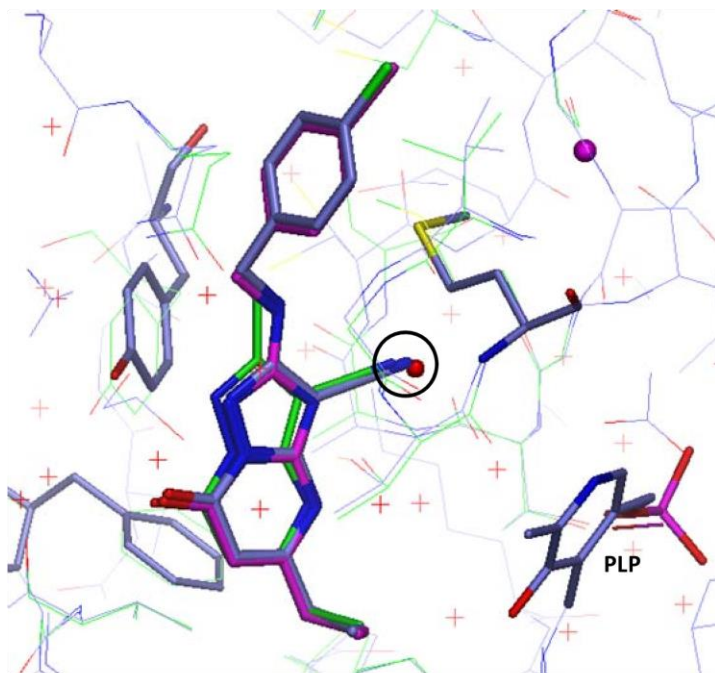
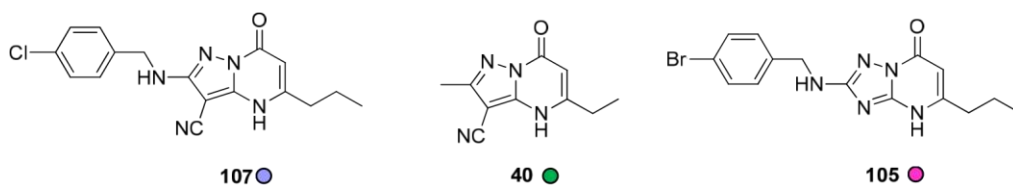


Figure 2.59 Crystal structure of compound **107** (●) and **40** (●) overlaid with compound **105** (●)

From work carried out elsewhere within our laboratory,¹¹⁴ initial SAR showed that the nitrile was preferred. Although the nitrile was not in an optimal angle to make an H-bonding interaction, replacement with a carboxylic acid or amide to interact directly with the protein was shown not to be favourable. Methylation of the pyrimidinone nitrogen reduced potency suggesting that an H-bond donor might be preferred. From the crystal structure, the pyrimidinone nitrogen is involved in a network of H-bonding interactions *via* water molecules. Thus, addition of a methyl group would disrupt the water molecule network of interaction and be detrimental to potency. Methylation of the pyrimidinone carbonyl also ablated potency confirming that interaction with the Tyr173 residue was important for potency. The initial SAR associated with cluster 6 is summarised in Figure 2.60.

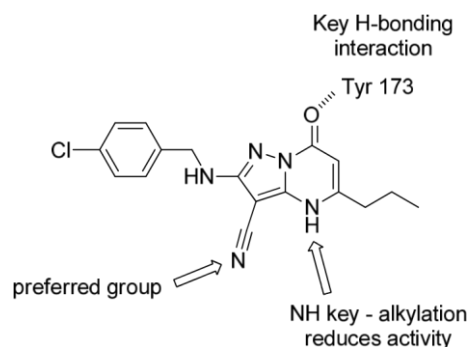


Figure 2.60 Initial SAR

2.4.2 Research Objective

From these initial data, the key objective was thus to fully explore SAR on this series to identify the best tool molecule for *in vivo* studies. Consequently, chemistry was focussed on exploring SAR around three key areas: the benzyl amine in the induced lipophilic pocket (in blue), the linker (in pink) and the lipophilic pocket (in green) where the propyl chain bound (Figure 2.61). Optimisation of the benzylamine ring (in blue) was carried out by other members of our laboratory,¹¹⁴ whereas the focus of the author's work was on exploring alternative linkers and alternative alkyl chains in the lipophilic pocket.

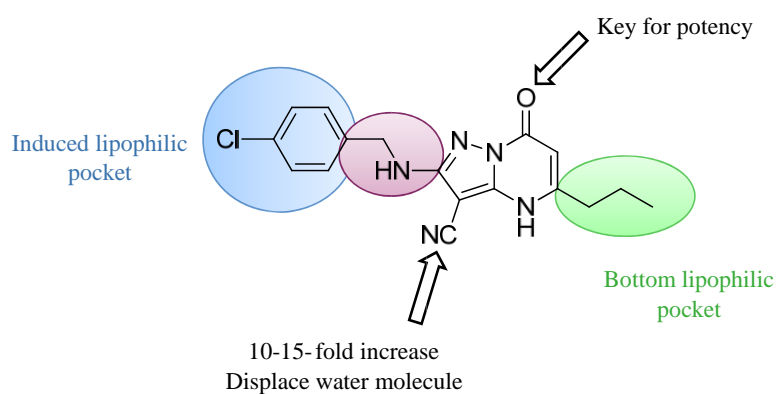


Figure 2.61 SAR exploration

2.4.3 Results and Discussion

2.4.3.1 Pyrazolo[1,5- α]pyrimidinone Chemistry

The pyrazolo[1,5- α]pyrimidinone core **110** has been widely used in drug design and appears in a variety of biologically active molecules.¹¹⁵⁻¹¹⁸ It has also been used within a versatile intermediate in the synthesis of various biologically active molecules as shown in Figure 2.62.¹¹⁹⁻¹²²

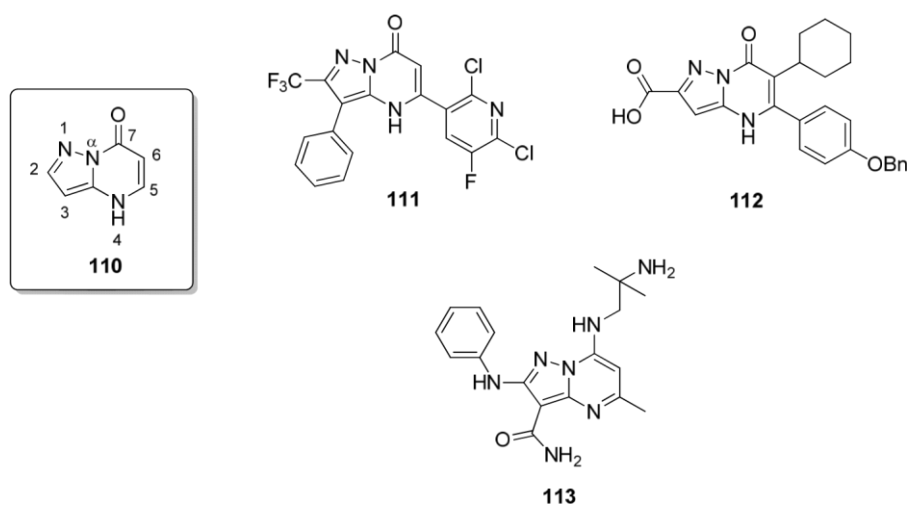
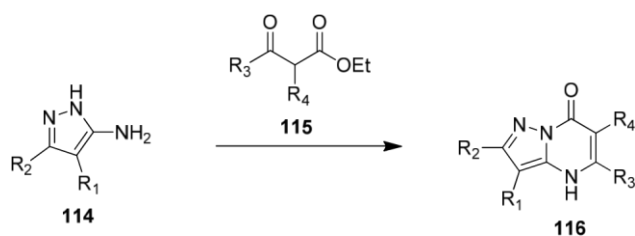


Figure 2.62 Biologically active molecules containing the pyrazolo[1,5- α]pyrimidin-7-one core

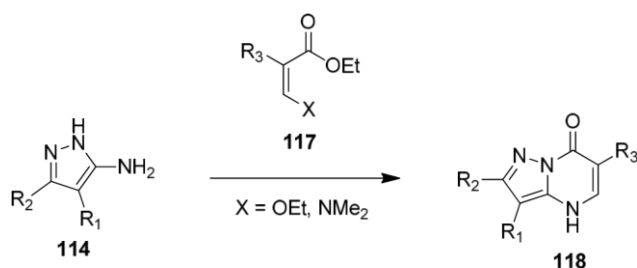
111 Kv7/KCNQ potassium channel activators;¹¹⁶ **112** inhibitor of hepatitis C virus polymerase;¹¹⁵ **113** c-Src kinase inhibitor.¹²²

Due to its synthetic versatility, the pyrazolo[1,5- α]pyrimidinone core has received a considerable amount of interest in the literature.¹²³⁻¹²⁸ A common synthetic route involves the condensation of a 5-amino-1*H*-pyrazole **114** with β -keto esters **115** (Scheme 2.12).^{115,116,129} This route allows the introduction of substituents at both the 5- and 6-positions.



Scheme 2.12

An alternative route involves the condensation of a 5-amino-1H-pyrazole **114** with ethoxypropenoates or dimethylaminopropenoates **117** (Scheme 2.13).^{123-125,127}



Scheme 2.13

Analogue such as **119** targeted in this work (Figure 2.63) are novel molecules not represented in the literature. The closest precedent is from Mukaiyama and coworkers who described the synthesis of 2-anilinopyrazolo-[1,5- α]pyrimidine derivatives **124**, in which they used analogues of compound **119** as intermediates as shown in Scheme 2.14.¹³⁰

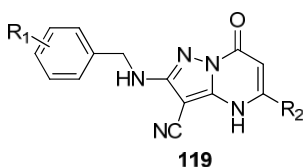
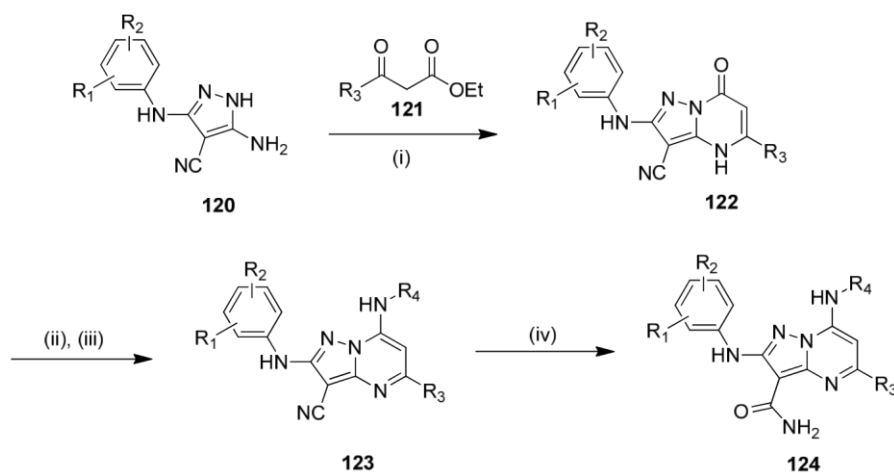


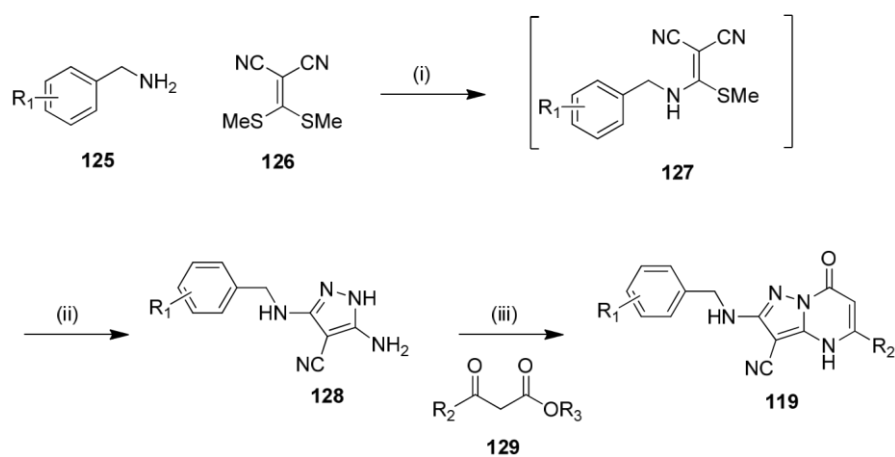
Figure 2.63



Reagents and conditions: (i) AcOH, reflux; (ii) POCl₃, DMF, 60 °C; (iii) R₄NH₂, NEt₃, NMP, rt; (iv) NaOH, H₂O₂, 60 °C.

Scheme 2.14

Thus, a similar synthetic route was developed to prepare the aminopyrazolo[1,5 α]pyrimidine derivatives represented by **119**. The synthetic route was developed and optimised elsewhere in our laboratory and is described in Scheme 2.15.¹³¹ The Minked analogues **119** were prepared by reaction of the desired benzylamine **125** with [bis(methylthio)methylene]propanedinitrile **126**. The intermediate **127** was usually not isolated and hydrazine hydrate was directly added to the reaction mixture to form the corresponding aminopyrazole **128**. The final product **119** was then obtained by cyclisation using the desired β -keto ester **129** in acetic acid/water at reflux.



Reagents and conditions: (i) EtOH, reflux, 3 h; (ii) hydrazine hydrate, reflux, 1 h; (iii) AcOH/H₂O, 120 °C.

Scheme 2.15

2.4.3.2 Investigation of Alternative Linkers

As shown previously, compound **107** had good enzyme and cellular potency with good efficiency. The objective of this phase of the work was to establish whether the best linker had been identified. From consideration of the crystal structure, the NH linker did not appear to make any polar interactions with the protein. Therefore, several alternative linkers were investigated as shown in Figure 2.64.

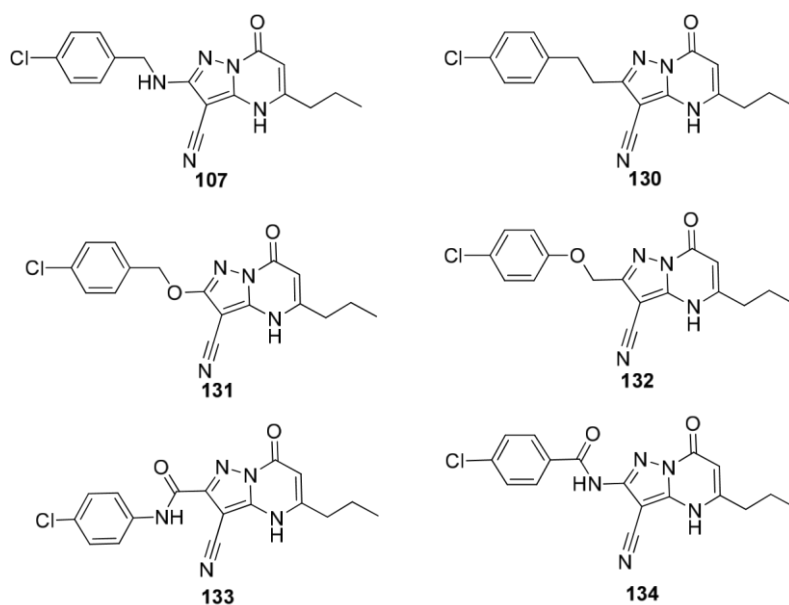


Figure 2.64 Alternative linkers

Work in this area focussed on synthesising the carbon linker **130** and the oxygen linker **131**. The remaining target compounds were synthesised elsewhere in our laboratory.¹³²

2.4.3.2.1 Carbon linker

The key intermediate for the synthesis of the carbon-linked compound **130** was the corresponding aminopyrazole intermediate **135** (Figure 2.65). Compound **135** can then be disconnected to give hydrazine and a dinitrile ethylene derivative **137**, analogous to the *N*-linked chemistry discussed above in Section 5.2.

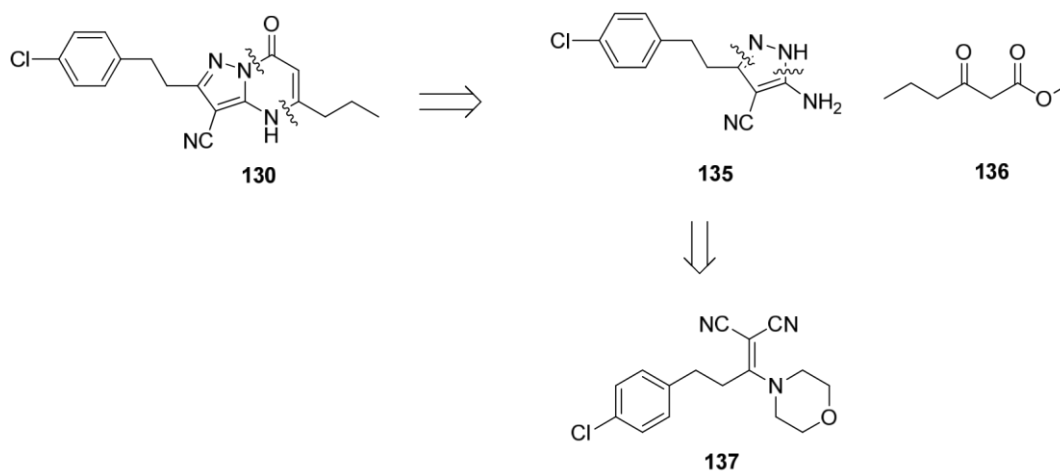
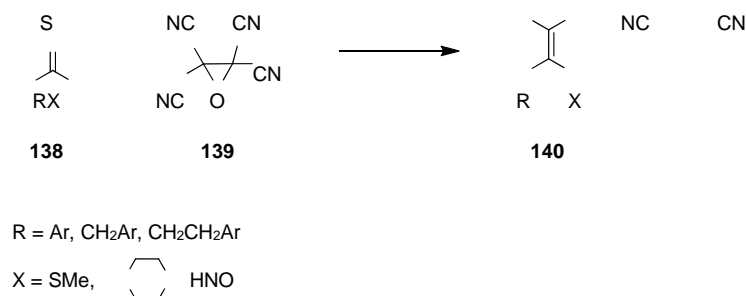


Figure 2.65 Retrosynthetic analysis of compound **130**

In relation to intermediate **137**, Tominaga and co-workers described the synthesis of carbon-linked dinitrile ethylene analogues by the reaction of thioamides or methyl dithiocarboxylates **138** with tetracyanoethylene oxide **139** in good yields (Scheme 2.16).^{133,134}

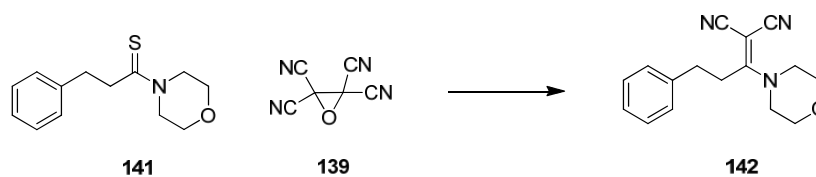


Reagents and conditions: (i) benzene, rt, 3-5 h, 69-91 %.

Scheme 2.16

Literature precedent has shown that compound **142**, a close analogue to **137**, was prepared by reaction of the thioamide **141** with tetracyanoethylene oxide **139** in good yield (Scheme 2.17).¹³⁴ In addition, thioamides are readily available in one step by the

Willgerodt-Kindler reaction discussed in more detailed below.¹³⁵ Based on this, the above method was selected for synthesis.



Reagents and conditions: (i) benzene, rt, 3-5 h, 79 %.¹³⁴

Scheme 2.17

A proposed mechanism for this reaction is described in Figure 2.66.¹³⁶ In the first instance, the thione sulfur attacks the epoxide **139** to form the intermediate **I**. Following this, carbonyl dicyanide is eliminated to form the carbanion **II**. Subsequently, the carbanion attacks the imine to form the thioepoxide **III**, which reopens to give the imine **IV**. Finally, elemental sulfur is eliminated to give the final alkene **142**.

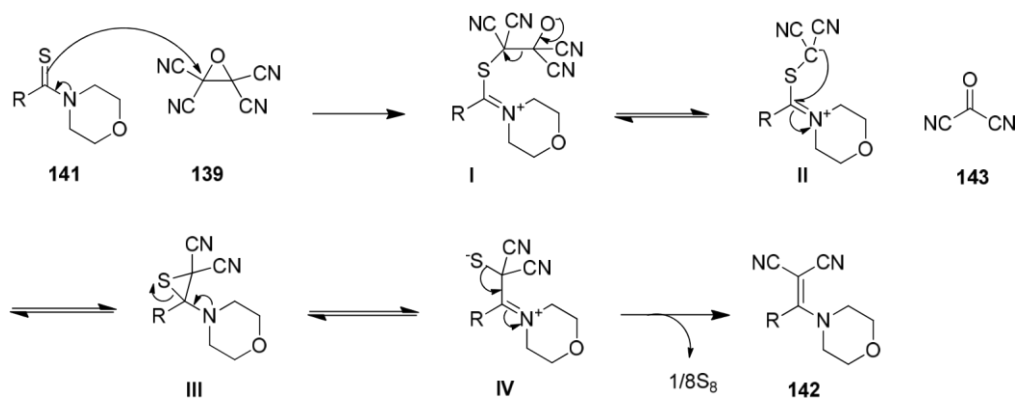
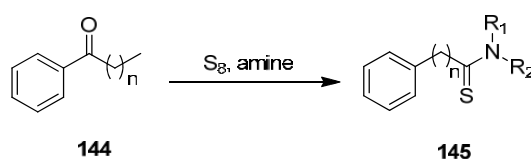


Figure 2.66 Proposed mechanism for the synthesis of dinitrile ethylene analogues

As discussed above, thioamides are readily available *via* the Willgerodt-Kindler reaction.^{135,137,138} The process involves the reaction of alkyl aryl ketones **144** with

sulfur and a primary or secondary amine to give thioamides **145** where the functional group has migrated to the end of the chain (Scheme 2.18).^{135,139}



Scheme 2.18 Willgerodt-Kindler reaction

Morpholine has been shown to be the most popular amine in this process as it is readily available and generally gives good yields. However, other primary and secondary amines have also been successfully used, including aniline, piperidine and, piperazine.¹³⁵ Originally, the Willgerodt-Kindler reaction was carried out with alkyl aryl ketones,¹³⁹ however, it has now been extended to other compounds such as aldehydes, amines and imines.¹³⁵ One limitation of the reaction was the high reaction temperature (around 200 °C) and long reaction time (several hours). More recently, however, several studies have demonstrated the efficiency of microwave heating.^{137,138} The reaction can be carried out in the microwave for a short period of time (in the region of 5 min) and in good yield.

A number of studies have been carried out to understand the mechanism of the reaction; however, there is still some debate in relation to the proposed reaction pathway.^{135,140} Several earlier studies showed that the reaction mechanism did not involve a rearrangement.^{135,141-144} Thus, the following mechanism was proposed for the reaction of acetophenone and morpholine (Figure 2.67).¹⁴⁵

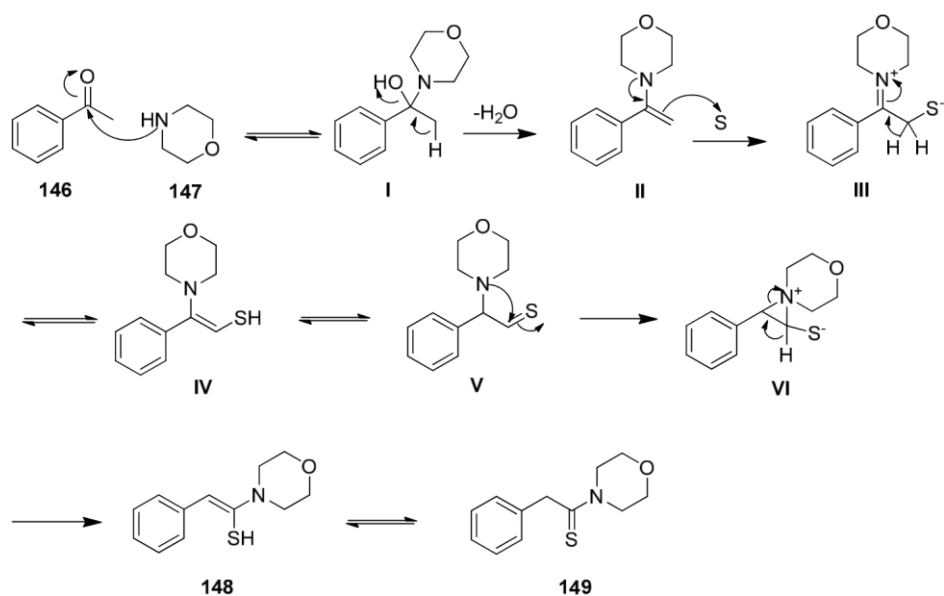


Figure 2.67 Proposed mechanism of the Willgerdt-Kindler reaction

In the first instance, morpholine **147** reacts with the ketone of acetophenone **146** to give the corresponding enamine **II** similarly to Carmack's mechanism.¹⁴⁰ Elemental sulfur then adds to the double bond to afford the terminal thiol **III**. Subsequently, the morpholine nitrogen attacks the thiocarbonyl to form an aziridinium system **VI**, which reopens to give the thioamide **149**.

Having stated this, in the case of longer alkyl chains, the above mechanism would not give the desired product **141** (Figure 2.68). The key intermediate **151** cannot give the desired final product **139**. Following the above scheme, this would involve the elimination of the methyl group giving the product **152**.

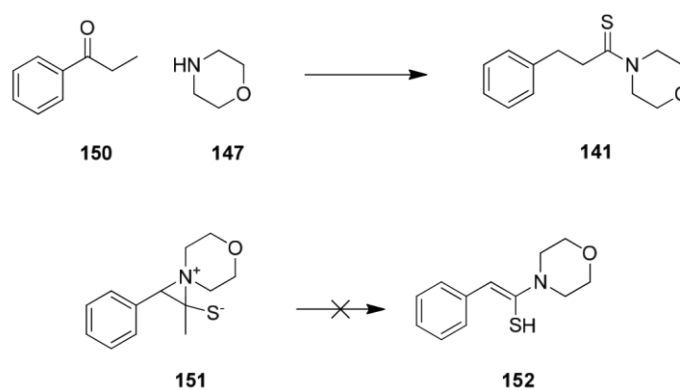


Figure 2.68 Mechanism of the Willgerdt-Kindler reaction with longer chain systems

In order to move along the chain, an alternative mechanism is needed. Several mechanisms have been proposed.¹³⁵ However, to date no clear consensus on an acceptable mechanism exists.

One proposed alternative mechanism for this reaction is described in Figure 2.69.¹⁴⁰ In the first instance, morpholine reacts with the ketone of acetophenone to give the corresponding enamine **II** similarly to the mechanism with acetophenone. Elemental sulfur then adds to the double bond to afford the intermediate **III**. The sulfur attacks the imine to form the thiirane **IV**, which after elimination of morpholine gives **V**. Morpholine then attacks the thiirane to give **VI**. Elemental sulfur then adds to the double bond and after elimination of elemental sulfur affords the intermediate **VIII**. Subsequently, the morpholine nitrogen attacks the thiocarbonyl to form an aziridinium system **XI**, which reopens to give the thioamide **141**.

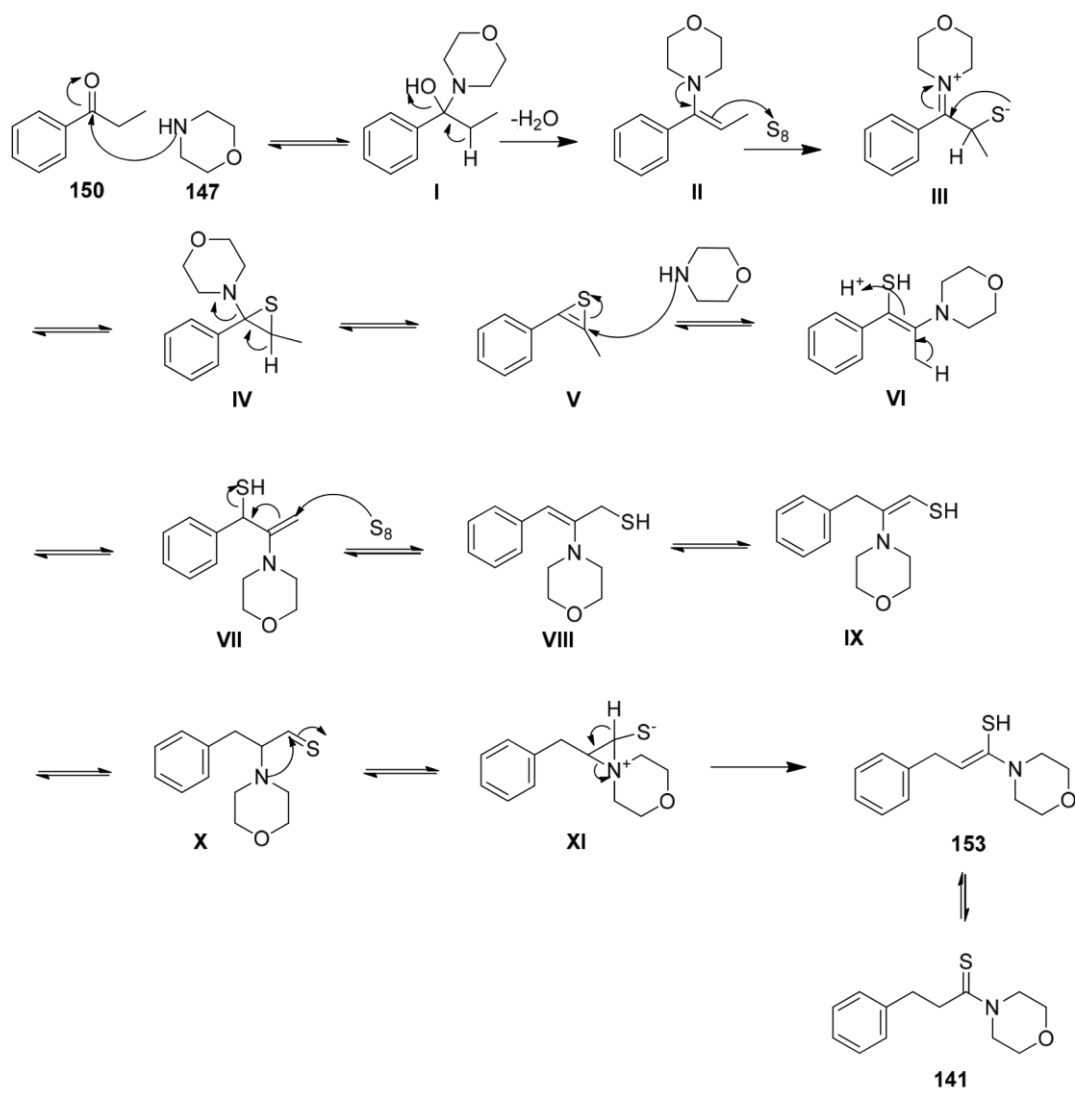
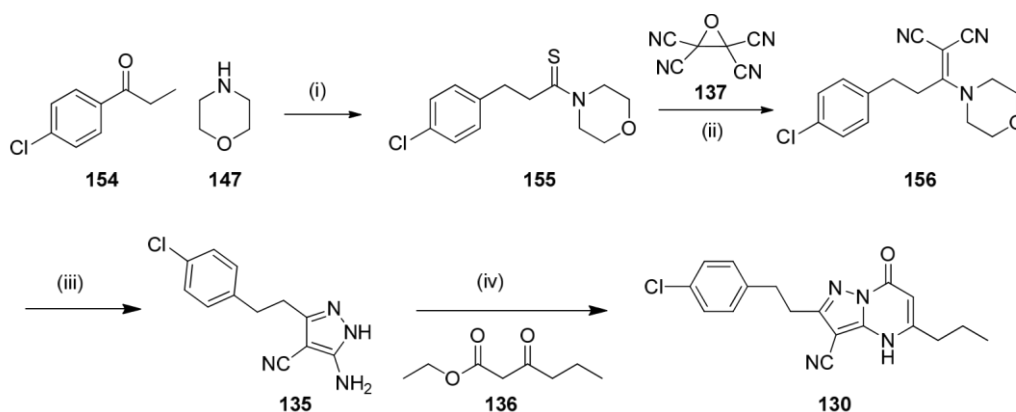


Figure 2.69 Proposed mechanism of Willgerdt-Kindler with longer alkyl chains

Returning to the synthesis of the target compounds, the requisite carbon-linked analogue **130** was prepared following the synthetic route described in Scheme 2.19.



Reagents and conditions: (i) sulfur, 130 °C, 24 h, 62%; (ii) toluene, rt, overnight, 49%; (iii) hydrazine hydrate, EtOH, reflux, 5 h, 73%; (iv) AcOH, reflux, 20 h, 59%.

Scheme 2.19

The desired thiomorpholine **155** was prepared from the ketone **154** using the Willderodt-Kindler reaction.¹³⁷ The reaction was carried out using conventional heating instead of the microwave conditions. A test reaction was initially carried out in the microwave but due to the high pressure and the unpleasant smell, it was found more practical to use conventional heating and a trap of bleach to contain the H₂S gas generated during the reaction. The isolated yield was good for two carbon chains^{137,138,146} and comparable to the yield reported by Salim and co-workers more recently,¹⁴⁷ in the reaction with sulfated tungstate as catalyst. The ethylene intermediate **156** was then prepared by reaction of the thioamide **155** with tetracyanoethylene oxide in excellent yield following the procedure of Taminoga and co-workers.¹³⁴ Reaction of **156** with hydrazine gave the desired pyrazole intermediate **135** again in good yield.¹³⁴ The final product **130** was then obtained by cyclisation using the desired β -keto ester in acetic acid at reflux.¹²²

2.4.3.2.2 Oxygen linker

Initially, a similar route to the *N*-linked analogues was investigated (see Section 5.2).¹²² Disconnection of the pyrimidone ring leads to the corresponding aminopyrazole intermediate **157**, which can be further disconnected to the dinitrile alkene intermediate **158**.

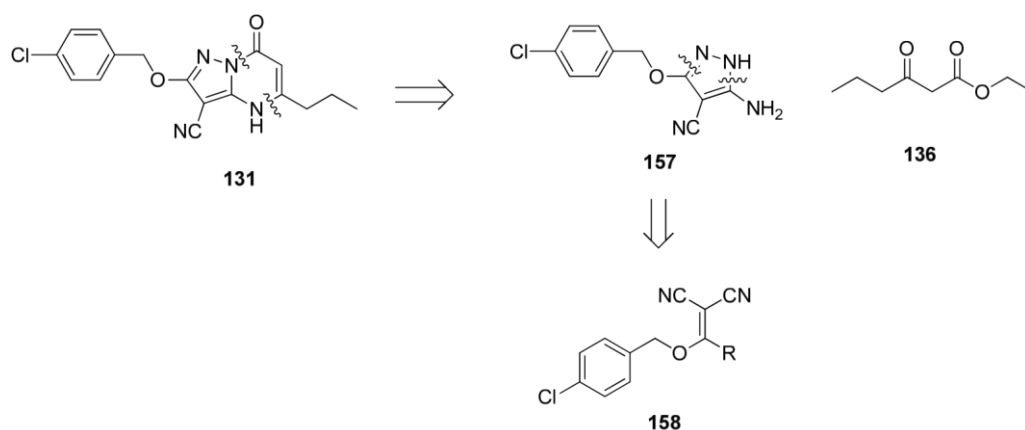
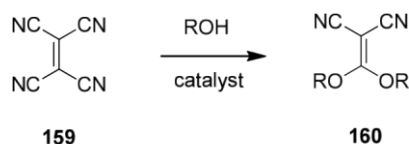


Figure 2.70 Retrosynthetic route to *O*-linked compound

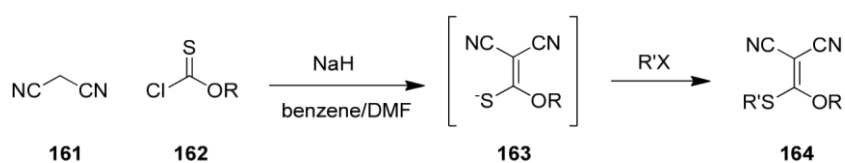
Literature precedent for the synthesis of intermediate **158** was limited. However, related analogues with alkoxy or phenoxy groups have been described.¹⁴⁸⁻¹⁵⁰

A common method to prepare dicyanoketene alkyl acetal **160** is by reaction of the alcohol with tetracyanoethylene **159** in presence of urea or diethylamine as catalyst (Scheme 2.20),^{148,150,151} with the reaction either carried out neat or in THF. In this way, compounds were obtained in moderate to good yields depending on the alcohol. However, generation of HCN during the reaction was not attractive as the first choice from our perspective due to its high toxicity.



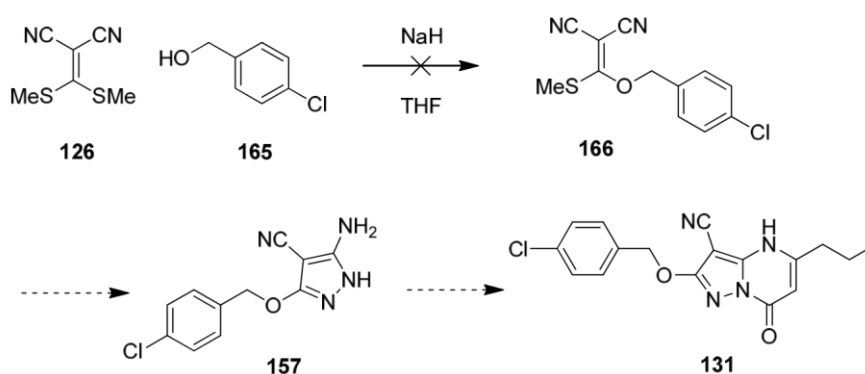
Scheme 2.20

An alternative method proposed by Nilsson described the synthesis of ketene *O,S*-acetals *via* thioacylation of malonitrile.¹⁴⁹ Thiocarbamoyl chlorides **162** react with malonitrile **161** to form the corresponding thiolate anion **163**, which is then directly alkylated to give the final product **164** as shown in Scheme 2.21. However, the method gave good results for aryl acetals but very poor yields for alkyl acetals (14%). Thus, this method was not considered further.



Scheme 2.21

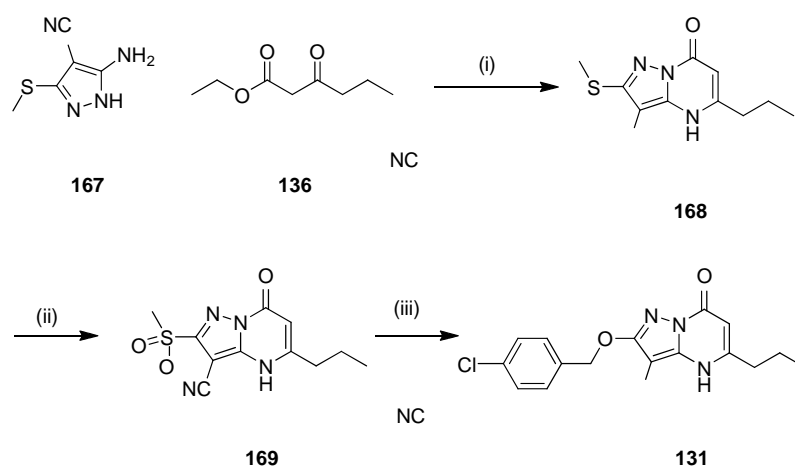
It was decided to initially attempt the conditions used for the *N*-linked analogues by reacting cyanoketene *S,S*-acetal **126** with the desired benzyl alcohol **165** (Scheme 2.22). Despite repeated attempts, the reaction was unsuccessful even after heating, with only starting material observed.



Reagents and conditions: (i) NaH, THF, rt to reflux.

Scheme 2.22

Based on this result, a new approach was investigated. Displacement of a methylsulfonyl group, which is a good leaving group, can be used to add nucleophiles to heteroaromatic ring systems. Based on all of the above, the *O*-linked analogue **131** was prepared following the synthetic route described in Scheme 2.23. Commercial compound **167** was condensed with the desired β -keto ester **136** in acetic acid at reflux to give the intermediate **168**. This thiol ether was oxidised to the sulfone **169** using mCPBA.¹⁵² Conversion to the sulfoxide proceeded quickly, while further conversion to the sulfone was much slower and required a longer reaction time. The final product **131** was obtained by displacement of the sulfone with (4chlorophenyl)methanol. The yield was low due to a mixture of unknown by-products being obtained and difficult purification due to poor solubility of the compound. Robust identification of by-products was not possible using LCMS analysis. In addition, due to the reaction scale, isolation of by-products was not carried out. However, sufficient material was obtained from the reaction and, thus, no further optimisation was carried out at the stage.



Reagents and conditions: (i) AcOH/H₂O (2:1), 120 °C, 86 h, 53%; (ii) mCPBA, DCM, 0 °C to rt, 4 days, 85%; (iii) NaH, (4-chlorophenyl)methanol, THF, 90 °C, 1 h, μ wave, 12%.

Scheme 2.23

While alternative linkers were being investigated, compound **170** was identified elsewhere in our laboratory,¹³¹ which showed good potency and efficiencies. Thus, the

4-chloro-2-fluorophenyl group was also selected for the *O*-linked analogue series as it could be prepared in one step from the sulfone intermediate **169** (Scheme 2.24).

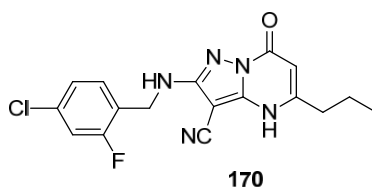
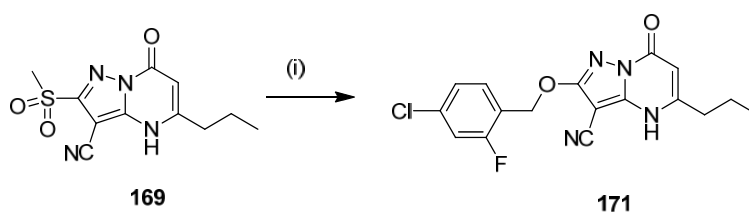


Figure 2.71 Molecule identified with good activity

The *O*-linked analogue **171** was prepared following the synthetic route described in Scheme 2.24. The final product **171** was obtained by displacement of the sulfone with (4-chloro-2-fluorophenyl)methanol in low yield. Similarly to compound **131**, the reaction gave a complex mixture of products and the desired product showed poor solubility in various organic solvents.



Reagents and conditions: (i) NaH, (4-chloro-2-fluorophenyl)methanol, THF, 90 °C, 1 h, μ wave, 12%.

Scheme 2.24

2.4.3.2.3 Biological Data

Following synthesis and characterisation, each of the new analogues was subjected to biochemical assay and the results on alternative linkers are summarised in Table 2.15.

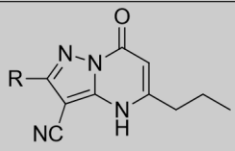
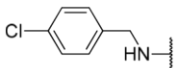
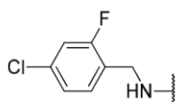
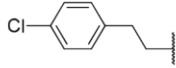
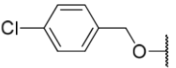
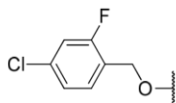
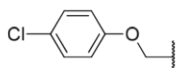
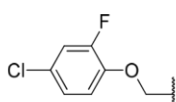
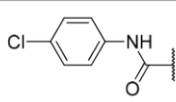
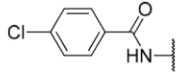
	pIC ₅₀	LE	LLE _{AT}	Chrom logD _{7.4}	CLND sol. (µg/mL)	Cell pIC ₅₀	BCATc pIC ₅₀
107 	7.1	0.41	0.36	2.90	144	6.2	6.0
170* 	7.3	0.40	0.35	2.91	≥ 155	6.5	6.6
130 	6.2	0.35	0.27	3.26	34	5.3 ^a	6.1
131 	6.6	0.38	0.33	3.49	16	n.d.	n.d.
171 	7.3	0.40	0.35	3.56	6	6.2	n.d.
132* 	6.7	0.38	0.32	3.16	162	5.3 ^a	5.7
172* 	6.5	0.36	0.31	3.20	≥ 185	<5.5	5.6
133* 	6.1	0.33	0.34	3.08	100	n.d.	n.d.
134* 	6.0	0.33	0.36	2.28	≥ 202	n.d.	n.d.

Table 2.15 Alternative linker data (*compounds synthesised elsewhere in our laboratory)

^a Compound reported pIC₅₀<5.5 in 1 out of the 2 test occasions.

All of the alternative linkers investigated showed a decrease in potency compared to the *N*-linked progenitor **107**. Both amide linkers **133** and **134** showed a drop of 10fold in potency and were not considered further at this stage. The carbon linker **130** showed nearly a 10-fold drop in potency and, thus, a decrease in ligand efficiency. In addition, replacement of the nitrogen by an extra carbon increased lipophilicity and reduced solubility significantly. Cellular potency was also reduced by around an order of magnitude. Thus, it was concluded that the carbon linker did not represent a good alternative to the *N*-linked system. The *O*-linkers **132** and **172** showed a drop in potency but maintained good ligand efficiencies. However, cellular potency was lower than the tool criteria and the *N*-linked analogues remained more attractive. On the other hand, the *O*-linked analogues **131** and **171** showed very encouraging results. Although compound **131** showed a slight drop in potency, the analogue **171** maintained good potency and good ligand efficiencies. Compound **171** also showed reasonable cellular potency. Interestingly, compound **131** showed very poor solubility as observed during its synthesis but compound **172** had comparatively good solubility. Thus, this aspect of the profile would need to be addressed for further development.

Based on the data in Table 2.15, compound **171** was progressed to X-ray crystallography in order to gain further insight into the SAR.⁸⁴ The crystal structure of compound **171** () showed a good overlay with the *N*-linked analogue **107** (Figure 2.72) suggesting that the two compounds might have similar SAR and that the directly *O*-linked series could be a good alternative, provided solubility could be improved.

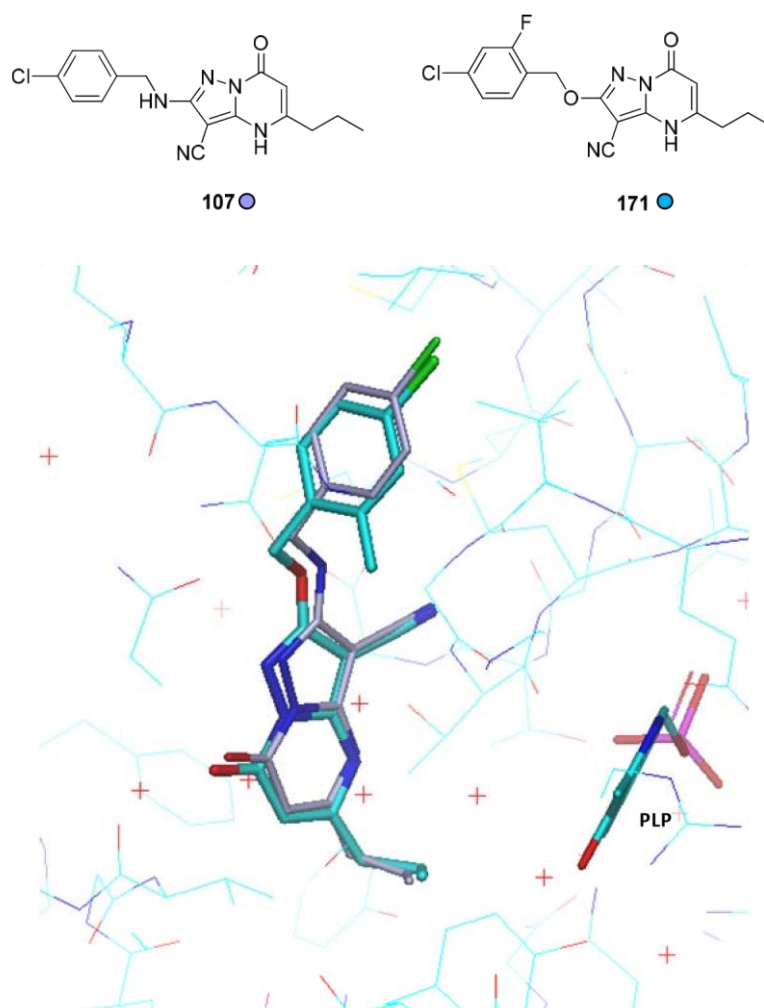
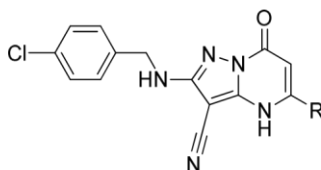


Figure 2.72 Crystal structure of compound **171** (●) overlaid with compound **107** (●)

2.4.3.3 Exploring the Lipophilic Pocket

Through analysis of the crystal structure of compound **107**, it was observed that the propyl chain did not optimally fill the volume of the lipophilic pocket and, thus, offer opportunity to improve potency further. A small set of longer and branched chain analogues were initially synthesised by other members of the team (Table 2.16).¹¹⁴ The ethyl analogue **173** showed a significant drop in potency (> 10-fold), suggesting that the extra length of the propyl chain (**107**) made favourable interaction with the protein. Addition of one extra carbon in the butyl analogue **174** maintained good potency and

efficiency. Interestingly, branched compounds (**175-176**) gave reduced potency and therefore efficiency. Although the benzyl compound **109** showed good enzyme potency, LE and LLE_{AT} were lower and solubility was sub-optimal also impacting on its cellular potency.



Cmpd	R	pIC ₅₀	LE	LLE _{AT}	Chrom logD _{7.4}	CLND sol. (µg/mL)	Cell pIC ₅₀
107		7.1	0.41	0.36	2.69	144	6.2
173		5.9	0.35	0.33	2.34	≥ 144	n.d.
174		7.4	0.41	0.34	3.38	109	6.7
175		6.6	0.36	0.30	3.26	≥ 133	5.7
176		6.9	0.36	0.28	3.87	75	6.2
109		7.0	0.34	0.30	3.23	26	5.9

Table 2.16 Initial SAR around lipophilic pocket¹¹⁴

In this next phase of the programme, the objective was to expand SAR while maintaining good physicochemical properties to select the optimum substituents for further studies. It was thus proposed to incorporate heteroatoms in the alkyl chains to reduce logP. As propyl and butyl chains were the most efficient, oxygen-containing chains were selected. The X-ray crystal structure also showed space in the binding site for bigger substituents. Therefore, cyclopentyl rings with heteroatoms were also selected. In addition, cluster 3 work (see section 3.3.4) revealed that a thiazole ring could interact with Lys202 in the PMP-form of the protein, which gave a significant increase in potency. Although the benzyl ring was not beneficial for cellular potency, thiazole and other aromatic heterocycles, which could interact with Lys202, were also designed for synthesis to establish whether a similar interaction could be achieved

in this cluster. In addition, introduction of heteroatoms in the aromatic ring should help to reduce logP and improve solubility.

Compounds selected for synthesis are summarised in Figure 2.73. For the nonaromatic rings, it was proposed that the racemate was initially tested and, if data were positive, the two enantiomers would then be separated and tested to identify the active enantiomer.

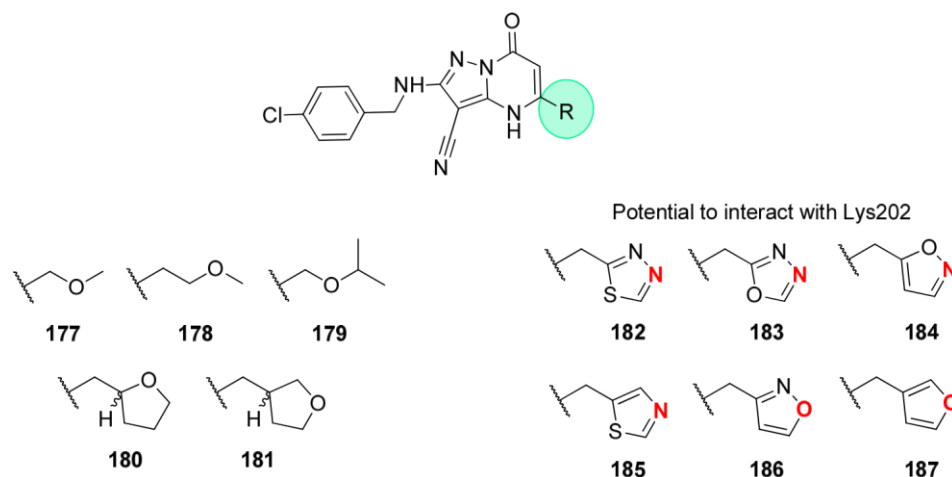
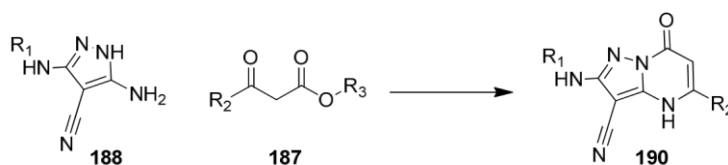


Figure 2.73 Compounds designed to improve physicochemical properties or interact with Lys202

2.4.3.3.1 Chemistry

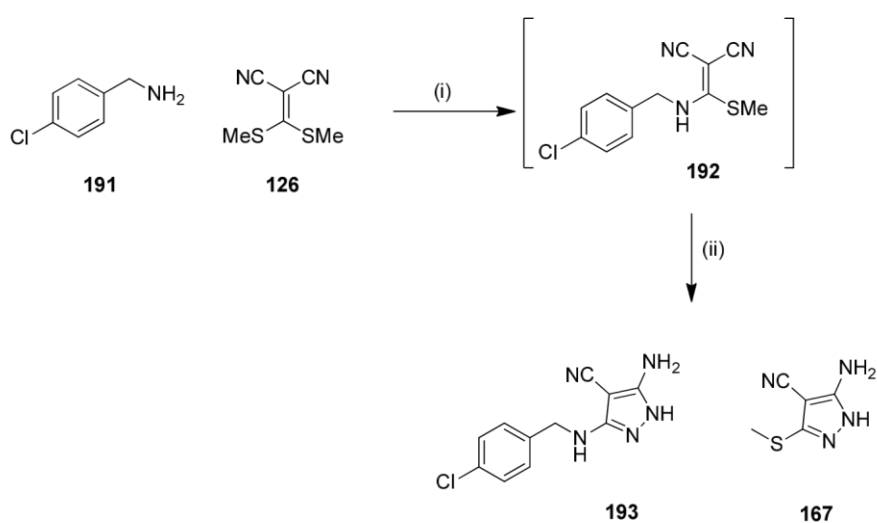
As discussed above, a common method to make pyrazolopyrimidinone derivatives **190** is by condensation of an aminopyrazole **188** with the desired β -keto ester **189** (Scheme 2.25). Accordingly, the target compounds were synthesised using the desired β -keto esters in acetic acid/water at reflux.



Reagents and conditions: (i) AcOH/H₂O (2:1), 120 °C.

Scheme 2.25

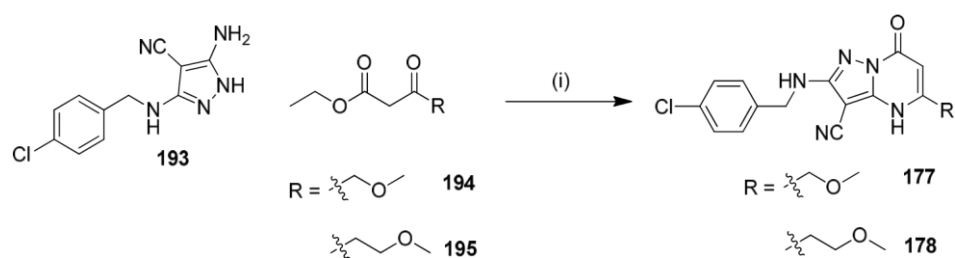
The key amino pyrazole intermediate **193** was synthesised on larger scale using the synthetic route previously optimised within our laboratory, as shown in Scheme 2.26.^{122,131} The amine **191** reacted with [bis(methylthio)methylene]propanedinitrile **126** to give the intermediate **192**, followed by cyclisation with hydrazine to produce the desired aminopyrazole **193**. As the reaction was carried out in one pot, residual [bis(methylthio)methylene]propanedinitrile **126** also reacted with hydrazine to generate the by-product **167**.



Reagents and conditions: (i) EtOH, reflux, 3 h; (ii) hydrazine hydrate, reflux, 5 h, 62% (**193**) over two steps; **167** not isolated.

Scheme 2.26

In the first instance, compounds **177** and **178** were obtained using the commercially available desired β -keto esters, as shown in Scheme 2.27.



Reagents and conditions: (i) AcOH/H₂O (2:1), 120 °C, 24 h, 44% (**177**), 25% (**178**).

Scheme 2.27

The yields obtained were somewhat lower than expected, especially in the case of compound **178**. LCMS of the reaction mixture during the preparation of compound **178** showed a more complex impurity profile, with less than 50 % by area of desired mass observed by LCMS. Two peaks with the desired mass were also observed ($R_t=0.83$, 39 % and $R_t=1.10$, 19 %). The major peak at 0.83 min was successfully isolated by MDAP. Full characterisation by NMR confirmed that desired product was obtained. The product at 1.10 min failed to be isolated and therefore could not be characterised by NMR. A possible structure for the by-product observed is shown in Figure 2.74. This implies that the amine reacts with the ester first, prior to condensation.

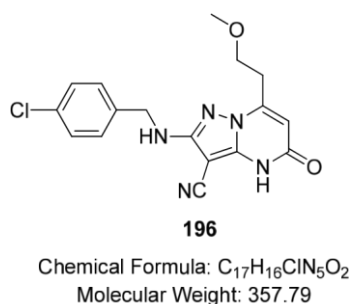


Figure 2.74

In principle, the reaction of aminopyrazole with β -keto esters can produce two isomers **197** and **198**, as shown in Figure 2.75, depending if the amine reacts with the ketone

or ester first. Given that a ketone is more reactive, product **199** should be the major product.

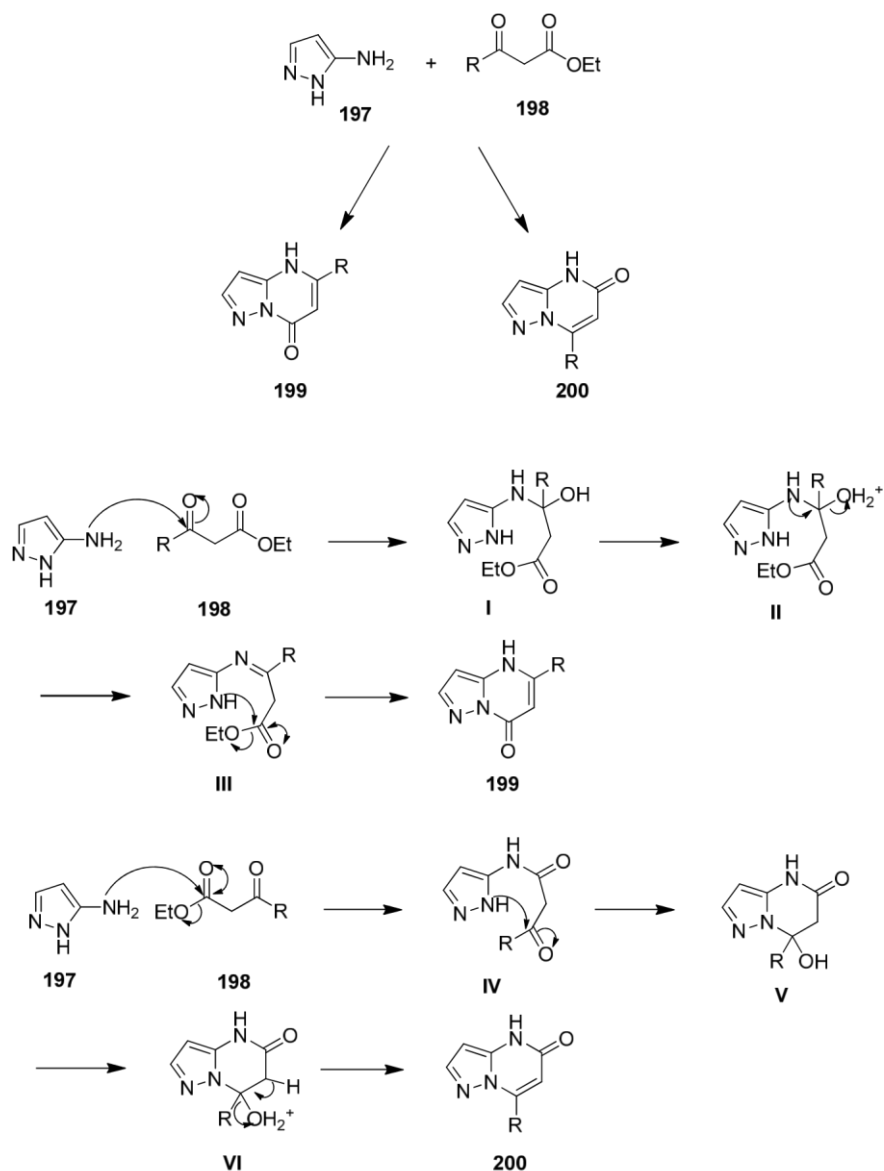
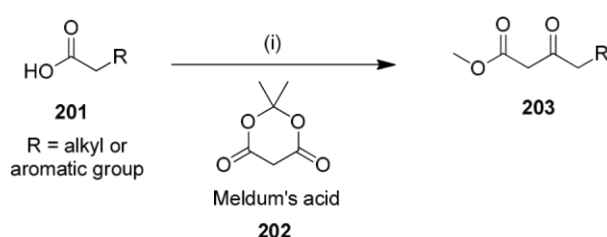


Figure 2.75

For the remaining target compounds, the requisite β -keto esters required had to be prepared prior the cyclisation. β -Keto esters are useful synthetic intermediates and a wide range of procedures have been developed to synthesise them.¹⁵³

Work in our laboratory had previously investigated different synthetic approaches to make β -keto esters and selected a method using Meldrum's acid,¹⁵⁴ which gave superior conversion to the target compounds. The crude mixture was generally used directly in the cyclisation step without purification. The reaction involved the condensation of Meldrum's acid **202** with an acyl chloride in the presence of pyridine, followed by decarboxylation in presence of methanol.¹⁵⁴ The precise conditions developed within our laboratory are described in Scheme 2.28.¹³¹



Reagents and conditions: (i) Thionyl chloride, pyridine, DCM, rt, 1 h followed by Meldrum's acid, DMAP, rt, 16 h; finally MeOH, reflux, 4 h.

Scheme 2.28

Originally, the mechanism proposed a nucleophilic attack of methanol onto one of the carbonyl groups from the Meldrum's acid intermediate **202**, followed by decarboxylation with loss of acetone to give the β -keto ester **203**.

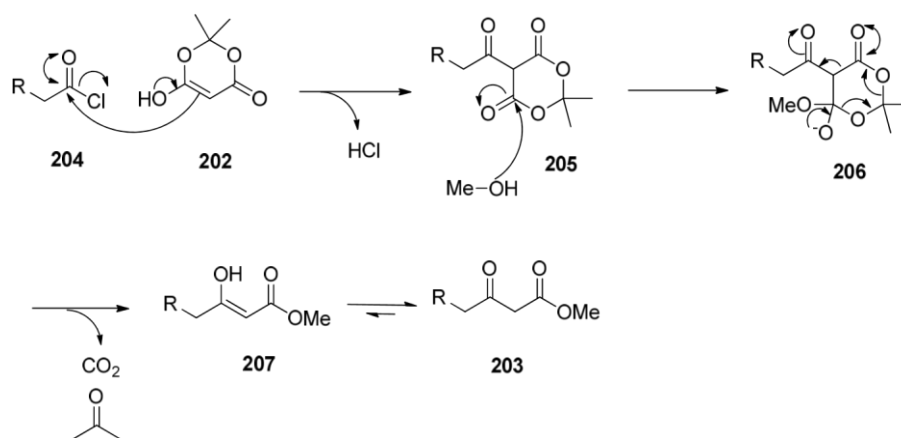


Figure 2.76

However, more recently, Xu and co-workers studied the reaction mechanism in more detail *via* IR and proposed a new mechanism *via* an α -oxoketene species **208**.¹⁵⁵ They have shown that the Meldrum's acid adduct **202** decomposed under heating into an α -oxoketene species **208**. Methanol then attacks the oxoketene to give the desired β -keto ester **203**.

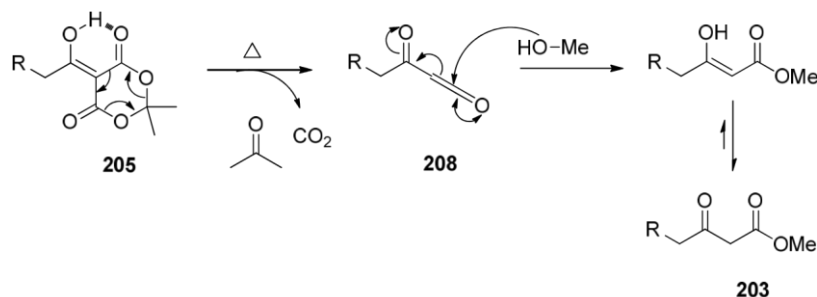


Figure 2.77

The alkyl acetic acid starting materials **209** (Figure 2.78) was available in our compound collection, which underpinned the synthesis of analogue **180**.

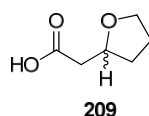
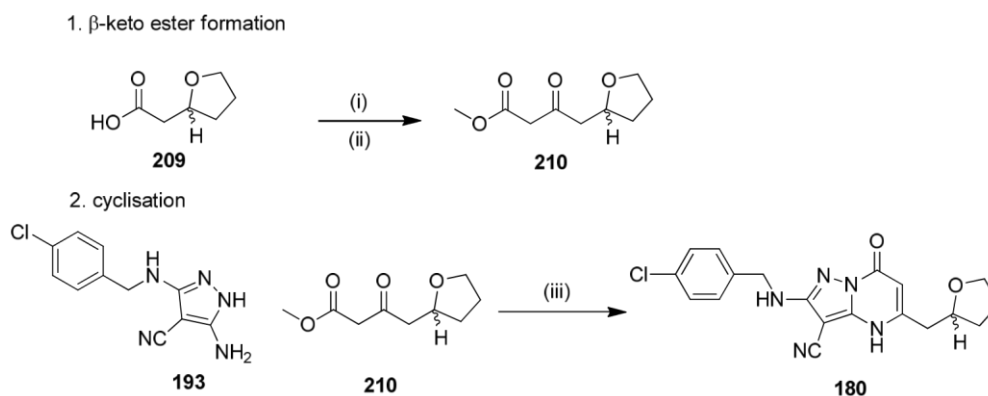


Figure 2.78

The β -keto ester **210** was thus prepared using the Meldrum's acid conditions described above, without recourse to isolation of the intermediates (Scheme 2.29). Compound **180** was subsequently accessed by cyclisation of the desired β -keto ester **210** and the aminopyrazole **193**.



Scheme 2.29

Compound **180** was isolated but contained unknown impurities observed by NMR after purification, therefore, the purity of the compound was not sufficient for submission to bioassay. At this stage not enough carboxylic acid was available to repeat the synthesis; therefore, it was decided to wait for the data from other compounds before remaking the starting material.

For compounds **179** and **181** (Figure 2.79), the requisite acetic acid starting materials were not available and, thus, would require synthesis. Accordingly, different synthetic routes were investigated.

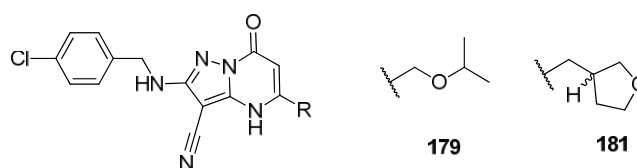
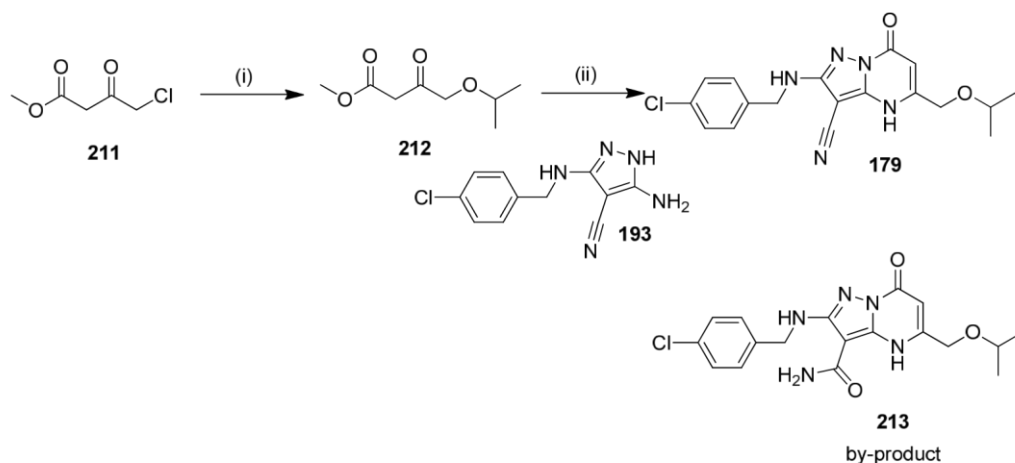


Figure 2.79

Compound **179** was synthesised following the route depicted in Scheme 2.30. The desired β -keto ester precursor **212** was prepared by reaction of the methyl 4-chloro3-

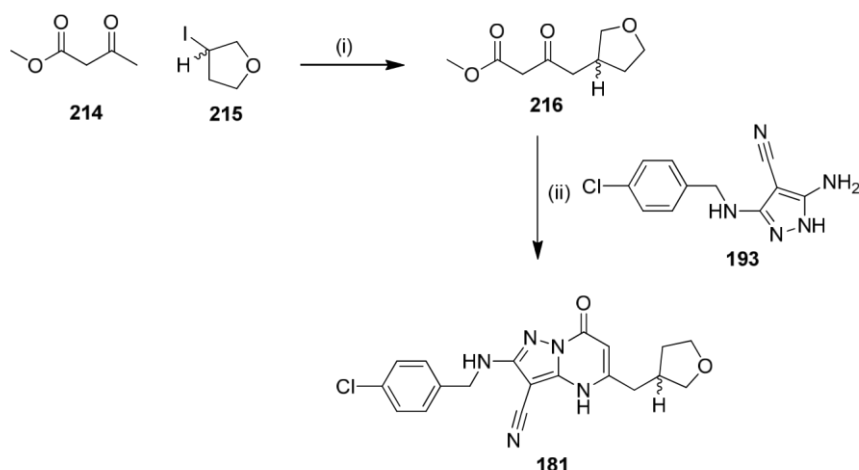
oxobutanoate **211** and isopropanol in presence of sodium hydride.¹⁵⁶ The product was again found to be volatile and needed the use of low vacuum to avoid loss through evaporation. Cyclisation with the amino pyrazole intermediate in acetic acid/water at reflux gave the desired final product **179**. One major by-product was isolated and corresponded to hydrolysis of the nitrile to the carboxamide **213**.



Reagents and conditions: (i) NaH, 2-propanol, Et₂O, rt, 1 h, then **211**, rt, 12 h; (ii) AcOH/H₂O (2:1), 120 °C, 2 days, 31% (**179**) over two steps, 12% (**213**) over two steps.

Scheme 2.30

Turning our attention to the tetrahydrofuran analogue **181** (Scheme 2.31), the desired β -keto ester **216** was prepared by reaction of the dianion methyl acetoacetate **214** and the iodide **215**.¹⁵⁷ The moderate yield obtained was suspected to be due to water solubility and the volatile nature of the compound. As sufficient material was obtained in this first attempt, the reaction was not repeated. Cyclisation with the amino pyrazole intermediate **193** in acetic acid/water at reflux gave the desired final product **181** in moderate yield. However, based on LCMS analysis, it was found that starting aminopyrazole remained (18 % by area), explaining the sub-optimal yield. It is anticipated that the yield could be improved in the future by adding additional β keto ester.



Reagents and conditions: (i) 1. nBuLi, DIPEA (2 eq.), THF, 0 °C, 1 h, 2. - 78 °C to rt, overnight; (ii) AcOH/H₂O (2:1), 120 °C, 24 h, 29% over two steps.

Scheme 2.31

In the case of the aromatic analogues, several acetic acid derived starting materials were available from either the our laboratory's building block collection or commercial sources, as shown in Figure 2.80.

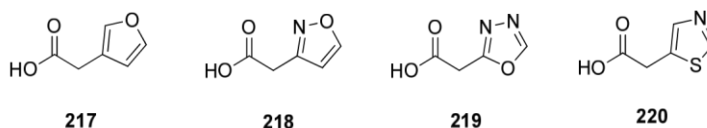
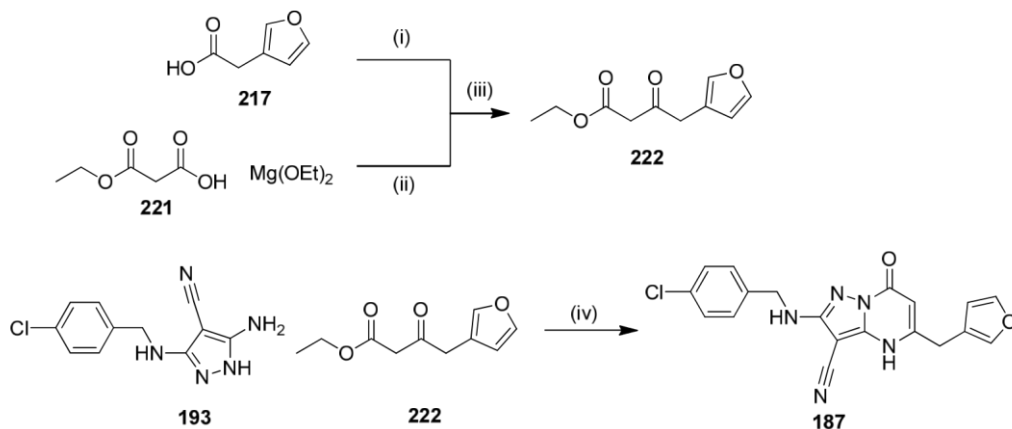


Figure 2.80 Intermediates available in house or from commercial suppliers

The Meldrum's acid conditions previously used were found to give low conversion to the desired β -keto esters and very complex mixtures unsuitable for the cyclisation step. A search of our laboratory's electronic lab notebook identified an alternative route (Scheme 2.32), which showed a cleaner reaction mixture and improved yield. These optimised conditions developed were therefore applied to make a range of heterocycle β -keto esters.^{158,159}

Compound **187** was prepared following the synthetic route described in Scheme 2.32. The carboxylic acid **217** was converted to the activated imidazolide using CDI and was

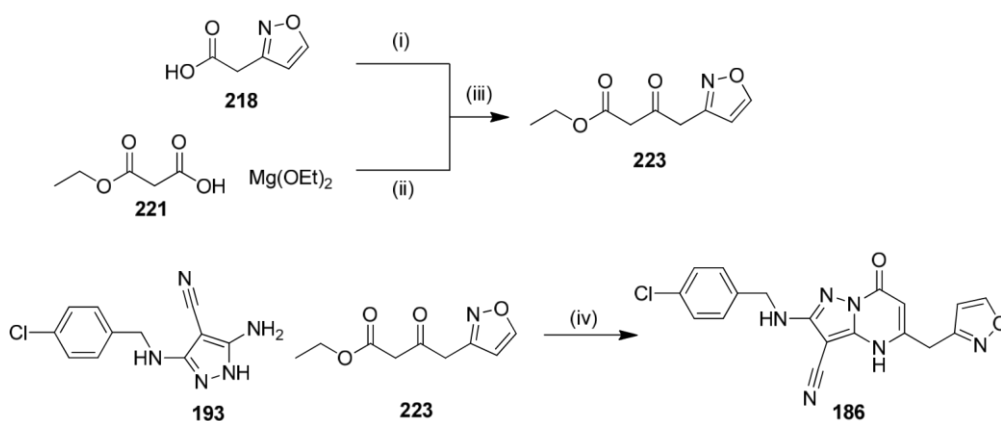
then treated without isolation with the magnesium salt of malonic acid.¹⁵⁸ The β -keto ester **222** was then reacted with the aminopyrazole intermediate **193** to give the desired final product **187**.



Reagents and conditions: (i) CDI, THF, rt, 20 h; (ii) THF, rt, 5 h then evaporated and redissolved in THF; (iii) rt, 6 h, 55%; (iv) AcOH/H₂O (2:1), 120 °C, 16 h, 45%.

Scheme 2.32

A similar route was applied to the synthesis of compound **186** (Scheme 2.33). The activated acid of **218** was treated with the magnesium salt of malonic acid to give the desired β -keto ester **223**.¹⁵⁸ The final compound **186** was then obtained by reaction between the β -keto ester **223** and the aminopyrazole **193**.



Reagents and conditions: (i) CDI, THF, rt, 3 days; (ii) THF, rt, 5 h then evaporated and redissolved in THF; (iii) rt, 16 h, crude; (iv) AcOH/H₂O (2:1), 120 °C, 16 h, 17% over two steps.

Scheme 2.33

These new conditions for the synthesis of β -keto ester have proven to give better yields and could be applied to the earlier molecules to improve yields in the event these analogues had to be revisited.

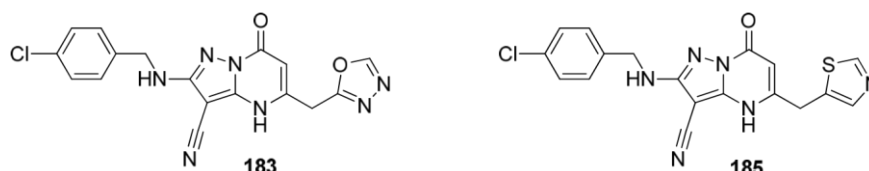
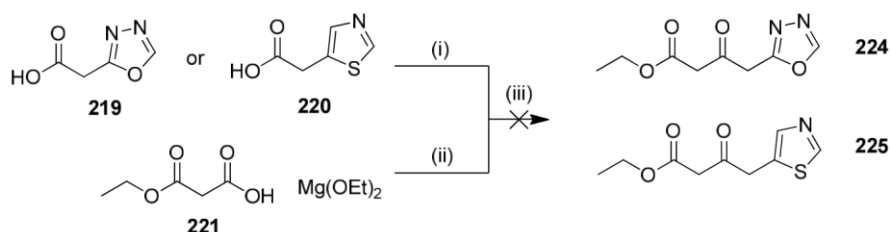


Figure 2.81

Synthesis of compounds **183** and **185** had proven to be more challenging (Figure 2.81). The required β -keto esters **224** and **225** could not be obtained using the previously employed CDI mediated conditions (Scheme 2.34).



Reagents and conditions: (i) CDI, THF, overnight; (ii) THF, rt, 5 h then evaporated and redissolved in THF; (iii) rt, 5 h.

Scheme 2.34

In both cases, no activated acid intermediate was observed by LCMS and thus, no β keto esters were formed. Only limited amounts of carboxylic acid **219** was available to investigate further conditions. Based on this, the Meldrum's acid conditions were applied to compound **220**. However, no desired β -keto ester was formed.

Finally, for compounds **182** and **184**, the carboxylic acid intermediates were not available and the alternative synthetic routes involved several steps to prepare the desired β -keto esters. At this stage of the programme, it was decided to wait for the data on the other heterocycles before investigating further the synthesis these two compounds.

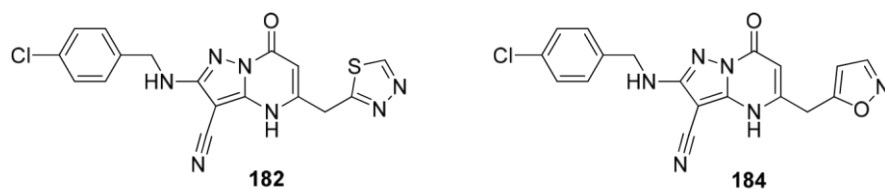
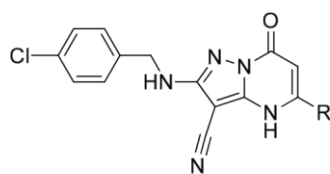


Figure 2.82

2.4.3.3.2 Biological Data

Following synthesis and characterisation, each of the new analogues was tested in the BCATm assay. The biological data on the alkyl units and saturated ring systems are shown in Table 2.17.



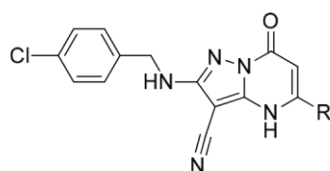
Cmpd	R	pIC ₅₀	LE	LLE _{AT}	Chrom logD _{7.4}	CLND sol. (µg/mL)
107*		7.1	0.41	0.36	2.9	144
177		5.4	0.31	0.36	1.94	162
174*		7.4	0.41	0.34	3.38	109
178		5.5	0.30	0.35	2.14	152
176*		6.9	0.36	0.28	3.87	75
179		5.7	0.30	0.32	2.57	≥ 181
180		5.0	0.25	0.29	2.18	n.d.

Table 2.17 Biological data on alkyl chain modification *Compounds synthesised elsewhere in our laboratory¹¹⁴

Attempts to incorporate an oxygen atom in the alkyl chains were consistently shown to reduce potency significantly (e.g **177**, **178** and **179**). Similarly, introduction of heteroatoms in the cyclopentyl ring to afford the tetrahydrofuran reduced potency (e.g. **180**). These results confirmed the hypothesis made from the crystal structure, which showed that this region of the pocket was fairly lipophilic in nature, favouring hydrophobic contacts. Based on all the above, the propyl (**107**) and butyl (**175**) chains were the most efficient aliphatic substituents.

However, by contrast, introduction of heterocycles in this region was more successful (Table 2.18) and showed that some heteroatoms were tolerated as noted previously in

cluster 3. Although compound **186** showed a small reduction in potency, LE and LLE_{AT} have been maintained and solubility has been greatly improved. More interestingly, compound **187** showed an increase in potency and ligand efficiencies. Lipophilicity has been reduced and solubility improved compared to the phenyl analogue **109**. In addition, compound **187** showed a similar profile to compound **107** in term of enzyme potency and physicochemical properties. This result suggested that the compound might make a useful interaction with the protein. In cluster 3 the thiadiazole compound **102** has been shown to give an increase in potency through interaction with Lys202 residue by stabilising the PMP-form of the protein. Accordingly, compound **187** was submitted to X-ray crystallography and cellular assay to further understand its potency and assess its potential as a new lead.



Cmpd	R	pIC ₅₀	LE	LLE _{AT}	Chrom logD _{7.4}	CLND sol. (µg/mL)	Cell pIC ₅₀
107		7.1	0.41	0.36	2.90	144	6.2
109		7.0	0.34	0.30	3.23	26	5.9
186		6.3	0.32	0.37	2.30	≥ 177	< 4.9
187		7.5	0.38	0.37	2.86	149	5.8

Table 2.18 Biological data

Disappointingly, compound **187** showed a significant drop in cellular potency compared to compound **109**, which could not be explained by looking at simple properties related to cell permeability, such as solubility and lipophilicity. Other ongoing studies in our laboratory around the induced lipophilic pocket led to the identification of non aromatic alternatives,¹⁶⁰ which thus could be combined with these newly identified heterocycle rings to give compounds which overall would have fewer aromatic rings and a different physicochemical profile.

X-ray crystallography of compound **187** showed good overlay with the propyl analogue **107** (Figure 2.83). However, the furan ring did not stabilise the PMP-form of the protein *via* interaction with Lys202 as previously observed with compound **102**. Therefore, the furan ring might optimally fill the binding site making favourable contacts but does not permit PMP interactions.

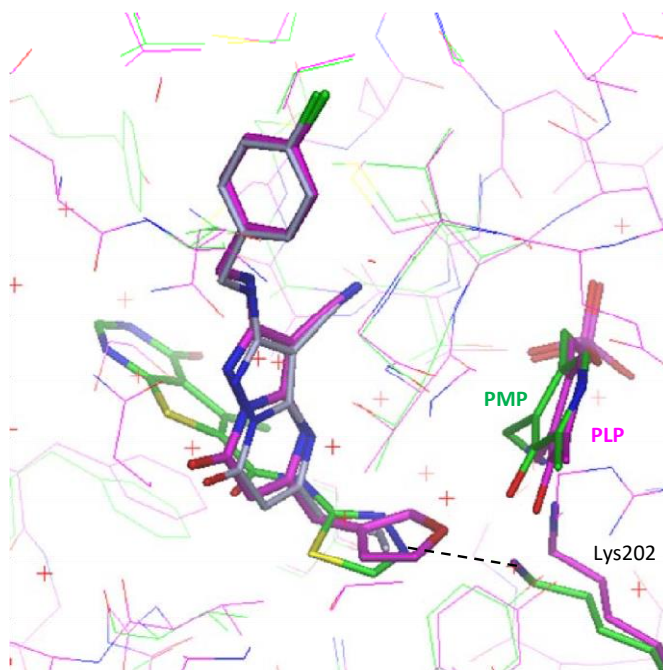
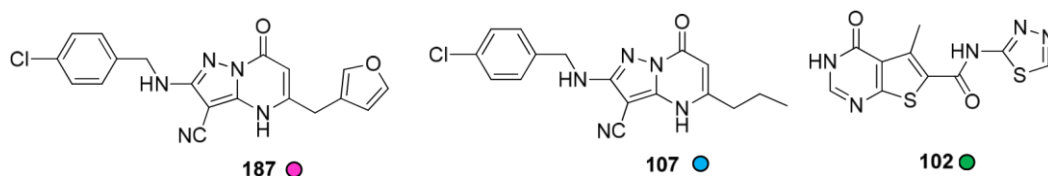


Figure 2.83 Crystal structure of compound **187** (●) overlaid with compounds **107** (●) and **101** (●)

2.4.3.3.3 Future Work

Following this interesting result and by analogy with cluster 3, it would be very interesting to prepare the thiadiazole analogue to establish whether a similar interaction

with the protein is possible but also investigate other heterocycles to fully understand SAR in this region (Figure 2.84). Given the fact that a number of compounds within the series as a whole met the pre-determined tool criteria, this effort was transferred to other members of our laboratories for further lead optimisation activities.

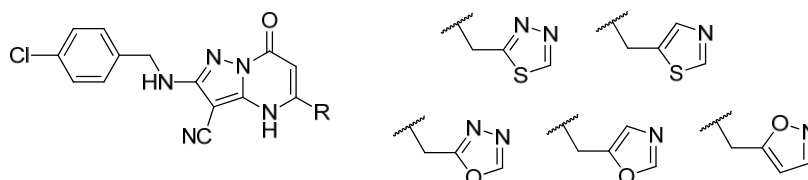


Figure 2.84

2.4.4 Conclusion

Within this cluster, two key areas have been evaluated and this work has demonstrated significant potential for further lead optimisation efforts. Alternative linkers have been identified, with the *O*-linked analogue **171** maintaining good potency and ligand efficiencies as compared to *N*-linked analogues and could offer a different PK profile. On the other hand, investigation around the propyl chain in the lipophilic pocket allowed identification of an area for further optimisation. Although the initial compound **187** showed lower cellular potency, the SAR generated indicated that heterocycles were tolerated in this region and could increase enzyme potency by fully occupying the binding site. Thus, further exploration could identify more optimal heterocyclic motifs such as the thiadiazole identified in cluster 3. However, having four aromatic rings in the molecule could be detrimental in terms of developability^{20,111} and should also be reduced. Work on-going elsewhere in our laboratory around the induced lipophilic pocket allowed identification of nonaromatic alternatives,¹⁶⁰ which accordingly could be combined with the heterocycle rings suggested here to give compounds without an excessive number of aromatic rings and potentially increased potency.

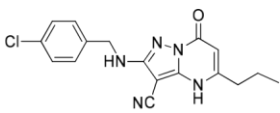
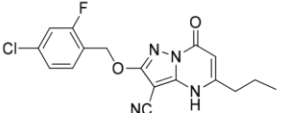
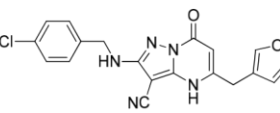
Cmpd	107	171	187
Structure			
BCATm pIC ₅₀	7.1	7.3	7.5
LE, LLE _{AT}	0.41, 0.36	0.40, 0.35	0.38, 0.37
Chrom logD _{7.4}	2.90	3.56	2.86
CLND sol. (µg/mL)	126	6	149
Cell pIC ₅₀	6.2	6.2	5.8
BCATc pIC ₅₀	6.0	n.d.	n.d.

Table 2.19 Cluster 6 compounds

2.5 Overall Conclusions

The aim of the project was to identify a tool molecule derived from FBDD, which was suitable for target validation, as at present no small molecule inhibitors of BCATm have been reported.

FBDD screening of BCATm using a combination of biochemical and biophysical assays was successful in the identification of diverse starting points. The overall hit rate was around 6% and, consequently, much higher than a standard HTS screening ($\leq 1\%$) showing the benefit of using a fragment-based approach as well as multiple screening technologies. From this exercise, 11 protein-ligand structures were solved by X-ray crystallography and after analysis of their binding mode and growth vectors, they were categorised into seven clusters providing a variety of starting points. This clustering was based on binding mode and not more traditional 2D similarity. Based on this, careful analysis of their interactions, ligand efficiencies, data from related analogues and potential synthetic direction allowed the prioritisation of clusters. Chemistry was initiated on three clusters identified as the promising starting points. This process was able to identify a wide range of novel ligands and binding modes never seen before with this target. Initial fragment optimisation was established using our chemical libraries, which allowed rapid expansion of SAR around the fragment. Additionally, leveraging data generated from parallel hit finding approaches such as HTS proved to be of value in further developing SAR around the clusters.

Using knowledge of the structural requirements for binding, cluster 3 hit **30** was successfully optimised to a high lead quality molecule. New interactions with the protein were incorporated by careful analysis of superimposed X-ray structures. Both structural information from this fragment series but also data from other screening methods (*vide infra*) were combined to design optimum molecules. From this exercise compound **53** was identified, which showed improved potency and solubility with good LE and LLE_{AT}. Subsequent X-ray structure of the compound confirmed the

original design hypothesis, with a key H-bonding interaction with Lys79 as observed in other clusters. In addition, our diversity-based approach around the lipophilic pocket led to the discovery of a compound with a novel binding mode and a new mode of action. The thiadiazole moiety of compound **102** made a key new interaction with the Lys202 from the PMP-form of the protein. To date, all the molecules bound to the PLP-form of the protein, where Lys202 is covalently bound to the PLP co-factor. In this instance, compound **102** stabilised the PMP-form of the protein by forming a favourable H-bonding interaction with Lys202. This is a good example of protein flexibility and how characterisation of potentially binding ligands can identify unexpected protein movement. This novel compound offers the opportunity to explore a different mode of action and its potential effect on the target, and also shows the value of using more diverse array based approaches to complement structure based design techniques.

Cmpd	30	53	102
Structure			
BCATm pIC ₅₀	4.2 ^a	6.0	6.7
LE, LLE _{AT}	0.38, 0.344	0.34, 0.45	0.48, 0.63
Chrom logD _{7.4}	-0.71	0.44	0.10
CLND sol. (µg/mL)	≥ 73	164	66
Cell pIC ₅₀	n.d.	< 4.3	5.5
BCATc pIC ₅₀	3.5	5.6	6.0

Table 2.20 Cluster 3 lead compounds

^aCompound reported inactive (pIC₅₀<4.2) in 3 out of the 34 test occasions.

Finally, within cluster 6, several areas were investigated to understand SAR and identify the most potent and efficient molecules. An alternative *O*-linker analogue **171** was successfully identified, with good potency and ligand efficiencies. Hybrid

compounds of cluster 6 and cluster 3, which demonstrated a novel mode of action, allowed the identification of compound **187**, which maintained good enzyme potency and has shown to fill the pocket optimally. Although this compound showed low cellular potency, combination of this new heterocyclic moiety with a non-aromatic left-hand side could deliver molecules with improved potency and favourable DMPK profile. Overall, the data generated on cluster 6 successfully allowed identification of areas for further lead optimisation and contributed to the selection of a tool molecule for *in vivo* target validation.

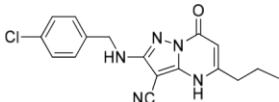
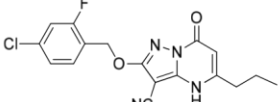
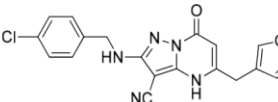
Cmpd	107	171	187
Structure			
BCATm pIC ₅₀	7.1	7.3	7.5
LE, LLE _{AT}	0.41, 0.36	0.40, 0.35	0.38, 0.37
Chrom logD _{7.4}	2.90	3.56	2.86
CLND sol. (µg/mL)	126	6	149
Cell pIC ₅₀	6.2	6.2	5.8
BCATc pIC ₅₀	6.0	n.d.	6.3

Table 2.21 Cluster 6 compounds

In conclusion, data generated from across all the clusters developed as part of this programme significantly contributed to the design of a novel series of molecules which, for the first time, were suitable for use in critical *in vivo* experiments to determine the validity of BCATm as an anti-obesity target.

Chapter 3

Discovery and Optimisation of Oral PI3K δ Inhibitors

3.1 Biological Background

3.1.1 Asthma

Asthma is one of the most common respiratory diseases particularly in developed countries. As of 2011, over 235 million people worldwide were affected by asthma and approximately 250,000 people die every year from the disease.^{161,162} Asthma is a chronic inflammatory disease of the airways characterised by airway inflammation, airflow obstruction, increased mucus production, and bronchial hyperresponsiveness. During an asthma attack, the airways become narrow reducing the flow of air going in and out of the lungs (Figure 3.1). This leads to difficulty in breathing, coughing, wheezing, and chest tightness. On the basis of the symptoms and their severity, the patients can be divided into mild, moderate, and severe asthma.¹⁶² The causes of asthma are not well understood but are thought to be due to a combination of genetic predisposition and environmental factors.^{162,163} The causes can differ from person to person and an individual can have several triggers. Common triggers are allergens (e.g. house dust mites, pet fur, pollen), tobacco smoke, air pollution, chest infections, irritant chemicals, and physical exercise.

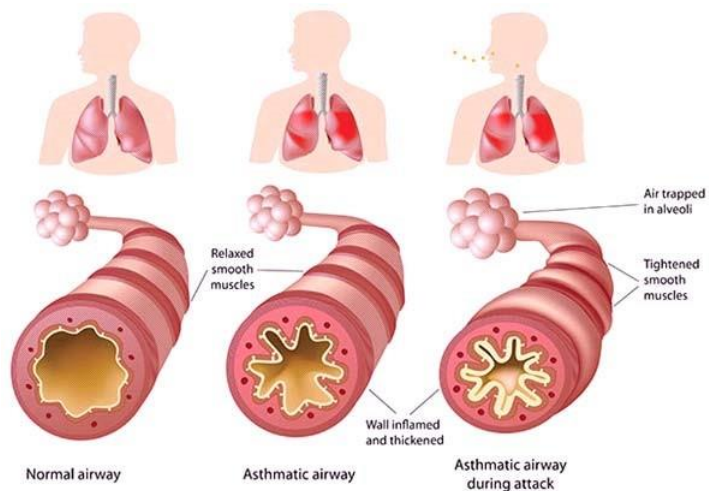


Figure 3.1 Normal airway and asthmatic airway¹⁶⁴

In asthmatic patients, inhaled allergens trigger an allergic inflammatory response involving excessive activation of T helper type 2 (Th2) cells (Figure 3.2).^{163,165} Once activated, the Th2 cells release several cytokines (e.g. IL-4, IL-5, and IL-13), which in turn activate B-cells, mast cells and eosinophils. These then release mediators such as histamines, prostaglandins, and leukotrienes, leading to airway inflammation and mucus overproduction. Targeting the inflammatory process by interfering with some of the key components within the immune response provides a range of opportunities for therapies.

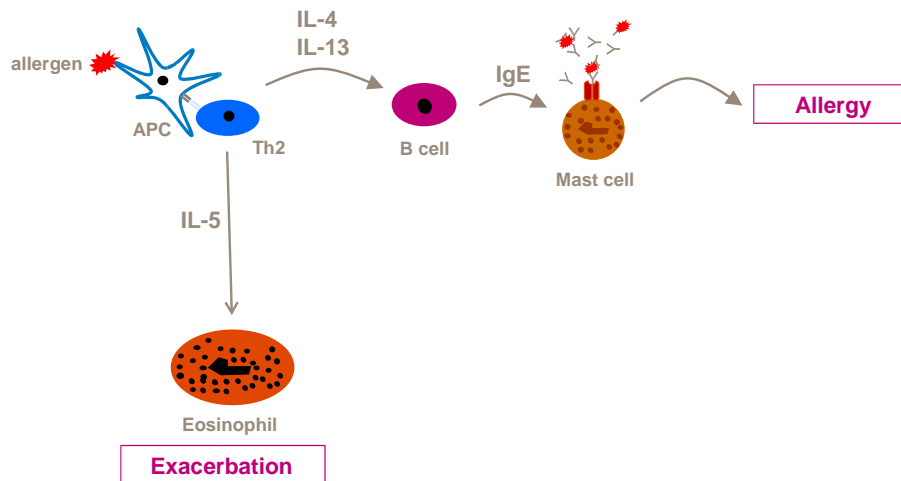


Figure 3.2 Inflammatory response in asthma
 APC = antigen-presenting cell; IgE=immunoglobulin E (antibody)

Currently, drug treatments for asthma relieve airway inflammation and help to control symptoms, but do not provide a cure. Accordingly, asthma treatment can be classified in two categories: relievers and controllers.^{162,163,166}

Relievers are short-term medications used when needed to relieve shortness of breath (e.g. the bronchodilator Salbutamol **226**, an inhaled short-acting β 2-agonist - Figure 3.3). They relax muscles around the airway, which opens the airways and allow more air in and out of the lungs.

On the other hand, controllers are long-term medications that are taken daily to keep asthma under control.¹⁶² Several therapies are available for the chronic management of asthma.^{163,166}

Inhaled corticosteroids (ICS, e.g. fluticasone propionate **227**) are the most effective anti-inflammatory drugs currently available for long-term treatment.¹⁶² They reduce airway inflammation and help to prevent asthma attacks. They need to be taken on a daily basis for prolonged periods to see the benefits. Some patients respond poorly to corticosteroids and need higher doses or add-on therapies (inhaled long-acting β 2agonists). They can, however, sometimes cause hoarseness of the voice, a sore throat, and a mouth infection, such as thrush, but these can be minimised by rinsing the mouth and cleaning teeth after their administration. At higher doses, which require the use of oral steroids, some more severe side effects can be observed such as infections, cataracts, and osteoporosis.^{162,167}

Inhaled long-acting β 2-agonists (LABA), such as Salmeterol **228**, relax the airway muscles, which open the airway and ease breathing.^{162,168} However, they do not reduce the airway inflammation and are thus only used as add-on therapies to inhaled corticosteroids. The combination of the two treatments allows the patient to reduce corticosteroid doses and to control asthma more effectively than corticosteroids on their own.¹⁶⁹

Alternative treatment options are cysteinyl-leukotriene receptor antagonists (e.g. Montelukast **229**).¹⁷⁰ They reduce airway inflammation and bronchoconstriction with minimal side effects. However, clinical studies have revealed that leukotriene modifiers are less effective than inhaled corticosteroids or inhaled long-acting β 2-agonists.¹⁶²

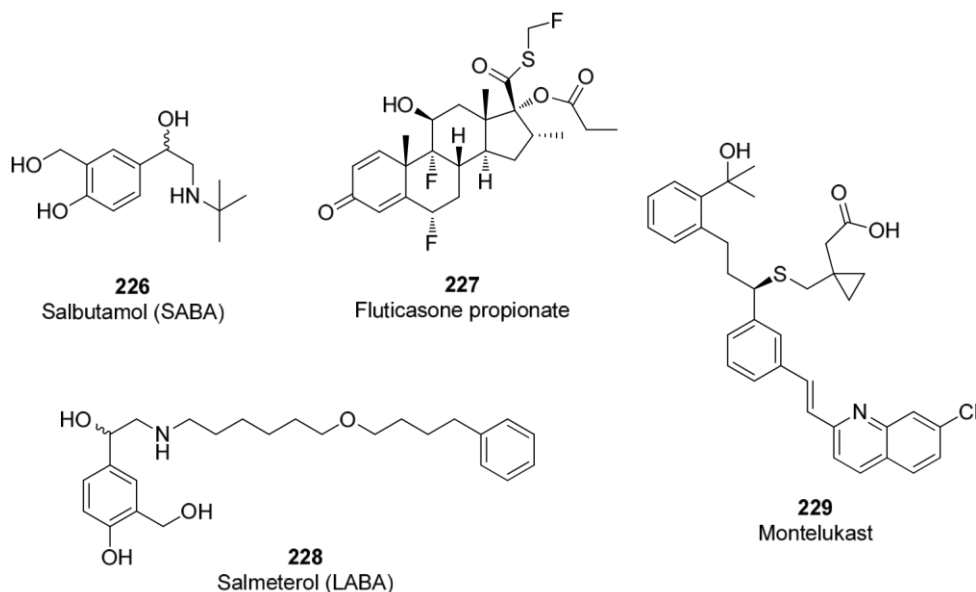


Figure 3.3 Asthma long-term-medication

Specific IgE monoclonal antibodies such as Omalizumab (Xolair®, injection once or twice a month) have been shown to be effective in 60-80% of patients.¹⁷¹ However, such treatment remains very expensive and is thus restricted to patients with severe asthma, which cannot be controlled with high doses of corticosteroids.

Although several therapies are currently available for the treatment of asthma, they are limited by their side effects, efficacy, compliance, and cost. Thus, there is a real need for new effective therapies with an improved overall profile. With these issues in mind, the lipid kinase PI3K δ has emerged as a potential new target for the treatment of

asthma. In the last 20 years, several studies have demonstrated that PI3K δ plays a key role in immune cell signalling and, thus, in inflammatory processes (Figure 3.4).^{165,172-174} Studies conducted in our laboratories have recently confirmed that PI3K δ is a promising target for allergic asthma as it is involved in activation of T-cells, B-cells, and mast cells.¹⁷⁵ The inhibition of PI3K δ should inhibit allergen driven responses in T-cells and B-cells and, thus, prevent the release of key mediators (IL-4, IL-5, IL-13) and reduce eosinophilia (an abnormally high number of eosinophils, a type of white blood cells, in the blood).

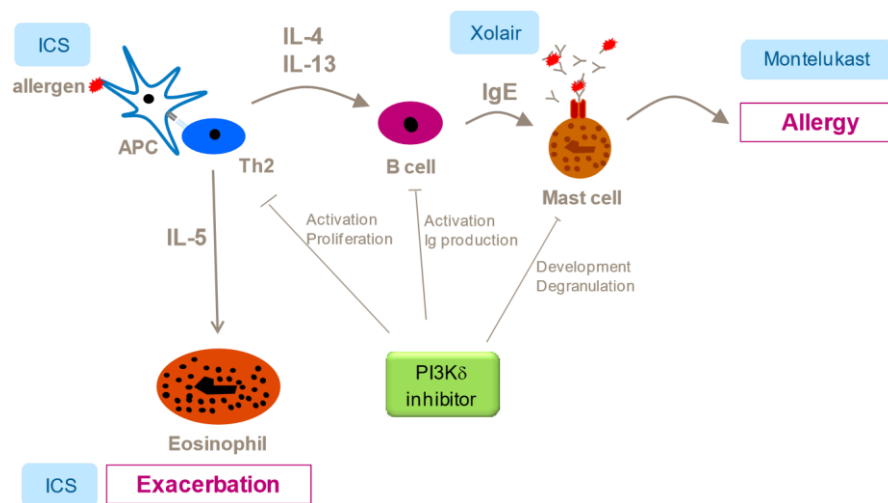


Figure 3.4 Role of PI3K δ in inflammatory response in asthma compared to current drugs

3.1.2 The PI3K Family

Phosphoinositide 3-kinases (PI3Ks) play a central role in cell signalling functions including cell growth, proliferation, migration, and survival.¹⁷⁶⁻¹⁷⁹ PI3Ks are lipid kinases that phosphorylate the 3-position of the inositol lipid ring of phosphatidylinositol (PIP) using adenosine triphosphate (ATP) (Figure 3.5). The phosphatase and tensin homolog (PTEN) reverses the process.

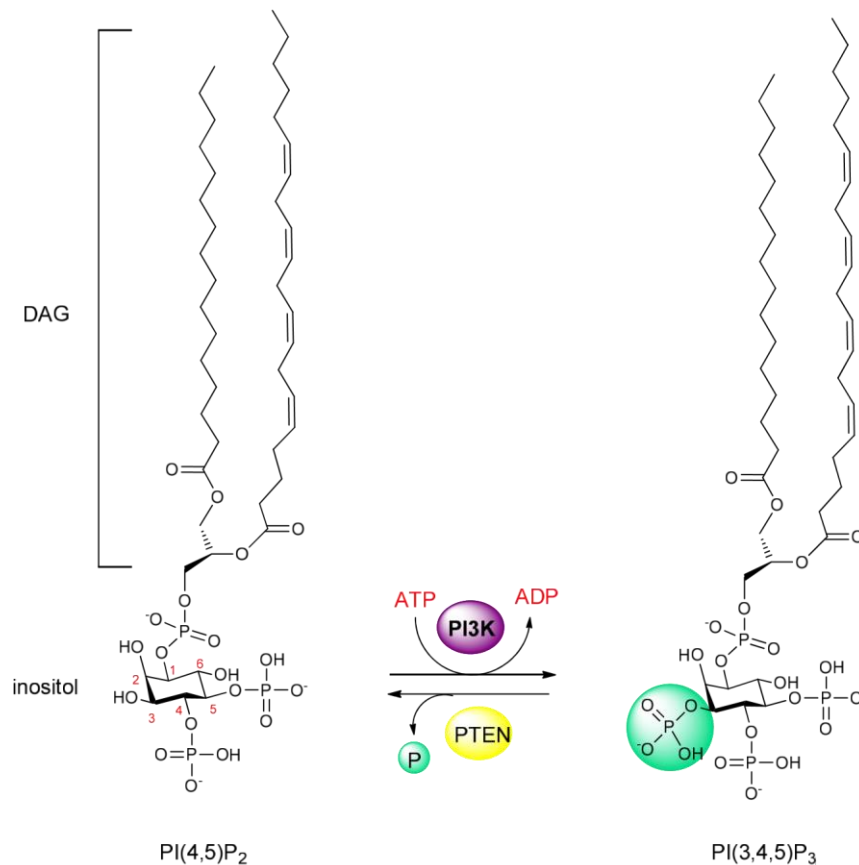


Figure 3.5 PI3K enzyme reaction

PIPs are basic building blocks of the intracellular membrane and are comprised of an inositol ring linked *via* a phosphate group to diacylglycerol (DAG). The inositol ring has five free hydroxyl groups and three of them have been found to be phosphorylated in the cell (3-OH, 4-OH and 5-OH).¹⁸⁰ In total, eight distinct PIP species have been identified (Figure 3.6).

The PI3Ks that have been identified are divided into three classes (I, II and III) on the basis of their structural and functional aspects.^{177,179,181} Class I PI3Ks comprise four isoforms (α , β , δ and γ), which convert the cell membrane phospholipid PI(4,5)P₂ into PI(3,4,5)P₃ (blue, Figure 3.6). Class II PI3Ks comprise three isoforms (C2 α , C2 β and C2 γ), which can phosphorylate PI into PI3P and PI4P into PI(3,4)P₂. Finally, class III PI3K, Vps34 (vasuolar protein sorting-associated protein 34), phosphorylates PI to

generate PI3P.^{180,181} The reactions catalysed by PI3Ks in the cell are highlighted in Figure 3.6.

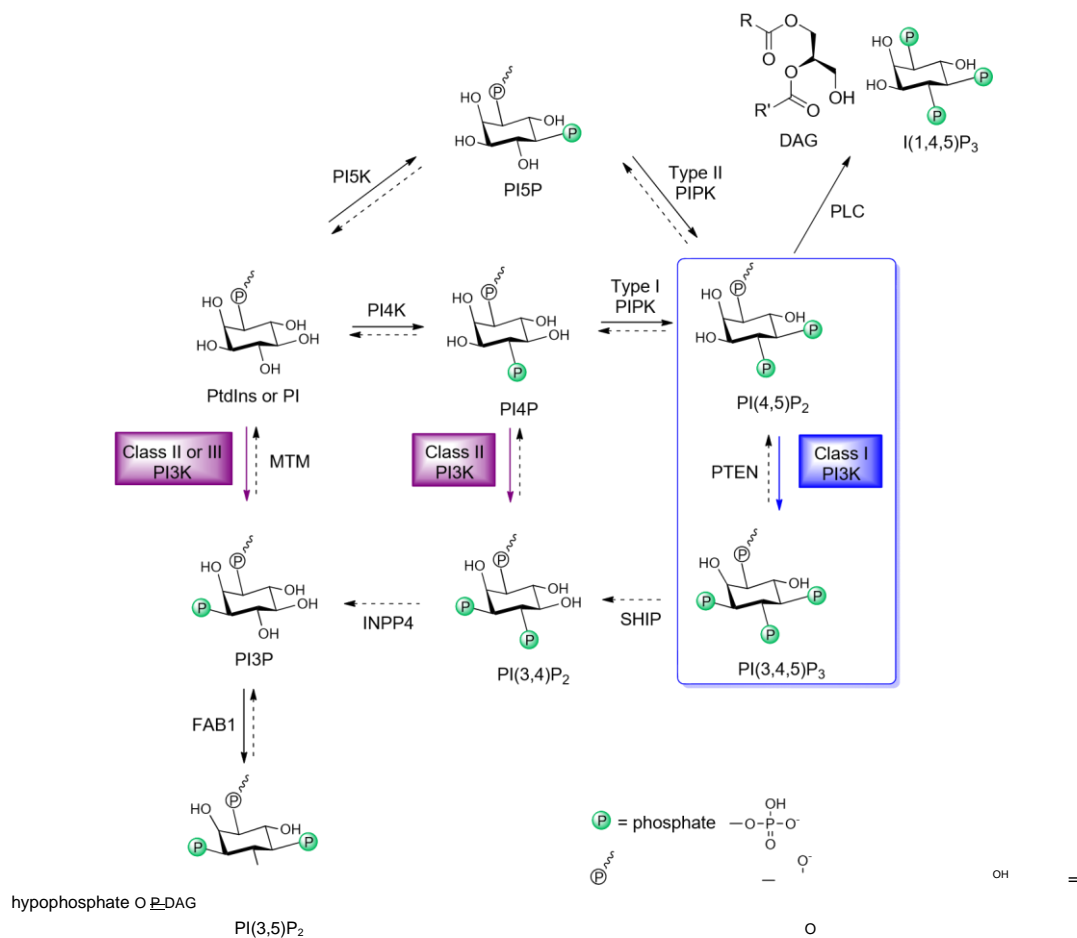


Figure 3.6 Reactions catalysed by PI3Ks in cell¹⁸⁰

DAG = diacylglycerol; Fab1 = 1-phosphatidylinositol 3-phosphate 5-kinase; INPP4 = inositol polyphosphate-4-phosphatase; MTM = myotubularin; PI4K = phosphoinositide 4-kinase; PI5K = phosphoinositide 5-kinase; PIPK = Phosphatidylinositol phosphate kinases; PLC = phospholipase C; PI = phosphatidylinositol; PIP = phosphatidylinositol phosphate; PTEN = phosphatase and tensin homolog; SHIP = SH2 domain-containing inositol 5-phosphatase.

Class I PI3Ks are the most studied and validated targets from a drug discovery perspective. Class I is subdivided in two additional categories: class IA, which includes PI3K α , PI3K β and PI3K δ , and class IB, which only includes PI3K γ .¹⁷⁹

PI3K α and PI3K β isoforms are ubiquitously expressed, while PI3K δ and PI3K γ are mainly expressed in leukocytes, giving the opportunity to specifically target inflammatory diseases.¹⁸²

PI3Ks are heterodimers constituted of a catalytic subunit (p110) and a Src-homology 2 (SH2) domain-containing regulatory subunit (Figure 3.7).^{177,181,183} Class IA catalytic subunits can form heterodimers with five different isoforms of regulatory subunit: p85 α , p55 α , p50 α , p85 β and p55 γ (often referred to as p85). By contrast, p110 γ (class IB) is only associated with a p101 regulatory subunit. Class IA isoforms are activated by growth factor-stimulation of receptor tyrosine kinases, *via* interaction of their regulatory subunits with tyrosine-phosphorylated motif (YXXM). Class IB is similarly activated by G-protein coupled receptors (GPCRs). PI3K activity is further enhanced by interaction with GTP-RAS.

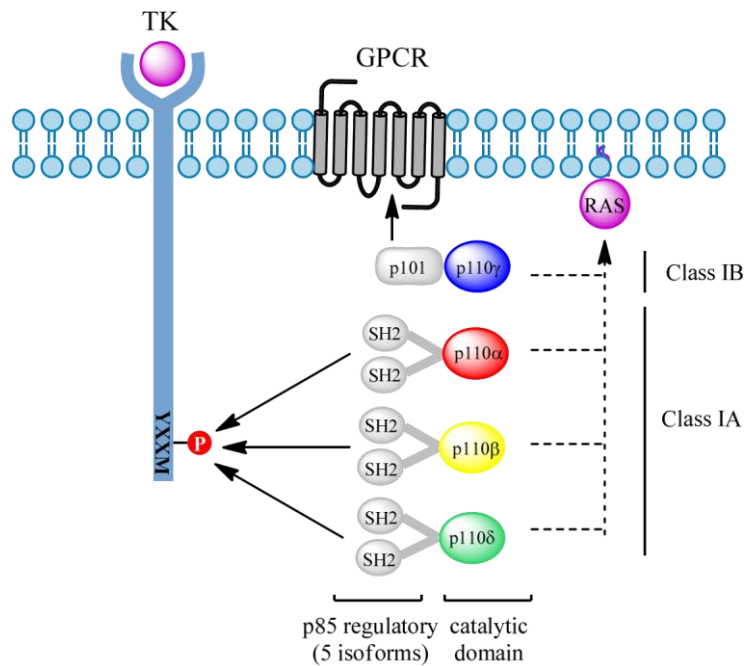


Figure 3.7 Class I PI3K isoforms and their recruitment

Upon receptor activation, PI3Ks convert PI(4,5)P₂ (PIP₂) into PI(3,4,5)P₃ (PIP₃) (Figure 3.8), an important secondary messenger for a variety of signal transduction pathways including cell growth, differentiation, and apoptosis. PI(3,4,5)P₃ is down regulated by either PTEN or SHIP *via* dephosphorylation (Figure 3.6). PI(3,4,5)P₃ generated at the surface of the membrane acts as a membrane tether of proteins containing a pleckstrin homology (PH) domain including protein kinases AKT/PKB and PDK1.^{180,181,184} PDK1 is then activated and, in turn, phosphorylates AKT, which is fully activated by mTOR (Figure 3.8). Once fully activated, AKT activates other downstream proteins, which are important to immune cell functions.^{184,185}

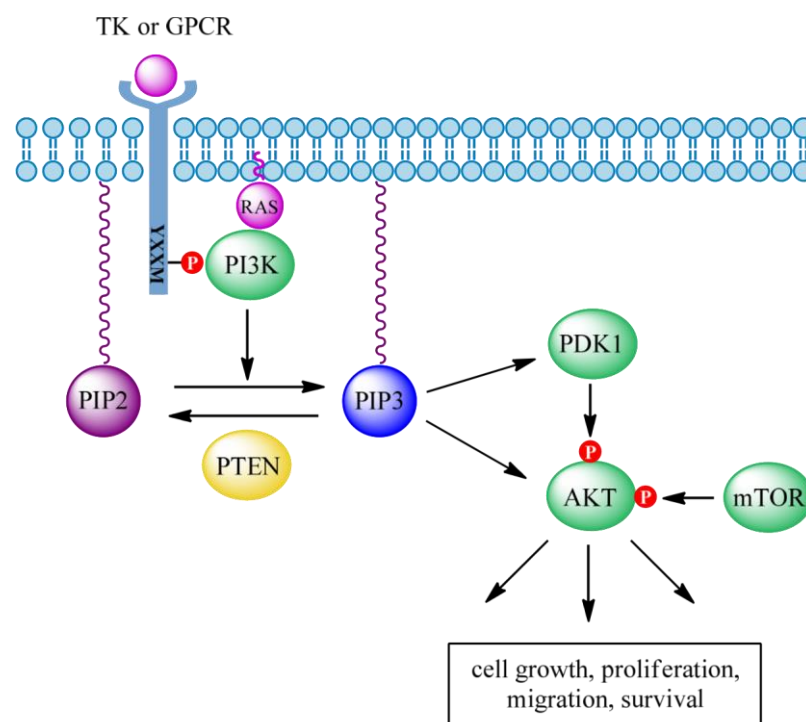


Figure 3.8 Simplified PI3K signalling pathway

3.1.3 PI3K δ Structure and Selective Inhibition

The catalytic subunit of PI3K (p110) consists of five domains (Figure 3.9): an Nterminal adaptor-binding domain (ABD) that binds to p85 (not present in the crystal structure as the domain is cleaved during purification in the crystallography construct),

a RAS-binding domain (), a C2 domain () that likely binds to the cell membrane, a helical domain of unknown function (), the kinase domain (N-lobe and C-lobe). The ATP-binding site is part of the catalytic subunit and is situated between the C-lobe and N-lobe of the kinase domain.

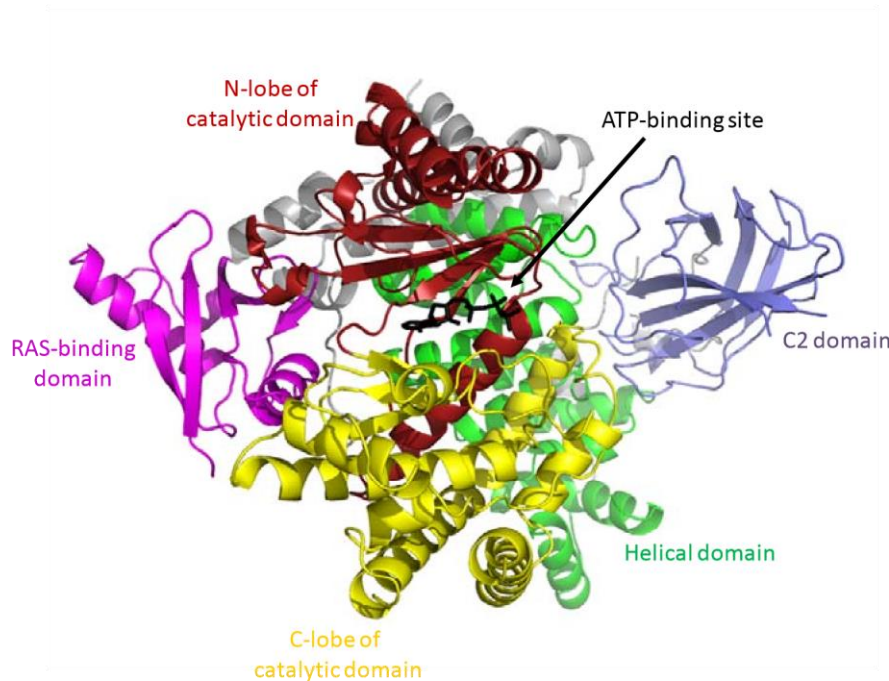
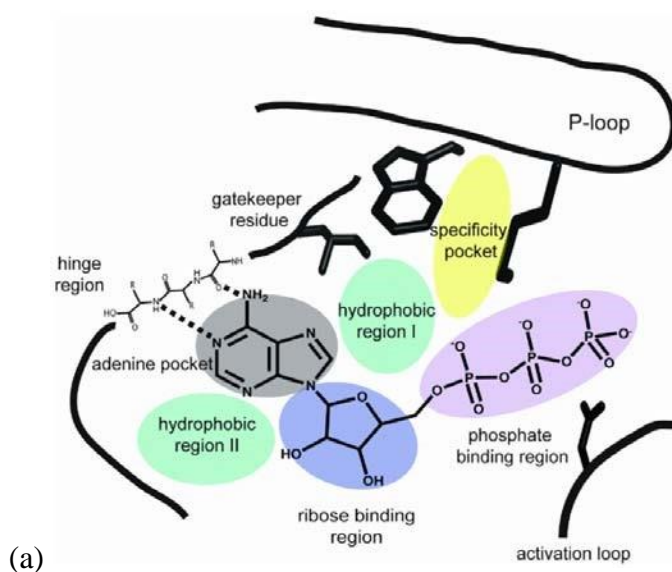


Figure 3.9 p110 δ crystal structure in complex with ATP (2.2 Å) generated in our own laboratory (mouse protein)¹⁸⁶

The majority of the small molecule inhibitors of kinases target the ATP-binding site.¹⁸⁷ Since the ATP-binding site is conserved across the different kinases, selectivity is one of the most important challenges in the discovery of kinase inhibitors. Although the ATP-binding site is quite conserved, the adjacent areas not occupied by ATP are more variable and allow the design of selective inhibitors.¹⁸⁷ In addition, PI3Ks are lipid kinases and their ATP site differs from protein kinases as described below, offering further potential for the design of selective inhibitors.

The ATP-binding site can be divided into five regions important for binding (Figure 3.10): an adenine pocket (near the so-called hinge), an affinity pocket (also known as hydrophobic pocket I, buried region), a hydrophobic region II (solvent exposed), a

ribose binding region, and a phosphate binding region.^{188,189} Kinase inhibitors usually occupy the adenine pocket and make two to three H-bonding interactions with the hinge region *via* its acceptor-donor-acceptor H-bonding pattern. Hinge binding motifs typically consist of flat heterocyclic ring systems.¹⁸⁷ Contrary to protein kinase inhibitors, lipid kinase inhibitors tolerate one to three interactions with the hinge region. In addition, from experience in prosecuting lipid kinase targets in our laboratories, the hinge region has demonstrated the ability to accommodate some 3D-shaped binding motifs, which usually imparts good selectivity over protein kinases. The ribose and phosphate binding sites are rarely exploited. Affinity and selectivity is usually achieved by growing towards the hydrophobic regions. The gatekeeper residue can restrict access to the hydrophobic region I depending on its size and, thus, can contribute to selectivity. In PI3K, the gatekeeper residue is an isoleucine residue, which forms part of the wall of the hydrophobic pocket I and helps to make the PI3K pocket distinct from protein kinases in size and shape.¹⁸⁹ The isoleucine residue is shifted further up and away from the adenine ring of ATP compared to a protein kinase gatekeeper providing more space near the hinge. This space is closed by a conserved Tyr residue (Tyr813 in PI3K δ , Figure 3.10), which is directly in contact with ATP, in contrast to protein kinases. This could explain why more 3D-character is tolerated in lipid kinases such as morpholine hinge binders (Figure 3.11). Based on all the above, selectivity over protein kinases is usually not an issue.



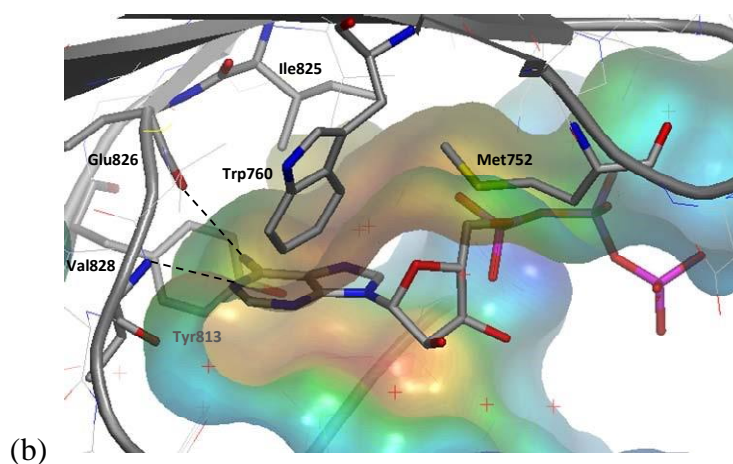
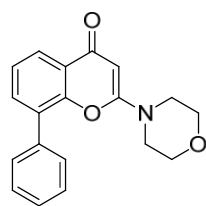
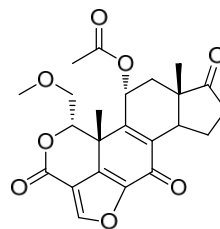


Figure 3.10 (a) PI3K ATP-binding site schematic¹⁸⁹
(b) PI3K δ crystal structure in complex with ATP¹⁸⁶

Within the class I PI3K family, the four isoforms are highly homologous and selectivity between the isoforms can be challenging.^{189,190} Two non-selective PI3K inhibitors (LY294004 **230** and wortmannin **231**, Figure 3.11) have been widely used as tools to investigate and understand the role of PI3K enzymes in cellular function.¹⁹¹ Pan-inhibitors of the PI3K class have also been shown to be useful for the treatment of cancer,¹⁹² such as GDC-0941 (**232**) from Roche (Figure 3.11) currently in Phase I clinical trials for the treatment of breast cancer.



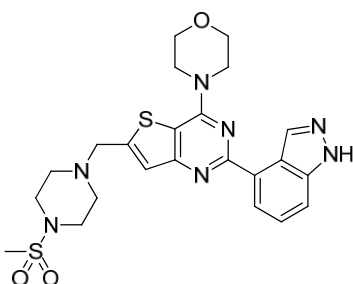
230 LY294004



231 wortmannin

Figure 3.11

Pan-PI3K inhibitors



232 GDC-0941

However, due to the fairly ubiquitous distribution of PI3K α and PI3K β and their vital role for development, their unnecessary inhibition might result in serious adverse effects. Indeed, genetic ablation of PI3K α and PI3K β has shown to result in early embryonic lethality.^{193,194} In addition, PI3K α is also involved in insulin signalling and glucose metabolism.¹⁹⁵ Thus, their inhibition could be detrimental when targeting the related PI3K δ driven diseases. By contrast, however, PI3K δ and PI3K γ knock-out mice are viable but are immune deficient, suggesting that inhibition of these targets is a therapeutically viable approach.¹⁹⁶⁻¹⁹⁸

More recently, several selective PI3K δ inhibitors have been reported in the literature (Figure 3.12) along with structural hypotheses behind the isoform selectivity, and some of these compounds have entered clinical trials.^{188,191,199-201} For example, GS1101 (**234**) originally from Calistoga and now Gilead, a derivative of the selective IC-87114 (**233**), has recently been approved for the treatment of acute myeloid leukemia and B-

cell chronic lymphoid leukemia.²⁰² GSK2269557 (**235**) developed in our own laboratories is currently in Phase II clinical trials for the treatment of COPD.²⁰³

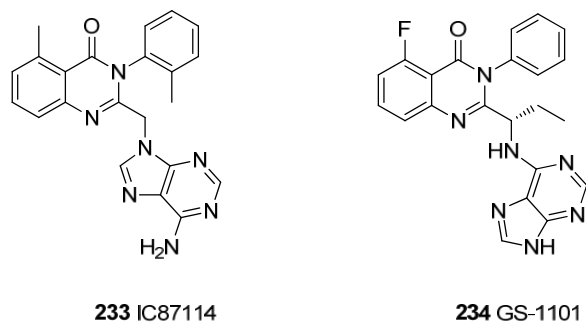
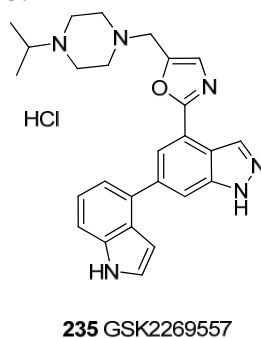


Figure 3.12 Selective PI3K δ inhibitors



Biological data of these selective PI3K δ inhibitors generated in our assays are shown in Table 3.1.

Compounds	233	234	235
administration	oral	oral	inhaled
pIC ₅₀ (δ)	6.9	8.1	9.4
LE, LLE _{AT}	0.32; 0.31	0.36; 0.31	0.39; 0.32
pIC ₅₀ (α , β , γ)	<4.6; <4.6; 5.0	5.0; 5.8; 6.6	5.2; 5.6; 5.0 ^a

fold-selectivity (α , β , γ)	200; 200; 80	1,259; 200; 32	> 6,000
chromlogD_{7.4}	3.4	3.2	2.5
PFI	8.4	8.2	7.6

Table 3.1 Biological data of known selective PI3K δ inhibitors in our assay

^aCompound reported inactive (pIC₅₀ < 4.6) in one out of the nine test occasions.

Most of the selective PI3K δ inhibitors are propeller-shaped in nature (e.g. **233** ●, Figure 3.13).¹⁸⁸ Murine crystal structures indicate that these inhibitors stabilise a conformational change that opens a novel pocket between Trp760 and Met752, referred to as the specificity pocket (Figure 3.10).¹⁸⁸ In PI3K α and PI3K β isoforms, this region is less flexible and this conformational change is not possible.^{188,189} For example, compound **233** exhibits 80-200 fold selectivity over the other PI3K isoforms and greater selectivity (400-4,000 fold) over related kinases C2 β , Vps34, DNA-PK, and, mTOR, and no activity over an additional 402 kinases.²⁰² More recently, a second group of inhibitors have been reported, which do not induce the selectivity pocket but pack against Trp760 making favourable hydrophobic contacts (e.g. **235** ●, Figure 3.13).^{188,200,203} Trp760 is conserved across other PI3K isoforms, however the residues that interact with Trp760 are not. A key difference is a threonine residue found at position 750 in PI3K δ . In other isoforms, the residue corresponding to Thr750 is a larger lysine or arginine residue, which reduces access to the face of Trp760 and, thus, gives opportunity to design selective inhibitors.^{188,200} Compared to the propeller-shaped inhibitors, this approach is less validated as only few examples have been reported.^{188,200,201} The inhaled compound **235** developed elsewhere in our laboratories took advantage of this approach to gain excellent PI3K δ selectivity (> 6,000 fold-selectivity over PI3K isoforms and more than 250 kinases).²⁰³

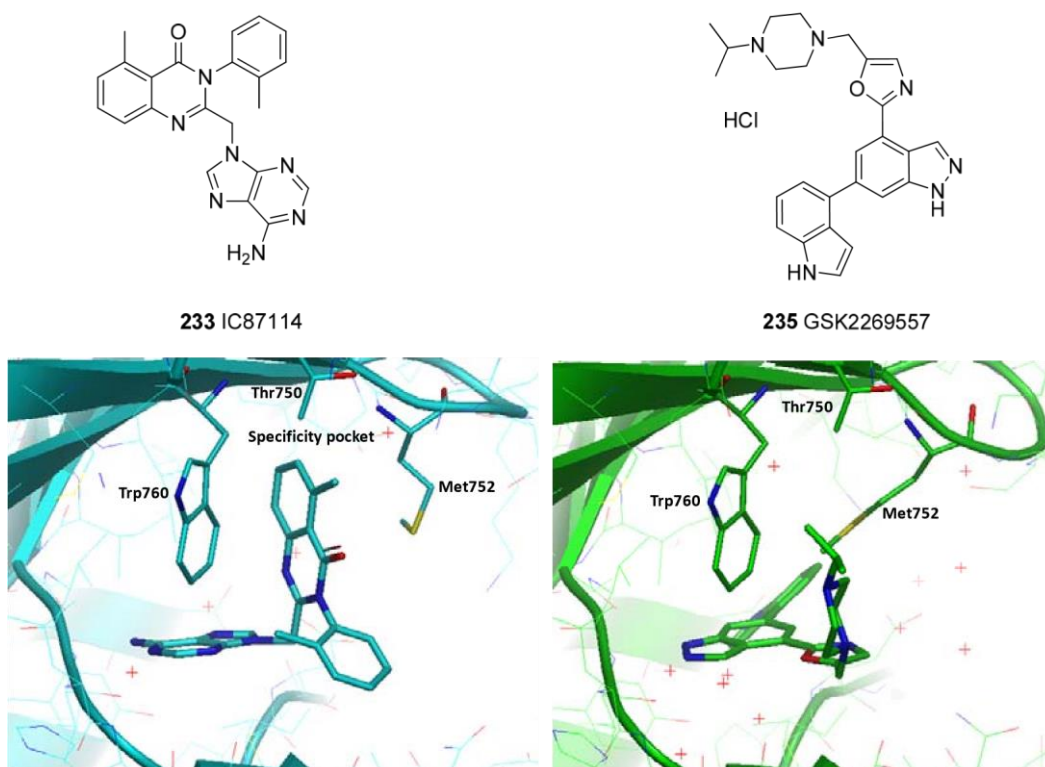


Figure 3.13 Crytal structures of PI3K δ in complex with inhibitors IC-87114 **233** (●, 2.2 Å - pdb 2X38)¹⁸⁸ and GSK2269557 **236** (●, 2.4 Å - in house)¹⁸⁶

3.2 Aims

As discussed above, previous research in our group had identified a selective PI3K δ inhibitor, which is dosed through the inhaled route. The objective of this research effort was to identify a selective inhibitor of PI3K δ for the treatment of respiratory diseases suitable for oral dosing. The candidate molecule needs to combine good human whole blood potency (hWB), isoform and kinase selectivity, appropriate physicochemical properties for an oral drug, and a suitable pharmacokinetic profile for once daily dosing.

The target candidate profile is described in Table 3.2.

PI3K δ hWB pIC ₅₀	≥ 7
-------------------------------------	----------

LE, LLE_{AT}	≥ 0.3
chromlogD_{7.4}	< 4
Ar ring	≤ 3
selectivity	> 100 -fold against PI3K isoforms and key kinases
CLND solubility	> 200 $\mu\text{g/mL}$
FaSSiF solubility	> 100 $\mu\text{g/mL}$
off-target activity	No hERG, P450 issues
PK profile	Suitable for once daily oral dose

Table 3.2 Candidate Profile

The human whole blood potency target of $\text{pIC}_{50} \geq 7$ was chosen in accordance with known PI3K δ inhibitors (e.g. oral PI3K δ inhibitor GS-1101 **234**, hWB $\text{pIC}_{50} = 6.7$ in our hands)²⁰⁴ and should facilitate achieving the desired *in vivo* efficacy. Greater than 100-fold selectivity over PI3K isoforms is required to avoid potentially toxic side effects. As discussed above, PI3K α and PI3K β play a vital role for development and their inhibition would result in serious adverse effects. Accordingly, selectivity over other lipid kinases and protein kinases is therefore key to avoid potential side effects. As intimated previously, selectivity over protein kinases is usually achieved by making one H-bonding interaction with the hinge and exploiting the affinity pocket. Isoform selectivity can be achieved by either exploiting the specificity pocket or interaction with Trp760.

Throughout our optimisation trajectory, it was important to tightly control physicochemical properties in order to reduce the risk of toxicity and increase the probability of achieving good pharmacokinetic profile.^{8,9,12} A useful metric proposed by Young *et al.* to achieve this suggested that the molecules should have chromlogD_{7.4} below four and no more than three aromatic rings.^{16,20} Indeed, highly lipophilic compounds are more likely to be insoluble and, thus, poorly absorbed. In addition, molecules of this nature tend to be extensively metabolised (greater affinity towards

cytochrome P450 enzymes)²⁰⁵ and be highly protein bound, which means little of the drug would be available to exert its action at the target of interest. In terms of measured physicochemical properties, chemi-luminescent nitrogen detection (CLND) solubility is considered high above 200 µg/mL. CLND solubility is a high throughput method used in our laboratories, which provides a good measure of the kinetic solubility of compounds.²⁰⁶ For more advanced compounds, FaSSIF (Fasted State Simulated Intestinal Fluid) solubility, which uses a biologically relevant gastrointestinal media and solid compound, is also measured. FaSSIF solubility is more relevant for oral administration and a target of greater than 100 µg/mL is found to increase the probability of good absorption. The FaSSIF solubility assay was a lower throughput than the CLND solubility assay and is therefore reserved for key compounds. There are also many off-target activities that are undesirable in a drug candidate, such as hERG inhibition, which would potentially result in cardiovascular side effects.²⁰⁷ Consequently, activity at any of these anti-targets must be avoided.

The general pharmacokinetic parameters considered in our laboratory to be suitable for an oral drug are listed in Table 3.3.^{208,209}

	Desired profile
Clearance Cl_b	< 1/3 liver blood flow rat < 26 mL/min/kg
Half-life $t_{1/2}$	rat ~ 2 h
V_{dss}	1-4 L/kg
Bioavailability F%	> 30 %

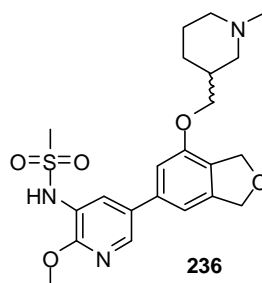
Table 3.3 Desired PK Profile for once daily oral dose

Clearance (Cl_b) links the rate of elimination to the drug concentration. It is defined as the volume of blood cleared of drug per unit of time and is linked to metabolism. The

greater the metabolism, the higher the clearance. High clearance may result in low exposure, low bioavailability, and a short half-life. On the other hand, low clearance might result in accumulation and potentially raise risks of toxicity associated with the compound. Ideally for an oral drug, clearance should be lower than 1/3 of liver blood flow (LBF in rat is approximately 78 mL/min/kg). The volume of distribution (V_{dss}) corresponds to the partitioning of the drug in the body between plasma and the rest of the body. If the volume of distribution is too low for a target in the tissues, the drug may not reach the site of action and the half-life may be low. It can also reflect high plasma protein binding (PPB). The half-life ($t_{1/2}$) corresponds to the time required to reduce the drug concentration by half. It thus depends on clearance and volume of distribution. For a once daily oral drug, rat $t_{1/2}$ should be approximately 2 h.^{208,209} Finally, oral bioavailability (F%) defines how much drug is absorbed after an oral dose. It corresponds to the fraction of drug that reaches the systemic circulation after oral absorption. The levels of bioavailability are determined by a combination of absorption through the gut and first pass metabolism through the liver.

3.3 Lead Series – Dihydrobenzofuran Template

At the inception of this work, a series of potent and moderately selective molecules had been identified as a result of earlier efforts in our laboratories.²¹⁰ The lead molecule **236** (racemic mixture initially, Figure 3.14) showed good enzyme potency, good overall physicochemical properties for an oral drug and achieved the target hWB potency of 7.0. However, the compound had only moderate selectivity against PI3K isoforms.



PI3Kδ pIC₅₀	8.3
LE, LLE_{AT}	0.37 ; 0.35
PI3K pIC₅₀ Fold selectivity	α 6.4 β 6.7 ^a γ 5.8 α 79 β 40 γ 316
PI3Kδ hWB pIC₅₀	7.1
chromlogD_{7.4}	2.2
CLND solubility	≥ 230 $\mu\text{g/mL}$

Figure 3.14 Lead PI3K δ inhibitor **236**

Colour coding: green = desired; orange = borderline; red = undesired ^aCompound failed to fit a curve in one out of the six test occasions

3.3.1 Research Objective

From consideration of the profile of the lead compound **236** above, the objective of the current study was to improve isoform selectivity of the lead molecule **236** whilst keeping the physicochemical properties in an acceptable range for an oral drug.

Compound **236** was successfully crystallised in the murine PI3K δ active site (3.0 Å) as shown in Figure 3.15 to confirm the binding mode and suggest ways to improve selectivity.¹⁸⁶

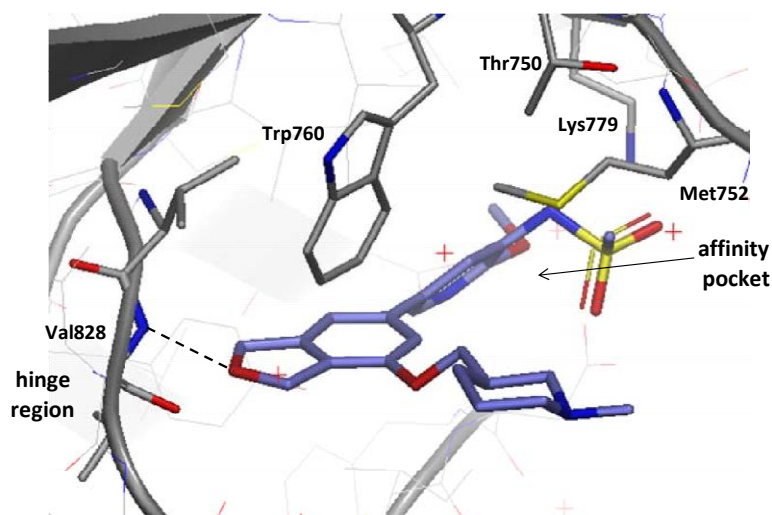


Figure 3.15 Crystal structure of PI3K δ in complex with lead compound **236** (3.0 Å)

Analysis of this structure revealed that the oxygen of the dihydrobenzofuran ring forms a key hydrogen bond with Val828 in the hinge region. Lipid kinases such as PI3K δ have the ability to accommodate an sp^3 -hinge binder, which furnishes good selectivity over other protein kinases but also offers advantages in terms of physicochemical properties of the molecules. Indeed, kinase hinge binders encountered in the literature are often flat and aromatic similar to the adenine moiety in ATP, which can impact on the physicochemical properties of the molecules (e.g. solubility).¹⁸⁷ From this crystal structure, Lys779 is pointing toward the sulfonamide NH and, thus, could potentially make an interaction with the ligand. Previous work around the pyridine sulfonamide had indicated that this moiety was key for activity.²¹⁰ It is believed that the sulfonamide is deprotonated at physiological pH due to its relative acidity (measured $pK_a = 7.6$) and thus would make a stronger interaction with the Lys residue. The compound does not induce the selectivity pocket as observed with other PI3K δ selective inhibitors (propeller-shape inhibitors, see section 1.3). However, selectivity could be achieved by interacting with Trp760 in a similar manner to the progenitor inhaled compound **236**. As mentioned previously, the residues corresponding to Thr750 are larger in other PI3K isoforms (Lys or Arg), which reduce access to the face of Trp760 and, thus, offers opportunity to design selective inhibitors. Recently, it has been shown that packing

against the indole ring of Trp760 was favourable and increased isoform selectivity (see section

3.1.3).^{200,201}

The crystal structure suggested there was space to add substituents on the piperidine group of **236** towards Trp760 (Figure 3.16). As it is mainly solvent exposed and presents no clear interaction with the protein, it was hypothesised that other substituents could be added to improve selectivity of the compound. Additional steric bulk on the piperidine ring (e.g. Me, *i*-Pr) might be able to pack against Trp760 and improve selectivity.

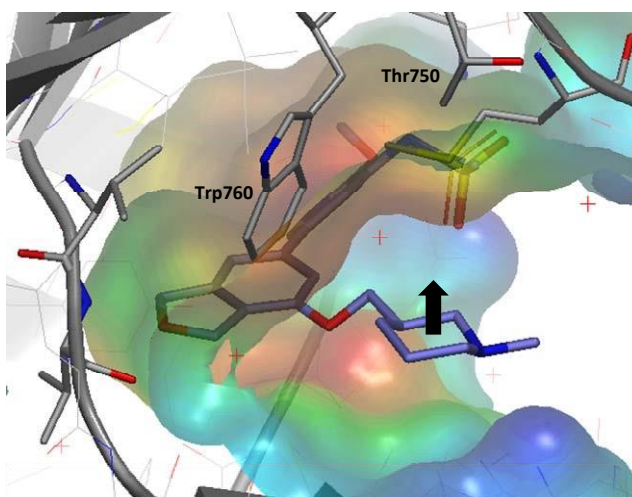


Figure 3.16 Crystal structure of PI3K δ in complex with lead compound **236** showing potential to grow towards Trp760 from the piperidine ring

A selection of compounds was thus designed to increase selectivity through interaction with Trp760. Based on this, initial studies focused on the introduction of an isopropyl group on the piperidine ring to test our hypothesis as described in Figure 3.17. Both the NH and *N*-Me analogues were planned. Previously, the NH piperidine analogue had shown poor permeability and *N*-methylation improved this significantly by

removing a hydrogen bond donor. Amines tend to ionise under physiological conditions, which can lead to poor membrane penetration due to the polarity of the molecule. If a molecule is too polar, it will not be able to cross the fatty exterior of the cell membrane by passive diffusion. However, by adding a lipophilic group around the NH, the associated polarity will be masked by lipophilicity, which will potentially impact favourably on permeability.

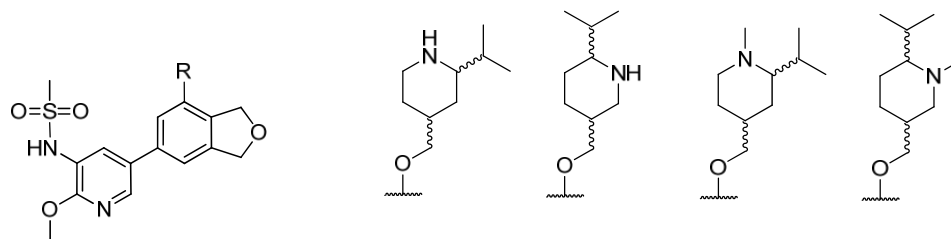


Figure 3.17 Target molecules designed to improve selectivity of the lead series

3.3.2 Results and Discussion

3.3.2.1 Retrosynthetic Analysis

A retrosynthetic approach to make the desired compounds is described in Figure 3.18. The first disconnection of compound **237** at the phenol junction led to the dihydrobenzofuran phenol **239** and the alcohol **238**. Subsequently, the desired dihydrobenzofuran **239**, previously prepared by other members of our laboratories,²¹¹ was synthesised by [2+2+2] alkyne cyclotrimerisation from compounds **240** and **241**.

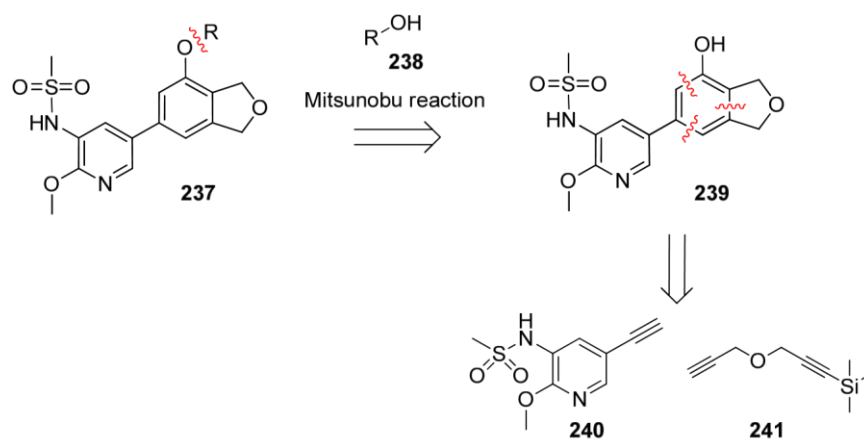
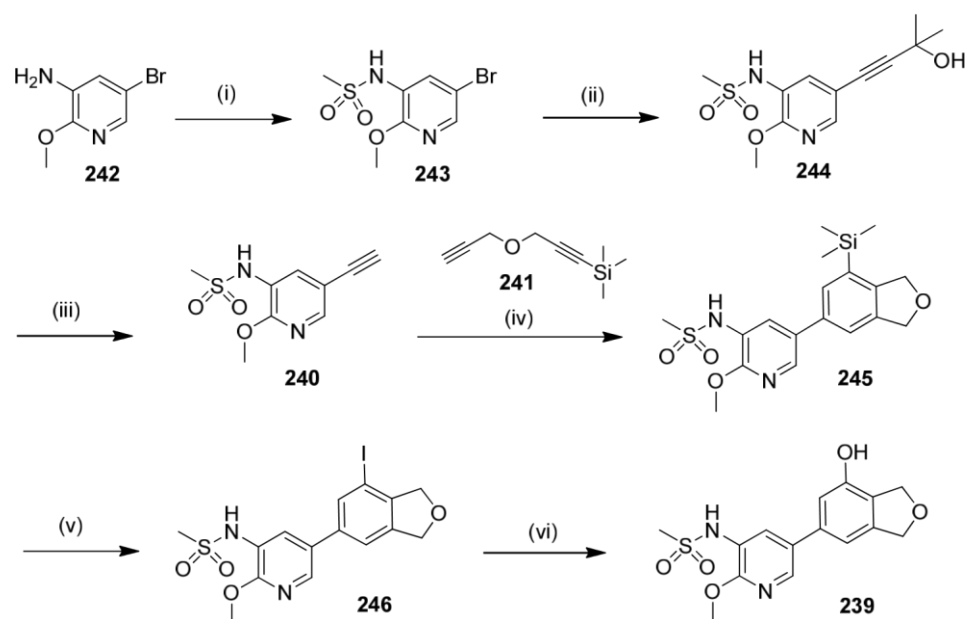


Figure 3.18 Retrosynthetic analysis

The forward synthetic route to make the dihydrobenzofuran phenol intermediate **239**, previously developed elsewhere in our group,²¹¹ is summarised in Scheme 3.1.



Reagents and conditions: (i) MeSO_2Cl , Py, MeCN, rt, 3 h, 80%; (ii) 2-methylbut-3-yn-2-ol, CuI, $\text{Pd}(\text{PPh}_3)_2\text{Cl}_2$, Et_3N , 2Me-THF, 85 °C, 37 h followed by rt, 2 days, 79%; (iii) KOH, *i*-PrOH, reflux, overnight, 73%; (iv) $\text{RuCp}^*(\text{cod})\text{Cl}$ (10 mol%), CPME, rt, 2 h, 66%; (v) ICl, DCM, -10 °C-rt, 1 h, 80%; (vi) $n\text{Bu}_4\text{NOH}$, 2-methylquinolin-8-ol, CuI, DMSO, μwave , 120 °C, 2 h, 62%.

Scheme 3.1

Alkyne [2+2+2] cyclotrimerisation is a common and efficient method to synthesise the dihydrobenzofuran moiety.²¹² In line with this, Yamamoto and co-workers have reported a highly efficient and *meta*-regioselective ruthenium-catalysed [2+2+2] cyclotrimerisation of unsymmetrical 1,6-diynes.²¹³ In addition, the ruthenium catalyst has shown to be tolerant to a wide range of functionality. Based on this encouraging precedent, this method was selected for use within our laboratory in order to construct the current template. Firstly, the desired silyl diyne intermediate **241** was prepared by reaction of the corresponding symmetric ether diyne with LHMDS and TMSCl following the procedure of Cheng and co-workers.²¹⁴ The alkyne **240** was prepared in three steps from the amino starting material **242**. The requisite sulfonamide intermediate **243** was obtained by reaction of the amine **242** with methylsulfonyl chloride in presence of pyridine. Subsequently, the alkyne group was introduced using a Sonogashira approach from **243**, followed by removal of the tertiary alcohol using potassium hydroxide to give the desired alkyne intermediate **240**. The dihydrobenzofuran intermediate **245** was then obtained by [2+2+2] cyclotrimerisation using a ruthenium catalyst and the desired alkyne pyridine **240** as described by Yamamoto and co-workers.²¹³ The trimethylsilyl group was subsequently converted to the corresponding iodide intermediate **246** through iododesilylation using iodine chloride.^{215,216} Finally, the desired phenol intermediate **239** was obtained by hydroxylation of the aryl iodide **246** with tetrabutylammonium hydroxide in presence of copper(I) iodide and 2-methylquinolin-8-ol, as recently reported by Paul and co-workers.²¹⁷ At the outset of this work, both intermediates **239** and **246** were available in large quantities in our laboratories.

In the initial stages of this optimisation effort, the main focus was on the synthesis of the protected piperidine alcohol intermediates **247** and **248** for the Mitsunobu step (Figure 3.19). Use of a suitable protecting group (in this case benzyl) was required to avoid side reactions during the Mitsunobu step.

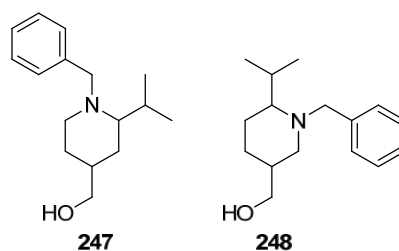


Figure 3.19 Piperidine alcohol intermediates

Substituted piperidines can be prepared by a variety of methods.²¹⁸ A simple and straightforward strategy is by hydrogenation of the corresponding pyridines. The retrosynthetic strategy described in Figure 3.20 was thus selected to prepare the target piperidine alcohols. It was reasoned that alcohol **247** could be obtained by reduction of the corresponding ester **249**, which itself could be formed by protection of the amine **250**. The piperidine system **250** could be obtained by hydrogenation of the corresponding pyridine intermediate **251**. In turn, disconnection of pyridine **251** led to commercially available compound **252**. The requisite isopropyl group can easily be introduced *via* a Suzuki-Miyaura coupling.

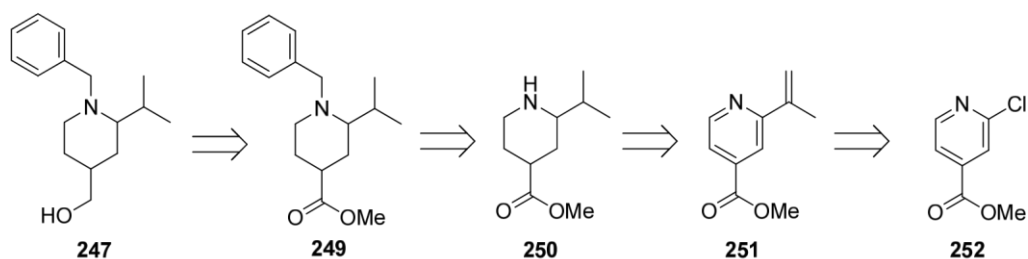


Figure 3.20 Retrosynthetic analysis of piperidine alcohol **247**

A similar approach can be applied to the piperidine alcohol **248** by starting from the commercially available pyridine **256** (Figure 3.21).

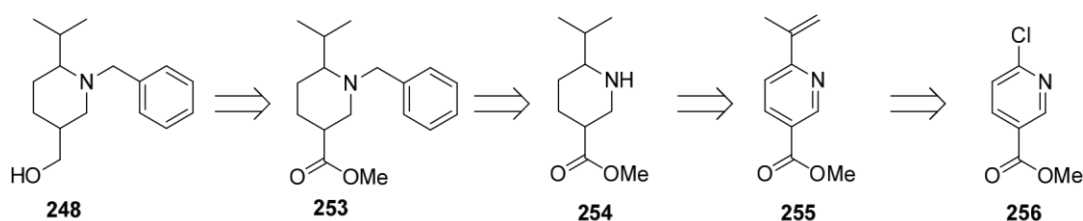


Figure 3.21 Retrosynthetic analysis of piperidine alcohol **248**

3.3.2.2 Synthesis of Piperidine **247**

3.3.2.2.1 Suzuki-Miyaura Coupling

The first step corresponds to the introduction of the isopropene group *via* a Suzuki-Miyaura coupling of the chloropyridine. The Pd-catalysed Suzuki-Miyaura reaction is one of the most efficient and popular transformations for C-C bond formation due to its versatility.^{219,220} The key advantages that make it so popular are the mild reaction conditions and the commercial availability of a range of boronic acids. In addition, the reagents are easy to handle and less toxic than in comparison to other methods (e.g. organostannanes). The reaction is not affected by the presence of water and tolerates a broad range of functional groups.

First disclosed in 1979,²²¹ the Suzuki-Miyaura reaction involves the reaction of an aryl/vinyl organoboron **258** with an aryl/vinyl halide **257** catalysed by palladium (Figure 3.22).

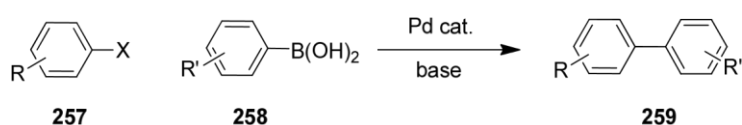


Figure 3.22 Suzuki-Miyaura reaction

Traditionally, the reaction used aryl bromides and iodides. However, triflates ($\text{OSO}_2\text{CF}_3 = \text{OTf}$) are also now commonly used. As the rate determining step is

oxidative addition, the choice of the aryl halides plays an important role in the rate of the reaction (relative reactivity: R-I > R-OTf > R-Br >> R-Cl). Originally, aryl chlorides were avoided due to their slow reactivity. However, as they are abundant and cheap, there has been considerable attention to develop conditions that would promote the reaction of aryl chlorides.²¹⁹

The mechanism of the reaction is described in Figure 3.23.^{222,223} The first step consists of an oxidative addition of Pd⁰ (**I**) with the aryl halide to afford the Pd^{II} complex (**II**). The halide is then displaced by the base to give a more reactive complex (**III**).²²³ The base also activates the boron reagent, which can then react with the intermediate (**III**) *via* transmetalation to give the organopalladium species (**V**). Finally, reductive elimination gives the desired product **259** and regenerates the palladium catalyst.

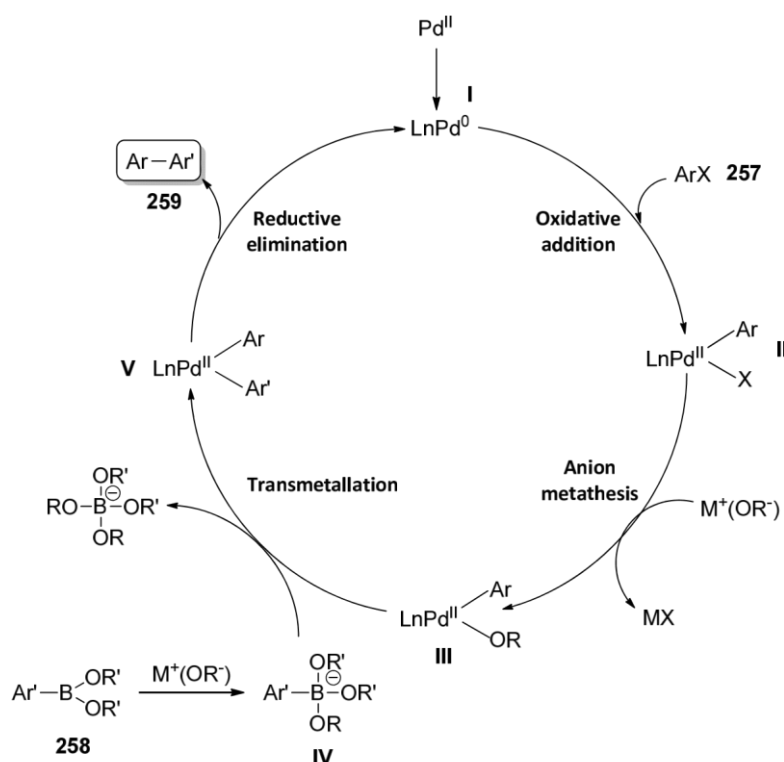
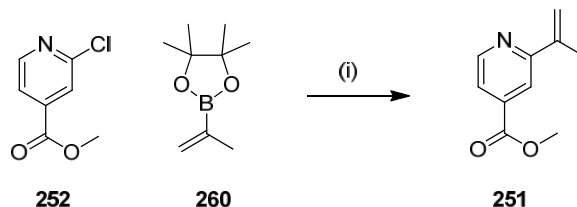


Figure 3.23 Mechanism of Suzuki-Miyaura reaction

The synthesis of the desired intermediate **251** was previously reported by Whelligan and co-workers and thus offered a good starting point.²²⁴ The conditions used in this publication are described in Scheme 3.2.

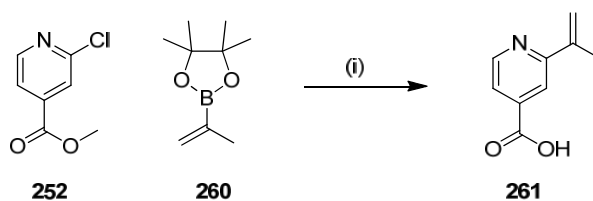


Reagents and conditions: (i) SPhos (6 mol%), Pd(OAc)₂ (3 mol%), K₃PO₄, MeCN/H₂O (3:2), 120 °C, 1 h, 31%.

Scheme 3.2 Literature preparation of compound **251** by Whelligan and co-workers²²⁴

The reaction was catalysed by palladium(II) acetate in presence of SPhos and potassium phosphate as base. Dialkylbiaryl phosphine ligands have been extensively used in cross coupling reactions due to their stability and wide scope.²²⁵ SPhos has shown to be particularly efficient, easy to handle and, thus, seemed a reasonable choice.²²⁶ The low yield was attributed to the partial hydrolysis of the ester and it was reasoned that this could be improved by further optimisation of the conditions such as the ratio of water in the reaction.

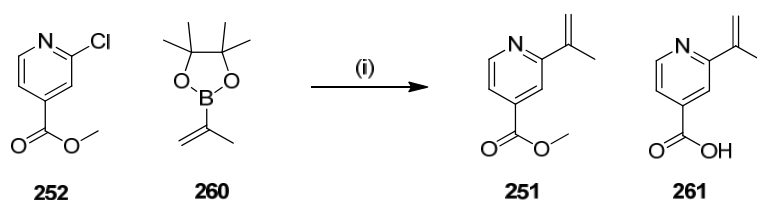
Initially, these conditions were applied, and in our hands resulted in complete conversion to the carboxylic acid analogue (**261**) as shown in Scheme 3.3 (observed by LCMS, product not isolated). As observed by Whelligan and co-workers, the carboxylic acid product was difficult to isolate from the aqueous layer and, thus, it was decided to tune the conditions to obtain the desired ester.



Reagents and conditions: (i) SPhos (7 mol%), Pd(OAc)₂ (3 mol%), K₃PO₄, MeCN/H₂O (3:2), 130 °C, 1 h, μ wave, product not isolated.

Scheme 3.3

The conditions investigated to maximise formation of the desired ester product **251** are summarised in Table 3.4.



Reagents and conditions: (i) SPhos (10 mol%), Pd(OAc)₂ (6 mol%), K₃PO₄, MeCN/H₂O, μ wave.

Scheme 3.4

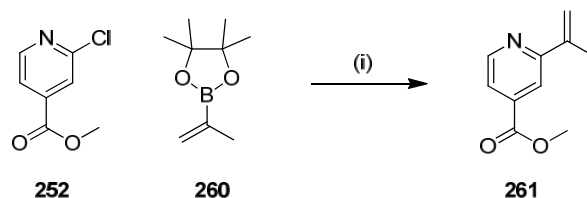
Entry	MeCN/H ₂ O ratio	T (°C)	t (h)	LCMS %area		
				252	251	261
1*	3:2	130 °C	1	0	0	100
2	3:2	100 °C	1	0	37	55
3	10:1	100 °C	1	9	67	1
4	10:1	120 °C	1	4	70	4

Table 3.4 Suzuki conditions screening *

SPhos (7 mol%), Pd(OAc)₂ (3 mol%)

Reduction of temperature to 100 °C (entry 2) reduced the formation of the carboxylic acid, however the acid still remained as the major product. Based on this, it was believed that water present in the reaction mixture was also influencing the ester hydrolysis. Further examination of the literature to convert chloropyridine to the isopropene analogue revealed that a range of conditions have been used but also the

ratio of solvent/water was very variable (between 1:1 to 10:1).²²⁷⁻²²⁹ In order to reduce the carboxylic acid formation, a ratio of acetonitrile/water 10:1 was attempted (entry 3). Under these conditions, little carboxylic acid product was observed but at 100 °C starting material remained. Accordingly, the temperature was increased to 120 °C in order to achieve better conversion (entry 4). In these conditions, some starting material and carboxylic acid by-product remained but the desired product was the major component of the reaction mixture. At this stage, no further optimisation was attempted and these conditions were thus selected for the synthesis of intermediate **251** (Scheme 3.5). On scale-up, starting material was fully consumed and only 7% of carboxylic acid by-product was observed by LCMS. The final product **251** was isolated by normal phase chromatography to give the pure desired material in 55% yield.



Reagents and conditions: (i) SPhos (10 mol%), Pd(OAc)₂ (8 mol%), K₃PO₄, MeCN/H₂O (10:1), 120 °C, 1 h, μ wave, 55%.

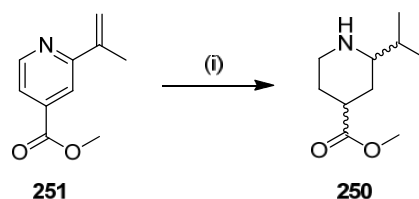
Scheme 3.5 Optimised conditions for the synthesis of the vinyl pyridine **261**

3.3.2.2.2 Reduction of Pyridine

In the next step, the pyridine ring was hydrogenated to the piperidine analogue with concomitant reduction of the isobutene group. Hydrogenation is an efficient way to access piperidines, provided the corresponding pyridine analogue is easily accessible. A variety of catalysts such as PtO₂, Raney Ni, RuO₂, Rh/C and Pd/C, have been described to fully reduce pyridines.²³⁰⁻²³² One drawback is that this method requires harsh reaction conditions (high temperature and pressure), which are not compatible with all functionalities. Milder conditions have been investigated *via* the hydrogenation

of more reactive pyridinium salts and pyridine *N*-oxides.²³³⁻²³⁵ More recently, metal-free direct hydrogenation has also been investigated.²³⁶

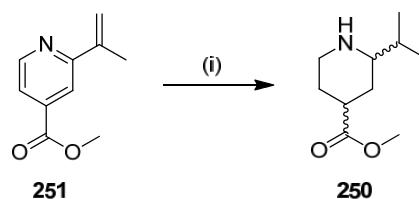
Whelligan and co-workers reported direct hydrogenation of compound **251** using platinum oxide (8 mol%) in acetic acid at 50 °C under 50 psi pressure in moderate yield (43%) as described in Scheme 3.6.²²⁴



Reagents and conditions: (i) PtO₂ (8 mol%), H₂, AcOH, 50 °C, 50 psi, 18 h, 43%.

Scheme 3.6 Literature preparation of compound **250** by Whelligan and co-workers²²⁴

Accordingly, these conditions were first investigated as the product could be obtained in one step. In an effort to improve the yield of the previously described process, the reaction was carried out at a variety of temperatures (Table 3.5). The reactions were followed qualitatively by TLC and LCMS, with the disappearance of starting material being monitored in each case.



Reagents and conditions: (i) PtO₂ (x mol%), H₂, AcOH, T, 4 bar, 18 h.

Scheme 3.7

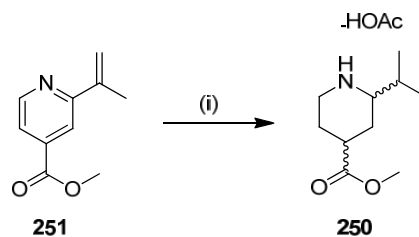
Entry	PtO ₂ (mol%)	T (°C)	t (h)	LCMS	TLC
1	8	30 °C	18	251 observed	251 observed
2	8	50 °C	18	251 observed	251 observed
3	8	80 °C	18	251 observed	251 observed

4	16	50 °C	18	no 251	no 251
---	----	-------	----	---------------	---------------

Table 3.5 Screening of hydrogenation conditions

At 30 °C and 50 °C, starting material remained. Increasing the temperature to 80 °C appeared to improve the conversion to desired product but starting material still remained (weaker LCMS signal and TLC spot). It was thus decided to increase the catalyst loading to 16 mol% and keep the temperature at 50 °C in order to achieve full conversion (entry 4).

Based on this small survey of reaction conditions, the pyridine **251** was hydrogenated in acetic acid in the presence of PtO₂ (17 mol%) at 60 °C under 4 bar pressure to give quantitative conversion to the desired piperidine **250**, as the acetic acid salt (Scheme 3.8).



Reagents and conditions: (i) PtO₂ (17 mol%), H₂, AcOH, 60 °C, 4 bar, 4 h, no isolated yield – crude product progressed.

Scheme 3.8

Initial attempts to isolate the product using a basic aqueous work-up resulted in no material being recovered. Thus, the crude product was directly used in the next step, using an excess of base to neutralise residual acetic acid. In order to improve the isolation of the compound, an SCX cartridge could be used in the future.

NMR analysis of the crude product showed two sets of signals suspected to correspond to the *cis*- and *trans*-diastereoisomers (ratio 1:4 *trans/cis* from -OCH₃ signals H11 ~3.6

ppm, Figure 3.24). This was also observed by other groups when carrying similar reactions.²³⁰ In most cases, a mixture of diastereoisomers is observed with variable ratio. The diastereoselectivity obtained could be improved by investigating different catalysts and reaction conditions. For example, Steiner *et al.* have demonstrated that diastereoselectivity could be improved on their system by using mixed catalysts (Pd-Rh).²³⁷ We elected to proceed with the mixture, which would be separated later. In any case, as at this stage it was not known which geometry would be preferred in terms of kinase inhibition, therefore having a mixture would allow us to obtain all the diastereoisomers in one synthetic protocol.

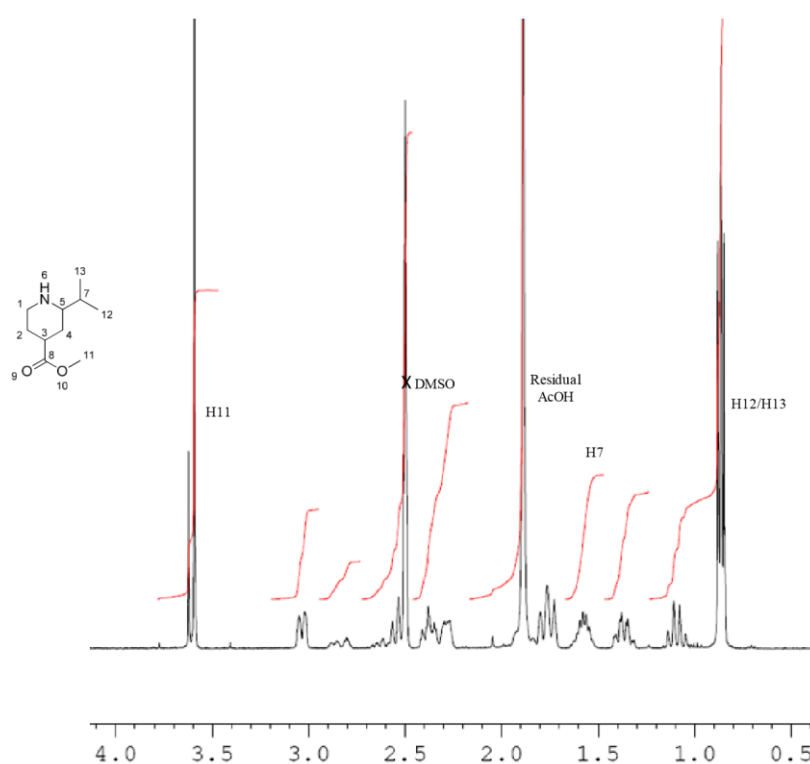
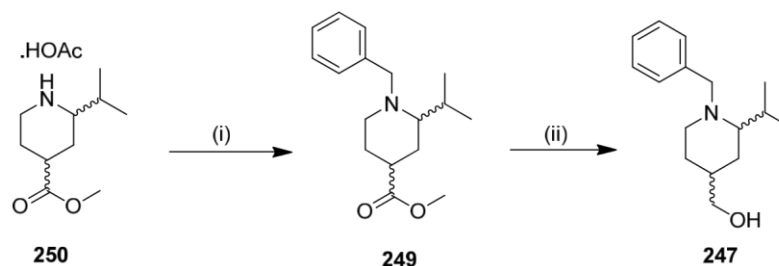


Figure 3.24 ¹H NMR spectra of crude product **250**

3.3.2.2.3 Reduction of Ester into Alcohol

To avoid any potential side reaction during the Mitsunobu step, the amine was first protected. To facilitate convenient monitoring of the reaction by LCMS, the benzyl

protecting group was selected. In addition, the benzyl group could be removed under hydrogenolysis conditions at the same time as the *para*-methoxybenzyl protecting group, which was to be utilised on the sulfonamide portion of the final target compound. The protection of piperidine **250** was carried out using benzyl bromide and potassium carbonate in acetonitrile (Scheme 3.9). The final product **249** was isolated using an aqueous work-up. Given the small amount of compound obtained, it was decided to progress the crude mixture to the next step without any purification.



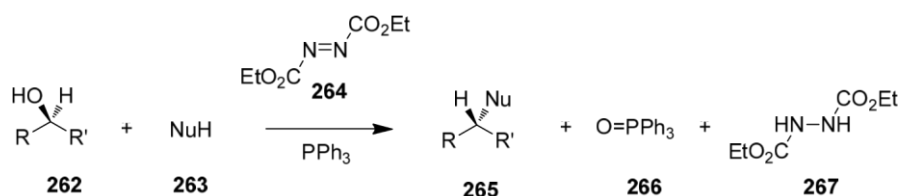
Reagents and conditions: (i) BnBr, K₂CO₃, MeCN, rt, 2 h, crude; (ii) DIBAL-H, THF, -78 °C to 0 °C, 25 h, 17% over three steps including previous hydrogenation.

Scheme 3.9

Finally, the ester was reduced using DIBAL-H as reducing agent, which had been shown to work well on similar systems previously prepared within our laboratories.²³⁸ On this system, the reduction was found to be slow and even after addition of extra equivalents of DIBAL-H, the reaction could not be driven beyond 70% conversion by LCMS (% by area). Conversion to the desired alcohol could be improved by investigating alternative reducing agents such as LiAlH₄. However, the decision was taken to isolate the desired product at this level of conversion and, accordingly, the crude product was purified by normal phase chromatography. Although TLC indicated good separation of the two diastereoisomers, they could not be isolated in satisfactory purity. LCMS and NMR analysis of the purified mixture showed a diastereomeric ratio of 4:1 *cis/trans*. To improve the yield, purification by SCX column could be used both after the hydrogenation and the piperidine protection to isolate the intermediates. However, at this stage of the project, a sufficient amount of the desired intermediate was obtained to prepare the desired final compounds for testing.

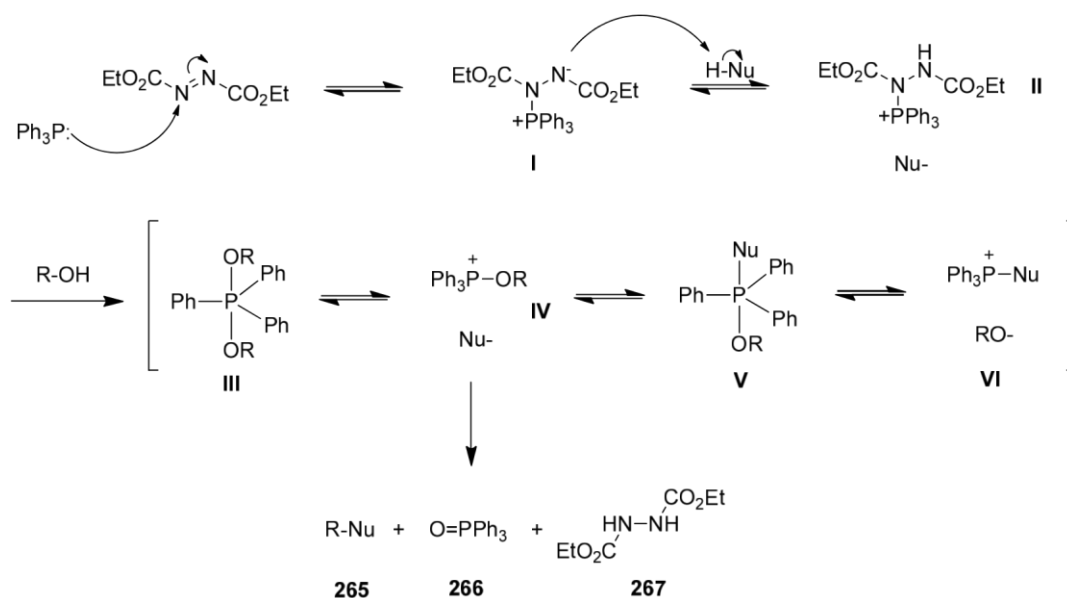
3.3.2.2.5 Mitsunobu Reaction

The diastereoisomeric alcohol mixture **247** was then coupled to the phenol intermediate *via* the Mitsunobu reaction. The Mitsunobu reaction is an efficient way to convert a phenol to a phenyl ether due to the acidity of the phenolic proton. The Mitsunobu reaction converts an alcohol group **262** to a variety of functional groups using an acid nucleophile **263**. The traditional conditions use triphenylphosphine (PPh₃) and diethyl azodicarboxylate (DEAD, **264**) or diisopropyl azodicarboxylate (DIAD) to alkylate the nucleophile as shown in Scheme 3.10.^{239,240} Secondary alcohols undergo an inversion of stereochemistry.



Scheme 3.10 Mitsunobu reaction

The mechanism has been widely studied to identify the intermediates formed and their roles.²⁴⁰⁻²⁴⁴ The proposed mechanism for the Mitsunobu reaction is described in Scheme 3.11. Initially, triphenylphosphine attacks DEAD to form a betaine intermediate **I**, which then deprotonates the nucleophile (pK_a < 11). The alcohol can then attack the phosphorus **II** to generate intermediate **IV**. The precise ratio of intermediates formed depends on the nucleophile pK_a and the solvent polarity.^{241,242,244} The active intermediate **IV** can then undergo an S_N2 displacement to generate the desired product and triphenylphosphine oxide.



Scheme 3.11 Mitsunobu mechanism

A key limitation of the Mitsunobu reaction is the removal of the triphenylphosphine oxide by-product, as well as the unreacted triphenylphosphine, which are waterinsoluble. Alternative phosphines or azodicarboxylates have been developed to facilitate isolation of the desired product (Figure 3.25).^{245,246} For example, pyridylmodified phosphines (e.g. **268**) can be removed with dilute aqueous HCl work-up. Additionally, the DEAD variant, di-*tert*-butyl azodicarboxylate (DTBAD, **269**) has been developed which decomposes during acidic work-up to generate volatile byproducts.

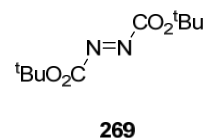
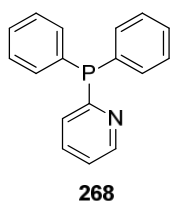
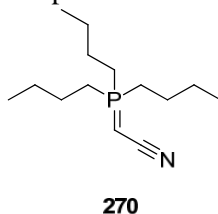
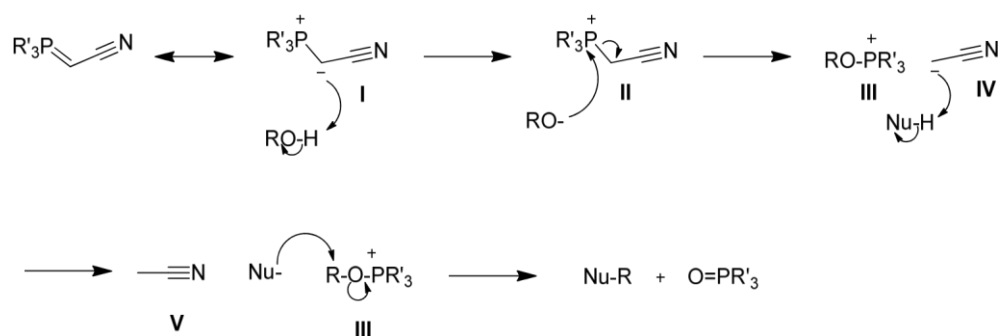


Figure 3.25 Examples of Mitsunobu reagents



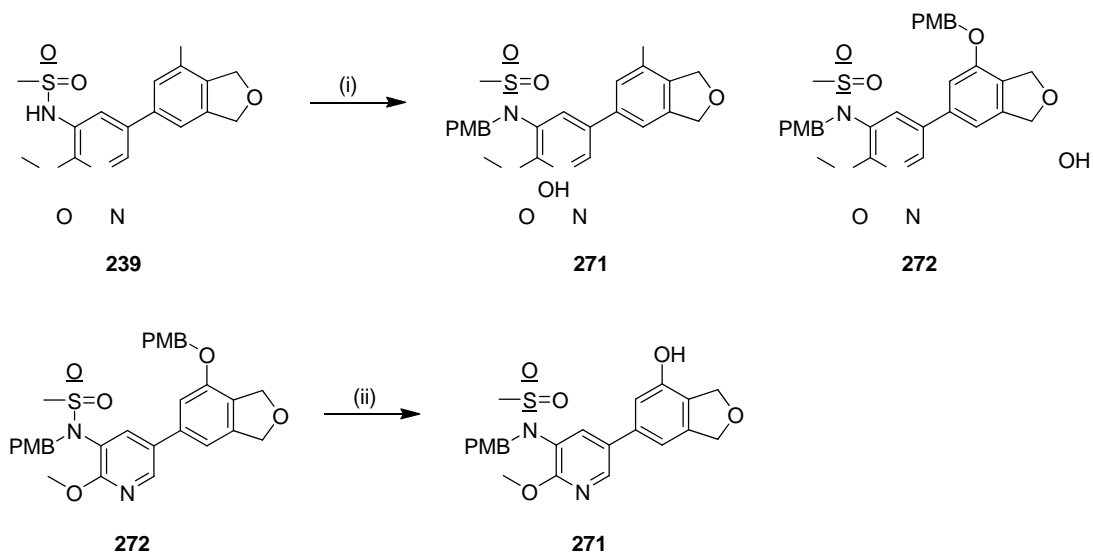
Following on from these developments, Tsunoda and co-workers reported a particularly effective reagent, cyanomethylenetriethylphosphorane (CMBP, **270**).²⁴⁷ This new reagent combines the triphenylphosphine and the diethyl azodicarboxylate into a single species, a phosphorane ylide. CMBP is less active at room temperature than other reagents but forms acetonitrile and tributylphosphine oxide as byproducts, which are more easily removed in comparison to traditional Mitsunobu reagent by-products. It also allows the use of less acidic nucleophiles.

The proposed mechanism is described in Scheme 3.12. In this case, the ylide acts as both the reducing agent and the base. The ylide **I** deprotonates the alcohol, then the resulting alkoxide attacks the phosphonium part of the ylide **II**. The resulting anion **IV** is protonated by the acid species to give acetonitrile. The conjugate base (Nu^-) can then react with the alkoxy phosphonium **III** to generate the desired product and the phosphine oxide by-product.



Scheme 3.12

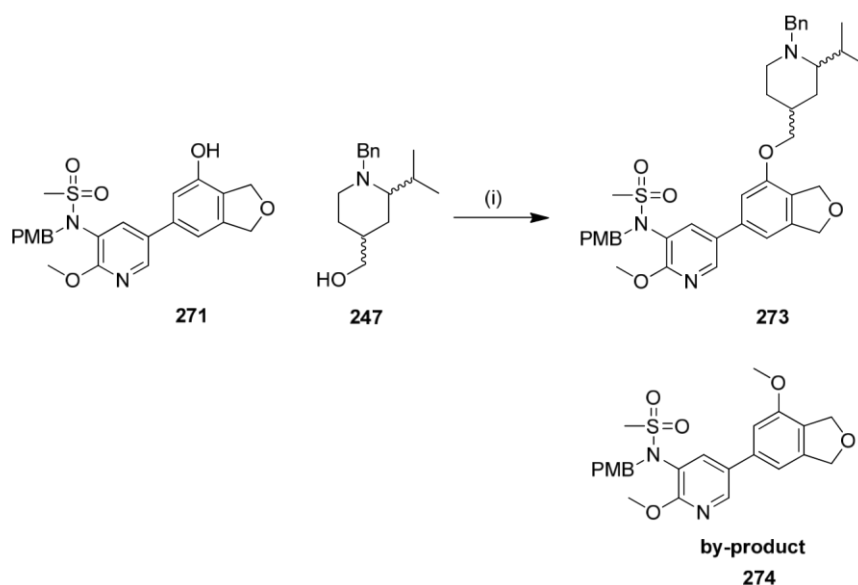
Prior to applying these conditions to our system, the acidic sulfonamide NH of the phenol intermediate **239** required protection to avoid a competing side reaction. The intermediate **239** was reacted with *para*-methoxybenzyl (PMB) bromide in DMF at room temperature to give the desired intermediate **271** (Scheme 3.13). During the reaction, bis-PMB by-product **272** was also observed. The PMB group could selectively be removed from the phenol ring using TFA at room temperature for 30 min in moderate yield after purification.



Reagents and conditions: (i) PMBBr, K_2CO_3 , DMF, rt, 2 h, 64% (**271**), 29% (**272**); (ii) TFA, DCM, rt, 30 min, 56%.

Scheme 3.13

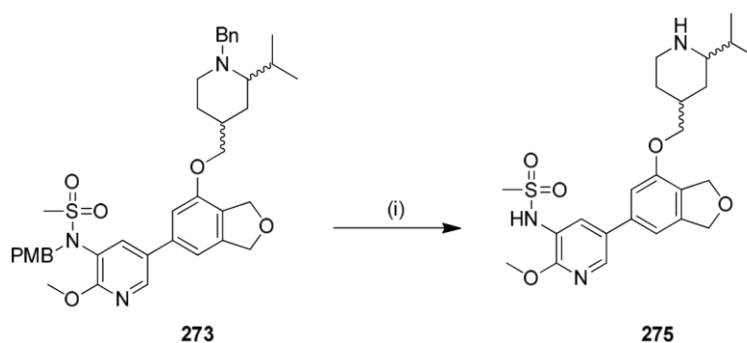
The piperidine alcohol mixture **247** was coupled to phenol **271** using CMBP in toluene at 120 °C for 1 h in a microwave reactor as described in Scheme 3.14. The product was purified twice by normal phase chromatography to give the desired product in 80% purity. LCMS also showed a component with molecular weight 14 Da above the expected mass compared to the phenol starting material **271**. Analysis of the batch of starting material **271** used revealed that residual MeOH was present and, thus, could have reacted in the Mitsunobu conditions to give by-product **274**. At this stage, the product was not repurified but instead progressed to the next step.



Reagents and conditions: (i) CMBP, toluene, 120 °C, 1 h, 99%, 80% **273** by LCMS.

Scheme 3.14

Finally, both protecting groups (PMB and Bn) were removed by hydrogenation using the H-cube and palladium on carbon as catalyst (Scheme 3.15). The final product was purified by MDAP to afford the desired product **275** as a diastereomeric mixture.



Reagents and conditions: (i) H₂, 10% Pd/C, EtOAc/EtOH (1:4), 50 °C, 1 mL/min, H-cube, 39%.

Scheme 3.15

Although compound **275** had been successfully isolated, there was an insufficient quantity of material to carry out *N*-methylation of the piperidine ring. At this stage, it was decided to await biological data on compound **275** prior to attempting resynthesis.

Analytical chiral HPLC of mixture **275** showed good separation of the four diastereoisomers (Figure 3.26), with two predominant diastereoisomers suspected to correspond to the *cis*-enantiomers, which was later confirmed by NMR analysis.

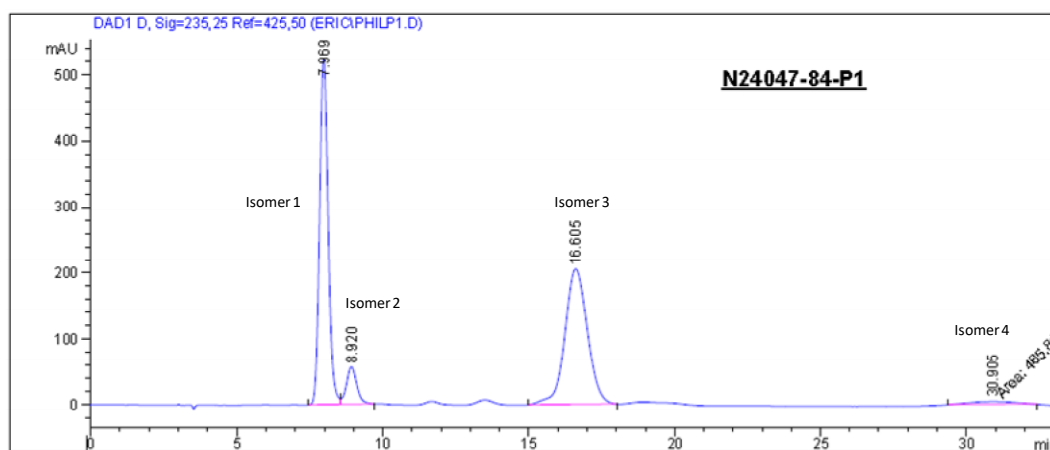


Figure 3.26 Chiral HPLC spectra of diastereomeric mixture **275**

Isomer 1 – Rt = 7.97 min, 45 % by area; Isomer 2 – Rt = 8.92 min, 6 % by area; Isomer 3 – Rt = 16.60 min, 47 % by area; Isomer 4 – Rt = 30.30 min, 2 % by area.

The four diastereoisomers were successfully separated by chiral HPLC purification to give the corresponding diastereoisomers (**276-279**).²⁴⁸ Chiral purity was then confirmed by analytical chiral HPLC in comparison to the racemic mixture. Isomer 1 (**276**) and isomer 4 (**279**) were isolated in 100% e.e. and isomer 2 (**277**) and isomer 3 (**278**) were isolated in 93.2% e.e.

The relative geometry was then determined by ¹H NMR and ROESY (Figure 3.27). For the *cis*-diastereoisomers (**276** and **278**), the relative geometry was determined from **276** spectrum, of which the analytical sample had more defined peaks. H27 (axial, 1.75 ppm) showed three large coupling constants: one geminal coupling and therefore, two diaxial couplings with H26 and H28 ($J_{\text{H27-H26}} = 11.2$ Hz and $J_{\text{H27-H28}} = 12.5$ Hz) confirming that both H26 and H28 were axial (Figure 3.28). In addition, ROESY correlations were observed between H26 (axial, 2.4 ppm) and H28 (axial, 1.85 ppm - Figure 3.30).

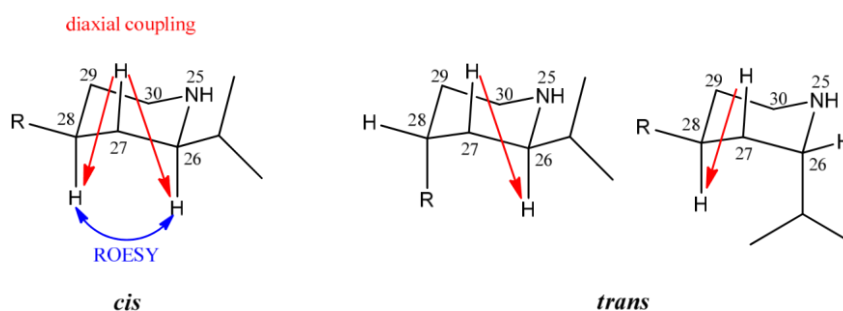


Figure 3.27 Key correlations observed in *cis/trans*-diastereoisomers

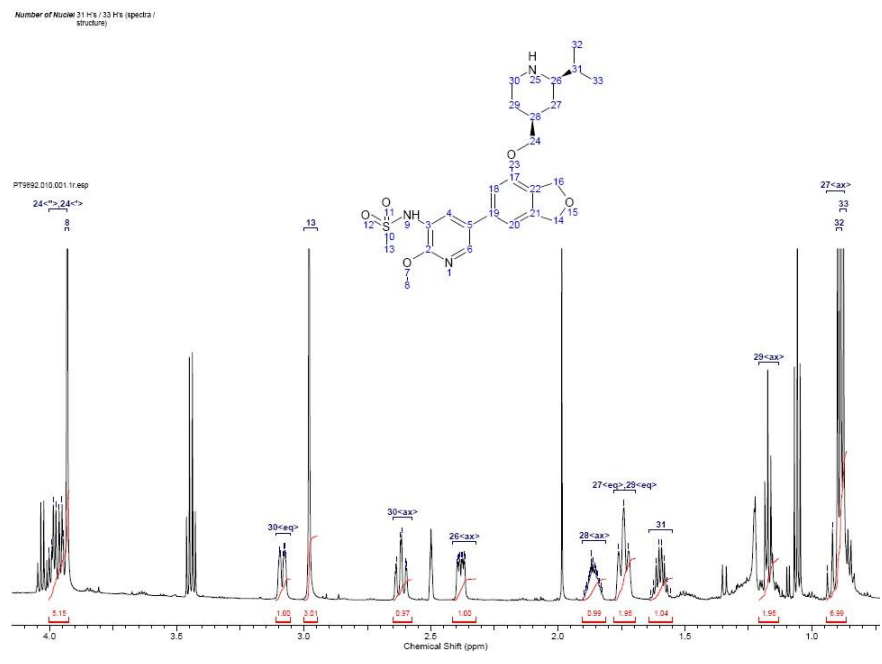


Figure 3.28 ¹H NMR spectrum of *cis*-diastereoisomer (isomer 1, 276)

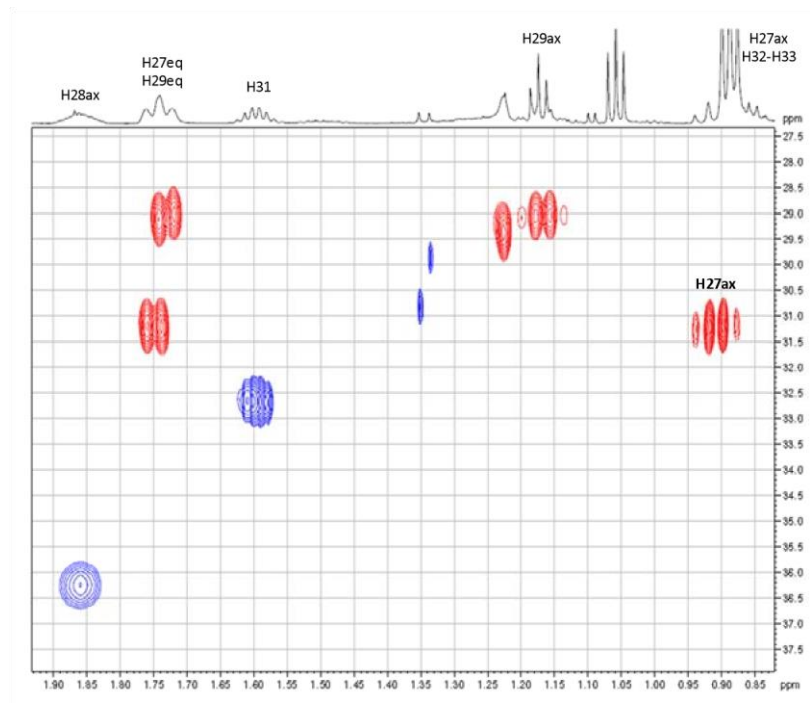


Figure 3.29 HSQC spectra of *cis*-diastereoisomer (isomer 1, 276)

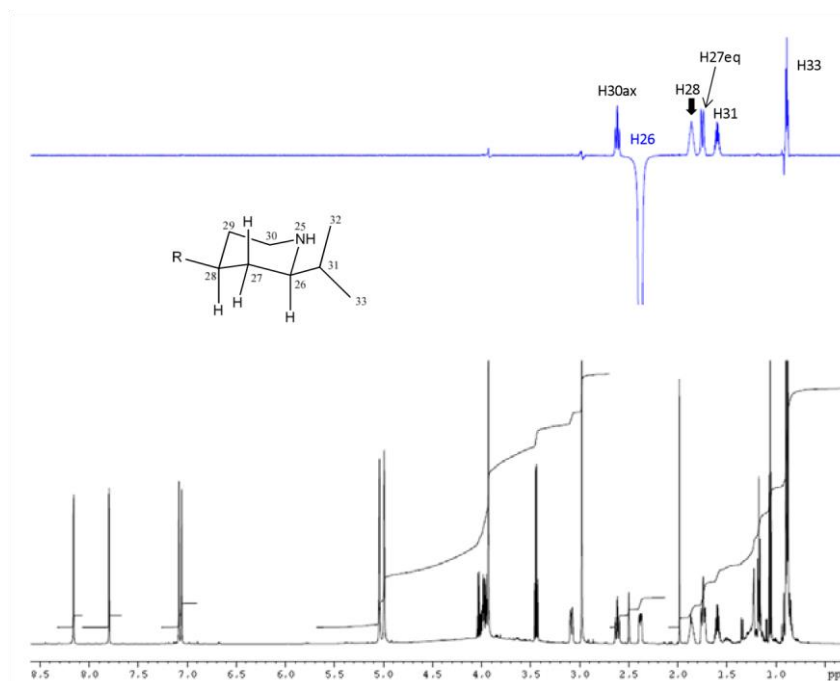


Figure 3.30 1D ROESY spectra of *cis*-diastereoisomer (isomer 1, **276**)

For the *trans*-diastereoisomer (**278** and **279**), no correlation was observed between H26 and H28 in the corresponding ROESY experiment. H27 proton signals overlapped with other signals and, thus, the coupling constants could not be used. The chemical shift difference between pairs of methylene protons (e.g. H27) were smaller than observed for the *cis* compound, suggesting an average between the two possible chair forms, which will be probably of similar energy (Figure 3.27).

The four diastereoisomers isolated are summarised in Figure 3.31. Only the relative stereochemistry could be determined from the NMR study.

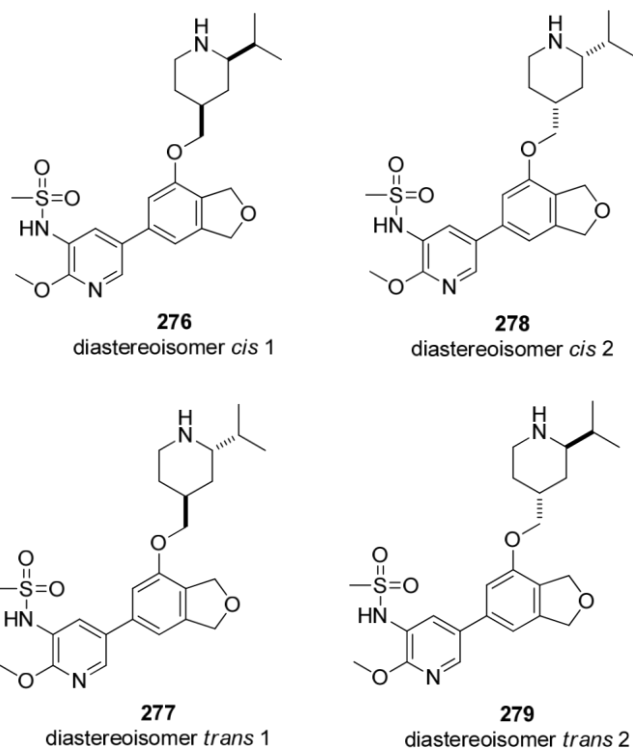
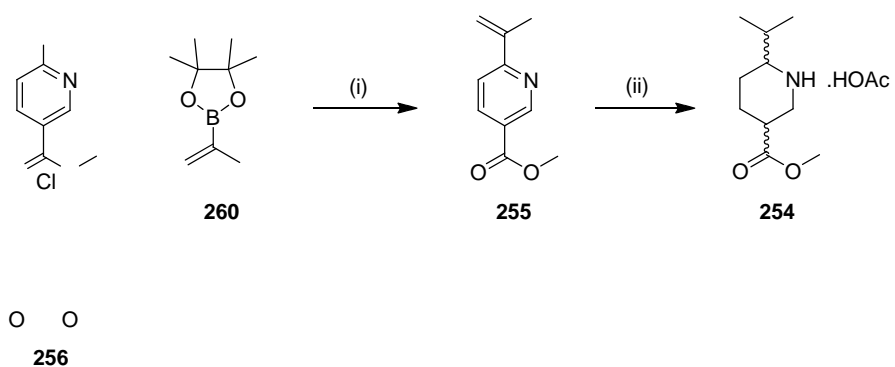
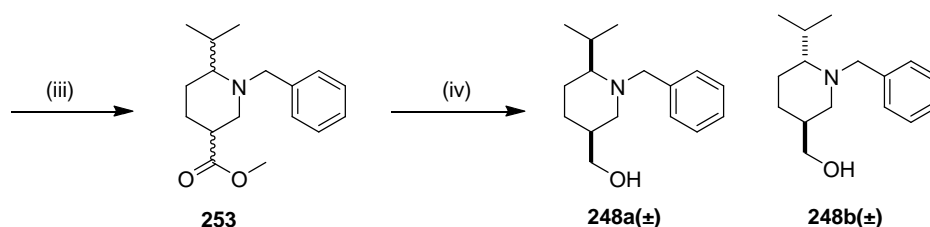


Figure 3.31 Diastereoisomer structures

3.3.2.3 Synthesis of Piperidine 248

A similar approach to that described above (Section 3.1) was applied in parallel for the synthesis of piperidine **248**. The synthetic route is described in Scheme 3.16.





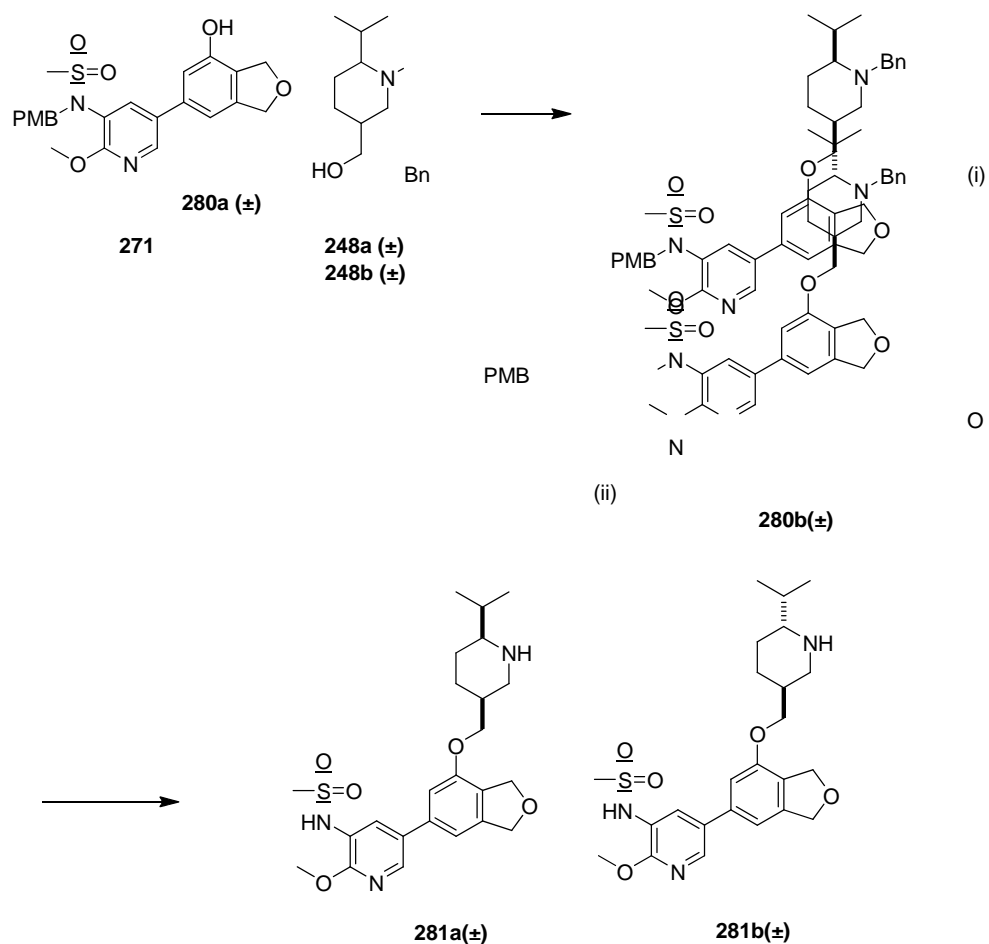
Reagents and conditions: (i) SPhos (10 mol%), Pd(OAc)₂ (8 mol%), K₃PO₄, MeCN/H₂O (10:1), 120 °C, 1 h, μ wave, 46%; (ii) PtO₂ (16 mol%), H₂, AcOH, 60 °C, 4 bar, 5 h, quantitative conversion; (iii) BnBr, K₂CO₃, MeCN, rt, overnight; (iv) DIBAL-H, THF, -78 °C, 15 min, then 0 °C, 1.5 h, 44% (**248a**), 11% (**248b**), over two steps.

Scheme 3.16 Synthesis of piperidine alcohols **248a** and **248b**

Firstly, the isopropene group was introduced *via* a Suzuki-Miyaura coupling of the chloropyridine to give the desired product **255** in moderate yield (46%). Under these optimised conditions, 8% of carboxylic acid analogue and 10% of remaining starting material were present in the mixture, contributing to the lower yield. The intermediate was hydrogenated with platinum oxide (16 mol%) in acetic acid. Conversion to piperidine **254** was quantitative by TLC and LCMS. No purification was carried out at this stage; the crude product was directly progressed to the protection step. Protection of the piperidine was carried out using benzyl bromide and potassium carbonate in acetonitrile. The desired diastereoisomeric mixture **253** was isolated by aqueous work-up without additional purification. Finally, the ester was reduced using DIBAL-H in good yield. At this stage, the diastereoisomers were successfully separated by normal phase chromatography in a 4:1 ratio. The overall yield for the total of the two diastereoisomers was 25% over 4 steps.

The two diastereoisomers **248a** and **248b** were then individually coupled to the phenol intermediate **271** *via* the Mitsunobu reaction using CMBP as the selected phosphorane ylide (Scheme 3.17) and the desired products **280a** and **280b** were isolated in acceptable purity by normal phase chromatography. At this point, it was found that unreacted piperidine alcohol intermediates **248a** and **248b** had co-eluted with the desired products **280a** and **280b** therefore the respective mixtures were progressed to

the next step without further purification. Finally, both protecting groups (PMB and Bn) were removed by hydrogenation using palladium as catalyst. The racemic mixtures were purified by MDAP to afford the pure desired products **281a** and **281b**.



Reagents and conditions: (i) CMBP, toluene, 120 °C, 1 h; (ii) H₂, Pd/C, EtOAc/EtOH (1:4), 50 °C, Hcube, 48% (**281a**), 39% (**281b**) over 2 steps.

Scheme 3.17

The relative geometry of each diastereomeric pair (**281a-281b**) was again confirmed by investigating H-H coupling in ¹H NMR (Figure 3.32).

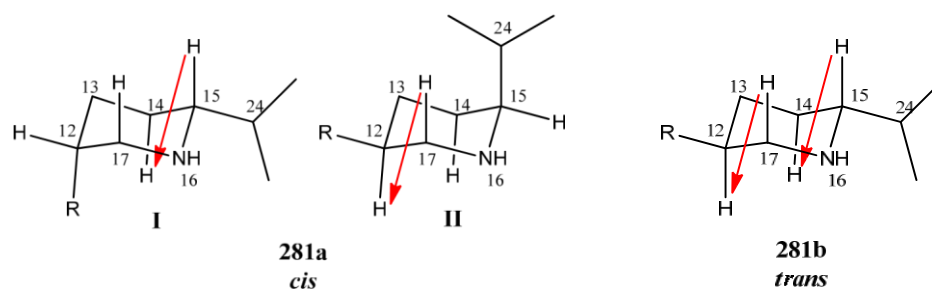


Figure 3.32 Key correlations observed in *cis/trans* diastereoisomers

For the *cis*-diastereoisomers (**281a**), two conformations can be envisaged with the *i*Pr and the DHB core either in axial or equatorial (**I** and **II**, Figure 3.32). In the proton NMR, both H17 protons showed one large coupling believed to correspond to the geminal interaction ($J_{\text{H17-H17}} = 12.2$ Hz) and one smaller coupling ($J_{\text{H12-H17}} = 2.7$ and 3.4 Hz), which thus indicated no axial-axial coupling but equatorial-equatorial or equatorial-axial. Therefore, H12 was identified as being equatorial suggesting that conformation **I** was observed by NMR. For proton H15, the interpretation was more challenging as several signals overlapped and coupling constants were not well defined. Decoupling of the multiplet H13 and H24 (1.50-1.65 ppm) left one large coupling for H15 and H14_{ax} ($J_{\text{H14-H15}} \sim 10$ Hz) suggesting that H15 was indeed axial.

For the *trans*-diastereoisomers (**281b**), one H17 proton (2.36 ppm) appeared as a triplet with $J = 11.4$ Hz suggesting that H12 was axial. For proton H15, decoupling of overlapping signals suggested a large coupling between H15 and H14 confirming that H15 was axial.

Each racemic mixture was then resolved by chiral HPLC purification to afford the four final products (**282-285**).²⁴⁹ Their chiral purity was then confirmed by analytical chiral HPLC in comparison to the racemic mixture (Figure 3.33 and Figure 3.34). The *cis*-enantiomers showed very good separation by chiral HPLC and delivered chirally pure products in excellent e.e. (98.8-100%). The separation for the *trans*-enantiomers was

found to be more challenging and enantiomer **285** was isolated with a slightly lower but still acceptable ee of 94.6%.

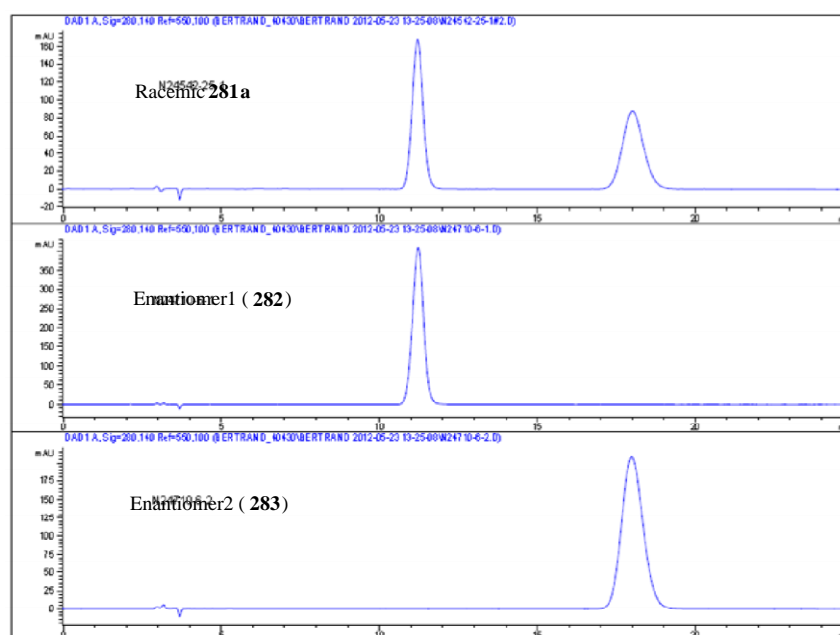


Figure 3.33 Chiral HPLC spectra of *cis*-diastereoisomers **282-283** compared to the initial diastereomeric mixture **281a**

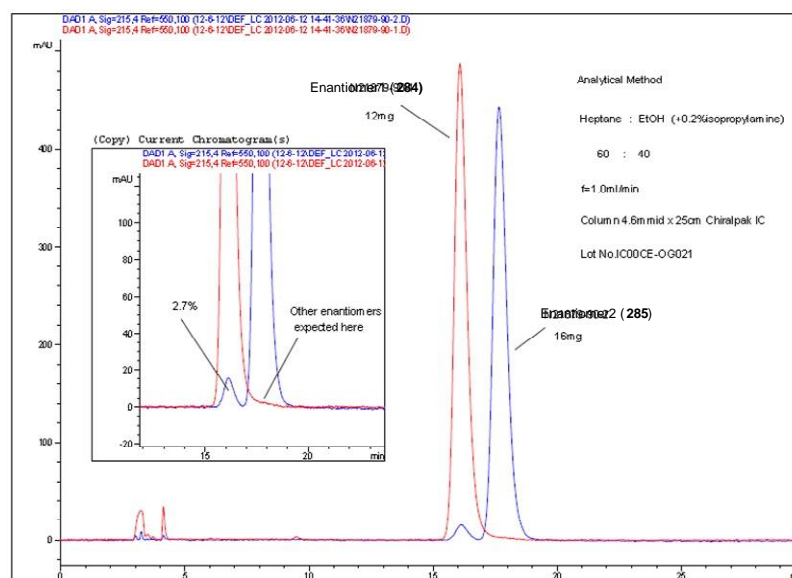


Figure 3.34 Chiral HPLC spectra of *trans*-diastereoisomers **284-285** compared to the initial diastereomeric mixture **281b**

The four diastereoisomers isolated are summarised in Figure 3.35.

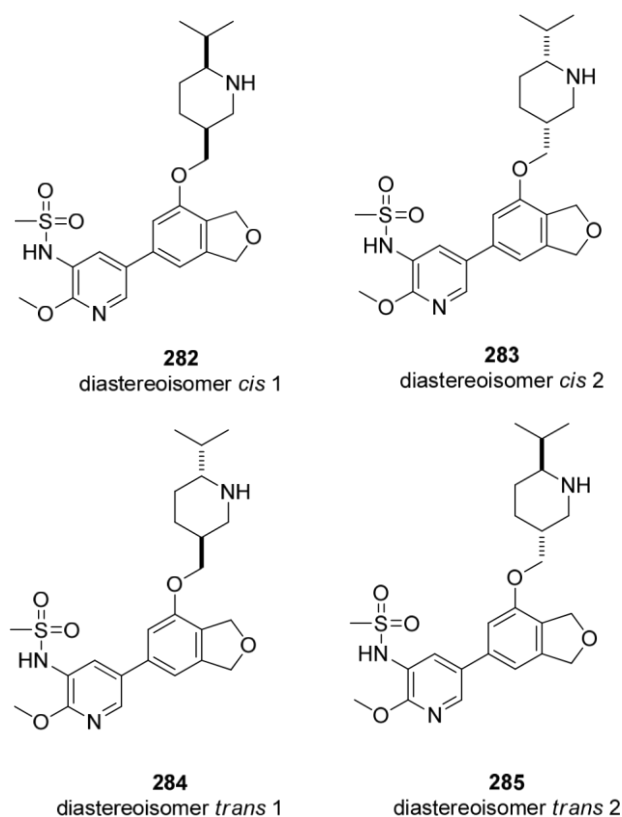
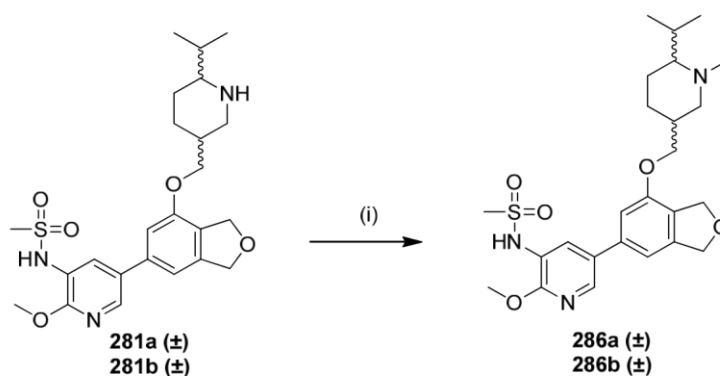


Figure 3.35 Diastereoisomer structures

Both racemic mixtures **281a** and **281b** were also methylated *via* an EschweilerClarke reaction²⁵⁰ using formaldehyde in acetic acid (Scheme 3.18). The methylation on the *trans*-mixture **281b** was found to be very slow due to the steric hindrance of the isopropyl group. For the *cis*-isomer, a mixture of the isopropyl unit in equatorial and axial positions, as shown in Figure 3.32, will be present in the reaction conditions. When the isopropyl group is in the axial position (**II**), the NH is less sterically hindered allowing faster reaction. After addition of several equivalents of formaldehyde and heating at 80 °C in the microwave for 10 h in total, only 50% conversion to desired product by LCMS was achieved. The desired products were subsequently isolated in moderate yield after purification by MDAP.



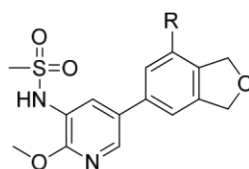
Reagents and conditions: (i) H₂C(O), HCO₂H, 80 °C, 1-10 h, microwave, 40% (**286a** ± *cis*), 22% (**286b** ± *trans*).

Scheme 3.18

Due to the small quantity of material isolated, the two *trans*-enantiomers could not be separated by chiral purification and were instead directly progressed to biological testing as a racemic mixture. Although the two *cis*-enantiomers showed good separation by analytical chiral HPLC analysis, they could not be separated in sufficient purity during the larger scale chiral HPLC purification. Therefore, only the racemic mixture was tested at this stage, with the expectation that single enantiomers could be subsequently isolated based on the biological data.

3.3.2.4 Biological Results

All the pure diastereoisomers described above were progressed to the relevant biological assays. Table 3.6 summarises the data generated on the NH isopropyl analogues. In each case, the new compounds are compared to the enantiomerically pure form of lead compound **267**, compound **287**, as all compounds have been isolated as enantiomerically pure diastereoisomers.



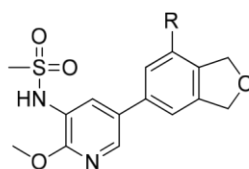
R*									
	287	276	278	277	279	282	283	284	285
pIC ₅₀ (δ)	8.3	8.8	7.5	8.2	7.8	7.9	8.0	7.7	7.9
X-fold selectivity α, β, γ	20 32 398	200 50 631	31 100 159	63 13 126	20 32 79	100 13 126	100 20 316	50 25 100	32 40 126
hWB pIC ₅₀	7.1	6.9	5.9	6.9	6.2 ^a	6.4	7.0	6.4	6.7
Chrom logD _{7.4}	2.2	2.7	2.6	2.5	2.5	2.9	3.0	2.8	2.8
CLND sol. (μg/mL)	≥ 268	102	≥ 56	≥ 131	≥ 115	167	≥ 188	≥ 211	130
Perm. (nm/sec)	400	149	190	170	130	400	425	410	400

Table 3.6 Biological data of isopropyl analogues *Only the relative stereochemistry is known ^aCompound failed to fit a curve in 1 out of the 3 test occasions.

Most of the compounds have good to excellent CLND solubility and permeability, confirming that the isopropyl group was able to mask the polarity of the NH as predicted. The 4-substituted analogues (**282-285**) have increased permeability compared to their 3-substituted analogues (**276-279**). The compounds with the 3isopropyl group (**276-279**) generally also showed relatively lower CLND solubility suggesting that crystal packing might be more important with the isopropyl at this position. The selectivity profile was improved overall in comparison to the initial lead **287** but was variable across the compounds. In general, the data showed no clear trend, although the *cis*-diastereoisomers tended to be somewhat more selective than their *trans*-analogues. One potential explanation could be that the *cis* geometry allowed a

better interaction with the key Trp760 residue, resulting in better selectivity. Three compounds in particular, **276**, **277** and **283**, showed an encouraging overall profile. They achieved the hWB pIC₅₀ target with good physicochemical properties. Compounds **276** and **283** had the best overall profile of all the analogues in this subset. They both showed encouraging selectivity, although there is potential for selectivity over the β isoform to be further improved. Disappointingly, compound **276**, which showed very good enzyme potency, had a bigger loss of potency in whole blood (2 orders of magnitude) resulting in similar cell potency (pIC₅₀ 6.9) to the parent piperidine compound **287**. Analysis of the data associated with compound **276** revealed no clear explanation why that would be the case. Compound **276** (PPB 79%) showed similar plasma protein binding to **287** (PPB 73%) and reasonable levels of permeability suggesting cell penetration is not an issue.

The data for the *N*-methylated compounds are summarised in Table 3.7. As stated above, only the racemic mixtures were tested at this stage as the individual diastereoisomers could not be separated given the quantities of material available. Therefore, the compounds are compared to their NH racemic analogues and lead compound **236** (racemic).



R					
	236	281a rac.	286a rac.	281b rac.	286b rac.
pIC₅₀ (δ)	8.3	8.0	8.1	8.0	7.8
X-fold selectivity (α, β, γ)	79 40 316	79 13 316	100 63 398	32 32 398	40 50 200
hWB pIC₅₀	7.1	6.3	6.7	6.5	6.8
chromlogD_{7.4}	2.2	3.0	4.5	2.8	3.6
CLND sol. (μg/mL)	≥ 230	≥ 196	14	13	≥ 229
Perm. (nm/sec)	310	530	890	330	740

Table 3.7

As expected, *N*-methylation of the piperidine NH has improved permeability of the compounds and resulted in slightly higher cellular potency compared to their racemic NH analogues. Selectivity over related PI3K isoforms was slightly improved for the *cis* analogue **286a**, however, the compound showed very poor solubility, which reflected its relatively high lipophilicity. It would be interesting to separate the two *cis*-enantiomers to delineate the profile of the best one. However, due to the poor solubility and high lipophilicity of the compound, no further work was carried out at this stage. The free NH analogues exhibited good solubility and permeability and avoid potential *N*-dealkylation as their metabolic fate, which could result in high clearance. Collectively, this data also indicated that good permeability can be achieved by adding a bulky group, which effectively masks the polarity of the free NH of the secondary amine.

Compound **276** was crystallised in the PI3K δ active site (2.5 Å, ●), as shown in Figure 3.36, to confirm its binding mode and to attempt to understand the increase in selectivity observed.¹⁸⁶ The density for the ligand and the active site residues was good; however the isopropyl group was not well resolved in the electron density maps. Compound **276** showed a good overlay with the initial lead compound **236** (○). The oxygen of the DHB ring forms a key interaction with Val828 at the hinge and the NH sulfonamide is in a good position to make an H-bonding interaction with Lys779 in the affinity pocket. Although the selectivity observed with compound **276** has been improved compared to **279**, inspection of the crystal structure suggests that interaction with Trp760 was not optimal. Indeed, the observed selectivity over the other isoforms, in particular PI3K β is still moderate compared to other compounds, which take advantage of the interaction with Trp760, supporting this view. Overlay with our inhaled lead compound **235** (●, Figure 3.36), which exhibits exquisite selectivity over the three isoforms (> 6,000-fold), revealed that the isopropyl group of **276** was positioned at the entrance of the pocket created by Trp760, Thr750 and Met752 and, thus, was not interacting optimally with Trp760. In addition, as the isopropyl group is not sufficiently large to fill the small pocket, it might not fully clash with Lys or Arg at position 750 in other isoforms (Thr750 in PI3K δ). Thus, to improve selectivity further, a larger or longer substituent might be preferable.

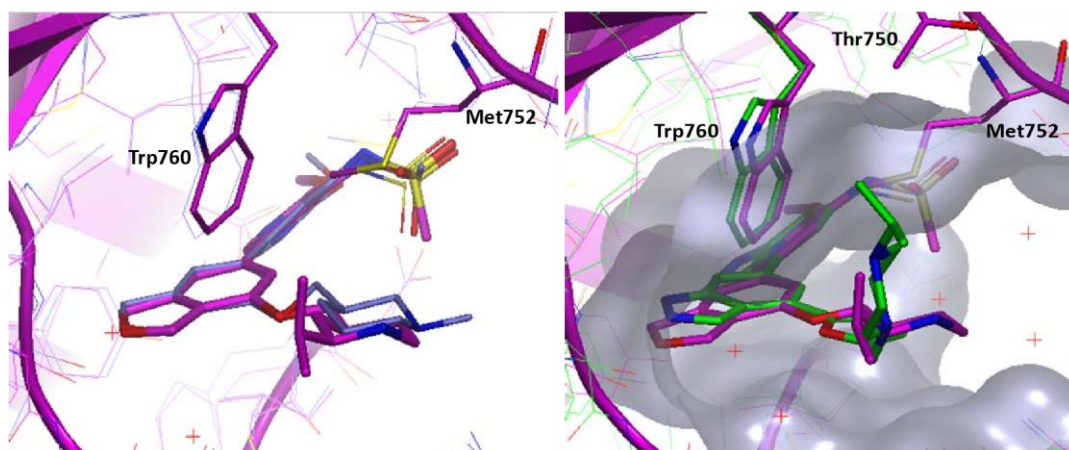
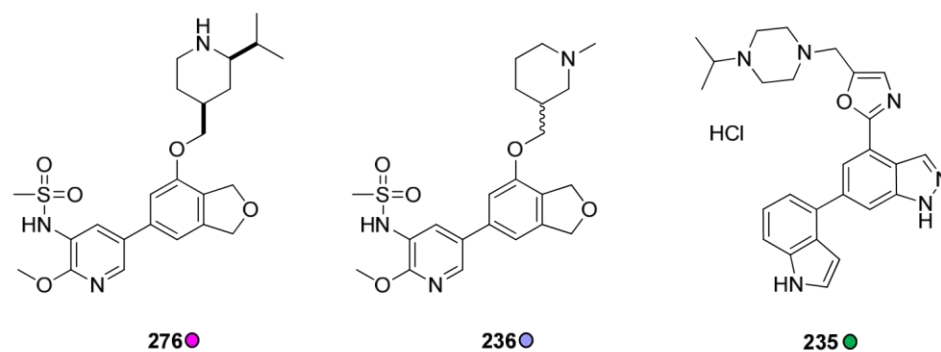


Figure 3.36

- (a) crystal structures of PI3K δ in complex with inhibitors **276** (●) and **236** (●)
 (b) crystal structures of PI3K δ in complex with inhibitors **276** (●) and **235** (●)

Having stated this, due to the lipophilicity of the piperidine analogue **287** (clogP of 2.8), there was limited space for optimisation within the bounds of desired range for clogP using this template. Accordingly, efforts next focused on a set of morpholinederived analogues. Compound **288** (Table 3.8), which had been synthesised by another member of our laboratory,²⁵¹ had a similar profile to the piperidine with lower lipophilicity (Table 3.8). Therefore, the next set of compounds was designed using the morpholine group (Figure 3.37). The (*R*)-enantiomer was confirmed to be the preferred stereoisomer by using an enantiomerically pure alcohol starting material during the synthesis.

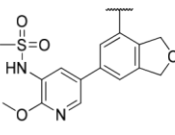
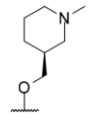
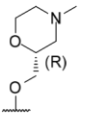
	 287	 288
pIC₅₀ (δ)	8.3	8.0
X-fold selectivity (α, β, γ)	20 31 398	50 79 63
hWB pIC₅₀ (δ)	7.1	6.6
clogP	2.8	2.2
CLND sol. (μg/mL)	≥ 268	≥ 212
Perm. (nm/sec)	400	495

Table 3.8

From consideration of the previously established SAR, addition of bulky groups at the 3-position of the piperidine (e.g. *i*-Pr) was thought to improve potency and selectivity. Therefore, both *i*-Pr and cyclobutyl substituents were selected for synthesis (Figure 3.37). In addition, from consideration of previous data and structural information, longer substituents might further improve selectivity by reaching further into the pocket formed by Trp760 and Thr750. However, by increasing the size of the alkyl substituent, lipophilicity will increase as well and could easily approach the undesirable range. Thus, the dimethyl ethanol group (e.g. **291**) was selected as it reduced lipophilicity of the molecules while retaining steric bulk in the desired region for selectivity.

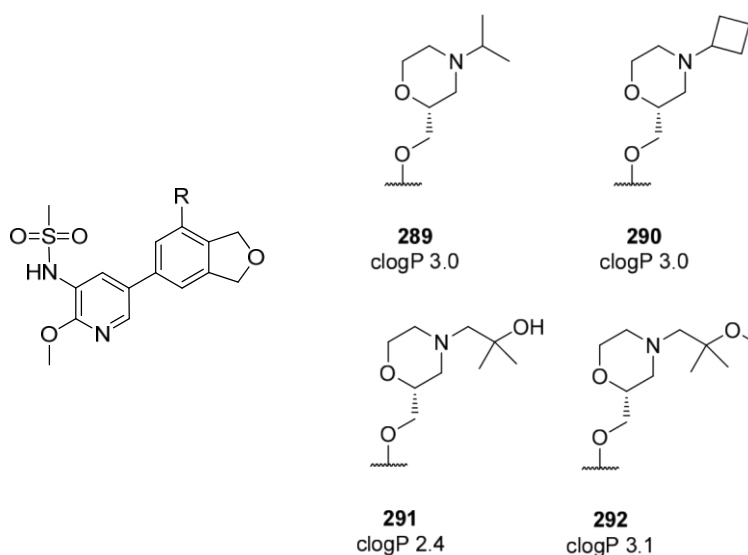
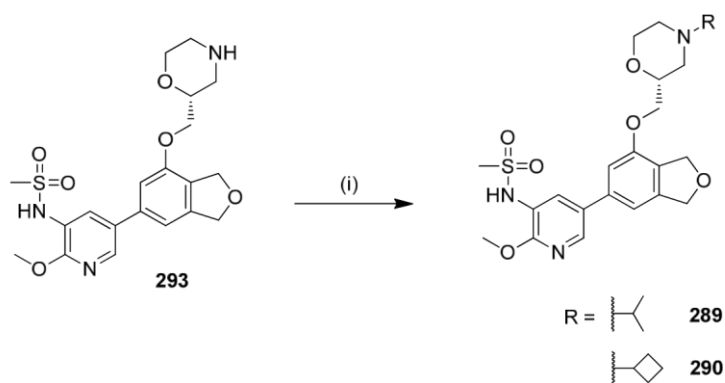


Figure 3.37

3.3.2.5 Morpholine Chemistry

3.3.2.5.1 Cyclobutyl Analogue

The morpholine intermediate **293** was previously prepared by another member of our laboratory *via* the Mitsunobu reaction discussed above on the appropriately protected morpholine alcohol.²⁵¹ The (*R*)-intermediate was used at the outset to obtain the preferred enantiomer without chiral separation. The desired products **289-290** were obtained by reductive amination in the presence of triacetoxyborohydride and the desired ketone in THF as shown in Scheme 3.19. The final compounds were purified by MDAP to give the target compounds **289-290** in good yield.

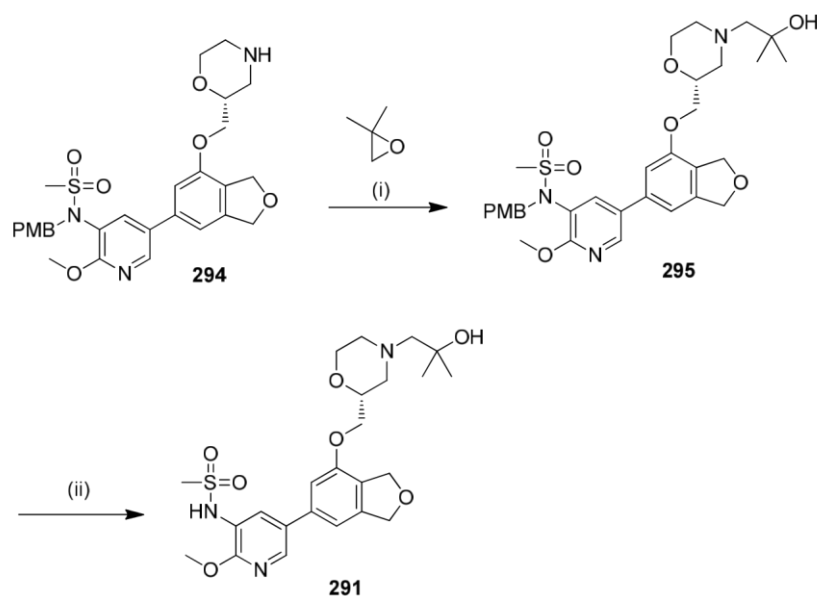


Reagents and conditions: (i) $\text{NaBH}(\text{OAc})_3$, THF, rt, 73% (**289**), 69% (**290**).

Scheme 3.19

3.2.5.2 Dimethylhydroxyl Analogue

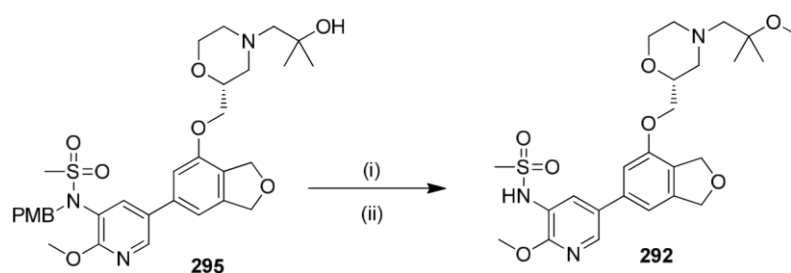
The dimethyl hydroxyl analogue was prepared using dimethylepoxyde and iron trichloride in acetonitrile at 60 °C (Scheme 3.20).²⁵² The reaction was particularly slow and required addition of several equivalents of both reagents for complete conversion. The intermediate **295** was not purified at this stage and progressed directly to the deprotection step; the PMB protecting group was removed using TFA at 70 °C in a microwave reactor. In this way, the final product **291** was isolated in 32% yield over the two steps.



Reagents and conditions: (i) FeCl_3 , CH_3CN , $60\text{ }^\circ\text{C}$, 35 h; (ii) TFA, DCM, $70\text{ }^\circ\text{C}$, 2 h, μwave , 32% over two steps.

Scheme 3.20

The methyl analogue was prepared following a similar synthetic route (Scheme 3.21). The crude product **295** was methylated using sodium hydride and methyl iodide in DMF.^{253,254} Due to the hindrance of the alcohol, it was expected to be a very slow reaction and this was confirmed in practice. To drive alkylation to completion, the reaction was stopped, worked up and resubjected to the reaction conditions several times to achieve 66% conversion. At this stage, the decision was taken to proceed to the next step. The PMB protecting group was removed using TFA and the product was purified by MDAP. The overall yield was 11% over the three steps with purification performed only at the last step.



Reagents and conditions: (i) MeI, NaH, THF then DMF, rt, 7 days; (ii) TFA, DCM, 70 °C, 2 h, μ wave, 11 % over 2 steps.

Scheme 3.21

3.3.2.6 Biological Results

The biological data on the morpholine compounds are summarised in Table 3.9.

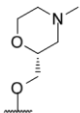
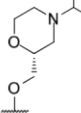
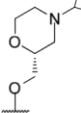
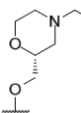
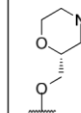



					
	288	289	290	291	292
pIC₅₀ δ	8.0	8.2	8.7	8.8	9.1
X-fold selectivity (α, β, γ)	50 79 63	251 200 159	316 398 200	631 1259 316	501 1585 316
hWB pIC₅₀	6.6	6.5	6.4 ^a	7.1	7.0
clogP	2.2	3.0	3.0	2.4	3.1
chromlogD_{7.4}	3.1	4.0	4.7	4.0	5.5
CLND sol. (μg/mL)	≥ 212	≥ 216	≥ 201	≥ 221	208
Perm. (nm/sec)	495	190	520	450	690

Table 3.9

^aCompound failed to fit a curve in 1 out of the 5 test occasions.

Overall, the subset of compounds prepared showed very promising data. They all demonstrated higher enzyme potency, good cellular potency and excellent selectivity

(> 150-fold) compared to the progenitor compound **288**, as hypothesised when bulky groups are introduced in this region, which then have the potential to favourably stack against Trp760. The observed drop-off in the cell-based assay was slightly higher on these new molecules than had been previously observed in this series. Although the molecules had a low clogP, measured chromlogD_{7.4} revealed a much higher degree of lipophilicity, probably linked to reduction in basicity due to the morpholine ring. The plasma protein binding was between 85 and 90% for the four compounds compared to 76% for compound **288**, which could account potentially for the greater reduction in hWB potency for these systems. Each of the compounds also showed good solubility and high permeability.

Compound **291** was crystallised in the PI3K δ active site (2.2 Å, ) , as shown in Figure 3.38, to confirm its binding mode and our selectivity hypothesis.¹⁸⁶ Compound **291** showed a good overlay with the compound **276** (); the key interactions with Val828 at the hinge and Lys779 in the affinity pocket were maintained. However, with the introduction of larger substituents, the morpholine ring had changed orientation and the dimethyl alcohol was in a good position in order to interact with Trp760, which confirmed our selectivity hypothesis. Overlay with our inhaled compound **235** (, Figure 3.37) revealed that the dimethyl alcohol substituent was in a similar position to the isopropyl group on the piperazine ring of **235**, providing further support to the proposed selectivity hypothesis. The crystal structure showed that by packing against Trp760, the dimethyl alcohol moiety is filling the space below Thr750, not accessible in other isoforms due to the presence of a lysine or arginine residue, which robustly explains the observed selectivity data.

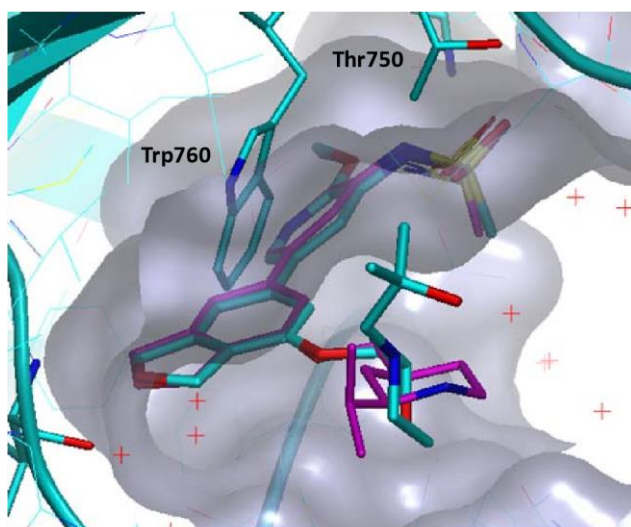
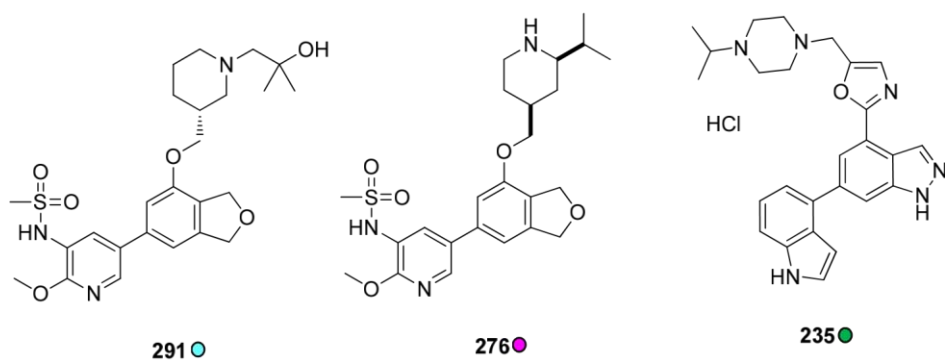


Figure 3.38 Crystal structures of PI3K δ in complex with inhibitors 291 ● and 276 ●

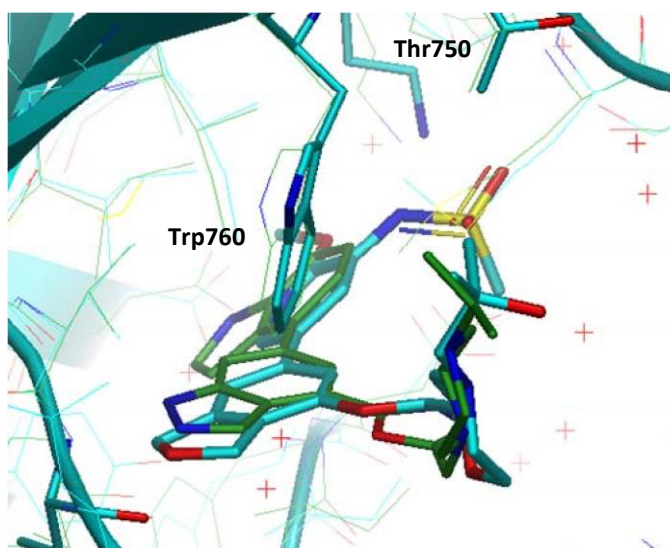


Figure 3.39 Crystal structures of PI3K δ in complex with inhibitors 291 ● and 235 ●

3.3.3 Summary and Conclusions

The aim of this research programme was to improve the selectivity of a series of dihydrobenzofuran containing oral PI3K δ inhibitors. Using prior knowledge on PI3K δ selectivity, a first set of compounds with good physicochemical properties and improved potency and selectivity over lead compound **287** were designed and synthesised (e.g **276**, Table 3.10). The data generated clearly showed improvement over the progenitor compound **287** with increased enzyme potency and selectivity over PI3K α and γ . A subsequent crystal structure of compound **276** indicated suboptimal interaction with Trp760, which resulted in low selectivity over the PI3K β isoform (50-fold), in accordance with earlier experience with this target class.

Building on the above findings, bulkier substituents were included on the morpholine template **288** to improve PI3K β selectivity, while keeping the physicochemical properties in an acceptable range. The new set of compounds thus designed, again delivered an improvement in both potency and selectivity compared to progenitor compounds (**287** and **288**), robustly meeting our objective (e.g **291**, Table 3.10). These compounds showed excellent selectivity over all the other PI3K isoforms (> 150-fold) and allowed the identification of a candidate molecule to progress to *in vivo* studies. A crystal structure of compound **291** confirmed that the compound made a more optimal interaction with Trp760 resulting in excellent selectivity.

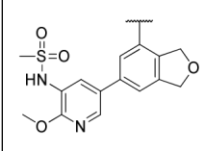
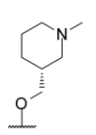
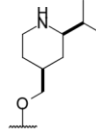
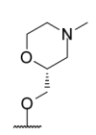
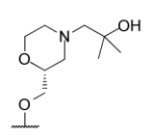
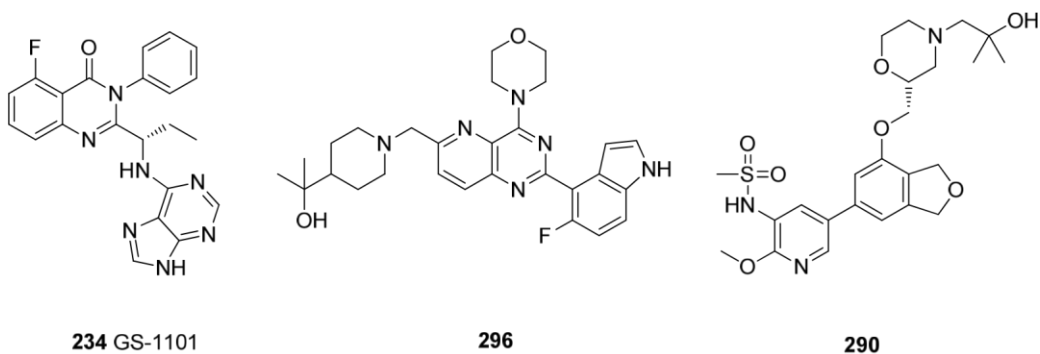
					
		287	276	288	291
pIC ₅₀ (δ)		8.3	8.8	8.0	8.8
X-fold selectivity α, β, γ		20 31 398	200 50 631	50 79 63	631 1259 316
hWB pIC ₅₀ (δ)		7.1	6.9	6.6	7.1
clogP		2.8	4.0	2.2	2.4
ChromlogD _{7.4}		2.2	2.7	3.1	4.0
CLND sol. (μg/mL)		≥ 268	102	≥ 212	≥ 221
Perm. (nm/sec)		400	149	495	450

Table 3.10 Progenitor compounds and associated leads

These novel, selective PI3K δ inhibitors (e.g. **291**, > 300-fold over the three other isoforms) showed improved potency and selectivity, particularly in relation to PI3K β and γ , to known oral inhibitors (e.g. **234** and **296** Table 3.11) and maintained good physicochemical properties compatible with oral dosing. These new compounds have moderate lipophilicity and a low number of aromatic rings, reducing risk of toxicity going forward according to the theory of Young *et al.*¹⁶ In addition, these compounds confirmed that interaction with Trp760 can deliver excellent selectivity over the three related PI3K isoforms, with improvement compared to the previously disclosed propeller-shape inhibitors (e.g. **234**), thus validating our approach towards this novel class of highly selective oral PI3K δ inhibitors.



Compounds	234	296*	291
Intended route of administration	oral	oral	oral
pIC ₅₀ (δ)	8.1	8.4	8.8
LE, LLE _{AT}	0.36; 0.31	0.31; 0.30	0.34; 0.36
fold-selectivity	1000	340	631
α/δ, β/δ, γ/δ	159 40	200 410	1259 316
clogP	3.6	3.1	2.4
ChromlogD _{7.4}	3.2	3.4 ¹	4.0
Ar ring	5	4	2

Table 3.11

*Data not generated in our assays; ¹calculated value

3.3.4 Future Work

When the compounds were progressed to *in vivo* pharmacokinetic studies, they all showed very high clearance (e.g. **291** Cl_b = 167 mL/min/kg). The next step for further work in this series would be to gain a more complete understanding of what drives the high clearance observed. Initially, *in vivo* Met ID of the best compounds would help to determine if a major metabolite is responsible for the high clearance. With these data in hand, a new strategy to block the metabolite site could be investigated. The compounds designed in this thesis showed good drug-like physicochemical properties

alongside excellent selectivity and, thus, could deliver a good quality drug candidate if clearance can be reduced, leading to satisfactory exposure *via* the oral route.

3.4 Fragment Series – Benzoxazine Template

3.4.1 Background

Elsewhere in our laboratories,²⁵⁵ a fragment screening effort had been initiated in order to identify a back-up series to the current lead exemplified by **236** for PI3K δ (see section 3.3 Lead Series). The screening cascade, which was used in this work to identify hit compounds, is summarised in Figure 3.40.

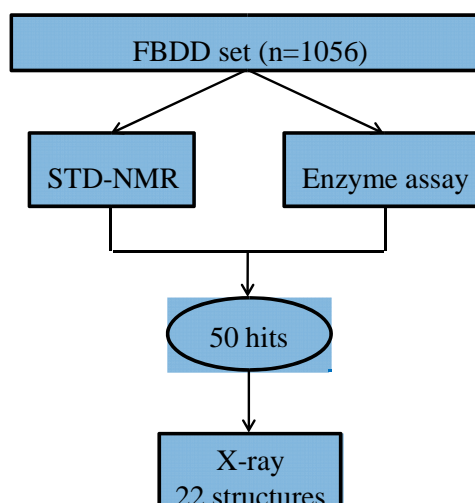


Figure 3.40 Screening cascade

The fragment set available in our laboratories was screened against PI3K δ in a high concentration biochemical TR-FRET²⁰⁴ assay (100 mM) and a STD-NMR⁹⁸ assay. From this exercise, 50 potential binders which were identified by STD-NMR also showed biochemical potency, representing a 5% hit rate. These dual hits were initially selected to ensure the greatest chance of success by crystallography.⁹⁵ These hits were then progressed to X-ray crystallography and 22 compounds produced crystal structures.¹⁸⁶ For this target, crystallography was carried out by soaking and the overall success rate of X-ray crystallography was considered moderate (44%). As discussed in Chapter 1, the soaking technique is very useful as it is a high throughput method compared to co-crystallisation and, thus, allows structures to be identified quickly.

However, soaking experiments can suffer from the destruction of the crystal during the experiment. Additionally, solubility issues with certain compounds at high concentration can result in a failure to produce a crystal structure. A selection of the fragment hits identified from this exercise is shown in Figure 3.41.

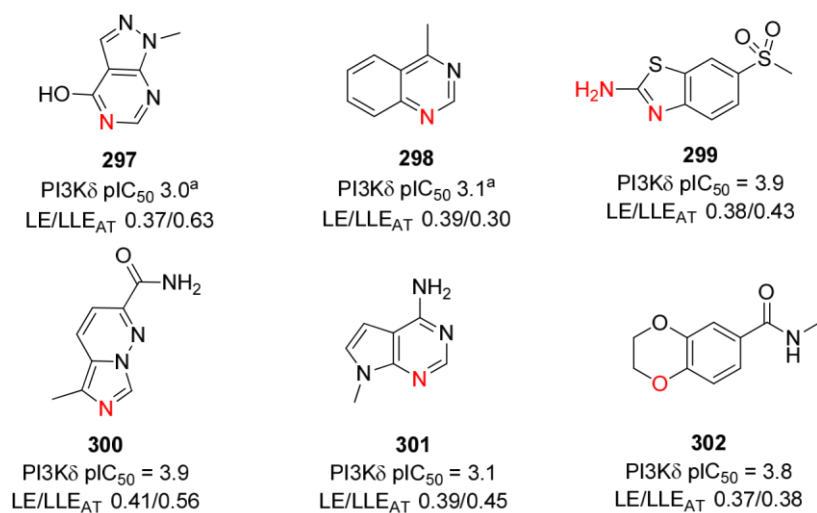


Figure 3.41 Examples of fragment hits identified
 red atom = hinge interaction

^a Compound reported inactive (pIC₅₀ < 2.78) in 1 out of the 2 test occasions.

Most of the fragments identified were flat aromatic systems (Figure 3.41), which represented less novelty compared to the current series and other known kinase hinge binders.¹⁸⁷ The identification of more sp³-containing hinge binding groups was a key goal in order to improve the physicochemical properties,^{16,20,111} as well as to identify more novel binders in what is a highly competitive area of research. Therefore, fragment hit **302**, which exhibited more sp³-character, was initially selected for optimisation. In addition, fragment **302** showed reasonable potency in the biochemical assay (pIC₅₀ = 3.8) with good levels of ligand efficiency and only one aromatic ring.

The crystal structure of fragment **302** () revealed that the compound bound in the ATP-binding site and made a key interaction with Val828 at the hinge region through the

232

dioxane ring (Figure 3.42). Interestingly, the amide substituent showed no apparent H-bonding interaction with the protein. However, it was reasoned that this could offer a good vector to grow the fragment and improve potency. Overlay of fragment **302** (●) with compound **303** (●), an exemplar from another series developed on in our laboratories,²¹⁰ suggested an additional vector from which to grow as indicated by the black arrow in Figure 3.42. From previous experience in our laboratories, it was known that the pyridine sulfonamide group gives a significant increase in potency by binding in the affinity pocket of the kinase.

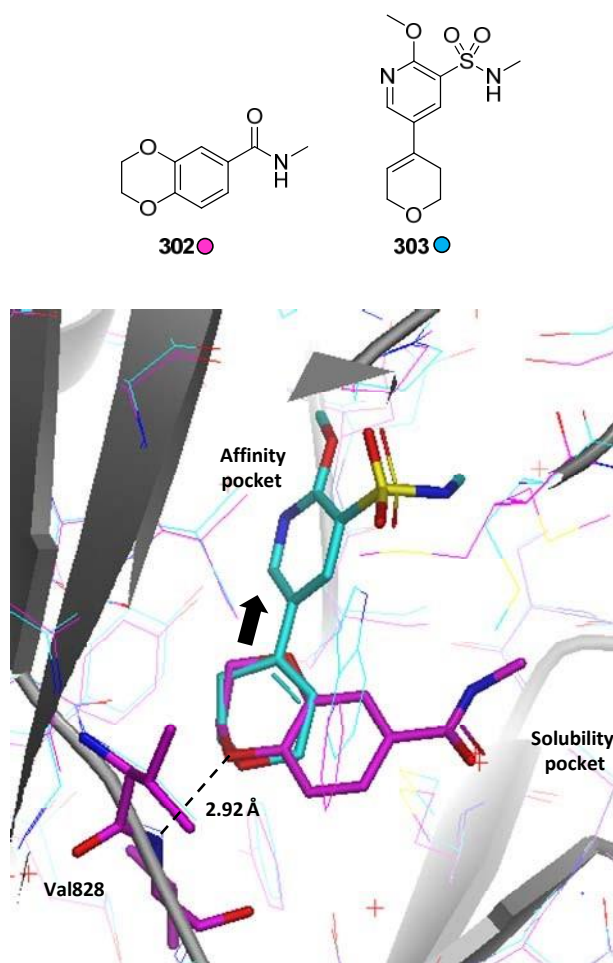


Figure 3.42 Crystal structure of PI3K δ in complex with fragment **302** (●) and hit **303** (●)

Synthesis of compound **304**, conducted within our laboratory,²⁵⁶ had already confirmed that the two series could be merged, delivering reasonable ligand efficiencies (Figure 3.43).

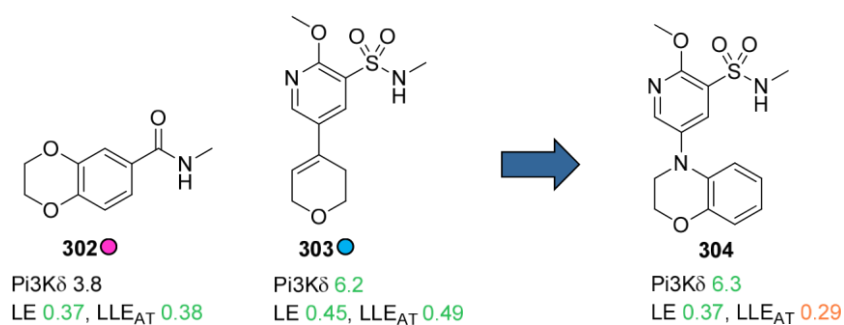
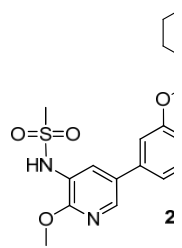


Figure 3.43 Fusion of fragment hit **302** and compound **303**

Although compound **304** did not show improved potency compared to its progenitor compound **303** and, thus, had somewhat reduced ligand efficiency, the phenyl ring in compound **304** provided additional growth vectors to further optimise the compound, providing an opportunity to remedy the reduction in ligand efficiency.

3.4.2 Aims and Optimisation Goals

The objective of this phase of the research was to identify good growth vectors from compound **304** towards the solubility pocket (see section 1.3) to initially increase potency to a level similar to the lead series exemplified by compound **236** as described in Chapter 3, section 3.3 (Figure 3.44), then to establish SAR and, thus, better understand the potential of this new series.



PI3Kδ pIC₅₀	8.3
LE, LLE_{AT}	0.37 ; 0.35
PI3K pIC₅₀ Fold selectivity	α 6.4 β 6.7 γ 5.8 α 79 β 40 γ 316
PI3Kδ hWB pIC₅₀	7.1
chromlogD_{7.4}	2.2
CLND solubility	\geq 230 μ g/mL

Figure 3.44 Lead PI3K δ inhibitor **236**

Colour coding: green = desired; orange = borderline; red = undesired ^aCompound failed to fit a curve in one out of the six test occasions

Overlay of the fragment hit **302** (○) with the lead compound **236** (●) suggested that both the 6- and 7-positions could access the solubility pocket, which had been used in the DHB series to improve both potency and selectivity (black arrow in Figure 3.45). Targeting the 7-position would explore a novel area of the pocket, not previously examined with the DHB series. In addition, expansion towards the solubility pocket might also allow access to Trp760 to improve selectivity.

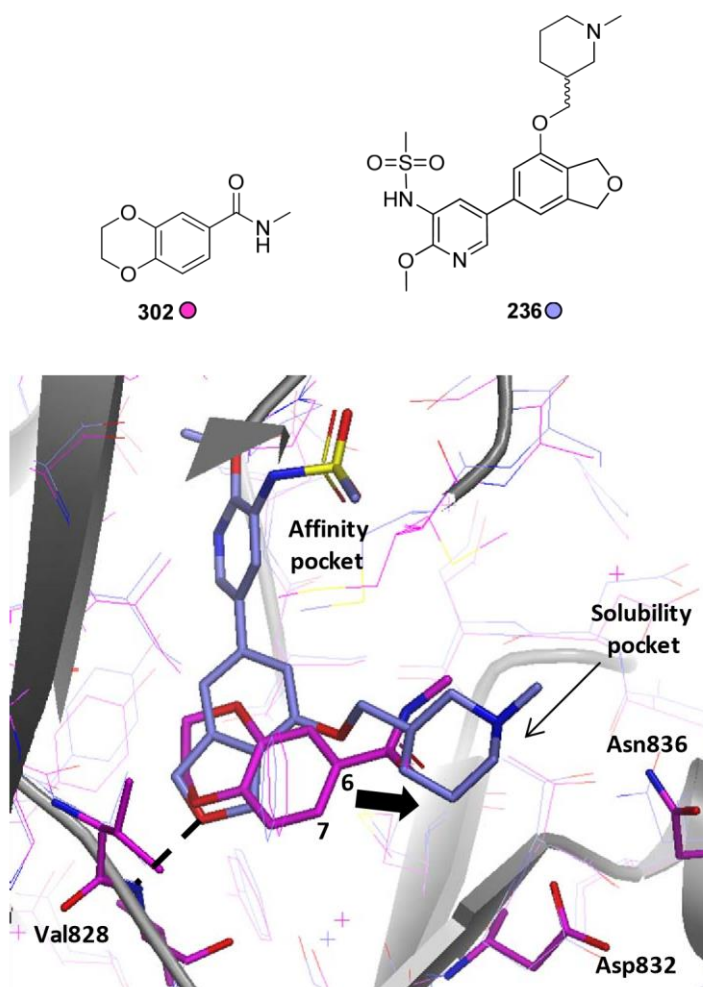


Figure 3.45 Crystal structure of PI3K δ in complex with fragment **302** (●) and lead **236** (●) indicating a potential growth vector

The crystal structures revealed that the 6-position of the benzoxazine system should access a very similar region of the pocket usually occupied by the DHB series (**236** ●, Figure 3.45). Thus, using established SAR from the DHB series, hybrid compounds were designed accordingly as shown in Figure 3.46. The full synthesis will be described in the subsequent section.

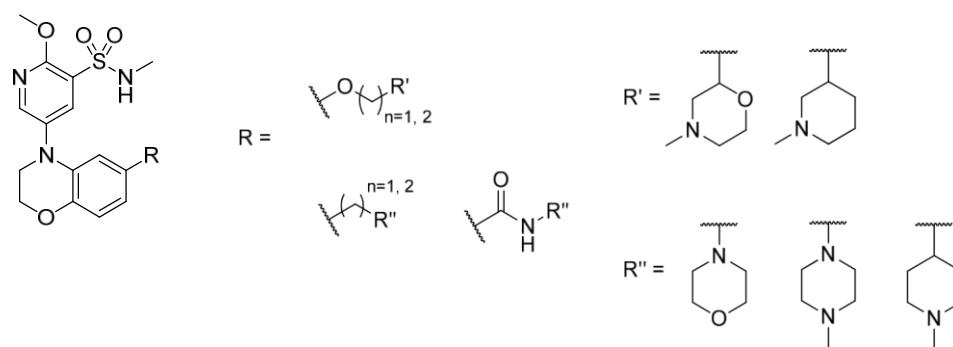


Figure 3.46 Target molecules to explore the 6-position

Initially, the pyridine sulfonamide moiety was fixed and efforts focused on investigating a range of linkers from the 6-position to explore and identify the preferred vector. The *O*-linker was selected as a direct comparison to the DHB series although the exact positions are slightly different. The *C*-linker was also investigated to understand the role of the oxygen but also to explore chain length. Consideration of the crystal structure of fragment hit **302** (●, Figure 3.45) suggested that an amide linker might also be suitable to access the desired region. The position of the substituent would be different compared to an oxygen or carbon linker and thus could access a slightly different part of the protein, which may lead to differences in potency and selectivity. *N*-linkers were initially discarded from the 6-position as the crystal structure showed no real advantage in terms of interaction and, thus, would avoid introduction of an aromatic amine as they can be mutagenic (see section 3.4.3.3.1).²⁵⁷ However, from the crystal structure, *N*-aryl amides might be of interest in derivatising the 7-position due to the close proximity of a water molecule in the crystal structure. In order to rapidly evaluate the linkers, simple terminal substituents such as morpholine, piperazine, or piperidine were selected as they were easily accessible and had demonstrated promising potency on the lead series **236**. It was proposed that more complex substituted groups could be investigated once the best linker was identified.

As mentioned above, the 7-position of the benzene ring (**302** ●, Figure 3.45) could potentially access the solubility pocket *via* a novel vector and accordingly this was

investigated further. As this position had not been explored previously, a structurebased approach was used to select the initial linkers. The objective was initially to confirm that an increase in potency could be achieved from this position. The crystal structure showed the presence of a conserved water molecule close to this position and it was hypothesised that a suitable linker could be designed to interact with this water (Figure 3.47). Examination of the H-bonding network suggested that an Hbond donor would be preferred as the water molecule is already involved in two Hbonding interactions with two carbonyl moieties present in the protein backbone. The pocket is also quite narrow in this region compared to the 6-position and, thus, an amide linker might function well in order to stay flat and avoid any potential clash with the protein surface. Docking studies also confirmed that an amide linker with the NH directly attached to the phenyl ring should be in good range to interact with the observed water molecule. By contrast, a reverse amide analogue with the carbonyl attached directly to the phenyl ring might potentially clash with Ser831 carbonyl (Figure 3.48).

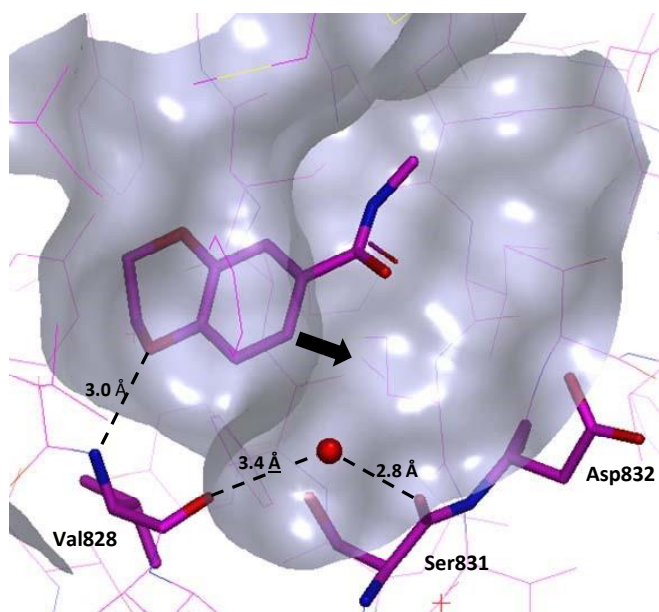


Figure 3.47 Crystal structure of PI3K δ in complex with fragment 302 (●)
Conserved water interacting with Val828 and Ser831

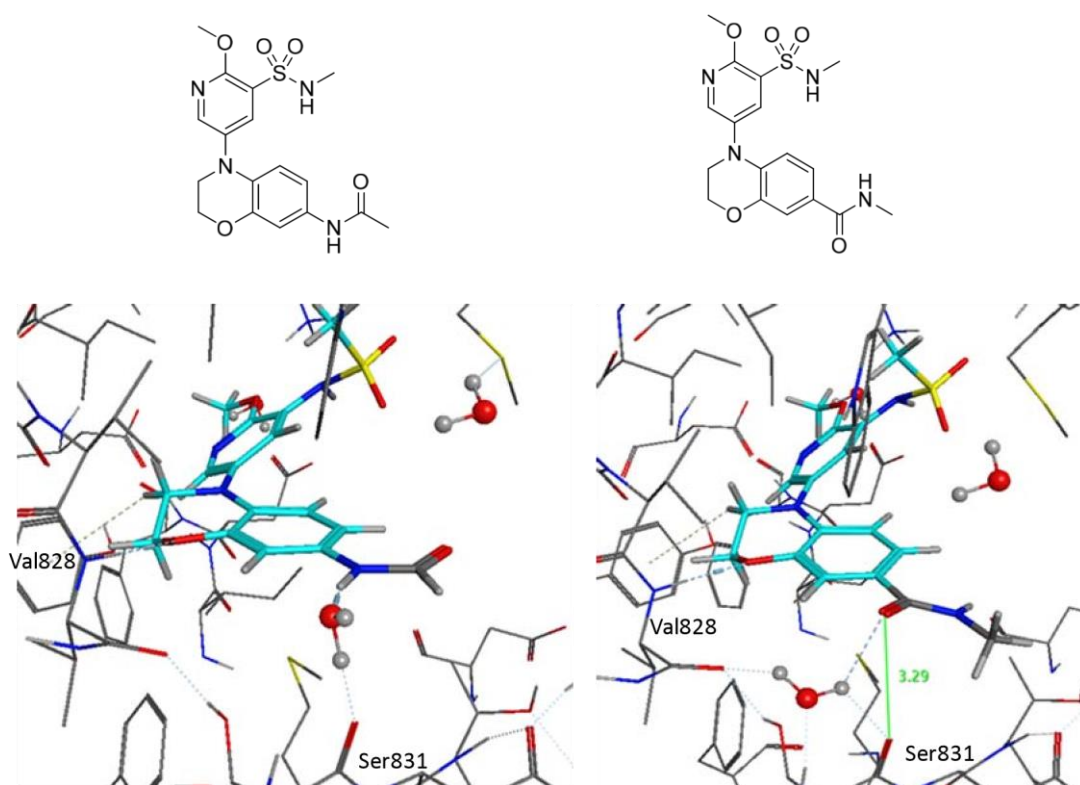


Figure 3.48 Docking structure of amide derivatives at the 7-position

Accordingly, both forward and reverse amides were synthesised to confirm our hypothesis. Initially, a small set of analogues were designed to evaluate the potential of this position as the compound would access a slightly different part of the pocket compared to the lead series **236** (Figure 3.49). Based on the structure, a basic centre might be able to interact with protein residues around this region (e.g. Asp832, Figure 3.47). The synthesis of these compounds is described in the next section 3.4.3.

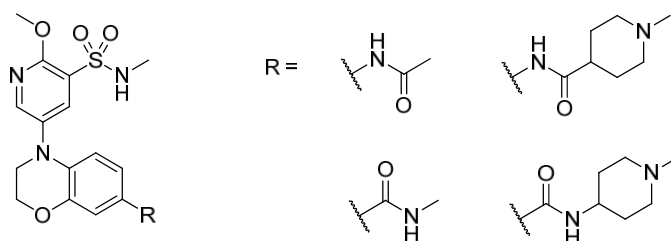


Figure 3.49 Target molecules to explore the 7-position

3.4.3 Results and Discussion

In this section, the author was responsible for both the design of novel target compounds as well as the synthetic routes towards the desired targets, in addition to full interpretation of all the associated results and data. All the practical chemistry described was carried out in collaboration with an external synthesis partner.²⁵⁸ Full characterisation was subsequently carried out by the author.

3.4.3.1 Chemistry at the 6-position

3.4.3.1.1 *O*-Linker

The four targets in this subset of potential inhibitors selected for synthesis are shown in Figure 3.50. The piperidine and morpholine substituents were selected to enable a direct comparison to the DHB lead series. Although these are not the preferred groups in terms of selectivity based on our earlier experience in prosecuting PI3K δ , they are synthetically more accessible, and would initially confirm if the SAR is transferable between the two series.

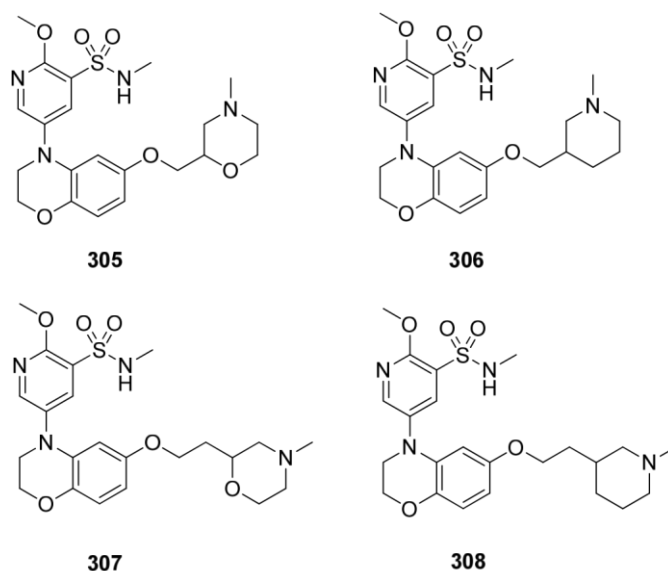


Figure 3.50 *O*-linker targets

Retrosynthetic analysis suggested three key disconnections (Figure 3.51). The first disconnection between the pyridine ring and the benzoxirane core led to the bicyclic system represented by **310**. Subsequently, disconnection at the aryl ether junction would lead to the phenol intermediate **311** and the appropriate alcohol substituents, which could be introduced *via* Mitsunobu reaction. It was reasoned that intermediate **311** could then be obtained in two steps from the commercially available benzoxazinone **312**.

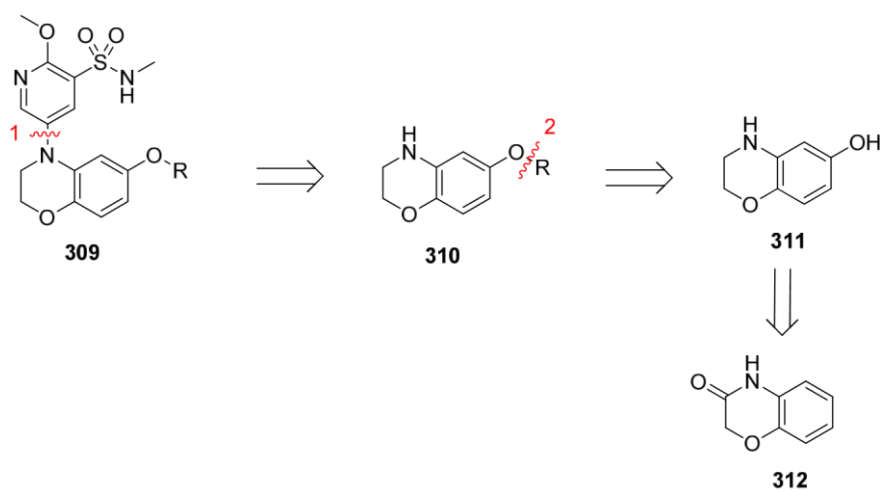
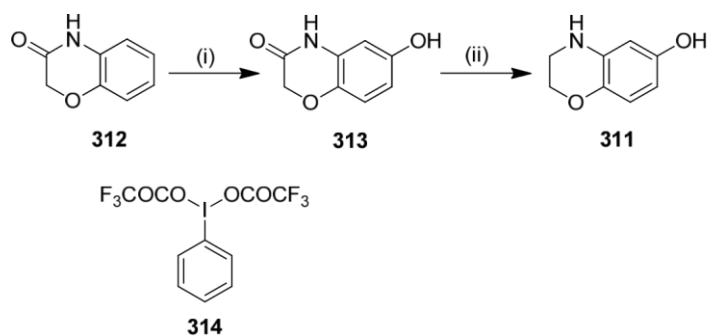


Figure 3.51 Retrosynthetic analysis of *O*-linker analogues

a. Phenol Synthesis

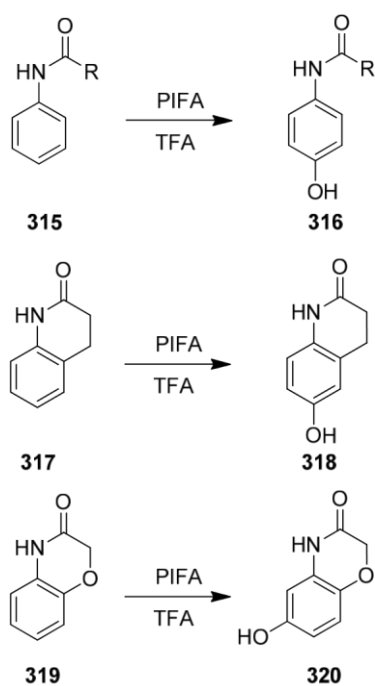
The phenol intermediate **311** was prepared from the commercially available benzoxazinone **312** using a procedure described by Itoh and co-workers (Scheme 3.22).²⁵⁹ The phenol functionality was selectively introduced in the *meta*-position with respect to the nitrogen by treatment of **312** with phenyliodine bis(trifluoroacetate) (PIFA, **314**) in TFA at reflux. The spectral data obtained was consistent with that previously reported in the literature for the same compound.²⁶⁰ With quantities of **313** in hand, the amide was then reduced using $\text{BH}_3\cdot\text{DMS}$ complex in THF to afford **311** in moderate yield.²⁶⁰



Reagents and conditions: (i) PIFA (**314**), TFA, reflux, 20 min, 55%; (ii) $\text{BH}_3\cdot\text{DMS}$, THF, rt, 1 h, 41%.

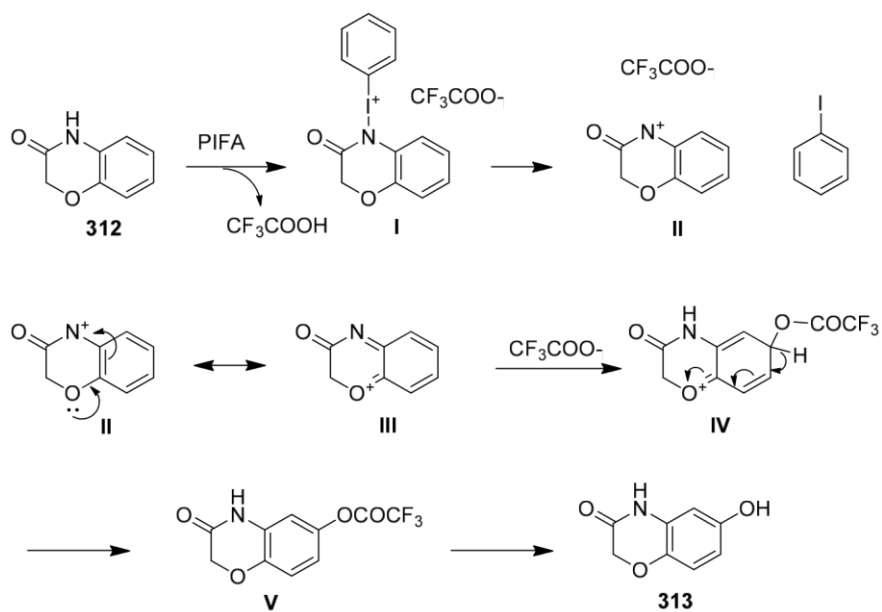
Scheme 3.22

In relation to the formation of the phenol, Itoh and co-workers have found that reaction of acetanilide **315** with PIFA in TFA introduced a hydroxyl group in the *para*-position of the phenyl ring (Scheme 3.23).²⁵⁹ Similar results were obtained with lactams such as **317**. However, in the case of the benzoxazinone ring in **319**, the oxygen has a stronger electronic effect than the nitrogen and directs the hydroxylation in the position *para* to the oxygen instead of the nitrogen. In previous work using concentrated sulfuric acid in methanol on **319**, they obtained a mixture of both the *meta*- and *para*-benzoxazinone compounds.²⁶¹



Scheme 3.23

The following mechanism was proposed by Itoh and co-workers (Scheme 3.24) to account for the regioselectivity observed.²⁵⁹

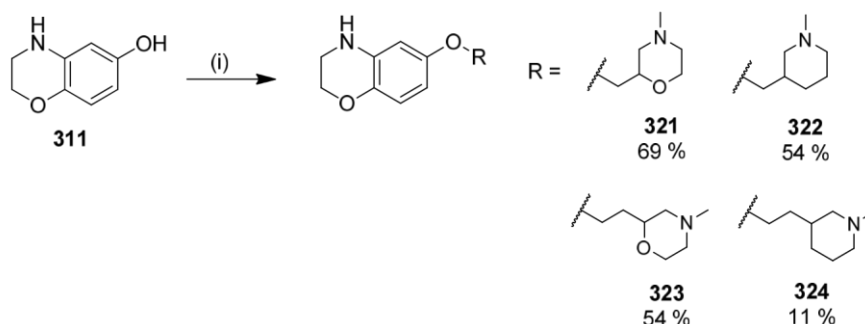


Scheme 3.24 Mechanism of benzoxazinone hydroxylation using PIFA²⁵⁹

In the first instance, PIFA reacts with the amide nitrogen to give intermediate **I**. Cleavage of the N-I bond then generates the nitrenium ion **II**. In the case of benzoxazinone intermediate **II**, a relatively more stable resonance form (**III**) can be drawn, and subsequently the charge can be trapped by trifluoroacetate anion to give **V**. Hydrolysis of **V** during the work-up gives the desired product **313**.

b. Mitsunobu Reaction

The desired alcohols were then coupled to the phenol intermediate **311** via a Mitsunobu reaction using CMBP previously employed on the lead series **236** in section 3.2.2.5 (Scheme 3.25).²⁴⁷ Isolated yields were usually good after normal phase purification, except for compound **324**, where the purification was more challenging resulting in the comparatively low yield.



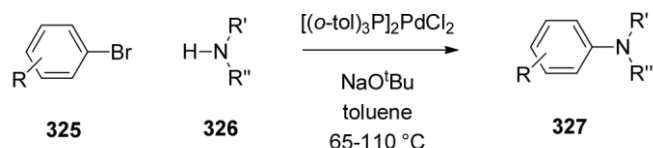
Reagents and conditions: (i) ROH, CMBP, toluene, 120 °C, 1 h.

Scheme 3.25

c. Buchwald-Hartwig Coupling

The Pd-catalysed *N*-arylation or Buchwald-Hartwig reaction is one of the most popular and valuable transformation for the synthesis of aromatic C-N bonds.²⁶² Prior to the discovery of this reaction, harsh conditions were employed to carry out this

transformation using organotin reagents and stoichiometric catalyst.^{263,264} Therefore, alternative routes were extensively investigated to identify milder conditions. In 1995, Buchwald and Hartwig simultaneously demonstrated that the coupling reaction could be carried out with free amines instead of organotin reagents in presence of palladium catalyst and a bulky base (Scheme 3.26).^{265,266}



Scheme 3.26 *N*-aryl conditions reported by Buchwald²⁶⁵

Since then, Buchwald and Hartwig have significantly expanded the scope of the reaction to include a wide range of aryl halides (e.g. Ar-Cl), amines, and ligands whilst increasing the overall efficiency of the reaction. Breakthroughs in this area have typically been driven by the implementation of novel ligands. Initially, the first generation catalyst (e.g. P(*o*-tol)₃) were found to be effective for coupling aryl bromides and secondary amines.^{265,266} The development of bidentate ligands such as BINAP, dppf, and XantPhos facilitated the coupling of primary amines and aryl iodides and triflates.^{262,267-270} More recently, more sterically hindered ligands (dialkylbiaryl monophosphine ligands such as XPhos, RuPhos - Figure 3.52) have been developed and have now been reported to be the most effective.^{262,271-273}

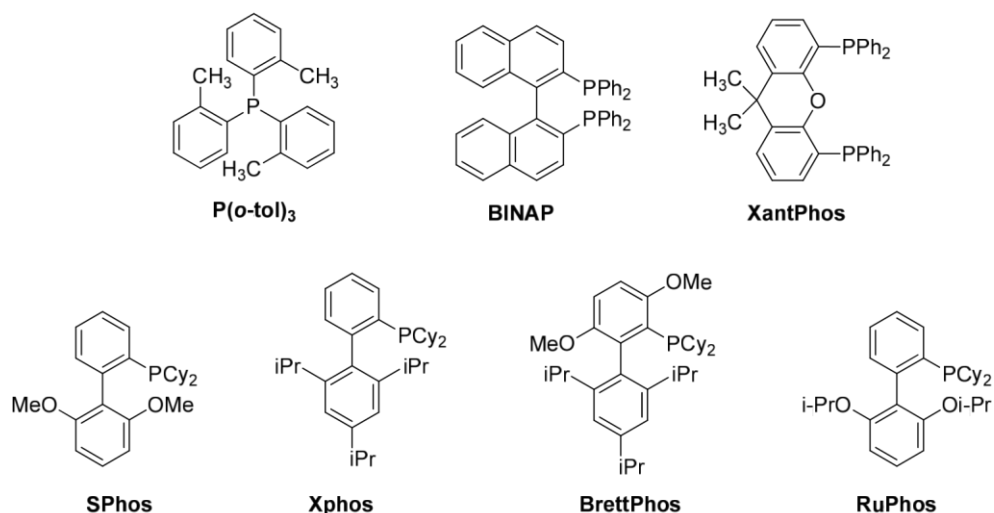


Figure 3.52 Ligands for Buchwald-Hartwig coupling

In terms of the Pd-catalyst component, Pd(OAc)₂ and Pd₂(dba)₃ have been widely used. The most common bases used in the coupling reaction include NaO^tBu, Cs₂CO₃, NaOMe and LiHMDS. NaO^tBu is widely used and often gives the highest reaction rate.²⁶²

Despite all these efforts, the conditions required for the reaction still remain largely substrate dependent.²⁶² Indeed, the nature of the coupling partners has an influence on the rate of oxidative addition, amine binding, and reductive elimination. The choice of ligand employed also plays a role in the rate with electron-rich ligands enhancing oxidative addition, whilst steric bulk controls reductive elimination. These factors with the added choice of base, solvent, and temperature make the reaction far from trivial and often require screening of a range of reaction conditions.

A general catalytic cycle of the reaction is described in Figure 3.53.²⁷⁴ The first step consist of an oxidative addition of Pd⁰ with the aryl halide to afford the Pd^{II} complex (II). The amine then coordinates to the Pd^{II} to form complex III. Upon deprotonation of the amine, the complex IV is generated. The final step is a reductive elimination

resulting in the formation of the desired product **X** and the regeneration of the palladium catalyst **I**.

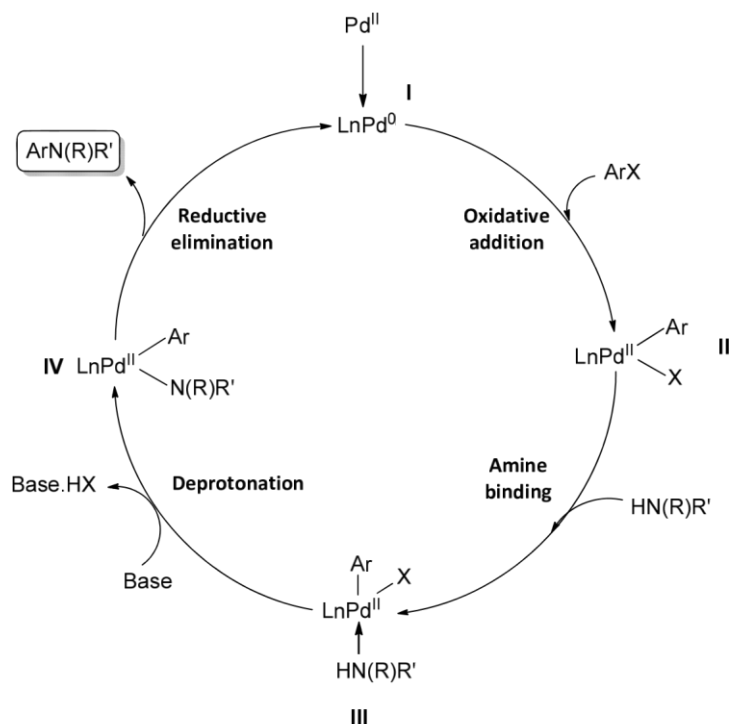
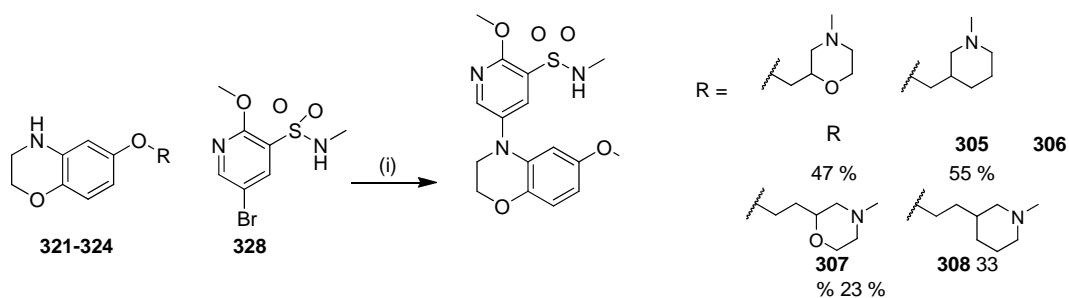


Figure 3.53 Mechanism of Buchwald-Hartwig reaction

Given its noted utility, the Buchwald-Hartwig coupling was selected to synthesise the final products **306-309** (Scheme 3.27). The commonly used Pd₂(dba)₃ catalyst and NaO^tBu base were selected in the first instance. XPhos is commonly used in our laboratories for these transformations and has shown to be efficient with heteroaryl halides. Using these conditions, yields were moderate and some of the compounds required multiple purification attempts to obtain the desired purity for testing, resulting in lower yields. At this stage of the project, alternative conditions were not investigated.



Reagents and conditions: (i) Pd₂(dba)₃, XPhos, NaO^tBu, toluene, 120-130 °C, 30 min.

Scheme 3.27

3.4.3.1.2 One Carbon Linker

The two targets described in Figure 3.54 were selected to evaluate the efficacy of a one carbon linker between the core and the putative solubilising groups. Overlay between fragment **302** and lead molecule **236** suggested that one methylene spacer may position the morpholine and piperazine ring in a similar region of the protein to that accessed by the piperidine in compound **236** (Figure 3.45).

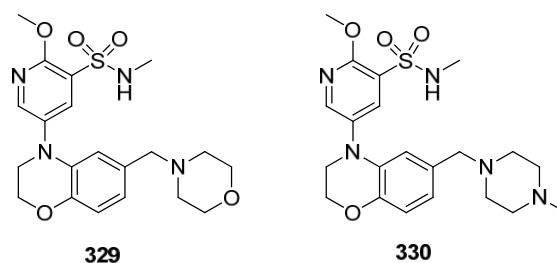


Figure 3.54

Retrosynthetic analysis indicated two key disconnections (Figure 3.55). Firstly, the disconnection between the pyridine ring and the benzoxirane led to benzoxirane intermediate **332**. Disconnection at the linker junction would lead to the commercially available bromo intermediate **333**, which could conceivably react with potassium trifluoroborate adducts e.g. **334** to introduce the desired amine groups.^{275,276} However, the availability of a range of the desired trifluoroborate salts might be limited.

Alternatively, disconnection at the amine junction would lead to the aldehyde **335**, which could be obtained from the bromo intermediate **333**. Although this route would involve one additional step, it would allow rapid exploration of different amines once the desired aldehyde intermediate **335** was obtained. Accordingly, this latter option was selected for synthesis.

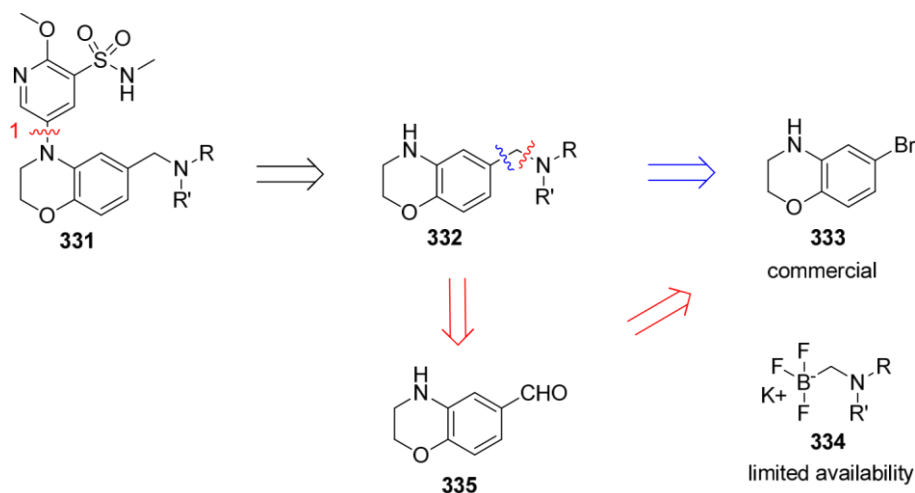
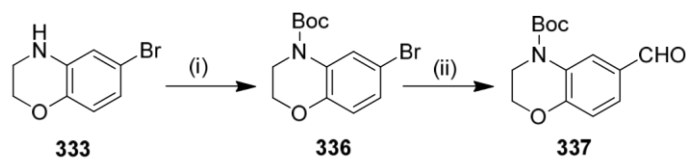


Figure 3.55 Retrosynthetic analysis

a. Aldehyde Synthesis

To avoid side reactions during the reductive amination step, the nitrogen of the benzoxirane ring required protection. Boc protecting groups are commonly used to protect amines as they are introduced and removed easily.²⁷⁷ They are stable in basic conditions and can be straightforwardly removed in acidic conditions, which was compatible for the subsequent steps. Boc protection of the benzoxazine ring has been reported in the literature and, thus, similar conditions were applied.²⁷⁸ The intermediate **333** was reacted with Boc anhydride in presence of triethylamine and DMAP to obtain the desired Boc protected intermediate **336** in excellent yield (Scheme 3.28). The aldehyde was then introduced by lithiation followed by reaction with DMF following literature conditions.²⁷⁹

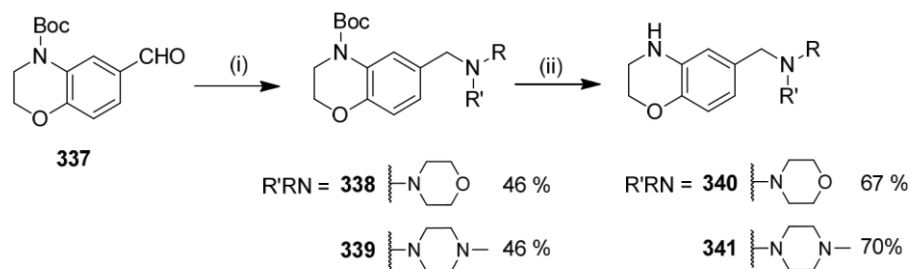


Reagents and conditions: (i) Boc_2O , TEA, DMAP, DCM, rt, overnight, 95%; (ii) $n\text{-BuLi}$, THF, $-78\text{ }^\circ\text{C}$, 10 min, then DMF, 10 min, 44%.

Scheme 3.28

b. Reductive Amination

With the requisite aryl aldehyde intermediate **337** in hand, the desired amines were introduced by reductive amination using sodium cyanoborohydride in the presence of acetic acid (Scheme 3.29).²⁸⁰ Following this procedure, the Boc protecting group was removed with HCl in dioxane in good yields.



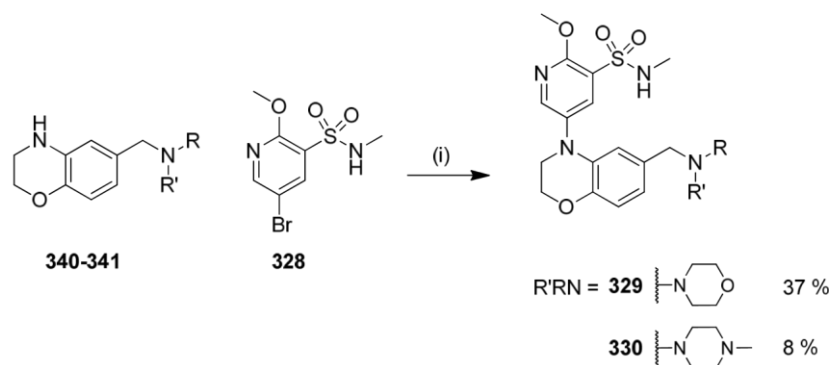
Reagents and conditions: (i) $\text{RR}'\text{NH}$, AcOH, DCM/MeOH (4:1), $0\text{-}5\text{ }^\circ\text{C}$ to rt, overnight followed by NaCNBH_4 , $0\text{ }^\circ\text{C}$ to rt, 3 h; (ii) HCl, dioxane, $0\text{-}5\text{ }^\circ\text{C}$, 5 h.

Scheme 3.29

c. Buchwald-Hartwig Coupling

Pyridine sulfonamide **328** was introduced using a Buchwald-Hartwig coupling (Scheme 3.30). The conditions previously identified on this system were applied

without further optimisation. The yield was comparatively low for compound **330** due to difficulty in the purification.



Reagents and conditions: (i) $\text{Pd}_2(\text{dba})_3$, XPhos, NaO^tBu , toluene, $130\text{ }^\circ\text{C}$, 30 min.

Scheme 3.30

3.4.3.1.3 Two Carbon Linker

As discussed previously, exploration of the linker length was considered to be a viable strategy to explore SAR. Accordingly, the targets described in Figure 3.56 were selected for synthesis as the crystal structure of compound **237** suggested these could be accommodated. Besides tuning primary potency, a longer chain might give a different profile in terms of selectivity with respect to the other PI3K isoforms.

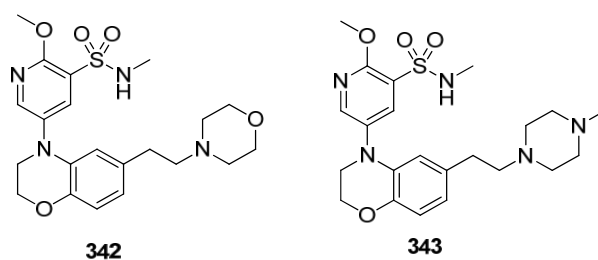


Figure 3.56

From a retrosynthetic perspective, and as previously proposed, disconnection 1 between the pyridine ring and the core led to benzoxirane intermediate **345** (Figure 3.57). Disconnection 2 at the linker junction would lead to the commercially available bromo intermediate **333**. However a survey of vendor databases indicated that the choice of desired trifluoroborate salts to accompany this would be very limited. From analysis of the literature and experience elsewhere in our laboratories, an alternative route *via* intermediate **347** was found, which could be obtained from commercially available benzoxazinone **312** *via* Friedel-Crafts acylation and reduction. This route would then enable the introduction of a wide range of amines.

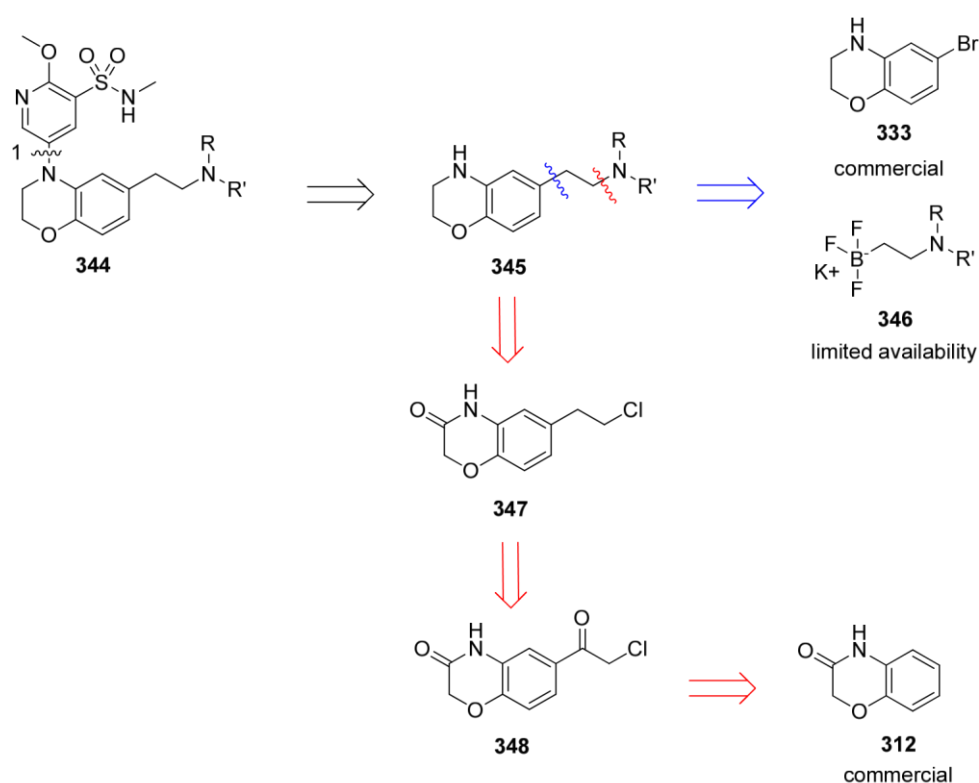


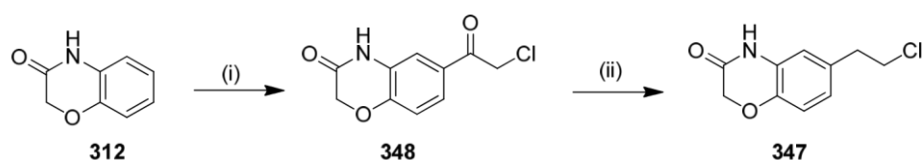
Figure 3.57 Retrosynthetic analysis of two carbon linker

a. Friedel-Crafts Acylation

As synthesis relating to intermediate alkyl chloride **347** has been reported in the literature,^{281,282} a similar synthetic route was investigated. The carbon chain was

introduced by Friedel-Crafts acylation followed by reduction of the carbonyl using triethylsilane. The Friedel-Crafts reaction is a powerful method to introduce substituent on an aromatic ring *via* electrophilic aromatic substitution. Alkylation reactions can potentially give polyalkylated products since the product can be more reactive than the original substrate and, thus, the acylation reaction is a valuable alternative.

Accordingly, intermediate **347** was prepared following reported conditions (Scheme 3.31).^{281,282} The commercially available benzoxazinone **313** was acylated *via* Friedel-Crafts using 2-chloroacetyl chloride in presence of aluminium trichloride. Acylation could occur in both the *ortho*- and *para*-position to the oxygen or nitrogen, as they are both electron-donating groups. However we reasoned that the acetyl group on the nitrogen makes the amine slightly less-electron donating than the oxygen ether and, thus, acylation should occur preferentially *ortho* or *para* with respect to the oxygen. The *ortho*-position is more hindered, favouring the *para*-position. This was confirmed by comparing the NMR spectral detail obtained with literature data. The carbonyl was then reduced using triethylsilane in presence of TFA to give the desired intermediate **347** in excellent yield.²⁸²

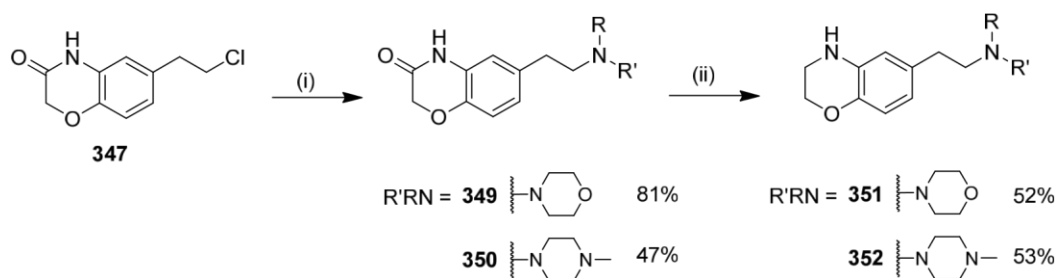


Reagents and conditions: (i) 2-chloroacetyl chloride, AlCl₃, DCM, 0 to 20 °C, 12 h, 69%; (ii) Et₃SiH, TFA, 0 °C to rt, overnight, 92%.

Scheme 3.31

b. Amine Synthesis

Having synthesised the appropriate alkyl halide **347**, the desired amine substituents were introduced by alkylation in the presence of potassium iodide in DMF (Scheme 3.32). The benzoxazinone ring was then reduced using $\text{BH}_3 \cdot \text{DMS}$ complex.

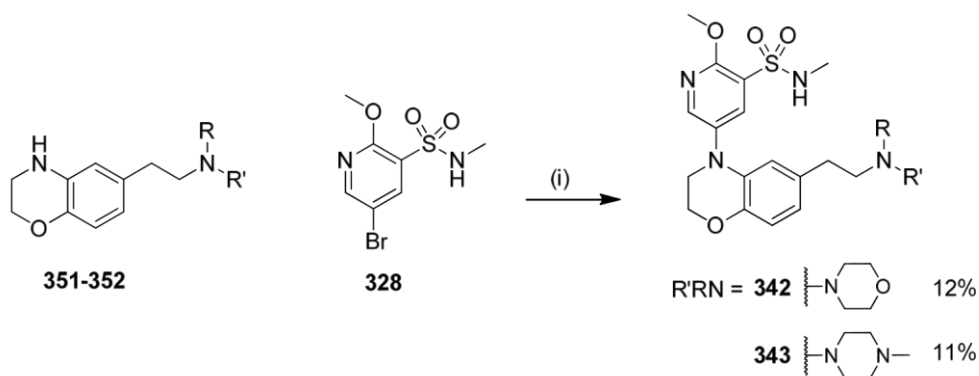


Reagents and conditions: (i) $\text{RR}'\text{NH}$, KI, DMF, rt, 4 h, then 110 °C, 4-16 h; (ii) $\text{BH}_3 \cdot \text{DMS}$, THF, rt, 70 min.

Scheme 3.32

c. Buchwald-Hartwig Coupling

Finally, to complete the synthesis of the target homologated systems, the benzoxirane rings **351-352** were coupled to the pyridine sulfonamide **328** using the Buchwald conditions developed previously (Scheme 3.33). Although yields were low due to extended purification procedures, this approach delivered the final products in sufficient quantities for biological testing and, thus, no further optimisation was attempted at this stage of the programme.



Reagents and conditions: (i) $\text{Pd}_2(\text{dba})_3$, XPhos, NaO^tBu , toluene, 130 °C, 30 min.

Scheme 3.33

3.4.3.1.4 Amide Linker

As outlined earlier, the original fragment **302** exhibited an amide moiety and expansion in this region was considered to be attractive in terms of enhancing potency. Accordingly, the targets described in Figure 3.58 were selected for synthesis.

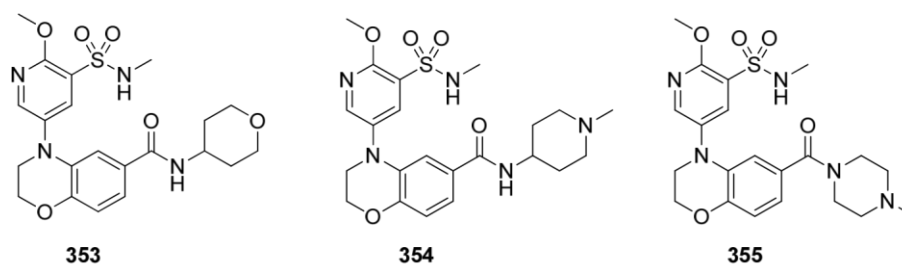


Figure 3.58

For the amide analogues, the two disconnections proposed could be carried out in any order, however, the most efficient route is as proposed in Figure 3.59. The first disconnection at the amide junction led to key carboxylic acid intermediate **357**. Disconnection 2 between the pyridine ring and the benzoxirane led to the commercially available benzoxirane ring **358**.

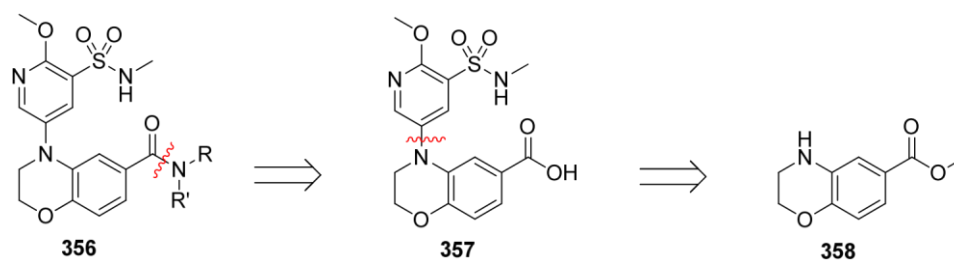
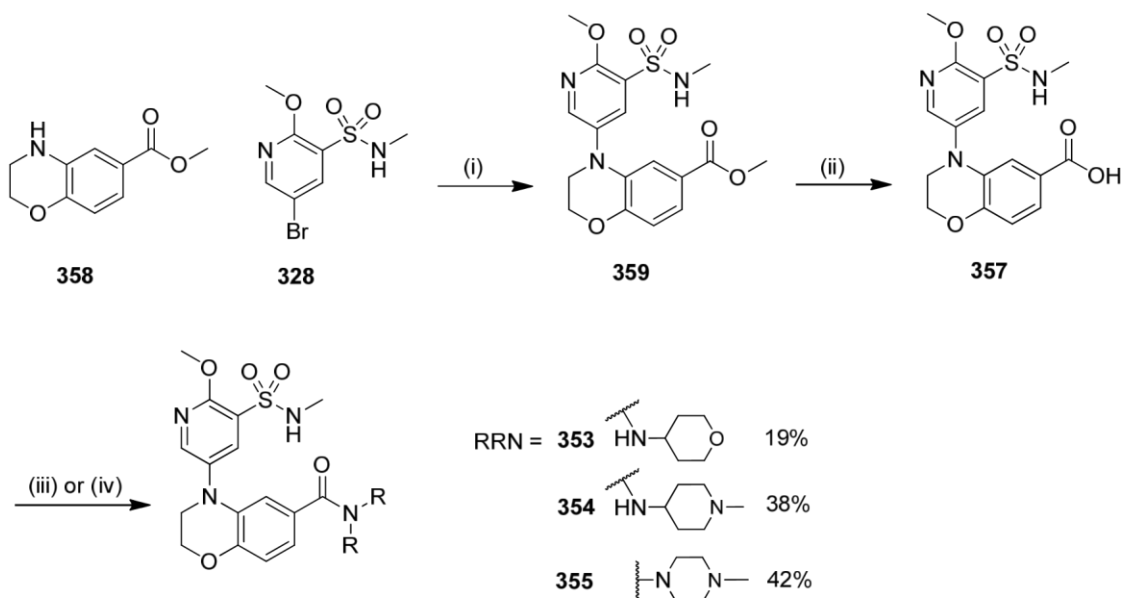


Figure 3.59 Retrosynthetic analysis of amide linker

The target molecules **353-355** were prepared according to Scheme 3.34. The commercially available benzoxazine ester **358** was coupled to the pyridine sulfonamide **328** by the previously described Buchwald protocol, and the ester was hydrolysed using standard conditions. The final products were obtained by amide coupling using HATU or T₃P.



Reagents and conditions: (i) Pd₂(dba)₃, XPhos, NaO^tBu, toluene, 130 °C, 30 min, 33%; (ii) LiOH, THF/H₂O, rt, 5 h, 65%; (iii) **353-354** RRNH₂, HATU, DIPEA, DMF, rt, 3-4 h; (iv) **355** RRNH₂, T₃P, Et₃N, DMF, rt, 60 h.

Scheme 3.34

3.4.3.2 Derivatisation at the 7-position

As indicated previously, an alternative vector for expansion of the benzoxazine template was accessible from the 7-position of the ring. In this case, synthesis of both the forward and reverse amides was considered and, based on this, the four targets described in Figure 3.60 were initially selected.

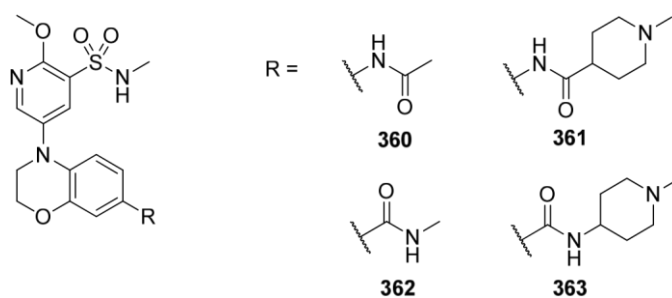


Figure 3.60 Targets to explore the 7-position

For both linkers, the first disconnection would be at the amide junction to lead to the amine and carboxylic acid intermediates **365** and **368**, respectively (Figure 3.61). Subsequent disconnection between the pyridine ring and the benzoxirane and functional group interconversion led to the commercially available starting materials **366** and **369**. Introduction of the pyridine sulfonamide group early in the synthesis will enable rapid access to the final compounds.

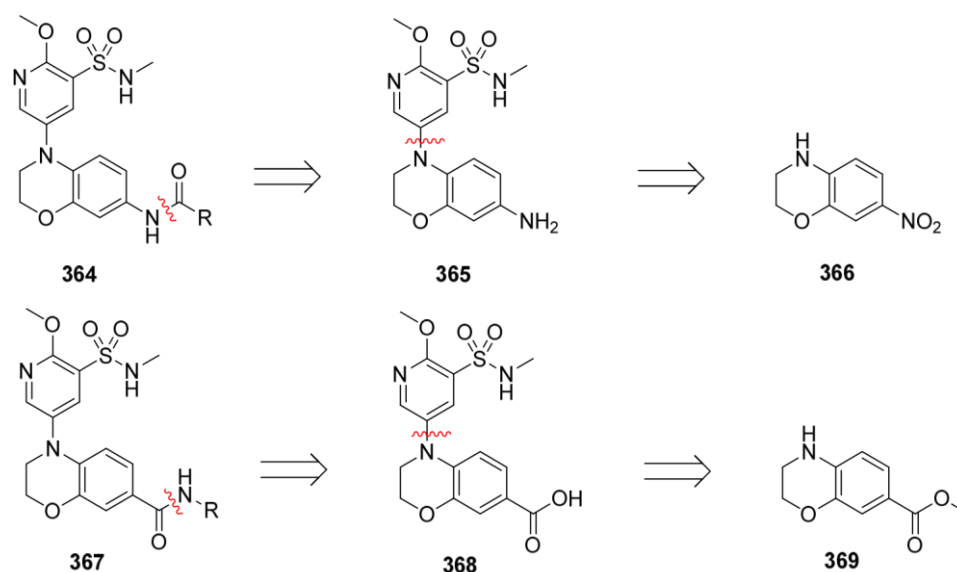
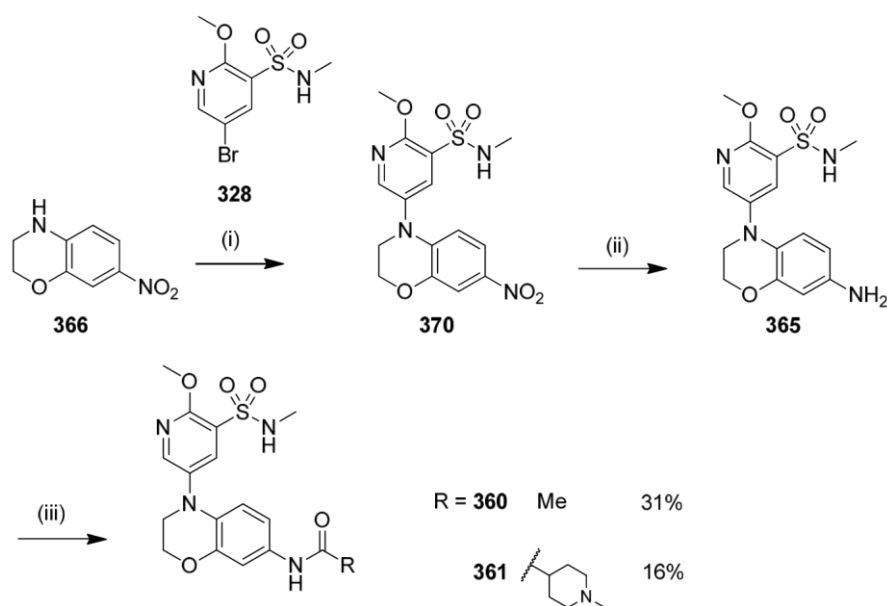


Figure 3.61 Retrosynthetic analysis

For both routes, chemistry previously developed for elaboration of the 6-position was applied, as discussed above.

The target molecules **360** and **361** were prepared according to Scheme 3.35. The commercially available nitro benzoxazine **366** was coupled to the pyridine sulfonamide **328** by Buchwald-Hartwig chemistry using conditions previously established and in moderate yield (see section 4.3.1.3). The nitro group was then reduced by hydrogenation using palladium on carbon to give the amine intermediate **365** in excellent yield. Finally, the desired products **360-361** were obtained by amide coupling using standard conditions of EDC, HOBt and DIPEA in DCM.¹⁰⁹ Poor yields were obtained due to difficult purification.

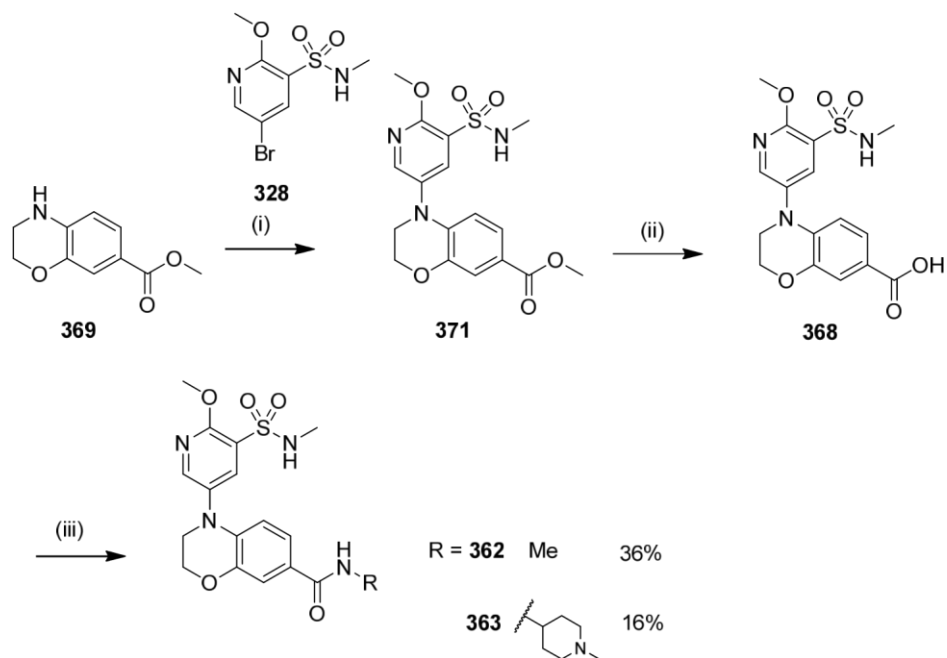


Reagents and conditions: (i) Pd₂(dba)₃, XPhos, NaO^tBu, toluene, 130 °C, 2 h, 38%; (ii) H₂, Pd/C, EtOAc, 60 psi, 2 h, 96%; (iii) RCO₂H, EDC, HOBt, DIPEA, DCM, rt, 16 h. **Scheme**

3.35

Returning to the synthesis of the forward amide systems, the target molecules **362** and **363** were prepared according to Scheme 3.36. The commercially available benzoxazine ester **369** was coupled to the pyridine sulfonamide **328** again by using previously developed Buchwald chemistry. The ester was then hydrolysed using LiOH in a mixture of THF/water before the desired products **362** and **363** were obtained by amide coupling in this instance using CDI in DMF.¹⁰⁹ Yields of the final coupling step were again low. Alternative amide coupling conditions could be investigated in attempts to

improve these yields. HATU, for example, gave higher yields in the synthesis of the 6-position series. To improve reactivity further, conversion to the acid chloride could also be considered as a good alternative.¹⁰⁹



Reagents and conditions: (i) Pd₂(dba)₃, XPhos, NaO^tBu, toluene, 130 °C, 2 h, 25%; (ii) LiOH, THF/H₂O, rt, 16 h, 89%; (iii) RNH₂, CDI, DMF, 50 °C, 16 h. **Scheme 3.36**

3.4.3.3 Biological Results

3.4.3.3.1 Biological Results on 6-substituted Benzoxazines

Following synthesis, all the compounds described above were progressed to the relevant biological assays. The tables below summarise the data generated on the

6-substituted analogues. In each case, the new compounds are compared to the initial fragment hit **304** and the relevant DHB analogues **236** and **288** (Figure 3.62).

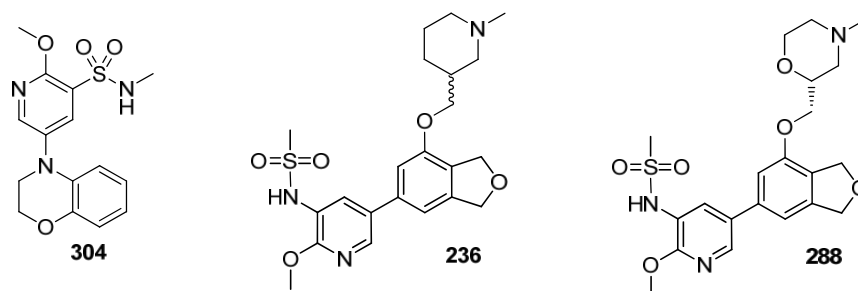
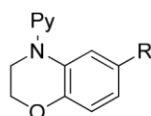


Figure 3.62

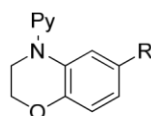


Cmpd	R	pIC ₅₀ δ (LE/LLE _{AT})	X-fold selectivity α, β, γ	hWB pIC ₅₀	Chrom logD _{7.4}
236	N/A	8.3 0.37; 0.35	79; 40; 316	7.1	2.2
304	H	6.3 0.38; 0.29	16; 32; 16	4.7 ^a	4.9
306		7.2 0.31; 0.26	32; 25; 40	5.9	2.7
308		7.5 0.31; 0.24	25; 50 ; 158	5.8 ^b	2.9
330		5.9 0.26; 0.22	6; 8; 10	n.d.	2.4
343		7.1 0.30; 0.31	10; 20; 32	5.7	2.5
354		7.7 0.32; 0.34	32; 20; 100	6.0	1.8
355		6.1 0.26; 0.26	25; 20; 32	5.1 ^c	2.7

Table 3.12 Biological results on the 6-position with piperidine/piperazine substituents

^a Compound failed to fit a curve in 2 occasions and reported inactive (pIC₅₀ < 4.4) in 1 occasion out of the 5 test occasions. ^b Compound failed to fit a curve in 3 out of the 6 test occasions.

^c Compound failed to fit a curve in 1 occasion and reported inactive (pIC₅₀ < 4.4) in 2 occasions out of the 5 test occasions.



Cmpd	R	pIC ₅₀ δ (LE/LLE _{AT})	X-fold selectivity α, β, γ	hWB pIC ₅₀	Chrom logD _{7.4}
288	N/A	8.0 0.35; 0.37	50; 79; 63	6.6	3.1
304	H	6.3 0.38; 0.29	16; 32; 16	4.7 ^a	4.9
305		7.0 0.30; 0.28	13; 32; 16	5.6	3.8
307		7.4 0.31; 0.27	50; 32; 40	5.5	4.0
329		6.1 0.28; 0.25	4; 8; 16	5.4 ^b	4.2
342		6.8 0.30; 0.26	8; 13; 8	6.0	3.9
353		7.5 0.32; 0.35	25; 316; 13	6.4 ^c	3.2

Table 3.13 Biological results on the 6-position with morpholine substituents

^aCompound failed to fit a curve in 2 occasions and reported inactive (pIC₅₀<4.4) in 1 occasion out of the 5 test occasions.

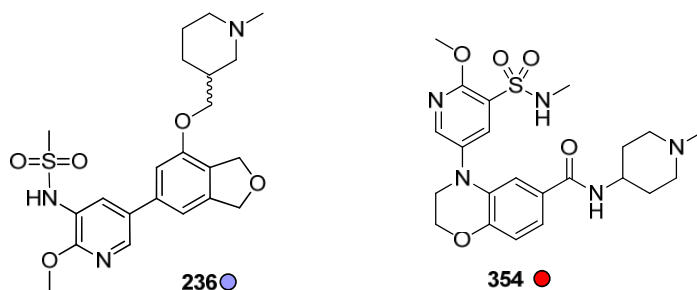
^bCompound failed to fit a curve in 1 out of the 5 test occasions. ^cCompound failed to fit a curve in 2 out of the 8 test occasions.

Most of the compounds tested for the 6-position delivered suboptimal enzyme potency and relatively low cellular potency compared to the DHB analogues **236** and **288**. The one carbon linker analogues (**329-330**) displayed a very poor overall profile suggesting that the linker length might be too short to reach the desired pocket. The crystal structure also suggested that the pocket near the benzoxirane ring is initially narrow and then opens up. Based on this, we reasoned that the morpholine system with the shorter linker might clash with the protein in this region. The two carbon linker

analogues (**342-343**) gave slightly higher potency, as did the *O*-linked compounds (**305-308**), supporting our view that longer chains were preferred.

However, the compounds suffered from low cellular potency compared to compounds **236** and **288**, especially in the cellular assay and thus also suboptimal lipophilic ligand efficiency. On the other hand, the amide linker compounds (**353-354**) showed a more promising overall profile. They maintained acceptable LE and LLE_{AT} compared to compounds **236** and **288** and showed encouraging cellular potency. Both compounds showed enhancement of selectivity. However, data on compound **355** indicated that the tertiary amide was less well tolerated. It is possible that the amide NH might be involved in interaction or the substituent might clash with the protein as the pocket is narrower near the benzoxazine ring.

Based on its biological data, compound **354** (2.8 Å, ●) was submitted to X-ray crystallography and a structure was successfully obtained (Figure 3.63).¹⁸⁶ The compound was shown to bind in the ATP-pocket as expected and made the key interaction with Val828 at the hinge region. The piperidine ring extended into the desired region where the equivalent moiety of compound **236** (●) was located but extended further into the pocket. The two compounds occupied a very similar part of the binding site resulting in very similar profiles. From consideration of the crystal structure of compound **354**, we reasoned that it was possible that the tertiary amide might clash with the protein as this region is narrower near the fused phenyl ring explaining the low potency associated with compounds such as **355**.



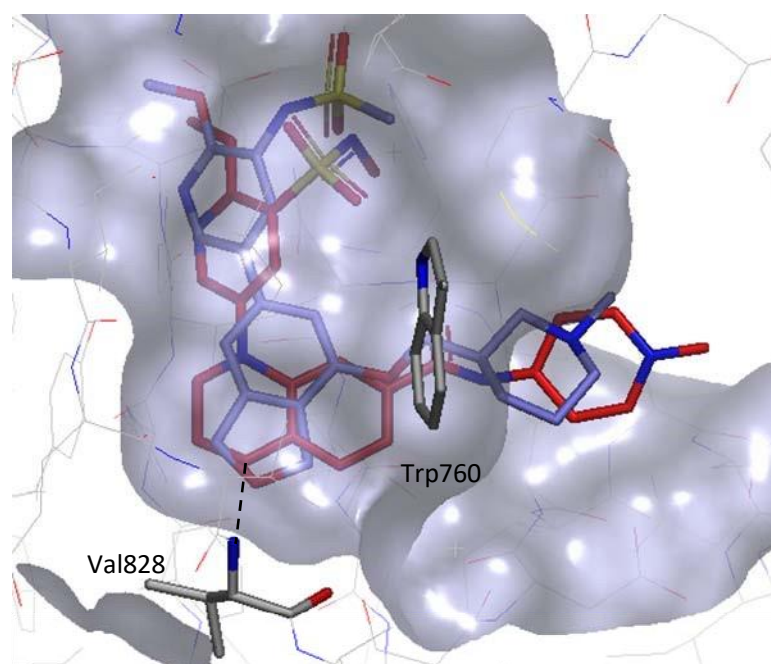


Figure 3.63 Crystal structure of PI3K δ in complex with **354** (●) and lead **236** (●)

As discussed in the introduction, we were aware that potency and selectivity could be improved by adding additional bulk around the piperidine ring in compound **236** to pack against Trp760, based on our experience with other classes of PI3K δ inhibitors. From the crystal structure, however, it was not clear if it would be possible to take advantage of the tryptophan interaction as the piperidine ring is further away from Trp760 compared to the corresponding ring in compound **236** and, thus, might not be able to optimally interact. As tertiary amides are not tolerated, we reasoned that it could potentially be interesting to try a smaller ring such as a pyrrolidine to access a slightly different vector or to add a CH₂ linker to direct the piperidine ring towards Trp760. Further analysis of the crystal structure revealed a number of residues in good range for additional interactions with the ligand (e.g. Asp832, Asn836). Based on this, it was hypothesised that these could be targeted to increase affinity and potentially selectivity. A further selection of amides were thus designed to test these hypotheses and evaluate if both potency and selectivity could be improved from this position (Figure 3.64).

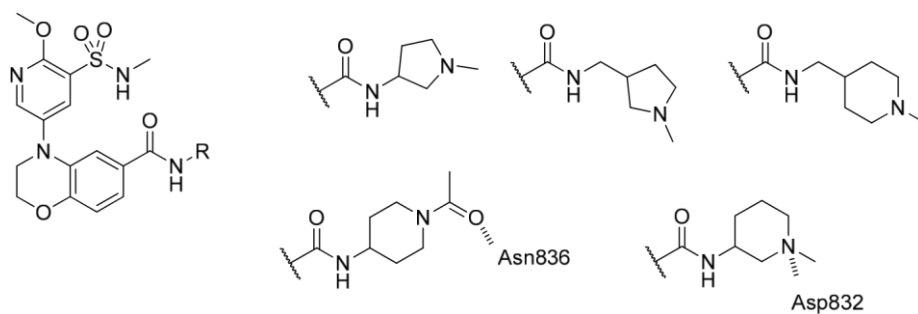
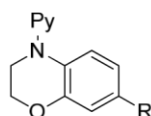


Figure 3.64

3.4.3.3.2 Biological Results on 7-substituted Benzoxazines

Biological results for this compound subset are summarised in Table 3.14. The compounds are compared to the initial fragment **304** and the DHB lead compound **236**.



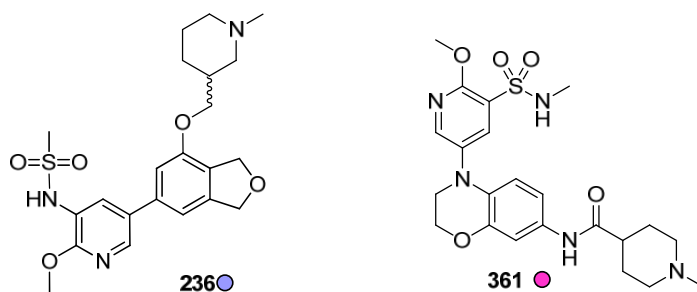
Cmpd	R	PI3K δ pIC ₅₀ (LE/LLE _{AT})	X-fold selectivity α, β, γ	hWB pIC ₅₀	Chrom logD _{7.4}
236	N/A	8.3 0.37; 0.35	79; 40; 316	7.1	2.2
304	H	6.3 0.38; 0.29	16; 32; 16	4.7 ^a	4.9
360		6.9 0.35; 0.34	25; 100; 5	5.7	2.5
361		8.1 0.34; 0.35	63; 2512; 398	6.1	1.5
362		6.1 0.31; 0.31	8; 40; 2	5.3	2.4
363		6.5 0.27; 0.29	50; 40; 100	5.1	1.4

Table 3.14 Biological results on the 7-substituted benzoxazines

^aCompound failed to fit a curve in 2 occasions and reported inactive (pIC₅₀<4.4) in 1 occasion out of the 5 test occasions.

The data generated confirmed that the amide with the NH directly attached to the phenyl ring (**360-361**) was preferred, as suggested by the crystal structure of compound **236**. Both compounds showed increased potency and lipophilic ligand efficiency compared to initial fragment **304**. Compound **361** showed a particularly encouraging profile as a novel lead compound. The compound had good enzyme potency with good efficiencies and excellent selectivity over PI3K β and PI3K γ compared to the lead series compound **236**. However, the compound suffered from a much lower than expected potency in the cellular assay resulting in sub-optimal potency compared to our cellular pIC₅₀ target of 7. One explanation for this could be the poor permeability of the compound (< 3 nm/sec) and this would need to be addressed in subsequent compounds alongside PI3K α selectivity.

A crystal structure of compound **361** (●) was also obtained confirming its binding mode (2.6 Å, Figure 3.65).¹⁸⁶ The compound participated in the expected key interaction with Val828 at the hinge region. From previous crystal structures (e.g. compound **302**), it was suspected that the amide NH was making a favourable interaction *via* a water molecule, although this was not observed in the new structure. It was also apparent that the piperidine ring was not making any additional interactions with the PI3K δ protein but when compared with compound **360**, it was hypothesised that it was accessing a new region that also appeared to give excellent selectivity over PI3K β and PI3K γ without packing against Trp760. Indeed, an overlay with lead compound **236** (●) showed that a novel area of the protein was accessed. Based on this structure, the piperidine nitrogen was suitably positioned to interact with proximal residues (e.g. Asp832). However, it was considered that the 3substituted piperidine might also be worthy of investigation in order to optimise the interaction with Asp832. From the crystal structure, it was not fully apparent that substituents on the piperidine ring might be able to pack against Trp760, which is known to be beneficial both for potency and selectivity, but was still worth investigating to fully understand SAR and potentially improve PI3K α selectivity.



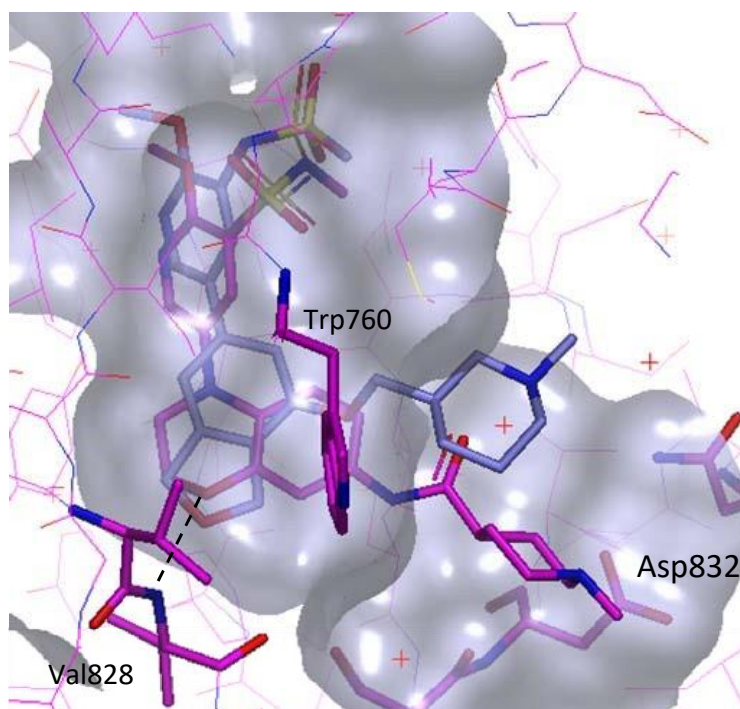


Figure 3.65 Crystal structure of PI3K δ in complex with fragment **361** (●) and **236** (●)

Given its encouraging overall profile, compound **361** was progressed to *in vivo* pharmacokinetic studies to generate a full profile around this series. The data are summarised in Table 3.15.

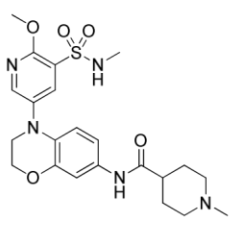
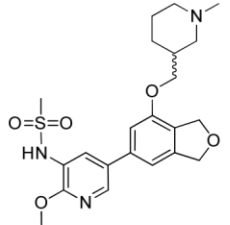
Structure	 361	 236
PI3Kδ pIC₅₀	8.1	8.3
hWB pIC₅₀	6.1	7.1
chromlogD_{7.4}	1.5	2.2
CLND sol. (μg/mL)	155	≥ 230
Perm. (nm/sec)	< 3	310
Rat Cl_b (mL/min/kg)	35	42
V_{dss} (L/kg)	4.3	1.4
T_{1/2} (h)	2.6	0.5
F (%)	n.d.	2 %

Table 3.15 Profile of compound **361**

The pharmacokinetic profile of compound **361** was very encouraging and showed significant improvement compared to lead compound **236**. In particular, the compound had a good half life and volume of distribution, and clearance was still moderate but encouraging. Permeability also remained an issue which would need to be addressed going forward.

A key concern with the series however was the embedded aromatic amine **365** (Figure 3.66), which could potentially lead to genotoxicity if liberated.²⁵⁷ Indeed, the amide bond could potentially be metabolically cleaved generating the aromatic amine metabolite **365**.

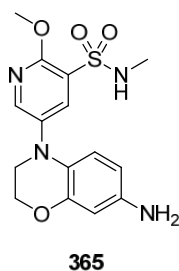


Figure 3.66 Aromatic amine for Ames testing

Aromatic amines are known to undergo metabolic activation that can lead to toxicity (Figure 3.67).²⁵⁷ In particular, they can be oxidised by CYP450 to form an aryl-Nhydroxylamine **I**. The hydroxyl group can be further activated by acetylation or sulfonation (**II**), which produces a reactive nitrenium ion **III**. This electrophile reacts with DNA, RNA, and proteins, which can ultimately lead to a cancer risk.

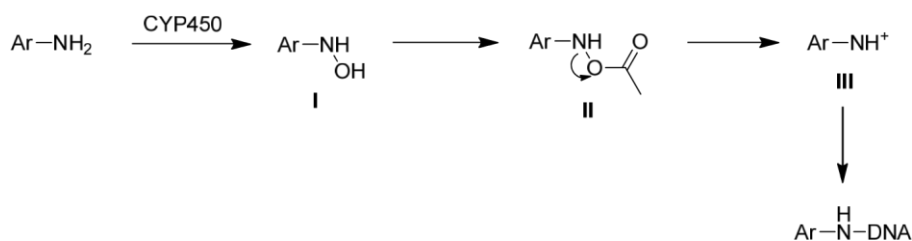


Figure 3.67 Metabolic activation of aromatic amines

To discharge any risk with the series prior further SAR exploration, the aromatic amine **365** was progressed to Ames testing. The Ames test is a biological assay to assess the mutagenic potential of a compound (ability to cause DNA mutations).²⁸³ A positive test indicates that the compound might be mutagenic and, thus, would result in stopping the progression of the compound. The test uses mutant strains of *Salmonella typhimurium*, which require histidine to grow and mutant strains of *Escherichia coli*, which require Tryptophan to grow. The assay consists of plating the bacteria on a medium containing minimum histidine or tryptophan to allow survival of cells but not proliferation. If the compound is mutagenic, a number of cells will revert to wild-type and grow on the medium. The more colonies formed, the more mutagenic the

compound. As stated above, aromatic amines require metabolic activation to become mutagenic. Therefore, to mimic metabolism, the liver S9 fraction (which contains cytosol and microsomes) is added to the test. Assays are then performed in presence and absence of S9-mix. Strains commonly used in our laboratories are *Salmonella typhimurium* strains TA98, TA100 TA1535 and TA1537 and *Escherichia coli* WP2 *uvrA* (pKM101). The aromatic amine **365** was tested in the five strains (\pm S9) and showed no mutagenetic effect, giving confidence to continue to work on this series.

3.4.3.4 Expanding Knowledge around 7-substituted Benzoxazines

From all these encouraging data, a new set of compounds was next designed to improve PI3K α selectivity and cellular potency. As discussed previously, selectivity could be obtained by packing against Trp760. However, from the crystal structure (Figure 3.65), it was not clear if interaction with Trp760 would be possible as the piperidine appeared slightly further away than the DHB piperidine substituents. From previous experience, it was reasoned that adding an isopropyl substituent on the piperidine ring would initially help to test this hypothesis. As mentioned above, the piperidine ring might not be the ideal ring to interact with Trp760, therefore a smaller ring such as a pyrrolidine ring might give different orientation. Targets designed to test these hypotheses and expand SAR are shown in Figure 3.68.

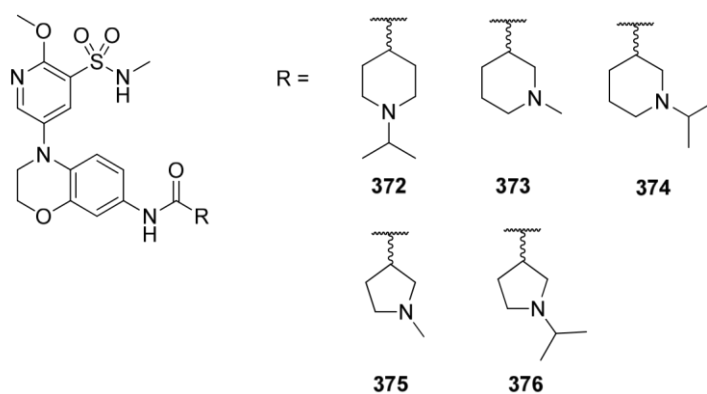
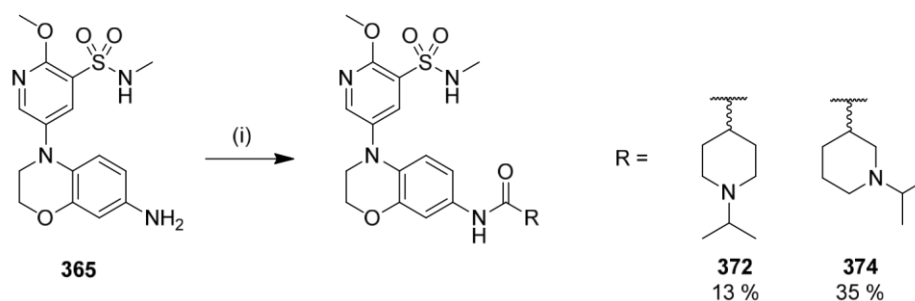


Figure 3.68 Targets designed to explore selectivity through interaction with Trp760

3.4.3.4.1 Chemistry

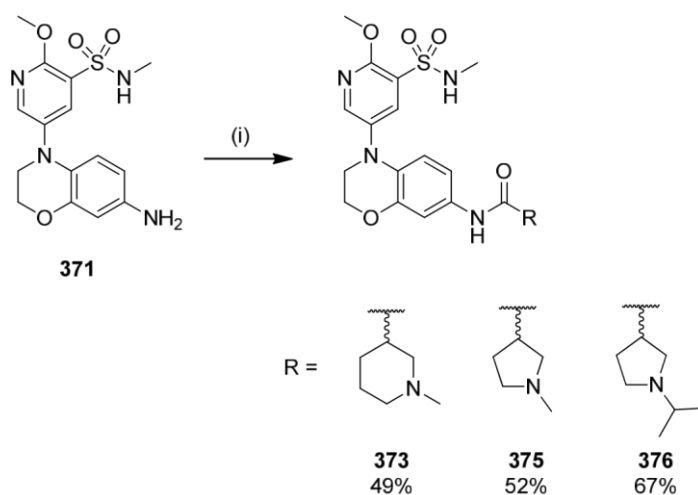
Compounds **372** and **374** were synthesised by amide coupling from the amine intermediate **365** using in this instance T₃P as coupling agent. As previously observed, the amide coupling yields were moderate to low due to poor reactivity and difficulty in the purification.



Reagents and conditions: (i) RCO₂H, T₃P 50% in DMF, DIPEA, EtOAc/DMF (10:1), 3-48 h.

Scheme 3.37

Further optimisation within our laboratory revealed that HATU as coupling reagent delivered the best yields and was thus selected as preferred coupling reagent for this transformation. Compounds **373**, **375** and **376** were synthesised by amide coupling from the amine intermediate **365** using HATU as coupling agent in good yields.



Reagents and conditions: (i) RCO₂H, HATU, DIPEA, DMF, rt, 1-16 h.

Scheme 3.38

3.4.3.4.2 Biological Results

With the *N*-substituted compounds in hand, the selectivity profile and physicochemical properties of each were then determined in comparison to the progenitor compound **361**. These data are summarised in Table 3.16.

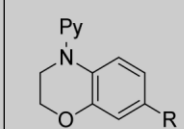
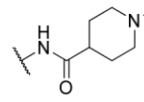
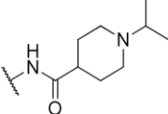
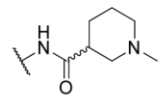
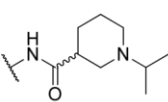
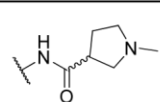
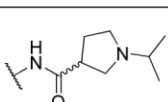
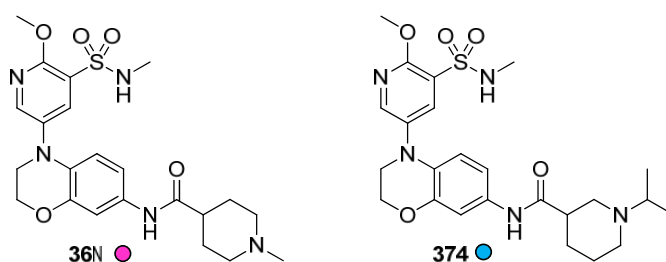
Cmpd		pIC ₅₀ δ LE/LLE _{AT}	X-fold selectivity α, β, γ	hWB pIC ₅₀	Chrom logD _{7.4}	CLND sol. (μg/mL)	Perm. (nm/sec)
361		8.1 0.34; 0.35	63 2512 398	6.1	1.5	155	< 3
372		8.1 0.32; 0.30	63 1259 501	6.2 ^a	1.8	≥ 209	< 3
373		7.5 0.31; 0.29	40 316 159	6.2	2.0	≥ 158	< 3
374		7.9 0.31; 0.26	50 1000 251	6.6	2.5	≥ 215	36
375		7.7 0.33; 0.33	50 631 200	6.7	1.7	≥ 193	< 3
376		7.7 0.31; 0.28	63 794 159	6.9	2.1	≥ 155	< 3

Table 3.16 Biological results on the 7-position

^aCompound failed to fit a curve in 2 out of the 10 test occasions.

Disappointingly, these new data showed no significant improvement in enzyme potency or selectivity compared to **361**. However, compounds **374-376** showed a slight increase in cellular potency. Compound **376** reached the desired cell potency. Selectivity at PI3K α and permeability still need to be improved. On the other hand, compound **374** showed slight increase in permeability, confirming that the desired profile could be achieved by exploring further the SAR in this region.

A crystal structure of compound **374** (●) was also obtained to confirm whether this molecule fulfilled our hypothesis (Figure 3.69).¹⁸⁶ The compound made the expected key interaction with Val828 at the hinge region. The amide NH was appropriately positioned in order to make an interaction *via* the water molecule discussed previously. However, the density for the iPr piperidine was not particularly good, and the exact position of the substituent could not be fully confirmed. Two poses could be envisaged, one where the addition of the iPr group caused the piperidine ring to adopt the desired conformation to pack against Trp760 (as shown in Figure 3.69) and one where the piperidine ring adopt a similar pose to **361** (●), which would explain the selectivity profile observed. If the piperidine adopts the desired conformation, the iPr group should clash with the Lys or Arg residues corresponding to Thr750 in PI3K δ . We reasoned that bulkier substituents might push the piperidine ring to twist toward Trp760.



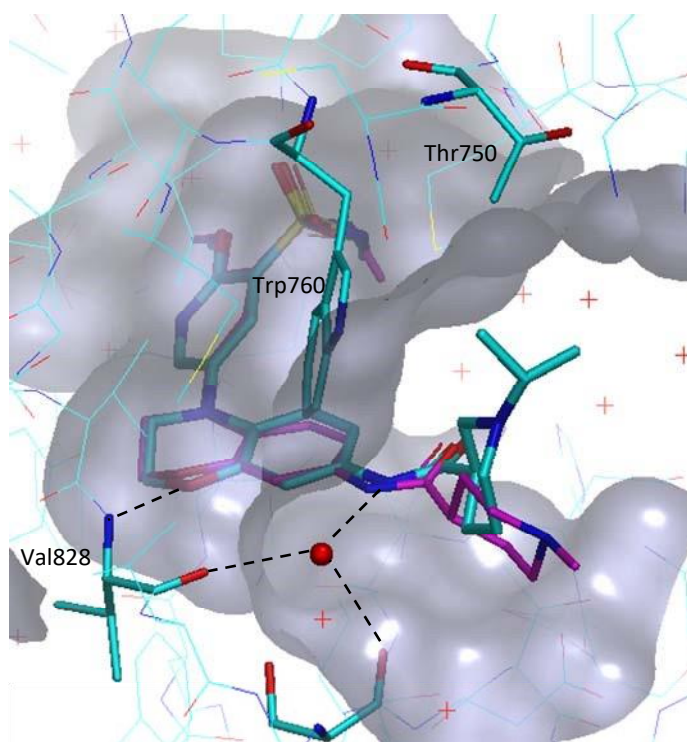


Figure 3.69 Crystal structure of PI3K δ in complex with **374** (●) and **361** (●)

A crystal structure of compound **372** (●) was also obtained, with good density for the ligand and the active site residues (Figure 3.70).¹⁸⁶ Again the compound made the expected key interaction with Val828 at the hinge region and *via* the water molecule as discussed previously. The piperidine ring occupied similar part of the protein to compound **361** (●) confirming once again that selectivity over PI3K β and PI3K γ can be achieved without interaction with Trp760. However, additional bulk did not result in increased potency or selectivity, providing no real advantage over **361**.

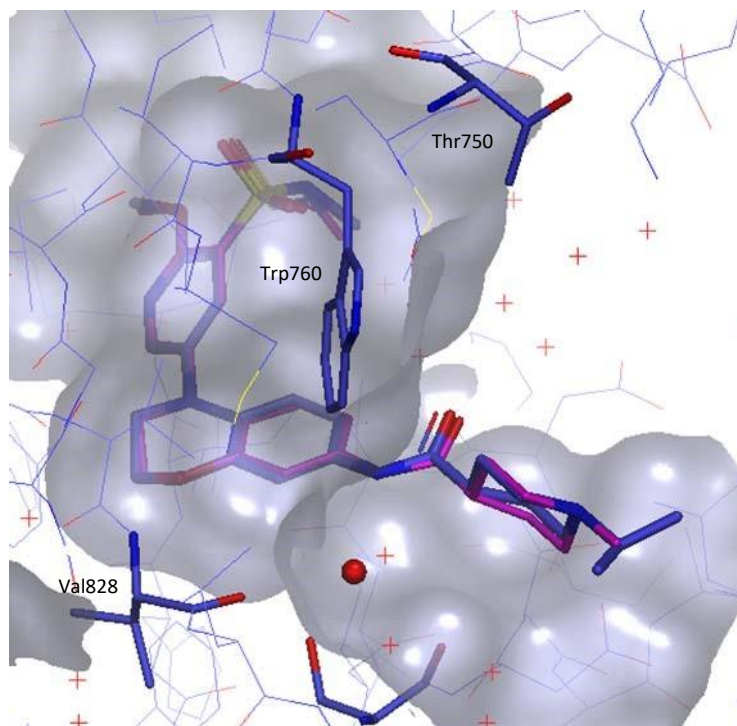
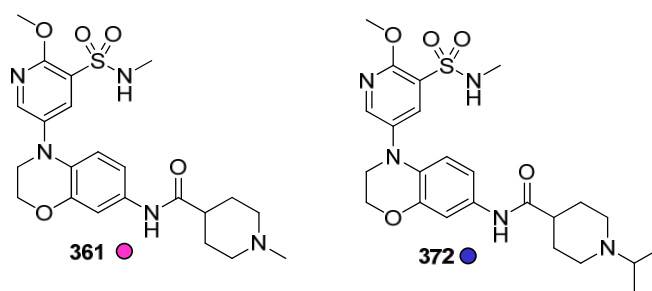


Figure 3.70 Crystal structure of PI3K δ in complex with **372** (●) and **361** (●)

From all the data obtained, it was reasoned that targeting the Trp shelf was still a viable strategy to improve PI3K α selectivity. As mentioned previously, Trp760 is conserved across other PI3K isoforms, however the residues that interact with Trp are not. The residue corresponding to Thr750 is larger in other isoforms (Arg or Lys) and thus reduces access to the face of Trp760. Thus, a new set of compounds was designed to favour interaction with Trp760 (Figure 3.71). As outlined above, it was hypothesised that longer, bulkier substituents might be able to pack against Trp760 more optimally. In addition, adding a CH₂ linker between the amide carbonyl and the piperidine ring might also orientate the ring toward the Trp residue and thus increase affinity and selectivity.

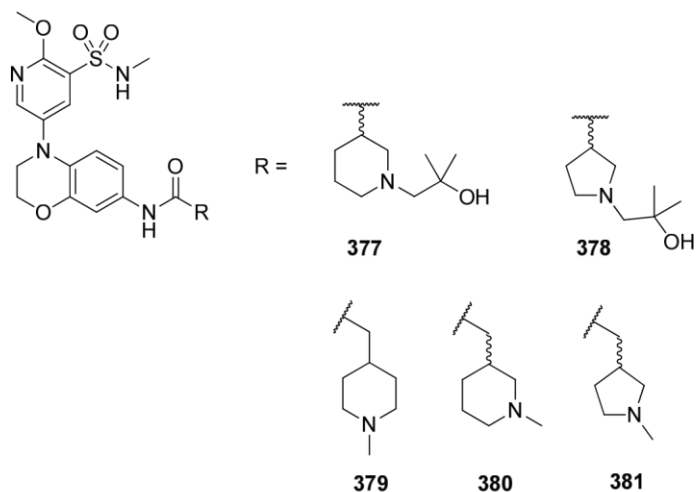
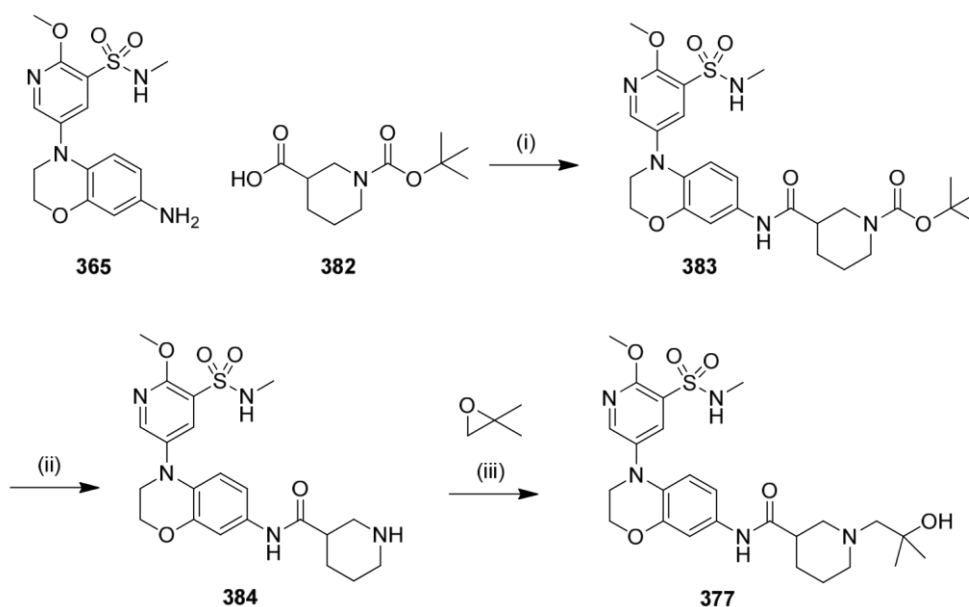


Figure 3.71 Targets designed to improve PI3K α selectivity through interaction with Trp760

3.4.3.4.3 Chemistry

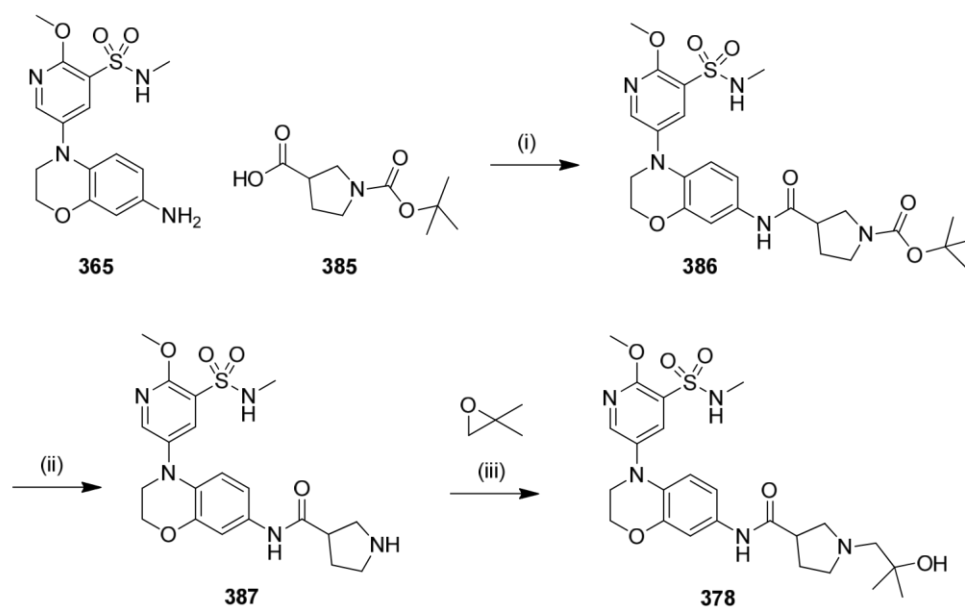
The dimethyl alcohol analogue **377** was prepared following Scheme 3.39. First, the key intermediate **383** was prepared by amide coupling from the amine intermediate **365** using HATU as coupling agent in excellent yield after purification. The Boc protecting group was removed using TFA. The dimethyl hydroxyl analogue **377** was prepared using dimethylepoxyde in ethanol at 90 °C.



Reagents and conditions: (i) HATU, DIPEA, DMF, rt, 16 h, 80%; (ii) TFA, DCM, rt, 2 h, quantitative; (iii) DIPEA, EtOH, sealed tube, 90 °C, 20 h, 51%. **Scheme**

3.39

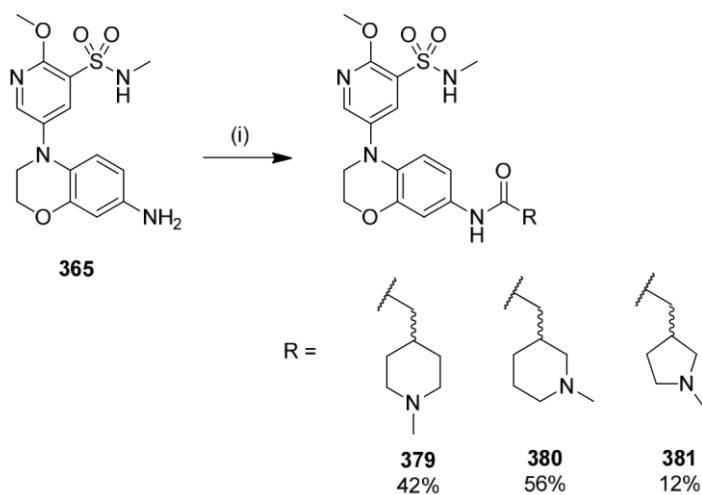
The dimethyl alcohol analogue **378** was prepared following Scheme 3.40. First, the key intermediate **386** was prepared by amide coupling from the amine intermediate **365** using HATU as coupling agent in good yield. The Boc protecting group was removed using TFA. The dimethyl hydroxyl analogue **378** was prepared using dimethylepoxy in ethanol at 90 °C.



Reagents and conditions: (i) HATU, DIPEA, DMF, rt, 1 h, 58%; (ii) TFA, DCM, rt, overnight, 53%; (iii) DIPEA, EtOH, 90 °C, over the weekend, 41%.

Scheme 3.40

Compounds **379-381** were prepared by amide coupling from the amine intermediate **365** using HATU as coupling agent (Scheme 3.41).



Reagents and conditions: (i) RCO₂H, HATU, DIPEA, DMF, rt, 3 h.

Scheme 3.41

3.4.3.4.4 Biological Results

Following synthesis, the new *N*-substituted compounds were progressed to the relevant assays to assess their selectivity profile in comparison to the progenitor **374**.

These data are summarised in Table 3.16.

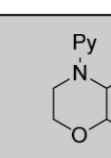
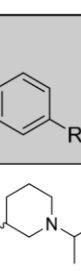

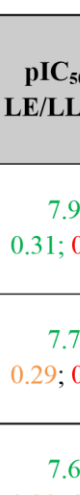





Cmpd		pIC ₅₀ δ LE/LLE _{AT}	X-fold selectivity α, β, γ	hWB pIC ₅₀	Chrom logD _{7.4}	CLND sol. µg/mL	Perm. nm/sec
374		7.9 0.31; 0.26	50 1000 251	6.6	2.5	≥ 215	36
377		7.7 0.29; 0.27	159 1585 251	6.6	3.3	≥ 210	20
378		7.6 0.29; 0.29	63 631 126	6.3 ^a	2.3	≥ 215	< 3
379		7.5 0.30; 0.29	40 398 159	6.4	1.6	≥ 215	< 3
380		7.9 0.32; 0.31	200 1259 316	6.7 ^b	1.9	≥ 189	< 3
381		7.7 0.32; 0.33	63 501 126	6.3	1.6	≥ 185	< 3
383		7.9 0.28; 0.22	398 2512 398	n.d.	5.4	22	170
384		7.4 0.32; 0.31	32 200 100	n.d.	1.7	≥ 155	< 3

Table 3.17 Biological results on the 7-position

^aCompound failed to fit a curve in 1 out of the 3 test occasions. ^bCompound failed to fit a curve in 2 out of the 12 test occasions.

These new data showed that the new compounds had similar potency to compound **374** but several compounds achieved the desired selectivity profile (> 100-fold over the three isoforms) with good enzyme potency. In particular, compounds **377** and **380** showed high selectivity for PI3K α , β and γ and have good enzyme and cellular potency alongside good physicochemical properties for an oral drug. The permeability of these compounds was still low and this would need to be further investigated. The smaller pyrrolidine ring (**378** and **381**) showed insufficient selectivity at PI3K α suggesting that the ring might not interact optimally with the Trp residue.

To confirm our selectivity hypothesis, both compounds **377** and **380** were progressed to crystallography.¹⁸⁶ The crystal structure of compound **377** (, 2.4 Å) showed that the piperidine ring adopted the desired conformation to pack against Trp760 (Figure 3.72).¹⁸⁶ In addition, the dimethyl hydroxy substituent was noted to reach high towards Thr750 and should thus clash with the larger residue found at this position in the other isoforms (Arg or Lys).

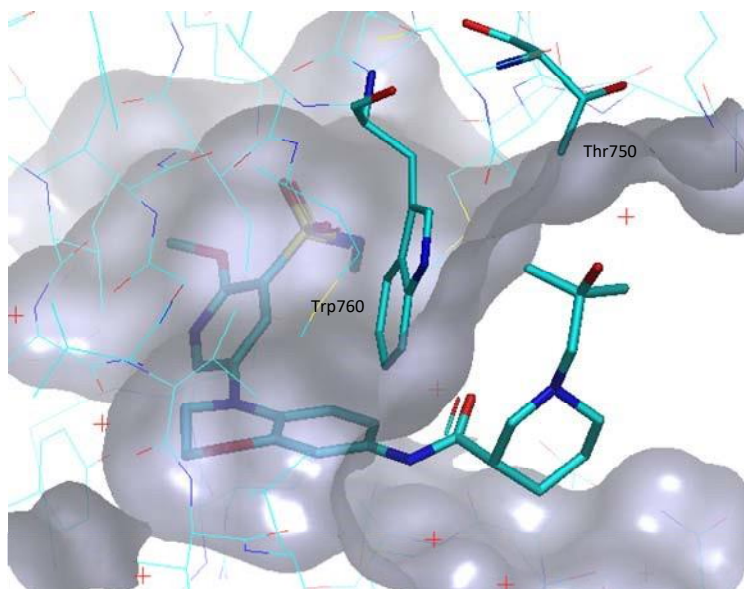


Figure 3.72 Crystal structure of PI3K δ in complex with **377** (●)
The crystal structure of compound **380** (●, 2.2 Å) further confirmed our original hypothesis.¹⁸⁶ The piperidine ring is bent toward the Trp residue allowing the methyl substituent to pack against Trp760, which resulted in good selectivity. Overlay with

377 (●) revealed that addition of larger substituents (e.g. *i*-Pr) on the piperidine ring might increase further the selectivity, as the methyl substituent is occupying the pocket fully.

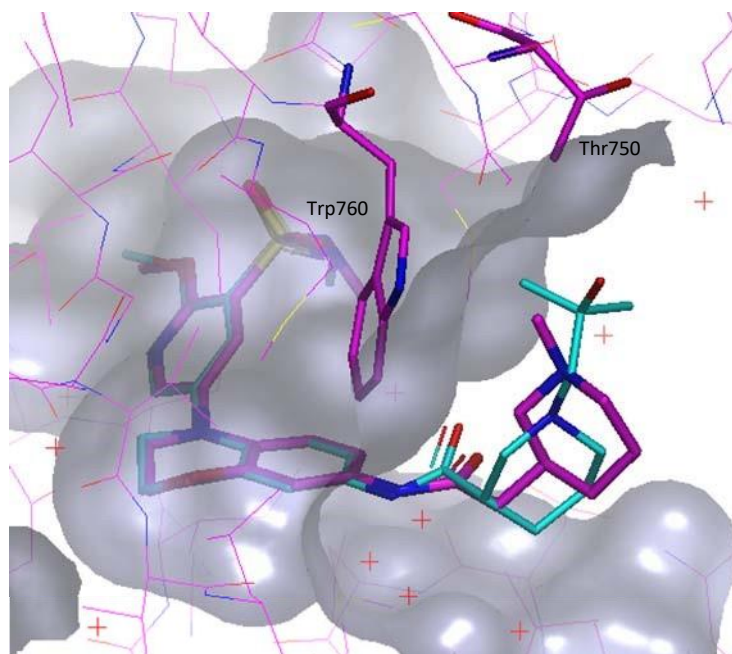
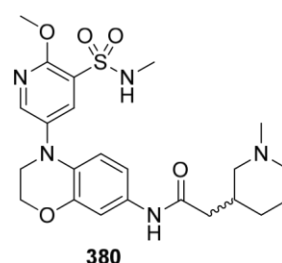
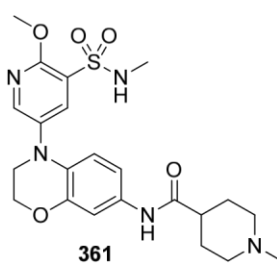
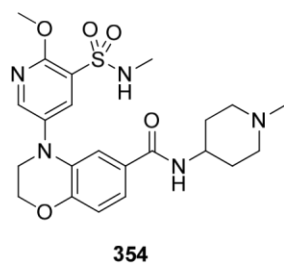
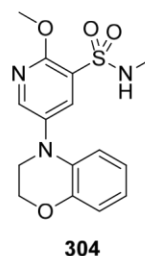
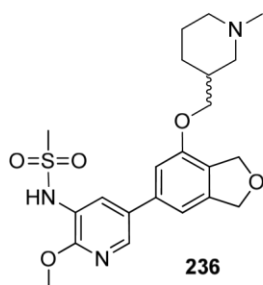


Figure 3.73 Crystal structure of PI3K δ in complex with **380** (●) and **377** (●)

3.4.4 Summary and Conclusions

The aim of the research was initially to evaluate the potential of a set of fragment hits as a novel lead series, through delineating SAR aimed at enhancing enzyme and cellular potency, alongside balancing good physicochemical properties for oral dosing. Using knowledge from the DHB lead series around the solubility pocket and structure-based design, two vectors were investigated from the 6- and 7-positions of the benzoxazine progenitor (**304**) and this delivered compounds with improved potency and good physicochemical properties compared to the progenitor fragment hit **304** (Table 3.18). Several linkers were evaluated at the 6-position and this work highlighted the amide linker as a preferred moiety to access the part of the protein where potency

could be improved (e.g. **354**). The compounds were not sufficiently selective at this stage but showed a similar profile to the initial DHB hit **236**, giving us confidence that selectivity could be improved once more preferred substituents could be incorporated. More interestingly, work around the 7-position identified a novel vector, where good potency and excellent selectivity over PI3K β and PI3K γ could be achieved without interaction with Trp760. Although the PI3K α selectivity remained lower than our target, the data showed an encouraging improvement compared to DHB lead **236**, delivering a good quality alternative lead compound **361**. These data also revealed a novel area in the binding area to obtain good selectivity without packing against Trp760 compared to DHB template (e.g. **236**). Addition of bulkier substituents at the 3-position of the piperidine ring (e.g. **377**) or a CH₂ spacer between the amide carbonyl and the piperidine ring (e.g. **380**) demonstrated that packing against Trp760 was also possible from the 7-position and delivered enhanced selectivity over the three PI3K isoforms. Several promising compounds were identified with encouraging cellular potency, IVC and good physicochemical properties delivering a new series for optimisation towards the discovery of a suitable oral PI3K δ inhibitor.



Compound	236	304	354	361	380
pIC ₅₀ (δ)	8.3	6.3	7.7	8.1	7.9
LE, LLE _{AT}	0.37; 0.35	0.38; 0.29	0.32; 0.34	0.34; 0.35	0.32; 0.31
X-fold selectivity α , β , γ	79 40 316	16 32 16	32 20 100	63 2512 398	200 1259 316
hWB pIC ₅₀ (δ)	7.1	4.7	6.0	6.1	6.7
ChromlogD _{7.4}	2.2	4.9	1.8	1.5	1.9
CLND sol. ($\mu\text{g/mL}$)	≥ 230	≥ 188	≥ 235	155	≥ 189
Perm. (nm/sec)	310	755	< 3	< 3	< 3
IVC rat	12	n.d.	n.d.	< 0.53	0.61

Table 3.18 Fragment hit and associated leads

3.4.5 Future Work

The work described in this chapter has identified several promising new compounds with encouraging cellular potency alongside excellent selectivity using existing knowledge and by exploiting a novel area of the protein not reported previously.

The next step for further work in this series would be to profile these new compounds *in vivo* and expand SAR to improve both cellular potency and permeability. Permeability within the series could be improved by removing or masking H-bond donors. Modification around the pyridine sulfonamide was not investigated in this work and might also help to improve potency and modulate the overall properties of the molecule to deliver a suitable oral PI3K δ inhibitor.

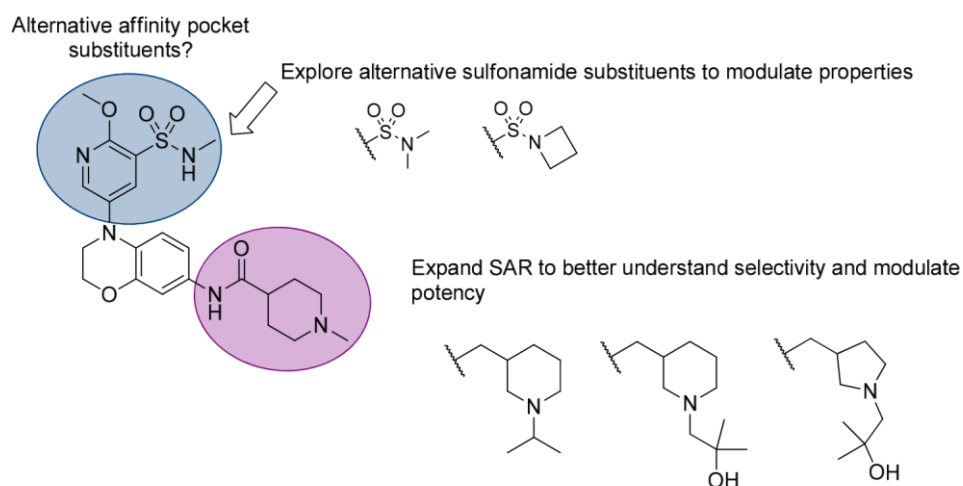


Figure 3.74 Proposed future work

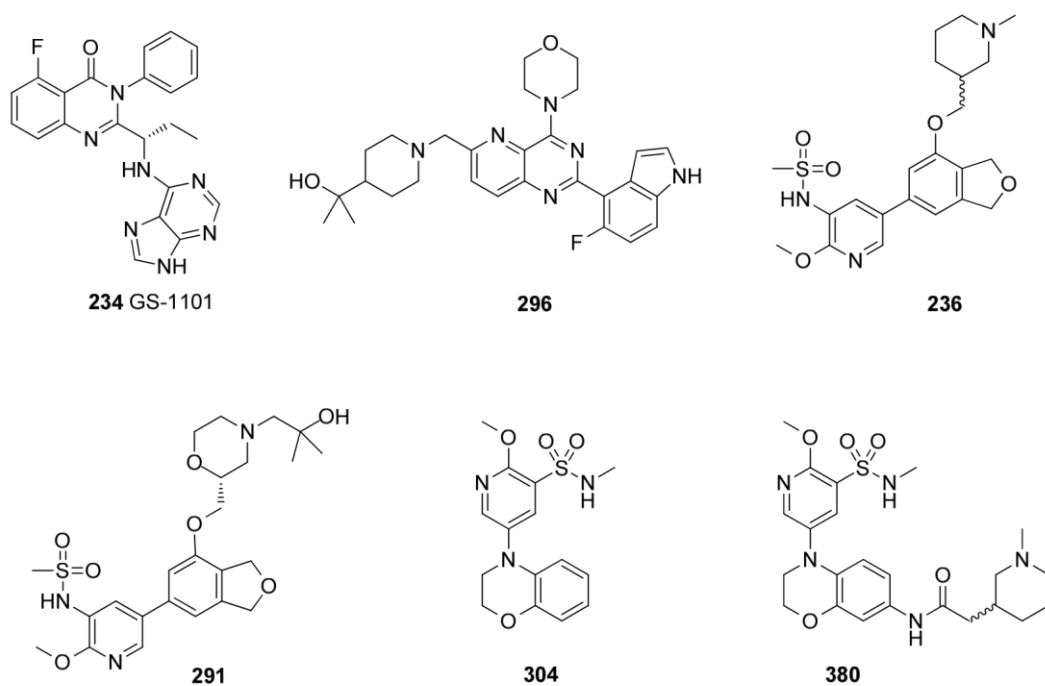
3.5 General Conclusions

The aim of the research was to identify potent and selective inhibitors of the lipid kinase PI3K δ with good physicochemical properties for oral dosing.

In the dihydrobenzofuran template, the original lead compound **236** had good enzyme and cellular potency but only moderate selectivity over the other PI3K isoforms. Using structure-based knowledge of PI3K δ selectivity, novel, selective PI3K δ inhibitors (> 300-fold over the three other isoforms) were identified. These inhibitors showed good enzyme and cellular potency (e.g. **291**, Table 3.19) comparable to known oral inhibitors (e.g. **234** and **296**), but with an improved selectivity profile and good overall physicochemical properties compatible with oral dosing. Crystal structures of the compounds confirmed our observation in other series that the key interaction with

Trp760 can deliver excellent selectivity over the three isoforms, and offer an advantage compared to the previously disclosed propeller-shape inhibitors (e.g. **234**), which retain some PI3K γ potency.

In the benzoxazine fragment template, structure-based design was employed to improve both potency and selectivity of the initial fragment **304** (Table 3.19) while maintaining good efficiency and physicochemical properties for oral delivery. Compounds showed encouraging cellular activity and improved selectivity over the initial DHB lead **7**. Work around both the 6- and 7-positions of the benzoxazine template explored a variety of linkers and generated meaningful SAR data, where both interaction with Trp760 and access to a novel vector delivered excellent selectivity (e.g. **379**). These data revealed a novel area in the protein to obtain selectivity without packing against Trp760, which has not been exploited before by known oral inhibitors (e.g. **234**, **296**). This work identified a novel lead series with an encouraging profile for optimisation towards the discovery of a suitable oral PI3K δ inhibitor for clinical development. In addition, this novel series already showed improvement compared to known inhibitors either in terms of selectivity and physicochemical properties and therefore represent useful assets going forward for the treatment of asthma through modulation of lipid kinase activity.



Compound	234	296*	236	291	380	304
administration	oral	oral	oral	oral	oral	-
pIC ₅₀ (δ)	8.1	8.4	8.3	8.8	7.9	6.3
LE, LLE _{AT}	0.36; 0.31	0.31; 0.30	0.37; 0.35	0.34; 0.36	0.32; 0.31	0.38; 0.29
fold-selectivity α/δ, β/δ, γ/δ	1000 159 40	340 200 410	79 40 316	631 1259 316	200 1259 316	16 32 16
clogP	3.6	3.1	2.8	2.4	3.0	4.7
ChromlogD _{7.4}	3.2	3.4 ¹	2.2	4.0	1.9	4.9
Ar ring	5	4	2	2	2	2
CLND sol. (μg/mL)	126	n.d.	≥ 200	221	≥ 189	≥ 188
Perm. (nm/sec)	n.d.	n.d.	390	450	< 3	755

Table 3.19

* Data not generated in our assays; ¹calculated value

Experimental

4.1 General procedures

All solvents and reagents, unless otherwise stated, were commercially available and were used without further purification. The purity of all compounds screened in the biological assays was examined by LCMS analysis and was found to be $\geq 95\%$ unless otherwise specified. The human biological samples were sourced ethically and their research use was in accord with the terms of the informed consents. All animal studies were ethically reviewed and carried out in accordance with Animals (Scientific Procedures) Act 1986 and the GSK Policy on the Care, Welfare and Treatment of Animals.

4.1.1 Nuclear Magnetic Resonance (NMR)

Proton nuclear magnetic resonance (^1H NMR) spectra were recorded using a Bruker AVI (400 MHz), Bruker Nano (400 MHz) or Bruker AVII+ (600 MHz) spectrometer (with cryoprobe) in the indicated solvent. Chemical shifts (δ) are reported in parts per million (ppm) relative to trimethylsilane and are internally referenced to the residual solvent peak. Coupling constants (J) are given in hertz (Hz) to the nearest 0.5 Hz. The following abbreviations are used for multiplicities: s = singlet; d = doublet; t = triplet; q = quadruplet; sxt = sextet; spt = septet; m = multiplet; dd = doublet of doublets; ddd = double double doublet; dt = doublet of triplets; br. = broad.

Carbon nuclear magnetic resonance (^{13}C NMR) spectra were recorded on using a Bruker AVI (400 MHz) or Bruker AVII+ (600 MHz) spectrometer and are proton decoupled. Chemical shifts (δ) are reported in parts per million (ppm).

4.1.2 Liquid Chromatography Mass Spectroscopy (LCMS)

Liquid Chromatography Mass Spectroscopy (LCMS) was conducted on either a Acquity UPLC BEH C₁₈ column (50 mm x 2.1 mm i.d. 1.7 μm packing diameter) at 40 °C eluting with either 10 mM ammonium bicarbonate in water adjusted to pH 10 with ammonia solution (solvent A) and acetonitrile (solvent B) or 0.1% v/v solution of formic acid in water (solvent A) and 0.1% v/v solution of formic acid in acetonitrile (solvent B). The UV detection is a summed signal from wavelength of 210 nm to 350 nm. The mass spectra were recorded on a Waters ZQ spectrometer using electrospray positive and negative mode.

The following elution gradients were used:

UPLC 2 min run formic acid

Time (min)	Flow rate (mL/min)	% solvent A	% solvent B
0	1	97	3
1.5	1	0	100
1.9	1	0	100
2.0	1	97	3

UPLC 2 min run high pH

Time (min)	Flow rate (mL/min)	% solvent A	% solvent B
0	1	99	1
1.5	1	3	97
1.9	1	3	97
2.0	1	99	1

4.1.3 Mass Directed Auto-Preparative (MDAP) Chromatography

Preparative mass directed HPLC (MDAP) was conducted on a Waters *MassLynx* system comprising of a Waters 515 pump with extended pump heads, Waters 2767 autosampler, Waters 996 photodiode array detector and Gilson 202 fraction collector on a XBridge C₁₈ column (30 mm x 100 mm i.d. 5µm packing diameter) or Sunfire C₁₈ column (30 mm x 150 mm i.d. 5µm packing diameter) at ambient temperature. The mobile phase was 0.1% v/v solution of formic acid in water or 10 mM ammonium bicarbonate in water adjusted to pH 10 with ammonia solution (solvent A) and 0.1% v/v solution of formic acid in acetonitrile or acetonitrile (solvent B). The UV detection is a summed signal from wavelength of 210 nm to 350 nm. Mass spectra were recorded on Waters ZQ mass spectrometer using alternate-scan positive and negative electrospray ionisation. The software used was *MassLynx* 3.5 with *FractionLynx* option or using equivalent alternative systems.

The elution gradients used were at a flow rate of 40 mL/min over 15 or 25 min:

Gradient A	5-30 % solvent B
Gradient B	15-55 % solvent B
Gradient C	30-85 % solvent B
Gradient D	50-99 % solvent B
Gradient E	80-99 % solvent B

The gradients employed are exemplified below with gradient A.

Gradient A

Time (min)	% A	% B
0	95	5
1	95	5
10	70	30
11	1	99
15	1	99

Time (min)	% A	% B
0	95	5
1	95	5

20	70	30
21	1	99
25	1	99

4.1.4 High Resolution Mass Spectroscopy (HRMS)

ESI (+) high resolution mass spectra (HRMS) were obtained on a Micromass Q-Tof 2 hybrid quadrupole time-of-flight mass spectrometer, equipped with a Z-spray interface, over a mass range of 100 – 1100 Da, with a scan time of 0.9 s and an interscan delay of 0.1 s. Reserpine was used as the external mass calibrant ($[M+H]^+ = 609.2812$ Da). The Q-Tof 2 mass spectrometer was operated in W reflectron mode to give a resolution (FWHM) of 16000-20000. Ionisation was achieved with a spray voltage of 3.2 kV, a cone voltage of 50 V, with cone and desolvation gas flows of 10-20 and 600 L/hr respectively. The source block and desolvation temperatures were maintained at 120 °C and 250 °C, respectively. The elemental composition was calculated using *MassLynx* v4.1 for the $[M+H]^+$ and the mass error quoted as ppm.

An Agilent 1100 liquid chromatograph equipped with a model G1367A autosampler, a model G1312A binary pump and a HP1100 model G1315B diode array detector was used. The method used was generic for all experiments. All separations were achieved using a Phenomenex Luna C18 (2) reversed phase column (100 x 2.1 mm, 3 μ m particle size). Gradient elution was carried out with the mobile phases as (A) water containing 0.1% (v/v) formic acid and (B) acetonitrile containing 0.1% (v/v) formic acid. The conditions for the gradient elution were initially 5% B, increasing linearly to 100% B over 6 minutes, remaining at 100% B for 2.5 min then decreasing linearly to 5% B over 1 min followed by an equilibration period of 2.5 min prior to the next injection. The flow rate was 0.5 mL/min, temperature controlled at 35 °C with an injection volume of between 2 to 5 μ L. All samples were diluted with DMSO (99.9%) prior to LCMS analysis.

4.1.5 Purification by column chromatography

Column chromatography was conducted on a CombiFlash® Rf,²⁸⁴ automated flash chromatography system, from Teledyne Isco using disposable, normal or reverse phase, SPE Redisep cartridges (4 g to 330 g). The CombiFlash® Rf uses RFID (Radio Frequency Identification Detector) technology to automate setting the parameters for purification runs and fraction collection. The system is equipped with a UV variable dual-wavelength and a Foxy® fraction collector enabling automated peak cutting, collection and tracking.

4.1.6 Phase separators

Isolute® phase separator cartridges²⁸⁵ are fitted with hydrophobic Teflon frit. They were used to separate chlorinated solvent from aqueous phase under gravity.

4.1.7 Isolute® 103

Isolute® 103 cartridges from Biotage are hydroxylated polystyrene-divinylbenzene co-polymer resin.²⁸⁵ They were used to extract organic compounds from aqueous solution using a catch and release protocol.

4.1.8 Microwave

Microwave chemistry was typically performed in Biotage sealed vessels, irradiating with a Biotage Initiator™ Microwave Synthesiser.²⁸⁵

4.1.9 H-cube®

Small scale hydrogenation chemistry was performed using a ThalesNano H-cube® continuous flow hydrogenation reactor.²⁸⁶ The reaction takes place on disposable packed catalyst cartridges, CatCarts®. Hydrogen is generated *in situ* by electrolysis of water. The reaction mixture can be heated up to 100 °C and pressurised up to 100 bar.

4.1.10 Melting point

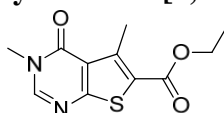
Melting points were measured on a Stuart automatic melting point apparatus, SMP40.²⁸⁷ The melting points were evaluated by eye and are in degree Celsius (°C). Melting points were measured on none crystalline products unless otherwise stated.

4.1.11 Infrared (IR) Spectroscopy

IR spectra were recorded from solid samples using a Perkin Elmer Spectrum One FTIR spectrometer fitted with a Perkin Elmer Universal ATR (Attenuated Total Reflectance) sampling accessory. Absorption frequencies are reported in wavenumbers (cm⁻¹). Only data for main functional groups and strong peaks are reported.

4.2 Experimental Procedures for Cluster 3 Template

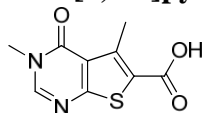
Ethyl 3,5-dimethyl-4-oxo-3,4-dihydrothieno[2,3-*d*]pyrimidine-6-carboxylate (**58**)



Potassium carbonate (1.3 g, 9.7 mmol) and iodomethane (0.6 mL, 9.7 mmol) were added to a solution of ethyl 5-methyl-4-oxo-3,4-dihydrothieno[2,3-*d*]pyrimidine-6carboxylate **57** (2.0 g, 8.4 mmol) in acetonitrile (150 mL) under nitrogen. The mixture

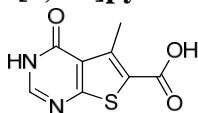
was stirred at 80 °C for 3 h under nitrogen. After cooling, water (150 mL) was added to the mixture and extracted with EtOAc (2 x 150 mL). The combined organic phases were passed through a hydrophobic frit, concentrated under reduced pressure and dried in a vacuum oven for 1 h to give the title product **58** as a white solid (2.1 g, 95%). mp 173-175 °C; ¹H NMR (400 MHz, DMSO-d₆) δ 8.53 (s, 1H), 4.31 (q, *J* = 7.1 Hz, 2H), 3.47 (s, 3H), 2.84 (s, 3H), 1.31 (t, *J* = 7.2 Hz, 3H); ¹³C NMR (101 MHz, DMSO-d₆) δ 164.8 (C), 161.7 (C=O), 158.0 (C=O), 151.0 (CH), 143.1 (C), 122.6 (C), 121.9 (C), 61.1 (CH₂), 33.4 (CH₃), 14.8 (CH₃), 14.1 (CH₃); LCMS (ESI, formic) *m/z* 253 [M+H]⁺, *R*_t = 0.89 min; HRMS (ESI) calcd for C₁₁H₁₃N₂O₃S [M+H]⁺ 253.0647, found 253.0636 (4.61 min); IR (ATR) cm⁻¹ 3060, 2983, 2939, 1700, 1680, 1573, 1249.

3,5-Dimethyl-4-oxo-3,4-dihydrothieno[2,3-*d*]pyrimidine-6-carboxylic acid (**30**)



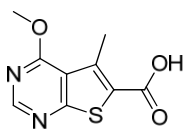
Lithium hydroxide, anhydrous (0.67 g, 28.1 mmol) was added to a solution of ethyl 3,5-dimethyl-4-oxo-3,4-dihydrothieno[2,3-*d*]pyrimidine-6-carboxylate **58** (2.0 g, 7.9 mmol) in a mixture of THF (40 mL), EtOH (5 mL) and water (10 mL). The mixture was stirred at room temperature for 3 days. Solvents were then evaporated under reduced pressure. The residue obtained was dissolved in water (50 mL) and the solution was acidified with 2 M aqueous HCl solution to pH 1. The resulting white precipitate was collected by filtration, washed with water and dried in a vacuum oven for 2 h to give the title product **30** as a white solid (1.6 g, 86 %). mp 275-278 °C; ¹H NMR (400 MHz, DMSO-d₆) δ 13.39 (br. s, 1H), 8.48 (s, 1H), 3.45 (s, 3H), 2.79 (s, 3H); ¹³C NMR (101 MHz, DMSO-d₆) δ 164.6 (C), 163.4 (C=O), 158.1 (C=O), 150.8 (Ar-CH), 142.3 (C), 123.5 (C), 122.8 (C), 33.5 (CH₃), 14.8 (CH₃); LCMS (ESI, formic) *m/z* 225 [M+H]⁺, *R*_t = 0.54 min; HRMS (ESI) calcd for C₉H₉N₂O₃S [M+H]⁺ 225.0334, found 225.0332 (3.34 min); IR (ATR) cm⁻¹ 3045, 2799, 2507, 1669, 1584, 1247.

5-Methyl-4-oxo-3,4-dihydrothieno[2,3-*d*]pyrimidine-6-carboxylic acid (**43**)



Lithium hydroxide, monohydrate (2.3 g, 55 mmol) was added to a solution of ethyl 5-methyl-4-oxo-3,4-dihydrothieno[2,3-*d*]pyrimidine-6-carboxylate **57** (4.0 g, 17 mmol) in a mixture of THF (50 mL), MeOH (25 mL) and water (8 mL). The mixture was stirred at room temperature for 16 h. Lithium hydroxide, monohydrate (1.0 g, 24 mmol) was added and the mixture was stirred for another 6 h. The mixture was then heated at 40 °C for 24 h. Solvent was evaporated under reduced pressure. The resulting crude product was dissolved in water and the mixture was acidified to pH 1 with 2 M aqueous HCl solution. The resulting precipitate was collected by filtration and dried in a vacuum oven overnight to give the title product as a pale pink solid (3.5 g, 99%). mp 300 °C (dec.), ¹H NMR (400 MHz, DMSO-*d*₆) δ 13.31 (br. s, 1H), 12.56 (br. s, 1H), 8.17 (s, 1H), 2.80 (s, 3H); ¹³C NMR (101 MHz, DMSO-*d*₆) δ 165.4 (C), 163.4 (C=O), 158.3 (C=O), 148.0 (Ar-CH), 142.4 (C), 123.9 (C), 123.1 (C), 14.7 (CH₃); LCMS (ESI, formic) *m/z* 211 [M+H]⁺, R_t = 0.45 min; HRMS (ESI) calcd for C₈H₇N₂O₃S [M+H]⁺ 211.0177, found 211.0172 (2.95 min); IR (ATR) cm⁻¹ 3072, 2880, 1667, 1586, 1262.

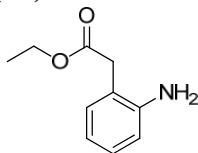
4-Methoxy-5-methylthieno[2,3-*d*]pyrimidine-6-carboxylic acid (**60**)



Methyl 4-chloro-5-methylthieno[2,3-*d*]pyrimidine-6-carboxylate **59** (500 mg, 2 mmol) was dissolved in MeOH (10 mL) under nitrogen. Sodium methoxide (223 mg, 4 mmol) was added and the mixture was stirred at room temperature for 2 h. The mixture was diluted in water (50 mL) and the solution was acidified with 2 M aqueous HCl solution. The mixture was extracted with DCM (2 x 50 mL). Insoluble material was collected by filtration to give the title product **60** as a white solid (280 mg, 55%). mp 280 °C (dec.); ¹H NMR (400 MHz, DMSO-*d*₆) δ 12.62 (br. s, 1H),

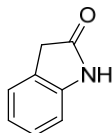
8.20 (s, 1H), 3.84 (s, 3H), 2.83 (s, 3H); LCMS (ESI, formic) m/z 225.07 $[M+H]^+$, R_t = 0.69 min.

Ethyl 2-(2-aminophenyl)acetate (62)



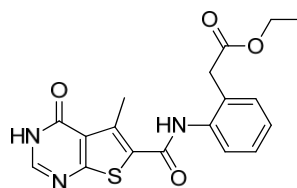
A solution of ethyl 2-(2-nitrophenyl)acetate **61** (200 mg, 0.96 mmol) in EtOH (40 mL) was hydrogenated using an H-cube (10% Pd/C catcart cartridge, 20 °C, full H₂). Solvent was evaporated under reduced pressure to give the title product **62** as an orange gum (148 mg, 86%). ¹H NMR (400 MHz, DMSO-d₆) δ 6.90 - 6.99 (m, 2H), 6.65 (dd, J = 7.8, 1.0 Hz, 1H), 6.51 (apparent dt, J = 7.4, 1.3 Hz, 1H), 4.84 (br. s, 2H), 4.07 (q, J = 7.0 Hz, 2H), 3.49 (s, 2H), 1.18 (t, J = 7.0 Hz, 3H); LCMS (ESI, formic) m/z 180 $[M+H]^+$, R_t = 0.70 min.

Upon standing the aniline cyclises to form the oxindole **63**.

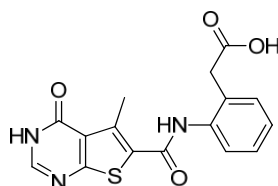


Purple gum, ¹H NMR (400 MHz, DMSO-d₆) δ 10.32 (br. s, 1H), 7.10 - 7.23 (m, 2H), 6.87 - 6.95 (m, 1H), 6.80 (d, J = 7.8 Hz, 1H), 3.45 (s, 2H); LCMS (ESI, formic) m/z 134 $[M+H]^+$, R_t = 0.57 min.

Ethyl 2-(2-(5-methyl-4-oxo-3,4-dihydrothieno[2,3-*d*]pyrimidine-6-carboxamido)phenyl)acetate (64)



HATU (141 mg, 0.37 mmol) and DIPEA (0.1 mL, 0.6 mmol) were added to a solution of 5-methyl-4-oxo-3,4-dihydrothieno[2,3-*d*]pyrimidine-6-carboxylic acid **43** (65 mg, 0.3 mmol) in DMF (1.5 mL). The mixture was stirred at room temperature for 10 min. Ethyl 2-(2-aminophenyl)acetate **62** (66 mg, 0.4 mmol) was then added and the mixture was stirred at room temperature for 16 h. Solvent was removed under a stream of nitrogen. The crude product was purified by reverse phase chromatography using formic acid MDAP (gradient B over 15 min) to give the title product **64** as a yellow solid (46 mg, 40%). ¹H NMR (400 MHz, DMSO-*d*₆) δ 12.56 (br. s, 1H), 9.75 (s, 1H), 8.17 (d, *J* = 3.8 Hz, 1H), 7.42 (br. d, *J* = 7.8 Hz, 1H), 7.29 - 7.36 (m, 2H), 7.19 - 7.28 (m, 1H), 4.04 (q, *J* = 7.0 Hz, 2H), 3.73 (s, 2H), 2.76 (s, 3H), 1.13 (t, *J* = 7.0 Hz, 3H); LCMS (ESI, formic) *m/z* 372 [M+H]⁺, *R*_t = 0.83 min. **2-(2-(5-Methyl-4-oxo-3,4-dihydrothieno[2,3-*d*]pyrimidine-6-carboxamido)phenyl)acetic acid (53)**



A solution of ethyl 2-(2-(5-methyl-4-oxo-3,4-dihydrothieno[2,3-*d*]pyrimidine-6-carboxamido)phenyl)acetate **64** (30 mg, 0.1 mmol) and lithium hydroxide (5.8 mg, 0.2 mmol) in a mixture of THF (0.4 mL), MeOH (0.2 mL) and water (0.07 mL) was stirred at room temperature for 2 h. Solvents were removed under a stream of nitrogen. The resulting crude product was dissolved in water (0.5 mL) and 2 M aqueous HCl solution was added. The resulting precipitate was collected by filtration and dried in a vacuum oven overnight to give the title product **53** as a brown solid (16 mg, 58%). mp 243-246 °C; ¹H NMR (400 MHz, DMSO-*d*₆) δ 12.55 (br. s, 1H),

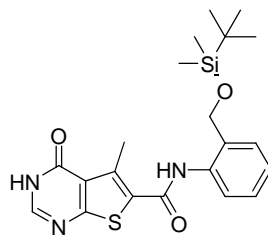
12.41 (br. s, 1H), 9.74 (s, 1H), 8.17 (d, $J = 3.7$ Hz, 1H), 7.46 (br. d, $J = 7.5$ Hz, 1H), 7.28 - 7.36 (m, 2H), 7.18 - 7.25 (m, 1H), 3.66 (s, 2H), 2.77 (s, 3H); ^{13}C NMR (151 MHz, DMSO- d_6) δ 172.5 (C=O), 164.2 (C), 160.7 (C=O), 158.3 (C=O), 147.4 (ArCH), 136.8 (C), 136.1 (C), 131.0 (C), 130.4 (C), 127.6 (Ar-CH), 127.2 (Ar-CH), 126.1 (Ar-CH), 126.0 (Ar-CH), 123.5 (C), 37.6 (CH₂), 14.9 (CH₃); LCMS (ESI, formic) m/z 344 [M+H]⁺, $R_t = 0.64$ min; HRMS (ESI) calcd for C₁₆H₁₄N₃O₄S [M+H]⁺ 344.0705, found 344.0695 (3.55min); IR (ATR) cm⁻¹ 3261, 3130, 3030, 2926, 2861, 1721, 1641, 1623, 1597, 1517.

2-(((*tert*-Butyldimethylsilyl)oxy)methyl)aniline (**78**)



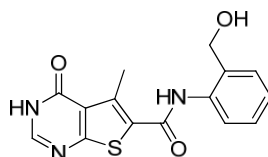
tert-Butyldimethylsilyl chloride (673 mg, 4.47 mmol) and imidazole (553 mg, 8.12 mmol) were added to a solution of (2-aminophenyl)methanol **77** (500 mg, 4.06 mmol) in DCM (6 mL). The reaction mixture was stirred at room temperature for 14 h. DCM (5 mL) and water (10 mL) were added and the organic layer was separated using a hydrophobic frit before being concentrated under reduced pressure to give the title product **78** as an orange liquid (889 mg, 92%). ^1H NMR (400 MHz, DMSO- d_6) δ 7.07 (br. d, $J = 7.3$ Hz, 1H), 6.96 (apparent dt, $J = 7.6, 1.5$ Hz, 1H), 6.62 (dd, $J = 7.8, 1.0$ Hz, 1H), 6.54 (apparent dt, $J = 7.4, 1.1$ Hz, 1H), 4.83 (br. s, 2H), 4.57 (s, 2H), 0.89 (s, 9H), 0.06 (s, 6H); LCMS (ESI, formic) m/z 238 [M+H]⁺, $R_t = 1.36$ min.

***N*-(2-(((*tert*-Butyldimethylsilyl)oxy)methyl)phenyl)-5-methyl-4-oxo-3,4-dihydrothieno[2,3-*d*]pyrimidine-6-carboxamide (79)**



HATU (230 mg, 0.60 mmol) and DIPEA (0.17 mL, 0.95 mmol) were added to a solution of 5-methyl-4-oxo-3,4-dihydrothieno[2,3-*d*]pyrimidine-6-carboxylic acid **43** (100 mg, 0.48 mmol) in DMF (1.5 mL). The mixture was stirred at room temperature for 5 min. 2-(((*tert*-butyldimethylsilyl)oxy)methyl)aniline **78** (140 mg, 0.59 mmol) was then added and the mixture was stirred at room temperature for 18 h. Solvent was evaporated under reduced pressure and the crude product was purified by reverse phase chromatography (43 g C18 column, 40-80 % CH₃CN + 0.1% formic acid in H₂O + 0.1% formic acid over 25 min) to give the title product **79** as a yellow solid (90 mg, 44%). ¹H NMR (400 MHz, DMSO-*d*₆) δ 12.57 (br. s, 1H), 9.63 (s, 1H), 8.18 (s, 1H), 7.60 (dd, *J* = 7.8, 1.0 Hz, 1H), 7.46 (dd, *J* = 7.5, 1.0 Hz, 1H), 7.32 (apparent td, *J* = 7.8, 1.7 Hz, 1H), 7.26 (apparent td, *J* = 7.5, 1.2 Hz, 1H), 4.77 (s, 2H), 2.80 (s, 3H), 0.87 (s, 9H), 0.06 (s, 6H). LCMS (ESI, formic) *m/z* 430 [M+H]⁺, *R*_t = 1.32 min.

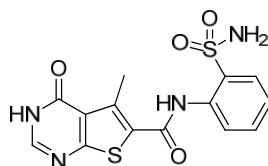
***N*-(2-(Hydroxymethyl)phenyl)-5-methyl-4-oxo-3,4-dihydrothieno[2,3-*d*]pyrimidine-6-carboxamide (54)**



TBAF (1 M in THF, 0.39 mL, 0.39 mmol) was added to a solution of *N*-(2-(((*tert*-butyldimethylsilyl)oxy)methyl)phenyl)-5-methyl-4-oxo-3,4-dihydrothieno[2,3-*d*]pyrimidine-6-carboxamide **79** (83 mg, 0.19 mmol) in THF (1 mL). The mixture was stirred at room temperature for 3 h. Saturated aqueous NaHCO₃ solution (10 mL) and EtOAc (10 mL) were added. The organic layer was separated and the aqueous was extracted with EtOAc (2 x 10 mL). The combined organic layers were

passed through a hydrophobic frit and concentrated under reduced pressure. The crude product was purified by reverse phase chromatography using the formic acid MDAP (gradient C over 15 min) to give the title product **54** as a white solid (36 mg, 59%). ¹H NMR (400 MHz, DMSO-d₆) δ 12.57 (br. s, 1H), 9.87 (br. s, 1H), 8.18 (s, 1H), 7.79 (br. d, *J* = 8.0 Hz, 1H), 7.40 (br. d, *J* = 7.5 Hz, 1H), 7.30 (br. t, *J* = 8.0 Hz, 1H), 7.19 (br. t, *J* = 7.5 Hz, 1H), 5.63 (br. s, 1H), 4.61 (s, 2H), 2.83 (s, 3H); LCMS (ESI, formic) *m/z* 316 [M+H]⁺, *R*_t = 0.67 min; HRMS (ESI) calcd for C₁₅H₁₄N₃O₃S [M+H]⁺ 316.0741, found 316.0756 (3.68 min).

5-Methyl-4-oxo-*N*-(2-sulfamoylphenyl)-3,4-dihydrothieno[2,3-*d*]pyrimidine-6-carboxamide (**55**)



HATU conditions

5-methyl-4-oxo-3,4-dihydrothieno[2,3-*d*]pyrimidine-6-carboxylic acid **43** (73 mg, 0.35 mmol) was dissolved in DMF (2.5 mL). HATU (158 mg, 0.42 mmol) and DIPEA (0.12 mL, 0.70 mmol) were added. The mixture was stirred at room temperature for 30 min. 2-aminobenzenesulfonamide **80** (120 mg, 0.70 mmol) was then added and the mixture was stirred at room temperature for 12 h. LCMS showed no reaction. The mixture was then heated at 40 °C for 3 h. LCMS showed no reaction.

CDI conditions

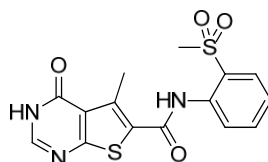
5-methyl-4-oxo-3,4-dihydrothieno[2,3-*d*]pyrimidine-6-carboxylic acid **43** (100 mg, 0.48 mmol) was dissolved in THF (4 mL). CDI (158 mg, 0.97 mmol) was added and

the mixture was stirred at room temperature for 1 h. LCMS showed conversion to the desired activated imidazole intermediate **81**. 2-aminobenzenesulfonamide **80** (98 mg, 0.57 mmol) was then added and the mixture was stirred at room temperature for 12 h. LCMS showed no desired product formed, only intermediate and starting material present.

Thionyl chloride conditions

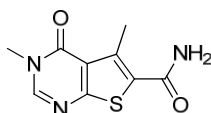
A solution of 5-methyl-4-oxo-3,4-dihydrothieno[2,3-*d*]pyrimidine-6-carboxylic acid **43** (60 mg, 0.29 mmol) in thionyl chloride (2 mL, 27 mmol) was refluxed for 20 h before the reaction mixture was concentrated under reduced pressure. A solution of 2-aminobenzenesulfonamide **80** (59.0 mg, 0.34 mmol) and DIPEA (0.1 mL, 0.6 mmol) in DMF (1.5 mL) was dried over molecular sieves (4 Å) and then added to the acid chloride intermediate under nitrogen. The reaction mixture was stirred at room temperature under nitrogen for 18 h. The crude product was purified by reverse phase chromatography using the formic acid MDAP (gradient A over 15 min) to give the title product **55** as orange solid (11 mg, 11%). ¹H NMR (400 MHz, DMSO-*d*₆) δ 12.56 (br. s, 1H), 8.17 (d, *J* = 3.5 Hz, 1H), 7.67 (dd, *J* = 8.0, 1.5 Hz, 1H), 7.29 - 7.36 (m, 1H), 6.84 (d, *J* = 8.3 Hz, 1H), 6.68 - 6.74 (m, 1H), 2.69 (s, 3H), amide NH and NH₂ protons not observed (exchangeable); LCMS (ESI, formic) *m/z* 364.97 [M+H]⁺, R_t = 0.62 min.

5-Methyl-*N*-(2-(methylsulfonyl)phenyl)-4-oxo-3,4-dihydrothieno[2,3-*d*]pyrimidine-6-carboxamide (**56**)



5-methyl-4-oxo-3,4-dihydrothieno[2,3-*d*]pyrimidine-6-carboxylic acid **43** (100 mg,

0.48 mmol) in thionyl chloride (2 mL, 27 mmol) was heated at 50 °C for 2 days before the mixture was concentrated under reduced pressure. A solution of DMF (1.5 mL) and DIPEA (0.2 mL, 1.1 mmol) dried over molecular sieves (4 Å) was added to the crude intermediate followed by 2-(methylsulfonyl)aniline **82** (250 mg, 1.5 mmol). The mixture was stirred at room temperature with molecular sieves under nitrogen for 16 h before being heated to 50 °C for a further 16 h. Starting material still remained by LCMS (24% area). The crude mixture was purified by reverse phase chromatography using the formic acid MDAP (gradient B over 15 min) to give the title product as a yellow solid (16 mg, 9%). ¹H NMR (400 MHz, DMSO-d₆) δ 8.19 - 8.24 (m, 2H), 7.96 (dd, *J* = 8.0, 1.5 Hz, 1H), 7.75 - 7.81 (m, 1H), 7.47 (td, *J* = 8.3, 1.0 Hz, 1H), 3.33 (s, 3H), 2.85 (s, 3H), amide NHs not observed (exchangeable); LCMS (ESI, formic) *m/z* 364 [M+H]⁺, *R*_t = 0.77 min. **3,5-Dimethyl-4-oxo-3,4-dihydrothieno[2,3-*d*]pyrimidine-6-carboxamide (83)**



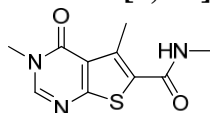
CDI (170 mg, 1 mmol) was added to a solution of 3,5-dimethyl-4-oxo-3,4-dihydrothieno[2,3-*d*]pyrimidine-6-carboxamide **30** (100 mg, 0.45 mmol) in THF (5 mL). The mixture was stirred at room temperature for 21 h. Further CDI (72.3 mg, 0.446 mmol) was added and the mixture was stirred for another 3 h. Ammonia gas was bubbled through the reaction mixture for 5 min and the reaction mixture was left to stir at room temperature for 1 h before the solvent was evaporated under reduced pressure. The resulting crude product was purified by reverse phase chromatography using high pH MDAP (gradient A over 15 min) to give the title product as a white solid (29 mg, 28%). mp > 300 °C; ¹H NMR (400 MHz, DMSO-d₆) δ 8.45 (s, 1H), 7.61 (br. s, 2H), 3.46 (s, 3H), 2.73 (s, 3H); LCMS (ESI, formic) *m/z* 224 [M+H]⁺, *R*_t = 0.44 min.

General procedure 1 for amide coupling

The appropriate amine (1.2 eq), HATU (1.2 eq) and DIPEA (2 eq) were added to a solution of 3,5-dimethyl-4-oxo-3,4-dihydrothieno[2,3-*d*]pyrimidine-6-carboxylic acid (1 eq) in DMF. The mixture was stirred at room temperature until reaction was

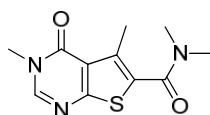
complete by LCMS. Water (50 mL) and EtOAc (50 mL) were added. The aqueous phase was extracted with EtOAc (2 x 50 mL). The organic layers were combined, passed through a hydrophobic frit and concentrated to dryness under reduced pressure. The resulting crude product was purified by reverse phase chromatography to give the desired final product.

***N*-3,5-Trimethyl-4-oxo-3,4-dihydrothieno[2,3-*d*]pyrimidine-6-carboxamide (84)**



N-3,5-Trimethyl-4-oxo-3,4-dihydrothieno[2,3-*d*]pyrimidine-6-carboxamide was prepared following the general procedure 1 using 3,5-dimethyl-4-oxo-3,4-dihydrothieno[2,3-*d*]pyrimidine-6-carboxylic acid **30** (100 mg, 0.45 mmol), methylamine (2 M in THF, 0.3 mL, 0.6 mmol), HATU (203 mg, 0.53 mmol) and DIPEA (0.16 mL, 0.90 mmol) in DMF (10 mL) for 3.5 h. Purification by reverse phase chromatography (gradient A over 15 min) gave the title product **84** as a white solid (20 mg, 18%). ¹H NMR (400 MHz, DMSO-*d*₆) δ 8.45 (s, 1H), 8.13 (br. s, 1H), 3.46 (s, 3H), 2.77 (d, *J* = 4.5 Hz, 3H), 2.70 (s, 3H); LCMS (ESI, formic) *m/z* 238 [M+H]⁺, *R*_t = 0.49 min.

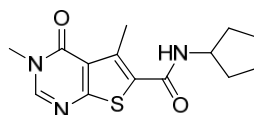
***N,N*-3,5-Tetramethyl-4-oxo-3,4-dihydrothieno[2,3-*d*]pyrimidine-6-carboxamide (85)**



N,N-3,5-Tetramethyl-4-oxo-3,4-dihydrothieno[2,3-*d*]pyrimidine-6-carboxamide was

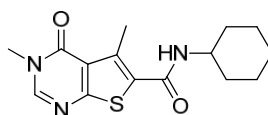
prepared following the general procedure 1 using 3,5-dimethyl-4-oxo-3,4-dihydrothieno[2,3-*d*]pyrimidine-6-carboxylic acid **30** (100 mg, 0.45 mmol), dimethylamine (2 M in THF, 0.3 mL, 0.6 mmol), HATU (203 mg, 0.53 mmol) and DIPEA (0.16 mL, 0.90 mmol) in DMF (10 mL) for 56 h, then 50 °C for 24 h. Purification by reverse phase chromatography (gradient A over 15 min) to give the title product as a yellow solid (13 mg, 11%). ¹H NMR (400 MHz, CDCl₃) δ 8.00 (s, 1H), 3.58 (s, 3H), 3.09 (br. s, 6H), 2.56 (s, 3H); LCMS (ESI, formic) *m/z* 252 [M+H]⁺, R_t = 0.54 min.

***N*-Cyclopentyl-3,5-dimethyl-4-oxo-3,4-dihydrothieno[2,3-*d*]pyrimidine-6-carboxamide (86)**



N-Cyclopentyl-3,5-dimethyl-4-oxo-3,4-dihydrothieno[2,3-*d*]pyrimidine-6-carboxamide was prepared following the general procedure 1 using 3,5-dimethyl-4-oxo-3,4-dihydrothieno[2,3-*d*]pyrimidine-6-carboxylic acid **30** (50 mg, 0.22 mmol), HATU (102 mg, 0.27 mmol), DIPEA (80 μL, 0.45 mmol) and cyclopentanamine (26 μL, 0.27 mmol) in DMF (5 mL) for 2 h. Purification twice by reverse phase chromatography using the formic acid MDAP (gradient B over 15 min) to give the title product **86** as a white solid (20 mg, 28%). mp 185-186 °C; ¹H NMR (400 MHz, CDCl₃) δ 8.03 (s, 1H), 5.82 (d, *J* = 6.3 Hz, 1H), 4.39 (apparent sxt, *J* = 6.8 Hz, 1H), 3.58 (s, 3H), 2.86 (s, 3H), 2.05 – 2.17 (m, 2H), 1.62 - 1.81 (m, 4H), 1.45 - 1.57 (m, 2H); LCMS (ESI, formic) *m/z* 292 [M+H]⁺, R_t = 0.78 min.

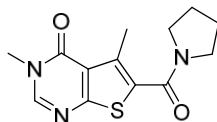
***N*-Cyclohexyl-3,5-dimethyl-4-oxo-3,4-dihydrothieno[2,3-*d*]pyrimidine-6-carboxamide (87)**



N-Cyclohexyl-3,5-dimethyl-4-oxo-3,4-dihydrothieno[2,3-*d*]pyrimidine-6-

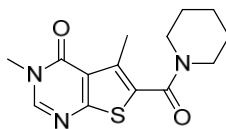
carboxamide was prepared following general procedure 1 using 3,5-dimethyl-4-oxo-3,4-dihydrothieno[2,3-*d*]pyrimidine-6-carboxylic acid **30** (100 mg, 0.45 mmol), cyclohexanamine (60 μ L, 0.53 mmol), HATU (203 mg, 0.53 mmol) and DIPEA (0.16 mL, 0.89 mmol) in DMF (10 mL) for 18 h. Purification by reverse phase chromatography (130g C18 column, 25-65% CH₃CN + 0.1% formic acid in H₂O + 0.1% formic acid) to give the title product **87** as white solid (90 mg, 63%). mp 221-223 °C; ¹H NMR (400 MHz, DMSO-*d*₆) δ 8.45 (s, 1H), 8.05 (d, *J* = 7.8 Hz, 1H), 3.65 - 3.77 (m, 1H), 3.47 (s, 3H), 2.67 (s, 3H), 1.77 - 1.88 (m, 2H), 1.67 - 1.75 (m, 2H), 1.50 - 1.63 (m, 1H), 1.21 - 1.40 (m, 4H), 1.04 - 1.19 (m, 1H); LCMS (ESI, formic) *m/z* 305.96 [M+H]⁺, *R*_t = 0.87 min.

3,5-Dimethyl-6-(pyrrolidine-1-carbonyl)thieno[2,3-*d*]pyrimidin-4(3*H*)-one (**88**)



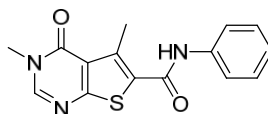
3,5-Dimethyl-6-(pyrrolidine-1-carbonyl)thieno[2,3-*d*]pyrimidin-4(3*H*)-one was prepared following procedure 1 using 3,5-dimethyl-4-oxo-3,4-dihydrothieno[2,3-*d*]pyrimidine-6-carboxylic acid **30** (80 mg, 0.36 mmol), DIPEA (0.12 mL, 0.71 mmol), HATU (163 mg, 0.43 mmol), pyrrolidine (35 μ L, 0.43 mmol), DMF (1.5 mL) overnight. Purification by reverse phase chromatography using formic acid MDAP (gradient A over 15 min) gave the title product **88** as orange solid (70 mg, 67%). mp 186-188 °C; ¹H NMR (400 MHz, DMSO-*d*₆) δ 8.47 (s, 1H), 3.50 (s, 3H), 3.46-3.50 (m, 4H), 2.50 (s, 3H), 1.89 (br. s, 4H); ¹³C NMR (101 MHz, DMSO-*d*₆) δ 163.0 (C), 161.5 (C=O), 157.9 (C=O), 149.6 (Ar-CH), 132.6 (C), 128.0 (C), 121.6 (C), 47.8 (CH₂), 45.7 (CH₂), 33.3 (CH₃), 25.3 (CH₂), 23.7 (CH₂), 14.9 (CH₃); LCMS (ESI, formic) *m/z* 278.09 [M+H]⁺, *R*_t = 0.63 min; HRMS (ESI) calcd for C₁₃H₁₆N₃O₂S [M+H]⁺ 278.0958, found 278.0954 (3.23 min).

3,5-Dimethyl-6-(piperidine-1-carbonyl)thieno[2,3-*d*]pyrimidin-4(3*H*)-one (89)



3,5-Dimethyl-6-(piperidine-1-carbonyl)thieno[2,3-*d*]pyrimidin-4(3*H*)-one was prepared following general procedure 1 using 3,5-dimethyl-4-oxo-3,4-dihydrothieno[2,3-*d*]pyrimidine-6-carboxylic acid **30** (80 mg, 0.36 mmol), piperidine (0.04 mL, 0.43 mmol), DIPEA (0.12 mL, 0.71 mmol), HATU (163 mg, 0.43 mmol), DMF (1.5 mL) overnight. Purification by reverse phase chromatography using the formic acid MDAP (gradient B over 15 min) to give the title product **89** as a white solid (70 mg, 64%). ¹H NMR (400 MHz, DMSO-*d*₆) δ 8.43 (s, 1H), 3.47 (br. s, 7H), 2.43 (s, 3H), 1.56 - 1.67 (m, 2H), 1.55-1.44 (m, 4H); LCMS (ESI, formic) *m/z* 292 [M+H]⁺, R_t = 0.74 min.

3,5-Dimethyl-4-oxo-*N*-phenyl-3,4-dihydrothieno[2,3-*d*]pyrimidine-6carboxamide (90)

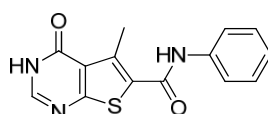


3,5-Dimethyl-4-oxo-*N*-phenyl-3,4-dihydrothieno[2,3-*d*]pyrimidine-6-carboxamide was prepared following general procedure 1 using 3,5-dimethyl-4-oxo-3,4-dihydrothieno[2,3-*d*]pyrimidine-6-carboxylic acid **30** (100 mg, 0.45 mmol), DIPEA (0.16 mL, 0.89 mmol), HATU (203 mg, 0.54 mmol), aniline (50 μL, 0.54 mmol), DMF (10 mL) for 16 h. Purification by reverse phase chromatography using the formic acid MDAP (gradient B over 15 min) gave the title product **90** as white solid (90 mg, 64%). mp 186-188 °C; ¹H NMR (400 MHz, DMSO-*d*₆) δ 10.25 (s, 1H), 8.50 (s, 1H), 7.68 (br. d, *J* = 7.5 Hz, 2H), 7.36 (br. t, *J* = 8.0 Hz, 2H), 7.07 - 7.16 (br. t, *J* = 7.5 Hz, 1H), 3.49 (s, 3H), 2.74 (s, 3H); LCMS (ESI, high pH) *m/z* 300 [M+H]⁺, R_t = 0.83 min.

General procedure 2 for amide coupling

HATU (1.2 eq) and DIPEA (2 eq) were added to a solution of 5-methyl-4-oxo-3,4-dihydrothieno[2,3-*d*]pyrimidine-6-carboxylic acid **43** (1 eq) in DMF (1.5 – 2.5 mL). The mixture was stirred at room temperature between 1 to 10 min. The appropriate amine (1.2 eq) was then added and the reaction mixture was stirred at room temperature until reaction was complete by LCMS. Solvent was then evaporated under reduced pressure. The resulting crude product was purified by reverse phase chromatography to give the desired final product. **5-Methyl-4-oxo-*N*-phenyl-3,4-dihydrothieno[2,3-*d*]pyrimidine-6-carboxamide**

(42)



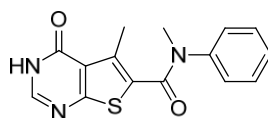
5-Methyl-4-oxo-*N*-phenyl-3,4-dihydrothieno[2,3-*d*]pyrimidine-6-carboxamide was prepared following general procedure 2 using 5-methyl-4-oxo-3,4-dihydrothieno[2,3-*d*]pyrimidine-6-carboxylic acid **43** (100 mg, 0.48 mmol), HATU (220 mg, 0.58 mmol), DIPEA (0.17 mL, 0.95 mmol) and aniline (50 μ L, 0.54 mmol) in DMF

(2.5 mL) for 1 h. Purification by reverse phase chromatography (C18 column, 1040% CH₃CN in 10 mM aqueous ammonium bicarbonate solution) gave the title product **42** as a pale yellow solid (87 mg, 64%). mp 276-278 °C; ¹H NMR (400 MHz, DMSO-*d*₆) δ 12.57 (br. s, 1H), 10.20 (s, 1H), 8.18 (s, 1H), 7.68 (d, *J* = 7.6 Hz, 2H), 7.36 (t, *J* = 7.9 Hz, 2H), 7.03 - 7.18 (m, 1H), 2.73 (s, 3H); ¹³C NMR (101 MHz, DMSO-*d*₆) δ 164.2 (C), 160.6 (C=O), 158.3 (C=O), 147.4 (Ar-CH), 138.5 (C), 136.4 (C), 128.7 (2C, Ar-CH), 127.9 (C), 124.0 (Ar-CH), 123.4 (C), 120.3 (2C, Ar-CH), 15.1 (CH₃); LCMS (ESI, high pH) *m/z* 286 [M+H]⁺, *R*_t = 0.72 min; HRMS (ESI) calcd for C₁₄H₁₂N₃O₂S [M+H]⁺ 286.0650, found 286.0646 (4.08 min); IR (ATR) cm⁻¹

¹

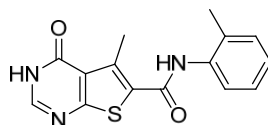
3294, 3062, 3020, 2929, 2866, 1656, 1634, 1595, 1580, 1529.

***N*,5-Dimethyl-4-oxo-*N*-phenyl-3,4-dihydrothieno[2,3-*d*]pyrimidine-6-carboxamide (91)**



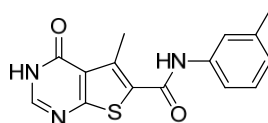
N,5-Dimethyl-4-oxo-*N*-phenyl-3,4-dihydrothieno[2,3-*d*]pyrimidine-6-carboxamide was prepared following general procedure 2 using 5-methyl-4-oxo-3,4-dihydrothieno[2,3-*d*]pyrimidine-6-carboxylic acid **43** (100 mg, 0.48 mmol), HATU (217 mg, 0.57 mmol), DIPEA (0.17 mL, 0.95 mmol) and *N*-methylaniline (60 μ L, 0.57 mmol) in DMF (2.5 mL) for 1 h. Purification by reverse phase chromatography (C18 column, 10-40% CH₃CN in 10 mM aqueous ammonium bicarbonate solution) gave the title product **91** as a pale yellow solid (68 mg, 48%). mp 257-259 °C; ¹H NMR (400 MHz, DMSO-*d*₆) δ 12.42 (br. s, 1H), 8.03 (s, 1H), 7.29 - 7.35 (m, 2H), 7.20 - 7.27 (m, 3H), 3.38 (s, 3H), 2.35 (s, 3H); LCMS (ESI, high pH) *m/z* 300 [M+H]⁺, *R*_t = 0.71 min.

5-Methyl-4-oxo-*N*-(*o*-tolyl)-3,4-dihydrothieno[2,3-*d*]pyrimidine-6-carboxamide (92)



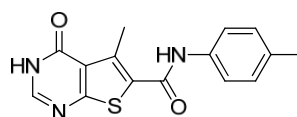
5-Methyl-4-oxo-*N*-(*o*-tolyl)-3,4-dihydrothieno[2,3-*d*]pyrimidine-6-carboxamide was prepared following general procedure 2 using 5-methyl-4-oxo-3,4-dihydrothieno[2,3-*d*]pyrimidine-6-carboxylic acid **43** (60 mg, 0.28 mmol), HATU (138 mg, 0.36 mmol), DIPEA (0.1 mL, 0.6 mmol) and *o*-toluidine (0.4 mL, 0.3 mmol) in DMF (1.5 mL) for 16 h. Purification by reverse phase chromatography using the formic acid MDAP (gradient B over 15 min) gave the title product **92** as yellow solid (32 mg, 37%). ¹H NMR (400 MHz, DMSO-*d*₆) δ 12.55 (br. s, 1H), 9.69 (s, 1H), 8.17 (s, 1H), 7.39 (br. d, *J* = 7.5 Hz, 1H), 7.28 (br. d, *J* = 7.0 Hz, 1H), 7.15 - 7.25 (m, 2H), 2.79 (s, 3H), 2.26 (s, 3H); LCMS (ESI, formic) *m/z* 300 [M+H]⁺, *R*_t = 0.78 min.

5-Methyl-4-oxo-*N*-(*m*-tolyl)-3,4-dihydrothieno[2,3-*d*]pyrimidine-6-carboxamide (93)



5-Methyl-4-oxo-*N*-(*m*-tolyl)-3,4-dihydrothieno[2,3-*d*]pyrimidine-6-carboxamide was prepared following general procedure 2 using 5-methyl-4-oxo-3,4-dihydrothieno[2,3-*d*]pyrimidine-6-carboxylic acid **43** (60 mg, 0.28 mmol), HATU (135 mg, 0.36 mmol), DIPEA (0.1 mL, 0.6 mmol) and *m*-toluidine (60 μ L, 0.57 mmol) in DMF (1 mL) at 50 $^{\circ}$ C for 4 h. Purification by reverse phase chromatography using the formic acid MDAP (gradient B over 15 min) gave the title product **93** as a white solid (39 mg, 46%). mp 250-253 $^{\circ}$ C; 1 H NMR (400 MHz, DMSO- d_6) δ 12.55 (br. s, 1H), 10.12 (s, 1H), 8.17 (s, 1H), 7.51 (s, 1H), 7.47 (d, J = 8.3 Hz, 1H), 7.23 (t, J = 7.8 Hz, 1H), 6.94 (d, J = 7.5 Hz, 1H), 2.73 (s, 3H), 2.31 (s, 3H); 13 C NMR (101 MHz, DMSO- d_6) δ 164.2 (C), 160.5 (C=O), 158.3 (C=O), 147.3 (CH), 138.4 (C), 137.9 (C), 136.3 (C), 128.5 (C), 128.0 (CH), 124.7 (CH), 123.4 (C), 120.8 (CH), 117.5 (CH), 21.1 (CH $_3$), 15.0 (CH $_3$); LCMS (ESI, formic) m/z 300 [M+H] $^+$, R_t = 0.85 min; HRMS (ESI) calcd for C $_{15}$ H $_{14}$ N $_3$ O $_2$ S [M+H] $^+$ 300.0801, found 300.0798 (4.21 min).

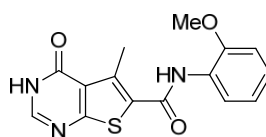
5-Methyl-4-oxo-*N*-(*p*-tolyl)-3,4-dihydrothieno[2,3-*d*]pyrimidine-6-carboxamide (94)



5-Methyl-4-oxo-*N*-(*p*-tolyl)-3,4-dihydrothieno[2,3-*d*]pyrimidine-6-carboxamide was prepared following general procedure 2 using 5-methyl-4-oxo-3,4-dihydrothieno[2,3-*d*]pyrimidine-6-carboxylic acid **43** (60 mg, 0.28 mmol), HATU (135 mg, 0.36 mmol), DIPEA (0.1 mL, 0.6 mmol) and *p*-toluidine (80 mg, 0.75 mmol) in DMF (1 mL) at 50 $^{\circ}$ C for 4 h. Purification by reverse phase chromatography using the formic acid MDAP (gradient B over 15 min) gave the title product **94** as a white solid

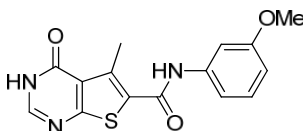
(39 mg, 45%). mp 272-275 °C; ¹H NMR (400 MHz, DMSO-d₆) δ 12.54 (br. s, 1H), 10.10 (s, 1H), 8.17 (s, 1H), 7.56 (d, *J* = 8.5 Hz, 2H), 7.16 (d, *J* = 8.3 Hz, 2H), 2.72 (s, 3H), 2.28 (s, 3H); ¹³C NMR (101 MHz, DMSO-d₆) δ 164.1 (C), 160.4 (C=O), 158.3 (C=O), 147.3 (Ar-CH), 136.2 (C), 136.0 (C), 133.1 (C), 129.0 (2C, ArCH), 128.0 (C), 123.4 (C), 120.3 (2C, Ar-CH), 20.5 (CH₃), 15.0 (CH₃); LCMS (ESI, formic) *m/z* 300 [M+H]⁺, *R*_t = 0.85 min; HRMS (ESI) calcd for C₁₅H₁₄N₃O₂S [M+H]⁺ 300.0801, found 300.0803 (4.19 min).

***N*-(2-Methoxyphenyl)-5-methyl-4-oxo-3,4-dihydrothieno[2,3-*d*]pyrimidine-6-carboxamide (95)**



N-(2-Methoxyphenyl)-5-methyl-4-oxo-3,4-dihydrothieno[2,3-*d*]pyrimidine-6-carboxamide was prepared following general procedure 2 using 5-methyl-4-oxo-3,4-dihydrothieno[2,3-*d*]pyrimidine-6-carboxylic acid **43** (96 mg, 0.46 mmol), HATU (206 mg, 0.54 mmol), DIPEA (0.16 mL, 0.91 mmol) and 2-methoxyaniline (0.1 mL, 0.89 mmol) in DMF (2 mL) at 50 °C for 20 h. Purification by reverse phase chromatography using the formic acid MDAP (gradient B over 15 min) gave the title product **95** as a white solid (55 mg, 38%). ¹H NMR (400 MHz, DMSO-d₆) δ 12.55 (br. s, 1H), 9.18 (s, 1H), 8.17 (s, 1H), 7.88 (dd, *J* = 7.9, 1.4 Hz, 1H), 7.15 - 7.21 (m, 1H), 7.09 - 7.13 (m, 1H), 6.97 (td, *J* = 7.6, 1.3 Hz, 1H), 3.87 (s, 3H), 2.83 (s, 3H); LCMS (ESI, formic) *m/z* 316 [M+H]⁺, *R*_t = 0.86 min.

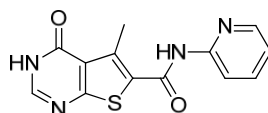
***N*-(3-Methoxyphenyl)-5-methyl-4-oxo-3,4-dihydrothieno[2,3-*d*]pyrimidine-6-carboxamide (96)**



N-(3-Methoxyphenyl)-5-methyl-4-oxo-3,4-dihydrothieno[2,3-*d*]pyrimidine-6-

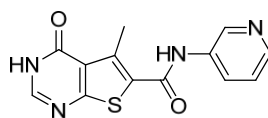
carboxamide was prepared following general procedure 2 using 5-methyl-4-oxo-3,4-dihydrothieno[2,3-*d*]pyrimidine-6-carboxylic acid **43** (60 mg, 0.29 mmol), HATU (135 mg, 0.36 mmol), DIPEA (0.10 mL, 0.57 mmol) and 3-methoxyaniline (64 μ L, 0.57 mmol) in DMF (1 mL) at 50 °C for 4 h. Purification by reverse phase chromatography using the formic acid MDAP (gradient B over 15 min) gave the title product **96** as a white solid (22 mg, 24%). ¹H NMR (400 MHz, DMSO-*d*₆) δ 12.56 (br. s, 1H), 10.18 (s, 1H), 8.18 (d, *J* = 3.01 Hz, 1H), 7.36 (m, 1H), 7.23 - 7.27 (m, 2H), 6.68 - 6.74 (m, 1H), 3.75 (s, 3H), 2.72 (s, 3H); LCMS (ESI, formic) *m/z* 316 [M+H]⁺, *R*_t = 0.79 min.

5-Methyl-4-oxo-*N*-(pyridin-2-yl)-3,4-dihydrothieno[2,3-*d*]pyrimidine-6-carboxamide (97)



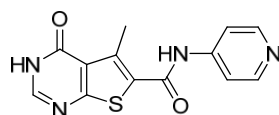
5-Methyl-4-oxo-*N*-(pyridin-2-yl)-3,4-dihydrothieno[2,3-*d*]pyrimidine-6-carboxamide was prepared following general procedure 2 using 5-methyl-4-oxo-3,4-dihydrothieno[2,3-*d*]pyrimidine-6-carboxylic acid **43** (65 mg, 0.31 mmol), HATU (141 mg, 0.37 mmol), DIPEA (0.1 mL, 0.57 mmol) and 2-aminopyridine (35 mg, 0.37 mmol) in DMF (1.5 mL) at 40 °C for 2 days. Purification by reverse phase chromatography (0-68 % MeOH in 10 mM aqueous ammonium bicarbonate solution over 36 min) gave the title product **97** as a off white solid (4 mg, 5%).; ¹H NMR (400 MHz, DMSO-*d*₆) δ 12.50 (br. s, 1H), 10.54 (s, 1H), 8.38 (d, *J* = 4.0 Hz, 1H), 8.16 (s, 1H), 8.07 (d, *J* = 8.3 Hz, 1H), 7.80 - 7.87 (m, 1H), 7.11 - 7.22 (m, 1H), 2.76 (s, 3H); LCMS (ESI, formic) *m/z* 287 [M+H]⁺, *R*_t = 0.61 min.

5-Methyl-4-oxo-*N*-(pyridin-3-yl)-3,4-dihydrothieno[2,3-*d*]pyrimidine-6-carboxamide (98)



5-Methyl-4-oxo-*N*-(pyridin-3-yl)-3,4-dihydrothieno[2,3-*d*]pyrimidine-6-carboxamide was prepared following general procedure 2 using 5-methyl-4-oxo-3,4-dihydrothieno[2,3-*d*]pyrimidine-6-carboxylic acid **43** (100 mg, 0.48 mmol), HATU (220 mg, 0.58 mmol), DIPEA (0.17 mL, 0.95 mmol) and pyridin-3-amine (57 mg, 0.61 mmol) in DMF (2.5 mL) for 1 h. Purification by reverse phase chromatography (5-20% acetonitrile in 10 mM aqueous ammonium bicarbonate solution over 18 min). The product was dissolved in MeOH and transferred in a vial for test to give the title product as MeOH solvate **98**, yellow solid (70 mg, 46%). ¹H NMR (400 MHz, DMSO-*d*₆) δ 12.59 (br. s, 1H), 10.39 (s, 1H), 8.84 (d, *J* = 2.5 Hz, 1H), 8.33 (dd, *J* = 4.8, 1.5 Hz, 1H), 8.19 (s, 1H), 8.07 - 8.14 (m, 1H), 7.40 (dd, *J* = 8.3, 4.8 Hz, 1H), 4.06 (d, *J* = 5.0 Hz, 1H, CH₃OH), 3.17 (d, *J* = 5.0 Hz, 3H, CH₃OH), 2.76 (s, 3H); LCMS (ESI, high pH) *m/z* 287 [M+H]⁺, R_t = 0.52 min.

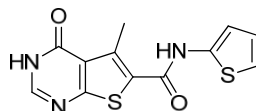
5-Methyl-4-oxo-*N*-(pyridin-4-yl)-3,4-dihydrothieno[2,3-*d*]pyrimidine-6-carboxamide (99)



5-Methyl-4-oxo-*N*-(pyridin-4-yl)-3,4-dihydrothieno[2,3-*d*]pyrimidine-6-carboxamide was prepared following general procedure 2 using 5-methyl-4-oxo-3,4-dihydrothieno[2,3-*d*]pyrimidine-6-carboxylic acid **43** (109 mg, 0.52 mmol), HATU (233 mg, 0.6 mmol), DIPEA (0.2 mL, 1.0 mmol) and pyridin-4-amine (148 mg, 1.6 mmol) in DMF (1.5 mL) at 50 °C for 48 h. Purification twice by reverse phase chromatography using formic acid MDAP (gradient A over 15 min) gave the title product **99** as white solid (5 mg, 3%). ¹H NMR (400 MHz, DMSO-*d*₆) δ 12.63 (br. s,

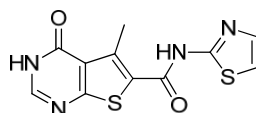
1H), 10.57 (br. s, 1H), 8.49 (apparent d, $J = 5.5$ Hz, 2H), 8.20 (s, 1H), 7.67 (apparent d, $J = 5.3$ Hz, 2H), 2.74 (s, 3H); LCMS (ESI, formic) m/z 287 $[M+H]^+$, $R_t = 0.40$ min.

5-Methyl-4-oxo-*N*-(thiophen-2-yl)-3,4-dihydrothieno[2,3-*d*]pyrimidine-6-carboxamide (100)



5-Methyl-4-oxo-*N*-(thiophen-2-yl)-3,4-dihydrothieno[2,3-*d*]pyrimidine-6-carboxamide was prepared following procedure 2 using 5-methyl-4-oxo-3,4-dihydrothieno[2,3-*d*]pyrimidine-6-carboxylic acid **43** (100 mg, 0.48 mmol), HATU (217 mg, 0.57 mmol) and DIPEA (0.17 mL, 0.97 mmol) in DMF (1.5 mL) and thiophen-2-amine (64 mg, 0.65 mmol) at 40 °C for 48 h. Purification by reverse phase chromatography using the formic acid MDAP (gradient B over 15 min) gave the title product **100** as white solid (21 mg, 15%). mp 250 °C (dec.); ^1H NMR (400 MHz, DMSO- d_6) δ 12.59 (br. s, 1H), 11.42 (s, 1H), 8.19 (d, $J = 4.0$ Hz, 1H), 7.05 (t, $J = 3.8$ Hz, 1H), 6.90 - 6.93 (m, 2H), 2.76 (s, 3H); ^{13}C NMR (101 MHz, DMSO- d_6) δ 164.4 (C), 158.5 (C=O), 158.2 (C=O), 147.6 (Ar-CH), 139.2 (C), 138.0 (C), 125.4 (C), 124.1 (C), 123.5 (Ar-CH), 117.9 (Ar-CH), 112.8 (Ar-CH), 15.1 (CH₃); LCMS (ESI, formic) m/z 292.03 $[M+H]^+$, $R_t = 0.74$ min; HRMS (ESI) calcd for C₁₂H₁₀N₃O₂S₂ $[M+H]^+$ 292.0214, found 292.0214 (4.01 min).

5-Methyl-4-oxo-*N*-(thiazol-2-yl)-3,4-dihydrothieno[2,3-*d*]pyrimidine-6-carboxamide (101)

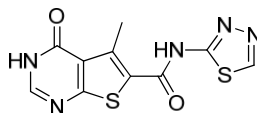


5-Methyl-4-oxo-*N*-(thiophen-2-yl)-3,4-dihydrothieno[2,3-*d*]pyrimidine-6-

carboxamide was prepared following procedure 2 using 5-methyl-4-oxo-3,4-dihydrothieno[2,3-*d*]pyrimidine-6-carboxylic acid **43** (100 mg, 0.48 mmol), HATU (217 mg, 0.57 mmol) and DIPEA (0.17 mL, 0.97 mmol) in DMF (1.5 mL) and 2-aminothiazole (66 mg, 0.66 mmol) at 40 °C for 48 h. Purification by reverse phase chromatography using the formic acid MDAP (gradient A over 15 min) gave the title product **101** as white solid (51 mg, 37%). ¹H NMR (400 MHz, DMSO-*d*₆)

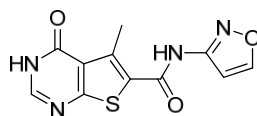
δ 12.89 (br. s, 1H), 12.51 (br. s, 1H), 8.15 (s, 1H), 7.48 (d, *J* = 4.3 Hz, 1H), 7.12 (d, *J* = 4.3 Hz, 1H), 2.87 (s, 3H); LCMS (ESI, formic) *m/z* 293.07 [M+H]⁺, *R*_t = 0.63 min.

5-Methyl-4-oxo-*N*-(1,3,4-thiadiazol-2-yl)-3,4-dihydrothieno[2,3-*d*]pyrimidine-6-carboxamide (**102**)



5-Methyl-4-oxo-*N*-(1,3,4-thiadiazol-2-yl)-3,4-dihydrothieno[2,3-*d*]pyrimidine-6-carboxamide was prepared following procedure 2 using 5-methyl-4-oxo-3,4-dihydrothieno[2,3-*d*]pyrimidine-6-carboxylic acid **43** (100 mg, 0.48 mmol), HATU (217 mg, 0.57 mmol) and DIPEA (0.17 mL, 0.97 mmol) in DMF (1.5 mL) and 2-amino-1,3,4-thiadiazole (62 mg, 0.61 mmol) at 40 °C for 48 h. DMSO (2 mL) was added to the reaction mixture and the whole mixture solubilised with heating. After cooling a solid precipitated out which was collected by filtration and dried in a vacuum oven overnight to give the title product **102** as yellow solid (70 mg, 50%). mp 350 °C (dec.); ¹H NMR (400 MHz, DMSO-*d*₆) δ 14.10 (br. s, 1H), 12.54 (br. s, 1H), 9.04 (br. s, 1H), 8.18 (d, *J* = 3.5 Hz, 1H), 2.89 (s, 3H); ¹³C NMR (126 MHz, DMSO-*d*₆) δ 167.6 (C), 166.7 (C=O), 158.5 (C=O), 146.2 (Ar-CH), 144.9 (Ar-CH), 135.6 (C), 134.2 (C), 124.2 (C), 109.5 (C), 14.8 (CH₃); LCMS (ESI, formic) *m/z* 294 [M+H]⁺, *R*_t = 0.38 min; HRMS (ESI) calcd for C₁₀H₈N₅O₂S₂ [M+H]⁺ 294.0119, found 294.0115 (3.22 min); IR (ATR) cm⁻¹ 3142, 3095, 3007, 2930, 1676, 1651, 1552.

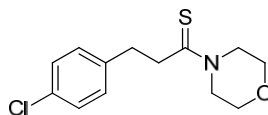
***N*-(Isoxazol-3-yl)-5-methyl-4-oxo-3,4-dihydrothieno[2,3-*d*]pyrimidine-6-carboxamide (103)**



A solution of 5-methyl-4-oxo-3,4-dihydrothieno[2,3-*d*]pyrimidine-6-carboxylic acid **43** (100 mg, 0.48 mmol) in thionyl chloride (2 mL, 27 mmol) was heated at 80 °C for 3 days before the reaction mixture was concentrated to dryness under reduced pressure. A solution of isoxazol-3-amine (160 mg, 1.9 mmol) and DIPEA (0.2 mL, 1.2 mmol) in DMF (1.5 mL) dried over molecular sieves (4 Å) was added to the crude and the mixture was stirred at room temperature with molecular sieves for 24 h. The crude reaction mixture was purified by reverse phase chromatography using formic acid MDAP (gradient A over 15 min) gave the title product **103** as white solid (18 mg, 14%). ¹H NMR (400 MHz, DMSO-*d*₆) δ 11.98 (br. s, 2H), 8.85 (d, *J* = 1.5 Hz, 1H), 8.19 (s, 1H), 6.97 (d, *J* = 1.8 Hz, 1H), 2.75 (s, 3H); LCMS (ESI, formic) *m/z* 277 [M+H]⁺, *R*_t = 0.57 min.

4.3 Experimental Procedures for Cluster 6 Template

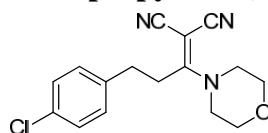
3-(4-Chlorophenyl)-1-morpholinopropane-1-thione (155)



A mixture of 1-(4-chlorophenyl)propan-1-one (2 g, 12 mmol), morpholine (4 mL,

46 mmol) and sulfur (0.77 g, 23.9 mmol), connected to a trap of bleach, was heated at 130 °C for 24 h under nitrogen. After cooling to room temperature, the mixture was poured into CHCl₃ (50 mL) and stirred with activated charcoal for 15 min. The mixture was filtered through Celite™ and evaporated under reduced pressure. The resulting residue was dissolved in EtOH and heated until complete dissolution. The solution was left to cool overnight. The precipitate formed was collected by filtration and dried in a vacuum oven for 3 h to give the title product **155** as a green solid (2.0 g, 62%). ¹H NMR (400 MHz, DMSO-d₆) δ 7.26 - 7.36 (m, 4H), 4.19 (t, *J* = 4.8 Hz, 2H), 3.74 (t, *J* = 4.7 Hz, 2H), 3.63 (t, *J* = 5.0 Hz, 2H), 3.51 (t, *J* = 4.7 Hz, 2H), 3.03 - 3.08 (m, 2H), 2.92 - 2.98 (m, 2H); LCMS (ESI, formic) *m/z* 270 [M+H]⁺, *R*_t = 1.08 min.

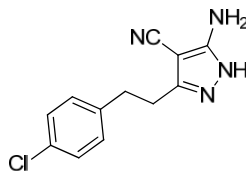
2-(3-(4-Chlorophenyl)-1-morpholinopropylidene)malononitrile (**156**)



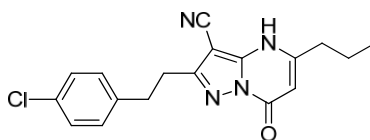
Tetracyanoethylene oxide (0.96 g, 6.7 mmol) in toluene (20 mL) was added dropwise to a solution of 3-(4-chlorophenyl)-1-morpholinopropane-1-thione **155** (1.5 g, 5.6 mmol) in toluene (20 mL) cooled to 0 °C under nitrogen. After complete addition, the mixture was stirred at room temperature overnight under nitrogen. Toluene was added and the organic was washed with saturated aqueous sodium carbonate solution. After several washes (10), the Merckoquant test still showed trace of cyanide. The toluene phase was washed with aqueous copper sulfate solution followed by brine. The brine wash was tested with Merckoquant test, which showed no trace of cyanide. The organic phase was separated, passed through a hydrophobic frit and evaporated under reduced pressure. The resulting residue was triturated with a minimum of MeOH. The solid was collected by filtration and dried in a vacuum oven overnight to give the title product **156** as a beige solid (688 mg, 41 %). The MeOH filtrate was evaporated under reduced pressure. The resulting crude product was purified by normal phase chromatography (20-100% *tert*-butylmethylether in cyclohexane over 58 min, 40 g SiO₂ column) to give additional title product **156** as light brown solid (830 mg, 49 %). ¹H NMR (400 MHz, DMSO-d₆) δ 7.39 (d, *J* = 8.3 Hz, 2H), 7.31 (d, *J* = 8.3 Hz, 2H),

3.75 (br. s, 4H), 3.65 - 3.71 (m, 4H), 2.77 - 2.91 (m, 4H); LCMS (ESI, formic) m/z 302 $[M+H]^+$, $R_t = 1.03$ min.

5-Amino-3-(4-chlorophenethyl)-1H-pyrazole-4-carbonitrile (**135**)



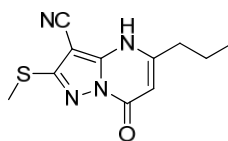
Hydrazine monohydrate (0.53 mL, 6.9 mmol) was added to a solution of 2-(3-(4-chlorophenyl)-1-morpholinopropylidene)malononitrile **156** (1.4 g, 4.6 mmol) in EtOH (10 mL). The reaction mixture was refluxed for 5 h under nitrogen. The mixture was left to cool overnight. Solvent was evaporated under reduced pressure and the resulting residue was triturated with water. The solid was collected under filtration and dried in a vacuum oven to give the title product **135** as a pale brown solid (836 mg, 73%). ^1H NMR (400 MHz, DMSO- d_6) δ 12.08 - 11.57 (2 br. s, 1H, two pyrazole isomers visible), 7.32 (d, $J = 8.0$ Hz, 2H), 7.21 (d, $J = 8.0$ Hz, 2H), 6.21 + 5.29 (2 br. s, 2H), 2.67 - 2.98 (m, 4H); LCMS (ESI, formic) m/z 247 $[M+H]^+$, $R_t = 1.07$ min. **5-Propyl-2-(4-chlorophenethyl)-7-oxo-4,7-dihydropyrazolo[1,5-*a*]pyrimidine-3-carbonitrile (**130**)**



A solution of 5-amino-3-(4-chlorophenethyl)-1H-pyrazole-4-carbonitrile **135** (90 mg, 0.37 mmol) and methyl 3-oxo-4-propylbutanoate (62 μL , 0.40 mmol) in acetic acid (1.5 mL) was refluxed for 20 h. Solvent was evaporated under reduced pressure. The resulting crude product was purified by reverse phase chromatography using the formic acid MDAP (gradient C over 15 min) to give the title product **130** as a white solid (73 mg, 59%). mp 264-267 $^\circ\text{C}$; ^1H NMR (400 MHz, DMSO- d_6) δ 13.09 (br. s, 1H), 7.32 - 7.36 (m, 2H), 7.26 - 7.30 (m, 2H), 5.81 (s, 1H), 3.03 (s, 4H), 2.55 (t, $J = 7.3$ Hz, 2H), 1.66 (apparent sxt, $J = 7.5$ Hz, 2H), 0.93 (t, $J = 7.4$ Hz, 3H); ^{13}C NMR (101 MHz,

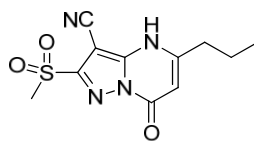
DMSO- d_6) δ 156.4 (C), 154.9 (C), 154.8 (C), 145.3 (C), 139.5 (C), 130.7 (C), 130.2 (2C, Ar-CH), 128.3 (2C, Ar-CH), 112.8 (C), 97.8 (CH), 74.0 (C), 33.9 (CH₂), 32.5 (CH₂), 28.8 (CH₂), 21.3 (CH₂), 13.3 (CH₃); LCMS (ESI, formic) m/z 341 [M+H]⁺, R_t = 1.03 min; HRMS (ESI) calcd for C₁₈H₁₈ClN₄O [M+H]⁺ 341.1164, found 341.1165 (4.77 min); IR (ATR) cm⁻¹ 3158, 3073, 2964, 2224, 1663, 1626, 1581.

2-(Methylthio)-7-oxo-5-propyl-4,7-dihydropyrazolo[1,5-*a*]pyrimidine-3carbonitrile (168)



5-Amino-3-(methylthio)-1*H*-pyrazole-4-carbonitrile (500 mg, 3.3 mmol) and ethyl 3-oxohexanoate (770 mg, 4.9 mmol) were dissolved in acetic acid (15 mL) and water (7.5 mL). The reaction mixture was heated at 120 °C for 20 h. Due to incomplete reaction, further ethyl 3-oxohexanoate (385 mg, 2.43 mmol) was added and the reaction mixture was heated at 120 °C for 66 h. The reaction was left to cool to room temperature and a few drops of water were added. The solid formed was collected by filtration under vacuum and dried in a vacuum oven for 4 h to give the title product **168** as an off-white solid (365 mg, 45%). The filtrate was evaporated under reduced pressure. The resulting crude product was purified by reverse phase chromatography using the formic acid MDAP (gradient B over 15 min) to give additional title product as a white solid (67 mg, 8%). ¹H NMR (400 MHz, DMSO- d_6) δ 13.12 (br. s, 1H), 5.82 (s, 1H), 2.62 (s, 3H), 2.54 (t, J = 7.3 Hz, 2H), 1.66 (sxt, J = 7.4 Hz, 2H), 0.93 (t, J = 7.4 Hz, 3H); LCMS (ESI, formic) m/z 249 [M+H]⁺, R_t = 0.72 min.

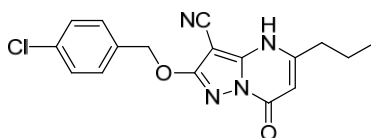
2-(Methylsulfonyl)-7-oxo-5-propyl-4,7-dihydropyrazolo[1,5-*a*]pyrimidine-3-carbonitrile (169)



A solution of 2-(methylthio)-7-oxo-5-propyl-4,7-dihydropyrazolo[1,5-*a*]pyrimidine-3-carbonitrile **168** (365 mg, 1.47 mmol) in DCM (15 mL) was cooled to 0 °C under nitrogen. mCPBA (805 mg, 3.73 mmol) was added and the reaction mixture was left to warm up to room temperature and then stirred for 4 days. Saturated aqueous sodium sulfite solution (10 mL) and saturated aqueous sodium bicarbonate solution (10 mL) were added to the reaction mixture and the mixture was extracted with DCM (2 x 40 mL). LCMS showed desired product only in the aqueous layer. The aqueous layer was passed through an isolute 103 column (packed with a hydroxylated polystyrene-divinylbenzene co-polymer) to remove inorganics. The desired product was eluted with MeOH (2 CV). The methanol fraction was evaporated under reduced pressure to give the title product **169** as a white solid (349 mg, 85%). ¹H NMR (400 MHz, DMSO-*d*₆) δ 13.54 (br. s, 1H), 6.00 (s, 1H), 3.44 (s, 3H), 2.60 (t, *J* = 7.5 Hz, 2H), 1.68 (sxt, *J* = 7.4 Hz, 2H), 0.94 (t, *J* = 7.4 Hz, 3H); LCMS (ESI, formic) *m/z* 281 [M+H]⁺, *R*_t = 0.61 min.

2-((4-Chlorobenzyl)oxy)-7-oxo-5-propyl-4,7-dihydropyrazolo[1,5-*a*]pyrimidine-

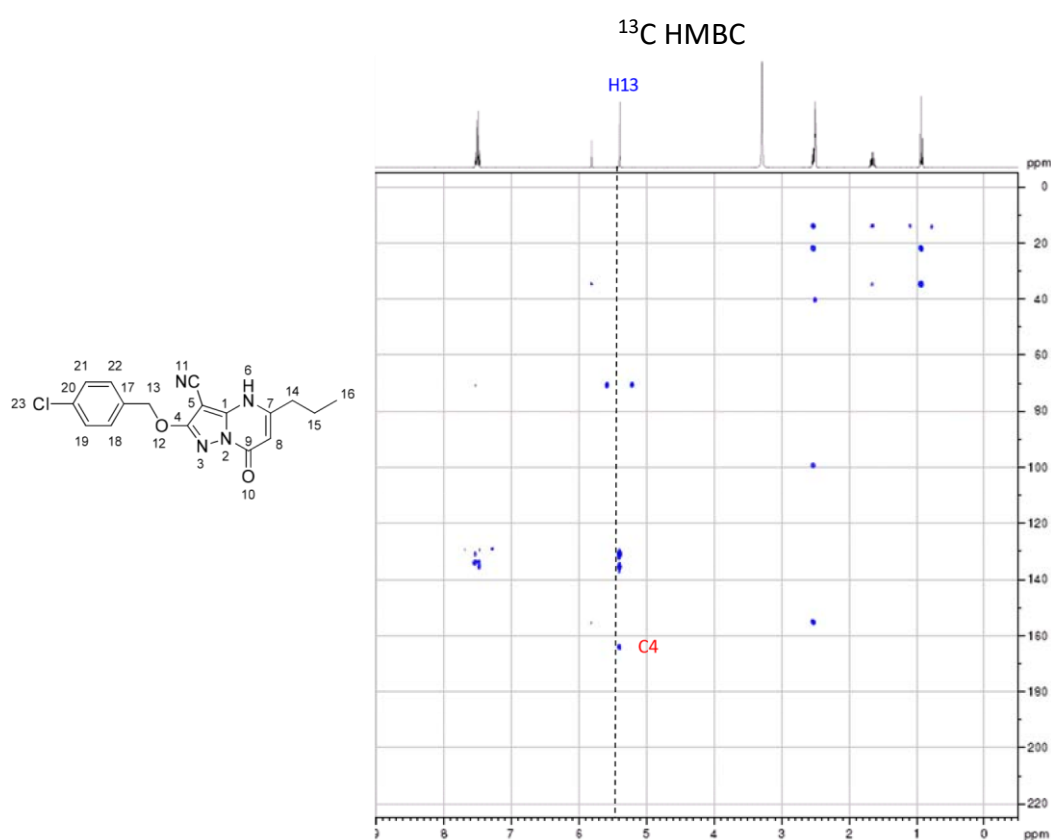
3-carbonitrile (131)



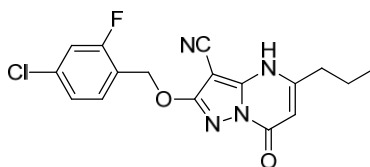
Sodium hydride (60% dispersion in mineral oil, 14 mg, 0.35 mmol) was suspended in THF (0.5 mL) in a microwave vial under nitrogen. (4-chlorophenyl)methanol (34 mg, 0.24 mmol) was added and the mixture was stirred at room temperature under nitrogen for 1 h. 2-(methylsulfonyl)-7-oxo-5-propyl-4,7-dihydropyrazolo[1,5*a*]pyrimidine-3-carbonitrile **169** (50 mg, 0.18 mmol) was then added and the reaction mixture was heated at 90 °C for 1 h in a microwave reactor. Water was added and the mixture was extracted with DCM (2 x 10 mL). LCMS showed

product mainly in the aqueous layer. The aqueous layer was evaporated under reduced pressure. The resulting crude product was purified by reverse phase chromatography using the formic acid MDAP (gradient C over 15 min) to give the title product **131** as a beige solid (7.6 mg, 12%). $^1\text{H NMR}$ (400 MHz, DMSO-d_6) δ 13.10 (br. s, 1H), 7.42 - 7.56 (m, 4H), 5.81 (s, 1H), 5.40 (s, 2H), 2.52 (t, $J = 7.3$ Hz, 2H, overlap with DMSO), 1.64 (sxt, $J = 7.4$ Hz, 2H), 0.93 (t, $J = 7.3$ Hz, 3H); LCMS (ESI, formic) m/z 343 $[\text{M}+\text{H}]^+$, $R_t = 1.01$ min.

HMBC showed correlation between CH_2 protons (H13) and pyrazole carbon (C4), as shown below, confirming the O-link connectivity.

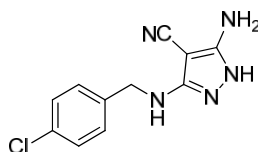


2-((4-Chloro-2-fluorobenzyl)oxy)-7-oxo-5-propyl-4,7-dihydropyrazolo[1,5-a]pyrimidine-3-carbonitrile (171)



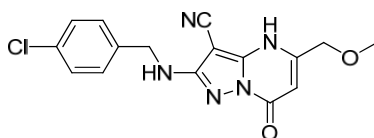
Sodium hydride (60% dispersion in mineral oil, 11 mg, 0.27 mmol) was suspended in THF (0.5 mL) in a microwave vial under nitrogen. (4-chloro-2-fluorophenyl)methanol (34 mg, 0.21 mmol) in THF (0.5 mL) was added and the mixture was stirred at room temperature under nitrogen for 1 h. 2-(Methylsulfonyl)-7-oxo-5-propyl-4,7-dihydropyrazolo[1,5-a]pyrimidine-3-carbonitrile **169** (50 mg, 0.18 mmol) was added and the reaction mixture was heated at 90 °C for 1 h in a microwave reactor. Water was added and solvents were evaporated under a stream of nitrogen. The resulting crude product was purified by reverse phase chromatography using the formic acid MDAP (gradient C over 15 min) to give the title product **171** as a white solid (8 mg, 12%). ¹H NMR (400 MHz, DMSO-d₆) δ 13.10 (br. s, 1H), 7.63 (apparent t, *J* = 8.2 Hz, 1H), 7.52 (dd, *J* = 10.0, 2.0 Hz, 1H), 7.37 (dd, *J* = 8.3, 1.8 Hz, 1H), 5.80 (s, 1H), 5.43 (s, 2H), 2.51 - 2.56 (m, 2H), 1.65 (sxt, *J* = 7.5 Hz, 2H), 0.93 (t, *J* = 7.4 Hz, 3H); LCMS (ESI, formic) *m/z* 361 [M+H]⁺, *R*_t = 1.03 min.

5-Amino-3-((4-chlorobenzyl)amino)-1H-pyrazole-4-carbonitrile (193)



A mixture of 2-(bis(methylthio)methylene)malononitrile (2.55 g, 15.0 mmol) and (4-chlorophenyl)methanamine (1.9 mL, 15 mmol) in EtOH (50 mL) was heated at reflux with a bleach scrubber on a stream of nitrogen for 3 h. Hydrazine (50% wt in water, 1 mL, 15 mmol) was added (dropwise over 1 min) and the reaction mixture was refluxed under nitrogen for 1 h. After this time, further hydrazine (50% wt in water, 0.5 mL, 8 mmol) was added and the reaction mixture was refluxed for 4 h. The reaction mixture

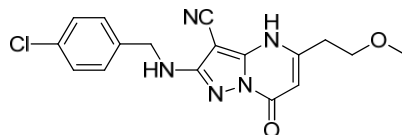
was cooled and all volatiles were removed under reduced pressure. The oily residue was triturated with water and a yellowish solid formed. The solid was collected by filtration under vacuum. The resulting crude product was purified by reverse phase chromatography (15–35% CH₃CN + 0.1% formic acid in H₂O + 0.1% formic acid over 30 min, 150 g C18 Gold column) to give the title product **193** as a white solid (2.3 g, 62%). ¹H NMR (400 MHz, DMSO-d₆) δ 10.92 (br. s, 1H), 10.59 (br. s, 1H), 7.33 (s, 4H), 6.03 (br. s, 2H), 4.21 (d, *J* = 5.77 Hz, 2H); LCMS (ESI, formic) *m/z* 248 + 250 [M+H]⁺, R_t = 0.73 min. **2-((4-Chlorobenzyl)amino)-5-(methoxymethyl)-7-oxo-4,7-dihydropyrazolo[1,5a]pyrimidine-3-carbonitrile (177)**



5-amino-3-((4-chlorobenzyl)amino)-1*H*-pyrazole-4-carbonitrile **193** (60 mg, 0.24 mmol) and methyl 4-methoxy-3-oxobutanoate (47 μL, 0.36 mmol) were dissolved in acetic acid (1.2 mL) and water (0.6 mL). The reaction mixture was heated at 120 °C for 24 h. Solvent was evaporated under reduced pressure. The resulting crude product was purified by reverse phase chromatography using the formic acid MDAP (gradient B over 15 min) to give the title product **177** as a white solid (37 mg, 44%).

¹H NMR (400 MHz, DMSO-d₆) δ 13.07 (br. s, 1H), 7.37 (s, 4H), 7.24 (br. s, 1H), 5.80 (s, 1H), 4.40 (d, *J* = 6.0 Hz, 2H), 4.31 (s, 2H), 3.34 (s, 3H); LCMS (ESI, formic) *m/z* 344 [M+H]⁺, R_t = 0.82 min.

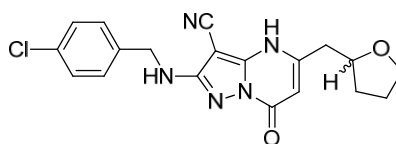
2-((4-Chlorobenzyl)amino)-5-(2-methoxyethyl)-7-oxo-4,7-dihydropyrazolo[1,5a]pyrimidine-3-carbonitrile (178)



5-Amino-3-((4-chlorobenzyl)amino)-1*H*-pyrazole-4-carbonitrile **193** (60 mg, 0.24

mmol) and methyl 5-methoxy-3-oxopentanoate (50 mg, 0.32 mmol) were dissolved in acetic acid (1.2 mL) and water (0.6 mL). The reaction mixture was heated at 120 °C for 24 h. LCMS showed two main peaks with the desired mass: $R_t=0.83$, 39% and $R_t=1.10$, 19%. Solvent was evaporated under reduced pressure. The crude product was purified by reverse phase chromatography using the formic acid MDAP (gradient B over 15 min) to give the title product **178** as a yellow solid (22 mg, 25%). mp 210 °C (dec.); $^1\text{H NMR}$ (400 MHz, DMSO-d_6) δ 12.85 (br. s, 1H), 7.36 (s, 4H), 7.22 (t, $J = 6.0$ Hz, 1H), 5.73 (s, 1H), 4.40 (d, $J = 6.3$ Hz, 2H), 3.60 (t, $J = 6.3$ Hz, 2H), 3.26 (s, 3H), 2.77 (t, $J = 6.3$ Hz, 2H); $^{13}\text{C NMR}$ (101 MHz, DMSO-d_6) δ 157.2 (C), 154.4 (C), 138.9 (C), 131.1 (C), 129.0 (2C, Ar-CH), 128.0 (2C, Ar-CH), 98.8 (CH), 69.6 (CH_2), 62.5 (C), 57.9 (CH_3), 44.8 (CH_2), 30.2 (CH_2). Three carbons too weak to assign: CN usually around 113 ppm and two C around 145 ppm and 152 ppm; LCMS (ESI, formic) m/z 358 $[\text{M}+\text{H}]^+$, $R_t = 0.83$ min; HRMS (ESI) calcd for $\text{C}_{17}\text{H}_{17}\text{ClN}_5\text{O}_2$ $[\text{M}+\text{H}]^+$ 358.1065, found 358.1062 (4.04 min).

2-((4-Chlorobenzyl)amino)-7-oxo-5-((tetrahydrofuran-2-yl)methyl)-4,7-dihydropyrazolo[1,5-*a*]pyrimidine-3-carbonitrile (180)

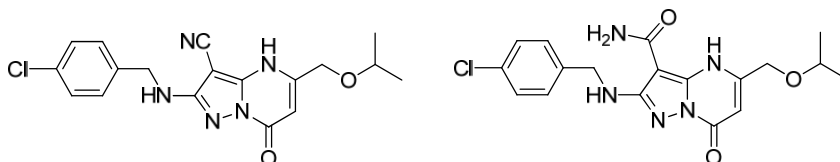


Thionyl chloride (0.28 mL, 3.8 mmol) was added slowly under nitrogen to a stirred mixture of 2-(tetrahydrofuran-2-yl)acetic acid (500mg, 3.8 mmol) and pyridine (0.78 mL, 9.6 mmol) in anhydrous DCM (17 mL). The mixture was stirred at room temperature for 20 min. Meldrum's acid (609 mg, 4.2 mmol) and DMAP (1.17 g, 9.6 mmol) were then added and the reaction mixture was stirred at room temperature under nitrogen for 6 h. Volatiles were evaporated under reduced pressure. DCM (20 mL) was added to the residue obtained and the mixture was washed with 1 M aqueous HCl solution (3 x 15 mL) followed by brine (15 mL). The aqueous layer was extracted with DCM (20 mL) and the organic layer was separated and passed through a hydrophobic frit. Solvent was evaporated under reduced pressure. The resulting residue was

dissolved in MeOH (10 mL) and the mixture was refluxed for 4 h under nitrogen. Solvent was evaporated to give a crude product containing methyl 3-oxo-4-(tetrahydrofuran-2-yl)butanoate **210** (400 mg).

A mixture of 3-amino-5-((4-chlorobenzyl)amino)-1*H*-pyrazole-4-carbonitrile **193** (50 mg, 0.2 mmol) and crude methyl 3-oxo-4-(tetrahydrofuran-2-yl)butanoate **210** (75 mg, 0.4 mmol) in acetic acid (2 mL) and water (1 mL) was heated at reflux for 66 h. As starting material remained, crude methyl 3-oxo-4-(tetrahydrofuran-2-yl)butanoate (140 mg) was added to the reaction mixture and the mixture was heated at reflux overnight. Water (5 mL) was added to the reaction mixture and all volatiles were evaporated under reduced pressure. The crude product was purified by reverse phase chromatography using the formic acid MDAP (gradient B over 15 min) to give impure desired product **180** (23 mg), mixture 70:30 by NMR. The pure desired product could not be isolated.

2-((4-Chlorobenzyl)amino)-5-(isopropoxymethyl)-7-oxo-4,7-dihydropyrazolo[1,5-*a*]pyrimidine-3-carbonitrile (179) and 2-((4chlorobenzyl)amino)-5-(isopropoxymethyl)-7-oxo-4,7-dihydropyrazolo[1,5*a*]pyrimidine-3-carboxamide (213)



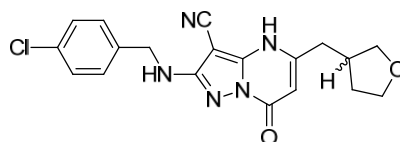
Propan-2-ol (0.2 mL, 2.7 mmol) was added to a suspension of sodium hydride (60% dispersion in mineral oil, 128 mg, 5.3 mmol) in diethyl ether (2 mL) under nitrogen and the resulting mixture was stirred at room temperature for 1 h. Methyl 4-chloro-3-oxobutanoate (0.16 mL, 1.33 mmol) was then added slowly and the reaction mixture was stirred at room temperature for 17 h. Water was added and the solvent was evaporated under reduced pressure. The residue was diluted with water and the pH was adjusted to 4 with 2 M aqueous HCl solution. The mixture was extracted with diethyl ether (3 x 10 mL). The combined organic phases were passed through a hydrophobic

frit and evaporated under reduced pressure to give the crude product, methyl 4-isopropoxy-3-oxobutanoate **212** (86 mg).

A mixture of 5-amino-3-((4-chlorobenzyl)amino)-1H-pyrazole-4-carbonitrile **193** (60 mg, 0.24 mmol) and crude methyl 4-isopropoxy-3-oxobutanoate **212** (84 mg, 0.48 mmol) in acetic acid (1.2 mL) and water (0.6 mL) was heated at 120 °C for 2 days. Solvent was then evaporated under reduced pressure. The crude product was purified by reverse phase chromatography using the formic acid MDAP (gradient C over 15 min) to give the title product **179** as a white solid (28 mg, 31% over two steps). mp 251-253 °C; ¹H NMR (400 MHz, DMSO-d₆) δ 13.01 (br. s, 1H), 7.37 (s, 4H), 7.25 (t, *J* = 6.0 Hz, 1H), 5.81 (s, 1H), 4.40 (d, *J* = 6.3 Hz, 2H), 4.35 (s, 2H), 3.69 (spt, *J* = 6.1 Hz, 1H), 1.15 (d, *J* = 6.0 Hz, 6H); LCMS (ESI, formic) *m/z* 372 [M+H]⁺, *R*_t = 0.93 min.

MDAP failed to collect the by-product. The waste was recovered and evaporated under reduced pressure. The crude product was purified by reverse phase chromatography using the formic acid MDAP (gradient B over 15 min) to give the by-product **213** as white solid (11 mg, 12%). ¹H NMR (600 MHz, DMSO-d₆) δ 11.18 (br. s, 1H), 7.34 - 7.41 (m, 4H), 7.19 - 7.34 (m, 2H), 6.87 (br. s, 1H), 5.76 (s, 1H), 4.49 (br. s, 4H), 3.68 (spt, *J* = 5.9 Hz, 1H), 1.17 (d, *J* = 5.9 Hz, 6H); LCMS (ESI, formic) *m/z* 390 [M+H]⁺, *R*_t = 0.84 min.

2-((4-Chlorobenzyl)amino)-7-oxo-5-((tetrahydrofuran-3-yl)methyl)-4,7-dihydropyrazolo[1,5-*a*]pyrimidine-3-carbonitrile (181)

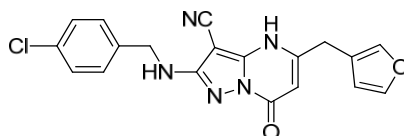


Diisopropylamine (0.82 mL, 5.75 mmol) was introduced in a round bottom flask under nitrogen. THF (2.5 mL) was added and the mixture was cooled to -78 °C. *n*BuLi (2.5 M in hexane, 2.3 mL, 5.8 mmol) was then added dropwise. The mixture was stirred at -78 °C for 30 min, and then warmed to 0 °C in an ice bath for 30 min. Ethyl 3-

oxobutanoate (0.29 mL, 2.3 mmol) was added at 0 °C and the mixture was stirred at 0 °C for 1 h. The mixture was then cooled to -78 °C and 3iodotetrahydrofuran (548 mg, 2.8 mmol) was added. The reaction mixture was stirred at -78 °C and left to warm to room temperature overnight. 2 M aqueous HCl solution (10 mL) was added and the mixture was extracted with diethyl ether (4 x 20 mL). The organic layers were combined and passed through a hydrophobic frit. The solvent was evaporated under reduced pressure to give crude ethyl 3-oxo-4-(tetrahydrofuran-3-yl)butanoate **216** (215 mg).

A mixture of 5-amino-3-((4-chlorobenzyl)amino)-1*H*-pyrazole-4-carbonitrile **193** (100 mg, 0.4 mmol) and crude ethyl 3-oxo-4-(tetrahydrofuran-3-yl)butanoate **216** (170 mg) in acetic acid (2 mL) and water (1 mL) was heated at 120 °C for 24 h. Solvent was evaporated under reduced pressure. The resulting crude product was purified by reverse phase chromatography using the formic acid MDAP (gradient B over 15 min) to give the title product **181** as a white solid (45 mg, 29% over two steps). mp 215-218 °C; ¹H NMR (600 MHz, DMSO-*d*₆) δ 12.82 (s, 1H), 7.33 - 7.39 (m, 4H), 7.25 (br. s, 1H), 5.74 (s, 1H), 4.40 (d, *J* = 6.2 Hz, 2H), 3.76 - 3.79 (m, 1H), 3.72 - 3.76 (m, 1H), 3.64 (q, *J* = 7.5 Hz, 1H), 3.34 (dd, *J* = 8.3, 5.4 Hz, 1H), 2.52 - 2.61 (m, 3H), 1.91 - 1.99 (m, 1H), 1.51 - 1.59 (m, 1H); ¹³C NMR (151 MHz, DMSO*d*₆) δ 157.2 (C), 154.4 (C), 151.7 (C), 145.8 (C), 138.9 (C), 131.1 (C), 129.0 (2C, ArCH), 128.0 (2C, Ar-CH), 112.9 (C), 98.7 (CH), 71.6 (CH₂), 66.8 (CH₂), 62.5 (C), 44.8 (CH₂), 37.5 (CH), 35.1 (CH₂), 31.0 (CH₂); LCMS (ESI, formic) *m/z* 384.14 [M+H]⁺, *R*_t = 0.83 min; HRMS (ESI) calcd for C₁₉H₁₉ClN₅O₂ [M+H]⁺ 384.1222, found 384.1218 (4.09 min); IR (ATR) cm⁻¹ 3409, 3063, 2934, 2862, 2209, 1680, 1578, 1546.

2-((4-Chlorobenzyl)amino)-5-(furan-3-ylmethyl)-7-oxo-4,7-dihydropyrazolo[1,5*a*]pyrimidine-3-carbonitrile (187)



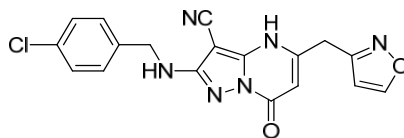
CDI (355 mg, 2.2 mmol) was added to a stirred solution of 2-(furan-3-yl)acetic acid

(250 mg, 2 mmol) in THF (7 mL) at room temperature under nitrogen. The mixture was stirred at room temperature for 20 h.

During this time, in a separate round bottom flask, magnesium ethoxide (250 mg, 2.2 mmol) was added to a stirred solution of 3-ethoxy-3-oxopropanoic acid (576 mg, 4.4 mmol) in THF (7 mL) at room temperature under nitrogen. The mixture was stirred at room temperature for 5 h. The solvent was evaporated under reduced pressure. The solid was then suspended in THF (4 mL) and added dropwise over 1 min to previously stirred CDI furanylacetate suspension. The resulting mixture was stirred at rt for 6 h. A saturated aqueous solution of sodium bicarbonate (20 mL) and EtOAc (20 mL) were added. The phases were separated. The aqueous was extracted with EtOAc (2 x 20 mL). The combined organic phases were passed through a hydrophobic frit and evaporated under reduced pressure to give the crude product, ethyl 4-(furan-3-yl)-3-oxobutanoate **222** as brown liquid (215 mg). LCMS (ESI, formic) m/z 197 $[M+H]^+$, R_t = 0.80 min, 57 % by area.

A mixture of 5-amino-3-((4-chlorobenzyl)amino)-1*H*-pyrazole-4-carbonitrile **193** (60 mg, 0.2 mmol) and crude ethyl 4-(furan-3-yl)-3-oxobutanoate **222** (160 mg) in acetic acid (1.2 mL) and water (0.6 mL) was heated at 120 °C for 16 h. Solvent was evaporated under reduced pressure. The resulting crude product was purified by reverse phase chromatography using the formic acid MDAP (30-85 % CH₃CN + 0.1 % formic acid in H₂O + 0.1 % formic acid over 15 min) to give the title product **187** as an orange solid (41 mg, 45%). ¹H NMR (400 MHz, DMSO-*d*₆) δ 12.99 (br s, 1H), 7.57 - 7.65 (m, 2H), 7.36 (s, 4H), 7.22 (t, *J* = 5.9 Hz, 1H), 6.47 (s, 1H), 5.61 (s, 1H), 4.40 (d, *J* = 6.3 Hz, 2H), 3.69 (s, 2H); ¹³C NMR (101 MHz, DMSO-*d*₆) δ 157.2 (C), 154.5 (C), 143.5 (Ar-CH), 140.6 (Ar-CH), 138.9 (C), 131.1 (C), 129.0 (2C, Ar-CH), 128.0 (2C, Ar-CH), 119.9 (C), 113.1 (C), 111.2 (CH), 98.3 (CH), 62.6 (C), 44.8 (CH₂), 27.4 (CH₂), one carbon too weak to assign usually 152 ppm; LCMS (ESI, formic) m/z 380.16 $[M+H]^+$, R_t = 0.93 min; HRMS (ESI) calcd for C₁₉H₁₉ClN₅O₂ $[M+H]^+$ 380.0909, found 380.0905 (4.11 min); IR (ATR) cm⁻¹ 3395, 2821, 2209, 1664, 1625,

1593, 1571. **2-((4-Chlorobenzyl)amino)-5-(isoxazol-3-ylmethyl)-7-oxo-4,7-dihydropyrazolo[1,5-a]pyrimidine-3-carbonitrile (186)**



CDI (191 mg, 1.2 mmol) was added to a stirred solution of 2-(isoxazol-3-yl)acetic acid (150 mg, 1.2 mmol) in THF (5 mL) at room temperature under nitrogen. The mixture was stirred at room temperature for 3 days.

During this time, in a separate round bottom flask, magnesium ethoxide (149 mg, 1.3 mmol) was added to a stirred solution of 3-ethoxy-3-oxopropanoic acid (350 mg, 2.7 mmol) in THF (5 mL) at room temperature under nitrogen. The mixture was stirred at room temperature for 5 h. The solvent was evaporated under reduced pressure. The solid was then suspended in THF (2 mL) and added dropwise over 1 min to previously stirred suspension. The resulting mixture was stirred at rt for 16 h. A saturated aqueous solution of sodium bicarbonate (20 mL) and EtOAc (20 mL) were added. The phases were separated and the aqueous was extracted with EtOAc (2 x 20 mL). The combined organic phases were passed through a hydrophobic frit and evaporated under reduced pressure to give the crude product, ethyl 4-(isoxazol-3-yl)-3-oxobutanoate **223**, as a yellow gum (200 mg). LCMS (ESI, formic) m/z 198 $[M+H]^+$, $R_t = 0.62-0.64$ min, 69 % by area.

A mixture of 5-amino-3-((4-chlorobenzyl)amino)-1*H*-pyrazole-4-carbonitrile **193** (60 mg, 0.24 mmol) and crude ethyl 4-(isoxazol-3-yl)-3-oxobutanoate **223** (149 mg) in acetic acid (1.2 mL) and water (0.6 mL). The reaction mixture was heated at 120 °C for 16 h. Solvent was evaporated under reduced pressure. The crude product was purified by reverse phase chromatography using the formic acid MDAP (gradient B over 15 min) to give the title product **186** as a white solid (16 mg, 17% over two steps). ^1H NMR (400 MHz, DMSO- d_6) δ 13.20 (br. s, 1H), 8.89 (d, $J = 1.3$ Hz, 1H), 7.36 (s, 4H), 7.24 (br. s, 1H), 6.61 (d, $J = 1.5$ Hz, 1H), 5.70 (s, 1H), 4.40 (d, $J = 6.3$ Hz, 2H), 4.01 (s, 2H); LCMS (ESI, formic) m/z 381 $[M+H]^+$, $R_t = 0.84$ min.

4.4 Experimental Procedures for Dihydrobenzofuran Template

Methyl 2-(prop-1-en-2-yl)isonicotinate (**251**) Suzuki conditions screening

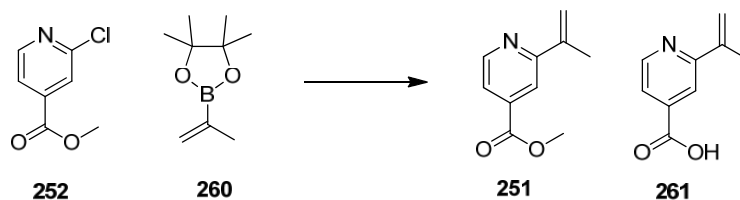


Table 4 Entry 1

Methyl 2-chloroisonicotinate (50 mg, 0.29 mmol), isopropenylboronic acid pinacol (0.11 mL, 0.58 mmol), SPhos (8 mg, 0.02 mmol), Pd(OAc)₂ (2.0 mg, 8.7 μmol) and potassium phosphate (124 mg, 0.583 mmol) were combined in acetonitrile (1 mL) and water (0.7 mL). The reaction mixture was heated at 130 °C for 1 h in a microwave reactor. LCMS showed complete conversion to the carboxylic acid product **261**. Product not isolated. LCMS (ESI, high pH) *m/z* 164 [M+H]⁺, *R_t* = 0.39 min.

Table 4 Entry 2

Methyl 2-chloroisonicotinate (25 mg, 0.15 mmol), isopropenylboronic acid pinacol (0.050 mL, 0.27 mmol), SPhos (6.0 mg, 0.015 mmol), Pd(OAc)₂ (2.0 mg, 8.7 μmol) and potassium phosphate (55 mg, 0.26 mmol) were combined in acetonitrile (0.5 mL) and water (0.3 mL). The reaction mixture was heated at 100 °C for 1 h in a microwave reactor to afford a mixture of **251** and **261** by LCMS. Products not isolated. LCMS (ESI, high pH) *m/z* 164 [M+H]⁺, *R_t* = 0.40 min (55%, **261**); *m/z* 178 [M+H]⁺, *R_t* = 0.96 min (37%, **251**).

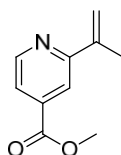
Table 4 Entry 3

Methyl 2-chloroisonicotinate (25 mg, 0.15 mmol), isopropenylboronic acid pinacol (0.050 mL, 0.27 mmol), SPhos (6 mg, 0.015 mmol), Pd(OAc)₂ (2 mg, 8.7 μmol) and potassium phosphate (55 mg, 0.26 mmol) were combined in acetonitrile (0.5 mL) and water (0.05 mL). The reaction mixture was heated at 100 °C for 1 h in a microwave reactor to afford a mixture of **251**, **252** and **261** by LCMS. Products not isolated. LCMS (ESI, high pH) *m/z* 164 [M+H]⁺, R_t = 0.40 min (1%, **261**); *m/z* 172 [M+H]⁺, R_t = 0.82 min (9%, **252**); *m/z* 178 [M+H]⁺, R_t = 0.96 min (67%, **251**).

Table 4 Entry 4

Methyl 2-chloroisonicotinate (25 mg, 0.15 mmol), isopropenylboronic acid pinacol (0.050 mL, 0.27 mmol), SPhos (6.0 mg, 0.015 mmol), Pd(OAc)₂ (2 mg, 8.7 μmol) and potassium phosphate (55 mg, 0.26 mmol) were combined in acetonitrile (0.5 mL) and water (0.05 mL). The reaction mixture was heated at 120 °C for 1 h in a microwave reactor to afford a mixture of **251**, **252** and **261** by LCMS. Products not isolated. LCMS (ESI, high pH) *m/z* 164 [M+H]⁺, R_t = 0.38 min (4%, **261**); *m/z* no clear ionisation [M+H]⁺, R_t = 0.79 min (4%, **252**); *m/z* 178 [M+H]⁺, R_t = 0.93 min (70%, **251**).

Methyl 2-(prop-1-en-2-yl)isonicotinate (**251**)



Methyl 2-chloroisonicotinate (1.0 g x 2, 12 mmol), isopropenylboronic acid pinacol (2.0 mL x 2, 21 mmol), SPhos (250 mg x 2, 1.22 mmol), Pd(OAc)₂ (110 mg x 2, 0.980 mmol) and tripotassium phosphate (2.5 g x 2, 24 mmol) were combined in acetonitrile (12 mL x 2) and water (1.2 mL x 2). The reaction mixtures were heated at 120 °C for 1 h in a microwave reactor. Water (150 mL) and DCM (150 mL) were added. The organic layer was collected. The aqueous layer was extracted with DCM (100 mL). The combined organic layers were washed with water (100 mL). The organic layer was collected, passed through a hydrophobic frit and concentrated under

reduced pressure. The resulting crude product was purified by normal phase chromatography (330 g pre-packed silica column, 0 to 15% EtOAc in cyclohexane gradient) to give the title product **251** as a pale pink oil (1.14 g, 55%). ¹H NMR (400 MHz, DMSO-d₆) δ 8.77 (br. d, *J* = 4.8 Hz, 1H), 7.98 (s, 1H), 7.72 (br. d, *J* = 4.0 Hz, 1H), 6.00 (br. s, 1H), 5.41 (br. s, 1H), 3.91 (s, 3H), 2.18 (s, 3H); LCMS (ESI, high pH) *m/z* 178 [M+H]⁺, R_t = 0.96 min.

Methyl 2-isopropylpiperidine-4-carboxylate (**250**) Pyridine reduction screening

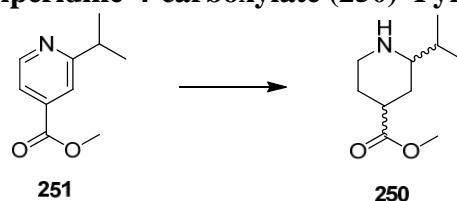


Table 5 Entry 1

PtO₂ (3.0 mg, 0.013 mmol) was charged to the hydrogenation vessel followed by a solution of methyl 2-(prop-1-en-2-yl)isonicotinate **251** (30 mg, 0.17 mmol) in acetic acid (2 mL). The mixture was hydrogenated using hydrogen gas (4 bar) at 30 °C for 18 h. TLC and LCMS showed starting material **251** remaining.

Table 5 Entry 2

PtO₂ (3.0 mg, 0.013 mmol) was charged to the hydrogenation vessel followed by a solution of methyl 2-(prop-1-en-2-yl)isonicotinate **251** (30 mg, 0.17 mmol) in acetic acid (2 mL). The mixture was hydrogenated using hydrogen gas (4 bar) at 50 °C for 18 h. TLC and LCMS showed starting material **251** remaining.

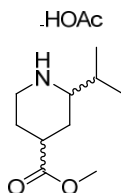
Table 5 Entry 3

PtO₂ (3.0 mg, 0.013 mmol) was charged to the hydrogenation vessel followed by a solution of methyl 2-(prop-1-en-2-yl)isonicotinate **251** (30 mg, 0.17 mmol) in acetic acid (2 mL). The mixture was hydrogenated using hydrogen gas (4 bar) at 80 °C for 18 h. TLC and LCMS showed starting material **251** remaining but TLC showed less starting material present compared to entry 1 and 2.

Table 5 Entry 4

PtO₂ (6.0 mg, 0.026 mmol) was charged to the hydrogenation vessel followed by a solution of methyl 2-(prop-1-en-2-yl)isonicotinate **251** (30 mg, 0.17 mmol) in acetic acid (2 mL). The mixture was hydrogenated using hydrogen gas (4 bars) at 50 °C for 18 h. TLC and LCMS showed complete reaction.

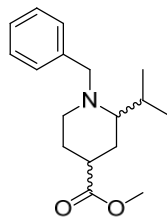
Methyl 2-isopropylpiperidine-4-carboxylate (**250**)



PtO₂ (245 mg, 1.08 mmol) was charged to the hydrogenation vessel followed by a solution of methyl 2-(prop-1-en-2-yl)isonicotinate **251** (1.14 g, 6.43 mmol) in acetic acid (60 mL). The mixture was hydrogenated using hydrogen gas (4 bar) at 60 °C for 4 h. The mixture was filtered through a cartridge of celite and concentrated under reduced pressure to give the title product **250** as an acetate salt, colourless oil (2.3 g).

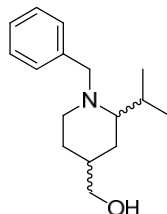
¹H NMR indicates a mixture of diastereoisomers ratio 4:1. **Isomer 1** (major isomer):
¹H NMR (400 MHz, DMSO-d₆) δ 8.13 - 10.40 (br. s, 2H), 3.59 (s, 3H), 3.00 - 3.07 (m, 1H), 2.50 - 2.58 (m, 1H), 2.33 - 2.43 (m, 1H), 2.24 - 2.32 (m, 1H), 1.89 (s, 3H), 1.76 (apparent t, *J* = 15.1 Hz, 2H), 1.51 - 1.65 (m, 1H), 1.30 - 1.43 (m, 1H), 1.09 (apparent q, *J* = 12.1 Hz, 1H), 0.86 (apparent t, *J* = 6.2 Hz, 6H). **Isomer 2** (minor isomer): ¹H NMR (400 MHz, DMSO-d₆) δ 8.13 - 10.40 (br. s, 2H), 3.62 (s, 3H), 2.77 - 2.91 (m, 2H), 2.60 - 2.69 (m, 1H), 2.33 - 2.43 (m, 1H), 1.82 - 1.95 (m, 2H), 1.89 (s, 3H), 1.51 - 1.65 (m, 2H), 1.30 - 1.43 (m, 1H), 0.86 (apparent t, *J* = 6.2 Hz, 6H). Note that some signals from the two isomers are overlapping. Compound not visible by LCMS.

Methyl 1-benzyl-2-isopropylpiperidine-4-carboxylate (**249**)



Methyl 2-isopropylpiperidine-4-carboxylate, acetate salt **250** (2.2 g, 6.40 mmol th. corr.) was dissolved in acetonitrile (20 mL) under an atmosphere of nitrogen. Potassium carbonate (2.2 g, 16 mmol) was added followed by benzyl bromide (0.84 mL, 7.0 mmol). The mixture was stirred at room temperature under an atmosphere of nitrogen for 2 h. Water (100 mL) was added and the product was extracted with EtOAc (2 x 100 mL). The combined organic layers were passed through a hydrophobic frit and concentrated under reduced pressure to give the crude title product **249** as a yellow gum (1.39 g), which was used directly in the next step without further purification. LCMS (ESI, high pH) m/z 276 $[M+H]^+$, $R_t = 1.40$ min, m/z 276 $[M+H]^+$, $R_t = 1.44$ min, mixture of diastereoisomers.

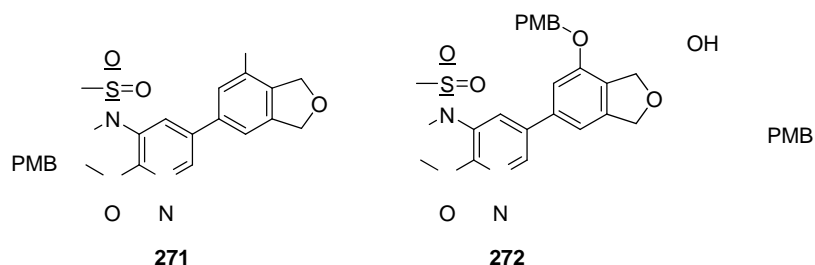
(1-Benzyl-2-isopropylpiperidin-4-yl)methanol (**247**)



Methyl 1-benzyl-2-isopropylpiperidine-4-carboxylate, crude **249** (1.39 g, 5.05 mmol) was dissolved in THF (30 mL) under an atmosphere of nitrogen and the mixture was cooled to -78 °C. A solution of DIBAL-H in THF (1 M, 10 mL, 10 mmol) was added and the mixture was stirred at -78 °C for 15 min, then at 0 °C for 1.5 h. The mixture was quenched with aq. HCl solution (2 M) and extracted with EtOAc (2 x 100 mL). The aqueous phase was collected and basified with sat. aq. NaHCO_3 solution (pH ~ 8) and extracted with EtOAc (2 x 200 mL). The combined organic phases were passed through a hydrophobic frit and concentrated under reduced pressure. LCMS of the resultant crude product showed incomplete reaction. The crude product was

redissolved in THF (10 mL) under nitrogen and the mixture was cooled to -78 °C. A solution of DIBAL-H in THF (1 M, 3 mL, 3 mmol) was added and the reaction mixture was stirred at -78 °C for 15 min, then at 0 °C for 7 h. A further portion of a solution of DIBAL-H in THF (1 M, 3 mL, 3 mmol) was then added and the mixture was stirred at 0 °C to room temperature for 16 h. The mixture was quenched with aq. HCl solution (2 M) and extracted with EtOAc (100 mL). The aqueous phase was collected and basified with sat. aq. NaHCO₃ solution (pH ~ 8) and extracted with EtOAc (2 x 100 mL). The combined organic phases were passed through a hydrophobic frit and concentrated under reduced pressure. The resulting crude product was purified by normal phase chromatography (80 g pre-packed silica column, 0 to 50% EtOAc (+ 1% Et₃N) in cyclohexane (+ 1% Et₃N) gradient) to give the title product **247** as a yellow gum (270 mg, 17% over 3 steps). ¹H NMR indicates a mixture of **247** diastereoisomers ratio 4:1. **Isomer 1** (major isomer): ¹H NMR (400 MHz, DMSO-d₆) δ 7.26 - 7.39 (m, 4H), 7.19 - 7.25 (m, 1H), 4.38 (t, *J* = 5.4 Hz 1H), 4.08 (d, *J* = 13.5 Hz, 1H), 3.23 (apparent t, *J* = 5.8 Hz, 2H), 2.95 (d, *J* = 13.5 Hz, 1H), 2.64 - 2.79 (m, 1H), 2.20 - 2.32 (m, 1H), 1.97 - 2.06 (m, 1H), 1.88 (td, *J* = 12.1, 2.4 Hz, 1H), 1.58 - 1.66 (m, 1H), 1.42 - 1.51 (m, 1H), 1.30 - 1.39 (m, 1H), 0.98 (qd, *J* = 12.2, 3.7 Hz, 1H), 0.75 - 0.95 (m, 7H). **Isomer 2** (minor isomer): ¹H NMR (400 MHz, DMSO-d₆) δ 7.27 - 7.33 (m, 4H), 7.18 - 7.25 (m, 1H), 4.34 - 4.41 (m, 1H), 3.78 (d, *J* = 13.9 Hz, 1H), 3.68 (d, *J* = 13.7 Hz, 1H), 3.20 - 3.28 (m, 2H), 2.67 - 2.79 (m, 1H), 2.42 - 2.48 (m, 1H), 2.09 - 2.15 (m, 1H), 2.03 - 2.09 (m, 1H), 1.64 - 1.72 (m, 1H), 1.15 - 1.55 (m, 4H), 0.85 - 0.95 (m, 6H); note that some signals from the two isomers are overlapping. LCMS (ESI, high pH) *m/z* 248 [M+H]⁺, *R*_t = 1.13 min (79%), *m/z* 248 [M+H]⁺, *R*_t = 1.22 min (21%).

***N*-(5-(7-Hydroxy-1,3-dihydroisobenzofuran-5-yl)-2-methoxypyridin-3-yl)-*N*-(4methoxybenzyl)methanesulfonamide (271) and *N*-(2-methoxy-5-(7-((4methoxybenzyl)oxy)-1,3-dihydroisobenzofuran-5-yl)pyridin-3-yl)-*N*-(4methoxybenzyl)methanesulfonamide (272)**

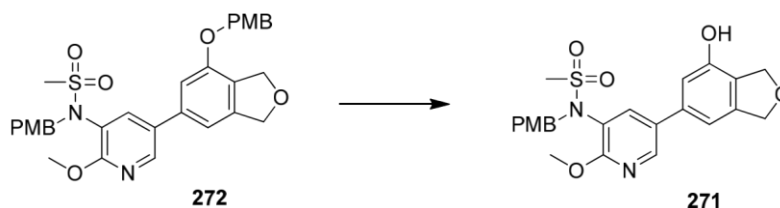


N-(5-(7-hydroxy-1,3-dihydroisobenzofuran-5-yl)-2-methoxypyridin-3-yl)methanesulfonamide (1.96 g, 5.83 mmol) was dissolved in DMF (25 mL) under nitrogen. Potassium carbonate (1.6 g, 11.6 mmol) was added followed by 1(bromomethyl)-4-methoxybenzene (1.3 mL, 8.8 mmol) slowly. The reaction mixture was stirred at room temperature under nitrogen for 2 h. Both desired product **271** and bis alkylated product **272** have been formed. The mixture was filtered and concentrated under reduced pressure. The resulting crude product was purified by normal phase chromatography (330 g pre-packed Redisep silica cartridge; 0 to 5% MeOH in DCM gradient). The two products were not separated. The mixture was repurified by normal phase chromatography (330 g pre-packed Redisep silica cartridge; 30 to 70% EtOAc in cyclohexane gradient) to give the title product **271** as a white solid (1.7 g, 64%) and the by-product **272** as a yellow gum (978 mg, 29%).

Product 271 - $^1\text{H NMR}$ (400 MHz, DMSO-d_6) δ 9.79 (s, 1H), 8.30 (d, $J = 2.5$ Hz, 1H), 7.56 (d, $J = 2.5$ Hz, 1H), 7.18 (apparent d, $J = 8.6$ Hz, 2H), 6.75 - 6.90 (m, 4H), 4.96 (apparent d, $J = 16.9$ Hz, 4H), 4.72 (br. s, 2H), 3.98 (s, 3H), 3.68 (s, 3H), 3.15 (s, 3H); LCMS (ESI, high pH) m/z 457 $[\text{M}+\text{H}]^+$, $R_t = 1.00$ min.

Product 272 - $^1\text{H NMR}$ (400 MHz, DMSO-d_6) δ 8.39 (d, $J = 2.5$ Hz, 1H), 7.64 (d, $J = 2.5$ Hz, 1H), 7.38 (apparent d, $J = 8.6$ Hz, 2H), 7.20 (apparent d, $J = 8.6$ Hz, 2H), 7.02 (d, $J = 2.9$ Hz, 2H), 6.95 (apparent d, $J = 8.6$ Hz, 2H), 6.83 (d, $J = 8.6$ Hz, 2H), 5.15 (s, 2H), 4.99 (apparent d, $J = 16.1$ Hz, 4H), 4.73 (br. s, 2H), 3.98 (s, 3H), 3.75 (s, 3H), 3.66 (s, 3H), 3.17 (s, 3H); LCMS (ESI, high pH) m/z 577 $[\text{M}+\text{H}]^+$, $R_t = 1.29$ min.

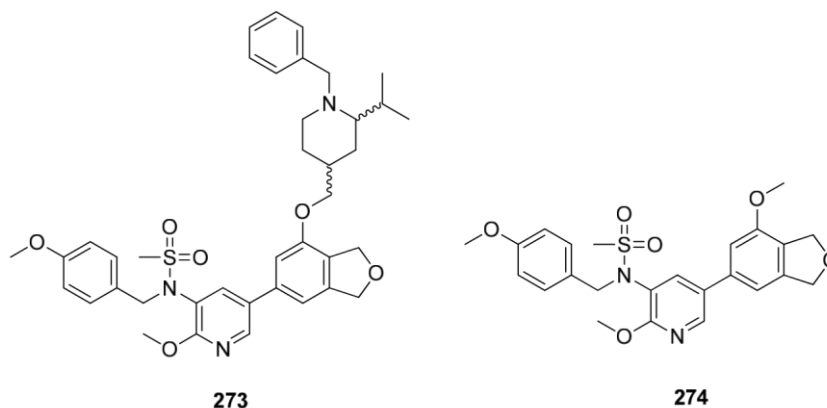
***N*-(5-(7-Hydroxy-1,3-dihydroisobenzofuran-5-yl)-2-methoxypyridin-3-yl)-*N*-(4-methoxybenzyl)methanesulfonamide (**271**)**



N-(2-methoxy-5-(7-((4-methoxybenzyl)oxy)-1,3-dihydroisobenzofuran-5-yl)pyridin-3-yl)-*N*-(4-methoxybenzyl)methanesulfonamide **272** (978 mg, 1.70 mmol) was dissolved in DCM (20 mL) under nitrogen. TFA (10 mL, 130 mmol) was added slowly and the mixture was stirred at room temperature for 30 min. The mixture was concentrated under reduced pressure. The resulting residue was diluted in sat. aq. sodium bicarbonate solution (50 mL) and EtOAc (50 mL). The two phases were separated and the aqueous layer was back extracted with EtOAc (50 mL). The combined organic phases were passed through a hydrophobic frit and concentrated under reduced pressure. The resulting crude product was purified by normal phase chromatography (120 g pre-packed Redisep silica cartridge; 30 to 70% EtOAc in cyclohexane gradient) to give the title product **271** as a white solid (435 mg, 56%).

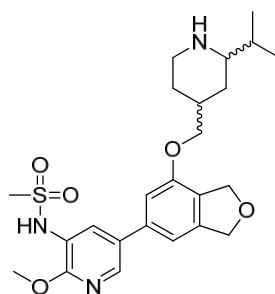
¹H NMR (400 MHz, DMSO-*d*₆) δ 9.79 (s, 1H), 8.30 (d, *J* = 2.2 Hz, 1H), 7.55 (d, *J* = 2.2 Hz, 1H), 7.18 (apparent d, *J* = 8.6 Hz, 2H), 6.75 - 6.90 (m, 4H), 4.96 (apparent d, *J* = 16.9 Hz, 4H), 4.72 (br. s, 2H), 3.98 (s, 3H), 3.68 (s, 3H), 3.15 (s, 3H); LCMS (ESI, high pH) *m/z* 457 [M+H]⁺, *R*_t = 1.00 min.

***N*-(5-(7-((1-Benzyl-2-isopropylpiperidin-4-yl)methoxy)-1,3-dihydroisobenzofuran-5-yl)-2-methoxypyridin-3-yl)-*N*-(4-methoxybenzyl)methanesulfonamide (**273**)**



N-(5-(7-hydroxy-1,3-dihydroisobenzofuran-5-yl)-2-methoxypyridin-3-yl)-*N*-(4-methoxybenzyl)methanesulfonamide **271** (270 mg, 0.591 mmol), (1-benzyl-2-isopropylpiperidin-4-yl)methanol **247** (220 mg, 0.889 mmol) and CMPB (2(tributylphosphoranylidene)acetonitrile) (0.5 mL, 1.9 mmol) were combined in a microwave vial with toluene (4 mL). The mixture was heated at 120 °C for 1 h in a microwave reactor. Solvent was evaporated under reduced pressure. The resulting crude product was purified by normal phase chromatography (120 g pre-packed silica column, 0 to 100% EtOAc in cyclohexane gradient) to give impure desired product **273** (523 mg). The crude product was repurified by normal phase chromatography (80 g pre-packed silica column, 20 to 80% EtOAc in cyclohexane gradient) to give the title product **273** as orange gum (403 mg, 99%, 80% by LCMS), which was used directly in the next step. LCMS (ESI, high pH) m/z 471 $[M+H]^+$, R_t = 1.17 min (20%, **274**), m/z 636 $[M+H]^+$, R_t = 1.65 min (51%), m/z 636 $[M+H]^+$, R_t = 1.67 min (26%). No NMR data collected. Product directly progressed to the next step without further purification.

***N*-(5-(7-((2-Isopropylpiperidin-4-yl)methoxy)-1,3-dihydroisobenzofuran-5-yl)-2-methoxypyridin-3-yl)methanesulfonamide (**275**)**



N-(5-(7-((1-Benzyl-2-isopropylpiperidin-4-yl)methoxy)-1,3-dihydroisobenzofuran-5-yl)-2-methoxypyridin-3-yl)-*N*-(4-methoxybenzyl)methanesulfonamide **273** (323 mg, 0.471 mmol) was dissolved in EtOAc (10 mL) and EtOH (40 mL). The mixture was hydrogenated using the H-cube (settings: 50 °C, full H₂, 1 mL/min flow rate) and 10% Pd/C CatCart as the catalyst. The mixture was concentrated under reduced pressure. The resulting crude product was purified by MDAP (High pH, method B) to give the title product **275** as a white solid (88 mg, 39%). ¹H NMR (400 MHz, DMSO-*d*₆) δ 8.14 - 8.19 (m, 1H), 7.79 (d, *J* = 2.3 Hz, 1H), 7.03 - 7.13 (m, 2H), 5.04 (br. s, 2H), 4.99 (br. s, 2H), 4.09 - 4.19 (m, 0.5H), 3.94 - 4.01 (m, 1.5H), 3.93 (s, 3H), 3.03 - 3.11 (m, 0.75H), 2.98 (s, 3H), 2.79 - 2.86 (m, 0.5H), 2.55 - 2.66 (m, 1H), 2.322.41 (m, 0.75H), 2.18 - 2.27 (m, 0.25H), 1.80 - 1.91 (m, 0.75H), 1.69 - 1.78 (m, 2H), 1.49 - 1.68 (m, 1.5H), 1.11 - 1.21 (m, 0.75H), 0.89 (apparent dd, *J* = 6.8, 4.8 Hz, 6.75H), 2 NH not visible; LCMS (ESI, high pH) *m/z* 476 [M+H]⁺, *R*_t = 0.80 min (16% by area), *m/z* 476 [M+H]⁺, *R*_t = 0.81 min (84% by area).

Analytical chiral HPLC using a Chiralpak AD-H column and 50% EtOH in heptane (0.1% isopropylamine v/v) showed separation of the 4 isomers. The diastereoisomer mixture **275** was thus separated by chiral chromatography using a Chiralpak AD-H column and the following stepped gradient was used: 25:75 EtOH/heptane (0.2% isopropylamine v/v) to elute isomer 1 (**276**) and isomer 2 (**277**) then 50:50 EtOH/heptane (0.2% isopropylamine v/v) to elute isomer 3 (**278**) and finally an EtOH wash to isolate isomer 4 (**279**). The compounds were individually analysed by chiral

HPLC to confirm their purity and by NMR to confirm relative stereochemistry of each enantiomer.

Isomer 1 – *cis* diastereoisomer *N*-(5-(7-(((2*R,4*S**)-2-Isopropylpiperidin-4-yl)methoxy)-1,3-dihydroisobenzofuran-5-yl)-2-methoxypyridin-3-yl)methanesulfonamide (276)**

Brown gum (29 mg) ; ee 100% (7.97 min); ¹H NMR (DMSO-d₆, 600 MHz) δ 8.16 (d, *J* = 2.2 Hz, 1H), 7.80 (d, *J* = 2.2 Hz, 1H), 7.09 (s, 1H), 7.06 (s, 1H), 5.04 (s, 2H), 4.99 (s, 2H), 3.93 - 4.00 (m, 2H), 3.93 (s, 3H), 3.05 - 3.11 (m, 1H), 2.98 (s, 3H), 2.62 (td, *J* = 12.2, 2.3 Hz, 1H), 2.38 (ddd, *J* = 11.2, 5.2, 1.9 Hz, 1H), 1.86 (ttt, *J* = 12.5, 6.5, 6.0 Hz, 1H), 1.69 - 1.78 (m, 2H), 1.60 (qd, *J* = 7.0, 5.2 Hz, 1H), 1.13 - 1.21 (m, 1H), 0.89 (apparent t, *J* = 7.0 Hz, 7H), 2 NH not visible; ¹³C NMR (126 MHz, DMSO-d₆) δ 156.8 (Ar-C), 154.0 (Ar-C), 142.3 (Ar-C), 139.3 (Ar-CH), 139.2 (ArC), 130.4 (Ar-CH), 130.0 (Ar-C), 126.1 (Ar-C), 124.2 (Ar-C), 111.9 (Ar-CH), 109.5 (Ar-CH), 73.6 (CH₂), 73.2 (CH₂), 71.4 (CH₂), 61.6 (CH), 54.0 (CH₃), 46.1 (CH₂), 40.9 (CH₃), 36.3 (CH), 32.7 (CH), 31.3 (CH₂), 29.1 (CH₂), 19.3 (CH₃), 18.8 (CH₃); LCMS (ESI, formic) *m/z* 476 [M+H]⁺, *R*_t = 0.74 min; HRMS (ESI) calcd for C₂₄H₃₄N₃O₅S [M+H]⁺ 476.2219, found 476.2218 (7.71 min); IR (ATR) cm⁻¹ 2921, 2853, 1599, 1461, 1397, 1293, 1196.

Isomer 2 - *trans* diastereoisomer *N*-(5-(7-(((2*S,4*S**)-2-Isopropylpiperidin-4-yl)methoxy)-1,3-dihydroisobenzofuran-5-yl)-2-methoxypyridin-3-yl)methanesulfonamide (277)**

7 mg; ee 93.2% (8.92 min); ¹H NMR (DMSO-d₆, 600 MHz) δ 8.18 (d, *J* = 2.2 Hz, 1H), 7.80 (d, *J* = 2.4 Hz, 1H), 7.12 (s, 1H), 7.09 (s, 1H), 5.05 (s, 2H), 4.99 (d, *J* = 1.5 Hz, 2H), 4.09 - 4.19 (m, 2H), 3.93 (s, 3H), 2.98 (s, 3H), 2.78 - 2.85 (m, 2H), 2.54 (ddd, *J* = 9.2, 6.9, 2.8 Hz, 1H), 2.19 - 2.26 (m, 1H), 1.64 - 1.71 (m, 2H), 1.58 - 1.65 (m, 1H), 1.51 - 1.58 (m, 1H), 1.43 - 1.51 (m, 1H), 0.88 (d, *J* = 6.6 Hz, 3H), 0.86 (d, *J* = 6.8 Hz, 3H), 2 NH not visible; LCMS (ESI, formic) *m/z* 476 [M+H]⁺, *R*_t = 0.74 min.

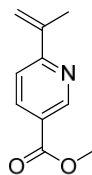
Isomer 3 – *cis* diastereoisomer *N*-(5-(7-(((2*R,4*S**)-2-Isopropylpiperidin-4-yl)methoxy)-1,3-dihydroisobenzofuran-5-yl)-2-methoxypyridin-3-yl)methanesulfonamide (278)**

Brown gum (32 mg); ee 93.2% (16.6 min); ¹H NMR (400 MHz, DMSO-*d*₆) δ 8.16 (d, *J* = 2.0 Hz, 1H), 7.80 (d, *J* = 2.3 Hz, 1H), 7.09 (s, 1H), 7.06 (s, 1H), 5.04 (s, 2H), 4.99 (s, 2H), 3.94 - 4.00 (m, 2H), 3.93 (s, 3H), 3.03 - 3.11 (m, 1H), 2.98 (s, 3H), 2.60 (td, *J* = 12.2, 2.3 Hz, 1H), 2.38 (ddd, *J* = 11.3, 5.2, 2.0 Hz, 1H), 1.80 - 1.90 (m, 1H), 1.69 - 1.78 (m, 2H), 1.52 - 1.63 (m, 1H), 1.11 - 1.21 (m, 1H), 0.89 (apparent dd, *J* = 6.8, 4.5 Hz, 7H), 2 NH not visible; ¹³C NMR (126 MHz, DMSO-*d*₆) δ 156.8 (Ar-C), 154.0 (Ar-C), 142.3 (Ar-C), 139.3 (Ar-CH), 139.1 (Ar-C), 130.4 (Ar-CH), 129.9 (ArC), 126.1 (Ar-C), 124.3 (Ar-C), 111.9 (Ar-CH), 109.5 (Ar-CH), 73.6 (CH₂), 73.2 (CH₂), 71.4 (CH₂), 61.6 (CH), 54.0 (CH₃), 46.1 (CH₂), 40.9 (CH₃), 36.3 (CH), 32.8 (CH), 31.3 (CH₂), 29.2 (CH₂), 19.3 (CH₃), 18.9 (CH₃); LCMS (ESI, formic) *m/z* 476 [M+H]⁺, *R*_t = 0.73 min; HRMS (ESI) calcd for C₂₄H₃₄N₃O₅S [M+H]⁺ 476.2219, found 476.2216 (7.75 min); IR (ATR) cm⁻¹ 2922, 2853, 1599, 1564, 1461, 1396, 1293, 1195.

Isomer 4 - *trans* diastereoisomer *N*-(5-(7-(((2*S,4*S**)-2-Isopropylpiperidin-4-yl)methoxy)-1,3-dihydroisobenzofuran-5-yl)-2-methoxypyridin-3-yl)methanesulfonamide (279)**

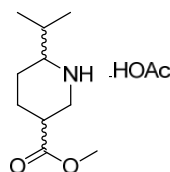
5 mg; 100% ee (30.9 min); ¹H NMR (400 MHz, DMSO-*d*₆) δ 8.10 (d, *J* = 2.27 Hz, 1H), 7.76 (d, *J* = 2.27 Hz, 1H), 7.10 (s, 1H), 7.07 (s, 1H), 5.04 (s, 2H), 4.98 (s, 2H), 4.08 - 4.18 (m, 2H), 3.91 (s, 3H), 2.93 (s, 3H), 2.75 - 2.81 (m, 2H), 2.43 - 2.48 (m, 1H), 2.16 - 2.25 (m, 1H), 1.56 - 1.68 (m, 3H), 1.43 - 1.55 (m, 2H), 0.86 (apparent dd, *J* = 9.7, 6.7 Hz, 6H), 2 NH not visible; LCMS (ESI, formic) *m/z* 476 [M+H]⁺, *R*_t = 0.75 min.

Methyl 6-(prop-1-en-2-yl)nicotinate (**255**)



Methyl 6-chloronicotinate (1.0 g x 3, 17.5 mmol), isopropenylboronic acid pinacol (1.9 mL x 3, 30 mmol), SPhos (240 mg x 3, 1.75 mmol), Pd(OAc)₂ (105 mg x 3, 1.40 mmol) and potassium phosphate (2.5 g x 3, 35 mmol) were combined in acetonitrile (12 mL x 3) and water (1.2 mL x 3). The 3 mixtures were heated at 120 °C for 1 h in a microwave reactor and then were combined. Water (150 mL) and DCM (150 mL) were added. The organic layer was collected and the aqueous layer was extracted with DCM (100 mL). The combined organic layers were washed with a further portion of water (100 mL). The organic layer was collected, passed through a hydrophobic frit and concentrated under reduced pressure. The resulting crude product was purified by normal phase chromatography (330 g pre-packed silica column, 0 to 15% EtOAc in cyclohexane gradient) to give the title product **255** as a white solid (1.44 g, 46%). ¹H NMR (400 MHz, CDCl₃) δ 9.18 (br. d, *J* = 2.2 Hz, 1H), 8.25 (dd, *J* = 8.3, 2.2 Hz, 1H), 7.56 (d, *J* = 8.3 Hz, 1H), 6.01 (s, 1H), 5.41 - 5.45 (m, 1H), 3.96 (s, 3H), 2.25 (s, 3H); LCMS (ESI, high pH) *m/z* 178 [M+H]⁺, *R*_t = 0.96 min.

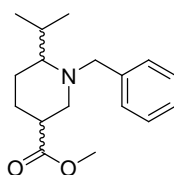
Methyl 6-isopropylpiperidine-3-carboxylate (**254**)



PtO₂ (295 mg, 1.30 mmol) was charged to the hydrogenation vessel followed by a solution of methyl 6-chloronicotinate **255** (1.44 g, 8.13 mmol) in acetic acid (80 mL). The mixture was hydrogenated using hydrogen gas (4 bar) at 60 °C for 5 h. The reaction mixture was filtered through a cartridge of celite and concentrated under reduced pressure. Toluene was added and solvent was evaporated under reduced pressure to give the title product **254** as an acetate salt, light brown oil (2.07 g, quantitative). ¹H NMR indicates a mixture of diastereoisomers ratio 4:1. **Isomer 1** (major isomer): ¹H

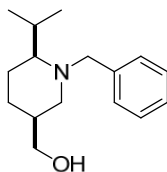
NMR (400 MHz, DMSO-d₆) δ 8.3 (br. s, 2H), 3.60 (s, 3H), 3.28 (td, $J = 12.4, 2.3$ Hz, 1H), 2.67 (dd, $J = 12.2, 3.7$ Hz, 1H), 2.44 - 2.51 (m, 1H), 2.10 - 2.17 (m, 1H), 2.00 - 2.08 (m, 1H), 1.90 (s, 6H), 1.39 - 1.55 (m, 3H), 1.13 - 1.25 (m, 1H), 0.78 - 0.85 (m, 6H); **Isomer 2** (minor isomer): ¹H NMR (400 MHz, DMSO-d₆) δ 8.3 (br. s, 2H), 3.57 (s, 3H), 3.11 - 3.18 (m, 1H), 2.44 - 2.55 (m, 1H), 2.31 - 2.38 (m, 1H), 2.10 - 2.18 (m, 1H), 1.99 (br. s, 1H), 1.90 (s, 3H), 1.56 - 1.66 (m, 1H), 1.42 - 1.52 (m, 1H), 1.32 - 1.41 (m, 1H), 0.98 - 1.10 (m, 1H), 0.78 - 0.85 (m, 6H). Note that some signals from the two isomers are overlapping.

Methyl 1-benzyl-6-isopropylpiperidine-3-carboxylate (**253**)

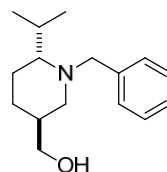


Methyl 6-isopropylpiperidine-3-carboxylate, acetate salt **254** (1.9 g, 7.8 mmol) was dissolved in acetonitrile (30 mL) under an atmosphere of nitrogen. Potassium carbonate (2.68 g, 19.4 mmol) was added followed by benzyl bromide (1.0 mL, 8.5 mmol). The reaction mixture was stirred at room temperature under an atmosphere of nitrogen overnight. Water (100 mL) was added and extracted with EtOAc (2 x 100 mL). The combined organic layers were passed through a hydrophobic frit and concentrated under reduced pressure to give the crude title product **253** as a yellow oil (2.2 g). No further purification was attempted, instead the crude material was used directly in the next step. LCMS (ESI, high pH) m/z no clear ionisation $[M+H]^+$, $R_t = 1.09$ min (43%), m/z 276 $[M+H]^+$, $R_t = 1.45$ min (10%), m/z 276 $[M+H]^+$, $R_t = 1.49$ min (40%).

((3*S, 6*S**)-1-Benzyl-6-isopropylpiperidin-3-yl)methanol (248a) and ((3*S**, 6*R**)-1-benzyl-6-isopropylpiperidin-3-yl)methanol (248b)**



248a (±)



248b (±)

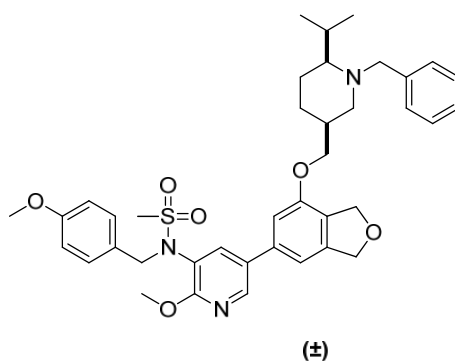
Methyl 1-benzyl-6-isopropylpiperidine-3-carboxylate, crude **253** (2.2 g, 7.8 mmol th. corr.) was dissolved in THF (50 mL) under an atmosphere of nitrogen and the mixture was cooled to -78 °C. A solution of DIBAL-H in THF (1 M, 16 mL, 16 mmol) was added and the mixture was stirred at -78 °C for 15 min, then at 0 °C for 1.5 h. The mixture was quenched with aq. HCl solution (2 M) and extracted with EtOAc (2 x 100 mL). The aqueous layer was then basified with sat. aq. NaHCO₃ solution (pH ~ 8) and extracted with further EtOAc (3 x 200 mL). The combined organic phases were passed through a hydrophobic frit and concentrated under reduced pressure. The resulting crude product was purified by normal phase chromatography (40 g and 80 g pre-packed silica columns, 0 to 50% EtOAc (+1% Et₃N) in cyclohexane (+1% Et₃N)) to give the two separate diastereoisomers **248a** (847 mg, 44%) and **248b** (212 mg, 11%).

Product 248a - yellow gum; ¹H NMR (400 MHz, DMSO-d₆) δ 7.26 - 7.33 (m, 4H), 7.17 - 7.24 (m, 1H), 4.25 (br. s, 1H), 3.87 (d, *J* = 13.8 Hz, 1H), 3.49 (d, *J* = 13.8 Hz, 1H), 3.30 - 3.35 (m, 1H), 3.17 - 3.25 (m, 1H), 2.52 - 2.58 (m, 1H), 2.33 (dd, *J* = 3.40, 13.0 Hz, 1H), 2.10 (apparent sxt, *J* = 6.8 Hz, 1H), 1.97 - 2.05 (m, 1H), 1.72 (d, *J* = 3.5 Hz, 1H), 1.55 - 1.65 (m, 1H), 1.34 - 1.49 (m, 3H), 0.90 (d, *J* = 6.8 Hz, 3H), 0.80 (d, *J* = 6.6 Hz, 3H); ¹³C NMR (101 MHz, DMSO-d₆) δ 141.0 (Ar-C), 128.7 (Ar-CH, 2C), 128.5 (Ar-CH, 2C), 126.9 (Ar-CH), 64.4 (CH), 64.2 (CH₂), 57.9 (CH₂), 50.9 (CH₂), 33.8 (CH), 26.7 (CH), 24.1 (CH₂), 20.9 (CH₃), 19.6 (CH₂), 18.8 (CH₃); LCMS (ESI, high pH) *m/z* 248 [M+H]⁺, *R*_t = 1.32 min; HRMS (ESI) calcd for C₁₆H₂₆NO [M+H]⁺ 248.2014, found 248.2016 (5.67 min); IR (ATR) cm⁻¹ 3343, 2929, 2865, 2793.

Product 248b, yellow gum; ¹H NMR (400 MHz, DMSO-d₆) δ 7.25 - 7.32 (m, 4H), 7.17 - 7.24 (m, 1H), 4.20 - 4.28 (m, 1H), 4.07 (apparent d, *J* = 13.6 Hz, 1H), 3.11 -

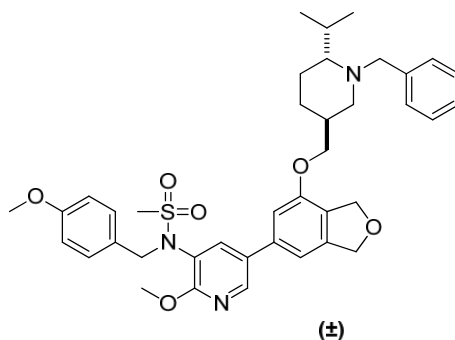
3.20 (m, 1H), 2.92 - 3.07 (m, 1H), 2.80 - 2.89 (m, 1H), 2.80 - 2.89 (m, 1H), 2.19 - 2.30 (m, 1H), 1.89 - 1.97 (m, 1H), 1.65 - 1.74 (m, 1H), 1.44 - 1.63 (m, 3H), 1.15 - 1.28 (m, 1H), 0.88 (apparent dd, $J = 6.8, 10.8$ Hz, 6H), 0.75 - 0.90 (m, 1H); LCMS (ESI, high pH) m/z 248 $[M+H]^+$, $R_t = 1.18$ min.

***N*-(5-(7-((1-Benzyl-6-isopropylpiperidin-3-yl)methoxy)-1,3-dihydroisobenzofuran-5-yl)-2-methoxypyridin-3-yl)-*N*-(4-methoxybenzyl)methanesulfonamide (280a)**



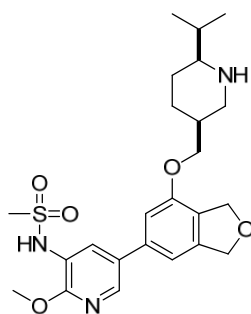
N-(5-(7-hydroxy-1,3-dihydroisobenzofuran-5-yl)-2-methoxypyridin-3-yl)-*N*-(4-methoxybenzyl)methanesulfonamide **271** (200 mg, 0.438 mmol), (1-benzyl-6-isopropylpiperidin-3-yl)methanol **248a** (271 mg, 1.09 mmol) and CMBP (0.35 mL, 1.3 mmol) were combined in a microwave vial in toluene (4 mL). The mixture was heated at 120 °C for 1 h in a microwave reactor. Solvent was removed under reduced pressure. The crude product was purified by normal phase chromatography (40 g prepacked silica column, 0 to 100% EtOAc in cyclohexane gradient) to give the title product **280a** (±) as a yellow oil (340 mg). ^1H NMR (400 MHz, DMSO- d_6) δ 8.41 (d, $J = 2.5$ Hz, 1H), 7.64 (d, $J = 2.5$ Hz, 1H), 7.16 - 7.26 (m, 7H), 6.99 (s, 1H), 6.89 (s, 1H), 6.81 (d, $J = 8.6$ Hz, 2H), 5.00 (br. s, 2H), 4.78 (d, $J = 12.5$ Hz, 1H), 4.73 (br. s, 2H), 4.63 (d, $J = 12.5$ Hz, 1H), 3.98 (s, 3H), 3.84 - 3.96 (m, 1H), 3.65 (s, 3H), 3.38 (d, $J = 13.5$ Hz, 1H), 3.17 (s, 3H), 2.71 (dd, $J = 12.8, 7.2$ Hz, 1H), 2.26 - 2.36 (m, 1H), 2.05 - 2.22 (m, 2H), 1.36 - 1.53 (m, 5H), 0.91 (apparent t, $J = 7.0$ Hz, 6H), 13% w/w residual EtOAc and 19% w/w **248a**; LCMS (ESI, high pH) m/z 686 $[M+H]^+$, $R_t = 1.69$ min (88%); m/z 248 $[M+H]^+$, $R_t = 1.32$ min (10% - **248a**). No further purification was carried out at this stage. The product was reacted directly in the next step.

***N*-(5-(7-((1-Benzyl-6-isopropylpiperidin-3-yl)methoxy)-1,3-dihydroisobenzofuran-5-yl)-2-methoxypyridin-3-yl)-*N*-(4-methoxybenzyl)methanesulfonamide (**280b**)**



N-(5-(7-Hydroxy-1,3-dihydroisobenzofuran-5-yl)-2-methoxypyridin-3-yl)-*N*-(4-methoxybenzyl)methanesulfonamide **271** (100 mg, 0.219 mmol), (1-benzyl-6-isopropylpiperidin-3-yl)methanol **248b** (85 mg, 0.34 mmol) and CMBP (0.17 mL, 0.66 mmol) were combined in a microwave vial in toluene (2 mL). The mixture was heated at 120 °C for 1 h in a microwave reactor. Solvent was removed under reduced pressure. The crude product was purified by normal phase chromatography (50 g prepacked silica column, 0 to 100% EtOAc in cyclohexane gradient) to give the title product **280b** (±) as a yellow gum (152 mg, 92% by area in LCMS, quantitative). LCMS (ESI, high pH) m/z 686 [M+H]⁺, R_t = 1.67 min (92%), m/z 248 [M+H]⁺, R_t = 1.17 min (4% - alcohol starting material **248b**). No NMR data collected. No further purification was carried out at this stage and the product was progressed directly to the next step.

***N*-(5-(7-(*cis*-(6-Isopropylpiperidin-3-yl)methoxy)-1,3-dihydroisobenzofuran-5-yl)-2-methoxypyridin-3-yl)methanesulfonamide (**281a**)**



N-(5-(7-((1-Benzyl-6-isopropylpiperidin-3-yl)methoxy)-1,3-dihydroisobenzofuran-5-yl)-2-methoxypyridin-3-yl)-*N*-(4-methoxybenzyl)methanesulfonamide **280a** (340 mg, 68% w/w, 0.337 mmol th. corr.) was dissolved in a mixture of EtOH (40 mL) and EtOAc (10 mL). The mixture was hydrogenated using an H-cube (setting: Pd/C Catcart, Full H₂, 50 °C, 1 mL/min). Solvent was removed under reduced pressure to give the crude title product **281a** (\pm) as a yellow gum (213 mg, 90%). LCMS (ESI, high pH) m/z 476 [M+H]⁺, R_t = 0.98 min (100%).

A portion of the crude material was progressed to further purification and the rest was used directly in the next step without purification for the *N*-methylation.

112 mg of product were purified by reverse phase chromatography using the MDAP (high pH, method 30-85% B) to give the pure racemic title product **281a** (\pm) as a white solid (53 mg, 33% of total th. mass, corr. yield estimated 48% over two steps).

¹H NMR (DMSO-*d*₆, 400 MHz): δ 8.27 (d, J = 2.3 Hz, 1H), 7.84 (d, J = 2.3 Hz, 1H), 7.13 (s, 1H), 7.12 (s, 1H), 5.07 (s, 2H), 5.01 (s, 2H), 4.28 - 4.37 (m, 1H), 4.16 (dd, J = 9.5, 6.8 Hz, 1H), 3.97 (s, 3H), 2.99 - 3.05 (s, 4H), 2.75 (dd, J = 12.2, 3.4 Hz, 1H), 2.18 - 2.29 (m, 1H), 1.99 (br. s, 1H), 1.81 (d, J = 14.1 Hz, 1H), 1.50 - 1.65 (m, 2H), 1.43 (dd, J = 13.1, 3.0 Hz, 1H), 1.17 - 1.33 (m, 1H), 0.88 (apparent dd, J = 8.4, 6.9 Hz, 6H), 2 NH not visible; ¹³C NMR (101 MHz, DMSO-*d*₆) δ 156.2 (C), 153.6 (C), 141.8 (C), 139.9 (Ar-CH), 138.5 (C), 130.4 (Ar-CH), 130.0 (C), 125.8 (C), 122.1 (C), 111.4 (Ar-CH), 109.2 (Ar-CH), 73.1 (CH₂), 70.9 (CH₂), 68.2 (CH₂), 61.8 (CH₃), 53.6 (CH₃), 46.5 (CH₂), 40.6 (CH), 32.6 (CH), 31.5 (CH), 25.0 (CH₂), 23.8 (CH₂),

19.0 (CH₃), 18.6 (CH₃); LCMS (ESI, high pH) m/z 476.08 [M+H]⁺, R_t = 0.97 min; HRMS (ESI) calcd for C₂₄H₃₄N₃O₅S [M+H]⁺ 476.2207, found 476.2214 (3.8 min).

The racemic product **281a** (±) was confirmed as the *cis* diastereoisomer from H-H coupling analysis.

The two enantiomers were separated by chiral chromatography using a Chiralpak AD-H column and the following mobile phase was used: 60:40 heptane/EtOH (0.25% isopropylamine v/v) to isolate compounds **282** and **283**. The compounds were individually analysed by chiral HPLC using 60:40 heptane/EtOH (0.2% isopropylamine v/v) solvent to confirm their purity.

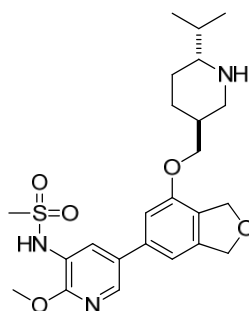
Enantiomer 1 *N*-(5-(7-(*cis*-(6-Isopropylpiperidin-3-yl)methoxy)-1,3-dihydroisobenzofuran-5-yl)-2-methoxypyridin-3-yl)methanesulfonamide (282)

Yellow solid (16 mg); mp 135-137 °C; ee 100% (14.7 min); $[\alpha]_D^{20} = +8.4^\circ$ (c 0.478, DMSO); ¹H NMR (400 MHz, DMSO-d₆) δ 8.24 (d, $J = 2.2$ Hz, 1H), 7.82 (d, $J = 2.2$ Hz, 1H), 7.11 (apparent d, $J = 6.8$ Hz, 2H), 5.72 (br. s, 1H), 5.05 (s, 2H), 4.99 (s, 2H), 4.31 (t, $J = 8.8$ Hz, 1H), 4.10 - 4.17 (m, 1H), 3.95 (s, 3H), 2.98 - 3.06 (m, 4H), 2.73 (dd, $J = 12.1, 3.30$ Hz, 1H), 2.16 - 2.26 (m, 1H), 1.97 (br. s, 1H), 1.73 - 1.83 (m, 1H), 1.50 - 1.62 (m, 2H), 1.35 - 1.47 (m, 1H), 1.20 - 1.31 (m, 1H), 0.86 (apparent dd, $J = 8.4, 7.0$ Hz, 6H), 1 NH not visible; ¹³C NMR (101 MHz, DMSO-d₆) δ 156.2 (C), 153.7 (C), 141.8 (C), 139.7 (Ar-CH), 138.6 (C), 130.2 (Ar-CH), 130.0 (C), 125.7 (C), 122.5 (C), 111.4 (Ar-CH), 109.1 (Ar-CH), 73.1 (CH₂), 70.9 (CH₂), 68.3 (CH₂), 62.0 (CH₃), 53.6 (CH₃), 46.7 (CH₂), 40.6 (CH), 32.7 (CH), 31.7 (CH), 25.2 (CH₂), 24.0 (CH₂), 19.0 (CH₃), 18.7 (CH₃); LCMS (ESI, high pH) m/z 476 [M+H]⁺, R_t = 0.97 min; HRMS (ESI) calcd for C₂₄H₃₄N₃O₅S [M+H]⁺ 476.2219, found 476.2222 (3.8 min); IR (ATR) cm⁻¹ 2924, 1600, 1459, 1396, 1330, 1143.

Enantiomer 2 *N*-(5-(7-(*cis*-(6-Isopropylpiperidin-3-yl)methoxy)-1,3-dihydroisobenzofuran-5-yl)-2-methoxypyridin-3-yl)methanesulfonamide (283)

Yellow solid (18 mg); mp 134-136 °C ; ee 98.8% (25.5 min); $[\alpha]_D^{20} = -8.4^\circ$ (c 0.473, DMSO); $^1\text{H NMR}$ (400 MHz, DMSO- d_6) δ 8.25 (d, $J = 2.2$ Hz, 1H), 7.82 (d, $J = 2.2$ Hz, 1H), 7.11 (apparent d, $J = 6.4$ Hz, 2H), 5.78 (br. s, 1H), 5.05 (s, 2H), 4.99 (s, 2H), 4.31 (t, $J = 8.9$ Hz, 1H), 4.10-4.17 (m, 1H), 3.95 (s, 3H), 2.98 - 3.06 (m, 4H), 2.74 (dd, $J = 12.0, 3.4$ Hz, 1H), 2.16 - 2.27 (m, 1H), 1.97 (br. s, 1H), 1.79 (s, 1H), 1.72 - 1.84 (m, 1H), 1.49 - 1.64 (m, 2H), 1.37 - 1.46 (m, 1H), 1.18 - 1.32 (m, 1H), 0.86 (apparent dd, $J = 8.8, 6.9$ Hz, 6H); $^{13}\text{C NMR}$ (101 MHz, DMSO- d_6) δ 156.2 (C), 153.7 (C), 142.8 (C), 139.8 (Ar-CH), 138.5 (C), 130.3 (Ar-CH), 130.0 (C), 125.7 (C), 122.4 (C), 111.4 (Ar-CH), 109.1 (Ar-CH), 73.1 (CH₂), 70.9 (CH₂), 68.3 (CH₂), 62.0 (CH₃), 53.6 (CH₃), 46.7 (CH₂), 40.6 (CH), 32.7 (CH), 31.7 (CH), 25.2 (CH₂), 24.0 (CH₂), 19.0 (CH₃), 18.7 (CH₃); LCMS (ESI, high pH) m/z 476.11 [M+H]⁺, $R_t = 0.97$ min; HRMS (ESI) calcd for C₂₄H₃₄N₃O₅S [M+H]⁺ 476.2219, found 476.2220 (3.8 min), IR (ATR) cm⁻¹ 2924, 1599, 1467, 1396, 1330, 1142.

***N*-(5-(7-(*trans*-(6-Isopropylpiperidin-3-yl)methoxy)-1,3-dihydroisobenzofuran-5-yl)-2-methoxypyridin-3-yl)methanesulfonamide (281b)**



N-(5-(7-((1-Benzyl-6-isopropylpiperidin-3-yl)methoxy)-1,3-dihydroisobenzofuran-5-yl)-2-methoxypyridin-3-yl)-*N*-(4-methoxybenzyl)methanesulfonamide **280b** (152 mg, 0.219 mmol th.corr.) was dissolved in a mixture of EtOH (20 mL) and EtOAc (5 mL). The mixture was hydrogenated using an H-cube (setting: Pd/C Catcart, Full H₂, 50 °C, 1 mL/min). Solvent was removed under reduced pressure. The crude product was

purified by reverse phase chromatography using MDAP (high pH, method 15-55%) to give the title product **281b** (\pm) as a white solid (41 mg, 39% over 2 steps). ^1H NMR (600 MHz, DMSO- d_6) δ 8.22 (d, $J = 1.8$ Hz, 1H), 7.82 (d, $J = 2.2$ Hz, 1H), 7.11 (s, 1H), 7.07 (s, 1H), 5.06 (s, 2H), 5.00 (s, 2H), 3.84 - 4.01 (m, 5H), 3.16 - 3.19 (m, 1H), 3.02 (s, 3H), 2.36 (t, $J = 11.4$ Hz, 1H), 2.20 - 2.25 (m, 1H), 1.80 - 1.92 (m, 2H), 1.63 - 1.68 (m, 1H), 1.54 (dd, $J = 12.7, 6.4$ Hz, 1H), 1.06 - 1.17 (m, 2H), 0.88 (dd, $J = 9.2, 7.0$ Hz, 6H), two NH not visible; LCMS (ESI, high pH) m/z 476 $[\text{M}+\text{H}]^+$, $R_t = 0.89$ min.

The racemic product **281b** was confirmed as *trans* isomer by ^1H NMR using H-H coupling.

The racemic mixture **281b** was separated by chiral chromatography using a Chiralpak IC column and the following mobile phase was used: 30:70 EtOH/heptanes (+ 0.2% isopropylamine) to isolate compounds **284** and **285**. The compounds were individually analysed by chiral HPLC using 60:40 heptane / EtOH (+ 0.2% isopropylamine) solvent to confirm their purity.

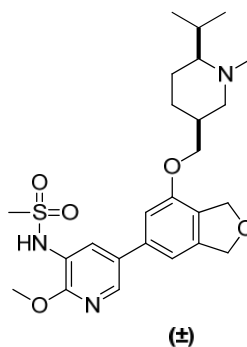
Enantiomer 1

***N*-(5-(7-(*trans*-(6-Isopropylpiperidin-3-yl)methoxy)-1,3-dihydroisobenzofuran-5yl)-2-methoxypyridin-3-yl)methanesulfonamide (284)** white solid (12 mg); 100% ee (16 min); ^1H NMR (400 MHz, DMSO- d_6) δ 8.21 (d, $J = 2.0$ Hz, 1H), 7.81 (d, $J = 2.0$ Hz, 1H), 7.10 (s, 1H), 7.06 (s, 1H), 5.05 (br. s, 2H), 4.99 (br. s, 2H), 3.88 - 4.01 (m, 5H), 3.13 - 3.20 (m, 1H), 3.01 (s, 3H), 2.35 (t, $J = 11.2$ Hz, 1H), 2.22 (br. s, 1H), 1.86 (br. s, 2H), 1.66 (br. s, 1H), 1.48 - 1.57 (m, 1H), 1.11 (d, 2H), 0.87 (apparent t, $J = 6.4$ Hz, 6H), 2 NH not visible; LCMS (ESI, high pH) m/z 476 $[\text{M}+\text{H}]^+$, $R_t = 0.88$ min; HRMS (ESI) calcd for $\text{C}_{24}\text{H}_{34}\text{N}_3\text{O}_5\text{S}$ $[\text{M}+\text{H}]^+$ 476.2219, found 476.2215 (7.80 min).

Enantiomer 2

N-(5-(7-(*trans*-(6-Isopropylpiperidin-3-yl)methoxy)-1,3-dihydroisobenzofuran-5-yl)-2-methoxypyridin-3-yl)methanesulfonamide (**285**) white solid (16 mg); 94.3% ee (17.8 min); ¹H NMR (400 MHz, DMSO-*d*₆) δ 8.21 (d, *J* = 2.3 Hz, 1H), 7.81 (d, *J* = 2.3 Hz, 1H), 7.10 (s, 1H), 7.06 (s, 1H), 5.05 (br. s., 2H), 4.99 (s, 2H), 3.87 - 4.01 (m, 5H), 3.13 - 3.20 (m, 1H), 3.01 (s, 3H), 2.35 (t, *J* = 11.5 Hz, 1H), 2.21 (d, *J* = 5.5 Hz, 1H), 1.79 - 1.91 (m, 2H), 1.65 (d, *J* = 9.3 Hz, 1H), 1.54 (dq, *J* = 6.6, 12.8 Hz, 1H), 1.11 (d, *J* = 8.8 Hz, 2H), 0.87 (t, *J* = 6.4 Hz, 6H), 2 NH not visible; LCMS (ESI, high pH) *m/z* 476 [M+H]⁺, *R*_t = 0.88 min; HRMS (ESI) calcd for C₂₄H₃₄N₃O₅S [M+H]⁺ 476.2219, found 476.2213 (7.78 min).

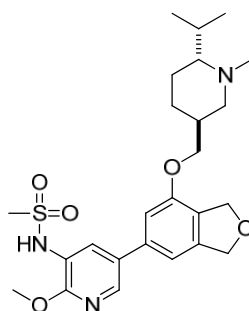
N-(5-(7-(*cis*-(6-Isopropyl-1-methylpiperidin-3-yl)methoxy)-1,3-dihydroisobenzofuran-5-yl)-2-methoxypyridin-3-yl)methanesulfonamide (**286a**)



N-(5-(7-((6-Isopropylpiperidin-3-yl)methoxy)-1,3-dihydroisobenzofuran-5-yl)-2-methoxypyridin-3-yl)-*N*-(4-methoxybenzyl)methanesulfonamide **281a** (100 mg, 0.210 mmol), formaldehyde (37% w/w in water, 0.140 mL, 1.88 mmol) in formic acid (88% w/w in water, 0.800 mL, 18.4 mmol) were placed in a microwave vial. The reaction mixture was heated at 80 °C for 1 h in a microwave reactor. Solvent was removed under reduced pressure. The crude product was partitioned between sat. aq. NaHCO₃ solution (5 mL) and DCM (5 mL). The aqueous layer was extracted a second time with DCM (5 mL). The combined organic layers were passed through a hydrophobic frit and concentrated under reduced pressure. The crude product was purified by reverse phase chromatography using MDAP (high pH, method 50-99%) to give the title racemic

product **286a** (\pm) as a white solid (41 mg, 40%). $^1\text{H NMR}$ (600 MHz, DMSO-d_6) δ 9.32 (br. s, 1H), 8.30 (d, $J = 2.2$ Hz, 1H), 7.85 (d, $J = 1.8$ Hz, 1H), 7.12 (s, 2H), 5.06 (s, 2H), 5.01 (s, 2H), 4.30 (t, $J = 8.6$ Hz, 1H), 4.14 (dd, $J = 9.2, 7.0$ Hz, 1H), 3.97 (s, 3H), 3.07 (s, 3H), 2.86 (d, $J = 11.4$ Hz, 1H), 2.23 (dd, $J = 11.7, 3.3$ Hz, 1H), 2.13 (s, 3H), 2.02 - 2.11 (m, 2H), 1.73 - 1.82 (m, 1H), 1.65 - 1.72 (m, 1H), 1.43 - 1.53 (m, 1H), 1.26 - 1.41 (m, 2H), 0.76 - 0.89 (m, 6H); LCMS (ESI, formic) m/z 490 $[\text{M}+\text{H}]^+$, $R_t = 0.74$ min.

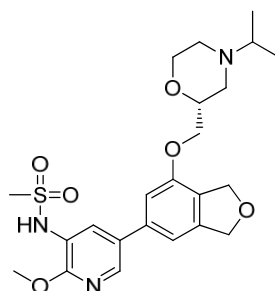
***N*-(5-(7-(*trans*-(6-Isopropyl-1-methylpiperidin-3-yl)methoxy)-1,3-dihydroisobenzofuran-5-yl)-2-methoxypyridin-3-yl)methanesulfonamide (286b)**



N-(5-(7-((6-Isopropylpiperidin-3-yl)methoxy)-1,3-dihydroisobenzofuran-5-yl)-2-methoxypyridin-3-yl)-*N*-(4-methoxybenzyl)methanesulfonamide **281b** (40 mg, 0.084 mmol), formaldehyde (37% w/w in water, 0.10 mL, 1.3 mmol) and formic acid (88% w/w in water, 0.40 mL, 9.2 mmol) were placed in a microwave vial. The reaction mixture was heated at 80 °C for 1 h in a microwave reactor. An additional portion of formaldehyde (37% w/w in water, 0.10 mL, 1.3 mmol) was added and the reaction mixture was heated in a microwave reactor at 80 °C for 4 h. A further portion of formaldehyde (37% w/w in water, 0.1 mL, 1.3 mmol) was added and the reaction was heated at 80 °C in a microwave reactor for 2 h. The reaction mixture was reheated at 80 °C for 3 h in a microwave reactor. LCMS showed starting material remaining. The mixture was concentrated under reduced pressure. The crude product was purified twice by reverse phase chromatography using the high pH MDAP (method 30-85%) to give the title product **286b** (\pm) as a brown solid (9 mg, 22%). $^1\text{H NMR}$ (400 MHz, DMSO-d_6) δ 9.33 (br. s, 1H), 8.25 (d, $J = 2.3$ Hz, 1H),

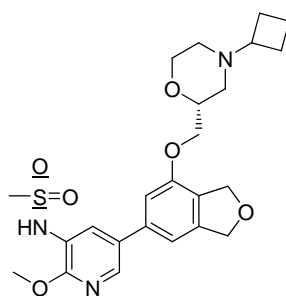
7.83 (d, $J = 2.3$ Hz, 1H), 7.1 (s, 1H), 7.05 (s, 1H), 5.05 (br. s, 2H), 5.00 (br. s, 2H), 3.84 - 4.03 (m, 5H), 3.03 (s, 3H), 2.97 (d, $J = 10.1$ Hz, 1H), 2.14 (s, 3H), 2.06 (td, $J = 6.9, 3.9$ Hz, 1H), 1.89 - 2.00 (m, 1H), 1.84 (t, $J = 11.0$ Hz, 2H), 1.59 - 1.67 (m, 1H), 1.49 - 1.58 (m, 1H), 1.09 - 1.25 (m, 1H), 0.94 - 1.07 (m, 1H), 0.85 (d, $J = 6.8$ Hz, 3H), 0.78 (d, $J = 6.8$ Hz, 3H); LCMS (ESI, high pH) m/z 490 $[M+H]^+$, $R_t = 1.11$ min.

(*R*)-*N*-(5-(7-((4-Isopropylmorpholin-2-yl)methoxy)-1,3-dihydroisobenzofuran-5-yl)-2-methoxypyridin-3-yl)methanesulfonamide (289)



(*R*)-*N*-(2-methoxy-5-(7-(morpholin-2-ylmethoxy)-1,3-dihydroisobenzofuran-5-yl)pyridin-3-yl)methanesulfonamide (75 mg, 0.17 mmol) and propan-2-one (0.24 mL, 1.63 mmol) were mixed in THF (1.5mL) under nitrogen for 10 min. sodium triacetoxyborohydride (102 mg, 0.481 mmol) was then added. The mixture was stirred at room temperature for 1 h. The mixture was quenched with water and concentrated under reduced pressure. The crude product was purified by reverse phase chromatography using MDAP (high pH, 30-85% (B)) to give the title product **289** as a white solid (60 mg, 73%). ^1H NMR (400 MHz, DMSO- d_6) δ 9.33 (br. s, 1H), 8.29 (d, $J = 2.3$ Hz, 1H), 7.85 (d, $J = 2.3$ Hz, 1H), 7.12 (apparent d, $J = 6.3$ Hz, 2H), 5.05 (s, 2H), 5.00 (s, 2H), 4.08 - 4.18 (m, 2H), 3.96 (s, 3H), 3.83 (apparent d, $J = 11.1$ Hz, 1H), 3.71 - 3.78 (m, 1H), 3.46-3.55 (m, 1H), 3.05 (s, 3H), 2.81 (d, $J = 11.1$ Hz, 1H), 2.58 - 2.65 (m, 2H), 2.21 (dt, $J = 11.2, 3.3$ Hz, 1H), 2.09 (t, $J = 10.6$ Hz, 1H), 0.98 (dd, $J = 6.3, 1.3$ Hz, 6H); LCMS (ESI, high pH) m/z 478 $[M+H]^+$, $R_t =$

0.87 min. (**(*R*)-*N*-(5-(7-((4-Cyclobutylmorpholin-2-yl)methoxy)-1,3-dihydroisobenzofuran-5-yl)-2-methoxypyridin-3-yl)methanesulfonamide (290)**)



Sodium triacetoxyborohydride (29 mg, 0.14 mmol) was added to a mixture of (*R*)-*N*-(2-methoxy-5-(7-(morpholin-2-ylmethoxy)-1,3-dihydroisobenzofuran-5-yl)pyridin-3-yl)methanesulfonamide (20 mg, 0.046 mmol) and cyclobutanone (0.010 mL, 0.13 mmol) in THF (0.5 mL) under an atmosphere of nitrogen. The reaction was stirred at room temperature for 2 h. The reaction mixture was quenched with water and combined with the second batch below.

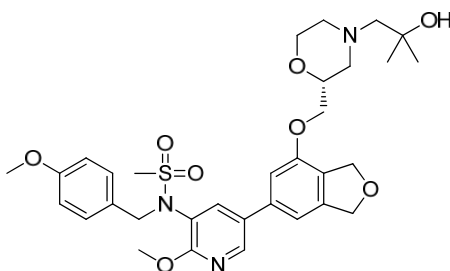
Sodium triacetoxyborohydride (102 mg, 0.482 mmol) was added to a mixture of (*R*)-*N*-(2-methoxy-5-(7-(morpholin-2-ylmethoxy)-1,3-dihydroisobenzofuran-5-yl)pyridin-3-yl)methanesulfonamide (70 mg, 0.16 mmol) and cyclobutanone (0.024 mL, 0.32 mmol) in THF (2 mL) under an atmosphere of nitrogen. The mixture was stirred at room temperature for 3 h. The reaction mixture was quenched with water, combined with the first batch and concentrated under reduced pressure. The crude product was purified by reverse phase chromatography using MDAP (high pH, 3085% (B)) to give the title product **290** as a white solid (70 mg, 69%). mp 135-137 °C; $[\alpha]_{\text{D}}^{20} = -14.3^{\circ}$ (c 1.011, DMSO); $^1\text{H NMR}$ (400 MHz, DMSO- d_6) δ 9.34 (br. s, 1H), 8.29 (d, $J = 2.3$ Hz, 1H), 7.85 (d, $J = 2.3$ Hz, 1H), 7.12 (d, $J = 6.0$ Hz, 2H), 5.05 (s, 2H), 4.99 (s, 2H), 4.14 (d, $J = 5.0$ Hz, 2H), 3.96 (s, 3H), 3.80 - 3.86 (m, 1H), 3.70 - 3.79 (m, 1H), 3.51 (dt, $J = 11.1, 2.4$ Hz, 1H), 3.06 (s, 3H), 2.78 (apparent d, $J = 11.1$ Hz, 1H), 2.72 (apparent t, $J = 7.4$ Hz, 1H), 2.60 (apparent d, $J = 11.1$ Hz,

1H), 1.91 - 2.01 (m, 2H), 1.83 - 1.91 (m, 1H), 1.71-1.83 (m, 3H), 1.59-1.69 (m, 2H);
¹³

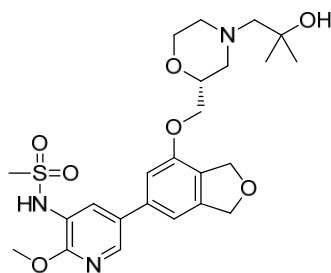
$^1\text{C NMR}$ (101 MHz, DMSO- d_6) δ 156.3 (C), 153.3 (C), 141.9 (C), 140.4 (Ar-CH), 138.3 (Ar-CH), 130.9 (C), 129.8 (C), 125.9 (C), 119.1 (C), 111.8 (Ar-CH), 109.4 (Ar-CH), 73.5 (CH), 73.0 (CH₂), 70.9 (CH₂), 69.4 (CH₂), 65.7 (CH₂), 59.8 (CH), 53.6 (CH₃), 50.8 (CH₂), 48.8 (CH₂), 40.7 (CH₃), 26.1 (CH₂, 2C), 14.1 (CH₂); LCMS (ESI, high pH) m/z 490 $[\text{M}+\text{H}]^+$, $R_t = 0.97$ min; HRMS (ESI) calcd for C₂₄H₃₂N₃O₆S

[M+H]⁺ 490.2007, found 490.2006 (3.5 min); IR (ATR) cm⁻¹ 2938, 1601, 1474, 1394, 1329, 1148.

(R)-N-(5-(7-((4-(2-Hydroxy-2-methylpropyl)morpholin-2-yl)methoxy)-1,3-dihydroisobenzofuran-5-yl)-2-methoxypyridin-3-yl)-N-(4-methoxybenzyl)methanesulfonamide (295)



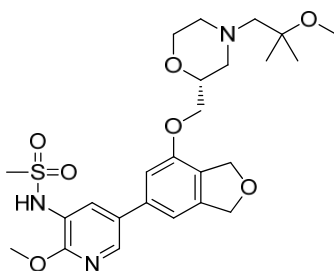
(R)-N-(2-Methoxy-5-(7-(morpholin-2-ylmethoxy)-1,3-dihydroisobenzofuran-5-yl)pyridin-3-yl)-N-(4-methoxybenzyl)methanesulfonamide (60 mg, 0.11 mmol) was suspended in acetonitrile (0.8 mL). FeCl₃ (5% w/w on Si, 70 mg, 0.022 mmol) and 2,2-dimethyloxirane (0.021 mL, 0.24 mmol) were added. The reaction mixture was heated at 60 °C overnight. LCMS (high pH) showed approx 5:4 ratio of SM to product. A further portion of 2,2-Dimethyloxirane (0.021 mL, 0.24 mmol) and FeCl₃ (5% w/w on Si, 35 mg, 0.011 mmol) in acetonitrile (0.2 mL) were added. The mixture was again stirred at 60 °C overnight. After this time, a further portion of 2,2dimethyloxirane (0.020 mL, 0.24 mmol) and FeCl₃ (5% w/w on Si, 36 mg, 0.011 mmol) were added and the mixture was stirred at 60 °C for a further 3 h. The mixture was then filtered through a 1 g silica cartridge, eluted with acetonitrile and the filtrate was concentrated under reduced pressure. The crude residue was diluted with water (15 mL) and extracted with EtOAc (2 x 15 mL). The combined organics were passed through a hydrophobic frit and concentrated under reduced pressure to give the title product **295** as a yellow gum (56 mg), which was used directly in the next step. LCMS (ESI, high pH) *m/z* 628 [M+H]⁺, R_t = 1.17 - 1.19 min (96%). No NMR data collected. **(R)-N-(5-(7-((4-(2-Hydroxy-2-methylpropyl)morpholin-2-yl)methoxy)-1,3-dihydroisobenzofuran-5-yl)-2-methoxypyridin-3-yl)methanesulfonamide (291)**



(*R*)-*N*-(5-(7-((4-(2-Hydroxy-2-methylpropyl)morpholin-2-yl)methoxy)-1,3-dihydroisobenzofuran-5-yl)-2-methoxypyridin-3-yl)-*N*-(4-methoxybenzyl)methanesulfonamide (56 mg, 0.089 mmol) was dissolved in DCM (1 mL) and TFA (0.5 mL, 6.5 mmol) was added. The mixture was heated at 70 °C for 1.5 h in a microwave reactor. A further amount of TFA (0.10 mL, 1.3 mmol) was added and the mixture was heated at 70 °C for 30 min in a microwave reactor before solvent was removed under reduced pressure. The crude product was purified by reverse phase chromatography using MDAP (formic acid, 5-30% (B)) to give the title product **291** as a white solid (28 mg). The product showed residual formic acid. The product was dissolved in a minimum of MeOH and passed through a 2 g SCX cartridge, pre-conditioned with MeOH. The product was washed with MeOH and eluted with 2 M NH₃ in MeOH solution. The solvent was removed under reduced pressure to give the title product **291** as a white solid (18 mg, 32% over two steps).

¹H NMR (400 MHz, DMSO-*d*₆) δ 9.29 (br. s, 1H), 8.32 (d, *J* = 2.3 Hz, 1H), 7.86 (d, *J* = 2.0 Hz, 1H), 7.13 (d, *J* = 6.8 Hz, 2H), 5.02 (d, *J* = 22.2 Hz, 4H), 4.05 - 4.19 (m, 3H), 3.97 (s, 3H), 3.78 (d, *J* = 11.1 Hz, 2H), 3.50 - 3.62 (m, 1H), 3.07 (s, 3H), 2.95 (d, *J* = 11.1 Hz, 1H), 2.77 (d, *J* = 11.1 Hz, 1H), 2.21 (s, 3H), 2.05 - 2.15 (m, 1H), 1.10 (s, 6H); LCMS (ESI, formic) *m/z* 508 [M+H]⁺, *R*_t = 0.59 min. (*R*)-*N*-(2-Methoxy-5-(7-((4-(2-methoxy-2-methylpropyl)morpholin-2-yl)methoxy)-1,3-dihydroisobenzofuran-5-yl)pyridin-3-yl)methanesulfonamide

(292)



(*R*)-*N*-(5-(7-((4-(2-Hydroxy-2-methylpropyl)morpholin-2-yl)methoxy)-1,3-dihydroisobenzofuran-5-yl)-2-methoxypyridin-3-yl)-*N*-(4-methoxybenzyl)methanesulfonamide **296** (125 mg, 0.199 mmol) was dissolved in THF (2 mL). Sodium hydride (60% w/w dispersion in mineral oils, 24 mg, 0.60 mmol) was added and the mixture was stirred at room temperature for 15 min. Iodomethane (0.050 mL, 0.80 mmol) was then added and the mixture was stirred at room temperature over the weekend (65 h). LCMS (high pH) showed only 8% of desired product at this stage. Sodium hydride (60% w/w dispersion in mineral oils, 24 mg, 0.60 mmol) was added and the mixture was stirred at room temperature for 30 min. Iodomethane (0.050 mL, 0.80 mmol) was then added and the reaction mixture was stirred at room temperature overnight. LCMS (high pH) showed little improvement. The reaction mixture was quenched with water (5 mL) and extracted with EtOAc (2 x 20 mL). The combined organic layers were passed through a hydrophobic frit and concentrated under reduced pressure. The resulting crude product was dissolved in THF (2 mL) under an atmosphere of nitrogen. Sodium hydride (60% w/w dispersion in mineral oils, 50 mg, 1.3 mmol) was added followed by iodomethane (62 μ L, 1.0 mmol) and the mixture was left to stir at room temperature for 20 h. LCMS (formic) showed 12% of the desired product. The reaction mixture was quenched with water (5 mL) and extracted with EtOAc (2 x 20 mL). The combined organic layers were passed through a hydrophobic frit and concentrated under reduced pressure. Sodium hydride (60% w/w dispersion in mineral oil, 10 mg, 0.25 mmol) was added to a solution of the resulting crude (130 mg, 0.207 mmol) in DMF (1 mL). The mixture was stirred for 20 min and then iodomethane (20 μ L, 0.32 mmol) was added. The mixture was stirred at room temperature overnight. Further sodium hydride (60% w/w dispersion in mineral oil, 10 mg, 0.25 mmol) was added and the mixture was stirred at room temperature. Iodomethane (20 μ L, 0.32

mmol) was added and the mixture was stirred at room temperature for 24 h. Additional sodium hydride (60% w/w dispersion in mineral oil, 10 mg, 0.25 mmol) was added and the reaction mixture was stirred at room temperature. Iodomethane (20 μ L, 0.32 mmol) was added and the reaction mixture was stirred at room temperature over the weekend. LCMS showed no change. The reaction was quenched with water and extracted with EtOAc. The organic layer was washed with water and after separation passed through a hydrophobic frit. Solvent was removed under reduced pressure. The resulting crude product was dissolved in DMF (2 mL). Sodium hydride (60% w/w dispersion in mineral oils, 72 mg, 1.8 mmol) was added and the mixture was stirred at room temperature for 15 min. Iodomethane (0.050 mL, 0.80 mmol) was then added and the reaction mixture was stirred at room temperature for 24 h. LCMS (high pH) showed 52% of desired product and 24 % of starting material. Sodium hydride (60% w/w dispersion in mineral oils, 30 mg, 0.75 mmol) was added and the mixture was stirred for 1 h. Iodomethane (0.050 mL, 0.80 mmol) was then added and the reaction mixture was left to stir at room temperature for 6 h. LCMS (high pH) showed 64% of desired product and 13 % of starting material. The reaction mixture was quenched with water (5 mL) and extracted with EtOAc (2 x 20 mL). The combined organic layers were passed through a hydrophobic frit and concentrated under reduced pressure. The crude product was dissolved in DMF (2 mL). Sodium hydride (60% w/w dispersion in mineral oils, 72 mg, 1.8 mmol) was added and the mixture was stirred at room temperature for 1 h. Iodomethane (0.050 mL, 0.80 mmol) was then added and the mixture was stirred at room temperature for 20 h. LCMS (high pH) showed no change: 66% of desired product and 11% of starting material. The mixture was quenched with water (5 mL) and extracted with EtOAc (2 x 20 mL). The combined organic layers were passed through a hydrophobic frit and evaporated under reduced pressure to give the crude title product **292** (148 mg). LCMS (ESI, high pH) m/z 642 $[M+H]^+$, R_t = 1.31 min, 68% by area.

The crude product **292** (148 mg) was mixed with TFA (1 mL) in DCM (1 mL). The reaction mixture was heated at 70 °C in a microwave reactor for 2 h. The mixture was concentrated under reduced pressure. The resulting crude product was purified by reverse phase chromatography using MDAP (high pH, 30-85% (B)) to give the title product **292** as a yellow solid (16 mg, 11% over 2 steps). 1H NMR (400 MHz, DMSO-

d₆) δ 9.32 (br. s, 1H), 8.29 (d, $J = 2.3$ Hz, 1H), 7.85 (d, $J = 2.3$ Hz, 1H), 7.13 (s, 1H), 7.11 (s, 1H), 5.05 (s, 2H), 4.99 (s, 2H), 4.05 - 4.18 (m, 2H), 3.96 (s, 3H), 3.73 - 3.81 (m, 2H), 3.55 (td, $J = 11.0, 2.4$ Hz, 1H), 3.08 (s, 3H), 3.05 (s, 3H), 2.94 (d, $J = 11.3$ Hz, 1H), 2.75 (apparent d, $J = 11.3$ Hz, 1H), 2.29 (apparent d, $J = 1.5$ Hz, 2H), 2.17 - 2.26 (m, 1H), 2.05 - 2.13 (m, 1H), 1.11 (s, 6H); LCMS (ESI, high pH) m/z 522 [M+H]⁺, $R_t = 1.00$ min.

References

References

1. Garnier, J. *Harv. Bus. Rev.* **2008**, *86*, 68-70.
2. Kola, I.; Landis, J. *Nat. Rev. Drug Discov.* **2004**, *3*, 711-716.
3. Paul, S. M.; Mytelka, D. S.; Dunwiddie, C. T.; Persinger, C. C.; Munos, B. H.; Lindborg, S. R.; Schacht, A. L. *Nat. Rev. Drug Discov.* **2010**, *9*, 203-214.
4. Butcher, E. C. *Nat. Rev. Drug Discov.* **2005**, *4*, 461-467.
5. Sams-Dodd, F. *Drug Discov. Today.* **2006**, *11*, 465-472.
6. Schreiber, S. L. *Science.* **2000**, *287*, 1964-1969.
7. Leeson, P. D.; Springthorpe, B. *Nat. Rev. Drug Discov.* **2007**, *6*, 881-890.
8. Price, D. A.; Blagg, J.; Jones, L.; Greene, N.; Wager, T. *Exp. Opin. Drug Metab. Toxicol.* **2009**, *5*, 921-931.
9. Hughes, J. D.; Blagg, J.; Price, D. A.; Bailey, S.; DeCrescenzo, G. A.; Devraj, R. V.; Ellsworth, E.; Fobian, Y. M.; Gibbs, M. E.; Gilles, R. W.; Greene, N.; Huang, E.; Krieger-Burke, T.; Loesel, J.; Wager, T.; Whiteley, L.; Zhang, Y. *Bioorg. Med. Chem. Lett.* **2008**, *18*, 4872-4875.
10. Gleeson, M. P. *J. Med. Chem.* **2008**, *51*, 817-834.
11. Waring, M. J. *Exp. Opin. Drug Discov.* **2010**, *5*, 235-248.
12. Leeson, P. D.; Empfield, J. R. *Annu. Rep. Med. Chem.* **2010**, *45*, 393-407.
13. Prous Science Integrity. <http://integrity.prous.com>
14. GVK Bio databases. <http://www.gvkbio.com/informatics.html>
15. Leo, A.; Hansch, C.; Elkins, D. *Chem. Rev.* **1971**, *71*, 525-616.
16. Young, R. J.; Green, D. V. S.; Luscombe, C. N.; Hill, A. P. *Drug Discov. Today.* **2011**, *16*, 822-830.
17. Valko, K.; Bevan, C.; Reynolds, D. *Anal. Chem.* **1997**, *69*, 2022-2029.
18. Valko, K. *J. Chromatogr. A.* **2004**, *1037*, 299-310.
19. Lipinski, C. A.; Lombardo, F.; Dominy, B. W.; Feeney, P. J. *Adv. Drug Delivery Rev.* **1997**, *23*, 3-25.
20. Ritchie, T. J.; MacDonald, S. J. F. *Drug Discov. Today.* **2009**, *14*, 1011-1020.

21. Hill, A. P.; Young, R. J. *Drug Discov. Today*. **2010**, *15*, 648-655.
22. Hann, M. M.; Leach, A. R.; Harper, G. J. *Chem. Inf. Comput. Sci.* **2001**, *41*, 856-864.
23. Oprea, T. I.; Davis, A. M.; Teague, S. J.; Leeson, P. D. J. *Chem. Inf. Comput. Sci.* **2001**, *41*, 1308-1315.
24. Carr, R. A. E.; Congreve, M.; Murray, C. W.; Rees, D. C. *Drug Discov. Today*. **2005**, *10*, 987-992.
25. Chessari, G.; Woodhead, A. J. *Drug Discov. Today*. **2009**, *14*, 668-675.
26. Murray, C. W.; Rees, D. C. *Nat. Chem.* **2009**, *1*, 187-192.
27. Barker, J.; Courtney, S.; Hestekamp, T.; Ullmann, D.; Whittaker, M. *Exp. Opin. Drug Discov.* **2006**, *1*, 225-236.
28. Schuffenhauer, A.; Ruedisser, S.; Marzinzik, A. L.; Jahnke, W.; Blommers, M.; Selzer, P.; Jacoby, E. *Curr. Top. Med. Chem.* **2005**, *5*, 751-762.
29. Congreve, M.; Carr, R.; Murray, C.; Jhoti, H. *Drug Discov. Today*. **2003**, *8*, 876-877.
30. Lipinski, C.; Hopkins, A. *Nature*. **2004**, *432*, 855-861.
31. Seidler, J.; McGovern, S. L.; Doman, T. N.; Shoichet, B. K. *J. Med. Chem.* **2003**, *46*, 4477-4486.
32. Gozalbes, R.; Carbajo, R. J.; Pineda-Lucena, A. *Curr. Med. Chem.* **2010**, *17*, 1769-1794.
33. Chung, C.-W. GlaxoSmithKline, R&D Platform Technology & Science, MDR Chemical Sciences UK, Unpublished work.
34. Francis, P. GlaxoSmithKline, R&D Platform Technology & Science, MDR Chemical Sciences UK, Unpublished work.
35. Mayer, M.; Meyer, B. *Angew. Chem. Int. Ed.* **1999**, *38*, 1784-1788.
36. Ludwig, C.; Guenther, U. L. *Front. Biosci.* **2009**, *14*, 4565-4574.
37. Mayer, M.; Meyer, B. *J. Am. Chem. Soc.* **2001**, *123*, 6108-6117.
38. Frederickson, M.; Callaghan, O.; Chessari, G.; Congreve, M.; Cowan, S. R.; Matthews, J. E.; McMenamin, R.; Smith, D. M.; Vinkovic, M.; Wallis, N. G. *J. Med. Chem.* **2008**, *51*, 183-186.

39. Wyatt, P. G.; Woodhead, A. J.; Berdini, V.; Boulstridge, J. A.; Carr, M. G.; Cross, D. M.; Davis, D. J.; Devine, L. A.; Early, T. R.; Feltell, R. E.; Lewis, E. J.; McMenamin, R. L.; Navarro, E. F.; O'Brien, M. A.; O'Reilly, M.;
Reule, M.; Saxty, G.; Seavers, L. C. A.; Smith, D. M.; Squires, M. S.; Trewartha, G.; Walker, M. T.; Woolford, A. J. A. *J. Med. Chem.* **2008**, *51*, 4986-4999.
40. Carvalho, A. L.; Trincao, J.; Romao, M. J. *Methods Mol. Biol.* **2010**, *572*, 31-56.
41. Orita, M.; Warizaya, M.; Amano, Y.; Ohno, K.; Niimi, T. *Exp. Opin. Drug Discov.* **2009**, *4*, 1125-1144.
42. Hubbard, R. E.; Davis, B.; Chen, I.; Drysdale, M. J. *Curr. Top. Med. Chem.* **2007**, *7*, 1568-1581.
43. Congreve, M.; Chessari, G.; Tisi, D.; Woodhead, A. J. *J. Med. Chem.* **2008**, *51*, 3661-3680.
44. Murray, C. W.; Verdonk, M. L. *J. Comput. -Aided Mol. Des.* **2002**, *16*, 741753.
45. Kuntz, I. D.; Chen, K.; Sharp, K. A.; Kollman, P. A. *Proc. Natl. Acad. Sci.* **1999**, *96*, 9997-10002.
46. Hopkins, A. L.; Groom, C. R.; Alex, A. *Drug Discov. Today.* **2004**, *9*, 430431.
47. Mortenson, P. N.; Murray, C. W. *J. Comput. -Aided Mol. Des.* **2011**, *25*, 663667.
48. Gill, A. L.; Frederickson, M.; Cleasby, A.; Woodhead, S. J.; Carr, M. G.; Woodhead, A. J.; Walker, M. T.; Congreve, M. S.; Devine, L. A.; Tisi, D.; O'Reilly, M.; Seavers, L. C. A.; Davis, D. J.; Curry, J.; Anthony, R.; Padova, A.; Murray, C. W.; Carr, R. A. E.; Jhoti, H. *J. Med. Chem.* **2005**, *48*, 414426.
49. Mortenson, Paul N. and Murray, Christopher W. Ligand Lipophilicity Efficiency - Assessing lipophilicity of fragments and early hits. Poster - Ligand Lipophilicity Efficiency - Assessing lipophilicity of fragments and early hits. 2009. 4-3-2009.
50. Murray, C. W.; Verdonk, M. L.; Rees, D. C. *Trends Pharmacol. Sci.* **2012**, *33*, 224-232.
51. Baker, M. *Nat. Rev. Drug Discovery.* **2013**, *12*, 5-7.
52. Fragments in the clinic: 2013 edition.
<http://practicalfragments.blogspot.co.uk/2013/01/fragments-in-clinic-2013edition.html> (accessed on Nov. 2014).
53. Bollag, G.; Hirth, P.; Tsai, J.; Zhang, J.; Ibrahim, P. N.; Cho, H.; Spevak, W.; Zhang, C.; Zhang, Y.; Habets, G.; Burton, E. A.; Wong, B.; Tsang, G.; West,

- B. L.; Powell, B.; Shellooe, R.; Marimuthu, A.; Nguyen, H.; Zhang, K. Y. J.; Artis, D. R.; Schlessinger, J.; Su, F.; Higgins, B.; Iyer, R.; D'Andrea, K.; Koehler, A.; Stumm, M.; Lin, P. S.; Lee, R. J.; Grippo, J.; Puzanov, I.; Kim, K. B.; Ribas, A.; McArthur, G. A.; Sosman, J. A.; Chapman, P. B.; Flaherty, K. T.; Xu, X.; Nathanson, K. L.; Nolop, K. *Nature*. **2010**, *467*, 596-599.
54. Bollag, G.; Tsai, J.; Zhang, J.; Zhang, C.; Ibrahim, P.; Nolop, K.; Hirth, P. *Nat. Rev. Drug Discov.* **2012**, *11*, 873-886.
 55. Tsai, J.; Lee, J. T.; Wang, W.; Zhang, J.; Cho, H.; Mamo, S.; Bremer, R.; Gillette, S.; Kong, J.; Haass, N. K.; Sproesser, K.; Li, L.; Smalley, K. S. M.; Fong, D.; Zhu, Y. L.; Marimuthu, A.; Nguyen, H.; Lam, B.; Liu, J.; Cheung, I.; Rice, J.; Suzuki, Y.; Luu, C.; Settachatgul, C.; Shellooe, R.; Cantwell, J.; Kim, S. H.; Schlessinger, J.; Zhang, K. Y. J.; West, B. L.; Powell, B.; Habets, G.; Zhang, C.; Ibrahim, P. N.; Hirth, P.; Artis, D. R.; Herlyn, M.; Bollag, G. *Proc. Natl. Acad. Sci.* **2008**, *105*, 3041-3046.
 56. Murray, C. W.; Carr, M. G.; Callaghan, O.; Chessari, G.; Congreve, M.; Cowan, S.; Coyle, J. E.; Downham, R.; Figueroa, E.; Frederickson, M.; Graham, B.; McMenamin, R.; O'Brien, M. A.; Patel, S.; Phillips, T. R.; Williams, G.; Woodhead, A. J.; Woolford, A. J. A. *J. Med. Chem.* **2010**, *53*, 5942-5955.
 57. Woodhead, A. J.; Angove, H.; Carr, M. G.; Chessari, G.; Congreve, M.; Coyle, J. E.; Cosme, J.; Graham, B.; Day, P. J.; Downham, R.; Fazal, L.; Feltell, R.; Figueroa, E.; Frederickson, M.; Lewis, J.; McMenamin, R.; Murray, C. W.; O'Brien, M. A.; Parra, L.; Patel, S.; Phillips, T.; Rees, D. C.; Rich, S.; Smith, D. M.; Trewartha, G.; Vinkovic, M.; Williams, B.; Woolford, A. J. A. *J. Med. Chem.* **2010**, *53*, 5956-5969.
 58. BMI classification. http://apps.who.int/bmi/index.jsp?introPage=intro_3.html (accessed on Oct. 2014).
 59. Obesity and overweight. <http://www.who.int/mediacentre/factsheets/fs311/en/> (accessed on Oct. 2014).
 60. Haslam, D. W.; James, W. P. *Lancet*. **2005**, *366*, 1197-1209.
 61. Dixon, J. B. *Mol. Cell. Endocrinol.* **2010**, *316*, 104-108.
 62. Hofbauer, K. G.; Nicholson, J. R.; Boss, O. *Annu. Rev. Pharmacol. Toxicol.* **2007**, *47*, 565-592.
 63. Lee, J.; Song, K. S.; Kang, J.; Lee, S. H.; Lee, J. *Curr. Top. Med. Chem.* **2009**, *9*, 564-596.
 64. Oh, S.; Kim, K. S.; Chung, Y. S.; Shong, M.; Park, S. B. *Curr. Top. Med. Chem.* **2009**, *9*, 466-481.
 65. Padwal, R. S.; Majumdar, S. R. *Lancet*. **2007**, *369*, 71-77.

66. Rucker, D.; Padwal, R.; Li, S. K.; Curioni, C.; Lau, D. C. W. *Br. Med. J.* **2007**, *335*, 1194-1199.
67. McNeely, W.; Benfield, P. *Drugs.* **1998**, *56*, 241-249.
68. She, P.; Reid, T. M.; Bronson, S. K.; Vary, T. C.; Hajnal, A.; Lynch, C. J.; Hutson, S. M. *Cell Metab.* **2007**, *6*, 181-194.
69. Halton, T. L.; Hu, F. B. *J. Am. Coll. Nutr.* **2004**, *23*, 373-385.
70. Layman, D. K.; Walker, D. A. *J. Nutr.* **2006**, *136*, 319S-323S.
71. She, P.; Zhou, Y.; Zhang, Z.; Griffin, K.; Gowda, K.; Lynch, C. J. *J. Appl. Physiol.* **2010**, *108*, 941-949.
72. Fried, S. K.; Watford, M. *Cell Metab.* **2007**, *6*, 155-156.
73. Jansonius, J. N. *Curr. Opin. Struct. Biol.* **1998**, *8*, 759-769.
74. John, R. A. *Biochim. Biophys. Acta, Protein Struct. Mol. Enzymol.* **1995**, *1248*, 81-96.
75. Grishin, N. V.; Phillips, M. A.; Goldsmith, E. J. *Protein Sci.* **1995**, *4*, 1291-1304.
76. Yoshimura, T.; Nishimura, K.; Ito, J.; Esakik, N.; Kagamiyama, H.; Manning, J. M.; Soda, K. *J. Am. Chem. Soc.* **1993**, *115*, 3897-3900.
77. Okada, K.; Hirotsu, K.; Sato, M.; Hayashi, H.; Kagamiyama, H. *J. Biochem.* **1997**, *121*, 637-641.
78. Hutson, S. *Prog. Nucleic Acid Res. Mol. Biol.* **2001**, *70*, 175-206.
79. Hutson, S. M.; Fenstermacher, D.; Mahar, C. J. *Biol. Chem.* **1988**, *263*, 3618-3625.
80. Hutson, S. M.; Wallin, R.; Hall, T. R. *J. Biol. Chem.* **1992**, *267*, 15681-15686.
81. Harper, A. E. *Ann. N. Y. Acad. Sci.* **1989**, *573*, 267-273.
82. Hall, T. R.; Wallin, R.; Reinhart, G. D.; Hutson, S. M. *J. Biol. Chem.* **1993**, *268*, 3092-3098.
83. Yennawar, N.; Dunbar, J.; Conway, M.; Hutson, S.; Farber, G. *Acta Crystallogr. Sect. D: Biol. Crystallogr.* **2001**, *D57*, 506-515.
84. Somers, D. GlaxoSmithKline, R&D Platform Technology & Science, MDR Chemical Sciences UK, Unpublished work.
85. Goto, M.; Miyahara, I.; Hirotsu, K.; Conway, M.; Yennawar, N.; Islam, M. M.; Hutson, S. M. *J. Biol. Chem.* **2005**, *280*, 37246-37256.

86. Hu, L. Y.; Boxer, P. A.; Kesten, S. R.; Lei, H. J.; Wustrow, D. J.; Moreland, D. W.; Zhang, L.; Ahn, K.; Ryder, T. R.; Liu, X.; Rubin, J. R.; Fahnoe, K.; Carroll, R. T.; Dutta, S.; Fahnoe, D. C.; Probert, A. W.; Roof, R. L.; Rafferty, M. F.; Kostlan, C. R.; Scholten, J. D.; Hood, M.; Ren, X. D.; Schielke, G. P.; Su, T. Z.; Taylor, C. P.; Mistry, A.; McConnell, P.; Hasemann, C.; Ohren, J. *Bioorg. Med. Chem. Lett.* **2006**, *16*, 2337-2340.
87. Hutson, S. M.; Berkich, D.; Drown, P.; Xu, B.; Aschner, M.; LaNoue, K. F. J. *Neurochem.* **1998**, *71*, 863-874.
88. Mendoza, R.; Petros, A. M.; Liu, Y.; Thimmapaya, R.; Surowy, C. S.; Leise, W. F.; Pereda-Lopez, A.; Panchal, S. C.; Sun, C. *Bioorg. Med. Chem. Lett.* **2011**, *21*, 5248-5250.
89. Ancellin, N. GlaxoSmithKline, R&D Metabolic Pathways Cardio TAU, France, Unpublished work.
90. Bingham, R.; Smith, S. GlaxoSmithKline, R&D Platform Technology & Science, Biological Sciences UK, Unpublished work.
91. Hitchcock, S. A.; Pennington, L. D. *J. Med. Chem.* **2006**, *49*, 7559-7583.
92. Wager, T. T.; Hou, X.; Verhoest, P. R.; Villalobos, A. *ACS Chem. Neurosci.* **2010**, *1*, 435-449.
93. Wager, T. T.; Chandrasekaran, R. Y.; Hou, X.; Troutman, M. D.; Verhoest, P. R.; Villalobos, A.; Will, Y. *ACS Chem. Neurosci.* **2010**, *1*, 420-434.
94. Frye, S. V. *Nat. Chem. Biol.* **2010**, *6*, 159-161.
95. Chung, C. *Acta Crystallogr. Sect. D: Biol. Crystallogr.* **2007**, *63*, 62-71.
96. Borthwick, J. GlaxoSmithKline, R&D Platform Technology & Science, MDR Chemical Sciences UK, Unpublished work.
97. Chung, C.-W.; Pickett, S. D. GlaxoSmithKline, R&D Platform Technology & Science, MDR Chemical Sciences UK, Unpublished work.
98. Spitzfaden, C. GlaxoSmithKline, R&D Platform Technology & Science, MDR Chemical Sciences UK, Unpublished work.
99. Bertrand, S.; Borthwick, J.; Pickett, S. D. GlaxoSmithKline, R&D Platform Technology & Science, MDR Chemical Sciences UK, Unpublished work.
100. Bertrand, S.; Borthwick, J.; Pickett, S. D.; Somers, D. GlaxoSmithKline, R&D, UK, Unpublished work.
101. Legon, A. C.; Millen, D. J. *Chem. Soc. Rev.* **1987**, *16*, 467-498.
102. Fischer, M.; Hubbard, R. E. *Molecular Interventions.* **2009**, *9*, 22-30.

103. Boehm, H. J. J. *Comput. -Aided Mol. Des.* **1994**, *8*, 243-256.
104. Leung, C. S.; Leung, S. S. F.; Tirado-Rives, J.; Jorgensen, W. L. *J. Med. Chem.* **2012**, *55*, 4489-4500.
105. Lunn, G.; Banks, B. J.; Crook, R.; Feeder, N.; Pettman, A.; Sabnis, Y. *Bioorg. Med. Chem. Lett.* **2011**, *21*, 4608-4611.
106. Pickett, S. D. GlaxoSmithKline, R&D Platform Technology & Science, MDR Chemical Sciences UK, Unpublished work.
107. Grinev, A. N.; Kaplina, N. V. *Khim. Geterotsikl. Soedin.* **1985**, 925-928.
108. Carpino, L. A. *J. Am. Chem. Soc.* **1993**, *115*, 4397-4398.
109. Montalbetti, C. A. G. N.; Falque, V. *Tetrahedron.* **2005**, *61*, 10827-10852.
110. Corey, E. J.; Venkateswarlu, A. J. *J. Am. Chem. Soc.* **1972**, *94*, 6190-6191.
111. Ritchie, T. J.; MacDonald, S. J. F.; Young, R. J.; Pickett, S. D. *Drug Discov. Today.* **2011**, *16*, 164-171.
112. Ritchie, T. J.; MacDonald, S. J. F. *Drug Discov. Today.* **2009**, *14*, 1011-1020.
113. Dodic, N. GlaxoSmithKline, R&D Metabolic Pathways Cardio TAU, France, Unpublished work.
114. Young, R. J.; Gummer, L. GlaxoSmithKline, R&D Platform Technology & Science, MDR Chemical Sciences UK, Unpublished work.
115. Deng, Y.; Shipps, G. W.; Wang, T.; Popovici-Muller, J.; Rosner, K. E.; Siddiqui, M. A.; Duca, J.; Cooper, A. B.; Cable, M. *Bioorg. Med. Chem. Lett.* **2009**, *19*, 5363-5367.
116. Qi, J.; Zhang, F.; Mi, Y.; Fu, Y.; Xu, W.; Zhang, D.; Wu, Y.; Du, X.; Jia, Q.; Wang, K.; Zhang, H. *Eur. J. Med. Chem.* **2011**, *46*, 934-943.
117. Coumar, M. S.; Wu, J. S.; Leou, J. S.; Tan, U. K.; Chang, C. Y.; Chang, T. Y.; Lin, W. H.; Hsu, J. T. A.; Chao, Y. S.; Wu, S. Y.; Hsieh, H. P. *Bioorg. Med. Chem. Lett.* **2008**, *18*, 1623-1627.
118. Selleri, S.; Bruni, F.; Costagli, C.; Costanzo, A.; Guerrini, G.; Ciciani, G.; Gratteri, P.; Bonaccini, C.; Aiello, P. M.; Besnard, F.; Renard, S.; Costa, B.; Martini, C. *J. Med. Chem.* **2003**, *46*, 310-313.
119. Mustazza, C.; Del Giudice, M. R.; Borioni, A.; Gatta, F. *J. Heterocycl. Chem.* **2001**, *38*, 1119-1129.
120. Wang, X.; Berger, D. M.; Salaski, E. J.; Torres, N.; Dutia, M.; Hanna, C.; Hu, Y.; Levin, J. I.; Powell, D.; Wojciechowicz, D.; Collins, K.; Frommer, E.; Lucas, J. *J. Med. Chem.* **2010**, *53*, 7874-7878.

121. Yoshida, M.; Mori, A.; Inaba, A.; Oka, M.; Makino, H.; Yamaguchi, M.; Fujita, H.; Kawamoto, T.; Goto, M.; Kimura, H.; Baba, A.; Yasuma, T. *Bioorg. Med. Chem.* **2010**, *18*, 8501-8511.
122. Mukaiyama, H.; Nishimura, T.; Shiohara, H.; Kobayashi, S.; Komatsu, Y.; Kikuchi, S.; Tsuji, E.; Kamada, N.; Ohnota, H.; Kusama, H. *Chem. Pharm. Bull.* **2007**, *55*, 881-889.
123. Elnagdi, M. H.; Elmoghayar, M. R. H.; Elgemeie, G. E. H. *Adv. Heterocycl. Chem.* **1987**, *41*, 319-376.
124. Gavrin, L. K.; Lee, A.; Provencher, B. A.; Masefski, W. W.; Huhn, S. D.; Ciszewski, G. M.; Cole, D. C.; McKew, J. C. *J. Org. Chem.* **2007**, *72*, 10431046.
125. Jakse, R.; Svete, J.; Stanovnik, B.; Golobic, A. *Tetrahedron.* **2004**, *60*, 46014608.
126. Kurasawa, Y.; Kim, H. S.; Takada, A.; Okamoto, Y. *J. Heterocycl. Chem.* **1990**, *27*, 2203-2205.
127. Nagahara, K.; Kawano, H.; Sasaoka, S.; Ukawa, C.; HIRAMA, T.; Takada, A.; Cottam, H. B.; Robins, R. K. *J. Heterocycl. Chem.* **1994**, *31*, 239-243.
128. Senga, K.; Novinson, T.; Wilson, H. R.; Robins, R. K. *J. Med. Chem.* **1981**, *24*, 610-613.
129. Elnagdi, M. H.; Elmoghayar, M. R. H.; Elgemeie, G. E. H. *Adv. Heterocycl. Chem.* **1987**, *41*, 319-376.
130. Mukaiyama, H.; Nishimura, T.; Shiohara, H.; Kobayashi, S.; Komatsu, Y.; Kikuchi, S.; Tsuji, E.; Kamada, N.; Ohnota, H.; Kusama, H. *Chem. Pharm. Bull.* **2007**, *55*, 881-889.
131. Young, R. J. GlaxoSmithKline, R&D Platform Technology & Science, MDR Chemical Sciences UK, Unpublished work.
132. Young, R. J.; Gummer, L.; Washio, Y. GlaxoSmithKline, R&D Platform Technology & Science, MDR Chemical Sciences UK, Unpublished work.
133. Tominaga, Y.; Matsuoka, Y.; Kohra, S.; Hosomi, A. *Heterocycles.* **1987**, *26*, 613-616.
134. Tominaga, Y.; Matsuoka, Y.; Oniyama, Y.; Uchimura, Y.; Komiya, H.; Hirayama, M.; Kohra, S.; Hosomi, A. *J. Heterocycl. Chem.* **1990**, *27*, 647660.
135. Brown, E. V. *Synthesis.* **1975**, 358-375.
136. Emayan, K.; English, R. F.; Koutentis, P. A.; Rees, C. W. *J. Chem. Soc., Perkin Trans. 1.* **1997**, 3345-3350.
137. Moghaddam, F. M.; Ghaffarzadeh, M. *Synth. Commun.* **2001**, *31*, 317-321.

138. Nooshabadi, M.; Aghapoor, K.; Darabi, H. R.; Mojtahedi, M. M. *Tetrahedron Lett.* **1999**, *40*, 7549-7552.
139. Kindler, K. *Justus Liebigs Ann. Chem.* **1923**, *431*, 187-230.
140. Carmack, M. J. *Heterocycl. Chem.* **1989**, *26*, 1319-1323.
141. Shantz, E. M.; Rittenberg, D. J. *Am. Chem. Soc.* **1946**, *68*, 2109-2110.
142. Dauben, W.; Reid, J. C.; Yankwich, P. E.; Calvin, M. J. *Am. Chem. Soc.* **1946**, *68*, 2117.
143. Dauben, W. G.; Reid, J. C.; Yankwich, P. E.; Calvin, M. J. *Am. Chem. Soc.* **1950**, *72*, 121-124.
144. Brown, E. V.; Cerwonka, E.; Anderson, R. C. *J. Am. Chem. Soc.* **1951**, *73*, 3735-3738.
145. Mundy, B. P.; Ellerd, M. G.; Favaloro, F. G. Jr. *Name reactions and reagents in organic synthesis, 2nd Edition*; John Wiley & Sons: 2005.
146. McMillan, F. H.; King, J. A. *J. Am. Chem. Soc.* **1948**, *70*, 4143-4150.
147. Salim, S. D.; Pathare, S. P.; Akamanchi, K. G. *Catal. Commun.* **2011**, *13*, 7881.
148. Middleton, W. J.; Engelhardt, V. A. *J. Am. Chem. Soc.* **1958**, *80*, 2788-2795.
149. Nilsson, N. H. *Tetrahedron.* **1974**, *30*, 3181-3184.
150. Masaki, Y.; Tanaka, N.; Miura, T. *Tetrahedron Lett.* **1998**, *39*, 5799-5802.
151. Aliagas, I.; Gradl, S.; Gunzner, J.; Mathieu, S.; Rudolph, J.; Wen, Z.; Wenglowisky, S. M. Patent WO2011025947, 2010.
152. Peruncheralathan, S.; Khan, T. A.; Ila, H.; Junjappa, H. *J. Org. Chem.* **2005**, *70*, 10030-10035.
153. Benetti, S.; Romagnoli, R.; De Risi, C.; Spalluto, G.; Zanirato, V. *Chem. Rev.* **1995**, *95*, 1065-1114.
154. Oikawa, Y.; Sugano, K.; Yonemitsu, O. *J. Org. Chem.* **1978**, *43*, 2087-2088.
155. Xu, F.; Armstrong, J. D., III; Zhou, G. X.; Simmons, B.; Hughes, D.; Ge, Z.; Grabowski, E. J. *J. Am. Chem. Soc.* **2004**, *126*, 13002-13009.
156. Carceller Gonzalez, E.; Virgili Bernado, M.; Marti Via, J.; Medina Fuentes, E. M. Patent WO2009077608, 2008.
157. Nguyen, V. T. H.; Bellur, E.; Appel, B.; Langer, P. *Synthesis.* **2006**, 28652872.
158. Brooks, D. W.; Lu, L. D. L.; Masamune, S. *Angew. Chem. Int. Ed. Engl.* **1979**, *18*, 72-74.

159. Humphreys, P. GlaxoSmithKline, R&D Immunoinflammation DPU, UK, Unpublished work.
160. Borthwick, J.; Pickett, S. D. GlaxoSmithKline, R&D Platform Technology & Science, MDR Chemical Sciences UK, Unpublished work.
161. Fact sheet on asthma (WHO).
<http://www.who.int/mediacentre/factsheets/fs307/en/index.html> (accessed on Sept. 2013).
162. Global strategy for asthma management and prevention.
http://www.ginasthma.org/local/uploads/files/GINA_Report_March13.pdf (accessed on Sept. 2013).
163. Martinez, F. D.; Vercelli, D. *Lancet*. **2013**, 382, 1360-1372.
164. Asthma and Airways (National Institute of Health).
<http://www.nlm.nih.gov/medlineplus/magazine/issues/fall11/articles/fall11pg4.html> (accessed on Sept. 2013).
165. Walker, C.; Thomas, M.; Edwards, M. J. *Drug Discov. Today: Disease Mechanisms*. **2006**, 3, 63-69.
166. Holgate, S. T.; Polosa, R. *Nat. Rev. Immunol.* **2008**, 8, 218-230.
167. Powell, H.; Gibson, P. G. *Med. J. Aust.* **2003**, 178, 223-225.
168. Palmqvist, M.; Persson, G.; Lazer, L.; Rosenborg, J.; Larsson, P.; Lotvall, J. *Eur. Respir. J.* **1997**, 10, 2484-2489.
169. Usmani, O. S.; Ito, K.; Maneechotesuwan, K.; Ito, M.; Johnson, M.; Barnes, P. J.; Adcock, I. M. *Am. J. Respir. Crit. Care Med.* **2005**, 172, 704-712.
170. Paggiaro, P.; Bacci, E. *Ther. Adv. Chronic Dis.* **2011**, 2, 47-58.
171. Holgate, S. T.; Djukanovic, R.; Casale, T.; Bousquet, J. *Clin. Exp. Allergy.* **2005**, 35, 408-416.
172. Ali, K.; Bilancio, A.; Thomas, M.; Pearce, W.; Gilfillan, A. M.; Tkaczyk, C.; Kuehn, N.; Gray, A.; Giddings, J.; Peskett, E.; Fox, R.; Bruce, I.; Walker, C.; Sawyer, C.; Okkenhaug, K.; Finan, P.; Vanhaesebroeck, B. *Nature*. **2004**, 431, 1007-1011.
173. Finan, P. M.; Thomas, M. J. *Biochem. Soc. Trans.* **2004**, 32, 378-382.
174. Lee, K. S.; Lee, H. K.; Hayflick, J. S.; Lee, Y. C.; Puri, K. D. *FASEB J.* **2006**, 20, 455-465.
175. Rowan, W. C.; Smith, J. L.; Affleck, K.; Amour, A. *Biochem. Soc. Trans.* **2012**, 40, 240-245.

176. Fruman, D. A.; Meyers, R. E.; Cantley, L. C. *Annu. Rev. Biochem.* **1998**, *67*, 481-507.
177. Foster, F. M.; Traer, C. J.; Abraham, S. M.; Fry, M. J. *J. Cell Sci.* **2003**, *116*, 3037-3040.
178. Jia, S.; Liu, Z.; Zhang, S.; Liu, P.; Zhang, L.; Lee, S. H.; Zhang, J.; Signoretti, S.; Loda, M.; Roberts, T. M.; Zhao, J. *Nature*. **2008**, *454*, 776-779.
179. Vanhaesebroeck, B.; Guillermet-Guibert, J.; Graupera, M.; Bilanges, B. *Nat. Rev. Mol. Cell Biol.* **2010**, *11*, 329-341.
180. Vanhaesebroeck, B.; Stephens, L.; Hawkins, P. *Nat. Rev. Mol. Cell Biol.* **2012**, *13*, 195-203.
181. Okkenhaug, K. *Annu. Rev. Immunol.* **2013**, *31*, 675-704.
182. Ward, S. G.; Finan, P. *Curr. Opin. Pharmacol.* **2003**, *3*, 426-434.
183. Walker, E. H.; Perisic, O.; Ried, C.; Stephens, L.; Williams, R. L. *Nature*. **1999**, *402*, 313-320.
184. Vanhaesebroeck, B.; Waterfield, M. D. *Exp. Cell Res.* **1999**, *253*, 239-254.
185. Manning, B. D.; Cantley, L. C. *Cell*. **2007**, *129*, 1261-1274.
186. Rowland, P.; Convery, M. GlaxoSmithKline, R&D Platform Technology & Science, CSci Biomolecular Sciences UK, Unpublished work.
187. Zhang, J.; Yang, P. L.; Gray, N. S. *Nat. Rev. Cancer*. **2009**, *9*, 28-39.
188. Berndt, A.; Miller, S.; Williams, O.; Le, D. D.; Houseman, B. T.; Pacold, J. I.; Gorrec, F.; Hon, W. C.; Liu, Y.; Rommel, C.; Gaillard, P.; Rueckle, T.; Schwarz, M. K.; Shokat, K. M.; Shaw, J. P.; Williams, R. L. *Nat. Chem. Biol.* **2010**, *6*, 244.
189. Williams, R.; Berndt, A.; Miller, S.; Hon, W. C.; Zhang, X. *Biochem. Soc. Trans.* **2009**, *37*, 615-626.
190. Marone, R.; Cmiljanovic, V.; Giese, B.; Wymann, M. P. *Biochim. Biophys. Acta, Proteins Proteomics*. **2008**, *1784*, 159-185.
191. Foster, J. G.; Blunt, M. D.; Carter, E.; Ward, S. G. *Pharmacol. Rev.* **2012**, *64*, 1027-1054.
192. Sutherlin, D. P.; Sampath, D.; Berry, M.; Castanedo, G.; Chang, Z.; Chuckowree, I.; Dotson, J.; Folkes, A.; Friedman, L.; Goldsmith, R.; Heffron, T.; Lee, L.; Lesnick, J.; Lewis, C.; Mathieu, S.; Nonomiya, J.; Olivero, A.; Pang, J.; Prior, W. W.; Salphati, L.; Sideris, S.; Tian, Q.; Tsui, V.; Wan, N. C.; Wang, S.; Wiesmann, C.; Wong, S.; Zhu, B. Y. *J. Med. Chem.* **2010**, *53*, 1086-1097.

193. Bi, L.; Okabe, I.; Bernard, D. J.; Nussbaum, R. L. *Mamm. Genome*. **2002**, *13*, 169-172.
194. Bi, L.; Okabe, I.; Bernard, D. J.; Wynshaw-Boris, A.; Nussbaum, R. L. *J. Biol. Chem.* **1999**, *274*, 10963-10968.
195. Knight, Z. A.; Gonzalez, B.; Feldman, M. E.; Zunder, E. R.; Goldenberg, D. D.; Williams, O.; Loewith, R.; Stokoe, D.; Balla, A.; Toth, B.; Balla, T.; Weiss, W. A.; Williams, R. L.; Shokat, K. M. *Cell*. **2006**, *125*, 733-747.
196. Okkenhaug, K.; Bilancio, A.; Farjot, G.; Priddle, H.; Sancho, S.; Peskett, E.; Pearce, W.; Meek, S. E.; Salpekar, A.; Waterfield, M. D.; Smith, A. J. H.; Vanhaesebroeck, B. *Science*. **2002**, *297*, 1031-1034.
197. Hirsch, E.; Katanaev, V. L.; Garlanda, C.; Azzolino, O.; Pirola, L.; Silengo, L.; Sozzani, S.; Mantovani, A.; Altruda, F.; Wymann, M. P. *Science*. **2000**, *287*, 1049-1053.
198. Jou, S. T.; Carpino, N.; Takahashi, Y.; Piekorz, R.; Chao, J. R.; Carpino, N.; Wang, D.; Ihle, J. N. *Mol. Cell. Biol.* **2002**, *22*, 8580-8591.
199. Ameriks, M. K.; Venable, J. D. *Curr. Top. Med. Chem.* **2009**, *9*, 738-753.
200. Murray, J. M.; Sweeney, Z. K.; Chan, B. K.; Balazs, M.; Bradley, E.; Castanedo, G.; Chabot, C.; Chantry, D.; Flagella, M.; Goldstein, D. M.; Kondru, R.; Lesnick, J.; Li, J.; Lucas, M. C.; Nonomiya, J.; Pang, J.; Price, S.; Salphati, L.; Safina, B.; Savy, P. P. A.; Seward, E. M.; Ultsch, M.; Sutherlin, D. P. *J. Med. Chem.* **2012**, *55*, 7686-7695.
201. Sutherlin, D. P.; Baker, S.; Bisconte, A.; Blaney, P. M.; Brown, A.; Chan, B. K.; Chantry, D.; Castanedo, G.; Depledge, P.; Goldsmith, P.; Goldstein, D. M.; Hancox, T.; Kaur, J.; Knowles, D.; Kondru, R.; Lesnick, J.; Lucas, M. C.; Lewis, C.; Murray, J.; Nadin, A. J.; Nonomiya, J.; Pang, J.; Pegg, N.; Price, S.; Reif, K.; Safina, B. S.; Salphati, L.; Staben, S.; Seward, E. M.; Shuttleworth, S.; Sohal, S.; Sweeney, Z. K.; Ultsch, M.; Waszkowycz, B.; Wei, B. *Bioorg. Med. Chem. Lett.* **2012**, *22*, 4296-4302.
202. Lannutti, B. J.; Meadows, S. A.; Herman, S. E. M.; Kashishian, A.; Steiner, B.; Johnson, A. J.; Byrd, J. C.; Tyner, J. W.; Loriaux, M. M.; Deininger, M.; Druker, B. J.; Puri, K. D.; Ulrich, R. G.; Giese, N. A. *Blood*. **2011**, *117*, 5915-5944.
203. Hamblin, N.; Down, K.; Harrison, Z.; Thomas, D.; Vituli, G. GlaxoSmithKline, R&D, Manuscript in preparation.
204. Rowedder, J.; Thomas, D. GlaxoSmithKline, R&D Platform Technology & Science, MDR Biological Sciences UK, Unpublished work.
205. Lewis, D. F. V.; Jacobs, M. N.; Dickins, M. *Drug Discov. Today*. **2004**, *9*, 530-537.

206. Bhattachar, S. N.; Wesley, J. A.; Seadeek, C. J. *Pharm. Biomed. Anal.* **2006**, *41*, 152-157.
207. Fermini, B.; Fossa, A. A. *Nat. Rev. Drug Discov.* **2003**, *2*, 439-447.
208. Edwards, C. GlaxoSmithKline, R&D Respiratory, Translational Sciences UK, Unpublished work.
209. Kerns, E. H.; Di, L. *Drug-like Properties: Concepts, Structure Design and Methods: From ADME to Toxicity Optimization*; Academic Press: 2014.
210. Hamblin, N.; Down, K.; Harrison, Z. GlaxoSmithKline, R&D Respiratory, Unpublished work.
211. Tame, C.; Peace, S.; Hamblin, N.; Down, K.; Harrison, Z. GlaxoSmithKline, R&D Respiratory, Unpublished work.
212. Shaaban, M. R.; El-Sayed, R.; Elwahy, A. H. M. *Tetrahedron.* **2011**, *67*, 6095-6130.
213. Yamamoto, Y.; Arakawa, T.; Ogawa, R.; Itoh, K. *J. Am. Chem. Soc.* **2003**, *125*, 12143-12160.
214. Chang, H. T.; Jeganmohan, M.; Cheng, C. H. *Org. Lett.* **2007**, *9*, 505-508.
215. Stock, L. M.; Spector, A. R. *J. Org. Chem.* **1963**, *28*, 3272-3274.
216. Price, S.; Williams, K.; Savy, P. P.; Dyke, H. J.; Montana, J. G.; Stanley, M. Patent WO2008024725, 2007.
217. Paul, R.; Ali, M. A.; Punniyamurthy, T. *Synthesis.* **2010**, 4268-4272.
218. Laschat, S.; Dickner, T. *Synthesis.* **2000**, 1781-1813.
219. Kotha, S.; Lahiri, K.; Kashinath, D. *Tetrahedron.* **2002**, *58*, 9633-9695.
220. Miyaura, N.; Suzuki, A. *Chem. Rev.* **1995**, *95*, 2457-2483.
221. Miyaura, N.; Yamada, K.; Suzuki, A. *Tetrahedron Lett.* **1979**, 3437-3440.
222. Matos, K.; Soderquist, J. A. *J. Org. Chem.* **1998**, *63*, 461-470.
223. Amatore, C.; Jutand, A.; Le Duc, G. *Chem. Eur. J.* **2011**, *17*, 2492-2503.
224. Whelligan, D. K.; Solanki, S.; Taylor, D.; Thomson, D. W.; Cheung, K. M.; Boxall, K.; Mas-Droux, C.; Barillari, C.; Burns, S.; Grummitt, C. G.; Collins, I.; van Montfort, R. L. M.; Aherne, G. W.; Bayliss, R.; Hoelder, S. J. *Med. Chem.* **2010**, *53*, 7682-7698.
225. Martin, R.; Buchwald, S. L. *Acc. Chem. Res.* **2008**, *41*, 1461-1473.

226. Barder, T. E.; Walker, S. D.; Martinelli, J. R.; Buchwald, S. L. *J. Am. Chem. Soc.* **2005**, *127*, 4685-4696.
227. Brown, W. D.; Jessen, C.; Stroebaek, D. Patent WO2011026891, 2010.
228. Boys, M. L.; Delisle, R. K.; Hicken, E. J.; Kennedy, A. Patent WO2012082689, 2011.
229. Kawata, S.; Matsumoto, K.; Nijima, M.; Takahashi, T. Patent WO2010122980, 2010.
230. Buffat, M. G. P. *Tetrahedron*. **2004**, *60*, 1701-1729.
231. Wu, J.; Tang, W.; Pettman, A.; Xiao, J. *Adv. Synth. Catal.* **2013**, *355*, 35-40.
232. Cheng, C.; Xu, J.; Zhu, R.; Xing, L.; Wang, X.; Hu, Y. *Tetrahedron*. **2009**, *65*, 8538-8541.
233. Ye, Z. S.; Chen, M. W.; Chen, Q. A.; Shi, L.; Duan, Y.; Zhou, Y. G. *Angew. Chem., Int. Ed.* **2012**, *51*, 10181-10184.
234. Seller, R. V.; Reshetov, P. V.; Kriven'ko, A. P. *Chem. Heterocycl. Compd.* **2001**, *37*, 797-821.
235. Zacharie, B.; Moreau, N.; Dockendorff, C. *J. Org. Chem.* **2001**, *66*, 5264-5265.
236. Liu, Y.; Du, H. *J. Am. Chem. Soc.* **2013**, *135*, 12968-12971.
237. Steiner, H.; Giannousis, P.; Pische-Jacques, A.; Blaser, H. U. *Top. Catal.* **2000**, *13*, 191-194.
238. Down, K. GlaxoSmithKline, R&D Respiratory, Unpublished work.
239. Mitsunobu, O. *Synthesis*. **1981**, 1-28.
240. Mitsunobu, O.; Yamada, M. *Bull. Chem. Soc. Jpn.* **1967**, *40*, 2380-2382.
241. Camp, D.; Jenkins, I. D. *J. Org. Chem.* **1989**, *54*, 3045-3049.
242. Camp, D.; Jenkins, I. D. *J. Org. Chem.* **1989**, *54*, 3049-3054.
243. Grochowski, E.; Hilton, B. D.; Kupper, R. J.; Michejda, C. J. *J. Am. Chem. Soc.* **1982**, *104*, 6876-6877.
244. Hughes, D. L.; Reamer, R. A.; Bergan, J. J.; Grabowski, E. J. *J. Am. Chem. Soc.* **1988**, *110*, 6487-6491.
245. Dembinski, R. *Eur. J. Org. Chem.* **2004**, 2763-2772.
246. But, T. Y. S.; Toy, P. H. *Chem. Asian J.* **2007**, *2*, 1340-1355.
247. Tsunoda, T.; Ozaki, F.; Ito, S. *Tetrahedron Lett.* **1994**, *35*, 5081-5082.

248. Knaggs, A. GlaxoSmithKline, R&D Platform Technology & Science, CSci Analytical Chemistry UK, Unpublished work.
249. Jackson, S. GlaxoSmithKline, R&D Platform Technology & Science, CSci Analytical Chemistry UK, Unpublished work.
250. Eschweiler, W. Ber. **1905**, 38, 880-882.
251. Harrison, Z. GlaxoSmithKline, R&D Respiratory, Unpublished work.
252. Iranpoor, N.; Tarrian, T.; Movahedi, Z. Synthesis. **1996**, 1473-1476.
253. Berthel, S. J.; Brinkman, J. Patent WO2009127546, 2009.
254. Cheng, H.; Smith, C. R.; Wang, Y.; Parrott, T. J.; Dress, K. R.; Nair, S. K.; Hoffman, J. E.; Le, P. T. Q.; Kupchinsky, S. W.; Yang, Y.; Cripps, S. J.; Huang, B. Patent WO2005108359, 2005.
255. Baldwin, I.; Fillmore, M.; Hamblin, N.; Down, K. GlaxoSmithKline, R&D Platform Technology & Science, CSci Medicinal Chemistry UK, Unpublished work.
256. Baldwin, I.; Sloan, L.; Washio, Y. GlaxoSmithKline, R&D Platform Technology & Science, CSci Medicinal Chemistry UK, Unpublished work.
257. Kerns, E. H.; Di, L. Toxicity. In *Drug-like Properties: Concepts, Structure Design and Methods - From ADME to Toxicity Optimisation*; Elsevier Ed.; Academic Press: 2014; pp 215-223.
258. GVK Bio, Unpublished work.
259. Itoh, N.; Sakamoto, T.; Miyazawa, E.; Kikugawa, Y. J. Org. Chem. **2002**, 67, 7424-7428.
260. Miller, S. C. Patent WO2009036351, 2008.
261. Sakamoto, T.; Hosoda, I.; Kikugawa, Y. J. Heterocycl. Chem. **1988**, 25, 1279-1281.
262. Surry, D. S.; Buchwald, S. L. Chem. Sci. **2011**, 2, 27-50.
263. Kosugi, M.; Kameyama, M.; Migita, T. Chem. Lett. **1983**, 927-928.
264. Paul, F.; Patt, J.; Hartwig, J. F. J. Am. Chem. Soc. **1994**, 116, 5969-5970.
265. Guram, A. S.; Rennels, R. A.; Buchwald, S. L. Angew. Chem. , Int. Ed. Engl. **1995**, 34, 1348-1350.
266. Louie, J.; Hartwig, J. F. Tetrahedron Lett. **1995**, 36, 3609-3612.
267. Wolfe, J. P.; Wagaw, S.; Buchwald, S. L. J. Am. Chem. Soc. **1996**, 118, 7215-7216.

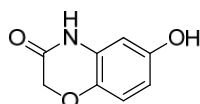
268. Driver, M. S.; Hartwig, J. F. *J. Am. Chem. Soc.* **1996**, *118*, 7217-7218.
269. Wolfe, J. P.; Buchwald, S. L. *J. Org. Chem.* **2000**, *65*, 1144-1157.
270. Guari, Y.; Van Es, D. S.; Reek, J. N. H.; Kamer, P. C. J.; Van Leeuwen, P. W. N. M. *Tetrahedron Lett.* **1999**, *40*, 3789-3790.
271. Huang, X.; Anderson, K. W.; Zim, D.; Jiang, L.; Klapars, A.; Buchwald, S. L. *J. Am. Chem. Soc.* **2003**, *125*, 6653-6655.
272. Charles, M. D.; Schultz, P.; Buchwald, S. L. *Org. Lett.* **2005**, *7*, 3965-3968.
273. Fors, B. P.; Watson, D. A.; Biscoe, M. R.; Buchwald, S. L. *J. Am. Chem. Soc.* **2008**, *130*, 13552-13554.
274. Shekhar, S.; Ryberg, P.; Hartwig, J. F.; Mathew, J. S.; Blackmond, D. G.; Strieter, E. R.; Buchwald, S. L. *J. Am. Chem. Soc.* **2006**, *128*, 3584-3591.
275. Darses, S.; Genet, J. P. *Chem. Rev.* **2008**, *108*, 288-325.
276. Molander, G. A.; Sandrock, D. L. *Org. Lett.* **2007**, *9*, 1597-1600.
277. Greene, T. W.; Wuts, P. G. M. *Protective Groups in Organic Synthesis, 2nd Edition*; 1991; p 473.
278. Bao, R.; Lai, C.; Qian, C. Patent WO2011130628, 2011.
279. Rueckle, T.; Jiang, X.; Gaillard, P.; Church, D.; Vallotton, T. Patent WO2004007491, 2003.
280. Borch, R. F.; Bernstein, M. D.; Durst, H. D. *J. Amer. Chem. Soc.* **1971**, *93*, 2897-2904.
281. Kumar, V. T.; Rao, S. K.; Narayana, L. V.; Dubey, P. K.; V, A. *Heterocycl. Commun.* **2003**, *9*, 51-56.
282. Bertani, B.; Borriello, M.; Bozzoli, A.; Bromidge, S. M.; Granci, E.; Leslie, C.; Serafinowska, H.; Stasi, L.; Vong, A.; Zucchelli, V. Patent WO2004046124, 2003.
283. Mortelmans, K.; Zeiger, E. *Mutat. Res.* **2000**, *455*, 29-60.
284. Combiflash Rf. www.isco.com (accessed on July 2012).
285. Biotage. <http://www.biotage.com> (accessed on July 2012).
286. H-cube. www.thalesnano.com/products/h-cube (accessed on July 2012).
287. Melting point apparatus. www.stuart-equipment.com (accessed on July 2012).

Appendix

Experimental Procedures for Benzoxazine Template

The experimental work was carried out by CRO. All the routes and conditions were designed and selected by the author. Full characterisation of key compounds were carried out by the author.

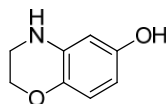
6-Hydroxy-2*H*-benzo[*b*][1,4]oxazin-3(4*H*)-one (313)



Bis(trifluoroacetoxy)iodobenzene (15.5 g, 36.0 mmol) in TFA (80 mL) was added to a stirred solution of 2*H*-benzo[*b*][1,4]oxazin-3(4*H*)-one (4.5 g, 30 mmol) in TFA (90 mL). The mixture was heated to reflux for 20 min. The mixture was then cooled and poured onto chilled water. Insoluble materials were filtered and the resulting filtrate was extracted with EtOAc (2 x 250 mL) and water (300 mL). The combined organic layers were dried with Na₂SO₄ and concentrated under reduced pressure. The crude was basified with NaHCO₃ solution and extracted with EtOAc (2 x 250 mL) and water (300 mL). The combined organic layers were dried with Na₂SO₄ and concentrated under reduced pressure. The resulting solid was washed with ether and EtOAc and finally dried in a vacuum oven to give the title product **313** as a brown solid (3.0 g, 55%). *R*_f (40% EtOAc in pet. ether) = 0.25; ¹H NMR (400 MHz, DMSO-*d*₆) δ 10.54 (s, 1H), 9.14 (s, 1H), 6.73 (d, *J* = 8.8 Hz, 1H), 6.36 (d, *J* = 2.8 Hz, 1H), 6.28 (dd, *J* = 8.7, 2.7 Hz, 1H), 4.43 (s, 2H); LCMS (ESI, formic) *m/z* 164

[*M*-H]⁻, *R*_t = 1.30 min.

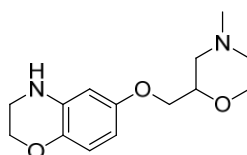
¹H NMR data consistent with those reported in literature. ²⁶⁰ **3,4-Dihydro-2*H*-benzo[*b*][1,4]oxazin-6-ol (311)**



6-Hydroxy-2*H*-benzo[*b*][1,4]oxazin-3(4*H*)-one **313** (2.0 g, 12 mmol) was dissolved

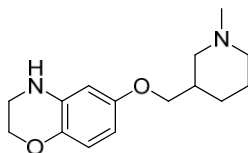
in THF (15 mL) under nitrogen. $\text{BH}_3\cdot\text{DMS}$ (2 M in THF, 24 mL, 48 mmol) was added slowly and the reaction mixture was stirred at room temperature for 70 min. The mixture was cooled to 0 °C and acidified with 2 N aqueous HCl solution. The mixture was then heated at reflux for 20 min, cooled to 0-5 °C and then basified with aqueous NaOH solution. The mixture was extracted with EtOAc (3 x 100 mL) and water. The combined organic layers were washed with water, separated and dried with Na_2SO_4 . Solvent was removed under reduced pressure. The resulting solid was washed with DCM followed by hexane and dried in a vacuum oven to give the title product **311** as a brown solid (1.0 g, 41%). R_f (40% EtOAc in pet. ether) = 0.35; LCMS (ESI, formic) m/z 152 $[\text{M}+\text{H}]^+$, R_t = 1.14 min.

6-((4-Methylmorpholin-2-yl)methoxy)-3,4-dihydro-2H-benzo[*b*][1,4]oxazine (321)



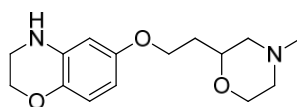
A solution of 3,4-dihydro-2 *H*-benzo[*b*][1,4]oxazin-6-ol **311** (150 mg, 0.992 mmol), (4-methylmorpholin-2-yl)methanol (325 mg, 2.48 mmol) and 2-(tributylphosphoranylidene)acetonitrile (0.78 mL, 2.98 mmol) in toluene (10 mL) under nitrogen was heated at 120 °C for 1 h in a sealed tube. The mixture was then diluted with water and extracted with EtOAc (3 x 100 mL). The combined organic layers were washed with water, dried over Na_2SO_4 and concentrated under reduced pressure. The resulting crude product was purified by normal phase chromatography (5% MeOH in DCM) to give the title product **321** as a brown solid (200 mg, 69%). R_f (10% MeOH in DCM) = 0.3; ^1H NMR (400 MHz, DMSO-d_6) δ 6.51 (d, J = 8.3 Hz, 1H), 6.13 (d, J = 2.9 Hz, 1H), 6.02 (dd, J = 8.7, 2.9 Hz, 1H), 5.72 (br. s, 1H), 3.99 - 4.07 (m, 2H), 3.65 - 3.83 (m, 4H), 3.45 - 3.58 (m, 1H), 3.22 - 3.26 (m, 2H), 2.51 - 2.80 (m, 2H), 2.19 (s, 3H), 1.90 - 2.05 (m, 1H), 1.70 - 1.90 (m, 1H); LCMS (ESI, formic) m/z 265 $[\text{M}+\text{H}]^+$, R_t = 1.19 min.

6-((1-Methylpiperidin-3-yl)methoxy)-3,4-dihydro-2H-benzo[*b*][1,4]oxazine (322)



A solution of 3,4-dihydro-2 *H*-benzo[*b*][1,4]oxazin-6-ol **311** (300 mg, 1.99 mmol), (1-methylpiperidin-3-yl)methanol (0.64 mL, 5.0 mmol) and 2-(tributylphosphoranylidene)acetonitrile (1.56 mL, 5.95 mmol) in toluene (25 mL) under nitrogen was heated to 120 °C for 1 h. The mixture was diluted with water and extracted with EtOAc (2 x 80 mL). The combined organic layers were dried over Na₂SO₄ and concentrated under reduced pressure. The resulting crude product was purified by normal phase chromatography (6 to 10% MeOH in DCM) to give the title product **322** as a brown oil (300 mg, 54%). *R*_f (10% MeOH in DCM) = 0.2; LCMS (ESI, formic) *m/z* 263 [M+H]⁺, *R*_t = 1.25 min.

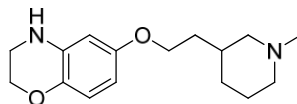
6-(2-(4-Methylmorpholin-2-yl)ethoxy)-3,4-dihydro-2H-benzo[*b*][1,4]oxazine (323)



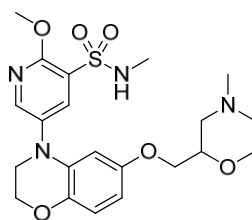
A solution of 3,4-dihydro-2*H*-benzo[*b*][1,4]oxazin-6-ol **311** (100 mg, 0.662 mmol), 2-(4-methylmorpholin-2-yl)ethanol (240 mg, 1.654 mmol) and 2-(tributylphosphoranylidene)acetonitrile (0.52 mL, 1.99 mmol) in toluene (3 mL) under nitrogen was heated to 120 °C for 1 h in a sealed tube. The mixture was then diluted with water and extracted with EtOAc (2 x 80 mL). The combined organic layers were dried over Na₂SO₄ and concentrated under reduced pressure. The resulting crude product was purified by normal phase chromatography (5% MeOH in DCM) to give the title product **323** as a brown solid (100 mg, 54%). *R*_f (10% MeOH in DCM) = 0.3; ¹H NMR (400 MHz, DMSO-*d*₆) δ 6.50 (d, *J* = 8.7 Hz, 1H), 6.13 (d, *J* = 2.9 Hz, 1H), 6.01 (dd, *J* = 8.7, 2.9 Hz, 1H), 5.70 (br. s, 1H), 4.02 (t, *J* = 4.6 Hz, 2H, 2H), 3.87 (t, *J* = 6.41 Hz, 2H), 3.71 - 3.79 (m, 1H), 3.51 - 3.60 (m, 1H), 3.47 (dt, *J* = 11.3, 2.5 Hz,

1H), 3.21 - 3.26 (m, 2H), 2.70 (d, $J = 11.4$ Hz, 1H), 2.59 (d, $J = 11.1$ Hz, 1H), 2.17 (s, 3H), 1.91 - 2.01 (m, 1H), 1.70 - 1.79 (m, 3H); no LCMS recorded.

6-(2-(1-Methylpiperidin-3-yl)ethoxy)-3,4-dihydro-2H-benzo[*b*][1,4]oxazine (324)

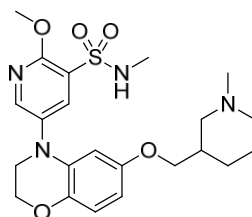


A solution of 3,4-dihydro-2H-benzo[*b*][1,4]oxazin-6-ol **311** (50 mg, 0.33 mmol), 2-(1-methylpiperidin-3-yl)ethanol (118 mg, 0.827 mmol), 2-(tributylphosphoranylidene)acetonitrile (0.26 mL, 0.99 mmol) in toluene (3 mL) under nitrogen was heated to 120 °C for 1 h in a sealed tube. The mixture was diluted with water and extracted with EtOAc (3 x 50 mL). The combined organic layers were dried over Na₂SO₄ and concentrated under reduced pressure. The resulting crude product was purified by preparative TLC to give the title product **324** as a brown solid (10 mg, 11%). R_f (20% MeOH in DCM) = 0.15; ¹H NMR (400 MHz, DMSO-*d*₆) δ 6.50 (d, $J = 8.8$ Hz, 1H), 6.12 (d, $J = 3.1$ Hz, 1H), 6.01 (dd, $J = 8.6, 2.9$ Hz, 1H), 5.70 (br. s, 1H), 4.02 (t, $J = 4.0$ Hz, 2H), 3.83 (t, $J = 6.4$ Hz, 2H), 3.21 - 3.25 (m, 2H), 2.68 - 2.81 (m, 2H), 2.20 (s, 3H), 1.65 - 1.75 (m, 3H), 1.40 - 1.64 (m, 4H), 0.82 - 0.96 (m, 2H); LCMS (ESI, formic) m/z 277 [M+H]⁺, $R_t = 3.17$ min. **2-Methoxy-N-methyl-5-(6-((4-methylmorpholin-2-yl)methoxy)-2Hbenzo[*b*][1,4]oxazin-4(3H)-yl)pyridine-3-sulfonamide (305)**



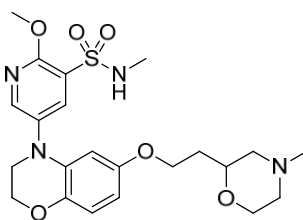
A solution of 6-((4-methylmorpholin-2-yl)methoxy)-3,4-dihydro-2H-benzo[*b*][1,4]oxazine **321** (150 mg, 0.567 mmol), 5-bromo-2-methoxy-N-methylpyridine-3-sulfonamide (239 mg, 0.851 mmol), XPhos (41 mg, 0.085 mmol) and sodium *tert*-butoxide (109 mg, 1.14 mmol) in toluene (10 mL) was degassed for 10 min. Pd₂(dba)₃ (52 mg, 0.057 mmol) was added and the mixture was heated to 130 °C for 30 min in a sealed tube. The mixture was diluted with water (50 mL) and

extracted with EtOAc (3 x 25 mL). The combined organic layers were washed with water, dried over Na₂SO₄ and concentrated under reduced pressure. The resulting crude product was purified by normal phase chromatography (10% MeOH in DCM) and then repurified by reverse phase chromatography (30 to 100% acetonitrile in 0.03 M ammonium acetate over 20 min). Fractions containing the desired product were combined and concentrated under reduced pressure. The resulting product was dissolved in EtOAc (100 mL) and washed with saturated NaHCO₃, brine and dried over on anhydrous Na₂SO₄ and concentrated under reduced pressure to give the title product **305** as a yellow solid (127 mg, 47%). *R*_f (10% MeOH in DCM) = 0.3; ¹H NMR (400 MHz, CDCl₃) δ 8.29 (d, *J* = 2.6 Hz, 1H), 8.09 (d, *J* = 2.6 Hz, 1H), 6.80 (d, *J* = 8.8 Hz, 1H), 6.35 (dd, *J* = 8.9, 2.7 Hz, 1H), 6.23 (d, *J* = 2.8 Hz, 1H), 5.03 (q, *J* = 5.3 Hz, 1H), 4.26 - 4.30 (m, 2H), 4.12 (s, 3H), 3.81 - 3.93 (m, 3H), 3.61 - 3.80 (m, 4H), 2.79 (apparent d, *J* = 11.4 Hz, 1H), 2.71 (d, *J* = 5.3 Hz, 3H), 2.64 (apparent d, *J* = 11.5 Hz, 1H), 2.30 (s, 3H), 2.14 (dt, *J* = 11.5, 3.4 Hz, 1H), 1.90 - 1.98 (m, 1H); LCMS (ESI, formic) *m/z* 465 [M+H]⁺, *R*_t = 3.48 min. **2-Methoxy-*N*-methyl-5-(6-((1-methylpiperidin-3-yl)methoxy)-2*H*benzo[*b*][1,4]oxazin-4(3*H*)-yl)pyridine-3-sulfonamide (306)**



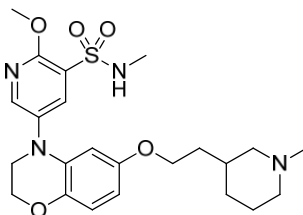
A solution of 6-((1-methylpiperidin-3-yl)methoxy)-3,4-dihydro-2*H*-benzo[*b*][1,4]oxazine **322** (20 mg, 0.076 mmol), 5-bromo-2-methoxy-*N*-methylpyridine-3-sulfonamide (27.9 mg, 0.099 mmol), XPhos (5.45 mg, 0.011 mmol), sodium *tert*-butoxide (14.7 mg, 0.152 mmol) in toluene (1 mL) was degassed for 5 min, then Pd₂(dba)₃ (6.98 mg, 7.62 μmol) was added. The reaction mixture was heated to 120 °C for 30 min. Water (20 mL) was added and product was extracted with EtOAc (3 x 30 mL). The combined organic layers were dried over Na₂SO₄ and the solvent was removed under reduced pressure. The resulting crude product was purified by preparative TLC (4% MeOH in DCM) to give the title product **306** as a pale yellow solid (20 mg, 55%). mp 102-103 °C; ¹H NMR (500 MHz, DMSO-*d*₆) δ 8.36 (s, 1H),

7.98 (s, 1H), 7.45 (br. s, 1H), 6.73 (d, $J = 8.8$ Hz, 1H), 6.30 (d, $J = 8.8$ Hz, 1H), 6.11 (br. s, 1H), 4.21 (br. s, 2H), 4.00 (s, 3H), 3.67 (br. s, 2H), 3.56 - 3.64 (m, 2H), 2.68 (d, $J = 9.9$ Hz, 1H), 2.56 (d, $J = 9.9$ Hz, 1H), 2.47 - 2.52 (br.s, 3H), 2.10 (s, 3H), 1.77 - 1.90 (m, 2H), 1.51 - 1.70 (m, 3H), 1.37 - 1.49 (m, 1H), 0.85 - 0.98 (m, 1H); ^{13}C NMR (126 MHz, DMSO- d_6) δ 156.3 (Ar-C), 153.4 (Ar-C), 147.7 (Ar-CH), 139.1 (Ar-CH), 137.1 (Ar-C), 136.2 (Ar-CH), 133.3 (Ar-C), 122.5 (Ar-C), 117.7 (Ar-CH), 106.3 (Ar-CH), 101.9 (Ar-CH), 71.2 (CH), 64.2 (CH $_2$), 59.1 (CH $_2$), 56.2 (CH $_2$), 54.7 (CH $_3$), 49.2 (CH $_2$), 46.9 (CH $_3$), 36.1 (CH), 29.2 (CH $_3$), 26.7 (CH $_2$), 24.6 (CH $_2$); LCMS (ESI, formic) m/z 463 [M+H] $^+$, $R_t = 2.12$ min; HRMS (ESI) calcd for C $_{22}$ H $_{31}$ N $_4$ O $_5$ S [M+H] $^+$ 463.2010, found 463.2007 (3.6 min); IR (ATR) cm^{-1} 2933, 1594, 1506, 1474, 1419, 1325, 1193, 1162. **2-Methoxy-*N*-methyl-5-(6-(2-(4-methylmorpholin-2-yl)ethoxy)-3,4-dihydro-2H-benzo[*b*][1,4]oxazin-4(3H)-yl)pyridine-3-sulfonamide (307)**



A solution of 6-(2-(4-methylmorpholin-2-yl)ethoxy)-3,4-dihydro-2H-benzo[*b*][1,4]oxazine **323** (150 mg, 0.539 mmol), 5-bromo-2-methoxy-*N*-methylpyridine-3-sulfonamide (227 mg, 0.808 mmol), XPhos (39 mg, 0.081 mmol) and sodium *tert*-butoxide (104 mg, 1.08 mmol) in toluene (5 mL) was degassed for 10 min under nitrogen. Pd $_2$ (dba) $_3$ (49 mg, 0.054 mmol) was added and the mixture was heated at 120 °C for 30 min in a sealed tube. Water (100 mL) was added and product was extracted with (3 x 80 mL). The combined organic layers were dried over Na $_2$ SO $_4$ and concentrated under reduced pressure. The crude product was purified by normal phase chromatography (10% MeOH in DCM) followed by reverse phase chromatography (60 to 100% acetonitrile/MeOH in 0.01 M ammonium acetate in water over 11 min). The fractions containing the desired product were combined and concentrated under reduced pressure. The resulting product was dissolved in EtOAc (100 mL) and washed with saturated NaHCO $_3$, brine and dried over anhydrous Na $_2$ SO $_4$

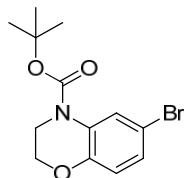
and concentrated under reduced pressure to give the title product **307** as a pale yellow gum (84 mg, 33%). ¹H NMR (400 MHz, CDCl₃) δ 8.29 (d, *J* = 2.6 Hz, 1H), 8.10 (d, *J* = 2.6 Hz, 1H), 6.80 (d, *J* = 9.0 Hz, 1H), 6.35 (dd, *J* = 8.8, 2.9 Hz, 1H), 6.19 (d, *J* = 2.6 Hz, 1H), 4.26 - 4.31 (m, 2H), 4.13 (s, 3H), 3.89 - 3.95 (m, 2H), 3.82 (dd, *J* = 11.6, 2.0 Hz, 1H), 3.64 - 3.69 (m, 3H), 2.71 (d, *J* = 5.0 Hz, 4H), 2.64 (d, *J* = 10.3 Hz, 1H), 2.28 (s, 4H), 1.77 - 1.87 (m, 4H); LCMS (ESI, formic) *m/z* 479 [M+H]⁺, *R*_t = 1.37 min. **2-Methoxy-*N*-methyl-5-(6-(2-(1-methylpiperidin-3-yl)ethoxy)-2*H*benzo[*b*][1,4]oxazin-4(3*H*)-yl)pyridine-3-sulfonamide (308)**



A solution of 6-(2-(1-methylpiperidin-3-yl)ethoxy)-3,4-dihydro-2*H*-benzo[*b*][1,4]oxazine **324** (150 mg, 0.543 mmol), 5-bromo-2-methoxy-*N*-methylpyridine-3-sulfonamide (229 mg, 0.814 mmol), XPhos (39 mg, 0.081 mmol) and sodium *tert*-butoxide (104 mg, 1.09 mmol) in toluene (10 mL) was degassed for 10 min under nitrogen. Pd₂(dba)₃ (50 mg, 0.054 mmol) was added and the reaction mixture was heated to 130 °C for 30 min in a sealed tube. The reaction mixture was diluted with water (50 mL) and product was extracted with EtOAc (3 x 75 mL). The combined organic layers were washed with water, separated and dried over Na₂SO₄. Solvent was removed under reduced pressure. The resulting crude product was purified by normal phase chromatography (10% MeOH in DCM) and then by reverse phase chromatography (20 to 100% acetonitrile in 0.01 M ammonium acetate over 20 min). The fractions containing the desired product were combined and concentrated under reduced pressure. The resulting product was dissolved in EtOAc (100 mL) and washed with saturated NaHCO₃, brine and dried over anhydrous Na₂SO₄ and concentrated under reduced pressure to give the title product **308** as a brown solid (60 mg, 23%). ¹H NMR (400 MHz, CDCl₃) δ 8.29 (d, *J* = 2.6 Hz, 1H), 8.11 (d, *J* = 2.6 Hz, 1H), 6.80 (d, *J* = 8.8 Hz, 1H), 6.34 (dd, *J* = 8.8, 2.9 Hz, 1H), 6.18 (d, *J* = 2.9 Hz, 1H), 5.19 (br. s, 1H), 4.23 - 4.33 (m, 2H), 4.13 (s, 3H), 3.84 (t, *J* = 6.5 Hz, 3H), 3.63 - 3.69 (m, 2H),

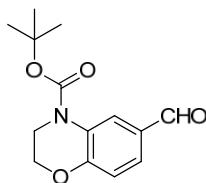
2.76 - 2.86 (m, 2H), 2.72 (s, 3H), 2.26 (s, 3H), 1.50 - 1.94 (m, 7H), 0.82 - 0.98 (m, 1H); LCMS (ESI, formic) m/z 477 [M+H]⁺, R_t = 1.59 min.

***tert*-Butyl 6-bromo-2*H*-benzo[*b*][1,4]oxazine-4(3*H*)-carboxylate (336)**



6-Bromo-3,4-dihydro-2*H*-benzo[*b*][1,4]oxazine (5.00 g, 23.4 mmol) was dissolved in DCM (100 mL). Triethylamine (9.8 mL, 70 mmol) and *N,N*-dimethylaminopyridine (400 mg, 3.27 mmol) were added and the mixture was stirred for 5 min. Di-*tert*-butyl dicarbonate (13.6 mL, 58.4 mmol) was added dropwise and the mixture was stirred overnight at room temperature. The reaction mixture was diluted with water (50 mL) and extracted with EtOAc (3 x 50 mL). The combined organic layers were washed with water, separated and then dried over Na₂SO₄. Solvent was removed under reduced pressure. The crude compound was purified by normal phase chromatography (5% EtOAc in pet. ether) to give the title product **336** as a pale yellow oil (7.0 g, 95%). R_f (20% EtOAc in pet. ether) = 0.6; ¹H NMR (400 MHz, DMSO-*d*₆) δ 8.01 (br. s, 1H), 7.12 (dd, J = 8.8, 2.4 Hz, 1H), 6.83 (d, J = 8.8 Hz, 1H), 4.18 - 4.22 (m, 2H), 3.76 - 3.81 (m, 2H), 1.49 (s, 9H).

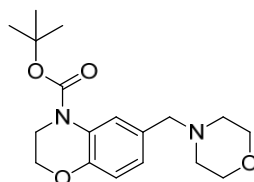
***tert*-Butyl 6-formyl-2*H*-benzo[*b*][1,4]oxazine-4(3*H*)-carboxylate (337)**



A solution of *tert*-butyl 6-bromo -2*H*-benzo[*b*][1,4]oxazine-4(3*H*)-carboxylate **336** (7.0 g, 22 mmol) in THF (100 mL) was cooled to -78 °C. *n*-butyllithium (42 mL, 67 mmol) was added dropwise and stirred for 10 min. DMF (17.2 mL, 223 mmol) was

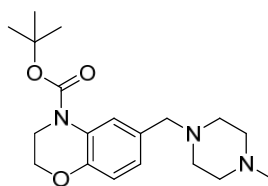
then added dropwise. The mixture was stirred for 10 min and then quenched with 5 mL of acetic acid and stirred at room temperature for 10 min. The mixture was then diluted with water (200 mL), extracted with EtOAc (3 x 100 mL). The combined organic layers were washed with 5% sodium bicarbonate aqueous solution, brine (100 mL) and then dried over Na₂SO₄. Solvent was removed under reduced pressure. The crude compound was purified by normal phase chromatography (10 % EtOAc in pet. ether) to give the title product **337** as a orange solid (3.0 g, 44%). *R_f* (20% EtOAc in pet. ether) = 0.45; ¹H NMR (400 MHz, CDCl₃) δ 9.87 (s, 1H), 8.38 (br. s, 1H), 7.55 (dd, *J* = 8.3, 2.0 Hz, 1H), 6.99 (d, *J* = 8.3 Hz, 1H), 4.33 (dd, *J* = 5.1, 4.1 Hz, 2H), 3.91 (dd, *J* = 5.3, 4.2 Hz, 2H), 1.59 (s, 9H); LCMS (ESI, formic) *m/z* 264 [M+H]⁺, *R_t* = 4.19 min.

***tert*-Butyl-6-(morpholinomethyl)-2*H*-benzo[*b*][1,4]oxazine-4(3*H*)-carboxylate (338)**



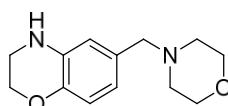
tert-Butyl-6-formyl-2*H*-benzo[*b*][1,4]oxazine-4(3*H*)-carboxylate **337** (1.5 g, 5.7 mmol) was dissolved in DCM (2 mL) and MeOH (0.5 mL). Morpholine (0.496 g, 5.70 mmol) was added followed by acetic acid (0.33 mL, 5.7 mmol) dropwise at 05 °C. The mixture was stirred overnight at rt. The mixture was cooled to 0 °C then NaCNBH₃ (358 mg, 5.70 mmol) was added. The reaction mixture was then stirred at rt for 3 h. The mixture was diluted with water (150 mL) and extracted with EtOAc (3 x 50 mL). The combined organic layer was washed with aqueous solution of ammonium chloride and water (50 mL). The organic layer was dried over Na₂SO₄. Solvent was removed under reduced pressure. The crude compound was purified by normal phase chromatography (40% EtOAc in pet. ether) to give the title product **338** as a red oil (1.0 g, 46%). *R_f* (30% EtOAc in pet. ether) = 0.5; ¹H NMR (400 MHz, CDCl₃) δ 7.72 (br. s, 1H), 6.95 (dd, *J* = 8.3, 2.0 Hz, 1H), 6.82 (d, *J* = 8.3 Hz, 1H), 4.24 (dd, *J* = 5.2, 4.1 Hz, 2H), 3.85 (dd, *J* = 5.2, 4.1 Hz, 2H), 3.67 - 3.73 (m, 4H), 3.41 (s, 2H), 2.30 - 2.56 (m, 4H), 1.61 (s, 9H); LCMS (ESI, formic) *m/z* 335

$[M+H]^+$, $R_t = 1.43$ min. ***tert*-Butyl-6-((4-methylpiperazin-1-yl)methyl)-2*H*-benzo[*b*][1,4]oxazine-4(3*H*)carboxylate (339)**



tert-Butyl-6-formyl-2*H*-benzo[*b*][1,4]oxazine-4(3*H*)-carboxylate **337** (1.5 g, 5.70 mmol) was dissolved in DCM (8 mL) and MeOH (2 mL). 1-methylpiperazine (0.63 mL, 5.7 mmol) was added dropwise at 0-5 °C followed by AcOH (0.33 mL, 5.7 mmol). The mixture was stirred overnight at rt. The mixture was cooled to 0 °C then NaCNBH₃ (358 mg, 5.70 mmol) was added. The reaction mixture was stirred at rt for 3 h. The mixture was diluted with water (100 mL) and extracted with EtOAc (2 x 50 mL). The combined organic layer was washed with water (50 mL) and dried over Na₂SO₄. Solvent was removed under reduced pressure. The crude compound was purified by normal phase chromatography (10% MeOH in DCM) to give the title product **339** as a red oil (1.0 g, 46%). R_f (10% MeOH in DCM) = 0.25; ¹H NMR (400 MHz, CDCl₃) δ 7.73 (br. s, 1H), 6.96 (dd, $J = 8.2, 1.9$ Hz, 1H), 6.83 (d, $J = 8.1$ Hz, 1H), 4.21-4.26 (m, 2H), 3.82 - 3.89 (m, 2H), 3.50 (s, 2H), 2.57 - 2.82 (m, 8H), 2.47 (s, 3H), 1.55 (s, 9H); LCMS (ESI, formic) m/z 348 $[M+H]^+$, $R_t = 5.10$ min.

6-(Morpholinomethyl)-3,4-dihydro-2*H*benzo[*b*][1,4]oxazine (340)



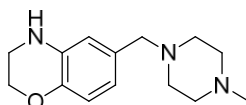
tert-Butyl 6-(morpholinomethyl)-2*H*-benzo[*b*][1,4]oxazine-4(3*H*)-carboxylate **338** (1.0 g, 3.0 mmol) was dissolved in 1,4-dioxane (3 mL) and cooled to 0-5 °C. HCl in dioxane (4 M, 15 mL, 60 mmol) was added dropwise and the reaction mixture was stirred for 5 h. Solvent was removed under reduced pressure. The resulting product was diluted with water (50 mL) and basified with aqueous NaHCO₃ solution. Product was then extracted with EtOAc (3 x 30 mL). The combined organic layer was washed

with water (50 mL), dried over Na₂SO₄. Solvent was removed under reduced pressure to give the title product **340** as a red oil (500 mg, 67%). *R*_f (EtOAc) = 0.35;

¹

¹H NMR (400 MHz, DMSO-*d*₆) δ 6.54 (d, *J* = 8.1 Hz, 1H), 6.51 (d, *J* = 2.0 Hz, 1H), 6.36 (dd, *J* = 8.0, 1.9 Hz, 1H), 5.70 (br. s, 1H), 4.07 (t, *J* = 4.2 Hz, 2H), 3.47 - 3.49 (m, 4H), 3.21 - 3.26 (m, 4H), 2.29 (br. s, 4H); LCMS (ESI, formic) *m/z* 235 [M+H]⁺, *R*_t = 1.17 min.

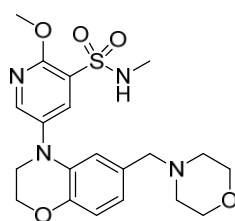
6-((4-Methylpiperazin-1-yl)methyl)-3,4-dihydro-2H-benzo[*b*][1,4]oxazine (341)



tert-Butyl 6-((4-methylpiperazin-1-yl)methyl)-2H-benzo[*b*][1,4]oxazine-4(3H)-carboxylate **339** (1.0 g, 2.9 mmol) was dissolved in 1,4-dioxane (3 mL) and cooled to 0-5 °C. HCl in dioxane (4 M, 15 mL, 60 mmol) was added dropwise and the reaction mixture was stirred for 5 h. Solvent was removed under reduced pressure. The resulting product was diluted with water (100 mL) and basified with aqueous NaHCO₃ solution. Product was then extracted with EtOAc (3 x 50 mL). The combined organic layer was washed with water (100 mL), dried over Na₂SO₄. Solvent was removed under reduced pressure to give the title product **111** as red oil

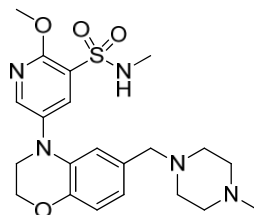
(500 mg, 70%). *R*_f (10% MeOH in DCM) = 0.25; ¹H NMR (400 MHz, DMSO-*d*₆) δ 6.53 (d, *J* = 8.1 Hz, 1H), 6.49 (d, *J* = 2.0 Hz, 1H), 6.34 (dd, *J* = 8.0, 2.0 Hz, 1H), 5.68 (br. s, 1H), 4.07 (t, *J* = 4.2 Hz, 2H), 3.57 (s, 2H), 3.20 - 3.27 (m, 2H), 2.22 - 2.36 (m, 8H), 2.13 (s, 3H).

2-Methoxy-*N*-methyl-5-(6-(morpholinomethyl)-2*H*-benzo[*b*][1,4]oxazin-4(3*H*yl)pyridine-3-sulfonamide (329)



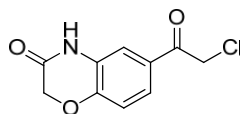
A solution of 6-(morpholinomethyl)-3,4-dihydro-2*H*-benzo[*b*][1,4]oxazine **340** (500 mg, 2.13 mmol), 5-bromo-2-methoxy-*N*-methylpyridine-3-sulfonamide (900 mg, 3.20 mmol), XPhos (153 mg, 0.320 mmol) and sodium *tert*-butoxide (410 mg, 4.27 mmol) in toluene (10 mL) was degassed for 5 min with nitrogen. Pd₂(dba)₃ (195 mg, 0.213 mmol) was added and the mixture was heated to 130 °C stirred for 30 min in a sealed tube. The mixture was diluted with water (100 mL) and extracted with EtOAc (50 mL). The combined organic layer was washed with water (100 mL) and dried over Na₂SO₄. Solvent was removed under reduced pressure. The crude product was purified by normal phase chromatography (50% EtOAc in pet. ether) and then repurified by reverse phase chromatography (60 to 100% acetonitrile/MeOH in 0.01 M ammonium acetate in water over 11 min). The fractions containing the desired product were combined and concentrated under reduced pressure. The resulting product was dissolved in EtOAc (100 mL) and washed with saturated NaHCO₃, brine and dried over anhydrous Na₂SO₄ and concentrated under reduced pressure to give the title product **329** as a pale yellow solid (348 mg, 37%). mp 79-81 °C; *R*_f (50% EtOAc in pet. ether) = 0.35; ¹H NMR (500 MHz, DMSO-*d*₆) δ 8.35 (s, 1H), 7.96 (s, 1H), 7.37 - 7.43 (m, 1H), 6.78 (d, *J* = 8.2 Hz, 1H), 6.65 (d, *J* = 8.2 Hz, 1H), 6.60 (s, 1H), 4.24 (br. s, 2H), 4.00 (s, 3H), 3.70 (br. s, 2H), 3.50 (br. s, 4H), 3.22 (s, 2H), 2.45 - 2.52 (m, 3H), 2.25 (br. s, 4H); ¹³C NMR (126 MHz, DMSO-*d*₆) δ 155.9 (Ar-C), 147.0 (Ar-CH), 144.2 (Ar-C), 137.6 (Ar-C), 135.6 (Ar-CH), 132.1 (Ar-C), 130.6 (Ar-C), 122.3 (Ar-C), 121.6 (Ar-CH), 117.1 (Ar-CH), 116.5 (Ar-CH), 66.6 (CH₂), 64.3 (CH₂), 62.5 (CH₂), 54.7 (CH₃), 53.4 (2 CH₂), 49.1 (2 CH₂), 29.2 (CH₃); LCMS (ESI, formic) *m/z* 433 [M-H]⁻, *R*_t = 3.75 min; HRMS (ESI) calcd for C₂₀H₂₇N₄O₅S [M+H]⁺ 435.1697, found 435.1685 (3.1 min); IR

(ATR) cm^{-1} 2805, 1508, 1474, 1419, 1327, 1298, 1259, 1161, 1112. **2-Methoxy-N-methyl-5-(6-((4-methylpiperazin-1-yl)methyl)-2Hbenzo[*b*][1,4]oxazin-4(3H)-yl)pyridine-3-sulfonamide (330)**



A solution of 6-((4-methylpiperazin-1-yl)methyl)-3,4-dihydro-2H-benzo[*b*][1,4]oxazine **341** (500 mg, 2.02 mmol), 5-bromo-2-methoxy-N-methylpyridine-3-sulfonamide (852 mg, 3.03 mmol), XPhos (145 mg, 0.303 mmol) and sodium *tert*-butoxide (389 mg, 4.04 mmol) in toluene (5 mL) was degassed for 5 min with nitrogen. $\text{Pd}_2(\text{dba})_3$ (185 mg, 0.202 mmol) was added and the reaction mixture was heated at 130 °C stirred for 30 min in a sealed tube. The mixture was diluted with water (100 mL) and extracted with EtOAc (3 x 50 mL). The combined organic layer was washed with (100 mL) and dried over Na_2SO_4 . Solvent was evaporated under reduced pressure. The crude compound was purified by normal phase chromatography (10% MeOH in DCM) and then purified by reverse phase chromatography (30 to 65% acetonitrile/MeOH in 0.1% formic acid in water over 12 min). The fractions containing the desired product were combined and concentrated under reduced pressure. The resulting product was dissolved in EtOAc (100 mL) and washed with saturated NaHCO_3 , brine and dried over anhydrous Na_2SO_4 and concentrated under reduced pressure to give the title product **330** as a pale yellow solid (71 mg, 8%). mp 100 °C (dec.); R_f (10% MeOH in DCM) = 0.2; ^1H NMR (500 MHz, DMSO-d_6) δ 8.34 (s, 1H), 7.95 (s, 1H), 7.41 (br. s, 1H), 6.77 (d, $J = 8.2$ Hz, 1H), 6.63 (d, $J = 8.2$ Hz, 1H), 6.57 (s, 1H), 4.24 (br. s, 2H), 4.00 (s, 3H), 3.69 (br. s, 2H), 3.21 (s, 2H), 2.46 - 2.51 (m, 3H), 2.24 (br. s, 8H), 2.10 (s, 3H); ^{13}C NMR (126 MHz, DMSO-d_6) δ 156.0 (Ar-C), 147.2 (Ar-CH), 144.1 (Ar-C), 137.6 (Ar-C), 135.7 (Ar-CH), 132.2 (Ar-C), 131.1 (Ar-C), 122.3 (Ar-C), 121.4 (Ar-CH), 117.1 (Ar-CH), 116.3 (Ar-CH), 64.3 (CH_2), 62.1 (CH_2), 55.1 (CH_2 , 2C), 54.7 (CH_3), 52.8 (CH_2 , 2C), 49.1 (CH_2), 46.2 (CH_3), 29.2 (CH_3); LCMS (ESI, formic) m/z 448 $[\text{M}+\text{H}]^+$, $R_t = 3.49$ min; HRMS (ESI) calcd for $\text{C}_{21}\text{H}_{30}\text{N}_5\text{O}_4\text{S}$ $[\text{M}+\text{H}]^+$ 448.2013, found 448.2009 (2.9 min); IR (ATR) cm^{-1}

2802, 1514, 1477, 1420, 1327, 1160. **6-(2-Chloroacetyl)-2H-benzo[*b*][1,4]oxazin-3(4*H*)-one (348)**



2*H*-benzo[*b*][1,4]oxazin-3(4*H*)-one (2.0 g, 13 mmol) was dissolved in DCM (100 mL). 2-chloroacetyl chloride (1.9 mL, 24 mmol) was added slowly. The mixture was cooled to 0 °C and anhydrous AlCl₃ (5.36 g, 40.2 mmol) was added in 5 equivalent portions. The temperature was then slowly raised 20 °C and the mixture was stirred for 12 h. The mixture was quenched into ice water containing HCl. The solid formed was collected by filtration to give the title product **348** as an off-white solid (2.1 g, 69% yield). *R*_f (30% EtOAc in pet ether) = 0.3; ¹H NMR (400 MHz, DMSO-*d*₆) δ 10.92 (s, 1H), 7.62 (dd, *J* = 8.4, 2.1 Hz, 1H), 7.47 (d, *J* = 2.2 Hz, 1H), 7.07 (d, *J* = 8.3 Hz, 1H), 5.10 (s, 2H), 4.70 (s, 2H); LCMS (ESI, formic) *m/z* 224 [MH]⁻, *R*_t = 3.37 min.

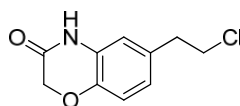
¹

H NMR consistent with data from commercial reagent (Aldrich CAS 26518-76-3).

¹

H NMR (400 MHz, DMSO-*d*₆) δ 10.90 (s, 1H), 7.62 (dd, *J* = 8.4 2.1 Hz, 1H), 7.48 (d, *J* = 2.0 Hz, 1H), 7.07 (d, *J* = 8.6 Hz, 1H), 5.08 (s, 2H), 4.70 (s, 2H).

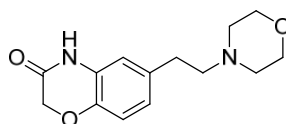
6-(2-Chloroethyl)-2H-benzo[*b*][1,4]oxazin-3(4*H*)-one (347)



A solution of 6-(2-chloroacetyl)-2*H*-benzo[*b*][1,4]oxazin-3(4*H*)-one **348** (2.0 g, 8.7 mmol) in TFA (5.4 mL, 70 mmol) was cooled to 0 °C and triethylsilane (3.3 mL, 20 mmol) was added dropwise. The reaction mixture was stirred under nitrogen at 0 °C for 10 min and then warmed to 45 °C for 20 min and then allowed to stir at room temperature overnight. The mixture was poured into ice, quenched with saturated NaHCO₃ and then extracted with EtOAc. The crude compound was purified by pentane washing to give the title product **347** as a pale yellow solid (1.8 g, 92%). *R*_f (30%

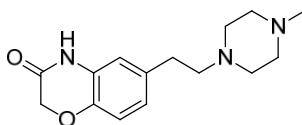
EtOAc in pet. ether) = 0.4; $^1\text{H NMR}$ (400 MHz, DMSO-d_6) δ 10.70 (s, 1H), 6.86 (d, $J = 8.0$ Hz, 1H), 6.83 (dd, $J = 8.1, 2.0$ Hz, 1H), 6.77 (d, $J = 2.0$ Hz, 1H), 4.53 (s, 2H), 3.77 (t, $J = 7.0$ Hz, 2H), 2.93 (t, $J = 7.0$ Hz, 2H); LCMS (ESI, formic) m/z 210 $[\text{M-H}]^-$, $R_t = 5.16$ min.

6-(2-Morpholinoethyl)-2H-benzo[*b*][1,4]oxazin-3(4H)-one (349)



6-(2-Chloroethyl)-2H-benzo[*b*][1,4]oxazin-3(4H)-one **347** (1.3 g, 6.1 mmol) was dissolved in DMF (15 mL). Potassium iodide (0.51 g, 3.07 mmol) was added followed by morpholine (1.6 mL, 18 mmol) at room temperature for 4 h and then heated to 110 °C for 4 h. The reaction mixture was diluted with ice water (2 x 150 mL) and extracted with EtOAc (2 x 150 mL). The combined organic layer was dried over Na_2SO_4 . Solvent was evaporated under reduced pressure. The crude compound was washed with pentane to give the title product **349** as a brown solid (1.3 g, 81%). R_f (10% MeOH in DCM) = 0.35 ; $^1\text{H NMR}$ (400 MHz, DMSO-d_6) δ 10.63 (s, 1H), 6.84 (d, $J = 8.1$ Hz, 1H), 6.71 - 6.79 (m, 2H), 4.51 (s, 2H), 3.57 (apparent t, $J = 4.5$ Hz, 4H), 2.58 - 2.66 (m, 2H), 2.36-2.46 (m, 6H).

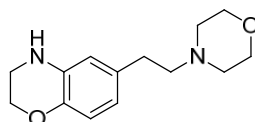
6-(2-(4-Methylpiperazin-1-yl)ethyl)-2H-benzo[*b*][1,4]oxazin-3(4H)-one (350)



6-(2-chloroethyl)-2H-benzo[*b*][1,4]oxazin-3(4H)-one **347** (1.5 g, 7.1 mmol) was dissolved in DMF (40 mL). Potassium iodide (0.588 g, 3.54 mmol) was added followed by 1-methylpiperazine (2.13 g, 21.3 mmol) at room temperature for 4 h and then heated to 110 °C for 16 h. The reaction mixture was diluted with EtOAc (2 x 100 mL) and washed with ice water twice. The combined organic layer was washed with brine and dried over Na_2SO_4 . Solvent was evaporated under reduced pressure.

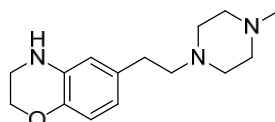
The crude compound was washed with pentane to give the title product **350** as a pale yellow solid (1.5 g, 47%, 61% area by LCMS). Progressed directly to the next step without further purification. R_f (10% MeOH in DCM) = 0.25; LCMS (ESI, formic) m/z 276 $[M+H]^+$, R_t = 2.89 min (61%).

6-(2-Morpholinoethyl)-3,4-dihydro-2H-benzo[b][1,4]oxazine (351)



6-(2-Morpholinoethyl)-2H-benzo[b][1,4]oxazin-3(4H)-one **349** (1.2 g, 4.6 mmol) was suspended in THF (30 mL) under nitrogen and $BH_3 \cdot DMS$ (2 M, 9.15 mL, 18.3 mmol) was added dropwise over 5 min. The mixture was stirred at room temperature for 70 min. The reaction mixture was cooled to 0 °C and acidified using 3 N HCl aqueous solution. After the addition, the reaction was refluxed for 10 min, cooled and basified with 6 N NaOH aqueous solution. Product was extracted with EtOAc twice. The combined organic layer was dried and concentrated under reduced pressure. The crude product was purified by normal phase chromatography (2% MeOH in DCM) to give the title product **351** as a off-white solid (600 mg, 52%). R_f (10% MeOH in DCM) = 0.32; 1H NMR (400 MHz, $DMSO-d_6$) δ 6.51 (d, J = 7.9 Hz, 1H), 6.38 (d, J = 2.0 Hz, 1H), 6.29 (dd, J = 8.0, 2.1 Hz, 1H), 5.61 (br. s, 1H), 4.06 (t, J = 4.4 Hz, 2H), 3.57 (apparent t, J = 4.6 Hz, 4H), 3.20 - 3.26 (m, 2H), 2.50 - 2.56 (m, 2H), 2.36 - 2.44 (m, 6H); LCMS (ESI, formic) m/z 249 $[M+H]^+$, R_t = 3.32 min.

6-(2-(4-Methylpiperazin-1-yl)ethyl)-3,4-dihydro-2H-benzo[b][1,4]oxazine (352)

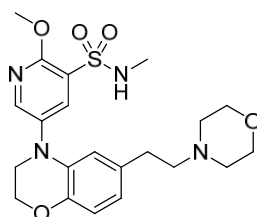


6-(2-(4-Methylpiperazin-1-yl)ethyl)-2H-benzo[b][1,4]oxazin-3(4H)-one **350** (400 mg, 1.45 mmol) was suspended in THF (20 mL) under nitrogen. $BH_3 \cdot DMS$ (2.91 mL, 5.81 mmol) was added dropwise over 5 min. The reaction mixture was stirred at

room temperature for 70 min. The reaction mixture was then cooled to 0 °C and acidified with 3 N HCl aqueous solution. The reaction mixture was refluxed for 10 min, cooled and basified with 6 N NaOH aqueous solution. Product was extracted with EtOAc. The combined organic layer was dried and concentrated under reduced pressure. The crude product was purified by normal phase chromatography (2% MeOH in DCM) to give the title product **352** as a off-white solid (200 mg, 53%).

LCMS (ESI, formic) m/z 262 $[M+H]^+$, R_t = 3.32 min.

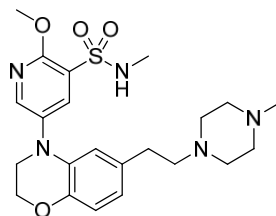
2-Methoxy-*N*-methyl-5-(6-(2-morpholinoethyl)-2*H*-benzo[*b*][1,4]oxazin-4(3*H*yl)pyridine-3-sulfonamide (342)



A solution of 6-(2-morpholinoethyl)-3,4-dihydro-2-*H*-benzo[*b*][1,4]oxazine **351** (500 mg, 2.01 mmol), 5-bromo-2-methoxy-*N*-methylpyridine-3-sulfonamide (736 mg, 2.62 mmol), XPhos (144 mg, 0.302 mmol) and sodium *tert*-butoxide (387 mg, 4.03 mmol) in toluene (30 mL). The mixture was degassed for 10 min. Pd₂(dba)₃ (184 mg, 0.201 mmol) was added and the reaction mixture was heated at 130 °C in sealed tube for 30 min. The reaction mixture was diluted with EtOAc (2 x 100 mL) and washed with water (100 mL). The combined organic layer was dried and concentrated under reduced pressure. The crude product was purified by normal phase chromatography (5% MeOH in DCM) followed by reverse phase chromatography (35 to 65% acetonitrile/MeOH in 0.01 M ammonium acetate in water over 15 min). The fractions containing the desired product were combined and concentrated under reduced pressure. The resulting product was dissolved in EtOAc (30 mL) and washed with saturated NaHCO₃, brine and dried over anhydrous Na₂SO₄ and concentrated under reduced pressure to give the title product **342** as a green solid (110 mg, 12%). R_f (10% MeOH in DCM) = 0.4; ¹H NMR (500 MHz, DMSO-*d*₆) δ 8.34 (br. s, 1H), 7.95 (br. s, 1H), 7.41 (br. s, 1H), 6.73 (br. s, 1H), 6.52 -

6.62 (m, 2H), 4.23 (br. s, 2H), 3.99 (s, 3H), 3.67 (br. s, 2H), 3.50 (br. s, 4H), 2.46 - 2.53 (m, 5H), 2.25 - 2.40 (m, 6H); ¹³C NMR (126 MHz, DMSO-d₆) δ 156.0 (Ar-C), 147.2 (Ar-CH), 143.3 (Ar-C), 137.6 (Ar-C), 135.7 (Ar-CH), 133.4 (Ar-C), 132.2 (Ar-C), 122.4 (Ar-C), 121.0 (Ar-CH), 117.2 (Ar-CH), 116.1 (Ar-CH), 66.6 (CH₂), 64.3 (CH₂), 60.7 (2 CH₂), 54.7 (CH₃), 53.7 (2 CH₂), 49.1 (CH₂), 32.2 (CH₂), 29.2 (CH₃); LCMS (ESI, formic) *m/z* 449.38 [M+H]⁺, R_t = 1.20 min; HRMS (ESI) calcd for C₂₁H₂₉N₄O₅S [M+H]⁺ 449.1853, found 449.1858 (3.2 min); IR (ATR) cm⁻¹ 2948, 2857, 1585, 1508, 1474, 1419, 1327, 1299, 1259, 1161, 1113.

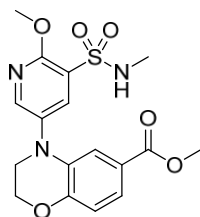
2-Methoxy-*N*-methyl-5-(6-(2-(4-methylpiperazin-1-yl)ethyl)-2*H*benzo[*b*][1,4]oxazin-4(3*H*)-yl)pyridine-3-sulfonamide (343)



A solution of 6-(2-(4-methylpiperazin-1-yl)ethyl)-3,4-dihydro-2*H*-benzo[*b*][1,4]oxazine **352** (600 mg, 2.30 mmol), 5-bromo-2-methoxy-*N*-methylpyridine-3-sulfonamide (839 mg, 2.98 mmol), XPhos (164 mg, 0.344 mmol) and sodium *tert*-butoxide (441 mg, 4.59 mmol) in toluene (40 mL) was degassed for 10 min. Pd₂(dba)₃ (210 mg, 0.230 mmol) was added and the reaction mixture was heated to 130 °C in sealed tube for 30 min. The reaction mixture was diluted with EtOAc (2 x 100 mL) and washed with water (100 mL). The combined organic layer was dried and concentrated. The crude compound was purified by normal phase chromatography (2% MeOH in DCM) and then by reverse phase chromatography (30 to 70% acetonitrile/MeOH in 10 mM ammonium acetate in water over 10 min). The fractions containing the desired product were combined and concentrated under reduced pressure. The resulting product was dissolved in EtOAc (30 mL) and washed with saturated NaHCO₃, brine and dried over anhydrous Na₂SO₄ and concentrated under reduced pressure to give the title product **343** (115 mg, 11%). mp 159-160 °C

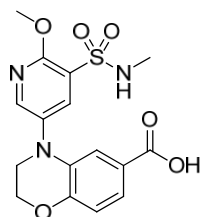
¹H NMR (400 MHz, DMSO-*d*₆) δ 8.34 (d, *J* = 2.6 Hz, 1H), 7.95 (d, *J* = 2.8 Hz, 1H), 7.42 (q, *J* = 4.8 Hz, 1H), 6.72 (d, *J* = 7.9 Hz, 1H), 6.51 - 6.60 (m, 2H), 4.19 - 4.25 (m, 2H), 3.99 (s, 3H), 3.65 - 3.70 (m, 2H), 2.44 - 2.52 (m, 7H), 2.23 - 2.37 (m, 8H), 2.11 (s, 3H); ¹³C NMR (126 MHz, DMSO-*d*₆) δ 156.0 (Ar-C), 147.2 (Ar-CH), 143.3 (Ar-C), 137.6 (Ar-C), 135.7 (Ar-CH), 133.5 (Ar-C), 132.2 (Ar-C), 122.4 (Ar-C), 121.0 (Ar-CH), 117.1 (Ar-CH), 116.1 (Ar-CH), 64.3 (CH₂), 60.4 (CH₂), 55.2 (2 CH₂), 54.7 (CH₃), 53.0 (2 CH₂), 49.1 (CH₂), 46.2 (CH₃), 32.6 (CH₂), 29.2 (CH₃); LCMS (ESI, formic) *m/z* 462 [M+H]⁺, *R*_t = 1.23 min; HRMS (ESI) calcd for C₂₂H₃₂N₅O₄S [M+H]⁺ 462.2170, found 462.2161 (3.0 min); IR (ATR) cm⁻¹ 2931, 2795, 1507, 1477, 1420, 1377, 1319, 1256, 1158.

Methyl 4-(6-methoxy-5-(*N*-methylsulfamoyl)pyridin-3-yl)-3,4-dihydro-2*H*benzo[*b*][1,4]oxazine-6-carboxylate (359)



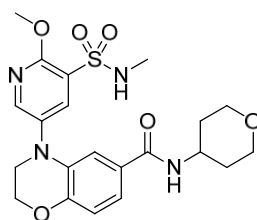
A solution of methyl 3,4-dihydro-2-*H*-benzo[*b*][1,4]oxazine-6-carboxylate (1.0 g, 5.2 mmol), 5-bromo-2-methoxy-*N*-methylpyridine-3-sulfonamide (2.18 g, 7.76 mmol), XPhos (0.370 g, 0.776 mmol) and sodium *tert*-butoxide (0.995 g, 10.4 mmol) in toluene (25 mL) was degassed for 5 min with nitrogen. Pd₂(dba)₃ (0.474 g, 0.518 mmol) was added and the mixture was heated at 130 °C for 30 min in a sealed tube. The reaction mixture was diluted with water (200 mL) and extracted with EtOAc (3 x 100 mL). The combined organic layer was washed with water (200 mL), dried over Na₂SO₄ and concentrated under reduced pressure. The crude compound was purified by normal phase chromatography (40% EtOAc in pet. ether) to give the title product **359** as a yellow solid (800 mg, 33%). *R*_f (30% EtOAc in pet.

ether) = 0.3; LCMS (ESI, formic) m/z 394 [M+H]⁺, R_t = 1.89 min. **4-(6-Methoxy-5-(*N*-methylsulfamoyl)pyridin-3-yl)-3,4-dihydro-2*H*benzo[*b*][1,4]oxazine-6-carboxylic acid (357)**



Methyl-4-(6-methoxy-5-(*N*-methylsulfamoyl)pyridin-3-yl)-3,4-dihydro-2*H*-benzo[*b*][1,4]oxazine-6-carboxylate (800 mg, 2.03 mmol) was suspended in THF (10 mL). LiOH (97 mg, 4.1 mmol) in water (10 mL) was added and the mixture was stirred for 5 h at room temperature. Solvent was removed under reduced pressure. The resulting crude product was acidified with citric acid. The solid obtained was filtered and washed with hexane and dried to give the title product **357** as a yellow solid (500 mg, 65%). R_f (EtOAc) = 0.2; ¹H NMR (400 MHz, DMSO-*d*₆) δ 12.52 (br. s, 1H), 8.41 (d, J = 2.6 Hz, 1H), 8.01 (d, J = 2.6 Hz, 1H), 7.47 (q, J = 5.0 Hz, 1H), 7.33 (dd, J = 8.3, 2.0 Hz, 1H), 7.14 (d, J = 2.0 Hz, 1H), 6.91 (d, J = 8.3 Hz, 1H), 4.33 - 4.40 (m, 2H), 4.02 (s, 3H), 3.68 - 3.79 (m, 2H), 2.47 - 2.52 (m, 3H).

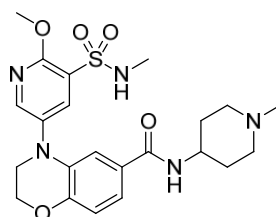
4-(6-Methoxy-5-(*N*-methylsulfamoyl)pyridin-3-yl)-*N*-(tetrahydro-2*H*-pyran-4-yl)-3,4-dihydro-2*H*-benzo[*b*][1,4]oxazine-6-carboxamide (353)



Tetrahydro-2*H*-pyran-4-amine (88 mg, 0.870 mmol) was dissolved in DMF (4 mL). 4-(6-methoxy-5-(*N*-methylsulfamoyl)pyridin-3-yl)-3,4-dihydro-2*H*benzo[*b*][1,4]oxazine-6-carboxylic acid **357** (300 mg, 0.791 mmol), DIPEA (0.35 mL, 1.98 mmol) and HATU (331 mg, 0.870 mmol) were added. The mixture was stirred at room temperature for 4 h. The mixture was diluted with ice water (30 mL)

and then extracted with EtOAc (2 x 30 mL). The combined organic layer was washed with brine, dried over Na₂SO₄ and concentrated under reduced pressure. The crude compound was purified by normal phase chromatography (10% MeOH in DCM) to give the title product **353** as a off-white solid (72 mg, 19%). *R_f* (10% MeOH in DCM) = 0.4; ¹H NMR (500 MHz, DMSO-*d*₆) δ 8.38 (s, 1H), 7.95 - 8.02 (m, 2H), 7.41 - 7.47 (m, 1H), 7.30 (d, *J* = 8.2 Hz, 1H), 7.15 (s, 1H), 6.88 (d, *J* = 8.2 Hz, 1H), 4.32 (br. s, 2H), 4.01 (s, 3H), 3.79 - 3.93 (m, 3H), 3.72 (br. s, 2H), 2.46 - 2.52 (m, 3H), 1.65 (br. d, *J* = 11.5 Hz, 2H), 1.42 - 1.55 (m, 2H), 2NH not visible; ¹³C NMR (126 MHz, DMSO-*d*₆) δ 165.3 (C=O), 156.4 (Ar-C), 147.6 (Ar-CH), 147.4 (Ar-C), 137.1 (Ar-CH), 136.2 (Ar-C), 132.6 (Ar-C), 127.8 (Ar-C), 122.6 (Ar-C), 119.8 (Ar-CH), 116.8 (Ar-CH), 115.0 (Ar-CH), 66.7 (2 CH₂), 64.8 (CH₂), 54.8 (CH₃), 48.7 (CH₂), 46.1 (CH), 32.9 (2 CH₂), 29.2 (CH₃); LCMS (ESI, formic) *m/z* 463 [M+H]⁺, *R_t* = 3.43 min; HRMS (ESI) calcd for C₂₁H₂₇N₄O₆S [M+H]⁺ 463.1646, found 463.1630 (4.2 min).

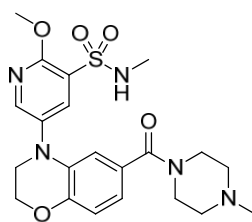
4-(6-Methoxy-5-(*N*-methylsulfamoyl)pyridin-3-yl)-*N*-(1-methylpiperidin-4-yl)3,4-dihydro-2Hbenzo[*b*][1,4]oxazine-6-carboxamide (354)



A solution of 1-methylpiperidin-4-amine (26.5 mg, 0.232 mmol), 4-(6-methoxy-5-(*N*-methylsulfamoyl)pyridin-3-yl)-3,4-dihydro-2H-benzo[*b*][1,4]oxazine-6-carboxylic acid **357** (80 mg, 0.211 mmol), DIPEA (92 μL, 0.53 mmol) and HATU (88 mg, 0.232 mmol) in DMF (3 mL) was stirred at room temperature for 3 h. The reaction mixture was diluted with ice water (30 mL) and then extracted with EtOAc (30 mL x 2). The combined organic was washed with brine, dried over Na₂SO₄ and concentrated under reduced pressure. The crude compound was purified by normal phase chromatography (10% MeOH in DCM) to give the title product **354** as a offwhite solid (40 mg, 38%). *R_f* (10 % MeOH in DCM) = 0.3; mp decomp. > 200 °C ¹H NMR (500 MHz, DMSO-*d*₆) δ 8.38 (d, *J* = 1.7 Hz, 1H), 7.96 (d, *J* = 1.9 Hz, 1H),

7.92 (d, $J = 7.7$ Hz, 1H), 7.44 (br. s, 1H), 7.29 (d, $J = 8.2$ Hz, 1H), 7.14 (s, 1H), 6.87 (d, $J = 8.2$ Hz, 1H), 4.32 (br. s, 2H), 4.01 (s, 3H), 3.72 (br. s, 2H), 3.57 - 3.66 (m, 1H), 2.71 (d, $J = 11.3$ Hz, 2H), 2.49 (br. s, 3H), 2.12 (s, 3H), 1.87 (t, $J = 11.4$ Hz, 2H), 1.65 (d, $J = 11.0$ Hz, 2H), 1.41 - 1.55 (m, 2H); ^{13}C NMR (126 MHz, DMSO- d_6) δ 165.4 (C=O), 156.3 (Ar-C), 147.6 (Ar-CH), 147.3 (Ar-C), 137.1 (Ar-C), 136.1 (ArCH), 132.6 (Ar-C), 127.9 (Ar-C), 122.6 (Ar-C), 119.8 (Ar-CH), 116.8 (Ar-CH), 115.0 (Ar-CH), 64.8 (CH₂), 55.0 (CH₂, 2C), 54.8 (CH₃), 48.7 (CH₂), 46.9 (CH), 46.4 (CH₃), 31.9 (CH₂, 2C), 29.2 (CH₃); LCMS (ESI, formic) m/z 476 [M+H]⁺, $R_t = 1.16$ min; HRMS (ESI) calcd for C₂₂H₃₀N₅O₅S [M+H]⁺ 476.1932, found 476.1949 (3.1 min); IR (ATR) cm⁻¹ 2940, 1639, 1606, 1543, 1503, 1477, 1420, 1379, 1325, 1265, 1158.

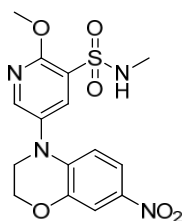
2-Methoxy-*N*-methyl-5-(6-(4-methylpiperazine-1-carbonyl)-2H-benzo[*b*][1,4]oxazin-3H)-yl)pyridine-3-sulfonamide (355)



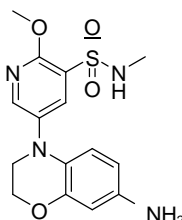
A solution of 4-(6-methoxy-5-(*N*-methylsulfamoyl)pyridin-3-yl)-3,4-dihydro-2H-benzo[*b*][1,4]oxazine-6-carboxylic acid **357** (103 mg, 0.271 mmol), propylphosphonic anhydride solution in DMF (0.23 mL, 0.39 mmol), triethylamine (0.11 mL, 0.79 mmol) in DMF (1 mL) was stirred for 30 min. 1-methylpiperazine (0.04 mL, 0.36 mmol) was added and the mixture was left to stir under nitrogen over the weekend. The mixture was concentrated under reduced pressure. The resulting crude product was purified by reverse phase chromatography using MDAP (high pH, method B) to give the title product **355** as an off-white solid (52 mg, 42%). mp 122.123 °C; ^1H NMR (500 MHz, DMSO- d_6) δ 8.40 (s, 1H), 8.00 (s, 1H), 7.38 - 7.46 (m, 1H), 6.88 (d, $J = 8.2$ Hz, 1H), 6.76 (d, $J = 8.2$ Hz, 1H), 6.57 (s, 1H), 4.32 (br. s, 2H), 4.01 (s, 3H), 3.72 (br. s, 2H), 3.40 (br. s, 4H), 2.49 (br. s, 3H), 2.21 (br. s, 4H), 2.14 (s, 3H); ^{13}C NMR (126 MHz, DMSO- d_6) δ 169.1 (C=O), 156.5 (Ar-C), 148.0 (ArCH), 145.9 (Ar-C), 136.8 (Ar-C), 136.3 (Ar-CH), 132.9 (Ar-C), 128.7 (Ar-C), 122.6 (Ar-

C), 119.6 (Ar-CH, 117.1 (Ar-CH, 114.3 (Ar-CH), 64.7 (CH₂), 55.4 (2 CH₂), 54.8 (CH₃), 48.6 (CH₂), 46.0 (CH₃), 29.2 (CH₃); 2 CH₂ not visible; LCMS (ESI, formic) *m/z* 462 [M+H]⁺, R_t = 0.58 min; HRMS (ESI) calcd for C₂₁H₂₈N₅O₅S [M+H]⁺ 462.1792, found 462.1806 (2.9 min); IR (ATR) cm⁻¹ 2940, 1638, 1508, 1480, 1416, 1325, 1298, 1260, 1159.

2-Methoxy-*N*-methyl-5-(7-nitro-2*H*-benzo[*b*][1,4]oxazin-4(3*H*)-yl)pyridine-3-sulfonamide (370)



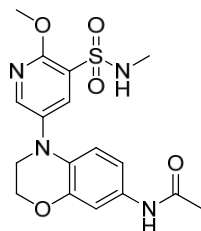
A solution of 7-nitro-3,4-dihydro-2*H*-benzo[*b*][1,4]oxazine (500 mg, 2.78 mmol), 5-bromo-2-methoxy-*N*-methylpyridine-3-sulfonamide (780 mg, 2.78 mmol), sodium *tert*-butoxide (533 mg, 5.55 mmol), XPhos (198 mg, 0.416 mmol) in dry toluene (20 mL) was degassed for 10 min. Pd₂(dba)₃ (254 mg, 0.278 mmol) was then added and the mixture was heated at 130 °C for 2 h. Water (35 mL) was added and product was extracted with EtOAc (2 x 50 mL). The combined organic layer was dried over sodium sulfate and concentrated under reduced pressure. The resulting crude product was purified by normal phase chromatography (50% EtOAc in hexane) to give the title product **370** as a yellow solid (400 mg, 38%). LCMS (ESI, formic) *m/z* 379 [MH]⁻, R_t = 2.31 min. **5-(7-Amino-2*H*-benzo[*b*][1,4]oxazin-4(3*H*)-yl)-2-methoxy-*N*-methylpyridine-3-sulfonamide (365)**



A solution of 2-methoxy-*N*-methyl-5-(7-nitro-2*H*-benzo[*b*][1,4]oxazin-4(3*H*)-yl)pyridine-3-sulfonamide **370** (450 mg, 1.18 mmol) in EtOAc (40 mL) was added to Pd/C (450 mg, 0.423 mmol) at room temperature. 60 psi of hydrogen was

then applied for 2 h. The mixture was filtered through celite and washed with EtOAc. The organic layer was concentrated under reduced pressure to give the title product **365** as a light green solid (400 mg, 96%). LCMS (ESI, formic) m/z 351 $[M+H]^+$, $R_t = 1.29$ min (70% by area).

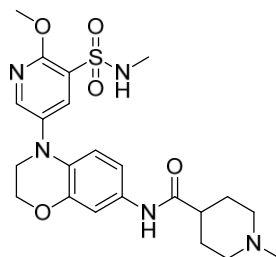
***N*-(4-(6-Methoxy-5-(*N*-methylsulfamoyl)pyridin-3-yl)-3,4-dihydro-2*H*benzo[*b*][1,4]oxazin-7-yl)acetamide (360)**



A solution of acetic acid (0.049 mL, 0.856 mmol), HOBt (114 mg, 0.742 mmol), EDC (164 mg, 0.856 mmol) and DIPEA (0.30 mL, 1.71 mmol) in DCM (8 mL) was stirred for 10 min. 5-(7-amino-2*H*-benzo[*b*][1,4]oxazin-4(3*H*)-yl)-2-methoxy-*N*-methylpyridine-3-sulfonamide **365** (200 mg, 0.571 mmol) was then added. The mixture was stirred under nitrogen at room temperature for 16 h. The mixture was quenched with saturated NaHCO_3 (20 mL) and extracted with DCM (2 x 20 mL). The combined organic layer was washed with water, brine and dried over anhydrous Na_2SO_4 and concentrated under reduced pressure. The crude product was purified by reverse phase chromatography (35% acetonitrile in 0.01 M ammonium acetate in water). The resulting solid was dissolved in DCM (20 mL), then washed with saturated NaHCO_3 (20 mL), water (20 mL) and brine (20 mL), dried over anhydrous Na_2SO_4 and concentrated under reduced pressure to give the title product **360** as pale green solid (70 mg, 31%). mp 200 °C (dec.); ^1H NMR (500 MHz, DMSO-d_6) δ 9.72 (s, 1H), 8.30 (s, 1H), 7.90 (s, 1H), 7.35 - 7.42 (m, 1H), 7.22 (s, 1H), 6.89 (d, $J = 8.5$ Hz, 1H), 6.61 (d, $J = 8.8$ Hz, 1H), 4.23 (br. s, 2H), 3.98 (s, 3H), 3.66 (br. s, 2H), 2.47 - 2.53 (m, 3H), 1.98 (s, 3H); ^{13}C NMR (126 MHz, DMSO-d_6) δ 168.2 (C=O), 155.7 (Ar-C), 146.4 (Ar-CH), 145.2 (Ar-C), 138.2 (Ar-C), 134.9 (Ar-CH), 133.4 (Ar-C), 127.8 (Ar-C), 122.4 (Ar-C), 116.8 (Ar-CH), 112.6 (Ar-CH), 108.7 (Ar-CH), 64.4 (CH_2), 54.7 (CH_3), 49.0 (CH_2), 29.2 (CH_3), 24.3 (CH_3); LCMS (ESI, 5 mM ammonium acetate) m/z 391

[M-H]⁻, R_t = 1.88 min; HRMS (ESI) calcd for C₁₇H₂₁N₄O₅S [M+H]⁺ 393.1227, found 393.1227 (3.9 min); IR (ATR) cm⁻¹ 2915, 1661, 1607, 1540, 1478, 1414, 1328, 1306, 1251, 1160.

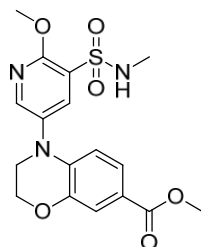
***N*-(4-(6-Methoxy-5-(*N*-methylsulfamoyl)pyridin-3-yl)-3,4-dihydro-2*H*benzo[*b*][1,4]oxazin-7-yl)-1-methylpiperidine-4-carboxamide (361)**



A solution of 1-methylpiperidine-4-carboxylic acid (90 mg, 0.63 mmol), HOBT (114 mg, 0.742 mmol), EDC (164 mg, 0.856 mmol) and DIPEA (0.30 mL, 1.71 mmol) in DCM (8 mL) was stirred for 10 min. 5-(7-amino-2*H*-benzo[*b*][1,4]oxazin-4(3*H*)-yl)-2-methoxy-*N*-methylpyridine-3-sulfonamide **365** (200 mg, 0.571 mmol) was added and the mixture was stirred under nitrogen at room temperature for 16 h. Water (15 mL) was added and product was extracted with EtOAc (2 x 20 mL). The combined organic layer was washed with brine and dried over anhydrous Na₂SO₄ and concentrated under reduced pressure. The crude product was purified by reverse phase chromatography (25 to 90% acetonitrile in 0.01 M ammonium acetate in water over 20 min). Fractions were collected and concentrated under reduced pressure. The resulting product was dissolved in 10% MeOH in DCM (20 mL) then washed with saturated NaHCO₃ (20 mL), water (20 mL) and brine (20 mL), dried over anhydrous Na₂SO₄ and concentrated under reduced pressure to give the title product **361** as a pale green solid (45 mg, 16%). mp 102-104 °C; ¹H NMR (400 MHz, DMSO-*d*₆) δ 9.62 (s, 1H), 8.30 (d, *J* = 2.8 Hz, 1H), 7.89 (d, *J* = 2.8 Hz, 1H), 7.38 (br. s., 1H), 7.24 (d, *J* = 2.3 Hz, 1H), 6.93 (dd, *J* = 8.7, 2.4 Hz, 1H), 6.61 (d, *J* = 8.8 Hz, 1H), 4.20 - 4.24 (m, 2H), 3.98 (s, 3H), 3.63 - 3.69 (m, 2H), 2.79 (apparent d, *J* = 11.4 Hz, 2H), 2.48 (s, 3H), 2.16 - 2.24 (m, 1H), 2.14 (s, 3H), 1.83 (dt, *J* = 11.5, 2.5 Hz, 2H), 1.56 - 1.73 (m, 4H); ¹³C NMR (101 MHz, DMSO-*d*₆) δ 173.0 (C=O),

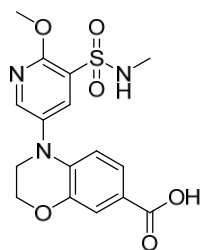
155.1 (Ar-C), 145.8 (Ar-CH), 144.7 (Ar-C), 137.7 (Ar-C), 134.3 (Ar-CH), 133.0 (Ar-C), 127.2 (Ar-C), 122.0 (Ar-C), 116.3 (Ar-CH), 112.1 (Ar-CH), 108.2 (Ar-CH), 63.9 (CH₂), 54.8 (CH₂, 2C), 54.1 (CH₃), 48.6 (CH₂), 46.1 (CH₃), 42.3 (CH), 28.7 (CH₃), 28.5 (CH₂, 2C); LCMS (ESI, 5 mM ammonium acetate) m/z 476 [M+H]⁺, R_t = 1.36 min; HRMS (ESI) calcd for C₂₂H₃₀N₅O₅S [M+H]⁺ 476.1962, found 476.1959 (3.4-3.6 min); IR (ATR) cm⁻¹ 2940, 1662, 1598, 1507, 1475, 1417, 1318, 1294, 1245, 1208, 1159.

Methyl-4-(6-methoxy-5-(*N*-methylsulfamoyl)pyridin-3-yl)-3,4-dihydro-2*H*benzo[*b*][1,4]oxazine-7-carboxylate (371)



A solution of methyl 3,4-dihydro-2 *H*-benzo[*b*][1,4]oxazine-7-carboxylate (200 mg, 1.04 mmol), 5-bromo-2-methoxy-*N*-methylpyridine-3-sulfonamide (320 mg, 1.14 mmol), sodium *tert*-butoxide (199 mg, 2.07 mmol) and XPhos (74.0 mg, 0.155 mmol) in toluene (7 mL) stirred at room temperature was purged with argon. Pd₂(dba)₃ (95 mg, 0.104 mmol) was then added and the mixture was heated to 130 °C in the sealed tube for 2 h. The mixture was filtered through celite and washed with EtOAc (20 mL). The filtrate was washed with water (20 mL), brine (20 mL) and dried over anhydrous Na₂SO₄. The crude product was purified by normal phase chromatography (40% EtOAc in hexane) to give the title product **371** as an off-white solid (100 mg, 25%). ¹H NMR (400 MHz, CDCl₃) δ 8.32 (d, *J* = 2.6 Hz, 1H), 8.12 (d, *J* = 2.6 Hz, 1H), 7.57 (d, *J* = 2.0 Hz, 1H), 7.45 (dd, *J* = 8.5, 2.0 Hz, 1H), 6.57 (d, *J* = 8.6 Hz, 1H), 4.38 (dd, *J* = 5.1, 3.8 Hz, 2H), 4.14 (s, 3H), 3.87 (s, 3H), 3.71 - 3.77 (m, 2H), 2.71 (d, *J* = 5.5 Hz, 3H); LCMS (ESI, formic) m/z 394 [M+H]⁺, R_t = 2.46 min.

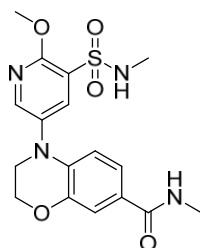
4-(6-Methoxy-5-(*N*-methylsulfamoyl)pyridin-3-yl)-3,4-dihydro-2*H*benzo[*b*][1,4]oxazine-7-carboxylic acid (368)



A solution of methyl-4-(6-methoxy-5-(*N*-methylsulfamoyl)pyridin-3-yl)-3,4-dihydro-2*H*-benzo[*b*][1,4]oxazine-7-carboxylate **371** (700 mg, 1.78 mmol) and LiOH (85 mg, 3.6 mmol) in THF (12 mL) and water (12 mL) was stirred at room temperature for 16 h. The mixture was concentrated under reduced pressure. The resulting crude was dissolved in water (15 mL), washed with EtOAc (25 mL). The aqueous layer was acidified with saturated KHSO₄ and extracted with EtOAc (2 x 15 mL). The organic layer was dried over anhydrous Na₂SO₄ and concentrated under reduced pressure to give the title product **368** as an off-white solid (600 mg, 89%).

¹H NMR (400 MHz, DMSO-*d*₆) δ 12.36 (br. s, 1H), 8.45 (d, *J* = 2.6 Hz, 1H), 8.05 (d, *J* = 2.6 Hz, 1H), 7.45 - 7.50 (m, 1H), 7.30 - 7.34 (m, 2H), 6.55 (d, *J* = 9.0 Hz, 1H), 4.32 - 4.36 (m, 2H), 4.03 (s, 3H), 3.75 - 3.79 (m, 2H), 2.47 - 2.52 (m, 3H); LCMS

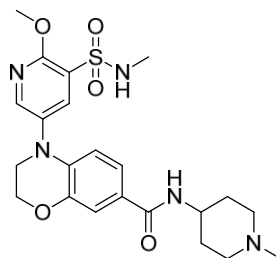
(ESI, 5 mM ammonium acetate) *m/z* 380 [M+H]⁺, *R*_t = 2.87 min. **4-(6-Methoxy-5-(*N*-methylsulfamoyl)pyridin-3-yl)-*N*-methyl-3,4-dihydro-2*H*benzo[*b*][1,4]oxazine-7-carboxamide (362)**



A solution of 4-(6-methoxy-5-(*N*-methylsulfamoyl)pyridin-3-yl)-3,4-dihydro-2*H*-benzo[*b*][1,4]oxazine-7-carboxylic acid **368** (80 mg, 0.21 mmol), CDI (85 mg, 0.53 mmol) in DMF (2 mL) was heated at 50 °C for 16 h. Methylamine (2 M in THF, 0.21 mL, 0.42 mmol) was added at 0 °C. The mixture was then stirred at rt for 3 h. The

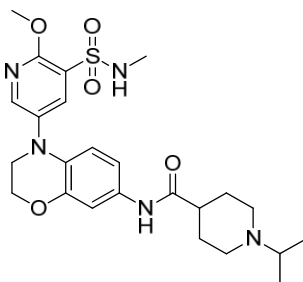
mixture was quenched with cold water (10 mL) and extracted with EtOAc (2 x 10 mL). The organic layer was washed with brine and dried over anhydrous Na₂SO₄ and concentrated under reduced pressure. The crude compound was triturated with diethylether (2 x 10 mL) and dried to give the title product **362** as an off-white powder (30 mg, 36%). ¹H NMR (600 MHz, DMSO-d₆) δ 8.40 (s, 1H), 8.11 (br. s, 1H), 8.01 (s, 1H), 7.41 (br. s, 1H), 7.33 (s, 1H), 7.23 (d, *J* = 7.7 Hz, 1H), 6.57 (d, *J* = 8.1 Hz, 1H), 4.32 (br. s, 2H), 4.01 (s, 3H), 3.74 (br. s, 2H), 2.47 - 2.52 (m, 3H), 2.72 (s, 3H); LCMS (ESI, formic) *m/z* 393 [M+H]⁺, R_t = 1.34 min.

4-(6-Methoxy-5-(*N*-methylsulfamoyl)pyridin-3-yl)-*N*-(1-methylpiperidin-4-yl)3,4-dihydro-2*H*-benzo[*b*][1,4]oxazine-7-carboxamide (363**)**



A solution of 4-(6-methoxy-5-(*N*-methylsulfamoyl)pyridin-3-yl)-3,4-dihydro-2*H*-benzo[*b*][1,4]oxazine-7-carboxylic acid **368** (150 mg, 0.395 mmol), CDI (160 mg, 0.988 mmol) in DMF (3 mL) was heated at 50 °C for 16 h. 1-methylpiperidin-4-amine (90 mg, 0.791 mmol) was then added at 0 °C. The mixture was stirred at room temperature for 3 h. The mixture was quenched with cold water (10 mL) and extracted with EtOAc (2 x 10 mL). The combined organic layer was washed with brine and dried over anhydrous Na₂SO₄ and concentrated under reduced pressure. The crude compound was dissolved in DCM (1 mL) and purified by normal phase chromatography (7% MeOH in DCM) to give the title product **363** as an off-white solid (30 mg, 16%). ¹H NMR (400 MHz, DMSO-d₆) δ 8.40 (d, *J* = 2.6 Hz, 1H), 8.00 (d, *J* = 2.6 Hz, 1H), 7.95 (d, *J* = 7.7 Hz, 1H), 7.41 - 7.48 (m, 1H), 7.37 (d, *J* = 1.8 Hz, 1H), 7.26 (dd, *J* = 8.6, 2.0 Hz, 1H), 6.58 (d, *J* = 8.6 Hz, 1H), 4.31 (br. s, 2H), 4.01 (s, 3H), 3.74 (br. s, 2H), 3.63 - 3.72 (m, 1H), 2.70 - 2.87 (m, 2H), 2.47 - 2.52 (m, 3H), 2.17 (s, 3H), 1.86 - 2.04 (m, 2H), 1.66 - 1.77 (m, 2H), 1.46 - 1.63 (m, 2H); LCMS (ESI, formic) *m/z* 476 [M+H]⁺, R_t = 1.39 min.

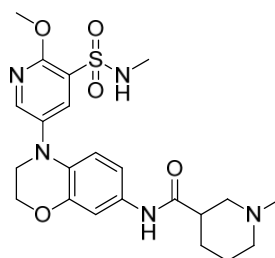
1-Isopropyl-N-(4-(6-methoxy-5-(*N*-methylsulfamoyl)pyridin-3-yl)-3,4-dihydro-2*H*-benzo[*b*][1,4]oxazin-7-yl)piperidine-4-carboxamide (372)



A solution of 5-(7-amino-2*H*-benzo[*b*][1,4]oxazin-4(3*H*)-yl)-2-methoxy-*N*-methylpyridine-3-sulfonamide **365** (54 mg, 0.154 mmol), 1-isopropylpiperidine-4-carboxylic acid (31.7 mg, 0.185 mmol) and DIPEA (0.081 mL, 0.462 mmol) in EtOAc (1 mL) and DMF (0.1 mL) was cooled to 0 °C and T₃P (50% in DMF, 0.135 mL, 0.231 mmol) was added dropwise. The mixture was allowed to warm at room temperature and stirred overnight. Additional DIPEA (0.081 mL, 0.462 mmol), T₃P (50% in DMF, 0.135 mL, 0.231 mmol) and 1-isopropylpiperidine-4-carboxylic acid (31.7 mg, 0.185 mmol) were added and the mixture was stirred at room temperature for 3 h. DIPEA (0.081 mL, 0.462 mmol), T₃P (50% in DMF, 0.135 mL, 0.231 mmol) and 1-isopropylpiperidine-4-carboxylic acid (31.7 mg, 0.185 mmol) were added and the reaction was stirred at room temperature overnight. The reaction mixture was then partitioned between EtOAc and 5% aqueous LiCl solution (5 mL). Phases were separated and aqueous sodium carbonate was added on the organic layer. The layers were separated, the aqueous phase was extracted with EtOAc (2 x 10 mL). The combined organic layers were washed with aqueous sodium carbonate. The organic layer was then passed through a hydrophobic frit and concentrated under reduced pressure to give crude product (53 mg). Analysis of the LiCl aqueous phase revealed desired product was present. The aqueous phase was passed through a 103 cartridge and product was eluting with MeOH. Solvent was concentrated under reduced pressure to give 75 mg of additional crude product. The combined crude products were purified by reverse phase chromatography using MDAP (high pH) to give the title product **372** (10 mg, 13%). ¹H NMR (400 MHz, DMSO-*d*₆) δ 9.58 (s, 1H), 8.29 (d, *J* = 2.8 Hz, 1H), 7.88 (d, *J* = 2.8 Hz, 1H), 7.37 (d, *J* = 4.8 Hz, 1H), 7.24 (d, *J* = 2.3 Hz, 1H), 6.93 (dd, *J*

= 8.8, 2.3 Hz, 1H), 6.60 (d, $J = 8.8$ Hz, 1H), 4.18 - 4.24 (m, 2H), 3.97 (s, 3H), 3.61 - 3.68 (m, 2H), 2.81 (d, $J = 11.3$ Hz, 2H), 2.65 (quin, $J = 6.6$ Hz, 1H), 2.45 - 2.52 (m, 3H), 2.15 - 2.25 (m, 1H), 2.08 (dt, $J = 11.6, 2.0$ Hz, 2H), 1.66 - 1.75 (m, 2H), 1.58 (dq, $J = 11.8, 3.8$ Hz, 2H), 0.95 (d, $J = 6.6$ Hz, 6H); LCMS (ESI, formic) m/z 504 $[M+H]^+$, $R_t = 0.88$ min.

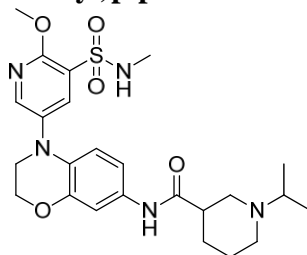
***N*-(4-(6-methoxy-5-(*N*-methylsulfamoyl)pyridin-3-yl)-3,4-dihydro-2*H*benzo[*b*][1,4]oxazin-7-yl)-1-methylpiperidine-3-carboxamide (373)**



1-Methylpiperidine-3-carboxylic acid (44 mg, 0.31 mmol) was dissolved in DMF (1.5 mL). HATU (113 mg, 0.297 mmol) and DIPEA (87 μ L, 0.50 mmol) were added and the mixture was stirred at room temperature for 10 min. 5-(7-Amino-2*H*benzo[*b*][1,4]oxazin-4(3*H*)-yl)-2-methoxy-*N*-methylpyridine-3-sulfonamide (71 mg, 0.20 mmol) was added and the mixture was stirred at room temperature for 1 h. Sat. aq. sodium bicarbonate solution (10 mL) was added and the mixture was extracted with EtOAc (10 mL). The aqueous phase was washed with further EtOAc (3 x 10 mL). The combined organics were passed through a hydrophobic frit and concentrated under reduced pressure. The crude product was purified by reverse phase chromatography using MDAP (high pH, 30-85%) and product obtained was dried in a vacuum oven overnight to give the title product 373 as a yellow solid (47 mg, 49%). ^1H NMR (400 MHz, DMSO- d_6) δ 9.75 (s, 1H), 8.30 (d, $J = 2.8$ Hz, 1H), 7.89 (d, $J = 2.8$ Hz, 1H), 7.38 (q, $J = 4.8$ Hz, 1H), 7.23 (d, $J = 2.3$ Hz, 1H), 6.92 (dd, $J = 8.8, 2.3$ Hz, 1H), 6.61 (d, $J = 8.8$ Hz, 1H), 4.20 - 4.25 (m, 2H), 3.98 (s, 3H), 3.62 - 3.69 (m, 2H), 2.81 (br. d, $J = 10.6$ Hz, 1H), 2.65 - 2.73 (m, 1H), 2.43 - 2.57 (m, 4H), 2.18 (s, 3H), 1.96 - 2.07 (m, 1H), 1.82 - 1.93 (m, 1H), 1.72 - 1.80 (m, 1H), 1.60 - 1.70 (m, 1H), 1.29 - 1.56 (m, 2H); LCMS (ESI, high pH) m/z 476 $[M+H]^+$, $R_t =$

0.92 min.

1-Isopropyl-*N*-(4-(6-methoxy-5-(*N*-methylsulfamoyl)pyridin-3-yl)-3,4-dihydro-2*H*-benzo[*b*][1,4]oxazin-7-yl)piperidine-3-carboxamide (374)



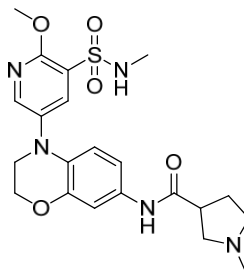
A mixture of 5-(7-amino-2*H*-benzo[*b*][1,4]oxazin-4(3*H*)-yl)-2-methoxy-*N*-methylpyridine-3-sulfonamide **365** (50 mg, 0.14 mmol), 1-isopropylpiperidine-3-carboxylic acid (27 mg, 0.16 mmol), T₃P (50% in DMF, 0.125 mL, 0.214 mmol) and DIPEA (75 μ L, 0.43 mmol) in EtOAc (1 mL) was stirred at room temperature for 5 min. Mixture remained a suspension so DMF (0.5 mL) was added. The solution was stirred at room temperature for 3 h. Saturated aqueous NaHCO₃ solution (5 mL) was added and the mixture was extracted with EtOAc (2 x 10 mL). The combined organic extracts were passed through a hydrophobic frit and concentrated under reduced pressure. The crude material was purified by reverse phase chromatography using MDAP (high pH) to give the title product **374** as a yellow solid (25 mg, 35%).

¹

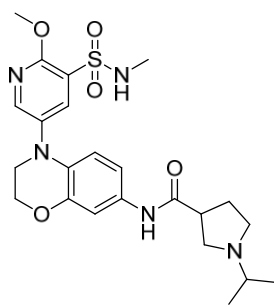
¹H NMR (400 MHz, CDCl₃) δ 10.90 (br. s, 1H), 8.24 (d, J = 2.8 Hz, 1H), 8.06 (d, J = 3.0 Hz, 1H), 7.21 (d, J = 2.3 Hz, 1H), 6.98 (dd, J = 8.7, 2.3 Hz, 1H), 6.67 (d, J = 8.8 Hz, 1H), 4.89 (q, J = 5.0 Hz, 1H), 4.29 (t, J = 4.3 Hz, 2H), 4.10 (s, 3H), 3.66 (t, J = 4.3 Hz, 2H), 3.08 (br. d, J = 11.8 Hz, 1H), 2.84 - 2.95 (m, 2H), 2.68 (d, J = 5.3 Hz, 3H), 2.59 - 2.63 (m, 1H), 2.46 (dd, J = 11.8, 2.8 Hz, 1H), 2.25 - 2.33 (m, 1H), 2.06 (d, J = 13.1 Hz, 1H), 1.71 - 1.85 (m, 1H), 1.12 (dd, J = 6.6, 2.0 Hz, 6H), 2 NH not visible; LCMS (ESI, formic) m/z 504 [M+H]⁺, R_t = 1.00 min.

From this point, the experimental work was carried out by the author.

***N*-(4-(6-methoxy-5-(*N*-methylsulfamoyl)pyridin-3-yl)-3,4-dihydro-2*H*benzo[*b*][1,4]oxazin-7-yl)-1-methylpyrrolidine-3-carboxamide (375)**



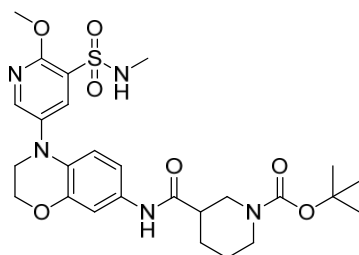
5-(7-amino-2*H*-benzo[*b*][1,4]oxazin-4(3*H*)-yl)-2-methoxy-*N*-methylpyridine-3-sulfonamide **365** (60 mg, 0.17 mmol) was dissolved in DMF (1.5 mL). DIPEA (90 μ L, 0.51 mmol), 1-methylpyrrolidine-3-carboxylic acid (45 mg, 0.35 mmol) and HATU (130 mg, 0.342 mmol) were added. The mixture was stirred at room temperature for 16 h. EtOAc (10 mL) and sat. aq. sodium bicarbonate (10 mL) were added. The organic layer was separated and the aqueous layer was extracted a second time with EtOAc (10 mL). The combined organic layers were passed through a hydrophobic frit and concentrated under a stream of nitrogen overnight. The crude product was purified by reverse phase chromatography using MDAP (high pH, 3085%) to give the title product 375 as a yellow solid (41 mg, 52%). ^1H NMR (400 MHz, DMSO- d_6) δ 9.66 (s, 1H), 8.30 (d, $J = 2.8$ Hz, 1H), 7.89 (d, $J = 2.8$ Hz, 1H), 7.34 - 7.40 (m, 1H), 7.24 (d, $J = 2.3$ Hz, 1H), 6.91 (dd, $J = 8.8, 2.5$ Hz, 1H), 6.61 (d, $J = 8.6$ Hz, 1H), 4.23 (t, $J = 4.0$ Hz, 2H), 3.98 (s, 3H), 3.66 (t, $J = 4.2$ Hz, 2H), 2.99 (quin, $J = 7.7$ Hz, 1H), 2.80 (t, $J = 8.6$ Hz, 1H), 2.56 - 2.64 (m, 1H), 2.43 - 2.50 (m, 4H), 2.37 (q, $J = 7.8$ Hz, 1H), 2.25 (s, 3H), 1.92-1.99 (m, 2H); LCMS (ESI, high pH) m/z 462 $[\text{M}+\text{H}]^+$, $R_t = 0.86$ min. **1-Isopropyl-*N*-(4-(6-methoxy-5-(*N*-methylsulfamoyl)pyridin-3-yl)-3,4-dihydro-2*H*-benzo[*b*][1,4]oxazin-7-yl)pyrrolidine-3-carboxamide, formic acid salt (376)**



5-(7-amino-2H-benzo[b][1,4]oxazin-4(3H)-yl)-2-methoxy-N-methylpyridine-3-sulfonamide **265** (60 mg, 0.17 mmol) was dissolved in DMF (1.5 mL). DIPEA (0.1 mL, 0.57 mmol), 1-isopropylpyrrolidine-3-carboxylic acid (57 mg, 0.36 mmol) and HATU (150 mg, 0.394 mmol) were added. The mixture was stirred at room temperature for 5 h. EtOAc (10 mL) and sat. aq. sodium bicarbonate (10 mL) were added. The organic layer was separated and the aqueous layer was extracted a second time with EtOAc (10 mL). The combined organic layers were passed through a hydrophobic frit and concentrated under a stream of nitrogen overnight. The crude product was purified by reverse phase chromatography using MDAP (high pH, 3085%) to give the title product **376** as a yellow solid (61 mg, 67%). ¹H NMR (400 MHz, DMSO-d₆) δ 9.75 (s, 1H), 8.30 (d, *J* = 2.7 Hz, 1H), 8.23 (s, 1H, formic acid), 7.89 (d, *J* = 2.7 Hz, 1H), 7.38 (br. s, 1H), 7.24 (d, *J* = 2.2 Hz, 1H), 6.91 (dd, *J* = 8.8, 2.2 Hz, 1H), 6.62 (d, *J* = 8.6 Hz, 1H), 4.23 (t, *J* = 3.9 Hz, 2H), 3.98 (s, 3H), 3.66 (t, *J* = 4.1 Hz, 2H), 2.95 - 3.05 (m, 2H), 2.76 - 2.84 (m, 1H), 2.52 - 2.68 (m, 3H), 2.48 (s, 3H), 1.93 - 2.00 (m, 2H), 1.06 (dd, *J* = 6.7, 2.20 Hz, 6H); ¹³C NMR (101 MHz, DMSO-d₆) δ 172.1 (C), 164.2 (CH-formic), 155.6 (C), 146.4 (Ar-CH), 145.1 (C), 138.1 (C), 134.8 (Ar-CH), 133.2 (C), 127.8 (C), 122.4 (C), 116.7 (Ar-CH), 112.6 (CH), 108.7 (CH), 64.3 (CH₂), 54.8 (CH₃), 54.6 (CH₂), 54.5 (CH), 51.3 (CH₂), 49.0 (CH₂), 43.7 (CH), 29.1 (CH₃), 28.1 (CH₂), 21.4 (CH₃, 2C); LCMS (ESI, high pH) *m/z* 490 [M+H]⁺, *R*_t = 0.95 min; HRMS (ESI) calcd for C₂₃H₃₂N₅O₅S [M+H]⁺ 490.2119, found 490.2123 (3.5min); IR (ATR) cm⁻¹ 2982, 1678, 1590, 1507, 1474, 1417, 1318, 1293, 1223, 1159.

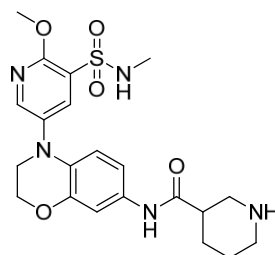
Compound was purified by high pH MDAP so formic was not expected. Compound might have been contaminated in blowdown unit or solvent from MDAP switched.

***tert*-Butyl 3-((4-(6-methoxy-5-(*N*-methylsulfamoyl)pyridin-3-yl)-3,4-dihydro-2*H*benzo[*b*][1,4]oxazin-7-yl)carbamoyl)piperidine-1-carboxylate (383)**



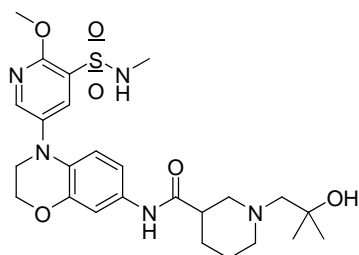
1-(*tert*-Butoxycarbonyl)piperidine-3-carboxylic acid (327 mg, 1.43 mmol) was dissolved in DMF (4 mL). DIPEA (0.38 mL, 2.18 mmol) and HATU (543 mg, 1.427 mmol) were added followed by 5-(7-amino-2*H*-benzo[*b*][1,4]oxazin-4(3*H*)yl)-2-methoxy-*N*-methylpyridine-3-sulfonamide **365** (250 mg, 0.713 mmol). The mixture was stirred at room temperature for 16 h. EtOAc (20 mL) and sat. aq. sodium bicarbonate (20 mL) were added. The organic layer was separated and the aqueous layer was extracted a second time with EtOAc (20 mL). The combined organic layers were passed through a hydrophobic frit and concentrated under reduced pressure. The crude product was purified by reverse phase chromatography (120 g C18 column, 40-90% acetonitrile + 0.1% formic acid in water + 0.1% formic acid over 12 CV) to give the title product **383** as a yellow solid (321 mg, 80%). ¹H NMR (400 MHz, DMSO-*d*₆) δ 9.77 (s, 1H), 8.30 (d, *J* = 2.8 Hz, 1H), 7.89 (d, *J* = 2.8 Hz, 1H), 7.37 (q, *J* = 4.8 Hz, 1H), 7.23 (d, *J* = 2.3 Hz, 1H), 6.93 (dd, *J* = 8.8, 2.3 Hz, 1H), 6.62 (d, *J* = 8.8 Hz, 1H), 4.23 (t, *J* = 4.0 Hz, 2H), 3.98 (s, 3H), 3.87 (br. d, *J* = 13.1 Hz, 1H), 3.66 (t, *J* = 4.2 Hz, 2H), 2.62 - 2.98 (m, 2H), 2.48 (br. s, 3H), 2.33 - 2.42 (m, 1H), 1.90 (d, *J* = 12.8 Hz, 1H), 1.69 (d, *J* = 13.1 Hz, 1H), 1.53 - 1.65 (m, 1H), 1.40 (s, 9H), 1.29 - 1.37 (m, 2H); LCMS (ESI, formic) *m/z* 462 [M+H]⁺ (deBoc fragment), *R*_t = 1.14 min.

***N*-(4-(6-Methoxy-5-(*N*-methylsulfamoyl)pyridin-3-yl)-3,4-dihydro-2*H*benzo[*b*][1,4]oxazin-7-yl)piperidine-3-carboxamide (384)**



tert-Butyl 3-((4-(6-methoxy-5-(*N*-methylsulfamoyl)pyridin-3-yl)-3,4-dihydro-2*H*benzo[*b*][1,4]oxazin-7-yl)carbamoyl)piperidine-1-carboxylate **383** (298 mg, 0.531 mmol) was dissolved in DCM (4 mL) under nitrogen. TFA (0.5 mL, 6.5 mmol) was added and the mixture was stirred at room temperature for 2 h. Sat. aq. sodium bicarbonate (10 mL) was added and the mixture was stirred for 10 min. DCM (10 mL) was added and the phases were separated using a hydrophobic frit. Solvent was removed under a stream of nitrogen over the weekend to give the title product **284** as a yellow solid (272 mg, quantitative). ¹H NMR (400 MHz, DMSO-*d*₆) δ 9.85 (s, 1H), 8.39 (s, 1H), 8.32 (d, *J* = 2.7 Hz, 1H), 7.90 (d, *J* = 2.7 Hz, 1H), 7.41 (br. s, 1H), 7.25 (d, *J* = 2.2 Hz, 1H), 6.94 (dd, *J* = 8.7, 2.3 Hz, 1H), 6.63 (d, *J* = 8.6 Hz, 1H), 4.21 - 4.27 (m, 2H), 4.00 (s, 3H), 3.65 - 3.71 (m, 2H), 3.09 (d, *J* = 10.0 Hz, 1H), 2.96 (d, *J* = 12.2 Hz, 1H), 2.73 (t, *J* = 11.2 Hz, 1H), 2.51 - 2.64 (m, 2H), 2.49 - 2.51 (m, 3H), 1.85 - 1.94 (m, 1H), 1.43 - 1.73 (m, 3H); LCMS (ESI, high pH) *m/z* 462 [M+H]⁺, *R*_t = 0.83 min.

1-(2-Hydroxy-2-methylpropyl)-*N*-(4-(6-methoxy-5-(*N*-methylsulfamoyl)pyridin-3-yl)-3,4-dihydro-2*H*-benzo[*b*][1,4]oxazin-7-yl)piperidine-3-carboxamide (377)



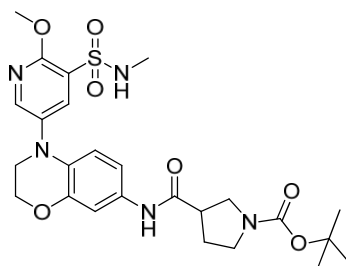
N-(4-(6-methoxy-5-(*N*-methylsulfamoyl)pyridin-3-yl)-3,4-dihydro-2*H*benzo[*b*][1,4]oxazin-7-yl)piperidine-3-carboxamide **384** (80 mg, 0.17 mmol) was dissolved in EtOH (2 mL). DIPEA (0.09 mL, 0.52 mmol) followed by 2,2-dimethyloxirane (0.06 mL, 0.68 mmol) were added. The mixture was stirred in a

sealed vial at 90 °C for 20 h. Solvent was removed under reduced pressure. The crude product was purified by reverse phase chromatography using MDAP (high pH, 30-85%) to give the title product **377** as a yellow solid (47 mg, 51%). mp 99-100 °C

1

¹H NMR (600 MHz, DMSO-d₆) δ 9.81 (s, 1H), 8.30 (d, *J* = 2.9 Hz, 1H), 7.89 (d, *J* = 2.9 Hz, 1H), 7.38 (br. s, 1H), 7.26 (d, *J* = 2.2 Hz, 1H), 6.96 (dd, *J* = 8.8, 2.2 Hz, 1H), 6.61 (d, *J* = 8.8 Hz, 1H), 4.22 (t, *J* = 4.0 Hz, 2H), 3.98 (s, 3H), 3.66 (t, *J* = 4.4 Hz, 3H), 2.87 (br. d, *J* = 9.9 Hz, 1H), 2.70 - 2.77 (m, 1H), 2.46 - 2.54 (m, 4H), 2.40 - 2.46 (m, 1H), 2.20 - 2.28 (m, 3H), 1.66 - 1.72 (m, 1H), 1.56 - 1.63 (m, 1H), 1.45 - 1.53 (m, 2H), 1.09 (s, 6H); ¹³C NMR (151 MHz, DMSO-d₆) δ 172.2 (C=O), 155.1 (Ar-C), 145.9 (Ar-CH), 144.6 (Ar-C), 137.7 (Ar-C), 134.3 (Ar-CH), 132.8 (Ar-C), 127.3 (Ar-C), 121.9 (Ar-C), 116.2 (Ar-CH), 112.3 (Ar-CH), 108.4 (Ar-CH), 70.3 (C), 68.6 (CH₂), 63.9 (CH₂), 57.7 (CH₂), 55.4 (CH₂), 54.1 (CH₃), 48.6 (CH₂), 43.4 (CH₂), 28.7 (CH), 27.9 (CH₃), 27.8 (CH₃), 26.9 (CH₂), 24.1 (CH₂); LCMS (ESI, high pH) *m/z* 534 [M+H]⁺, Rt = 1.01 min; HRMS (ESI) calcd for C₂₅H₃₆N₅O₆S [M+H]⁺ 534.2381, found 534.2383 (3.4min); IR (ATR) cm⁻¹ 2935, 1661, 1596, 1508, 1475, 1417, 1323, 1284, 1240, 1159.

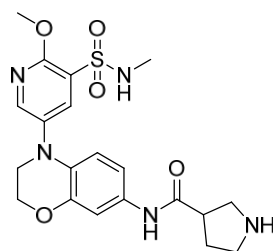
***tert*-Butyl 3-((4-(6-methoxy-5-(*N*-methylsulfamoyl)pyridin-3-yl)-3,4-dihydro-2*H*benzo[*b*][1,4]oxazin-7-yl)carbamoyl)pyrrolidine-1-carboxylate (**386**)**



1-(*tert*-Butoxycarbonyl)pyrrolidine-3-carboxylic acid (148 mg, 0.688 mmol) was dissolved in DMF (3 mL). DIPEA (0.19 mL, 1.09 mmol) and HATU (246 mg, 0.647 mmol) were added and the mixture was stirred at room temperature for 5 min. 5-(7Amino-2*H*-benzo[*b*][1,4]oxazin-4(3*H*)-yl)-2-methoxy-*N*-methylpyridine-3-sulfonamide **265** (152 mg, 0.434 mmol) was added and the mixture was stirred at

room temperature for 1 h. EtOAc (20 mL) and sat. sodium bicarbonate solution (20 mL) were added. The aqueous phase was washed with further EtOAc (20 mL). The combined organics were passed through a hydrophobic frit and solvent was removed under reduced pressure. The resulting crude purified by reverse phase chromatography (30 g, high pH, 30-85%) to give the title product as a yellow solid (137 mg, 58%). ¹H NMR (400 MHz, DMSO-d₆) δ 9.82 (s, 1H), 8.31 (d, *J* = 2.8 Hz, 1H), 7.89 (d, *J* = 2.5 Hz, 1H), 7.38 (q, *J* = 4.9 Hz, 1H), 7.23 (d, *J* = 2.3 Hz, 1H), 6.92 (dd, *J* = 8.8, 2.3 Hz, 1H), 6.62 (d, *J* = 8.6 Hz, 1H), 4.22 - 4.25 (m, 2H), 3.98 (s, 3H), 3.65 - 3.68 (m, 2H), 3.49 (dd, *J* = 10.5, 8.2 Hz, 1H), 3.32 - 3.43 (m, 2H), 3.25 (d, *J* = 6.8 Hz, 1H), 3.06 (br. s, 1H), 2.48 (s, 3H), 1.91 - 2.15 (m, 2H), 1.40 (s, 9H); LCMS (ESI, high pH) *m/z* 546 [M-H]⁻, *R*_t = 1.09 min.

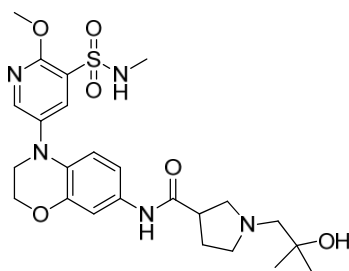
***N*-(4-(6-methoxy-5-(*N*-methylsulfamoyl)pyridin-3-yl)-3,4-dihydro-2*H*benzo[*b*][1,4]oxazin-7-yl)pyrrolidine-3-carboxamide (387)**



tert-Butyl 3-((4-(6-methoxy-5-(*N*-methylsulfamoyl)pyridin-3-yl)-3,4-dihydro-2*H*benzo[*b*][1,4]oxazin-7-yl)carbamoyl)pyrrolidine-1-carboxylate **386** (137 mg, 0.250 mmol) was dissolved in DCM (3 mL). TFA (0.19 mL, 2.50 mmol) was added and the mixture was stirred at room temperature overnight. Sat. sodium bicarbonate aqueous solution (10 mL) was added and the mixture was stirred at room temperature for 10 min. Water (15 mL) and DCM (20 mL) were then added and the phases were separated. The aqueous phase was extracted with further DCM (2 x 15 mL) and the combined organics were passed through a hydrophobic frit. Solvent was removed under reduced pressure to give the title product as a brown solid (59 mg, 53%). ¹H NMR (400 MHz, DMSO-d₆) δ 9.89 (s, 1H), 8.31 (d, *J* = 2.8 Hz, 1H), 7.89 (d, *J* = 2.8 Hz, 1H), 7.37 (br. s, 1H), 7.25 (d, *J* = 2.3 Hz, 1H), 6.93 (dd, *J* = 8.8, 2.3 Hz, 1H),

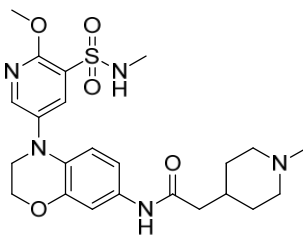
6.62 (d, $J = 8.8$ Hz, 1H), 4.21 - 4.26 (m, 2H), 3.98 (s, 3H), 3.62 - 3.71 (m, 2H), 3.14 - 3.22 (m, 2H), 2.9 - 3.11 (m, 3H), 2.48 (s, 3H), 2.00 - 2.11 (m, 1H), 1.89 - 1.98 (m, 1H), NH exchangeable; LCMS (ESI, high pH) m/z 448 $[M+H]^+$, $R_t = 0.51$ min.

1-(2-Hydroxy-2-methylpropyl)-*N*-(4-(6-methoxy-5-(*N*-methylsulfamoyl)pyridin-3-yl)-3,4-dihydro-2*H*-benzo[*b*][1,4]oxazin-7-yl)pyrrolidine-3-carboxamide (378)



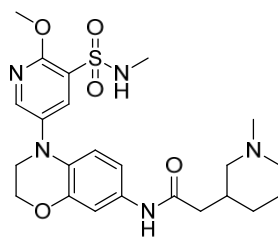
N-(4-(6-Methoxy-5-(*N*-methylsulfamoyl)pyridin-3-yl)-3,4-dihydro-2*H*-benzo[*b*][1,4]oxazin-7-yl)pyrrolidine-3-carboxamide **378** (59 mg, 0.13 mmol) was dissolved in EtOH (3 mL). DIPEA (0.07 mL, 0.40 mmol) followed by 2,2-dimethyloxirane (23 μ L, 0.26 mmol) were added. The mixture was heated to 90 °C for 1 h. Further 2,2-dimethyloxirane (15 μ L, 0.17 mmol) was added and the mixture was heated at 90 °C over the week-end. The solvent was removed under reduced pressure. The resulting crude product was purified by reverse phase chromatography using MDAP to give the title product as (28 mg, 41%). ^1H NMR (400 MHz, DMSO- d_6) δ 9.67 (s, 1H), 8.30 (d, $J = 2.8$ Hz, 1H), 7.89 (d, $J = 2.8$ Hz, 1H), 7.38 (br. s, 1H), 7.24 (d, $J = 2.3$ Hz, 1H), 6.92 (dd, $J = 8.8, 2.3$ Hz, 1H), 6.61 (d, $J = 8.8$ Hz, 1H), 4.21 - 4.25 (m, 2H), 4.05 (s, 1H), 3.98 (s, 3H), 3.64 - 3.68 (m, 2H), 2.88 - 3.00 (m, 2H), 2.71 - 2.79 (m, 1H), 2.54 - 2.63 (m, 2H), 2.47 - 2.48 (m, 1H), 2.35 (s, 2H), 1.88 - 1.96 (m, 2H), 1.09 (apparent d, $J = 1.0$ Hz, 6H); LCMS (ESI, high pH) m/z 520 $[M+H]^+$, $R_t = 0.90$ min.

***N*-(4-(6-Methoxy-5-(*N*-methylsulfamoyl)pyridin-3-yl)-3,4-dihydro-2*H*benzo[*b*][1,4]oxazin-7-yl)-2-(1-methylpiperidin-4-yl)acetamide (379)**



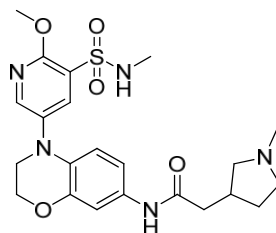
2-(1-Methylpiperidin-4-yl)acetic acid (54 mg, 0.343 mmol) was dissolved in DMF (1.5 mL). DIPEA (90 μ L, 0.514 mmol) and HATU (140 mg, 0.368 mmol) were added followed by 5-(7-amino-2*H*-benzo[*b*][1,4]oxazin-4(3*H*)-yl)-2-methoxy-*N*-methylpyridine-3-sulfonamide **265** (60 mg, 0.17 mmol). The mixture was stirred at room temperature for 3 h. EtOAc (10 mL) and sat. aq. sodium bicarbonate (10 mL) were added. The organic layer was separated and the aqueous layer was extracted a second time with EtOAc (10 mL). The combined organic layers were passed through a hydrophobic frit and concentrated under a stream of nitrogen. The crude product was purified by reverse phase chromatography using MDAP (formic acid, 30-85%) to give impure material. The product was repurified by reverse phase chromatography using MDAP (high pH, 15-55%) to give the title product **379** as a yellow solid (35 mg, 42%). ^1H NMR (400 MHz, DMSO- d_6) δ 9.66 (s, 1H), 8.30 (d, $J = 2.8$ Hz, 1H), 7.89 (d, $J = 2.8$ Hz, 1H), 7.38 (q, $J = 4.8$ Hz, 1H), 7.24 (d, $J = 2.3$ Hz, 1H), 6.91 (dd, $J = 8.7, 2.4$ Hz, 1H), 6.61 (d, $J = 8.8$ Hz, 1H), 4.19 - 4.26 (m, 2H), 3.98 (s, 3H), 3.62 - 3.68 (m, 2H), 2.71 (br. d, $J = 11.4$ Hz, 2H), 2.44 - 2.53 (m, 3H), 2.09 - 2.19 (m, 5H), 1.83 (dt, $J = 11.4, 2.5$ Hz, 2H), 1.53 - 1.73 (m, 3H), 1.20 (dq, $J = 12.0, 3.7$ Hz, 2H); LCMS (ESI, high pH) m/z 490 $[\text{M}+\text{H}]^+$, $R_t = 0.91$ min.

***N*-(4-(6-methoxy-5-(*N*-methylsulfamoyl)pyridin-3-yl)-3,4-dihydro-2*H*benzo[*b*][1,4]oxazin-7-yl)-2-(1-methylpiperidin-3-yl)acetamide (380)**



2-(1-Methylpiperidin-3-yl)acetic acid (55 mg, 0.350 mmol) was dissolved in DMF (1.5 mL). DIPEA (90 μ L, 0.51 mmol) and HATU (138 mg, 0.363 mmol) were added followed by 5-(7-amino-2*H*-benzo[*b*][1,4]oxazin-4(3*H*)-yl)-2-methoxy-*N*-methylpyridine-3-sulfonamide **265** (60 mg, 0.17 mmol). The mixture was stirred at room temperature for 3 h. EtOAc (10 mL) and sat. aq. sodium bicarbonate (10 mL) were added. The organic layer was separated and the aqueous layer was extracted a second time with EtOAc (10 mL). The combined organic layers were passed through a hydrophobic frit and concentrated under a stream of nitrogen overnight. The crude product was purified by reverse phase chromatography using MDAP (formic, 530%) to give the title product **380** as a yellow solid (47 mg, 56%). mp 90-93 $^{\circ}$ C 1 H NMR (400 MHz, DMSO- d_6) δ 9.65 (s, 1H), 8.30 (d, J = 2.8 Hz, 1H), 7.89 (d, J = 2.8 Hz, 1H), 7.37 (br. s, 1H), 7.24 (d, J = 2.3 Hz, 1H), 6.91 (dd, J = 2.3, 8.8 Hz, 1H), 6.61 (d, J = 8.8 Hz, 1H), 4.23 (t, J = 3.8 Hz, 2H), 3.98 (s, 3H), 3.66 (t, J = 4.0 Hz, 2H), 2.56 - 2.69 (m, 2H), 2.47 - 2.52 (m, 3H), 2.15 (d, J = 7.0 Hz, 2H), 2.11 (s, 3H), 1.97 (dd, J = 10.2, 6.9 Hz, 1H), 1.78 - 1.87 (m, 1H), 1.54 - 1.68 (m, 3H), 1.39 - 1.51 (m, 1H), 0.85 - 0.97 (m, 1H); 13 C NMR (151 MHz, DMSO- d_6) δ 169.6 (C=O), 155.1 (Ar-C), 145.9 (Ar-CH), 144.7 (Ar-C), 137.7 (Ar-C), 134.3 (Ar-CH), 132.8 (Ar-C), 127.3 (Ar-C), 121.9 (Ar-C), 116.3 (Ar-CH), 112.1 (Ar-CH), 108.2 (Ar-CH), 63.9 (CH $_2$), 61.3 (CH $_2$), 55.6 (CH $_2$), 54.1 (CH $_3$), 48.6 (CH $_2$), 46.3 (CH $_3$), 41.2 (CH $_2$), 33.1 (CH), 29.6 (CH $_2$), 28.7 (CH $_3$), 24.5 (CH $_2$); LCMS (ESI, high pH) m/z 490 [M+H] $^+$, Rt = 0.91 min; HRMS (ESI) calcd for C $_{23}$ H $_{32}$ N $_5$ O $_5$ S [M+H] $^+$ 490.2119, found 490.2116 (3.3min); IR (ATR) cm^{-1} 2931, 1655, 1599, 1507, 1474, 1416, 1329, 1294, 1244, 1160.

***N*-(4-(6-methoxy-5-(*N*-methylsulfamoyl)pyridin-3-yl)-3,4-dihydro-2*H*benzo[*b*][1,4]oxazin-7-yl)-2-(1-methylpyrrolidin-3-yl)acetamide, formic acid salt (381)**



2-(1-Methylpyrrolidin-3-yl)acetic acid (49 mg, 0.34 mmol) was dissolved in DMF (1.5 mL). DIPEA (90 μ L, 0.514 mmol) and HATU (130 mg, 0.342 mmol) were added followed by 5-(7-amino-2*H*-benzo[*b*][1,4]oxazin-4(3*H*)-yl)-2-methoxy-*N*-methylpyridine-3-sulfonamide **365** (60 mg, 0.17 mmol). The mixture was stirred at room temperature for 3 h. EtOAc (10 mL) and sat. aq. sodium bicarbonate (10 mL) were added. The organic layer was separated and the aqueous layer was extracted a second time with EtOAc (10 mL). The combined organic layers were passed through a hydrophobic frit and concentrated under a stream of nitrogen overnight. The crude product was purified by reverse phase chromatography using MDAP (formic acid, 530%) to give the title product **281** as a yellow solid (11 mg, 12%). ¹H NMR (400 MHz, DMSO-*d*₆) δ 9.71 (s, 1H), 8.30 (d, *J* = 2.8 Hz, 1H), 8.25 (s, 1H, formic), 7.89 (d, *J* = 2.8 Hz, 1H), 7.38 (br. s, 1H), 7.23 (d, *J* = 2.3 Hz, 1H), 6.91 (dd, *J* = 8.6, 2.3 Hz, 1H), 6.61 (d, *J* = 8.6 Hz, 1H), 4.23 (t, *J* = 4.3 Hz, 2H), 3.98 (s, 3H), 3.66 (t, *J* = 4.2 Hz, 2H), 2.71 (dd, *J* = 9.2, 7.7 Hz, 1H), 2.52-2.60 (m, 2H), 2.25-2.36 (m, 7H), 1.91-2.02 (m, 1H), 1.38-1.49 (m, 1H); LCMS (ESI, formic *m/z* 476 [M+H]⁺, Rt = 0.53 min.